New Approaches to the treatment of Schizophrenia and other Neuropsychiatric Disorders: Targeting α_2-adrenoceptors

A thesis presented to Trinity College Dublin, the University of Dublin, for the degree of Doctor of Philosophy

Aaron P. Keogh, B.A. (Mod.)

Trinity College Dublin

The University of Dublin

Based on research carried out under the supervision of Prof. Isabel Rozas

School of Chemistry

2019

Declaration

This thesis is submitted for the degree of Doctor of Philosophy to the University of Dublin, Trinity College and has not been submitted before for any degree or examination to this or any other university. Other than where acknowledged, all work described herein is original and carried out by the author alone. Permission is granted so that the Library may lend or copy this thesis upon request. This permission covers only single copies made for study purposes, subject to normal conditions of acknowledgment.

_____

Aaron P. Keogh

Abstract

Schizophrenia is a severe mental illness affecting 21 million people worldwide, resulting in cognitive impairments and negative symptoms that impact patients' ability to live a normal life. Almost all current antipsychotic drugs are dopamine D2 antagonists, which largely address only the positive symptoms. Effective treatments for negative symptoms and cognitive deficits remain unmet clinical needs. The α_{2C}-adrenoceptor (α_{2C}-AR) has been highlighted as a promising neuropsychiatric drug target with excellent therapeutic potential to treat affective and cognitive symptoms. Non-selective α_2-AR antagonism may compromise therapeutic utility; however, selective α_{2C}-AR antagonists have demonstrated pro-cognitive, antidepressant and antipsychotic actions in animal models of neuropsychiatric disorders.

This study takes a two-fold approach aimed at expanding our understanding of the structural characteristics required for receptor engagement of guanidine-based α_2-AR ligands. Firstly, a retrospective analysis of *hit* α_2-AR ligands developed over the last 20 years within the Rozas group was conducted, a selection of the most pertinent ligands were chosen to be synthesised and submitted for comprehensive pharmacological screening at the National Institute of Mental Health Psychoactive Drug Screening Program in the University of North Carolina, Chapel Hill, (USA).

A deeper understanding of the receptor engagement profiles exhibited by these compounds informed the design of novel derivatives that may display optimal pharmacological properties to become novel drug candidates for treatment of schizophrenia and other neuropsychiatric disorders. Hence, the influence of subtle structural modifications around the cationic moiety of current *hit* compounds on their affinity, activity and selectivity at the α_2-ARs was synthetically explored to elucidate and potentially improve the characteristics needed to impart the desired biological activity. Secondly, the subtype selectivity of some derivatives with structural similarities to known α_{2C}-AR ligands were studied in collaboration with Prof. Callado (University of the Basque Country, Spain), the results of which served as a base for the preparation of new derivatives currently awaiting pharmacological evaluation.

This work and the resultant outcomes constitute a strong foundation for future expansion and investigation of novel α_2-AR subtype selective ligands. The extensive receptor profiles compiled herein will serve as guidelines to assist in the development of new molecules with enhanced affinity and selectivity aimed at particular targets within the central nervous system and can be used in the development of drugs to treat a wide range of mental disorders.

Abbreviations

AC: adenylyl cyclase

ACh: Acetylcholine

Ad: Adrenaline

ADHD: Attention deficit hyperactivity disorder

AMPA: α-amino-3-hydroxy-5-methyl-4-isoxazolepropionic acid

AMY: Amygdala

AR: Adrenoceptor/adrenergic receptor

Ar: Argon

Asp: Aspartate

ATP: Adenosine triphosphate

Ca^{2+}: Calcium ions

cAMP: Cyclic adenosine monophosphate

CNS: Central nervous system

CHO: Chinese Hamster ovaries cells

CH_2Cl_2: Dichloromethane

COMT: Catechol *O*–methyl transferase

DA: Dopamine

DSM-V: Diagnostic and Statistical Manual of Mental Disorders, 5th Edition

DAG: Diacylgycerol

DRN: Dorsal raphe nucleus

EPS: Extrapyramidal symptoms

EtOAc: Ethyl acetate

Et_2O: Diethyl ether

FST: Forced swim test

Four A's: Ambivalence, autistic behaviour, blunted affect and loss of association

GPCR: G-protein coupled receptors

G proteins: Guanine nucleotide-binding proteins

GTP: Guanosine triphosphate

GDP: Guanosine diphosphate

GABA: γ-Aminobutyric acid

Glu: Glutamate

Gly: Glycine **HCl**: Hydrochloric acid

H: Histamine receptor

Hex: Hexanes

$HgCl_2$: Mercury (II) chloride

5-HT: 5-hydroxytryptamine/serotonin

IP_3: Inositol triphosphate

ITC: Isothiocyanate

KO: Knock-out

LC: Locus coeruleus

LSD: *D*-lysergic acid diethylamide

mAChR: Muscarinic acetylcholine receptor

MAO: Monoamine oxidase

MAT: Monoamine transporter

MAP: Mitogen-activated kinase

MC: Mesocortical

MDD: Major depressive disorder

MeCN: Acetonitrile

mGluR: Metabotropic glutamate receptors

MK-801: Dizoclipine

ML: Mesolimbic

NA: Noradrenaline

NAc: Nucleus accumbens

NEt_3: Triethylamine

NET: Noradrenaline transporter

NMDA: N-methyl-*D*-aspartate

NO: Nitrous oxide

NT: Neurotransmitter

PCP: Phencyclidine

PDSP: Psychoactive drug screening program

Pd/C: Palladium on carbon

PET: Positron emission tomography

PFC: Prefrontal cortex

PHL: *L*-phenylalanine

PIP_2: Phosphatidylinositol 4,5-bisphosphate

PKA: cAMP-dependent protein kinase A

PKC: Protein kinase C

PLC: Phospholipase C

PPP: Platelet poor plasma

PRP: Platelet rich plasma

SAR: Structure-activity relationship

SERT: Serotonin transporter

SNRI: Serotonin and noradrenaline reuptake inhibitor

SPECT: Single photon emission computerized tomography

SSRI: Selective serotonin reuptake inhibitor

SZ: Structure-selectivity relationship

TCA: Tricyclic antidepressant

TeCA: Tetracyclic antidepressant

TFA: Trifluoroacetic acid

THF: Tetrahydrofuran

TLC: Thin layer chromatography

VDCC: Voltage-dependant calcium channels

VTA: Ventral tegmental area

WHO: World Health Organization

WP: Washed platelets

Acknowledgements

Firstly, I want to express my deepest gratitude to my supervisor Prof. Isabel Rozas for believing in me and always encouraging me to pursue my ideas whilst providing support, trust and guidance over the past number years. Her door is always open and a pleasure to walk through as her constant compassion and reliable advice has provided reassurance and inspired hope during the most challenging times. My time in the Rozas group has allowed me to learn and grow, both professionally and personally, in more ways than I had ever expected and for that I will continue to value her not only as an excellent mentor but as a dear friend.

I have had the pleasure of working with some truly brilliant and talented people over the past four years. I am grateful to all former members of the Rozas groups, in particular Paddy, Michela, Viola, Cristina, Jagdeep and Filippo for all of their advice and expertise readily offered to assist and overcome many chemistry related issues. Together we formed a great team and I am lucky to call them true friends. I would also like to thank the current members of the Rozas group, Yemi, Helene and Nikolina, for their friendship and wish them well as they grow together into another great team.

Danielle Barnes, Lauren McSweeney and Keith Flanagan have been the most supportive, dependable and hilarious friends from day one, I will be forever indebted to each of them for everything they have done for me and all the great memories from coffee breaks and nights out have made the last four years unforgettable. Thanks also to Katie, Josh and Dylan whose great humour, advice, perspective and fun attitude have always been hugely appreciated, particularly when things weren't going well.A huge thanks to all the technical and administrative staff in the School of Chemistry. In particular, I would like to thank Dr. John O' Brien and Dr. Manuel Ruether for all of their assistance and expertise in all things NMR related; Dr. Martin Feeney and Dr. Gary Hessman for Mass Spectroscopy and Dr. Brendan Twamley X-ray crystallography for all of their assistance.

I must also acknowledge our collaborators in the pharmacology laboratory of Prof. Luis Callado at the UPV/EHU (Bilbao, Spain) for all the pharmacological assays. Thanks and credit are given for the screening services provided by Dr. Bryan Roth and the NIMH PDSP at the UNC (Chapel Hill, USA). My immense gratitude goes to Prof. Maria Santos-Martinez and Nadhim Kamil Hante from the TCD School of Pharmacy and Pharmaceutical Sciences for all their help, enthusiasm and expertise in all aspects of the human platelets study.

To my parents, Paula and Aidan, and my brother Colin – you all have always been there to support and guide me in different ways throughout this whole process. I can always depend on all of you for encouragement, support and help whenever needed – for this I am blessed and forever grateful. To my best friend and girlfriend Jenny – your unconditional love, kindness, dedication and patience have been ever-present in all aspects of my life and I can honestly say that I could not have done this without you.

Table of Contents

Chapter One
Introduction

1.1. Adrenergic receptors

Adrenergic receptors, adrenoceptors (ARs), are class A G-protein-coupled receptor (GPCR) transmembrane proteins which mediate physiological responses to endogenous catecholamine agonists adrenaline (Ad) and noradrenaline (NA). The investigation and original pharmacological classification of AR subtypes by Ahlquist *et al.*, designating α- and β-ARs, was based upon the observation that various natural and synthetic catecholamines induced different tissue-dependent responses. Specifically, α-ARs were shown to mediate most excitatory functions particularly in the cardiovascular system (*i.e.* vasoconstriction) and central nervous system (CNS) (*i.e.* neurotransmission). They were subdivided into α_1- and α_2-ARs in the 1970s through functional activity and ligand binding studies. Conversely, β-AR mediate most inhibitory functions, such as smooth muscle relaxation in the airways and vasculature, as well as one important excitatory function - cardiac contraction and increased heart rate.[1]

Presently, ARs are classified into two major alpha types, alpha1 (α_1), alpha2 (α_2) and three beta subtypes (β_1, β_2 and β_3)[2], which differ in their pharmacological specificity and tissue localization. Isolation, purification and molecular cloning methods have enabled alpha types to be further subdivided into genetically and functionally distinct subtypes:[3] α_{1A}, α_{1B} and α_{1D} as well as $\alpha_{2A/D}$, α_{2B} and α_{2C}.

The focus of this work is the development of compounds targeting receptors within the CNS, primarily α_2-ARs; however, both the β_1- and β_2-AR are the only ARs to date which have been successfully co-crystallized with multiple ligands in various activation states, the high resolution structures of which have been determined by X-ray crystallography.

In particular the β_2-AR has become a model system for hormone-activated GPCRs and has been subject to intensive experimental and computational studies yielding valuable insight into and understanding of GPCR structural biology, pharmacology, signalling and regulation.[4] Therefore, the β_2-AR will be utilized as a representative GPCR for the discussion of activation states, guanine nucleotide-binding proteins (G-proteins) and related ligand terminology.

1.1.2. G-Proteins Coupled Receptors and G-proteins

The crystallization and structural elucidation of bovine rhodopsin and the β_2-AR heralded a new age of GPCR based research facilitating advancements in numerous fields from structural biology and biochemistry to medicinal chemistry and drug discovery.[5] Up to 2016, crystal structures for 27 Class A GPCRs have been determined in either their active or inactive states, five of which have both active and inactive structures available including the β_2-AR.

GPCRs represent the largest family of druggable targets in the human genome with nearly a third of all prescribed medications designed to target them. GPCRs exhibit complex functional plasticity due to structural flexibility and their ability to adopt a range of ligand-specific conformational states. This further complicates GPCR-modulating drug design despite the availability of target crystal structures. The general secondary structure of a GPCR is depicted in Fig. 1.1.1, with an intracellular C-terminus and extracellular N-terminus.[6]

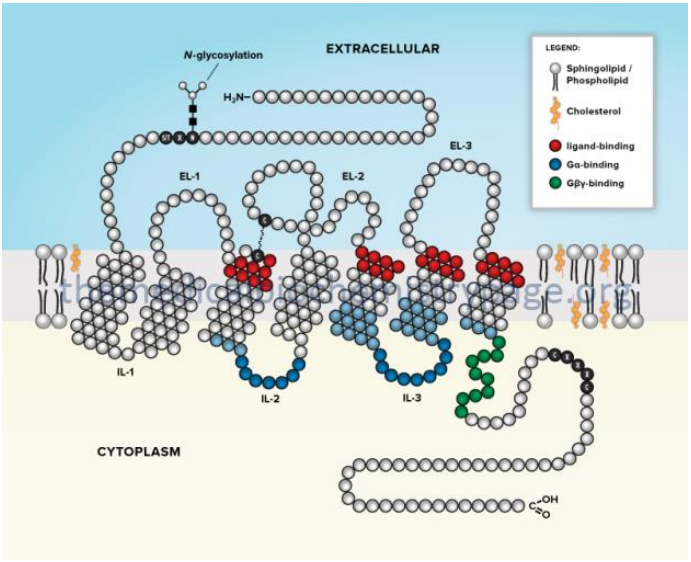

Figure 1.1.1 Generalised secondary structure of a GPCR.[7]

The transmembrane domain, comprised of seven hydrophobic transmembrane spanning α-helices TM1-7, is the key to effective transmission of a signal across the cytoplasm upon ligand binding to the extracellular side of GPCRs.[8] Ligand binding triggers rearrangement of residue contacts between the transmembrane helices leading to extensive conformational change of the cytoplasmic domains facilitating receptor activation together with receptor-mediated binding and allosteric activation of intracellular G-proteins.[6]

G-proteins are localized at the plasma membrane by an anchoring mechanism through lipid modification (myristoylation/palmitoylation) of an N-terminal glycine residue. Heterotrimeric G-proteins are comprised of three distinct subunits, a nucleotide-binding α-subunit (Gα) and a dimer composed of the β- and γ- subunits (Gβγ).[5] The Gβγ dimer, whilst acting as a Gα-independent signalling moiety capable of modulating effector systems, also plays an important role in controlling Gα-dependent signalling by acting as an anchorage point on the plasma membrane and assisting in coupling the G-protein complex to the proper receptor. [9]

Inactive G-proteins consists of the α-subunit bound to Guanosine diphosphate (GDP) tightly associated to the Gβγ dimer forming the inactive Gαβγ complex (Gα-GDP). According to the ternary complex model of GPCR activation, inactive G-proteins are recruited to the activated receptor (agonist bound) forming a ternary complex (Fig. 1.1.2).[5]

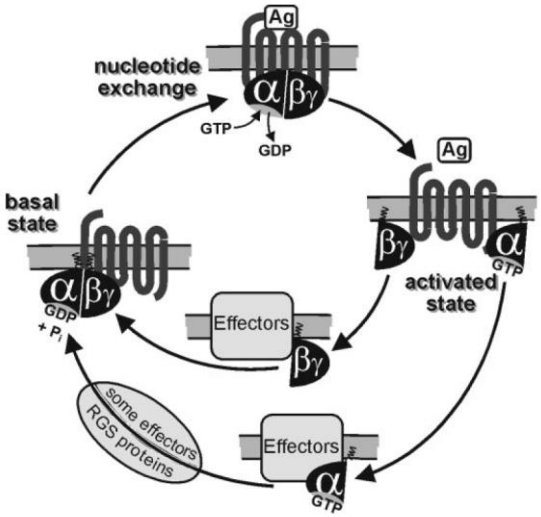

Figure 1.1.2. Functional cycle of G-protein activity.[10]

GPCR binding propagates conformational change to the Gαβγ complex inducing allosteric activation of the G-protein *via* guanine nucleotide exchange, Gα-GDP to Gα-Guanosine triphosphate (GTP), leading to rapid dissociation into free active subunits Gα-GTP and Gβγ. These subunits further propagate signal transduction *via* diffusion from the receptor to a plethora of effector systems and initiating intracellular signalling cascades.[11] The GTPase domain of the Gα subunit hydrolyses bound GTP to GDP reverting this subunit to its inactive state, subsequently controlling signal duration.[12]

The Gα subunit, containing the guanine nucleotide binding site and GTPase domain, is a crucial molecular signalling transducer which enables transmission of stimuli from GPCRs to intracellular effectors. There are four general subfamilies of G-proteins: $G_{i/o}$, G_s, $G_{q/11}$ and $G_{12/13}$ (Fig.1.1.3).[9] G_o, serendipitously discovered during purification of brain G_i protein, is the most abundant G-protein in the CNS which comprises between 0.5-1% of membrane proteins in the mammalian brain. $G\alpha_o$ transmits signals from numerous GPCRs to intracellular effectors including ion channels and enzymes (both membrane bound and cytosolic).[9]

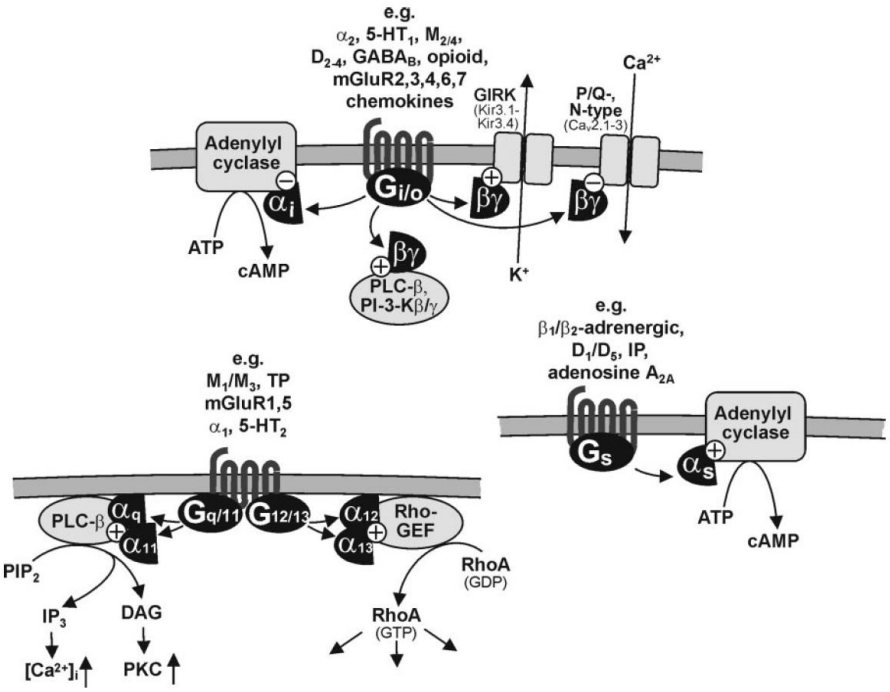

Figure 1.1.3. Schematic representation of the four general subfamilies of G-proteins- $G_{i/o}$, G_s, $G_{q/11}$ and $G_{12/13}$ and associated effector systems.[10]

Members of the $G_{i/o}$ family share more than 60% sequence identity and 70% similarity making them highly homologous. The three $G\alpha_i$ and two $G\alpha_o$ subunits are functionally similar *in vitro* but differ in their *in vivo* distribution.[9] Typically, α_2-AR couple to the $G_{i/o}$ family of G proteins which decrease the activity of adenylyl cyclase (AC), the enzyme which converts adenosine triphosphate (ATP) to cyclic adenosine monophosphate (cAMP), thereby decreasing cAMP levels.

The stimulatory G_s proteins increase AC activity whilst the $G_{q/11}$ family activates phospholipase C (PLC) which mediates protein kinase C (PKC) activation. Proteins G_q and G_{11} are expressed ubiquitously in the CNS.[13] In particular, the $G_{q/11}$ of α_1-ARs are coupled to and activate PLC, which converts phosphatidylinositol 4,5-bisphosphate (PIP_2) into inositol triphosphate (IP_3) and diacylgycerol (DAG), each of which act as second messengers.[14] The $G_{12/13}$ family are involved in the regulation of the GTPase Rho.[15] Many GPCRs exhibit promiscuous coupling to more than one G-protein, such as the β_2-AR which preferentially couples to G_s, as in Fig.1.1.4, but is also capable of activating $G_{i/o}$; conversely, the α_2-AR is known to couple to G_s as well as $G_{i/o}$ proteins.[16,17]

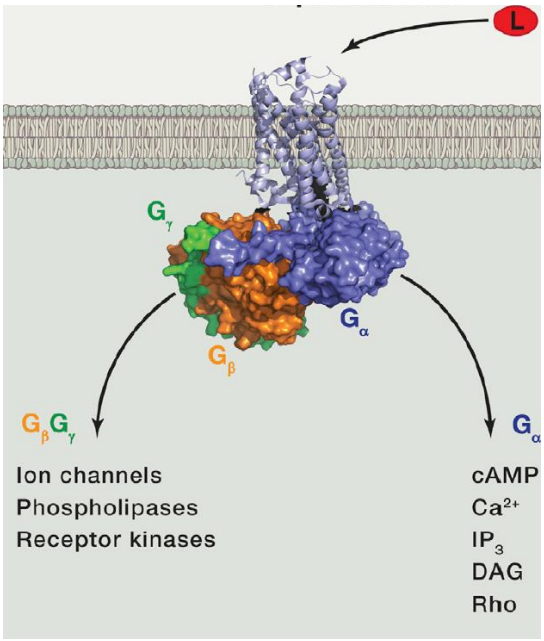

Figure 1.1.4. Modified diagram of β_2-AR activation and G-protein heterotrimer activation, dissociation and associated signalling casacades.[18]

1.1.3. Neurotransmitters and synaptic transmission

GPCRs are abundant in the CNS and comprise a large majority of the neurotransmitter (NT) receptors expressed throughout the nervous system. These receptors are major modulators of NT action and play an important role in synaptic transmission. There are two mechanisms by which neurons communicate with each other – direct transfer of intercellular signals *via* gap junctions at electrical synapses or the secretion of NTs at chemical synapses.[19] Neurotransmitters are divided into four classes:

1. The classical NTs - γ-aminobutyric acid (GABA), glycine (Gly), glutamate (Glu), acetylcholine (ACh), adenosine and ATP.
2. The monoaminergic NTs - dopamine (DA), NA, Ad, serotonin (5-hydroxytryptamine, 5-HT) and histamine.
3. The neuropeptides (*e.g.* vasopressin and neurotensin)
4. The membrane-permeable mediators nitric oxide (NO), endocannabinoids and other gaseous and lipidic NTs.[19]

Synaptic transmission is the strictly regulated mechanism by which neurons communicate with each other by the release of various NTs, principally between an axon terminal of the pre-synaptic neuron and dendritic spines of post-synaptic neurons. The vast majority of NTs are released by calcium (Ca^{2+})-dependent exocytosis from axon terminals, as shown in Fig. 1.1.5.[20]

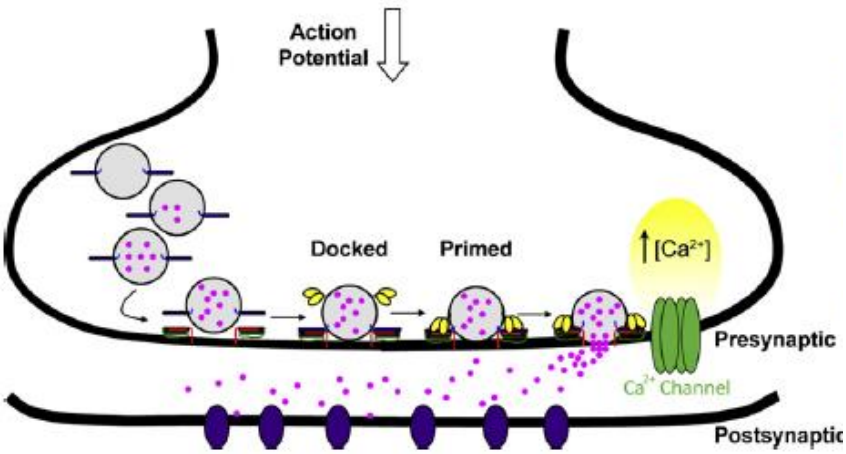

Figure 1.1.5. General scheme of synaptic transmission *via* Ca^{2+} dependant exocytosis. [20]

As the presynaptic membrane is depolarized, voltage-dependant Ca^{2+} channels (VDCCs) become activated causing an influx of Ca^{2+} ions which bind to synaptotagmin and calmodulin to facilitate synaptic vesicle fusion and NT exocytosis. This allows for efficient neuronal communication which is crucial to the normal functioning of the nervous system.[20]

1.2. Monoaminergic Neurochemistry

1.2.1. Central Adrenergic System

1.2.1.1. Noradrenergic neurotransmission

Many GPCRs, like α-ARs, are localised in both presynaptic and postsynaptic membrane terminals where they regulate both intra-synaptic and inter-synaptic communication.[19] All presynaptic autoreceptors in noradrenergic neurons are of the α_2 subtype and regulate the release of NA from noradrenergic terminals by a negative feedback mechanism.

The α_{2A} subtype is the predominant presynaptic autoreceptor within the CNS;[21] however, both α_{2B} and α_{2C} subtypes are also known to act as presynaptic autoreceptors (Fig. 1.2.1.). α_2-ARs are also located on non-adrenergic neurons, such as serotoninergic and cholinergic neurons, which are called α_2-heteroceptors and modify the release of other NTs such as these.[14] Noradrenergic neurons are localized in brainstem nuclei such as the locus coeruleus (LC) with almost every part of the brain innervated by noradrenergic axonal projections.[22]

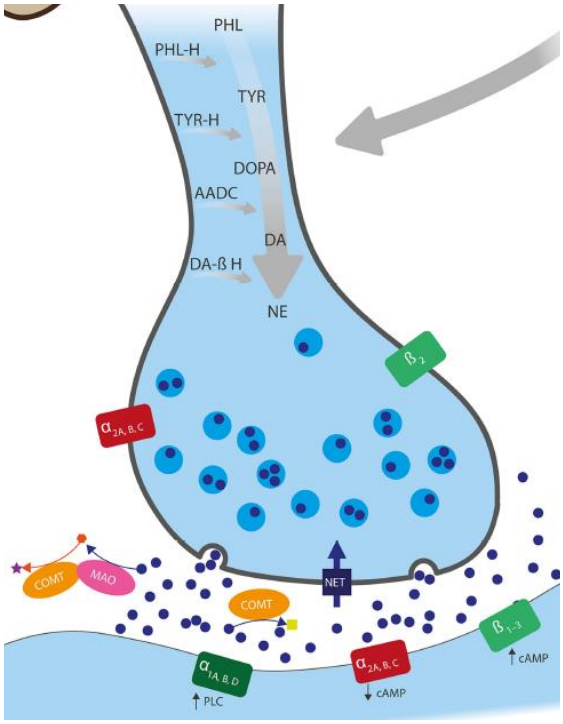

Figure 1.2.1. Schematic representation of a synapse between a noradrenergic neuron and post-synaptic cell expressing ARs. [*Key: Phenylalanine (PHL), phenylalanine hydroxylase (PHL-H), tyrosine (TYR), tyrosine hydroxylase (TYR-H), 3,4-dihydroxyphenylalanine (DOPA), aromatic amino acid decarboxylase (AADC), dopamine (DA), dopamine β-hydroxylase (DA-βH), noradrenline (NE), monoamine oxidase (MAO), catechol O-methyl transferase (COMT) and noradrenaline transporter (NET),cyclic adenosine monophosphate (cAMP) and phospholipase C (PLC).*][23]

Noradrenergic and dopaminergic neurons share a common biosynthetic pathway through which DA is synthesized and subsequently converted to NA, with both NTs deriving from the amino acid precursor *L*-phenylalanine (PHL).[24] NA and DA are degraded by catabolic enzymes monoamine oxidase (MAO) and catechol *O*-methyl transferase (COMT) to inactive metabolites such as homovanillic acid and normetanephrine.[25]

Sufficient stimulation of a noradrenergic neuron results in noradrenergic firing involving the propagation of an action potential towards the axon terminals which triggers Ca^{2+}-dependent exocytosis of NA into the synaptic cleft as detailed above. Once a threshold concentration of NA is reached within the synaptic cleft a negative feedback mechanism is initiated. This involves activation of presynaptic α_2-AR autoreceptors through binding of endogenous NA which activates the G-protein complex causing dissociation and releasing active $G\alpha_{i/o}$ and $G\beta\gamma$ subunits.[24]

Inhibition of AC by the active GTP bound $G\alpha_{i/o}$ subunit leads to a subsequent reduction in cAMP levels which prohibits Ca^{2+} influx *via* modulation of cyclic-nucleotide gated ion channels. The Gβγ subunit can directly inhibit VDCCs by stabilizing the channel in a less active conformational state and it can also activate GIRK K^+ channels and mitogen-activated (MAP) kinases ERK1/2. These intra-synaptic signalling cascades culminate to effectively inhibit synaptic vesicle exocytosis which subsequently terminates synaptic transmission by preventing further NA release, as shown in Fig.1.2.2.[26] NA is then either metabolised by MAO and COMT within the synaptic cleft or transported back into the neurons *via* NA transporters (NETs).

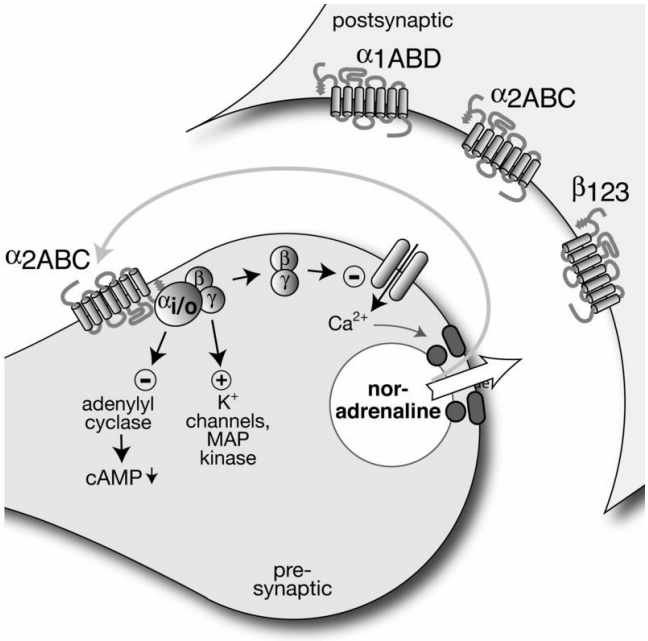

Figure 1.2.2. Presynaptic regulation of NA release *via* negative feedback mechanism.[26]

Amongst the α_2-AR subfamily, α_{2A} is the most widely distributed subtype within the CNS with α_{2A}-AR mRNA prominently expressed in the olfactory system, cerebral cortex, septal area basal ganglia area, amygdaloid body of the midbrain, cerebellum, pens and medulla whilst expression in the striatum is low. Besides, α_{2C}-ARs are predominantly located in the striatum and hippocampus, but are also present in much lower levels in the PFC. Finally, α_{2B}-AR have a limited presence in the CNS with only weak expression in the thalamus.[21]

1.2.1.2. The role of the noradrenergic system in neuropsychiatric disorders

α_2-AR are seen to be the principal regulatory receptors controlling noradrenergic neurotransmission and as such have been subject to intense investigation due to their potential role in many neuropsychiatric disorders such as major depressive disorder (MDD), schizophrenia (SZ) and attention deficit hyperactivity disorder (ADHD).[22] The understanding of the role that NA and its receptors play in these disorders has evolved over recent years, uncovering new hypothesis incorporating other monoaminergic NTs (i.e. DA and 5-HT) in the complex pathology of these disorders, highlighting their potential as unique therapeutic targets. In fact, the DA hypothesis is considered the classical neuropathological explanation for schizophrenic symptoms (discussed in section 1.5) and are the basis for all current antipsychotic drugs.[23]

The neuropathology of MDD and associated neuropharmacology of antidepressant drugs are some of the most rigorously investigated topics in the field of neuropsychiatric disorders. The classical monoaminergic theory of depression had long been considered the sole causative explanation for the illness, stipulating that deficits of NA and 5-HT in different parts of the brain were responsible for the symptoms of MDD. This theory was inspired by the therapeutic effectiveness of tricyclic antidepressants (TCAs), such as amitriptyline (**1**), imipramine (**2**) and desipramine (**3**) (Fig. 1.2.3).

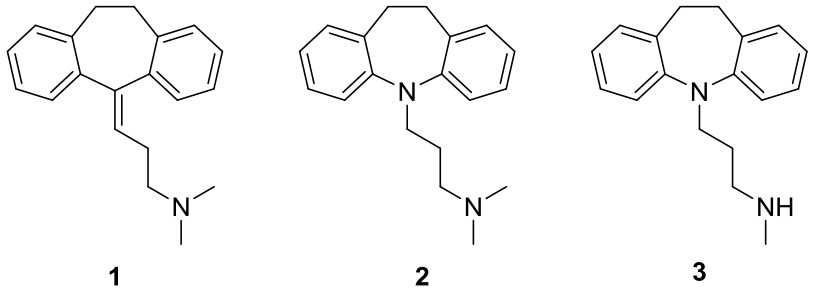

Figure 1.2.3. Structure of TCAs amitriptyline (**1**) and imipramine (**2**), both dual NA/5-HT re-uptake inhibitors (SNRIs), and desipramine (**3**), which is a selective NA re-uptake inhibitor (NRI).

These drugs increase synaptic availability of monoamine NTs by inhibiting monoamine reuptake through monoamine transporters (MATs), namely serotonin and noradrenaline transporters (SERTs and NETs respectively). [27]

Today it is widely accepted that this theory is an overly simplistic model of the complex pathophysiology of MDD; however, it still remains a central guiding component for the development of antidepressants.[28]

1.2.1.3. Relationship between Noradrenaline, Dopamine and Pre-frontal Cortex function

Enhancing monoamine neurotransmission has proven to be an effective approach to treat the symptoms of MDD. Selective 5-HT reuptake inhibitors (SSRIs), such as fluoxetine (**6**), and tetracyclic antidepressants, such as mirtazapine (**4**) and mianserin (**5**), are highly effective antidepressants utilized for the treatment of MDD (Fig. 1.2.4.). **6** is sold as a racemic mixture of *R*- and *S*-enantiomers, both being potent SSRIs; however, *R*-fluoxetine is also a moderate antagonist at the 5-HT_{2C} receptor.[28] **5** is an antagonist at presynaptic α_2-AR autoreceptors and 5-HT_{2C} receptors. **4** is considered a noradrenergic and specific serotonergic antidepressant as it is a potent antagonist of central α_2-AR auto- and heteroreceptors, selectively activating 5-HT_1 receptors and antagonising both 5-HT_{2C} and 5-HT_3 receptors, which in combination enhance both noradrenergic and serotonergic neurotransmission.[21]

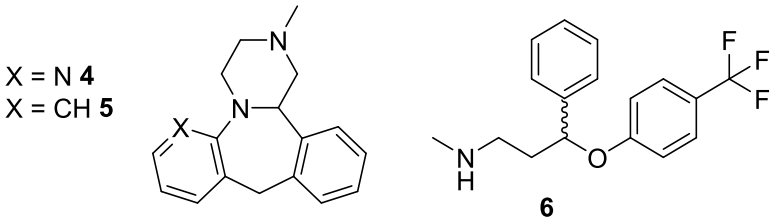

Figure 1.2.4. Structure of tetracyclic antidepressants mirtazapine (X = N, **4**) and mianserin (X = CH, **5**) and fluoxetine (**6**).

It is well established that the central adrenergic system regulates the midbrain dopaminergic system through a variety of different interactions.[29] Axonal projections of the dopaminergic neurons at the LC and ventral tegmental area (VTA) converge at the PFC where they play a crucial regulatory role in cognitive and emotional functions. Noradrenergic and dopaminergic dysfunction in this region is known to contribute to neuropsychiatric disorders such as aforementioned MDD and SZ. The α_2-ARs on LC-prefrontal noradrenergic neurons exert inhibitory control of noradrenergic firing and NA release in the medial PFC.

In particular, α_{2A}-AR are highly expressed along meso-prefrontal dopaminergic neurons and have been shown to act as heteroreceptors involved in controlling PFC DA release upon administration of α_2-ARs ligands.[30]

1.2.2 Dopaminergic System

DA is a NT involved in the regulation of different pathways implicated in cognitive functions, motor coordination and emotions.[29] Dopaminergic projects stem from the VTA in the midbrain to the cerebral cortex, known as the mesocortical (MC) pathway, from the VTA to the nucleus accumbens (NAc) known as the mesolimbic (ML) pathway and from the substantia nigra to the striatum termed the nigrostriatal pathway. There are two families of DA receptors all of which are GPCRs: D_1-like (D_1 and D_5 receptors) which are mainly post-synaptic and coupled to the G_s protein. The D_2-like receptor family (D_2, D_3 and D_4 receptors) couple to the G_i protein and are localized both pre- and post-synaptically.[31]

There is a wide distribution of DA receptors throughout the CNS, with D_1 and D_2 the most highly expressed subtypes. The NS, ML and MC areas such as the striatum, NAc, substantia nigra, olfactory bulb, amygdala (AMY) and frontal cortex all show high levels of D_1 expression. Highest levels of D_2 mRNA expression are found in the striatum, NAc, and olfactory tubercle with the substantia nigra, VTA, hypothalamus, septum, AMY and hippocampus also showing D_2 expression.[32] The other subtypes exhibit low levels of expression with only the D_3 subtype showing high levels of expression in limbic areas. As mentioned, dysfunction of DA neurotransmission is thought to underlie multiple neuropsychiatric illnesses including Parkinson's disease, SZ and MDD.[33]

As D_1 receptors are highly concentrated in the PFC, the role of the D_1-like receptor family in the regulation of cognitive function has been extensively researched. DA and NA provide an essential modulatory influence on the working memory and attentional functions of the PFC, with a landmark study by Brozoski *et al.*

These authors demonstrated that depletion of catecholamines from the dorsolateral PFC in rhesus monkeys was as detrimental to memory performance as actually removing the cortex itself. This highlights the sensitivity of the PFC and associated cognitive functions to subtle changes in levels of DA and NA stimulation.[34] This delicate modulatory balance of PFC DA and NA levels has been implicated in depressive and psychotic symptoms.

Microdialysis studies have shown that alterations in the levels of NA and DA in response to pharmacological treatment are linked as modifications of extracellular NA in the medial PFC also produces parallel changes in extracellular DA. Chemical or electronic stimulation of LC noradrenergic neurons led to a concomitant modification of NA and DA levels in the medial PFC, whilst only NA efflux was enhanced in the striatum. This evidence supports a common origin for NA and DA in the cerebral cortex perhaps with DA not only acting as a precursor to NA in noradrenergic neurons but also as co-transmitter. This relationship emphasises the utility of the noradrenergic system as a target for drugs to address deficits in superior cognitive functions such as those associated with SZ and MDD.[35]

Exposure to environmental or chemical stress has been shown to increase PFC DA release which can impair higher PFC functions in both animals and humans by activation of postsynaptic D_1 receptors (Fig. 1.2.5).[36] Low to moderate levels of NA improve PFC function, possibly *via* α_{2A}-ARs, whereas high concentrations of NA impair function. This impairment is thought to be due to binding of α_1-ARs (Fig. 1.2.5) as NA has a lower affinity for α_1 than α_2-ARs. These finding are relevant to SZ and MDD, as these stress-related disorders are known to be exacerbated or precipitated by stress exposure due to the inherent dysregulation of stress signalling pathways contributing to the neuropathology of these neuropsychiatric diseases.[37]

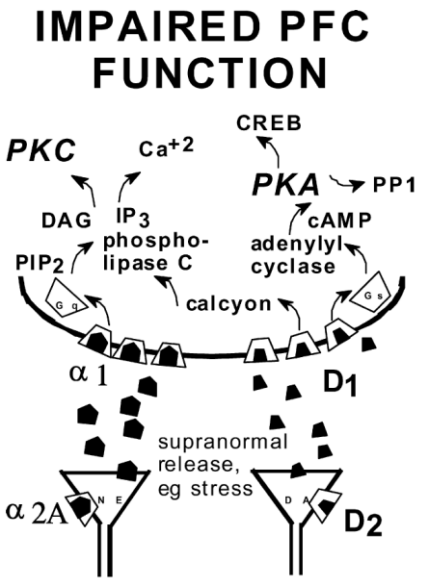

Figure Figure 1.2.5. Noradrenergic and dopaminergic mechanisms for stress induced impairment of PFC function.[37]

1.2.3. Serotonergic system

5-HT is a monoaminergic NT with highly complex receptor pharmacology. There are 14 subtypes of 5-HT receptors divided into seven major families, six of which consist of GPCRs (5-HT_1, 5-HT_2, 5-HT_4, 5-HT_5, 5-HT_6 and 5-HT_7) with only the 5-HT_3 family (5-$HT_{3A,}$ 5-HT_{3B}, 5-HT_{3C}, 5-HT_{3D} and 5-HT_{3E}) being pentameric ligand-gated ion channels (ionotropic). The 5-HT_1 (5-HT_{1A}, 5-HT_{1B}, 5-HT_{1D}, 5-HT_{1E} and 5-HT_{1F}) and 5-HT_5 receptor (5-HT_{5A} and 5-HT_{5B}) families' couple to $G_{i/o}$ whilst the 5-HT_2 receptors (5-$HT_{2A,}$ 5-HT_{2B} and 5-HT_{2C}) are $G_{q/11}$ coupled. The 5-HT_4, 5-HT_6 and 5-HT_7 receptor families are coupled to the stimulatory G_s family which activate AC.

Dual 5-HT_{1A} and 5-HT_7 antagonists have recently been shown to display antidepressant-like and anxiolytic-like effects in animal models of depression such as the forced swim test (FST) in mice and rats.[38] As mention before, the serotonergic system, together with the adrenergic and dopaminergic systems, is heavily implicated in generating antidepressant-like effects in animal models, with 5-HT receptors and SERTs playing crucial roles in the neuro-pharmacological mechanisms of numerous antidepressants such as **6**.[21]

1.2.4. Histaminergic system

Histamine is a monoamine NT produced both in neurons and mast cells within the CNS by the action of histidine decarboxylase on *L*-histidine. There is only a single site of neuronal histamine synthesis in the mammalian brain located in the hypothalamus, the tuberomammillary nucleus, the source of all histaminergic axonal projections.[39]

There are four different histamine receptors (H_{1-4}) all of which are GPCRs, but only H_{1-3} have been detected in the human PFC with limited H_4 expression in the hippocampus and cerebellum. H_1 and H_2 receptors are expressed post-synaptically throughout the CNS on both neuronal and glial cells with prominent roles in the cerebral cortex, striatum and hypothalamus. H_3 receptors are only expressed in neurons, where they act as both autoreceptors on histaminergic neurons and heteroreceptors in non-histaminergic neurons which regulate the release of other NT such as NA.[40] H_1 and H_2 receptors are $G_{q/11}$ and G_s coupled, respectively. H_3 receptors are $G_{i/o}$ coupled and hence activation leads to downregulation of cAMP-dependent PKA activation. In addition, H_3 receptors are negatively coupled to high-voltage activated Ca^{2+} channels which are involved in the presynaptic autoinhibition of histaminergic neurons.[39]

Histamine has been implicated in the pathology of numerous neurodegenerative disorders, such as SZ and Alzheimer's disease, with typical antipsychotics like chlorpromazine (**7**) initially developed as antihistaminic compounds and H_3 receptor antagonists, being shown to improve cognitive performance in animal models of Alzheimer's disease (Fig. 1.2.6).[40] Various changes in the histaminergic system have been discovered in the brains of people with SZ with published case reports and double-blind studies reporting famotidine (**8**), a H_2 antagonist, providing a positive therapeutic outcome on the negative symptoms of SZ.[39,41]

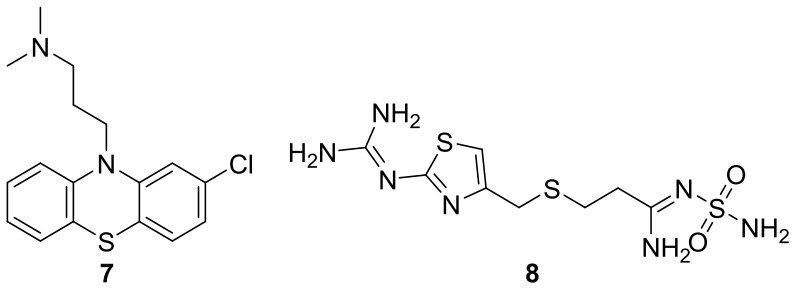

Figure 1.2.6. Structure of chlorpromazine (**7**, antipsychotic and antihistaminic) and famotidine (**8**, antihistaminic).

1.2.5. Targeting monoaminergic systems to treat neuropsychiatric disorders

The extensive modulatory roles and functional connectivity of the monoaminergic system (Fig. 1.2.7) makes it an attractive target in the treatment of a wide range of neuropsychiatric disorders.

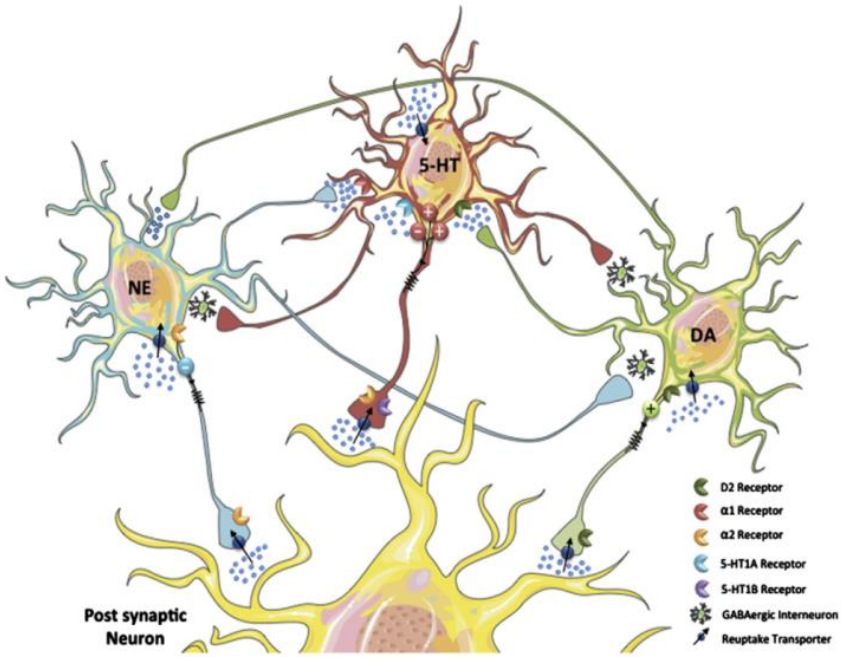

Figure 1.2.7. Functional connectivity of monoaminergic neurons.[42]

The prominent implication of these systems in the neuropathology of SZ and MDD (Fig. 1.2.8) further supports their utilization as pharmacological targets to relieve both cognitive dysfunctions and psychotic symptoms associated with these disorders.

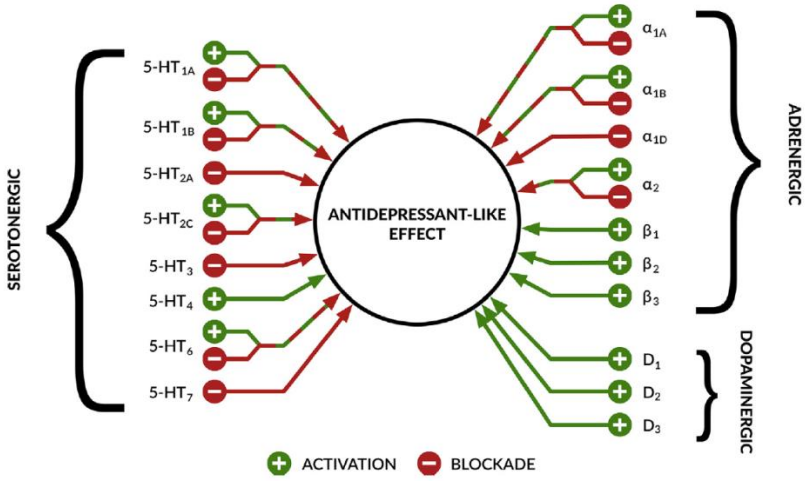

Figure 1.2.8. Contributions of central monoaminergic neurotransmission to generate antidressant-like effects.[21]

The noradrenergic system has been successfully targeted in the treatment of MDD, with the non-selective α_2-AR blockade proposed to contribute towards the therapeutic efficacy of anti-depressants (*e.g.* **4**) and atypical antipsychotic drugs (*e.g.* clozapine) (Fig. 1.2.9).[43] In particular, novel drugs capable of inducing an increase in the release of DA and NA in the PFC are expected to display potential clinical efficacy in the reduction of cognitive, depressive and negative symptoms in SZ.[44]

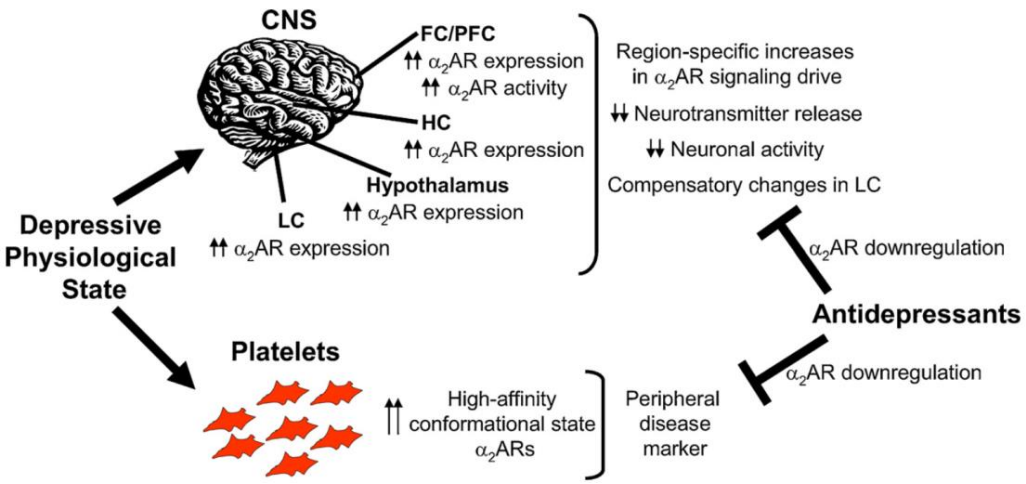

Figure. 1.2.9. Model for α_2-AR dysfunction in MDD.[45]

1.3. GPCR Ligands Pharmacology

Effective discussion and comparison of different GPCR ligands requires explanation of some key pharmacological concepts and the experimental techniques used to determine ligand properties such as affinity or activity. GPCRs exhibit constitutive activity which means that receptor mediated signalling can occur in the absence of a ligand due to spontaneous population of active receptor states. Ligands can bind to receptors in two general sites, a binding pocket which accommodates the endogenous ligand of the receptor called the orthosteric site or a pocket (allosteric) that is distinct from the orthosteric site that can modulate receptor activity/ligand binding. Bitopic ligands contain both orthosteric and allosteric moieties.[18] The activity of a ligand at a given receptor (Fig.1.3.1) is typically classified as one of the following:

Full agonist- Ligands that elicit maximum signal activation at the integrated pathway *i.e.* endogenous ligands.

Partial agonist- Ligands that elicit below maximal activity.

Inverse agonist- Ligands that inhibit constitutive receptor activity.

Neutral antagonist- Ligands that bind the receptor, but do not affect constitutive receptor activity.

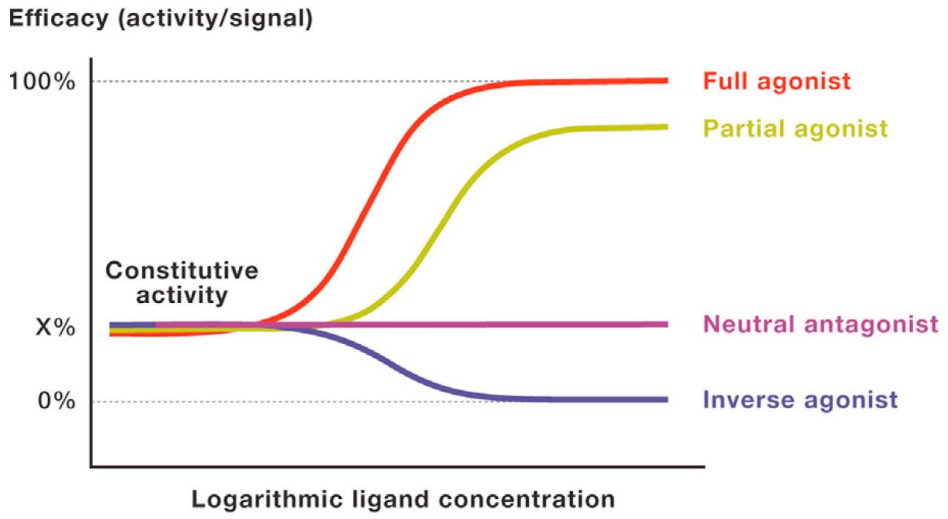

Figure 1.3.1. Key ligand activity classifications. [18]

1.3.1. Radioligand competition binding assays

Radioligand competition binding assays are used for affinity measurements (K_i determinations). These studies utilize standard ratiolabelled 'hot' ligands of known affinity (K_D) at a given concentration to measure the affinity of a competing ligand over a range of concentrations.[46] In a case of radioligand binding studies, the obtained data are fitted to a one-site curve-fitting equation with Prism 6.0 (GraphPad Software), and K_i values are estimated from best fit IC_{50} values using the Cheng−Prusoff equation:

$$K_i = \frac{IC_{50}}{1 + \frac{L_O}{K_D}}$$

Equation 1.3.1. The Cheng−Prusoff equation. L_O−labelled ligand concentration K_D−dissociation constant of labelled ligand.

1.3.2. GTP-γ-[^{35}S] Assay

The functional activity (agonist and/or antagonist) assay is sometimes referred to as a GTP exchange assay. A non-hydrolysable radiolabelled analogue of GTP is used in this assay. Thus, GTP is labelled on the gamma phosphate with ^{35}S (i.e. GTP-γ-[^{35}S]) to facilitate measurement of GPCR activation after the addition of a known agonist (Fig. 1.3.2.A) by measuring the amount of radiolabelled GTP bound to the cell membrane after washing away unbound GTP-γ-[^{35}S] (Fig. 1.3.2.B). Hydrolysable GTP cannot be used in this assay as it would be hydrolysed to GDP too rapidly, thereby removing the radiolabelled gamma phosphate from the bound radioligand leaving no radioisotope associated with the cell membrane for detection.[47]

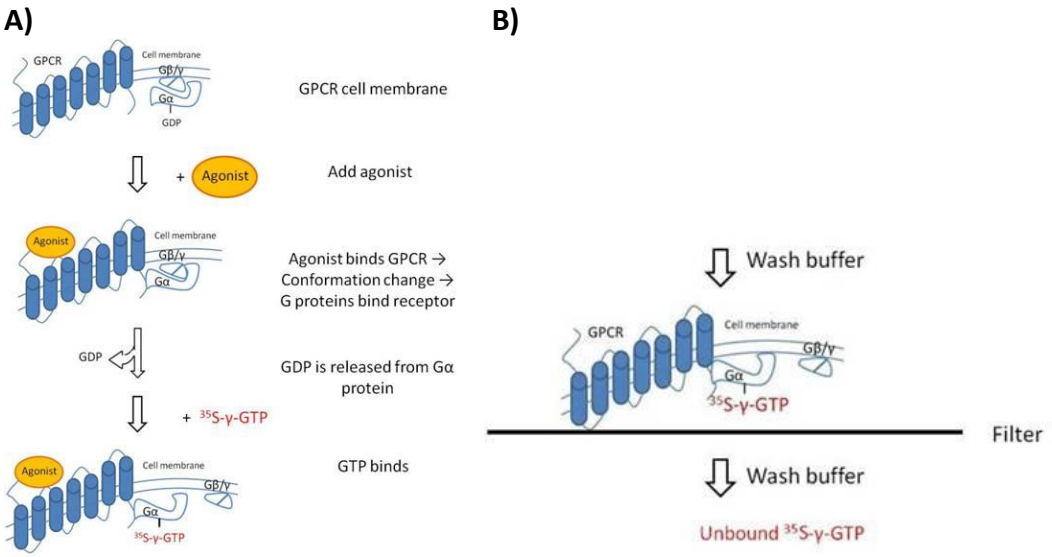

Figure 1.3.2. Steps involved in GTP-γ-[^{35}S] assay to assess ligand's functional activity in GPCRs.[48]

1.4. Background to Schizophrenia

The term schizophrenia is derived from the ancient Greek words *schizein* (to split) and *phren* (mind), which reflects the disorder or fragmented thinking of those suffering with the disorder. In 1891,[49] SZ was initially defined as '*dementia praecox'* (early dementia) by German psychiatrist Emil Krepalin until Eugen Bleuler, a German medical doctor and academic, termed it SZ in 1908. Bleuler introduced the concept of primary (the four As) and secondary (hallucination, delusions and asociality) symptoms of SZ.[50] This redefinition marked the beginning of the ongoing debate around the aetiology and classification of this well-known disorder.

The most recent version of the Diagnostic and Statistical Manual of Mental Disorders (DSM-V) defines the diagnosis of SZ based on the following criteria;

> 'Two (or more) of the following symptoms, each present for a significant portion of time during a 1-month period and should include at least 1, 2 or 3.
> 1. Delusions
> 2. Hallucinations
> 3. Disorganized speech
> 4. Grossly disorganized or catatonic behaviour
> 5. Negative symptoms (i.e. diminished emotional expression or avolition).'[51]

The symptoms of SZ have been reclassified since Bleuler's definition and, presently they are subdivided into three categories;[52]

Positive (psychotic) symptoms – Presence of abnormal behaviour such as delusions and hallucinations.

Primary negative symptoms of schizophrenia – Defined by the loss or lack of 'normal' social and interpersonal behaviours such as flattened affect, alogia, asociality, anhedonia, avolution and anergia.[53]

Cognitive deficits – Impaired attention, memory, language, executive and motor function.[54]

According to the World Health Organization (WHO), SZ is a severe and debilitating mental disorder which affects more than 21 million people worldwide.[55] SZ is more common and also manifests earlier in life among males with 12 million men vs. 9 million women currently diagnosed. SZ sufferers are 2/3 times more likely to die earlier than the general population, often as a result of physical illness. [56,57]

In comparison with other mental disorders, such as MDD, the occurrence of SZ is much less common, with a lifetime risk of approximately 1%. Despite this the severity of the disorder, associated morbidity and mortality as well as immense personal and societal costs justifies the necessity for improved treatment options.[58] It has been widely recognised that there is an unmet need for novel therapies which can help address the poorly treated aspects of this disorder.[59] The development of novel therapies requires exploration of alternative pharmacological treatment mechanisms beyond the scope of currently available drugs.[53]

1.4.1. Symptoms and Implicated Neuronal Pathways

SZ is a heterogeneous idiopathic mental disorder whose aetiology cannot be explained by a single unifying causative factor.[60] Instead, it is thought to stem from a complex interplay of a variety of influential factors (*e.g.* genetic,[58,61–65] developmental [66–69] and environmental).[70,71]

Its exact pathology is still largely unconfirmed; however, numerous studies have been conducted over several decades in an attempt to elucidate the nature of SZ's neuropathology.[72] The heterogeneity of SZ's symptoms indicates that they are the result of dysfunction in more than one region/pathway in the brain. Numerous neuropathological hypotheses have been proposed to explain the cause of these symptoms including the dopamine hypothesis[73,74] glutamate hypothesis[75,76] and serotonin hypothesis.[77,78]

1.4.2. Neuropathological Hypotheses of Schizophrenia

1.4.2.1. The Dopamine Hypothesis

The DA hypothesis is one of the most widely accepted theories of the neuropathology of SZ and it is for this reason that all current antipsychotic drugs are designed to affect dopaminergic neurotransmission. Numerous pharmacological studies showing that psychotic symptoms could be induced *via* administration of compounds which increase DA levels (*e.g.* amphetamine) and reversed by compounds which depleted DA levels (*e.g.* reserpine) have prompted the formulation of this hypothesis. [74] This theory proposes that the symptoms of SZ stem from dysfunction in dopaminergic mechanisms and activity in distinct brain regions. Positive symptoms are thought to stem from hyperdopaminergic activity in the subcortical ML pathway, which connects the VTA and NAc (Fig. 1.4.1). Hypo-dopaminergic activity in the MC pathway, linking the VTA to the PFC, has been linked to negative symptom and cognitive deficits.[73]

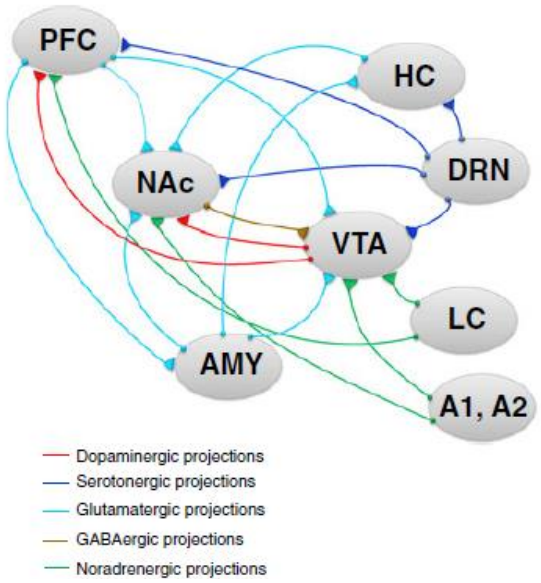

Figure 1.4.1. Functional connections between brain regions and their associated neurotransmitter (NT) projections. *AMY*: amygdala, *LC*: locus coeruleus, *DRN*: dorsal raphe nucleus, *HC*: hippocampus, *PFC*: prefrontal cortex, *NAc*: nucleus accumbens.[79]

The nigrostriatal pathway, extending from the substantia nigra to the dorsal striatum, has been implicated in the development of extrapyramidal symptoms (EPS), a collection of side effects such as tardive dyskinesia which are associated with early typical antipsychotic drugs.[33] Antipsychotic drugs have also been shown to affect the fourth DA pathway, the tubero-infundibular DA pathway, leading to prolactin elevation.[80] Typical/atypical antipsychotic drugs and their associated side effects will be discussed further in section 1.5.

1.4.2.2. The Glutamate Hypothesis

The glutamate hypothesis is the second leading theory of SZ neuropathology. Glutamatergic neurons act as the primary excitatory neurotransmission pathway in the brain and utilizes between 60-80% of total brain metabolic activity.[74] The extensive and important role of glutamatergic neurons would explain how dysfunction in this system could be catastrophic. Glutamatergic neurotransmission is mediated by two classes of glutamate receptors, metabotropic receptors and ionotropic receptors. Each class of glutamate receptors is further subdivided into three groups.

Metabotropic glutamate receptors (mGluR) are separated into mainly postsynaptic mGluR Group I (mGluR1 and mGluR5), largely presynaptic Group II (mGluR2 and mGluR3) and Group III (mGluR4, mGluR6, mGluR7 and mGluR8), which modulate NT release. Ionotropic glutamate receptors are named after the agonists first discovered to selectively activate each subtype: α-amino-3-hydroxy-5-methyl-4-isoxazolepropionic acid (AMPA), kainate and *N*-methyl-*D*-aspartate (NMDA).[81]

The first iteration of the glutamate hypothesis posited a simple deficit of glutamatergic neurotransmission in SZ; however, since then numerous discoveries have implicated a number of glutamate receptors playing diverse roles in the disorder.[82,83] The modified glutamate hypothesis, which currently prevails, highlights the primary role of NMDA receptor hypofunction.[84]As with the DA hypothesis, the glutamate hypothesis was based upon observations from pharmacological studies of non-competitive NMDA receptor antagonists (ketamine, phencyclidine (PCP) and dizoclipine (MK-801)) which cause immediate psychological effects that resembled schizophrenic symptoms.

To date, NMDA receptor antagonism is utilized as a model system for SZ, with the desired behavioural symptom model depending upon administration method (*i.e.* acute *vs.* chronic) and antagonist selection (*e.g.* PCP administration can mimic negative symptoms and cognitive deficits).[85,86] The mechanism by which NMDA receptor antagonists induce these symptoms and lead to downstream glutamate release is still under investigation. GABA, the principal inhibitory NT, has been implicated in this mechanism as NMDA receptor antagonists reduce GABAergic interneuron activity. Hippocampal and neocortical principal (pyramidal) neuron activity is controlled by GABAergic interneurons inhibition; therefore a reduction in this inhibitory activity leads to the ‘disinhibition’ of pyramidal neurons and increased pyramidal cell firing. This is known as the cortical disinhibition process (Fig. 1.4.2).[87]

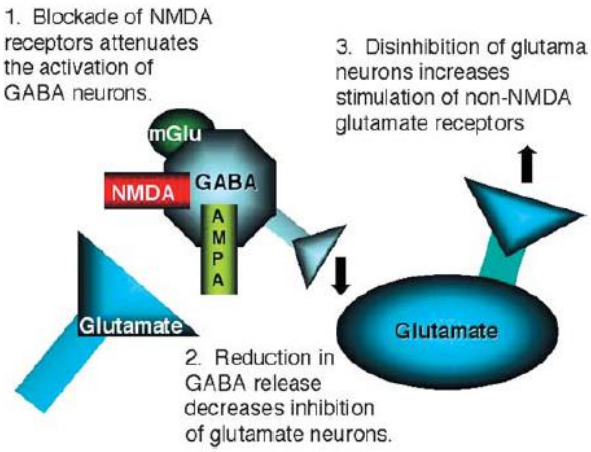

Figure 1.4.2. NMDA receptor blockade leading to cortical disinhibition.[76]

Recent studies suggest that glutamatergic dysfunction may lead to dopaminergic dysregulation *via* disinhibition of glutamatergic projections. A reduction in NMDA receptor availability and function on GABAergic interneurons can also cause disinhibition of glutamatergic projections onto midbrain DA neurons. This increases the release of glutamate along this pathway which, as an excitatory NT, causes amplified activation of dopaminergic neurons. These findings support the establishment of an integrated DA-glutamate hypothesis as a more universally coherent neuropathological explanation.[74]

1.4.2.3. Serotonin Hypothesis

The 5-HT hypothesis of SZ arose from studies examining the effects of psychedelic hallucinogens on the CNS. The initial 5-HT hypothesis was thought to involve 5-HT deficiency, as the 5-HT antagonistic activity of lysergic acid diethylamide (LSD) in smooth muscle preparations indicated that LSD was a 5-HT blocker. Once it was discovered that LSD could act to both mimic and antagonize 5-HT activity, the hypothesis was modified to consider an excess of 5-HT in SZ.

The two major classes of hallucinogens, indolamines (*e.g.* LSD) and phenethylamines (*e.g.* mescaline), have been shown to act as partial agonists at 5-HT_2 receptors, specifically the 5-HT_{2A} subtype. In fact, there is an excellent correlation between 5-HT_2 receptor affinity of hallucinogens and their hallucinogenic potency. [78]

Activation of 5-HT_{2A} receptors in the cerebral cortex, an area with a high concentration of this subtype, leads to enhanced glutamate release as indicated by an increase in glutamatergic excitatory post-synaptic potentials in the apical dendritic region of layer V pyramidal neurons. Hallucinogens also affect the LC by enhancing glutamatergic transmission; however, antipsychotic drugs can reverse these effects in the LC at doses which correlate with their 5-HT_{2A} affinity. The shared ability of psychedelic hallucinogens and NMDA receptor antagonists to increase glutamate release in the cerebral cortex, suggests that some common pathway may be involved in the similar psychomimetic effects of these two classes of drugs.[78] 5-HT receptors have also been proposed to play a critical role in the action of atypical antipsychotic drugs, discussed in section 1.5.[88,89]

1.5. Antipsychotic drugs: Typical and Atypical

The first antipsychotic drug to be serendipitously discovered was chlorpromazine (**7**), an aliphatic member of the phenothiazine class. This class of compounds were first utilized as drugs after Paul Erlich discovered the anti-malarial properties of methylene blue in 1891 which inspired further exploration of phenothiazine derivatives leading to the discovery of new anti-malarial, antihistaminic and anaesthetic drugs, as well as chlorpromazine.[90]

Chlorpromazine (**7**), haloperidol (**9**) and other typical antipsychotics (Fig. 1.5.1) were used as 'tranquilizers' for a wide range of psychiatric disorders for over ten years before their mechanism of action was discovered through numerous studies in the 1960s and 1970s. These studies found that typical antipsychotics acted as potent DA receptor antagonists.[91]

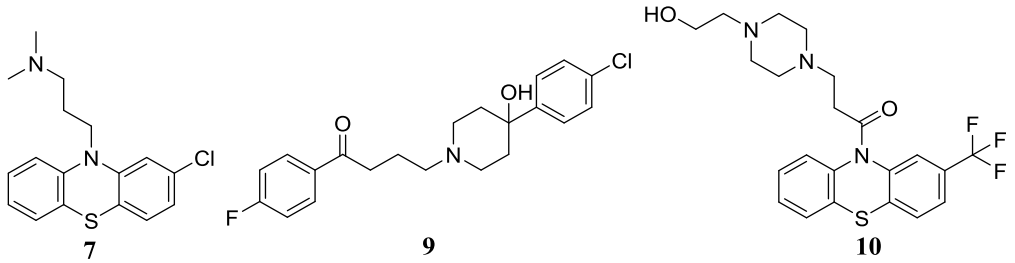

Figure 1.5.1. Structures of typical antipsychotic drugs: chlorpromazine (**7**), fluphenazine (**10**) and haloperidol (**9**).

Typical antipsychotics were a major development for the treatment of SZ; however, they were only successful in treating the positive or psychotic symptoms by reducing hyperdopaminergic activity in the ML-DA system through antagonism of DA D_2 receptors. Typical antipsychotics also display a significant side effect profile including EPS, hyperprolactinaemia, tardive dyskinesia and neuroleptic malignant syndrome.[92] The advent of neuro-receptor imaging techniques led to the discovery that these side effects were related to D_2 receptors occupancy, with the majority of typical antipsychotics displaying occupancy levels of 70-90% at clinical doses.

Positron emission tomography (PET) and single photon emission computerized tomography (SPECT) studies have indicated that antipsychotic drugs with D_2 receptors occupancy of >80% are associated with a significantly higher risk of EPS.[93] As mentioned in section 1.4.2.1, EPS are believed to occur as a result of D_2 antagonism of the nigrostriatal DA pathway, which is responsible for control of motor activity *via* the basal ganglia motor loop.[94] Prolactin elevation or hyperprolactinemia are also associated with D_2 antagonism which causes disinhibition of prolactin synthesis and release from lactotroph cells.[80]

The discovery of a new class of antipsychotic drugs, known as atypical antipsychotics, began with clozapine (**11**) (Fig. 5.1.2). This drug was first synthesised in 1958 at Wander Pharmaceuticals as part of a series of dibenzodiazepine tricyclics; however, these compounds were only active in some animal models of antipsychotic action compared with the aforementioned typical antipsychotics.[91] It was the unique therapeutic profile of **11** (antipsychotic effect without associated neuroleptic activity and minimal EPS), which defined it as the first atypical antipsychotic. Unfortunately, clozapine treatment was linked to life threatening agranulocytosis, a dangerously reduced white blood cell count, damaging the drug's reputation. Clozapine's utility saw a huge revival after a landmark double-blind study against chlorpromazine ("Study 30") displayed clozapine's superior clinical efficacy in treatment-resistant or refractory SZ.[90]

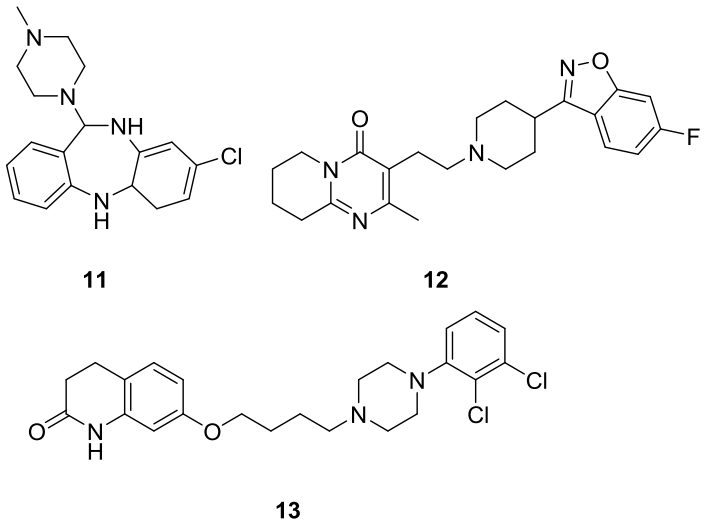

Figure 1.5.2. Structures of atypical antipsychotics**:** clozapine (**11**), risperidone (**12**) and aripiprazole (**13**).

Risperidone (**12**) and aripiprazole (**13**) (Fig. 1.5.2) are two commonly prescribed atypical antipsychotics used to treat SZ and ,like clozapine, each display striatal D_2 receptor occupancy below the EPS threshold of >80% at low dosage levels (2-3 mg/day for **12** and **13**, and 300-600 mg/day for **11**).[93,95]

The fundamental property of atypical antipsychotics that differentiates them from typical antipsychotics is their ability to produce an antipsychotic effect in the absence of EPS or prolactin elevation.[91] Even though not all atypical antipsychotics are devoid of these side effects, they are associated to a lesser extent than typical antipsychotics.[92] Atypical antipsychotics are however also associated with a number of additional side effects including metabolic disturbance (metabolic syndrome,[96] type II diabetes mellitus and hyperlipidemia), myocarditis, agranulocytosis, insomnia, dizziness and sexual side effects.[92,97] The broad range of side effects associated with the atypical antipsychotics can be attributed to their diverse polypharmacology, from which their atypicality is also thought to originate. The majority of atypical antipsychotics display different affinities and activity profiles for a number of receptors within the CNS including DA, 5-HT, histamine, muscarinic acetylcholine receptors (mAChR) and ARs).[98] The receptor profiles for a selection of typical antipsychotics (1st), atypical antipsychotics (2nd), and some common α-AR ligands are highlighted in Table 1.5.1 with the presented K_i values sourced from the National Institute of Mental Health (NIMH) Psychoactive Drug Screening Programme (PDSP) K_i database.[79,99]

Table 1.5.1. Binding affinities (K_i values) for first and atypical antipsychotics as well as α-AR agonists and antagonists at D_2 and α-AR subtypes. K_i values are sourced from the PDSP K_i database calculated from best fit IC_{50} values using the Cheng-Prusoff equation.[79,99]

Compound	**D_2** K_i (nM)	**α-AR** K_i (nM)			
		α_{1A}	**α_{2A}**	**α_{2B}**	**α_{2C}**
Antipsychotics					
Aripiprazole **13** (2nd)	0.66	26	74	102	37
Chlorpromazine **7** (1st)	4	0.28	184	27	46
Clozapine **11** (2nd)	256	1.64	142	26	34
Fluphenazine **10** (1st)	0.54	6.5	314.1	81.6	28.8
Haloperidol **9** (1st)	4	12	1130	80	550
Loxapine (2nd)	12	31	150.8	107.6	79.9
Molindone (1st)	63	2612	1097	557.8	172.6
Olanzapine (2nd)	31	115	314.1	81.6	28.8
Perphenazine (1st)	1.4	10	810.5	104.9	85.2
Pimozide (1st)	0.65	197.7	1593	821.1	376.5
Quetiapine (2nd)	245	22	3630	746.6	28.7
Risperidone **12** (2nd)	6.5	5	150.8	107.6	1.3
Sertindole (2nd)	9.1	1.8	640	450	450
Thioridazine (1st)	11	5	134.3	341.3	74.8
Thiothixene (1st)	0.63	11	79.9	50.2	51.9
Trifluoperazine (1st)	13	24	653.7	163.6	391.5
Ziprasidone (2nd)	9.7	18	160	48	59
α_2-AR ligands					
RX 821,002 (Ant.)	*n.d.*	*n.d.*	10	3.8	1.8
Guanfacine (Ag.)	*n.d.*	*n.d.*	50	1020	1120
(±)-Idazoxan (Ant.)	>10,000	*n.d.*	10	37	20
Clonidine (Ag.)	>10,000	*n.d.*	32	40	63
Mirtazapine (Ant.)	5454	*n.d.*	20	*n.d.*	18
n.d. = not determined; 2nd = second generaton or atypical; 1st = typical or typical; Ag. = Agonist; Ant. = Antagonist					

It is interesting to note that clozapine, quetiapine and to a lesser extent olanzapine display significantly lower affinity for D_2 receptors compared to α-ARs. These well established atypical antipsychotic drugs are reported to have unique therapeutic efficacy compared to other antipsychotics by exhibiting a measureable improvements on both the negative symptoms and cognitive deficits, poorly treated by other antipsychotic drugs, which may be related engagement with the noradrenergic system.[100–102] In fact, a number of atypical antipsychotics have been shown to act as α-AR antagonists.[79,103]

Numerous studies of the prototypical antipsychotic clozapine have shown that it displays superior efficacy in treating negative symptoms and cognitive deficits compared to typical antipsychotics.[102,104,105] The antagonistic activity of clozapine at α_1- and α_2-ARs has been implicated in the stabilization of the dysregulated central DA system in SZ.[106] It is generally expected that blocking α_1-ARs is responsible for supressing positive symptoms, whereas α_2-AR antagonism is thought to help treat the negative and cognitive symptoms.[23,107] The prevailing theory by which almost all clinically approved antipsychotics exert their action is the DA hypothesis, with both typical and atypical antipsychotics displaying prominent D_2 antagonism.[107] Even though the exact neurochemical basis for antipsychotic atypicality is still under investigation, an integrated 5-HT/DA hypothesis has been proposed, where potent 5-HT_{2A} receptor antagonism and mild D_2 antagonism (5-HT_{2A}/D_2 ratio) seem to be the most major pharmacological distinction between typical and atypical antipsychotic drugs.[88,91,108]

1.6. Adrenergic Targets for Antipsychotics

1.6.1. Targeting α2-ARs

Each of the three α_2-AR subtype (α_{2A}, α_{2B} and α_{2C}) are involved in a range of important physiological functions throughout the body, as illustrated in Fig. 1.6.1, and are preferentially associated with the $G_{i/o}$ family of G proteins.[79,109] Within the CNS, localization (both pre/post-synaptic and in distinct brain regions) and associated functions of α_2-AR subtypes vary.

Both the α_{2A}- and α_{2C}-subtypes act primarily as pre-synaptic auto-receptors which inhibit NA release through a negative feedback loop, whilst the α_{2B}-subtype plays a minimal role in the CNS with relation to nitrous oxide (NO) mediated analgesia in the spinal cord.[109–111] In particular, it has been shown that activation of post-synaptic α_{2A}-ARs in the PFC induce cognitive-enhancing effects, which could be utilized to address the cognitive deficits observed in SZ (*e.g.* impaired working memory, attention and learning). This provides the basis for the application of α_{2A}- selective agonists as potential pro-cognitive drug candidates.[79,112]

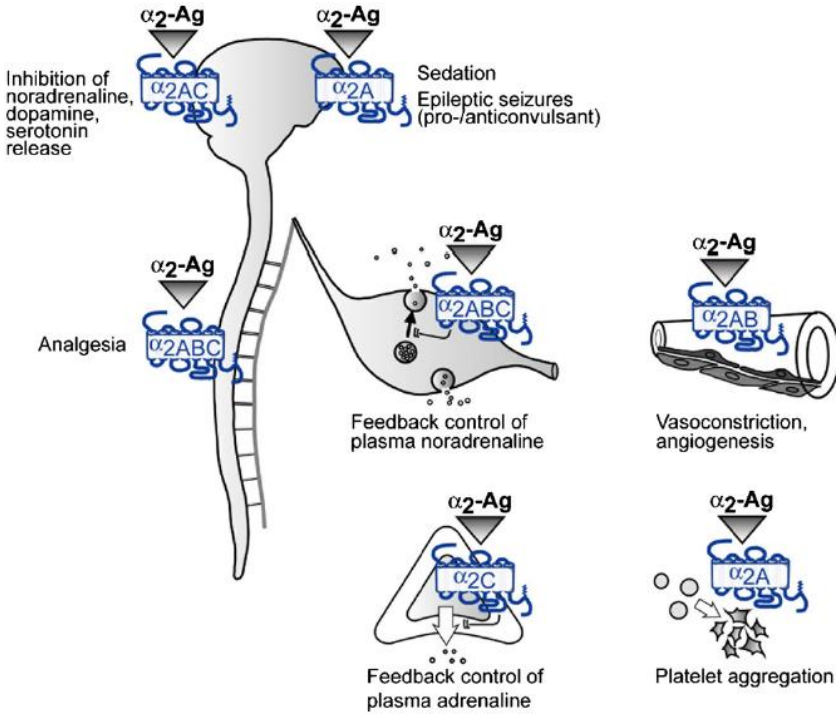

Figure 1.6.1. Overview of α_2-AR subtype specific functions.[109]

Some α_2-AR antagonists, such as mirtazapine and mianserin are being used as unlicensed adjunct treatments in combination with a number of antipsychotic drugs in order to help treat the negative symptoms and cognitive deficits of SZ. These drugs, typically used to treat MDD, antagonise central α_2-AR and multiple studies have shown them to cause DA efflux in the PFC in rodents when combined with D_2 antagonists (*e.g.* risperidone); which is thought to help enhance cognition and improve negative symptoms.[113–115]

Preclinical studies using behavioural animal models to evaluate novel antipsychotics, such as the conditioned avoidance response model, have shown that co-administration of a potent α_2-AR antagonist (*e.g.* idazoxan) with a sub-effective dose of a typical (**9**) or atypical antipsychotic (**12**) reduced the conditioned avoidance response significantly more than the antipsychotic drugs alone. This synergistic effect may provide a way to reduce the minimum effective dose of antipsychotic drugs required and could serve to increase efficacy and tolerability.[116]

1.6.2. Subtype selective α_2-AR antagonists

Several α_{2C}-AR selective or biased antagonists have been reported in the literature; however, a number of these compounds also display significant affinity and activity over other receptors. Compounds such as rauwolscine (**14**), ORM-10921 (**15**) and MK-912 (**16**) each containing a tetracyclic indoloquinolizine or benzofuro-quinolizine core, are potent α_{2C}–AR selective antagonists (Fig. 1.6.2).[117–119]

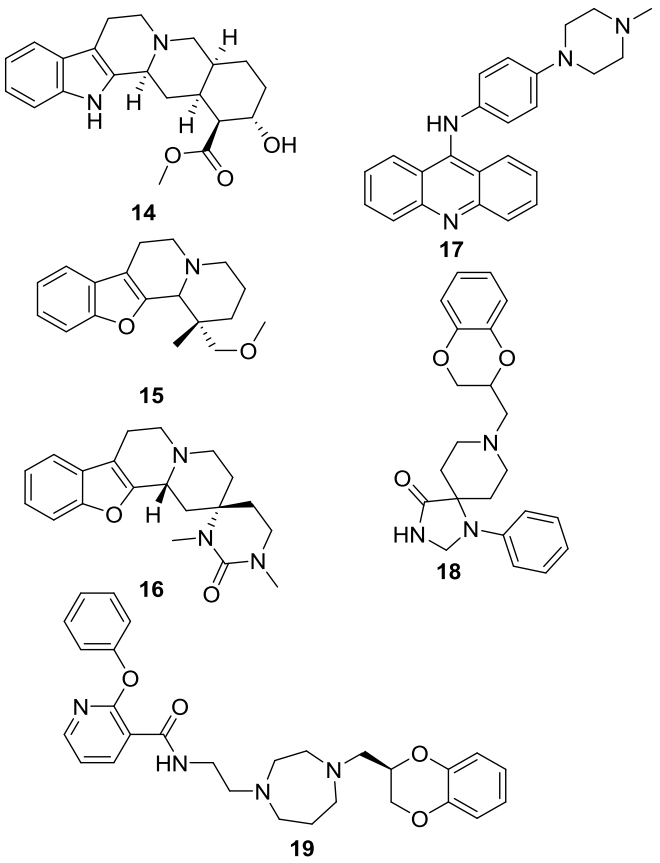

Figure 1.6.2. Selective α_{2C} antagonists previously reported in the literature: rauwolscine (**14**), ORM-10921 (**15**), MK-912 (**16**), JP-1302 (**17**), spiroxatrine (**18**) and nicotinamide derivative (**19**).

In particular, ORM-10921 (**15**, α_{2C}–AR K_i = 1.2 nM) has been shown to exhibit antipsychotic-like and antidepressant-like effects in behavioural animal models including PCP-induced pre-pulse inhibition (PPI) of acoustic startle and in the FST It also caused increased extracellular DA levels in the PFC shown by *in vivo* microdialysis studies.[120]

One of the most recently discovered α_{2C} selective antagonist, JP-1302 (**17**), displays affinity for the α_{2C}–AR of K_i = 28 nM in competition binding assays using transgenic Chinese hamster ovary (CHO) cells stably expressing the human α_2-AR subtypes. Compound **17** has also been shown to display antipsychotic-like and antidepressant-like effects in the PCP-induced PPI of acoustic startle model and the FST.[121–123] Additionally, **17** has also been utilized in the autoradiographic characterisation of α_{2C}-AR in the human striatum showing that a large proportion of α_2-ARs in the striatum are of the α_{2C} subtype and that α_2-AR subtype distribution patterns appear to be conserved in both rodents and humans, lending validity to research in rodent models.[124]

This research shows that α_{2C}-ARs are expressed at higher levels than α_{2A}-ARs, particularly in the NAc, whereas there is a relatively higher concentration of α_{2A}-ARs in the PFC.[79] Spiroxatrine (**18**)[125] and the nicotinamide derivative **19** (α_{2C}–AR K_i = 0.9 nM)[126] have also been identified as potent and selective α_{2C}-AR antagonists which exhibit antipsychotic-like effects in behavioural animal models. Both of these compounds were found to reduce impairment in the PCP-induced PPI of acoustic startle model This study also showed that transgenic mice over-expressing the α_{2C}-AR and α_{2A}-AR knockout (KO) mice both displayed increases in PPI.[79] The aforementioned studies provide substantial support that selective antagonism of the α_{2C}-AR may have therapeutic potential for the treatment of SZ, either as an independent therapy or adjunct treatment.[127] The mechanism by which blockade of the α_{2C}-AR leads to antipsychotic-like and antidepressant activity is thought to be twofold.

Firstly, due to its high concentration in the striatum, selective α_{2C}-AR antagonists should exert their primary effects in this region, in particular in the NAc. Blockade of α_{2C}-AR in the NAc causes increased DA release in the PFC, hence augmenting the hypodopaminergic state responsible in part for negative and cognitive symptoms.[43] Secondly, blockade of these receptors may help reduce the promiscuous binding of DA in the striatum.[37,79]

1.7. Previous work - α_2-adrenoceptor targeting and antidepressant research in the Rozas group

The Rozas group has been designing ligands to target α-ARs for over 20 years, initially targeting α_1-AR with series of bis-2-aminoimidazoline and bis-guanidine di(aminophenyl) derivatives for the treatment of benign prostatic hyperplasia.[128] This line of research uncovered the first α_2-AR *hit* compound, **20**, which proved to be a poor α_1-AR antagonist but was identified as a potent α_2-AR agonist (PFC α_2-AR K_i = 1.6 nM) in later studies (Fig. 1.7.1).[129]

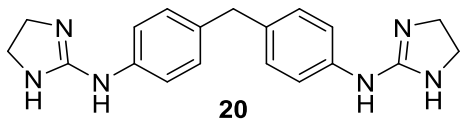

20

Figure 1.7.1. Structures of hit compound **20**.

The discovery of **20** inspired a series of *hit* generation strategies and structural activity relationship (SAR) studies involving various *mono*- and *bis*-(hetero)aryl α_2-AR ligands containing guanidine or 2-aminoimidazoline functionalities. These studies generated a number of *lead* compounds which displayed high affinity (K_i < 100 nM) and a variety of activities including potent α_2-AR agonists, partial agonists and neutral antagonists in pharmacological assays conducting in human PFC tissue in collaboration with the Callado group (Department of Pharmacology, University of the Basque Country UPV/EHU, Centro de Investigacion Biomedica en Red de Salud Mental, CIBERSAM, Spain).[129]

These assays included *in vitro* radioligand ([^{3}H]RX821002) competition binding assays and [^{35}S]GTPγS binding assays in human PFC tissue as well as *in vivo* microdialysis experiments in male Sprague-Dawley rats.[130–132]

The *lead* compounds identified by these studies will be divided into families in order to discuss and compare the key outcomes. Family **A** are based on **21**, one of the first *mono*-aryl guanidine *leads* to be identified and shown to elicit antidepressant-like effects *in vivo* (Fig.1.7.2).[133] This core and the related pyridine, thiophene and thiazole bioisosteric analogues showed the most consistent trend in activity with all *mono*- and *di*-substituted guanidine or 2-aminoimidazoline derivatives displaying neutral antagonist activity in human PFC tissue.[61,132] The benzene to thiophene replacement strategy generated the newest *lead* antagonist, **24** (PFC α_2-AR K_i = 31 nM), of this family to date.[134]

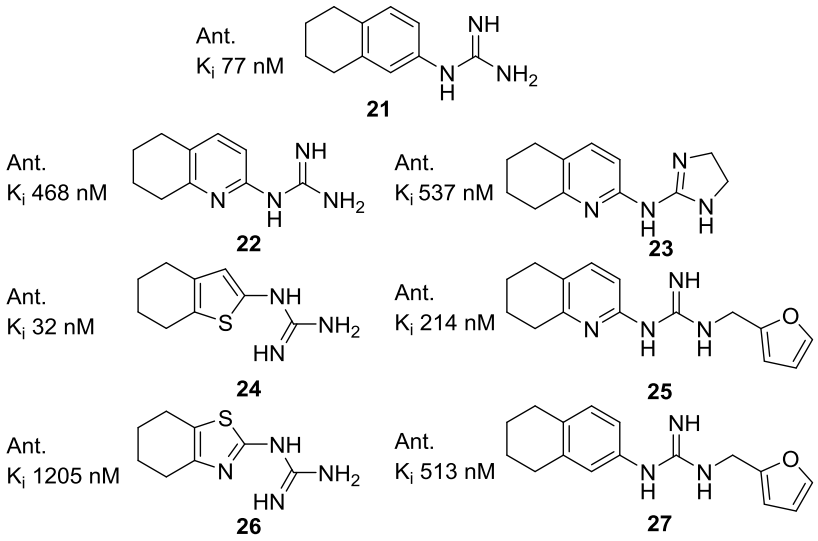

Figure 1.7.2. Structures of Family **A** lead antagonists and neutral antagonist compounds **21-27**.

Family **B** exemplifies the various strategies employed within the *hit*-to-*lead* optimization process for *mono*-aryl guanidine/2-aminoimidazoline analogues aiming to modify the α_2-AR profile of these compounds (Fig.1.7.3). Two approaches were applied to alter the activity of 2-aminoimidazoline agonist **28**. Firstly, modification of the cationic moiety from 2-aminoimidazoline to *mono*- (**29**) and *di*-substituted (**30**) guanidine, successfully altered the activity of the compounds to antagonists with concomitant reduction in affinity.

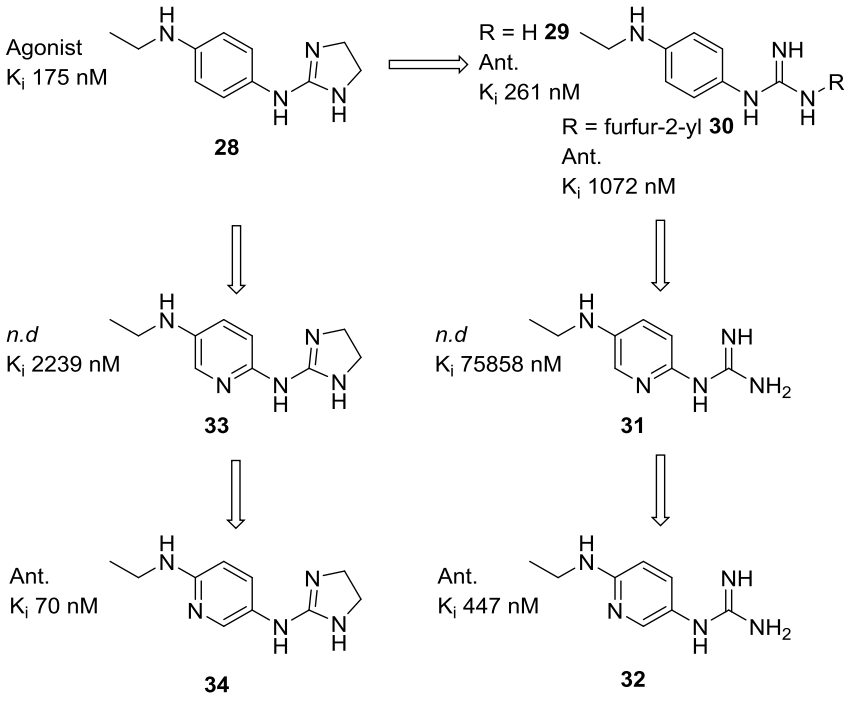

Figure 1.7.3. Structures of Family **B** as a result of *hit*-to-*lead* optimization.

Nonetheless, **29** was evaluated *in vivo* and displayed antidepressant-like properties and increased PFC NA release as measured by *in vivo* microdialysis experiments.[135] Secondly, a bioisosteric change of the aryl core furnishing pyridino-guanidine (**31** and **32**) and pyridino-(2-aminoimidazoline) (**33** and **34**) derivatives. The drastic drop in affinity for **31** and **33** precluded these analogues from activity measurement; however, **32** and **34** both displayed antagonist activity with **34** displaying the highest affinity (PFC α_2-AR K_i = 70 nM) not only for this family but for the entire pyridine analogue series.[132]

Family **C** highlights the dramatic differences in α_2-AR profile associated with different regioisomers of **28** (Fig. 1.7.4). Thus, the subtle change in aryl substitution from an *N*-ethylamino- to *N*,*N*-dimethylamino substituent gives **35** and **36** with higher affinity but displaying an inverse activity relationship to that of their regioisomeric analogues **29** and **28,** respectively.[131] Dramatic changes in ligand activity with minimal variation of ligand structure is a common phenomenon encountered by medicinal chemists targeting GPCRs.[136,137] Additional SAR studies were conducted to probe the orientation of the substituent on *di*-substituted guanidine derivatives, including the synthesis of conformationally restricted derivatives, **37** and **38**.[129,138]

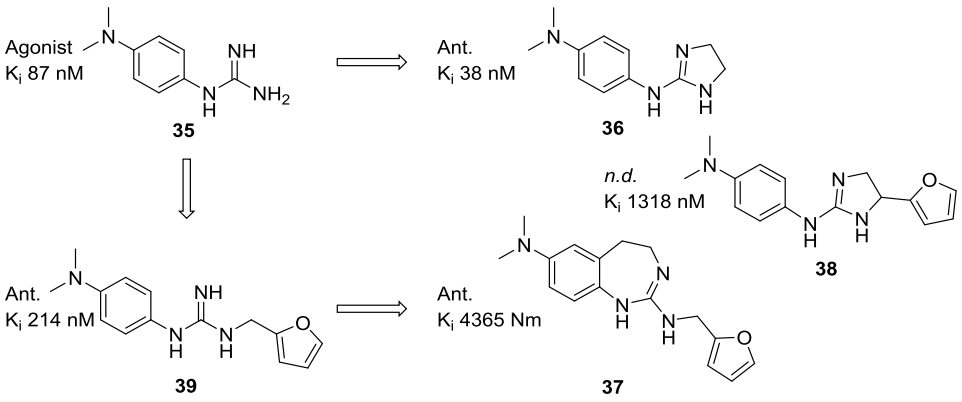

Figure 1.7.4. Structures of Family **C**.

Addition of a substituent to the guanidine moiety (**39**) favoured antagonistic activity as with family **B**; however, both substitution and conformational restriction greatly reduced the affinity of these analogues compared with **35** and **36**. Further pharmacological evaluation of **36** confirmed antagonistic activity with *in vivo* microdialysis experiments showing increased extracellular NA release after local and systemic administration.[129]

Family **D** represents the combined results of two large SAR studies involving *di*-aryl bis-cationic derivatives of **20** (Fig.1.7.5).[130] This collection of compounds have shown the highest affinities of all *di*-aryl α_2-AR ligands developed to date and display both partial agonist (**40**, **41** and **42**) and antagonist activity *in vitro* (**43**, **44** and **45**).[139]

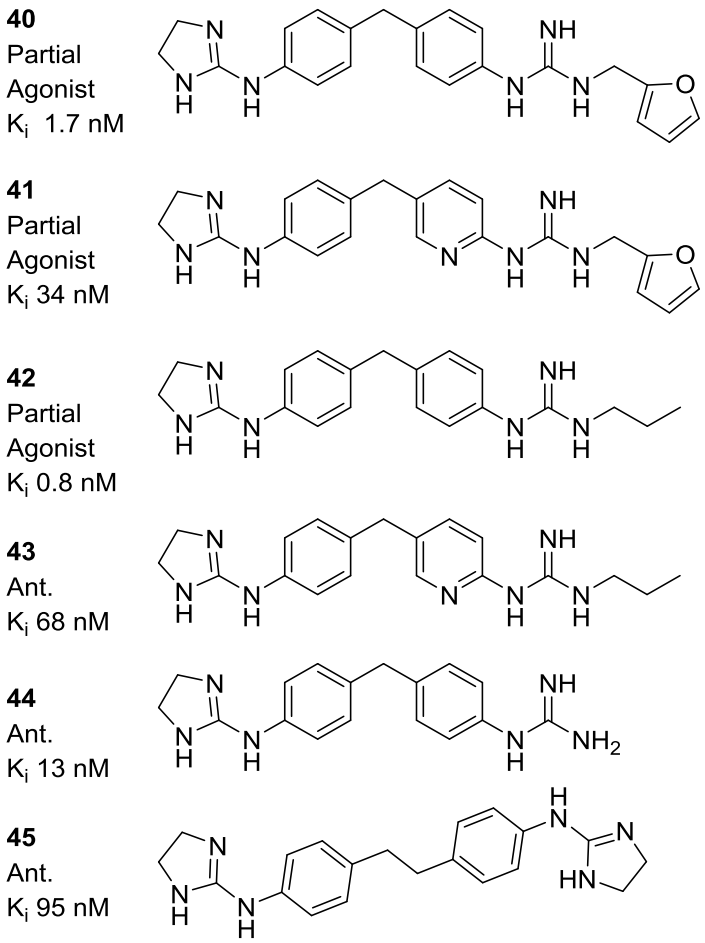

Figure 1.7.5. Structures of Family **D**.

Summarising, compounds **21**, **45** and **29** display potent antagonistic activity *in vitro* and have been shown to cause increased extracellular NA release in microdialysis assays in rats and exhibit antidepressant-like effects *in vivo* (Fig.1.7.6). The combined results obtained from each of these studies have defined these structures as the *lead* antidepressant candidates to undergo additional investigation.[133]

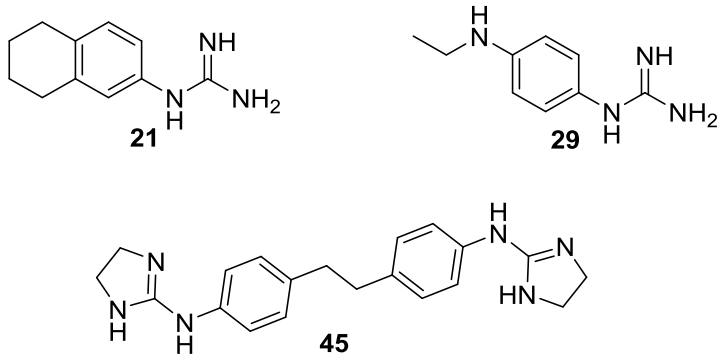

Figure 1.7.6. Structures of lead antidepressant compounds **21**, **45** and **29**.

Chapter Two
Objectives

2.1. Context

Over the past 20 years the Rozas group has employed a ligand-based drug design strategy to generate and optimise α_2-AR ligands (agonists and antagonists), which has led to a number of promising antidepressant drug candidates. This approach has generated a large library of both *mono*- and *di*-aryl guanidine and 2-iminoimidazolidine derivatives which have been subject to pharmacological evaluation. In collaboration with the pharmacology laboratory of Prof. Luis Callado at UPV/EHU (Bilbao, Spain), the α_2-AR engagement (affinity and activity) of these ligands has been determined by radioligand competion binding and [^{35}S]GTPγS functional assays in PFC brain tissue.[129,140]

This pharmacological data has been utilized in different structure activity SARs, comparative molecular field analysis and 3D pharmacophore studies which facilitated the selection and prioritisation of *lead* compounds. These *leads* have been further advanced to *in vivo* microdialysis experiments and behavioural tests (e.g. FST and TST) classically used to evaluate antidepressant-like activity.[133] Additionally, these compounds have been analysed using computational and molecular docking studies using homology models of the three α_2-AR subtypes.[132,134,138,141]

Despite the vast amount of information gained from these studies, it remains a challenge to rationalise and reconcile the observed pharmacological behaviour (α_2-AR affinity and activity) with shared structural features, even between closely related analogues. Therefore, it has proven very difficult to establish definitive SARs. Minor structural modifications of ligands which cause dramatic changes to their receptor interaction profiles is a regularly observed phenomenon in the development of GPCR targeting ligands.[137] Numerous reports in the literature show that even the most subtle of structural alteration can drastically impact the receptor profile of a wide variety of GPCR ligands.[136,137]

In terms of structural modifications which promote α_2-AR antagonist activity, one strategy developed within our group has proved consistently successful at converting *mono*-aryl guanidine and 2-iminoimidazolidine α_2-AR agonists to antagonists. Thus, bioisoteric replacement of the aryl component in these derivatives, from phenyl to an alternative heteroaromatic core such as pyridine, thiophene or thiazole, provides a reliable approach to convert agonists to antagonists, albeit with a concomitant reduction in binding affinity in most cases.[132,134] Addition of a substituent at the cationic moiety of aryl guanidine derivatives to form 1,3-disubstituted guanidines has also been effective at converting α_2-AR agonists to antagonists.[141]

2.2. General objectives

The objectives of this work are as follows:

1) Consolidate and refine our current understanding of the SARs utilising previously prepared ligands by conducting extensive screening for affinity in a panel of pertinent CNS targets.

2) Use the detailed pharmacological profiles derived from the screening process to prioritise a subset of candidate molecules to allow for a more focused synthetic approach by refining the scope of proposed derivatives.

3) Analyse a collection of rationally chosen compounds to determine whether they exhibit subtype selectivity for the α_{2C}-AR versus the α_{2A}-AR.

4) Utilize the subtype selectivity data obtained in the design and synthesis of a series of new derivatives incorporating core structures of known α_{2C}-AR selective antagonists such as acridine and quinoline cores.

5) Evaluate these newly prepared derivatives, using a range of pharmacological techniques, to determine which compounds exhibit desirable pharmacological profiles required to progress towards an application as novel treatments for SZ.

The approach towards achieving these objectives is two-fold. Firstly, as this work is the pioneering endeavour within the Rozas group aiming to discern the selectivity and specificity of some *hit* and *lead* α_2-AR ligands developed to date, a retrospective analysis of previously published compounds must be conducted. This will facilitate the selection of an appropriate series of *mono*-aryl guanidines and 2-aminoimidazolines which will be prepared and submitted for extensive pharmacological screening at the NIMH PDSP (UNC Chapel Hill). The comprehensive evaluation of the receptor engagement profiles exhibited by the members of this series will serve to enhance our understanding and possibly consolidate the SARs previously established for these compounds. This knowledge will inform the preparation of new derivatives designed to exhibit more refined and desirable pharmacological characteristics to allow their progression as *lead* compounds and potentially become novel drug candidates for the treatment of SZ.

Secondly, we intend to utilize alternative heterocyclic core structures (acridines and quinolines) in place of the *di*- and/or *mono*-aryl systems used up until now, in the design of novel α_2-AR ligands. This proposed substitution was informed by the structures of known α_2-AR subtype selective ligands *e.g.* JP-1302 (Fig. 1.6.2). *Hit* candidates found to exhibit optimal affinity and selectivity profiles, specifically antagonists with α_2-subtype selectivity, will progress to further stages of validation including investigation of their physiochemical properties and pharmacokinetic parameters.

The groups of CNS targets chosen for screening at the NIMH PDSP are depicted in Fig. 2.2.1 and include a range of GPCRs, ion channels and MATs. The pharmacological data generated from this screening will allow a detailed receptor profile to be constructed for each compound and may also facilitate the elucidation of specific structural motifs which favour receptor specificity and subtype selective binding. These receptor profiles will then be utilized in the design of new derivatives targeting the α_{2C}-AR that display improved receptor profiles and pharmacological behaviour.

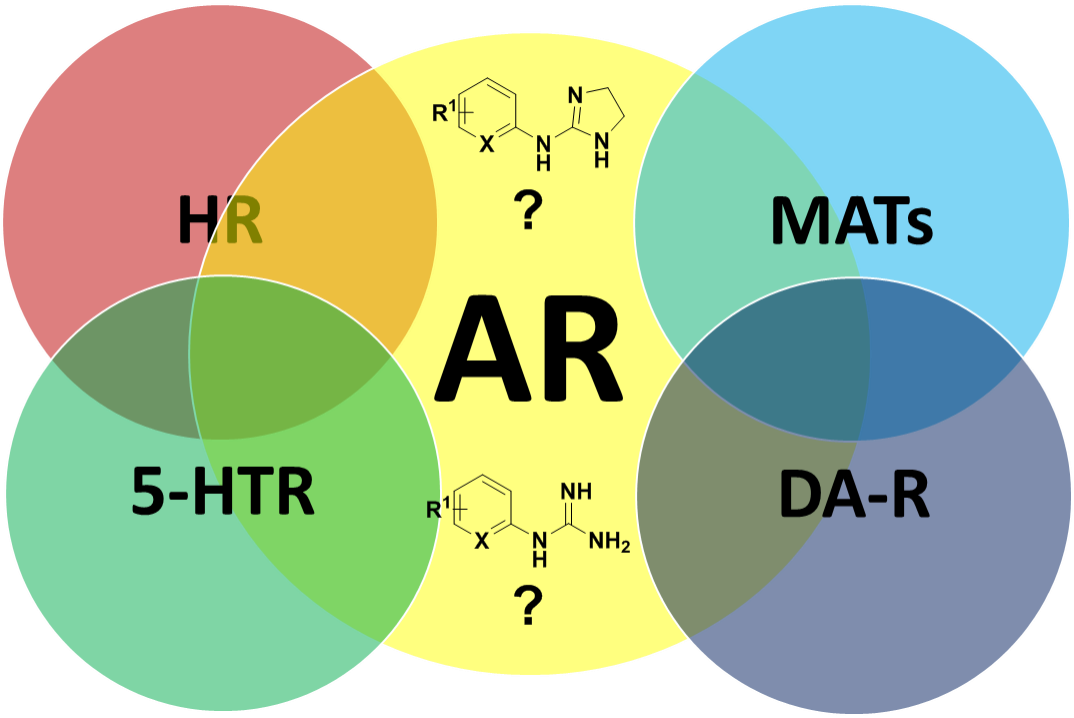

Figure 2.2.1. Schematic representation of the designated CNS targets selected for screening at the PDSP. *AR* = Adrenoceptors, *HR* = Histamine receptors, *MATs* = Monoamine transporters, *5-HTR* = Serotonin receptors, *DA-R* = Dopamine receptors.

2.3. Pharmacological objectives

All final compounds prepared throughout the course of this work will undergo preliminary pharmacological evaluation to determine their binding affinity for the α_2-AR in collaboration with the pharmacological laboratory of Prof. Luis Callado at UPV/EHU. These experiments are performed in human PFC brain tissue using competition radioligand binding assays against the α_2-AR selective radioligand [^{3}H]RX821002 to determine affinity.[142]

In addition, we intend to avail of the services provided by the NIMH PDSP to evaluate the affinity and subtype selectivity and/or specificity of a collection of α_2-AR ligands against a selection of 31 designated targets as summarised in Fig. 2.2.1. These detailed receptor profiles will then be employed to confirm the primary and secondary targets of these compounds which will assist in rationalising the pharmacological behaviour exhibited by these compounds.

These profiles will justify revised designation and prioritisation of *lead* compounds where appropriate, with the potential for these prioritised compounds to progress further into the *lead* optimization process and undergo additional pharmacological evaluation as potentially novel therapeutics for SZ. This screening will also inform the design of new *mono*-aryl guanidine and/or 2-aminoimidazoline derivatives with optimized affinity, selectivity and receptor binding profiles. These new compounds will contribute to the formulation of more definitive SARs.

Furthermore, a variety of core scaffolds will be investigated to potentially enhance α_2-AR engagement, with specific emphasis on compounds which exhibit distinct subtype selectivity between the three α_2-AR subtypes. In particular, compounds sharing common core structures with previously reported α_{2C}-selective compounds (i.e. JP-1302) will be studied. Accordingly, the affinity of a small 'in-house' library of compounds will be evaluated at the two major CNS α_2-AR subtypes, α_{2A} and α_{2C}, using a transgenic CHO cell-based subtype selectivity assay in collaboration with the pharmacological laboratory of Prof. Luis Callado at UPV/EHU. In the event that compounds are identified that display preferential affinity for the α_{2C} *vs.* α_{2A}-AR, further *in vitro* functional activity experiments will be conducted.

Another goal of this work is to prepare new derivatives and expand this collection of compounds based upon the results obtained. This will also help uncovered the structure selectivity relationships (SSR) within this group of compounds. High affinity compounds (K_i < 100 nM) will then be evaluated using [^{35}S]GTPγS binding functional assays to evaluate their activity and facilitate prioritisation of *hit* compounds. Designated *hit* compounds will be subsequently submitted to the NIMH PDSP and undergo more extensive pharmacological investigation.

2.4. Synthetic Objectives

Another aspect of this work involves investigating the effects of structural variation on the engagement of some *mono*-aryl *lead* compounds with α_2-ARs. We will primarily focus on α_2-AR's affinity and activity, with the potential to investigate subtype selectivity later on.

The specific structural modifications proposed consist of (i) ring expansion of 2-aminoimidazoline cationic moiety (blue) to the larger 2-amino-1,4,5,6-tetrahydropyrimidine moiety (red) and (ii) addition of substituents (R^2 and R^3) at 2-aminoimidazoline and 2-amino-1,4,5,6-tetrahydropyrimidine endocyclic nitrogens (Scheme 2.4.1).

Scheme 2.4.1. Outline of proposed structural modifications envisaged for this work.

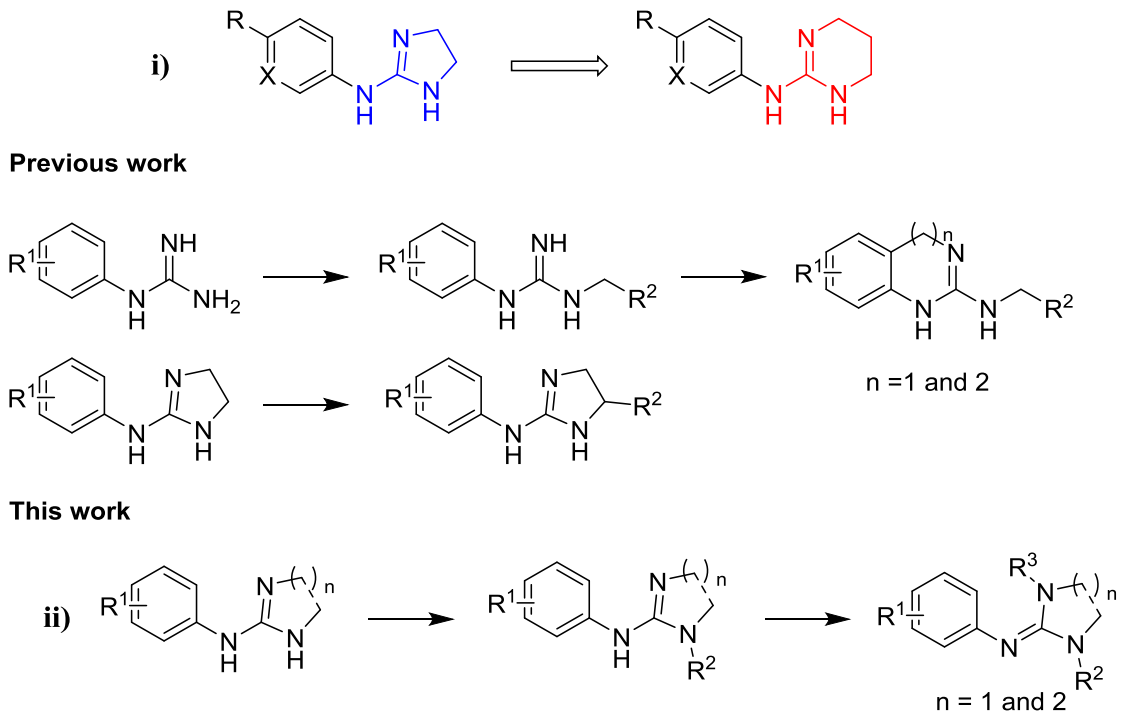

Firstly, we propose to investigate the impact of ring expansion, from 2-arylaminoimidazolines to 2-arylamino-1,4,5,6-tetrahydropyrimidines, on the α_2-AR profiles of representative members from the three families (A-C) of *lead* compounds developed within the Rozas group (Section 1.7). These analogues will serve as a representative series, preliminary evaluation of which will help identify the impact and potential utility of ring expansion which could be applied to other derivatives. Synthetic routes to the preparation of derivatives with substituents on the nitrogen atoms of both 2-arylaminoimidazolines and 2-arylamino-1,4,5,6-tetrahydropyrimidines rings will also be investigated using model systems and may be applied to the preparation of additional derivatives pending preliminary biological evaluation.

Synthesis and pharmacological evaluation of these initial 2-arylamino-1,4,5,6-tetrahydropyrimidines analogues (Fig. 2.4.1), with concomitant increase in polar surface area and lipophilicity, will highlight the implications of ring expansion on α_2-AR engagement. Subsequent comparison of these results with those of the corresponding *lead* analogues will establish any potential benefits exhibited by this ring expanded series.

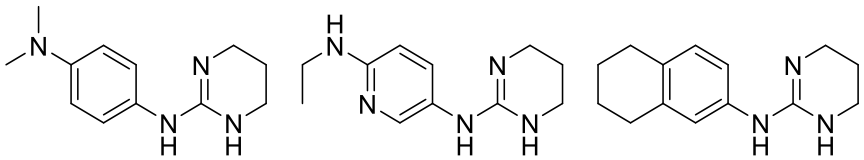

Figure 2.4.1. Proposed ring expansion series of representative analogues for families **A**-**C**.

Preparation of these analogues will require a thorough investigation of methodologies previously developed and utilized within the Rozas group to furnish 2-arylamino-1,4,5,6-tetrahydropyrimidines to identify the most suitable approach. A variety of synthetic routes to access 1-substituted-2-arylamino-1,4,5,6-tetrahydropyrimidines and 1-substituted-2-arylaminoimidazolines will be examined. The ultimate aim is to design a robust and versatile synthetic route of modular design utilizing readily available starting materials. This route can then enable the facile preparation of a series of analogues for SAR studies. Prior to this an extensive examination of published methodologies will also be conducted to inform synthetic design and selection of an optimal approach.

In summary, this work will constitute a strong foundation for future expansion and development of novel α_2-AR subtype selective ligands. The extensive receptor profiles compiled herein will serve as a set of guidelines to assist the design of new compounds aimed at targeting a specific subset of CNS targets with better affinity and specificity. The new compounds prepared throughout the course of this work will establish some of the core structural features necessary to impart optimal pharmacological properties required for the envisaged therapeutic application, whether it be for the treatment of SZ or MMD.

Chapter Three
Synthesis and screening of *mono*-aryl guanidine and cyclic guanidine analogues

3.1. Introduction

The hit generation and optimization process conducted within the Rozas group has furnished in excess of 100 promising hits and potential *lead* compounds with favourable α_2-AR engagement and desired pharmacological properties. A renewed approach is required to help progress and refine these *lead* compounds to allow the most promising *lead* compounds to be identified. Therefore, a more extensive panel of pharmacological screening is necessary to gain a broader understanding of the primary targets (on-targets) and secondary targets (off-targets) for each of these compounds within the CNS. This focused screening process will provide detailed receptor profiles that will aid the prioritization and development of new compounds exhibiting specificity and/or subtype selectivity for CNS-based targets of therapeutic interest.

The objectives of this chapter are to identify *mono*-aryl *lead* compounds which exhibit α_2-AR subtype selectivity and potentially elucidate a SSR for this series of compounds which can be applied to the design of future subtype selective derivatives. The pharmacological results obtained until now concerning affinity and functional activity have been unpredictable, significantly hindering the progression of the antidepressant research conducted within our group (Section 2.1.).

The data obtained from the proposed screening process may uncover compounds which display distinct polypharmacology, a property which has recently been highlighted to enhance the efficacy of potential drugs acting against GPCRs for psychiatric diseases.[143] The elevated therapeutic potential, accessible by means of harnessing polypharmacology, must also be balanced with the possibility of adverse effects through unwanted activity at 'antitargets'. As such, polypharmacology and antitarget selectivity are now seen as vital criteria which must be evaluated when identifying the most suitable *leads* in terms of affinity and activity against on-targets and selectivity vs. antitargets.

The target validation process may either reinforce our approach to *lead* identification and provide support for the proposed mechanism of action, or direct us to re-evaluate this process in order to identify *leads* which should progress to further optimization and derivatization.[144]

In-depth analysis of α_2-AR engagement (primarily measuring affinity with subsequent investigation of functional activity and subtype selectivity) may assist in the formulation of a hypothesis which can rationalise the impact of small structural changes on α_2-AR ligand affinity and correlate with the observed inversion of activity.

Therefore, the goal for this chapter is to establish a more detailed and refined description of the structural requirements to enhance the affinity and selectivity of *mono*-aryl guanidine and 2-aminoimidazoline ligands at the α_2-AR subtypes of interest, α_{2A} and α_{2C}. This information will advise the selection of appropriate substituents to enable the preparation of compounds with high specificity and affinity towards the different α_2-ARs.

3.1.1. Structure and subtype-specific functions of α_2-ARs

The α_2-ARs are known to mediate a wide range of physiological functions which makes them a highly attractive target with excellent therapeutic potential.[145] Unfortunately, the absence of any α_2-AR crystal structure is a major obstacle in drug design and development efforts. The lack of a crystal structure has prompted the development of homology models for the three α_2-AR subtypes which have been extensively reported through the literature.[146–149] Homology models of α_2-AR have proven useful in attempts to rationalise the structural characteristics of ligands which contribute to subtype selective binding;[147–149] however, without crystallographic evidence there is no definitive way to determine the validity of these predictions and hence determinants of selective binding remain elusive.[150]

Three distinct genes encode for the three α_2-AR subtypes present in humans and other mammals ($\alpha_{2A/D}$, α_{2B} and α_{2C}). These α_2-ARs are composed of 450–461 amino acid residues, 175 of which are conserved between the three receptor subtypes.[151]

The two highly conserved regions among these receptors are within the seven TM domains and the ligand accessible surface. Of the 33 amino acid residues which comprise the orthosteric binding cavity formed by TM2-TM7, 29 are identical for all three subtypes.[152]

In this chapter we will utilise a special indexing system, the Ballesteros–Weinstein nomenclature, which is used when discussing amino acids in GPCRs. In this system the letter denotes the amino acid and first number refers to the transmembrane helix (TM1-TM7) where the residue is located. The number after the decimal point refers to the residue position with respect to the most conserved residue in that helix.

This conserved residue is arbitrarily assigned the number 50.[153] A graphical representation of a generic GPCR which illustrates the Ballesteros–Weinstein nomenclature taken from the work of Venkatakrishnan *et al.* is shown in Fig. 3.1.1.[154]

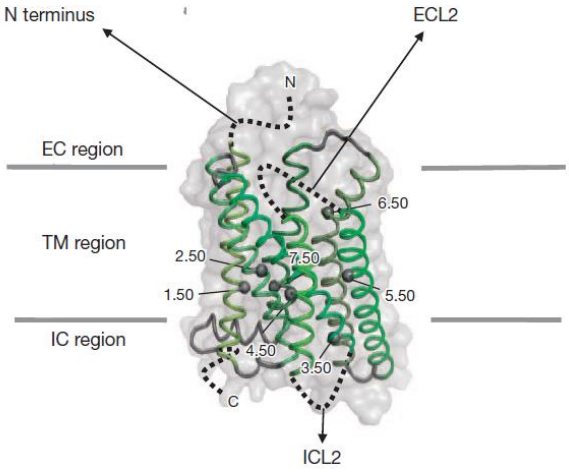

Figure 3.1.1. Illustration of the Ballesteros–Weinstein nomenclature on a generic GPCR. EC -Extracellular region, ECL2 - Extracellular loop 2, IC - Intracellular region and ICL2 - Intracellular loop 2.[154]

A common feature amongst all adrenoceptors is a conserved aspartate residue (D3.32) in TM-3 which acts as an electrostatic anchoring point for positively charged amino groups within ligands. Serine residues on TM-5 (S5.42, S/C5.43 and S5.46) are also known to be involved in hydrogen bonding with the catechol hydroxyl groups within catecholamines.

The α_{2A}- and α_{2C}-ARs are the only human adrenoceptors with a cysteine at position 5.43, while the human β_2- and α_{2B}-ARs both have a serine at position 5.43.

The cysteine residue C5.43 was thought to play a significant role in the binding of known agonists such as UK-14,304 to α_{2A}- and α_{2C}-ARs, but has been shown to be nonessential for receptor activation through site-directed mutagenesis studies.[155] An illustration of these key interactions is shown in Fig. 3.1.2 which depicts the key ligand-receptor interactions between adrenaline and the β_2-AR.

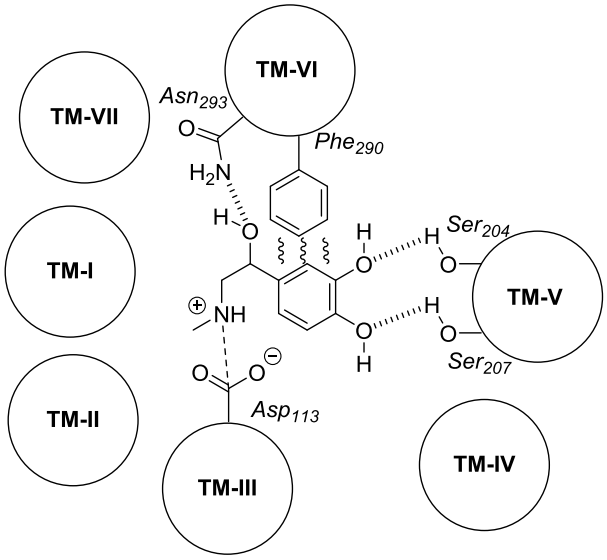

Figure 3.1.2. Illustration of key ligand-receptor interactions between adrenaline and the binding site of the β_2-AR.

Elucidation of the different physiological functions attributed to a given α_2-AR subtype remains challenging, largely due to a lack of sufficiently selective ligands which has limited the understanding about subtype-specific functions. It is known that α_2-ARs are widely distributed both in the central and peripheral nervous systems, with well-established tissue distribution within the brain. In particular, α_{2A}-ARs are abundantly expressed within the locus coeruleus whilst the α_{2B}-subtype are localised within the thalamic nuclei. The basal ganglia, olfactory tubercle, hippocampus and cerebral cortex are all known to express α_{2C}-AR. Studies involving KO or transgenic mice have yielded some important information about specific functions related to each subtype.[156]

Thus, the α_{2A}-AR subtype have been shown to mediate hypothermia, hypotension, sedation, analgesia and presynaptic inhibition of monoamine release and metabolism. The α_{2B}-subtype mediates hypertension and may be involved in developmental processes, whereas α_{2C}-ARs are thought to be involved in CNS processes such as startle reflex, stress response, locomotion, inhibition of adrenal catecholamine release and α_2-agonist mediated spinal analgesia.[3]

3.1.2. Design and development of selective α_2-AR Agonists

Pigini *et al.* have focused their research on the discovery and development of ligands endowed with preferential α_2-AR engagement, specifically the design of α_2-AR subtype selective agonists as novel analgesics. Their studies began by conservative modification of the aromatic moiety of a non-subtype selective α_2-AR antagonist **46** (Fig. 3.1.3). The introduction of polar functional groups, such as *m*-nitrophenyl, at the *ortho* position (R) of the phenyl system (compound **2**, Fig. 3.1.3) modulated the receptor interactions exhibited by **46** and led to significant and selective activation of the α_{2C}-AR. These studies also indicated that chirality, through comparison of results obtained for racemic and enantiomeric forms of **47**, was an important and influential factor for α_{2C}-AR agonism.[157]

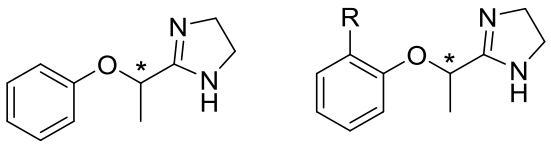

Antagonist
(±)-**46**

Agonists
R = *m*-NO_2Ph (±)-**47**
R = $CH_2CH{=}CH_2$ (±)-**48**
R = cyclopropyl (±)-**49**
R = cyclopentyl (±)-**50**
R = cyclohexyl (±)-**51**

Figure 3.1.3. Structures of compounds **1-6** reported by Pigini *et al.*[158]

The rationale thought to be responsible for converting the nonselective antagonist **46** to α_{2C}–selective agonist **47** was that *ortho* substitution (R in Fig. 3.1.3) allowed favourable interactions between the substituents and a highly conserved aromatic cluster in TM-VI, namely W6.48, F6.51 and F6.52. Furthermore, when R was substituted with groups of moderate steric bulk such as an allyl (**48**, Fig. 3.1.3) or cyclopropyl (**49**, Fig. 3.1.3) group, antagonism was retained at α_{2A}-AR and the α_{2C}-AR was potently activated; however, bulkier substituents (R= cyclopentyl, **50** and R= cyclohexyl, **51**; Fig. 3.1.3) resulted in indiscriminate activation of all three α_2-AR subtypes.[158,159]

These studies highlight how conservative structural modifications can result in drastic change to the α_2-AR activity and subtype-selectivity exhibited by ligands containing a common core. We will utilize a similar approach to identify a collection of α_2-AR ligands that exhibit preferential binding to the α_{2C}-AR and further we will use these core structures as templates in the development of new α_{2C}-selective antagonists. Extensive pharmacological screening of a series of α_2-AR ligands developed within our group (detailed in section 3.3.) will allow us to explore the secondary pharmacology of these ligands and inform the selection of the most promising and selective candidates for further development.

3.2. Synthetic Methodology

3.2.1 Synthesis of *mono*-aryl guanidines

There are numerous methodologies reported for the preparation of (hetero)-aryl and alkyl guanidines. This work is focused on the synthesis of (hetero)-aryl guanidine derivatives, therefore a summary of reported methods for their preparation shall be reviewed.

One of the most common utilized methods is *guanylation* which involves chemical transformation of a primary or secondary amine to build the guanidine core, typically as an *N,N'*-di-substituted guanidine, by reaction with a guanylating reagent (Scheme 3.2.1). These substiuents are usually electron-withdrawning protecting groups, such as Boc or Cbz, which enhance the electrophilic nature and activate the guanylating reagent, reduce the basicity and reactivity of the resulting guanidines thus facilitating their isolation and purificaction. Subsequent deprotection of these *N,N'*-di-substituted guanidine intermediates furnishes either the free base guanidine or the guanidinium salt depending on the protecting group.[160]

Scheme 3.2.1. A general guanylation reaction and deprotection to furnish a substituted guanidine.[161]

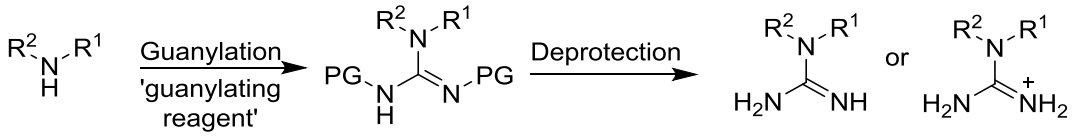

A number of reactive guanylating reagents have been developed for this transformation including thioureas and isothioureas, triflyl guanidines, aminoiminomethane-sulfonic acids (Fig. 3.2.1-A), pyrazole-1-carboxamidines (Fig. 3.2.1-B), chloroformamidines, triazole-carboxamidines and *S*-methylpseudothioureas (Fig. 3.2.1-C).[162]

The most straightforward route to access substituted guanidines involves reaction of an aryl or alkyl amine with an electrophilic thiourea derivative containing carbamate protecting groups (Fig. 3.2.1-**A**), using activating agents such as Mukaiyama's reagent (2-chloro-1-methylpyridinium iodide) or thiophilic metal salts ($HgCl_2$ or $CuCl_2$) and a tertiary amine (NEt_3) to accelerate the desulfurization.[163] Kim and Qian reported the use of (*N,N'*-di-*tert*-butoxycarbonyl)-thiourea (**52**) as the guanylating reagent with $HgCl_2$ and NEt_3 as activating agents for the preparation of *N*-aryl-*N',N''*-diBoc protected guanidines which has become the principal method adopted within the Rozas group. The application of this methodology for the preparation of the screening series will be discussed further in section 4.4. [164,165]

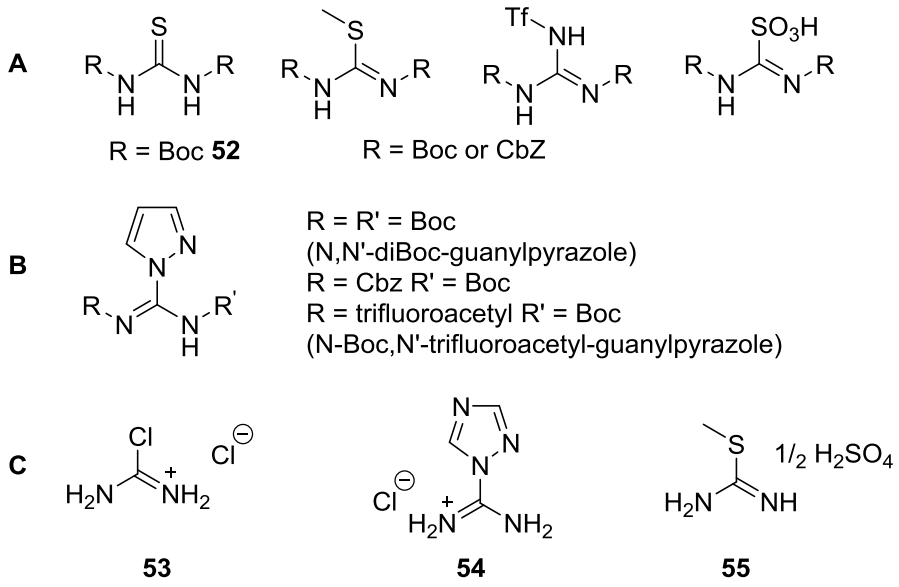

Figure 3.2.1. Structures of common guanylating reagents.[161]

Cunha *et al.* reported bismuth nitrate pentahydrate [$Bi(NO_3)_3.5H_2O$] as an environmentally benign alternative to $HgCl_2$ for the activation of the guanylation of *N*-aroylthioureas (i.e. *N*-benzoylthiourea) (Scheme 3.2.2).[165]

This method provides access to a range of 1,3-disubstituted *N*-aroylguanidines generating them in comparable yields to those achieved using $HgCl_2$ activation; nonetheless, reports on the use of this method are limited.[166,167]

A number of alternative reagents for the desulfurization of *N*-aroylthioureas have also been reported including *N*-iodosuccinimide (NIS),[168] iron trichloride ($FeCl_3$),[169] and EDCI.[170]

Scheme 3.2.2. Bismuth nitrate pentahydrate ($Bi(NO_3)_3 5H_2O$) mediated guanylation of N-benzoylthioureas.[165–167,171]

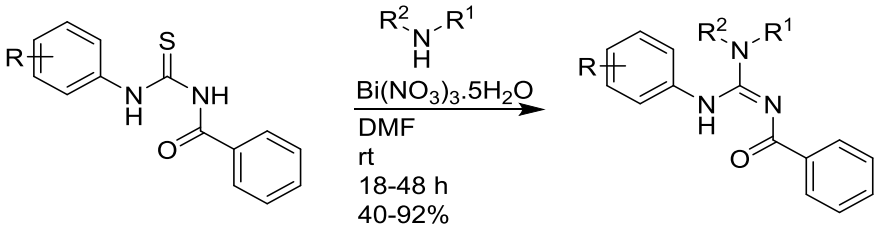

Typically, direct installation of the guanidine core utilizes reagents such as chloroformamidine hydrochloride (**53**), 1*H*-1,2,4-triazole-1-carboxamidine hydrochloride (**54**) and *S*-methylisothiourea hemisulfate (**55**); however, these reaction can suffer from poor yields and purification issues (Fig. 3.2.1-C)..[160,172,173] Direct guanylation of amino groups can also be achieved by addition of amines to cyanamides and acylcyanamides under harsh reaction conditions (reflux in concentrated aqueous H_2SO_4 or HCl), which can lead to decomposition of the reagents.[162]

Recently, alternative milder conditions utilizing Lewis acid catalysis ($AlCl_3$, TMSOTf and lanthanide(III) triflates) have proven to be highly effective for the preparation of aryl guanidines using cyanamide under aqueous conditions.[174] Catalytic guanylation reactions of amines with symmetrical and unsymmetrical carbodiimides have also become efficient and atom-economical methods to prepare *N*-substituted guanidines (Scheme 3.2.3). Extensive mechanistic studies have established that four different reaction mechanisms can be involved in heterogeneous and homogeneous catalysed guanylation reactions.[175]

Scheme 3.2.3. General scheme of amine addition (hydroamination) to carbodiimides.

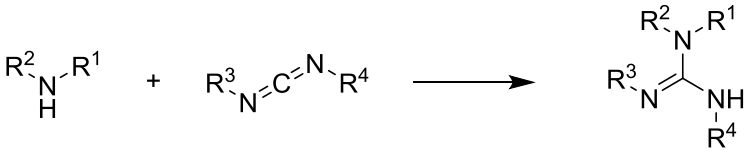

Conversley, *guanidinylation* reactions involve the installation of a preformed guanidine moeity (protected or masked) onto a (hetero)aromatic core using C-N bond forming reaction, often utilizing a copper or palladium catalysts (for example Scheme 3.2.4).[176] This reaction involves the nucelophilic aromatic substitution (NAS) of 2-chloro-5-nitropyridine using guanidinium hydrochloride which is converted to the free base *in situ* under strongly basic conditions.[132]

Scheme 3.2.4. Guanidylation of heteroaryl halide 2-chloro-5-nitropyridine by NAS.

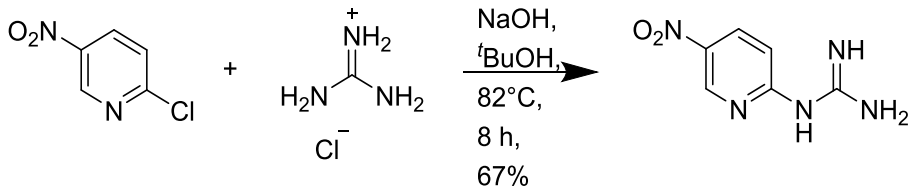

There are numerous literature reports of metal catalyzed guanidinylation reactions to prepare aromatic and heteroaromatic guanidines including many ligand-promoted Ullmann-type coupling reactions. A recent example from Ma *et al.* described the synthesis of symmetrical and unsymmetrical *N,N′*-diaryl guanidines using a CuI/*N*-methylglycine-catalyzed coupling reaction of guanidine nitrate with aryl halides (iodides and bromides).[177] This reaction gave *N,N′*-diaryl guanidines in good to excellent yields; however, as this reaction utilizes an unsubtituted guanidine which exhibits double nucelophilicity these conditions favour *N,N′*-diarylation and are unsuitable for the preparation of *N*-aryl guanidines. Schmitt *et al.* described a modified Ullmann reaction using CuOAc/*l*-proline as catalysts for the coupling of aryl halides and pseudohalides, with p-methoxybenzyl (PMB) guanidine as the guanidinylation agent. This provided *N*-mono(hetero)aryl guanidines in good yields after PMB-deprotection using TFA (Scheme 3.2.5).[178]

Scheme 3.2.5. Guanidylation using a CuOAc/*l*-proline catalysed reaction with p-methoxybenzyl (PMB) guanidine aryl halides.

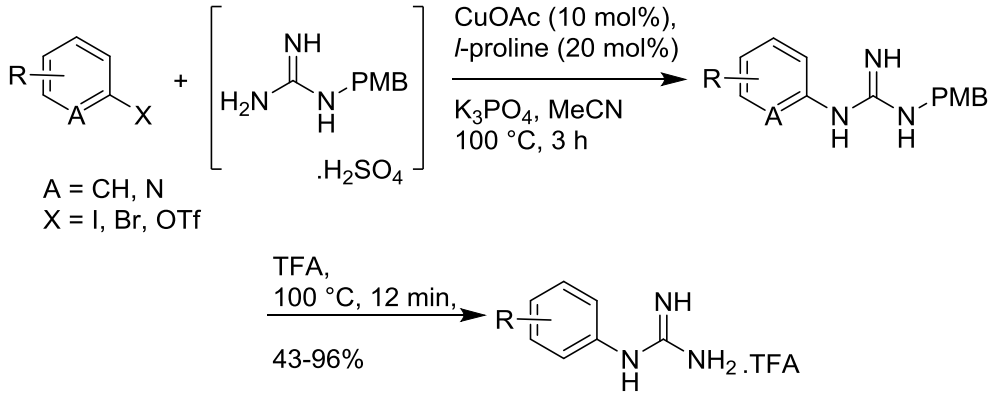

Shaw, Grayson and Rozas reported a method for preparation of aryl guanidines using the Pd-catalysed Buchwald-Hartwig coupling of aryl halides with 2-amino-4,6-dimethoxypyrimidine to give 2-(arylamino)pyrimidine intermediates (Scheme 3.2.6).[179] These are subsequently cleaved under acidic conditions furnishing aryl guanidinium hydrochloride salts in good to excellent yields. Two limiting factors which restrict the applicability and scope of this approach are the availability and cost of adequately substituted aryl halides and the harsh acid conditions required to liberate the desired guanidine hydrochloride chloride. These conditions are incompatible with certain acid sensitive functional groups and can lead to degradation of functionalities like cyano, acetamide, methyl ester and acid-labile protecting groups.

Scheme 3.2.6. Guanidylation using the Shaw, Grayson and Rozas method.

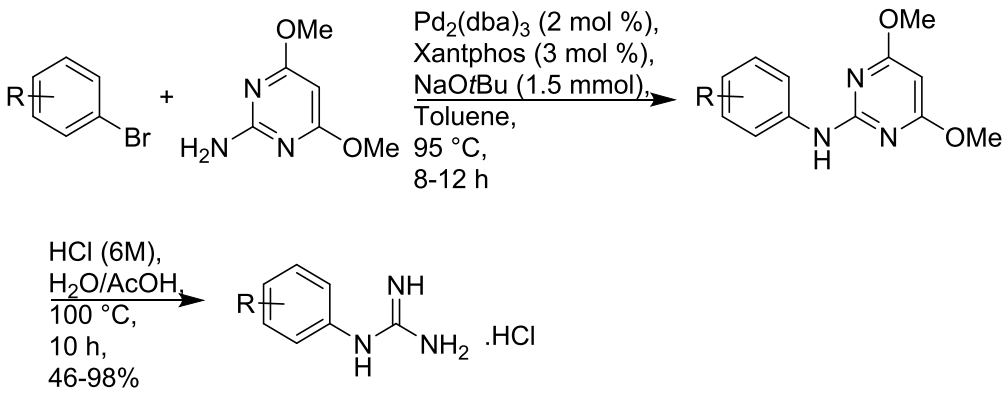

The Kim and Qian method has been most frequently utilized within the Rozas group to facilitate the facile and reliable preparation of a wide range of *N*-aryl guanidines (Scheme 3.2.7).[129,180] As such, this method has been retained for the preparation of the *N*-aryl guanidines α_2-AR ligands for screening at the PDSP (Section 3.4.).

Scheme 3.2.7. Kim and Qian method of guanylation using **52**.[164]

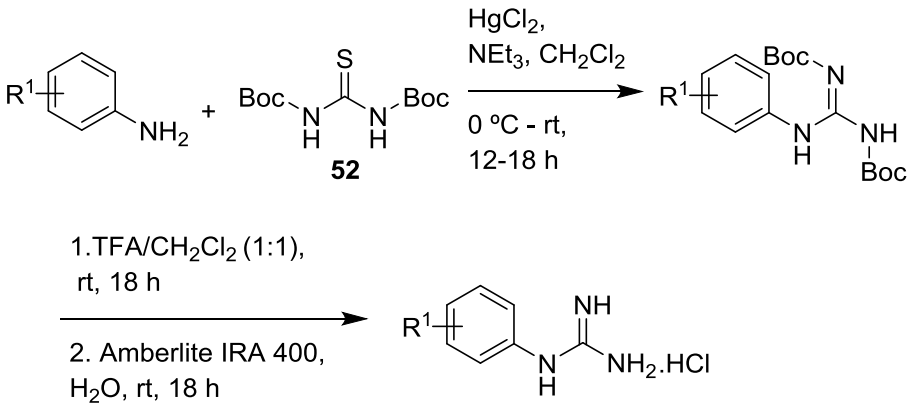

The proposed mechanism for this $HgCl_2$mediated reaction involves coordination of **52** sulphur to thiophilic Hg(II). This coordination enhances the electrophilic nature of the quaternary carbon and facilitates carbodiimide formation with elimination of mercury (II) sulfide (HgS) and triethylammonium hydrochloride. Subsequent nucleophilic attack of the amine followed by proton transfer affords *N,N'*-di(Boc)-*N''*-aryl guanidines (Scheme 3.2.8). These *N,N'*-di(Boc)-*N''*-aryl guanidines are very stable and readily purified using flash column chromatography.

A solution of trifluoroacetic acid (TFA) is used to remove the Boc protecting groups and form the corresponding guanidinium trifluoroacetate salt in excellent yields; however, due to the limited aqueous solubility of these salts, anion exchange resin (Amberlite IRA-400 chloride form) is used to form the more water soluble hydrochloride salts in high yield and purity.[130]

Scheme 3.2.8. Guanylation mechanism *via* $HgCl_2$ mediated desulfurization of (*N*,*N*-di-*tert*-butoxycarbonyl)thiourea yielding *N*-aryl-*N',N''*-diBoc protected mono-substituted guanidine.

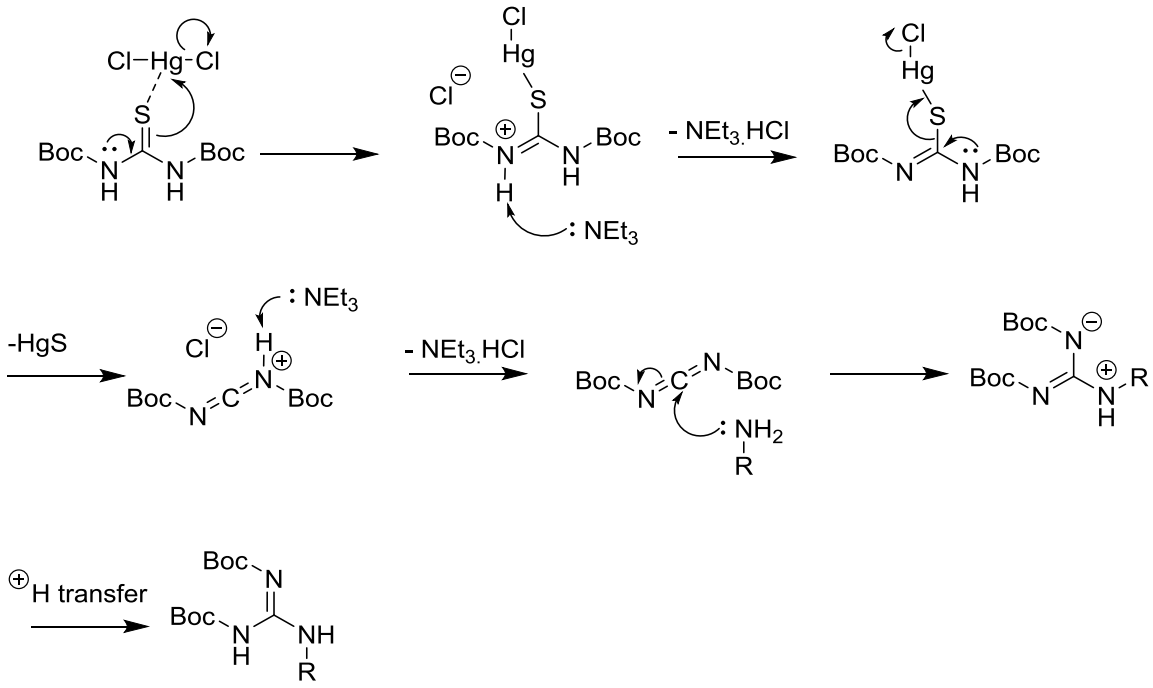

A modified version of this procedure developed within Rozas' group[181] will also be utilized in the preparation of the 2-arylamino imidazoline derivatives required for screening which will be discussed in section 3.2.2.

3.2.2. Synthesis of 2-arylaminoimidazolines

A number of α_2-AR agonists containing a 2-aminoimidazoline core, such as clonidine (**56**) and indanazoline (**57**), have been widely used in medicine as cardiovascular antihypertension agents, sedatives and vasoconstrictive agents (Fig. 3.2.2).[182]

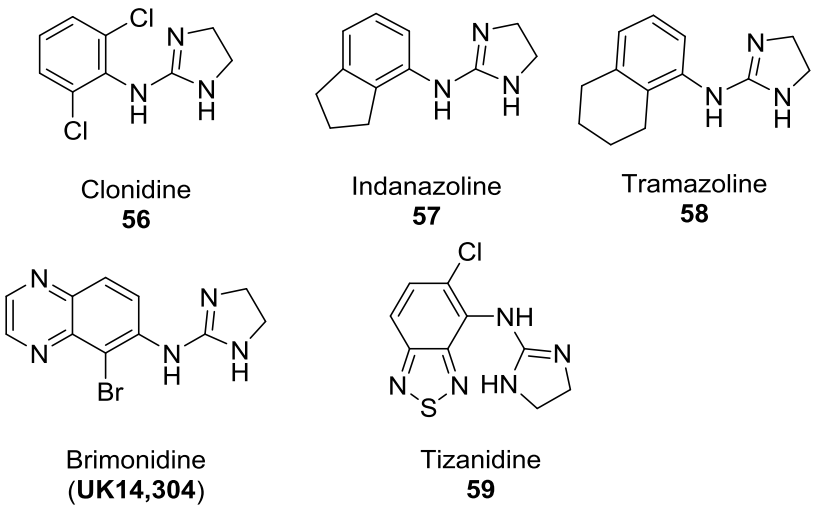

Figure 3.2.2. Structures of α_2-AR agonists containing a 2-aminoimidazoline core.

There are many reported methods for the preparation of 2-arylaminoimidazoline derivatives. Chapleo *et al*. reported the synthesis of clonidine analogues by treating 2-methylthio-2-imidazoline hydroiodide (**60**) with aromatic amines in the presence of pyridine (Scheme 3.2.9).[183]

Scheme 3.2.9. Preparation of 2-arylaminoimidazolidine derivatives from 2-methylthio-2-imidazoline hydroiodide.

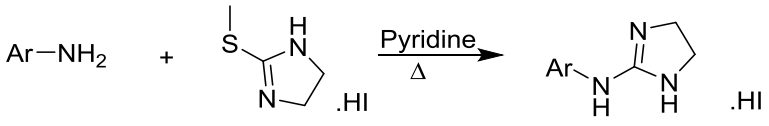

60

Alternatively, chlorination of imidazoline-2-one using phosphorous pentachloride can be used to give 2-chloro-4,5-dihydroimidazole, which is then reacted *in situ* with an aryl or alkyl amine to form the corresponding 2-aminoimidazolidine derivative (Scheme 3.2.10).[184]

Scheme 3.2.10. Preparation of 2-aminoimidazolidine derivatives from 2-chloro-4,5-dihydroimidazole.

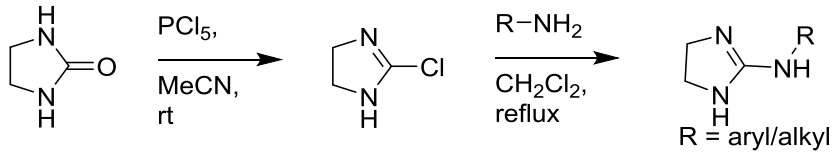

Originally, the most common approach was a three-step protocol involving the conversion of an aryl amine to an aryl isothiocyanate, further treating it with ethylene diamine; cyclization of the resulting thiourea intermediate was performed using a Lewis acid, commonly Hg(II) salts such as mercuric oxide (HgO) or acetate, $Hg(OAc)_2$ (Scheme 3.2.11).[185]

Scheme 3.2.11. Preparation of 2-aryliminoimidazolidine derivatives utilizing aryl isothiocyanates and ethylene diamine.

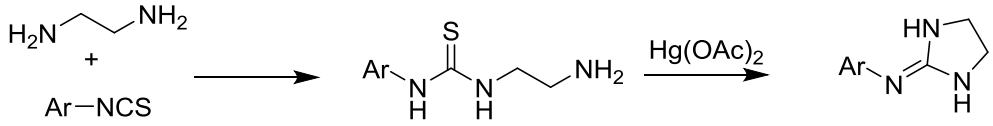

Preparation of 1-substituted-2-arylimino-2-imidazolidines involve a similar synthetic route with initial reaction an *N*-substituted ethylenediamine derivative and a phenyl isothiocyanate to give a thiourea intermediate which is subsequently cyclised using Hg^{2+} mediated guanylation reaction (Scheme 3.2.12).[186] This kind of reaction will be further discussed in Chapter 6.

Scheme 3.2.12. Synthesis of 1-substituted-2-phenylaminoimidazolines phenyl isothiocyanate.

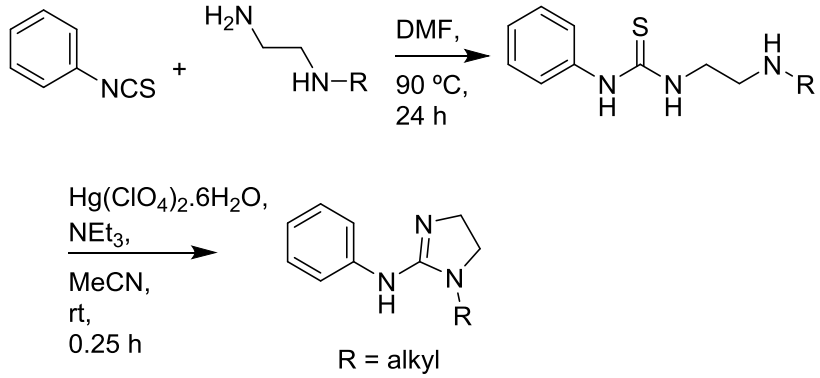

Similarly, Reynaud *et al.* reported a method which utilizes aryl isothiocyanates.[187] Conversion of the aryl isothiocyanates to an *N*-aryl-*O*-ethylthiocarbamate derivative is achieved by refluxing in ethanol and then it can be reacted with ethylene diamine to produce the 2-aryliminoimidazolidines, through cyclisation of the thiourea intermediate (Scheme 3.2.13).[187]

Scheme 3.2.13. Reynaud's method utilizing aryl isothiocyanates.[187]

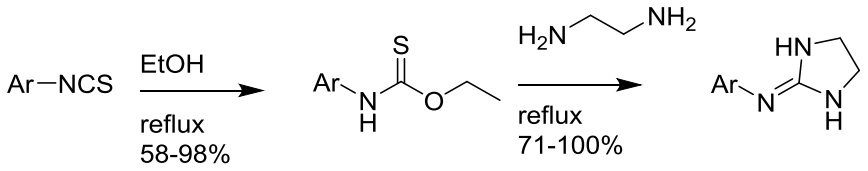

The Rozas and Dardonville method[128,188] requires the preparation of *N*,*N'*–bis-(*tert*-butoxycarbonyl)imidazolidine-2-thione (**61**) which involves Boc protection of 2-imidazolinethione using *di*-*tert*-butyl dicarbonate in the presence of an excess of sodium hydride suspended in anhydrous THF (Scheme 3.2.14).

Scheme 3.2.14. Synthesis of *N*,*N'*–*bis*-(*tert*-butoxycarbonyl)imidazolidine-2-thione (**61**) from 2-imidazolinethione.

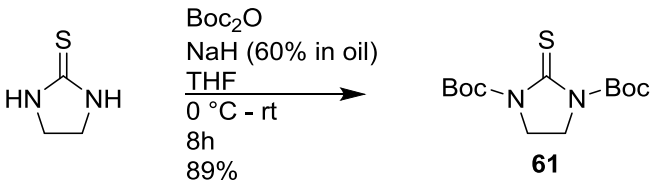

This procedure utilizes the same mild conditions as the Kim and Qian method ($HgCl_2$ and NEt_3) upon which it is based and, hence, tolerates a range of functional groups. The main advantage of this method is that it is compatible with poorly nucleophilic or labile amines such as anilines and aminopyridines allowing for the preparation of their 2-aryliminoimidazolidine derivatives, as their *bis*-Boc protected precursors, in good yields (Scheme 3.2.15).

Scheme 3.2.15. Rozas and Dardonville's method for the preparation of Boc protected 2-arylimino imidazolidine derivatives using **61**and $HgCl_2$.

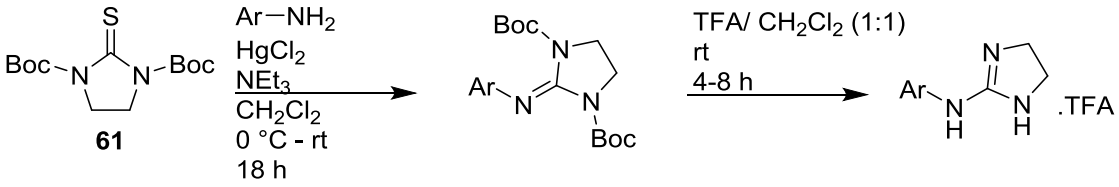

The mechanism by which this reaction occurs has not yet been confirmed; however, it is thought to proceed through an addition/elimination process due to the steric constrain of the cyclic thione (Scheme 3.2.16). The geometrical strain of the 5-membered ring system together with the lack of acid N-H protons would disfavour the formation of a carbodiimide, as proposed in Scheme 3.2.16. Instead, coordination is first thought to occur between the Boc-protected imidazolidine-2-thione and $HgCl_2$.

Scheme 3.2.16. Proposed addition/elimination guanylation mechanism *via* $HgCl_2$ mediated desulfurization of 1,3-bis-(*tert*-butoxycarbonyl)-2-methyl-2-thiopseudourea yielding *N*-aryl-*N',N''*-diBoc protected guanidine.

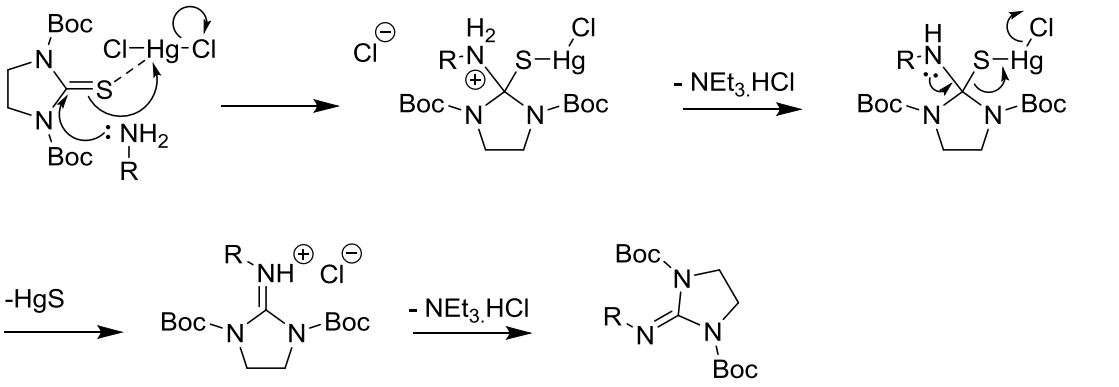

Hg(II) complexes with heterocyclic thiones have been previously reported including a 1:2 complex of $HgCl_2$ with 1,3-imidazole-2-thione and benzo-1,3-imidazole-2-thione (Fig. 3.2.3).[189,190] Coordination with Hg enhances the electrophilic nature of the C(=S) quaternary carbon and facilitates the concerted nucleophilic attack of the amine ('addition').

The resulting tetrahedral intermediate is then deprotonated and the desired Boc protected 2-aryliminoimidazolidine derivatives formed upon ‘elimination’ HgS (Scheme 3.2.16).

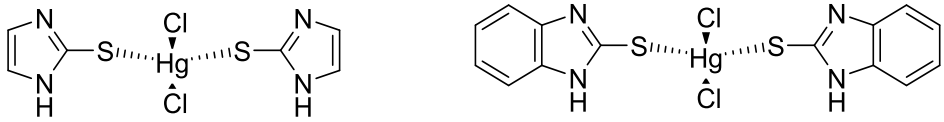

Figure 3.2.3. Structures of reported 1:2 Hg(II) complexes with 1,3-imidazole-2-thione and benzo-1,3-imidazole-2-thione.

A procedure reported by Mundal *et al.* involves a similar addition/elimination process in the reaction between the *N*-acylated-2-methylthio-2-imidazoline derivative (**62**) and aryl amines with loss of methane thiol instead of HgS (Scheme 3.2.17). This procedure was also found to be compatible with poorly nucleophilic anilines including heteroaromatic amines and anilines substituted with electron-withdrawing substitutents.[185]

Scheme 3.2.17. Preparation of 2-arylaminoimidazoline derivatives from **62** and aryl amines.

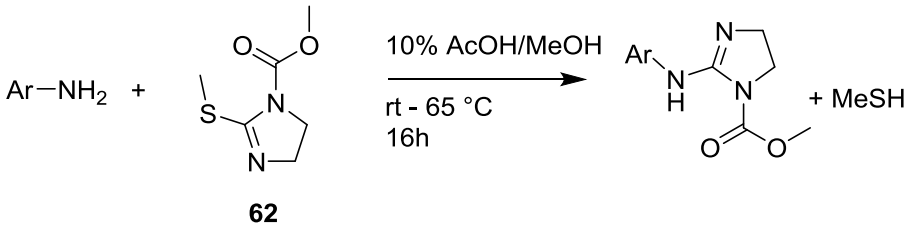

62

Previous work within our group with these Boc-protected 2-aryliminoimidazolidine derivatives has shown these derivatives to be extremely acid sensitive during purification on silica gel. This could result from a combination of both ring strain and the restrained imino tautomeric form which upon protonation may be susceptible to nucleophilic act. This could potentially lead either to endocyclic or to exocyclic cleavage and ultimately to degradation of the desired product (Scheme 3.2.18).

Scheme 3.2.18. Potential degradation pathways for Boc 2-aryliminoimidazolidine derivatives.

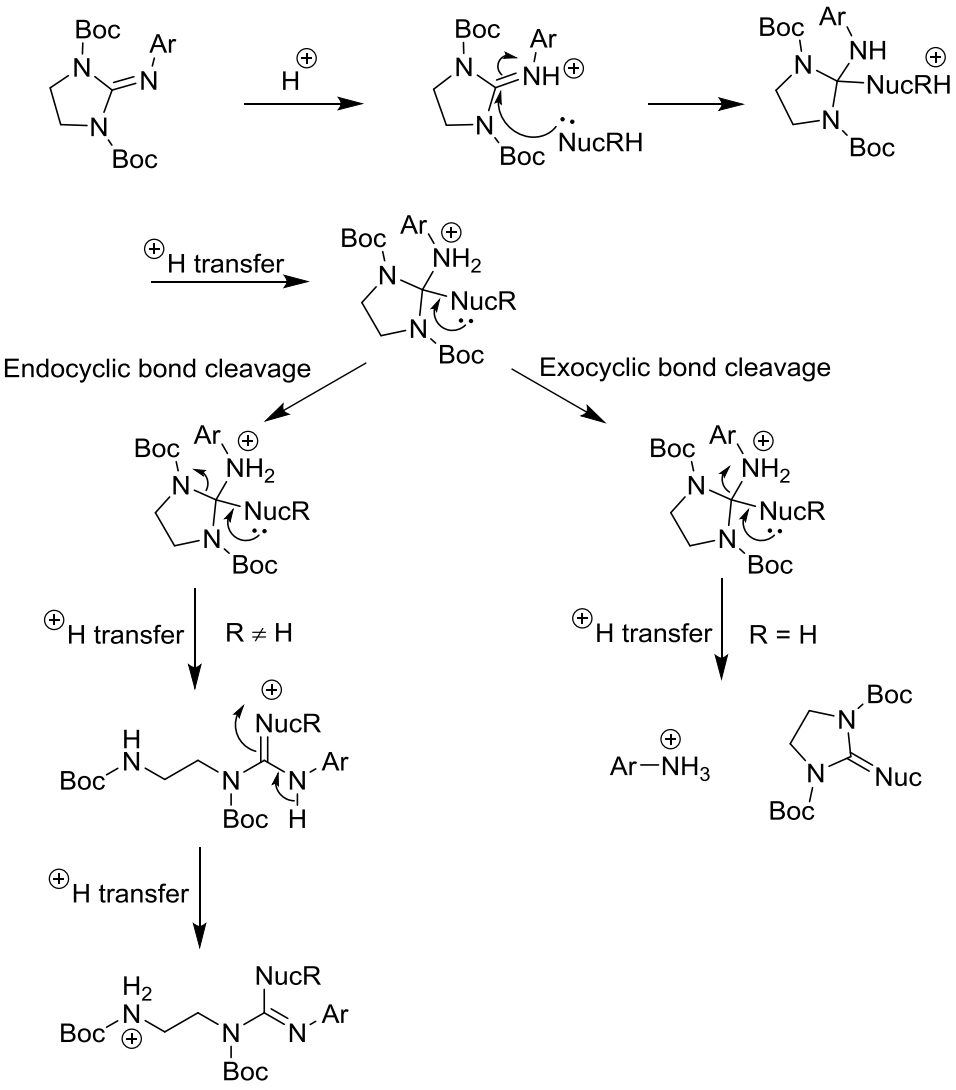

Hence, purification of these derivatives must be performed very quickly using alumina instead of silica gel. Additionally, NEt_3 treated (5%) non-polar eluent may also be required during loading of the alumina into the column to basify the stationary phase prior to purification.[132]

3.3. Synthesis of *mono*-aryl derivatives for screening

The compounds shown in Fig. 3.3.1 comprise the series of *mono*-aryl guanidine and 2-aminoimidazoline derivatives from our in-house library chosen for screening at the PDSP. The aryl guanidine derivatives (**63**, **64**, **65** and **66**) and 2-aminoimidazoline derivatives (**36**, **63b** and **69**) were synthesised as previously described in section 3.2.1, using $HgCl_2$ mediated guanidylation.[164]

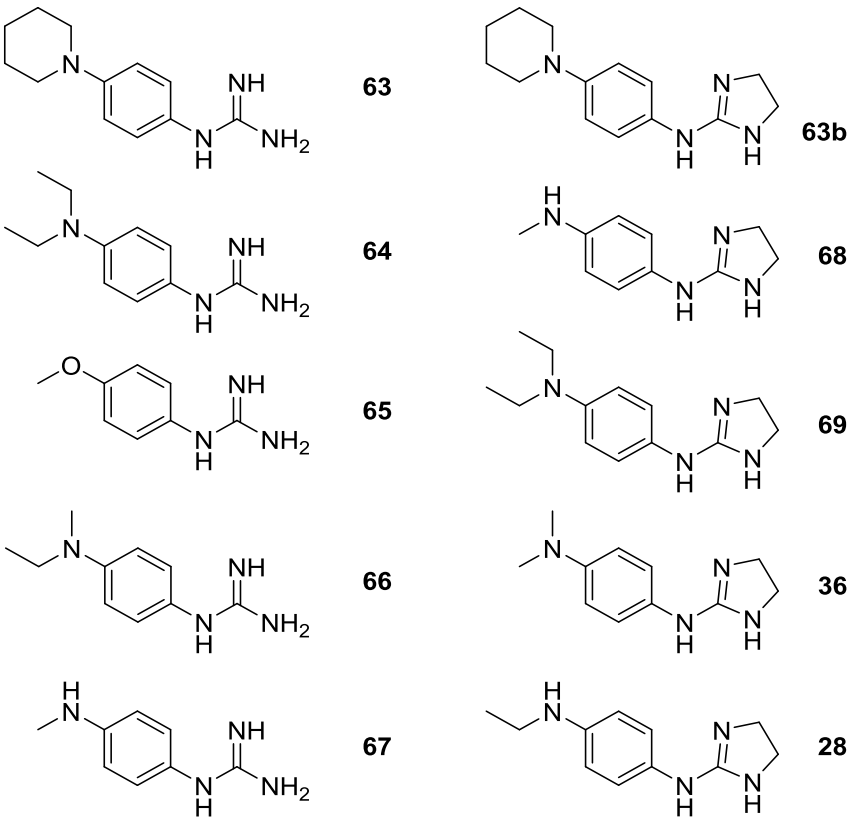

Figure 3.3.1. Structures of chosen α_2-AR ligands from our in-house library: mono-aryl guanidine derivatives (**63**, **64**, **65**, **66** and **67**) and 2-aminoimidazoline derivatives (**28**, **36**, **63b**, **68** and **69**).

Synthesis of these derivatives first required the preparation of **61** and **52**, obtained using reported methods for Boc protection of 2-imidazolinethione and thiourea (Scheme 3.2.14 and 3.3.1, respectively). **61** and **52** were obtained after recrystallization in good yields of 89% and 62%, respectively.

Scheme 3.3.1. Synthesis of **52** from thiourea.

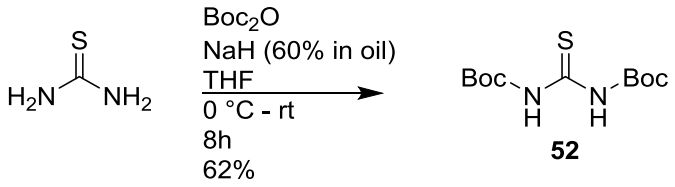

An overview of the synthetic route employed for the preparation of this series, as previously reported,[191] is shown in Scheme 3.3.2.

Scheme 3.3.2. Preparation of *mono*-aryl guanidine (**63**, **64**, **65**, **66** and **67**) and 2-aminoimidazoline derivatives (**28**, **36**, **63b**, **68** and **69**).

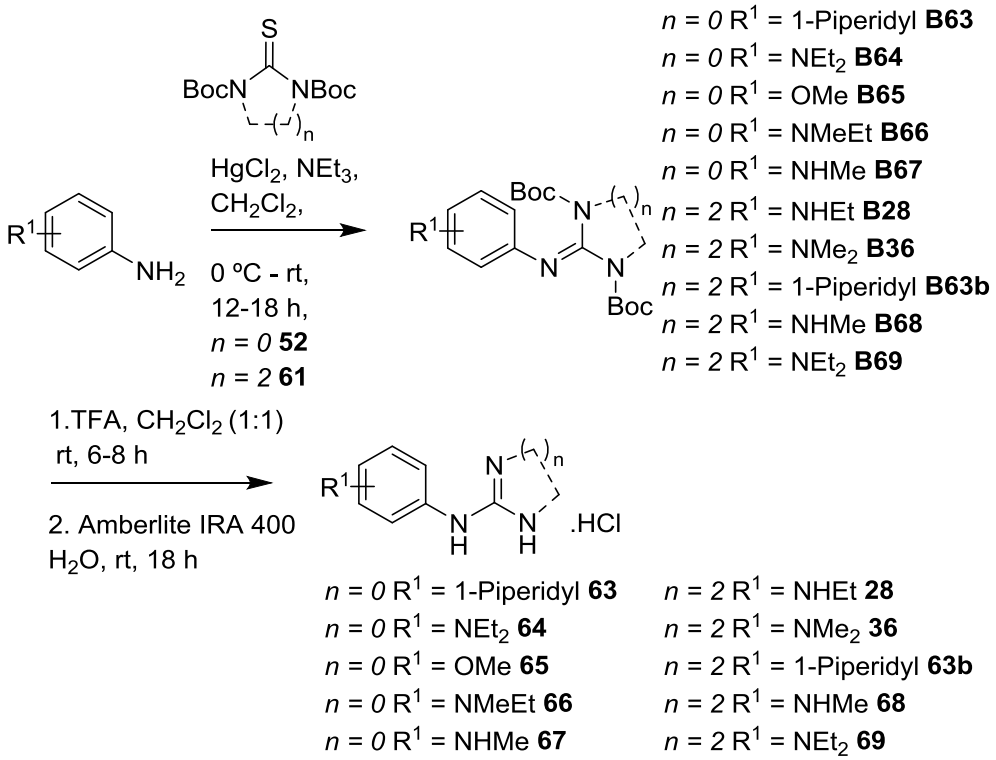

The only noteworthy deviations from the previously published synthesis, involved the preparation of the precursor diamines for **28**, **67** and **68**. Regarding the starting diamine for **67** and **68,** *N*-methyl-*p*-phenylenediamine (**70**), even though it was commercially available as the dihydrochloride salt, it was prohibitively expensive meaning that **70** would need to be synthesised.

The original synthesis of **67** and **68** first required the preparation of **70** starting from *p*-phenylenediamine which gave a very low overall yield of **70** (17%) after three steps (Scheme 3.3.3).[131]

Scheme 3.3.3. Original synthetic route to compound **70**.[131]

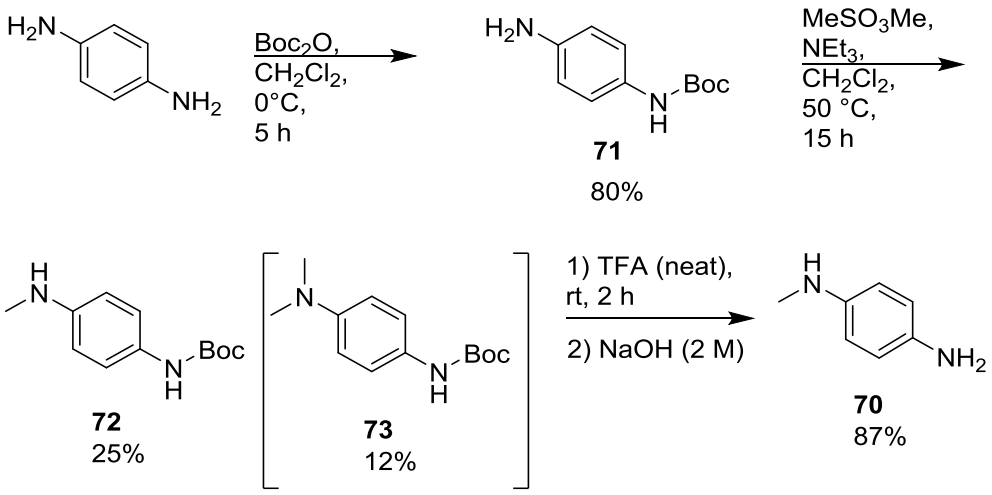

An alternative route was utilized starting from *N*-methyl-4-nitro-aniline (**74**) which allows for more direct entry to **70** using catalytic hydrogenation over palladium on carbon (Pd/C) to afford **70** in an excellent yield (Scheme 3.3.4).[192]

Scheme 3.3.4. Catalytic hydrogenation of **74** to **70**.[192]

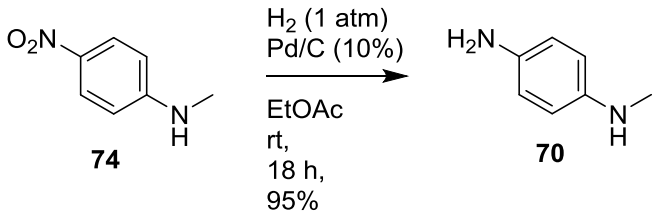

Likewise, preparation of **28** required non-commercially available *N*-ethyl-*p*-phenylenediamine (**75**) which had originally been prepared in a similar fashion to the *N*-methyl substituted analogue **70** as shown in Scheme 3.3.3, but in this work it was prepared by an alternative approach utilizing a hydride reduction of a commercially

available dianiline. Thus, *N*-acetyl-*p*-phenylenediamine (**76**) was reduced using an excess of lithium aluminium hydride ($LiAlH_4$), as shown in Scheme 3.3.5.

Scheme 3.3.5. $LiAlH_4$ reduction of **76** yielding **75**.

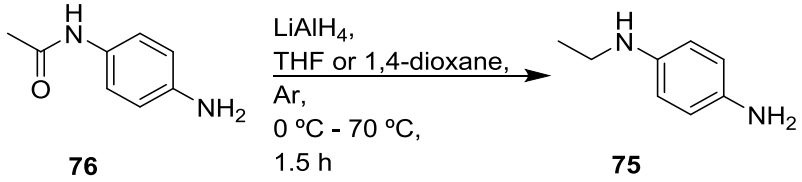

76 **75**

Initially, this reaction gave consistently low yields (20-30%) with formation of unidentified insoluble side products (red/black solid). Optimization of this reaction was conducted in an attempt to minimise the formation of the side product, including reducing the temperature, equivalents of $LiAlH_4$, and using an alternative reaction solvent. This process uncovered that **75** was temperature sensitive and was prone to degradation upon prolonged heating (>50 °C).

Unfortunately, the aforementioned reduction requires heating above this temperature to proceed at a reasonable rate and heating at 50 °C even with four equivalents of $LiAlH_4$ only furnished starting material after two hours. The solubility of **76** was also identified as a potential issue, since this compound is completely insoluble in diethyl ether and scarcely soluble in THF at room temperature. An alternative ethereal solvent, 1,4-dioxane, was examined and proved to give better results not only in terms of increased solubility, but also reaction yields. As such, the optimised reaction consisted in heating **76** in 1,4-dioxane with five equivalents of $LiAlH_4$ for 1.5 h, with close monitoring for consumption of **76**, to give **75** in an isolated yield of 56%. **75** was then utilized as previously reported in the synthesis of **28** (Scheme 3.3.2).

Considering that both **70** and **75** were both found to be thermally unstable and degraded to an undiscernible number of highly coloured unidentifiable side products over time, a potential explanation was sought. Examination of the literature regarding the stability and degradation of *p*-phenylenediamine derivatives revealed that these highly electron rich systems are prone to a number of different oxidative degradation

process resulting in bright coloured and poorly soluble by-products. For instance, *p*-phenylenediamine is transformed by (auto-)oxidation into benzoquinone diamine, Bandrowski's base (Fig. 3.3.2) and other highly coloured products. It is for this reason that it is commonly used in oxidative hair-dye formulations and tattoo inks. *p*-Phenylenediamine derivatives are also prone to oxidative polymerization and are used as precursors for the synthesis of azo dyes.[193]

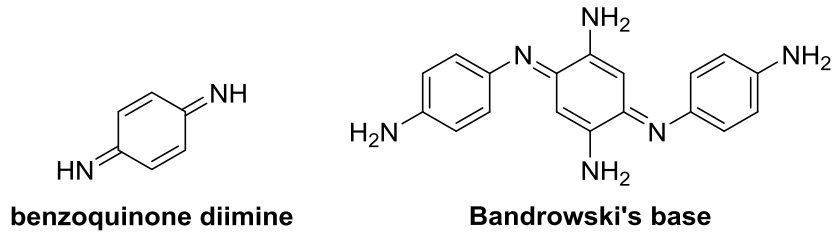

benzoquinone diimine **Bandrowski's base**

Figure 3.3.2. Structures of benzoquinone diimine and Bandrowski's base.

3.4. Pyridinoguanidine and pyridino-2-aminoimidazoline derivatives

Compounds **22**, **23** and **34**, shown in Fig. 3.4.1, were selected for screening; however, synthesis of these compounds requires the preparation of their corresponding aminopyridine precursors which are not commercially available.

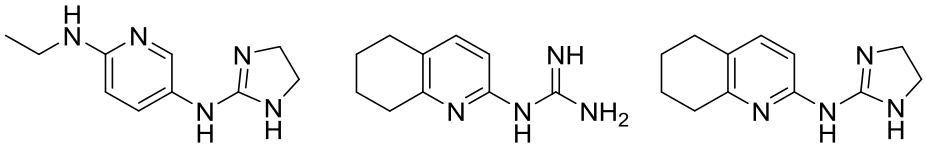

34 **22** **23**

Figure 3.4.1. Structures of compounds **22**, **23** and **34**.

3.4.1 Preparation of compound 34

The synthesis of **34** required the preparation of diamine **77**, starting from 2-aminopyridine (**78**) as shown in Scheme 3.4.1. This route involves acetylation of **78**

with acetic anhydride in pyridine to give 2-acetamidopyridine (**79**) in an excellent yield followed by lithium aluminium hydride reduction of **79** to give 2-(*N*-ethylamino)pyridine (**80**). Nitration using sulfuric acid (conc.) and potassium nitrate gave the nitro-pyridine derivative **81** in a 65% yield. Subsequent catalytic hydrogenation afforded **77** with an overall yield of 35% over 4 steps.

The procedure outlined in Scheme 3.3.2 using **61** was employed to give **82** in a good yield of 60%. Deprotection of **82** using the previously described method afforded **34** in a 90% yield as shown in Scheme 3.4.1.

Scheme 3.4.1. Preparation of **34** from **78**.

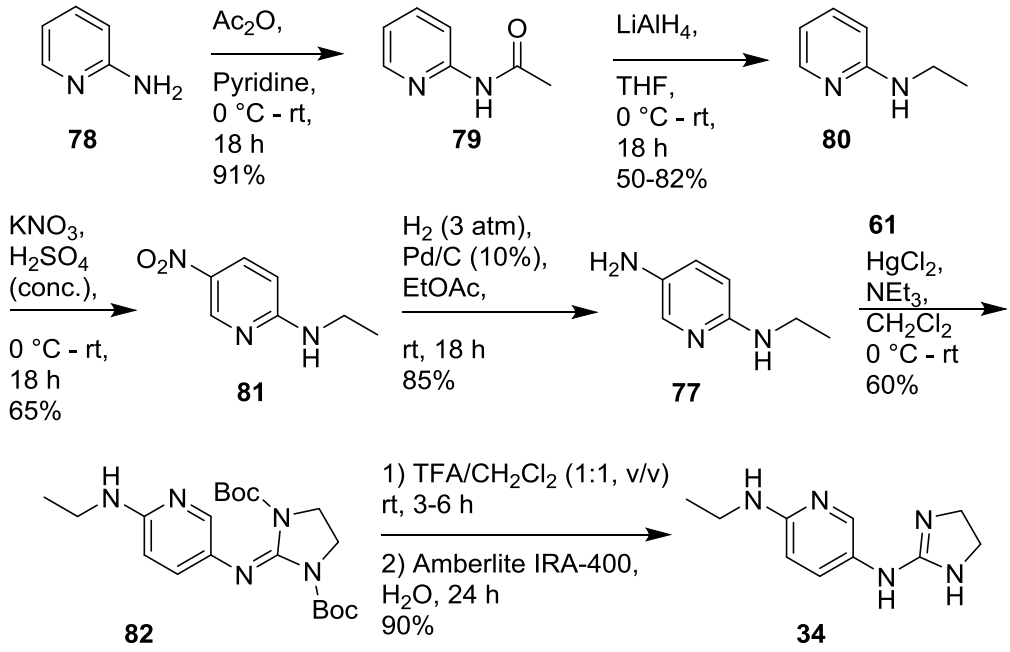

3.4.2 Preparation of 2-amino-5, 6, 7, 8-tetrahydroquinoline derivatives 22 and 23

In order to prepare compounds **22** and **23 (**Fig. 3.4.1), the starting 2-amino-5,6,7,8-tetrahydroquinoline (**83**) must be first synthesised as it is not commercially available. Hence, compound **83** was prepared from 3-(oxocyclohexyl) propanenitrile (**84**) following the procedure reported by Vijn *et al.* (Scheme 3.4.2).[194]

Scheme 3.4.2. Synthesis of **83** from **84** as reported by reported by Vijn *et al*.

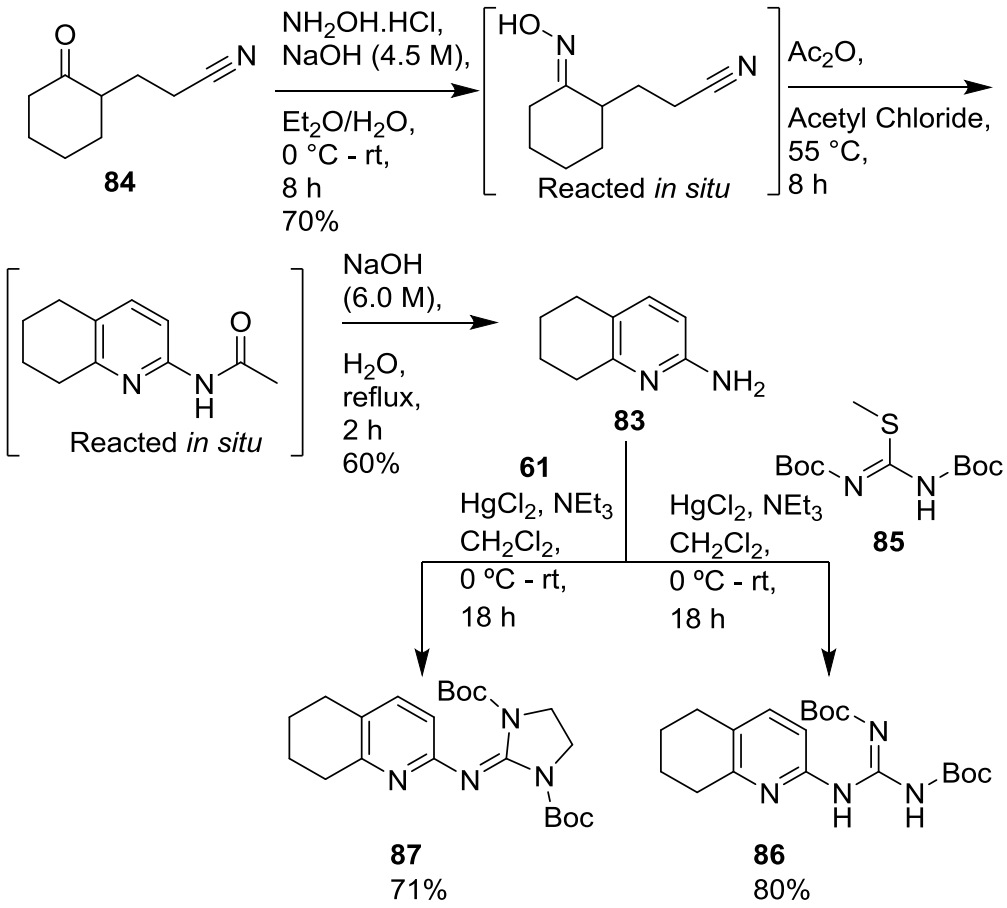

Once **83** was in hand, compounds **86** and **87** were prepared as previously reported by using $HgCl_2$ mediated guanylation using 1,3-bis(*tert*-butoxycarbonyl)-2-methyl-2-thiopseudourea (**85**) and **61**, respectively.[195] This procedure afforded **86** and **87** in good yields of 80% and 71% respectively. Subsequent deprotection with TFA and treatment with Amberlite IRA-400 resin furnished the desired hydrochloride salts **22** and **23** in 88% and 86% yields respectively.

3.5. Analysis of the purity of the chosen α_2–AR ligand series

The crude trifluoroacetate salts obtained after TFA deprotection of each corresponding Boc protected precursors were dissolved in H_2O and activated Amberlite IRA-400 chloride form resin was added in excess; then, the mixture was allowed to stir at room temperature for 18 h. The resin was removed by filtration, the aqueous layer washed with CH_2Cl_2 and concentrated *in vacuo* to afford the hydrochloride salts. ^1H and ^{19}F NMR confirmed lack of organic impurities and the absence of trifluoroacetic acid.

^1H NMR and melting point analysis matched with previously reported data.[130,132,142] HPLC analysis was conducted on all samples to assess purity and was found to match with previously reported data where available. A minimum HPLC purity of 95.0% was set for all compounds to be tested pharmacologically and all members of the series met this requirement prior to submission to the PDSP.

Dr. Daniel H. O'Donovan prepared compound **39** which was chosen to be the representative for the 1,3-disubstituted arylguanidine family as it displayed the highest α_2–AR binding affinity and antagonist activity of all the derivatives within this series (Fig. 3.5.1).[196]

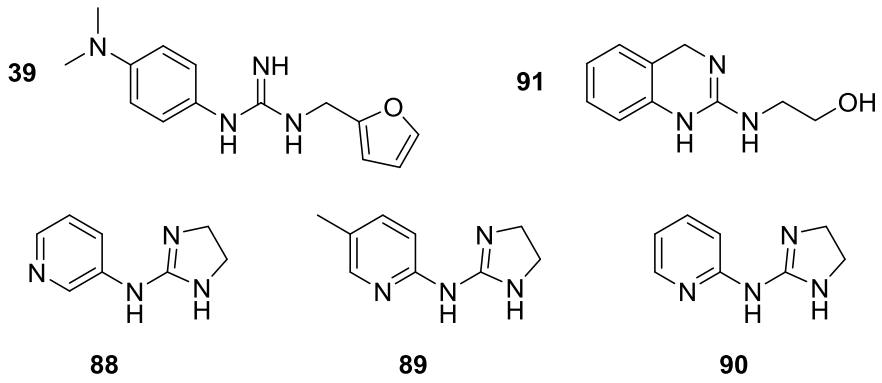

Figure 3.5.1. Structures of α_2-AR ligands **39**, **88**, **89**, **90** and **91** from the Rozas group 'in-house' compound library. These compounds were prepared by Dr. Daniel H. O'Donovan (**39**) and Dr. Brendan Kelly (**88**, **89**, **90** and **91**), respectively.

Another family of substituted 2-amino-1,4-dihydroquinazolines had been previously prepared to investigate the impact of conformationally restricting the cationic moiety.[197] This family together with compounds **88**, **89** and **90** were synthesised by Dr. Brendan Kelly. Compound **91** was chosen as the representative member of the family as it displayed both the highest α_2–AR affinity as well as antagonist activity (Fig. 3.5.1).[132] Each of these compounds, which form part of the Rozas' 'in-house' library of α_2–AR ligands, were rechecked for purity by ^{1}H NMR and HPLC analysis before being submitted to the PDSP.

3.6. Screening for selectivity of α_2-AR ligands at the PDSP

The mentioned series of *mono*-aryl guanidine and 2-aminoimidazoline α_2-AR ligands (shown in Fig. 3.3.1 and 3.4.1) were chosen to be screened for subtype selectivity at the α- and β-ARs and other sites for potential off-target receptor interactions, mostly at other biogenic amine GPCRs (Fig. 3.6.1). The PDSP is a contractor for the American NIMH which offers free screening of potential psychoactive drug candidates to academic research labs. Fortunately, the project application request we submitted outlining the rationale and justification for evaluating the pharmacological profiles of this series of related derivatives at 31 diverse receptors, ion channels and monoamine transporters (MATs) was approved.

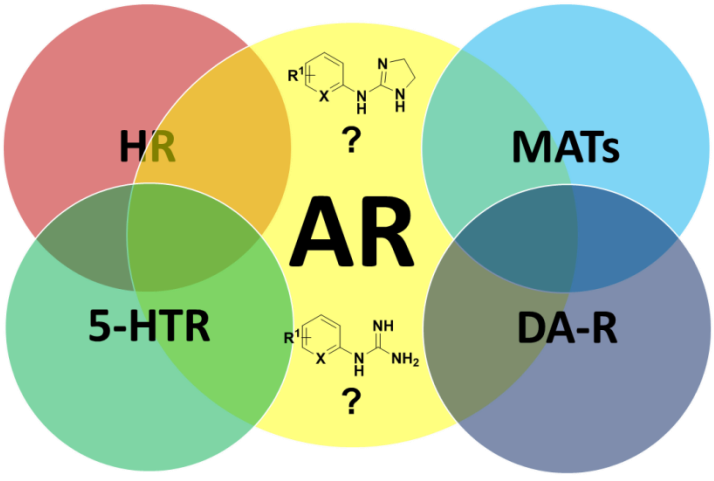

Figure 3.6.1. Schematic representation of the designated CNS targets selected for screening at the PDSP. *AR* = Adrenoceptors, *HR* = Histamine receptors, *MATs* = Monoamine transporters, *5-HTR* = Serotonin receptors, *DA-R* = Dopamine receptors.

Primarily, we aim to determine whether any members of the screening series exhibit appreciable affinities not only for adrenergic receptors (the priority in this work) but also for any other of the main biogenic amine receptors, namely histaminergic, dopaminergic and serotonergic receptors. Other targets to be examined include MATs and sigma receptors (σR). Exploring the off-target GPCR activities within this series will hopefully serve to unmask sets of SARs related to the binding of previously unconsidered targets and enlighten us about potential risks of secondary drug effects associated with this group of structures.

3.7. PDSP Screening results for α_2–AR Agonists and Antagonists

The results of the screening at the PDSP are discussed below with the most important ligand affinities highlighted and related reference made to the literature where relevant. Additional analysis of the data will conclude this section including discussion of observed trends and selection of candidates for further synthetic development and derivatization. Preparation of additional structural analogues will be proposed with the consideration of these results and may aim to reduce or accentuate certain off-target activities, depending on the identity of and nature of binding to possible secondary targets.[198]

The screening procedure involves a two-step process in which all of the compounds are screened in the *primary* assay to determine whether they displayed inhibition of binding (expressed as mean %-inhibition, N = 4 determinations) of a known radioligand at each receptor subtype. The default concentration for the *primary* assay is 10 μM with significant inhibition considered to be >50%.[199] Compounds exhibiting >50% inhibition for a given receptor subtype in the *primary* assay progress to the *secondary* assay. This allows for a distinct affinity value (K_i) to be measured from radioligand competition binding isotherms derived from competition binding assays using the same known radioligand as in the *primary* assay and a reference ligand for comparison.[200]

Extensive review of the literature was conducted in parallel with the screening process to identify any structurally similar ligands with reported affinities for other targets. This review uncovered many publications which described alternative targets for the same or closely related molecules as those chosen for screening. This information was

compiled and compared with the data gathered during the screening to help establish a better understanding of the polypharmacology within this series.

3.7.1. Affinity at monoamine transporters (MATs)

The human dopamine, noradrenaline and serotonin transporters (DAT, NET and SERT) are the three major MATs and have become important CNS targets for treating a range of neuropsychiatric disorders including PTSD, major depression, schizophrenia and a variety of anxiety disorders.[201,202]

Nonetheless, this work is concerned with selectively targeting the adrenergic system and compounds which exhibit substantial affinity for monoamine transporters would be unsuitable for development as subtype selective ligands.

3.7.1.1. Dopamine transporter (DAT)

All compounds were screened for affinity at the DAT in the primary assay which measures inhibition of the DAT radioligand **[^{3}H]WIN3542** (Fig. 3.7.1). Compound **39** (Fig. 3.7.1) was the only one in the series to display affinity for the DAT in the primary assay exhibiting 64.5% inhibition.

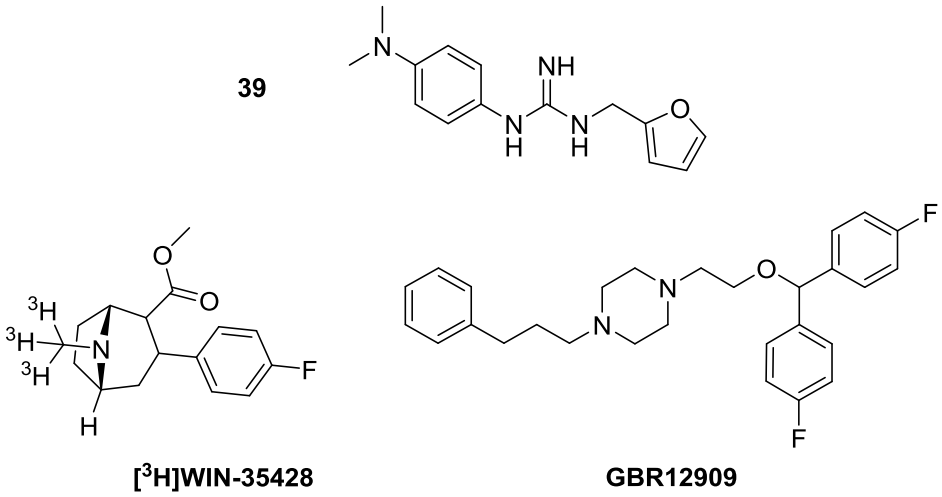

Figure 3.7.1. Structure of **39** and DAT antagonists **[^{3}H]-WIN35428** and vanoxerine (**GBR12909**) used in the DAT binding assays.

The secondary assay (competition binding) was conducted using **39** with **[^{3}H]WIN3542** as the radiolabelled "hot" ligand and vanoxerine (**GBR12909**, Fig. 3.7.1) as the "reference" high affinity DAT ligand. Vanoxerine had been in clinical trials for parkinsonism, major depression and cocaine addiction, but was found to lack efficacy and proved to be a potent blocker of hERG (i.e. cardiotoxic).[203]

The results obtained in this secondary assay for **39** gave a K_i value of 2 µM (Fig. 3.7.2). Even the low affinity for DAT exhibited by **39** is an undesirable pharmacological trait which disfavours **39** for potential development within the remit of this work.

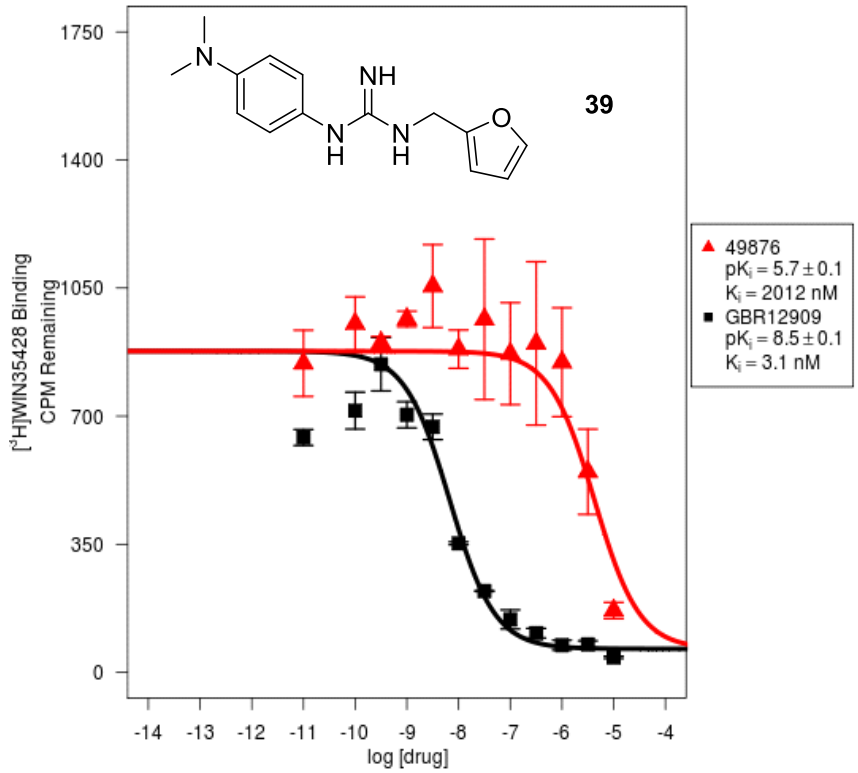

Figure 3.7.2.
Compound:
39
Receptor:
DAT
Hot Ligand:
[^{3}H]
WIN35428
Reference:
GBR12909

3.7.1.2. Noradrenaline transporter (NET)

Four of the compounds screened (**39**, **89**, **36** and **28**, Fig. 3.7.3) inhibited binding (>50% inhibition) of the NET radioligand **[^{3}H]-nisoxetine** (Fig. 3.7.3). These

compounds were subsequently analysed by competitive binding assay with **[^{3}H]-nisoxetine** as radioligand and **3** as reference to determine their affinity at the NET.

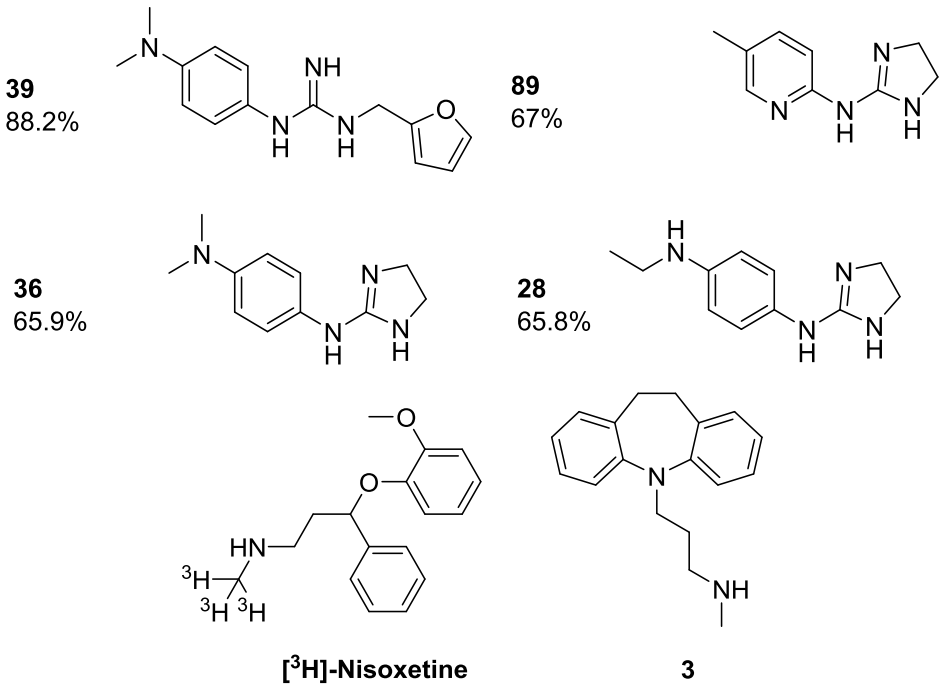

Figure 3.7.3. Structures of **39**, **89**, **36** and **28** (percentage inhibition from primary assay) and the known NET inhibitors **[^{3}H]-nisoxetine** and **3**.

All four compounds (**39**, **89**, **36** and **28**) displayed moderate affinity for the NET with **39** and **28** showing similar affinities (K_i = 343 nM and 364 nM, respectively). Both **89** and **36** had slightly lower NET affinities (K_i = 680 nM and 575 nM, respectively).

3.7.1.3. Serotonin transporter (SERT)

Known antidepressant agents, SSRIs such as fluoxetine (**1**) (Fig. 3.7.4) have been designed to inhibit only SERT and do not show strong affinity for NET or DAT; however, triple reuptake inhibitors such as nefopam exhibit high affinity and inhibitory activity at the three main monoamine transporters.[204]

Both the primary and secondary assays to measure affinity at SERT utilized **[^{3}H]-citalopram** as the radiolabelled "hot" ligand, in the secondary assay amitriptyline (**1**, tricyclic antidepressant, Fig. 3.7.4) was used as the reference ligand. Amitriptyline is an SNRI with prominent inhibition of SERT and moderate effects on NET.[204]

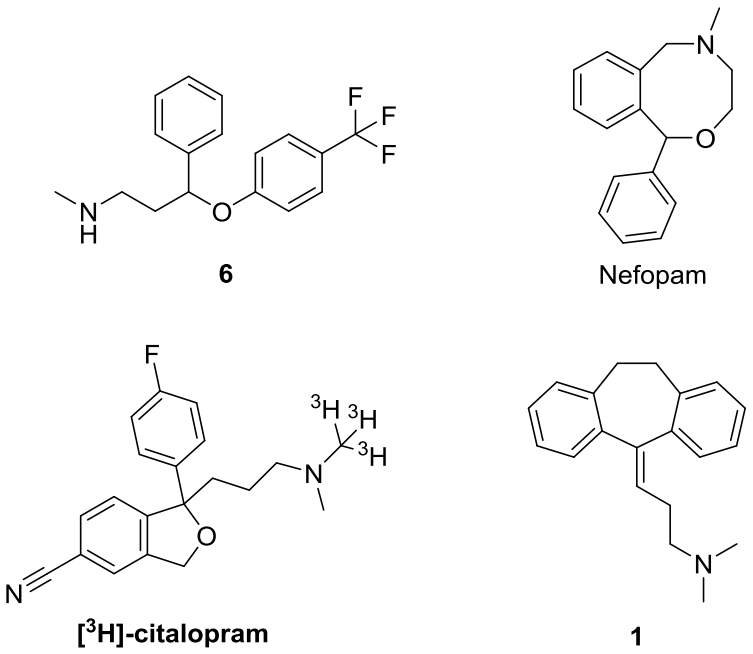

Figure 3.7.4. Structures of known SSRI antidepressant **6**, triple reuptake inhibitor nefopam as well as known SERT ligands **[^{3}H]-citalopram** and **1**.

The primary assay showed that compounds **34**, **22**, **39** and **91** inhibited **[^{3}H]-citalopram** binding to SERT to some extent (Fig. 3.7.5). These ligands subsequently progressed into the secondary assay to measure their affinity for SERT.

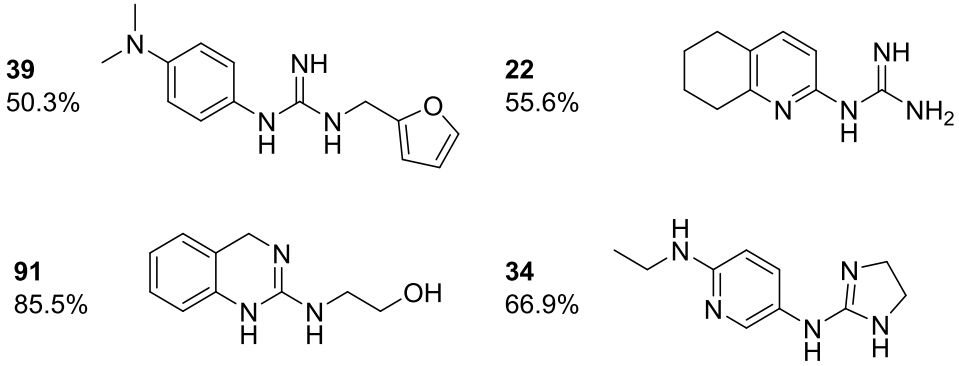

Figure 3.7.5. Structure and percentage SERT inhibition of **39**, **22**, **91** and **34**.

Intriguingly, despite having shown % inhibition above 50% in the primary assay **22** nor **34** both displayed K_i >10,000 nM for SERT in the secondary assay. In contrast, compounds **39** and **91** showed significant affinity for SERT in the secondary assay (K_i = 4529 nM and 566 nM, respectively). The lowest affinity for SERT was measured for **39**; however, when comparing the results obtained for the MATs tested **39** was the only ligand of the series to display affinity, albeit relatively low, for these three MATs.

3.7.2 Dopaminergic receptors

The selected compounds were screened for affinity at the following dopaminergic receptors: D_1-like (D_1 and D_5) and D_2-like (D_2, D_3 and D_4) receptors. As such, only two different radioligands are required to screen for affinity at all five DA receptors in the primary assay; D_1-like are screened using the tritiated D_1 antagonist **[^{3}H]-SCH23390**, whilst D_2-like screening utilizes the D_2 antagonist **[^{3}H]-*N*-methylspiperone** (Fig. 3.7.6).

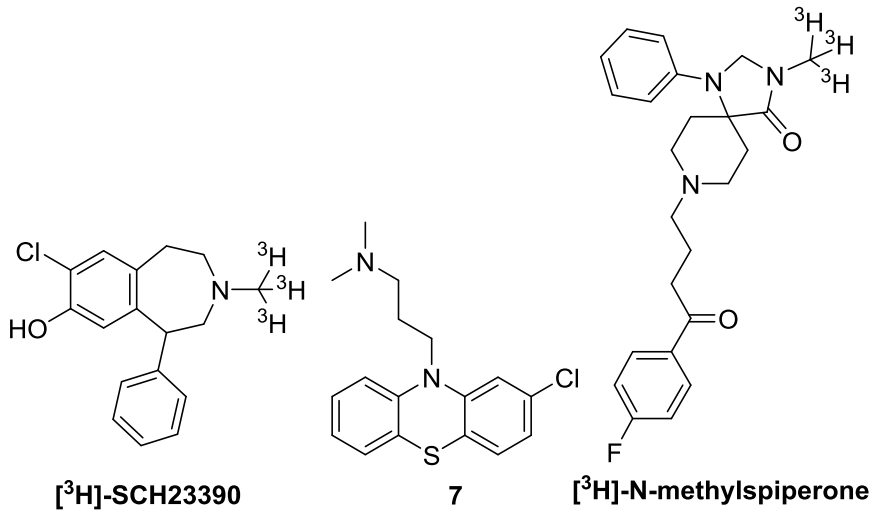

Figure 3.7.6. Structures of radiolabelled D_1 antagonist **[^{3}H]-SCH23390** and D_2 antagonists **[^{3}H]-*N*-methylspiperone** and **7**.

Fortunately, none of the compounds screened showed affinity for the D_2 or D_5 receptors and only two compounds, **91** and **22** (Fig. 3.7.7), displayed affinity for the D_4 receptor.

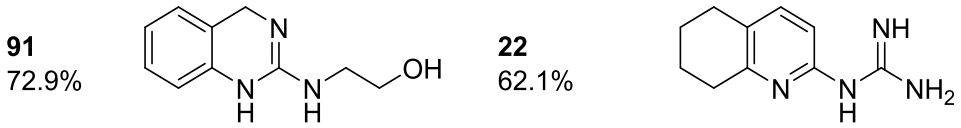

Figure 3.7.7. Structure and % inhibition of binding of **[^{3}H]-*N*-mehtylspiperone** of **91** and **22** at the D4 receptor.

Subsequently, **91** and **22** were analysed in the secondary assay which utilized the antipsychotic chlorpromazine (potent D_2 antagonist) as the reference ligand.[90] The measured binding affinities showed **22** displayed a low affinity (K_i = 2042 nM) compared to the very high affinity of **91** (K_i = 88 nM).

Compound **91** also exhibited affinity for the D_3 receptor (83% inhibition in the primary assay), which led to the secondary assay which was repeated twice giving two different K_i values (683 nM and 431 nM). This led to an average K_i value of 557 nM being reported. Compound **22**, which displayed poor affinity for the D_4 receptor (K_i = 2042 nM), showed affinity at the D_1 receptor with 58.3% inhibition of **[^{3}H]-SCH23390** binding in the primary assay. Thus, a secondary assay was conducted for **22** using **[^{3}H]-SCH23390** as the 'hot' ligand and (+)-butaclamol (Fig. 3.7.8), a dopamine receptor antagonist originally designed as a typical antipsychotic, as the reference ligand. The results of the competition binding assay indicated that **22** has a moderate affinity (K_i = 968 nM) for the D_1 receptor.

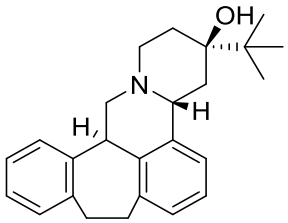

Figure 3.7.8. Structure of dopamine receptor antagonist (+)-butaclamol.

The results so far are encouraging as many of the compounds tested are devoid of affinity at dopaminergic receptors and, if any of these compounds is to be employed as an adjunctive treatment for schizophrenia, they must be compatible with conventional antipsychotic drugs.[116,205] Therefore, in order to avoid potentially detrimental drug-drug interactions these ligands should be devoid of affinity for the D_2 receptor, the primary target of mainstream antipsychotic drugs.[206]

To summarise the results so far, the antagonism enhancing effects of 1,3-disubstituted guanidines exemplified by **39** appears to be an unsuitable strategy to favour subtype selective ligands due to the indiscriminate binding of this compound to multiple targets including all three of the major monoamine transporters. Similarly, compound **91** does not represent a promising candidate for developing a highly selective ligand due to the wide range of receptors to which it binds. In spite of that, **91** may prove to be a unique starting point for the development of multi-target antidepressant drug candidates owing to the significant affinity it displays for some of the most commonly utilized antidepressant targets.

3.7.3 Sigma Receptors (σ_1 and σ_2)

Sigma receptors (σRs) are a relatively novel group of receptors which were originally discovered in the CNS of mammals in 1976 and were considered members of the orphan receptor class as no endogenous ligands were known for them. This changed when dimethyltryptamine was discovered to be an endogenous σR ligand. These non-opioid intracellular receptors are subdivided in two subtypes (σ_1R and σ_2R) and bind to diverse classes of psychotropic drugs such as benzomorphans (e.g. SKF-10047), pentazocine, cocaine, methamphetamine and methylenedioxymethamphetamine (MDMA) shown in Fig. 3.7.9.[207] Both σ_1R and σ_2R are extensively expressed within the CNS as well as many peripheral tissues. [208]

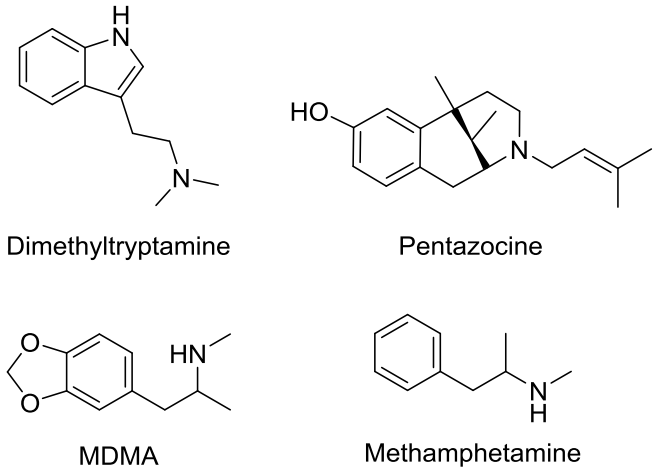

Figure 3.7.9 Structures of psychotropic σR ligands dimethyltryptamine, pentazocine, MDMA and methamphetamine.

It has been shown that σ_1Rs regulate a number of neurotransmitter systems including the glutamatergic, dopaminergic, serotonergic, noradrenergic and cholinergic systems.[207] The endogenous neurotransmitters from these systems interact with σ_1R what explains their role in the pathophysiology of mood and anxiety disorders (MDD), schizophrenia and dementia associated with Alzheimers disease. Hence, ligands which exhibit high affinity for σ_1R could be potential therapeutic agents for several neuropsychiatric disorders.[208] Accordingly, the series of compounds submitted to the PDSP were screened for affinity at both the σ_1R and σ_2R.

3.7.3.1 Sigma-1 Receptors (σ_1Rs)

The results obtained for the σ_1R assays which utilized the radiolabelled synthetic opioid **[^{3}H]-(+)-pentazocine** (Fig. 3.7.10) as the 'hot' ligand and the typical antipsychotic drug haloperidol (**9**) as the reference ligand indicate that compounds **91**, **39**, **22**, **23**, **64**, **66**, **36**, **67**, **69** and **63** bind to the σ_1R in the primary assay (81.1%, 80.7%, 87.1%, 84.4%, 80.8%, 74.3%, 54.7%, 89.3%, 76.2% and 69.8%, respectively).

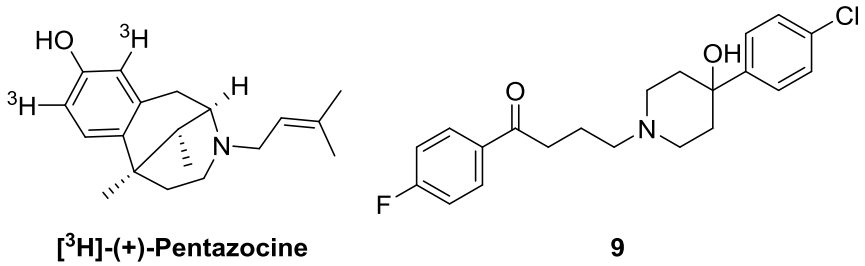

Figure 3.7.10. Structures of σ_1R ligands; radiolabelled **[^{3}H]-(+)-Pentazocine** and **9**.

Structural comparison of the compounds that exhibit the highest σ_1R affinity suggests that SAR may be derived for this class of compounds. In particular, comparison of the group of 4-aminophenyl substituted guanidines and 2-aminoimidazolines (**64**, **66**, **36**, **67**, **69** and **63**) reveals a trend (Fig. 3.7.11). Firstly, comparison of **68** (K_i > 10,000 nM) and **36** (K_i = 1029 nM) suggests that a tertiary amine alkyl substituted (-NMe_2) in *para* position enhances affinity for the σ_1R relative to a secondary amine (-NHMe).

This trend is supported further by the greatly enhanced affinity of the *N,N'*-diethyl-substituted derivative **69** (K_i = 163 nM). Once again, compounds **91** and **39** exhibited good affinity for the σ_1R (269 nM and 225 nM, respectively) providing additional evidence for the indiscriminate binding exhibited by these ligands.

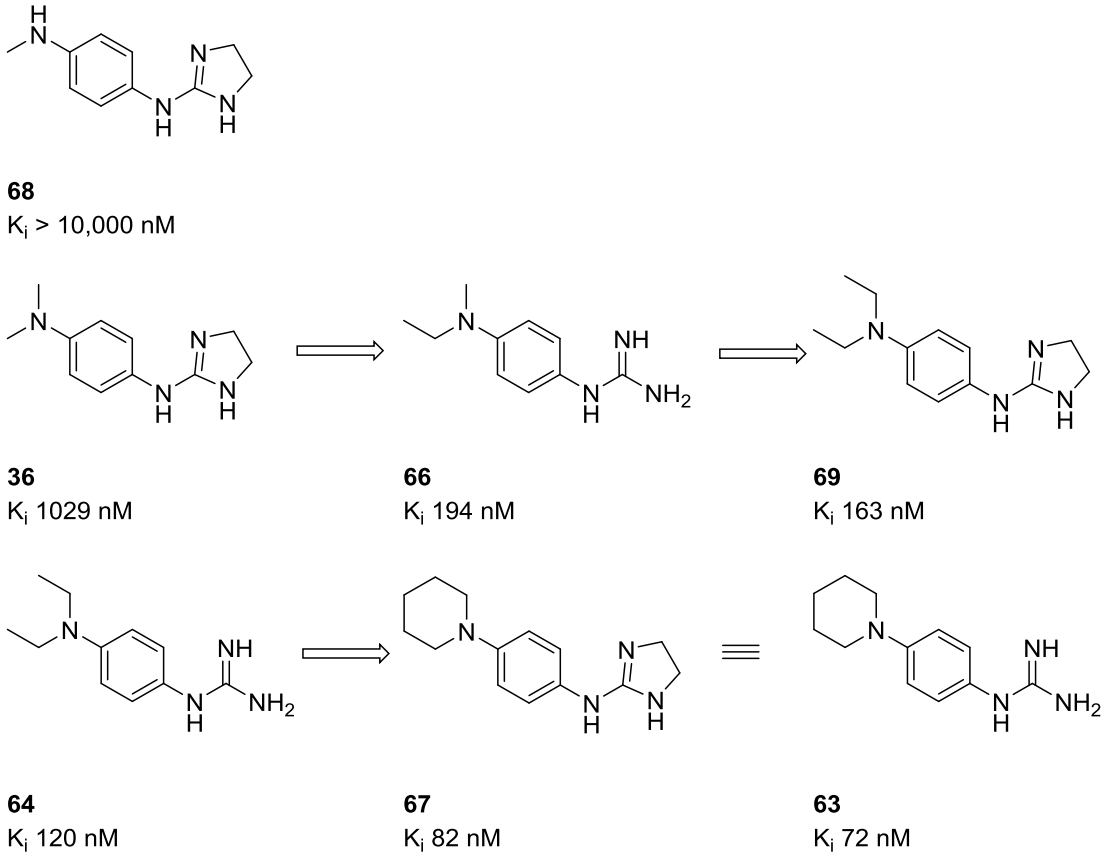

Figure: 3.7.11. Structure-affinity relationships identified within the screening series for σ_1R.

Furthermore, it appears that increasing the steric bulk of the alkyl substituents on the *para*-amino group of this series promotes increased affinity to the σ_1R (1-piperidyl > *N,N'*-diethyl > *N,N'*-dimethyl). Comparison of the σ_1R affinity for related guanidines and 2-aminoimidazoline analogues (i.e. **69** vs. **64** and **67** vs. **63**) indicates that the arylguanidine derivatives display 10-40 nM lower affinity values than their aryl-2-aminoimidazoline counterparts. Overall, these results suggest that increasing the steric bulk of the tertiary amine in the *para* position of this series of compounds enhances σ_1R affinity. Interestingly, one of the highest affinity ligands, **67,** was also found to exhibit affinity for the σ_2R (section 4.7.3.2) whilst its guanidine analogue, **63**, as well as any of the other σ_1R ligands, did not display affinity for the σ_2R. Both 2-amino-5,6,7,8-tetrahydroquinoline derivatives **23** and **22** showed good affinity for the σ_1R (K_i =179 nM and 266 nM). However, **22** (also showed affinity for the σ_2R (section 3.7.3.2), while its 2-aminoimidazoline counterpart **23** did not. The apparent σ_1R selectivity within this series is a unique finding and requires further investigation to determine the activity that these ligands exhibit upon σ_1R engagement.

3.7.3.2. Sigma-2 Receptors (σ_2Rs)

Four ligands (compounds **91**, **67**, **68** and **22**) were found to bind to the σ_2R and the results obtained for the primary assays were as shown below in Fig. 3.7.12.

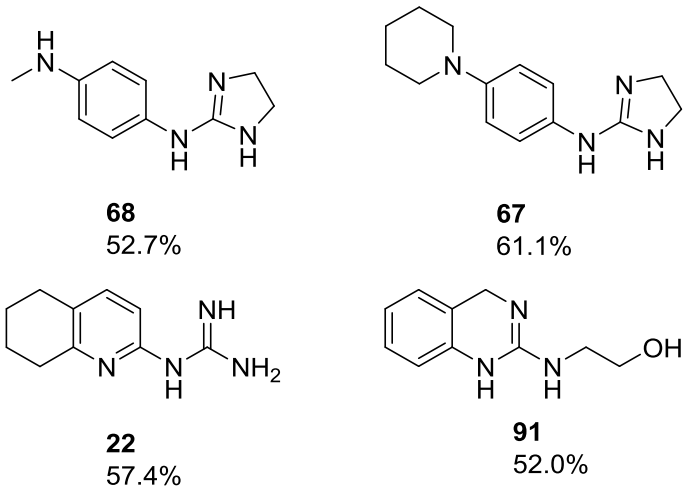

Figure: 3.7.12. Structures of ligands with affinity for the σ_2R.

The σ_2R affinity values for these ligands were then obtained in the secondary assay which utilized the radiolabelled nonselective σR agonist ditolylguanidine (**[^{3}H]-DTG)** as the 'hot' ligand and haloperidol as the reference ligand (Fig. 3.7.13).

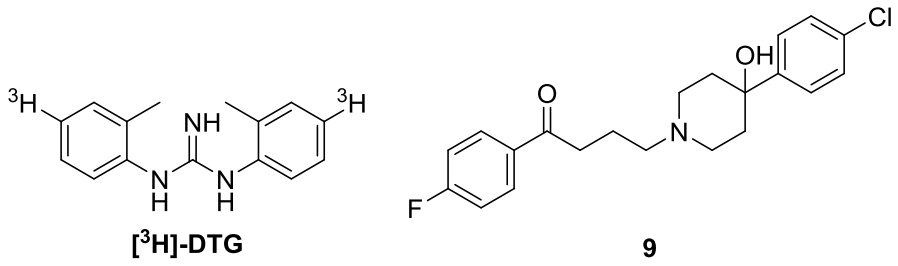

Figure: 3.7.13. Structures of σ_2R ligands; radiolabelled **[^{3}H]-DGT** and **9**.

Notably, only one of these four ligands (**68**) showed selective affinity for the σ_2R (K_i = 269 nM) versus σ_1R. The other three ligands did not exhibit selectivity among the two σR subtypes; however **67** and **22** did show higher affinity for the σ_1R (K_i 84 nM and 266 nM, respectively) than for the σ_2R (K_i 688 nM and 547 nM, respectively). Only **91** exhibited a slightly higher affinity for the σ_2R than for the σ_1R (K_i 178 nM vs. 269 nM).

3.7.4. Histamine receptors

The chosen compounds were screened at two different histamine receptors, H2 (primary target for the treatment of peptic ulcers) and H3 (presynaptic autoreceptors which inhibit histamine synthesis and release in the CNS), both of which are GPCRs.[209] These receptors are differentially expressed throughout the brain, including the PFC and NAc, where they have been implicated in the regulation of neurotransmission, facilitation of short term memory and immunomodulatory functions.[39,210] Alkyl- and aryl-guanidines and 2-aminoimidazolines feature in a number of different histamine ligands particularly in histamine H2 antagonists.[211]

N^{α}-guanylhistamine was one of the first H2 partial antagonists to be discovered which inspired the design and refinement of numerous guanidine containing H2 antagonists.[209,212,213] The evidence which implicated histaminergic neurons in neuropsychiatric diseases such as schizophrenia remains largely indirect; however, changes in histamine neuron activity in response to neuroleptics and the antipsychotic-like properties of H3 receptor antagonists/inverse agonists provide additional support for a role of histaminergic neurons in schizophrenia.[214]

3.7.4.1. Histamine H2 receptor

Nine of the ligands in the series displayed affinity for the H2 receptor in the secondary competition binding assays using H2-selective antagonist **[^{125}I]-iodoaminopotentidine** as the 'hot' ligand and the atypical antipsychotic asenapine as the reference ligand (Fig. 3.7.14).

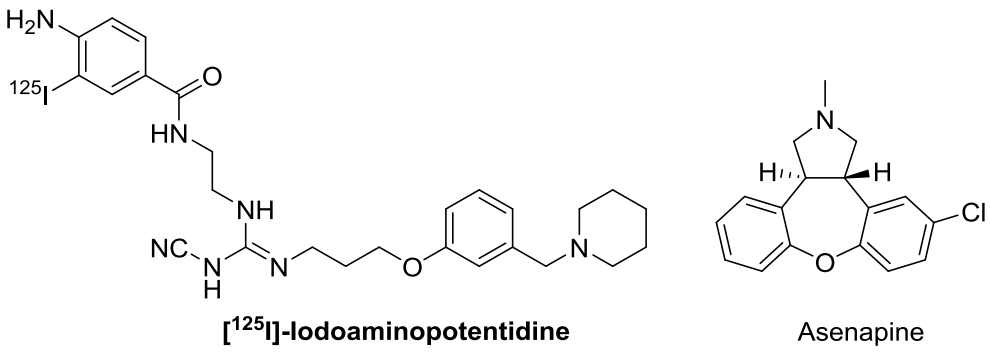

Figure 3.7.14. Structures of radiolabelled histamine H2-selective antagonist **[^{125}I]-iodoaminopotentidine** and asenapine as a reference ligand.

Only three of these nine ligands (compounds **22**, **23** and **91**) bind to the histamine H2 receptor with significant affinity (K_i = 80 nM, 202 nM and 58 nM, respectively) whereas the other ligands had relatively poor affinity (K_i <1000 nM). Analysis of the affinity values of related analogues starts to reveal the emergence of two trends. Firstly, comparison of **22** and **23** suggests that pyridinoguanidines may display better affinity than their 2-aminoimidazoline counterparts (Fig. 3.7.15). Moreover, comparison of **23** and **89** indicates that alkyl substitution at the 5- and 6-positions of the pyridine ring also enhances H2 receptor affinity.

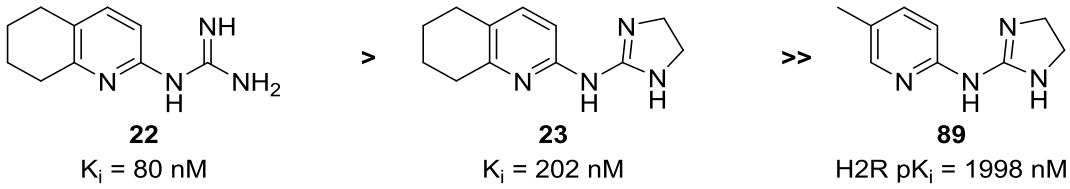

Figure 3.7.15. Trend in H2 receptor affinity between **22**, **23** and **89**.

A second trend can be observed for the aryl guanidine H2 receptor ligands (**64**, **66** and **67**), in which increasing the steric bulk and lipophilicity of the *para*-amino substituent serves to improve H2 receptor affinity (K_i = 2982 nM, 5773 nM and 7497 nM, respectively), albeit with relatively low affinity overall (Fig. 3.7.16).

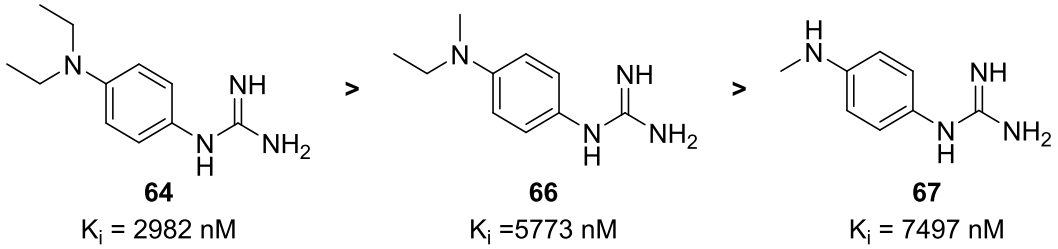

Figure 3.7.16. Trend in H2 receptor affinity for arylguanidine analogues **64**, **66** and **67**.

3.7.4.2. Histamine H3 receptor

Only **63** and **64** displayed affinity for the H3 receptor in competition binding assays using H3 receptor selective agonist **[^{3}H]-*N*-methylhistamine** as the 'hot' ligand and histamine as the reference ligand (K_i = 328 nM and 1380 nM, respectively). Structural comparison of these ligands shows high structural similarity; however, **64** displayed affinity both histamine H2 and H3 receptors (K_i = 1380 nM and 2982 nM, respectively) and **63** only displayed affinity for the H3 receptor (K_i = 328 nM). This would suggest that the subtle structural difference can favour preferential binding.

3.7.5. Serotonergic (5-HT) Receptors

The following three 5-HT receptor families were chosen for screening: 5-HT_1 receptors (5-HT_{1A}, 5-HT_{1B}, 5-HT_{1D}, and 5-HT_{1D} subtypes), 5-HT_2 receptors (5-HT_{2A}, 5-HT_{2B}, and 5-HT_{2C} subtypes) and the 5-HT_3 receptor. These receptors were selected as they all have been implicated in neurological and psychiatric disorders like schizophrenia and MDD as well as being involved in cognitive processes and regulation of neurotransmission.[38,215] These receptors are targets of many antidepressant and antipsychotic drugs which enhance their efficacy and atypicality whilst reducing side effects through greater therapeutic selectivity.[216,217]

The only non-GPCR members of the 5-HT receptor family are the 5-HT_3 receptors, which are ligand gated ion channels thought to play a role in both cognition and anxiety with a number of aryl guanidines reported to act as high affinity ligands.[218–220] A number of different radioligands for each of the subtypes of the chosen 5-HT receptors are utilized in the secondary competition binding assays (see structures in Fig. 3.7.17).[221]

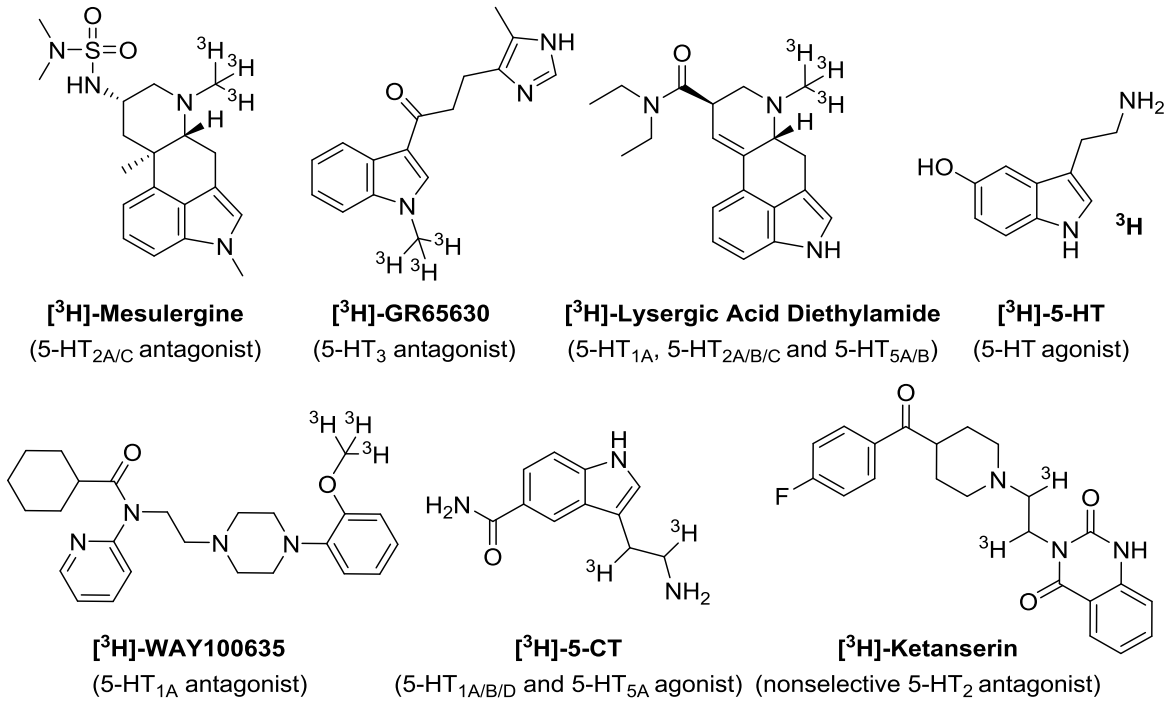

Figure 3.7.17. Structures of radiolabelled 5-HT receptor ligands **[^{3}H]-mesulergine**, **[^{3}H]-GR65630**, **[^{3}H]-5-CT**, **[^{3}H]-5-HT**, **[^{3}H]-WAY100635**, **[^{3}H]-LSD**, and **[^{3}H]-ketanserin** used in the secondary assays.

3.7.5.1. 5-HT$_1$ receptors

The series of ligands were screened against all 5-HT$_1$ receptor subtypes (5-HT$_{1A}$, 5-HT$_{1B}$, 5-HT$_{1D}$, and 5-HT$_{1E}$) and some of the compounds displayed selective affinity for one or more of the 5-HT$_1$ receptor subtypes with nine of them displaying good affinity for the 5-HT$_{1A}$ subtype. Each subtype will be discussed in turn detailing the ligands which display affinity along with the associated radioligand and reference ligand required for each assay.

3.7.5.1.1. 5-HT$_{1A}$ receptors

The 5-HT$_{1A}$ receptor is the most widespread 5-HT$_1$ receptor subtype in the human brain and has recently been shown to control the nigrostriatal release of DA in the pharmacotherapy of schizophrenia and Parkinson's disease which provides additional support for its relevance in this study.[216] Nine ligands (**34**, **36**, **39**, **63b**, **64**, **68**, **69** and **91**, Fig. 3.7.18) exhibited affinity for the 5-HT$_{1A}$ receptor in the primary assay (> 50%) and were subsequently analysed in the secondary assay to measure the affinity of each ligand for the 5-HT$_{1A}$.

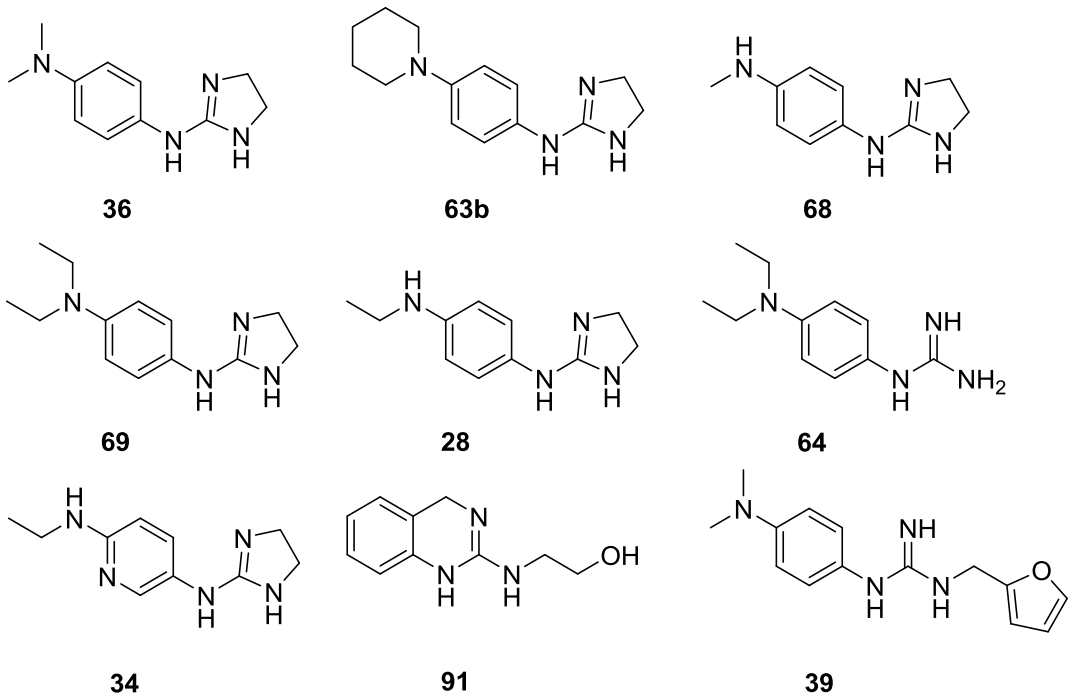

Figure: 3.7.18. Structures of ligands with affinity for the 5-HT$_{1A}$ receptor.

The radiolabelled 5-HT$_{1A}$ antagonist **[^{3}H]-WAY100635** was employed as the 'hot' ligand and the 5-HT$_{1A}$ agonist OH-DPAT was the reference ligand. Both **91** and **39**

exhibited binding at the 5-HT_{1A} receptor (K_i = 160 nM and 2144 nM, respectively), adding another target to their expanding polypharmacological profiles.

Comparison of the affinity values obtained for the 2-aminoimidazoline members of the series uncovers an interesting trend (Fig. 3.7.19). Substitution in the phenyl group with a *di*-alkyl amino system appears to enhance affinity (**36** K_i = 371 nM vs. **69** K_i = 103 nM, respectively) in comparison with the *mono*-alkyl amino analogues (**68** K_i = 969 nM vs. **28** K_i = 464 nM, respectively), which exhibit a 3-4 fold lower affinity.

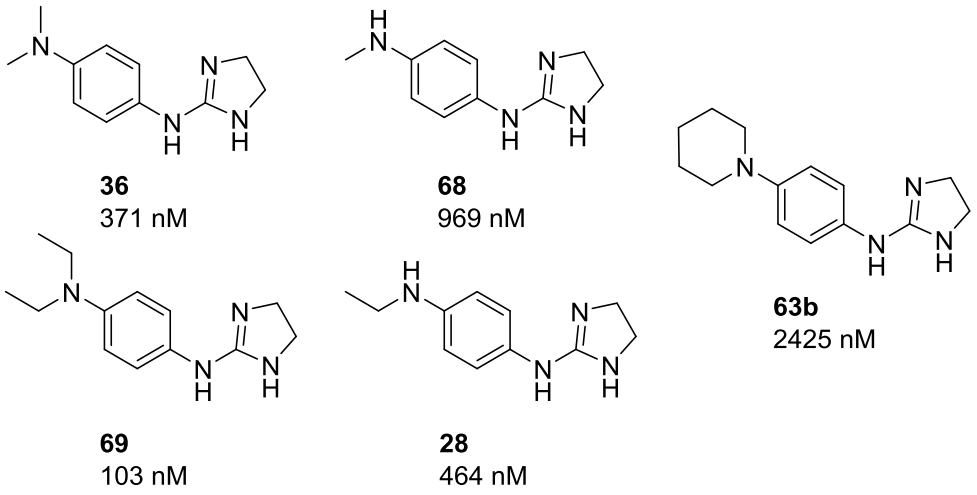

Figure 3.7.19. 5-HT_{1A} receptor affinity (K_i) trends for the 2-aminoimidazoline ligands.

Flexibility of the alkyl substituents in the amino group seems to be a crucial factor as the constrained cyclic piperidin-1-yl substituent in **63b** (K_i = 2425 nM) causes a drastic reduction in 5-HT_{1A} affinity. Similarly, replacement of the phenyl ring in **28** by a pyridine to give **34** also reduces the 5-HT_{1A} affinity (K_i = 772 nM). Furthermore, only one of the aryl guanidines within the series displayed 5-HT_{1A} affinity (**64**, K_i = 822 nM).

All of the ligands presented in Fig. 3.7.19 (with the exception of **36**) have been previously shown to act as α_2-AR agonists.[142] The activity of these ligands at the 5-HT_{1A} has not been determined in the current study; however, if these ligands also display agonistic activity at the 5-HT_{1A}, they would have beneficial applications in treating pain as both of these receptors are known to be involved in central nociceptive mechanisms.

A recent study by Mannelli *et al.*[215] describes a series of 2-substituted imidazoline derivatives which acted as dual 5-HT_{1A}/α_2-AR agonists and the synergistic stimulation of these receptors was shown to relieve neuropathic pain in a rat model. The subtype selective α_2-AR affinity of these ligands will be discussed in Section 3.7.6. Additionally, Nicolas *et al.* discovered that a number of α_2-AR ligands, such as clonidine, yohimbine and (±)-idazoxan, containing 2-substituted imidazolines exhibit marked affinity and agonist activity at the 5-HT_{1A} receptors.[222]

3.7.5.1.2. 5-HT_{1B} and 5-HT_{1D} receptors

Only **22** exhibited affinity for the 5-HT_{1B} and was subject to secondary assay to measure 5-HT_{1B} affinity utilizes radiolabelled **[^{3}H]-5-CT** as the 'hot' ligand and ergotamine as the reference ligand. These 'hot' and reference ligands are also used to measure the affinity at the 5-HT_{1D} receptor. There were only two other ligands within the series, **91** and **69**, which exhibited affinity for the 5-HT_{1D} receptor. The 5-HT_{1B} receptor affinity for **22** gave a K_i value of 792 nM and measurement 5-HT_{1D} receptor affinities for **91** and **69** gave K_i values of 1341 nM and 545 nM, respectively.

3.7.5.1.3. 5-HT_{1E} receptors

Only **69** was found to bind to the 5-HT_{1E} receptor. In this case, 5-HT was utilized as both the radioligand and reference ligand for secondary binding assay which showed **69** exhibited a K_i value of 751 nM at the 5-HT_{1E} receptor.

Compound **69** was the only ligand which exhibited affinity for three of the four 5-HT_1 receptor subtypes displaying affinity for the 5-HT_{1A}, 5-HT_{1D} and 5-HT_{1E} receptors (103 nM, 545 nM and 751 nM, respectively), whilst **91** bound to both the 5-HT_{1A} and 5-HT_{1D} subtypes (160 nM and 1341 nM, respectively).

3.7.5.2. 5-HT_2 Receptors

The 5-HT_2 receptor family is composed of three subtypes (5-HT_{2A}, 5-HT_{2B}, and 5-HT_{2C}) which are all GPCRs that couple to the G_q activating phospholipase C to trigger second messenger signalling pathways.

There is 75% homology in the transmembrane domain of the three 5-HT_2 receptor subtypes which makes the development of 5-HT2 subtype-specific ligands a complicated and delicate process.[223] Each 5-HT_2 receptor subtype has distinct regional distribution within the brain and it has been proposed that this could allow each subtype to mediate specific physiological functions.[224]

Many drug discovery programs targeting 5-HT_2 receptors are focused on different psychiatric disorders (5-HT_{2A} antagonists), sleep disorders (5-HT_{2A} antagonists), cluster headaches (5-HT_2 agonists), anxiety (5-$HT_{2B/2C}$ antagonists), obesity and addictive behaviours (5-HT_{2C} agonists).[225–227] A number of 5-HT_2 receptor modulators have shown potential utility as antipsychotic and antidepressant medications.[228–231]

There are many of non-selective 5-HT_2 receptor antagonists, such as ritanserin and mesulergine, which have been shown to block 5-HT_2 receptor-mediated effects. A range of atypical antipsychotics including clozapine (**11**) and aripiprazole (**13**) have also been reported to exhibit relatively high affinity and antagonist activity at the three 5-HT_2 receptor subtypes. In particular, **13** has been identified to display a higher antagonist affinity (EC_{50} = 11 nM) for the 5-HT_{2B} receptor subtype than at the 5-HT_{2A} or 5-HT_{2C} subtypes.[232]

3.7.5.2.1. 5-HT_{2A} Receptors

There were only three ligands in the series studied that exhibited affinity for the 5-HT_{2A} receptor: **91**, **39** and **22**. These three ligands progressed to the secondary assay to measure their affinity for the 5-HT_{2A} receptor using **[^{3}H]-ketanserin** as the 'hot' ligand and the atypical antipsychotic **11** as the reference ligand. The competition binding assay for **39** was conducted using the nonselective 5-HT_2 antagonist **[^{3}H]-LSD**. The only ligand which displayed reasonable affinity for the 5-HT_{2A} receptor was **22** (Ki = 960 nM) whereas **39** and **91** displayed poor affinity (K_i = 1146 nM and 1777 nM, respectively).

3.7.5.2.2. 5-HT_{2B} Receptors

The 5-HT_{2B} receptor subtype has gained much attention recently as a therapeutic target. These receptors play a crucial role in the long term behavioural and neurogenic effects of SSRIs such as **6**.[233]

Further studies have shown that these receptors are required for the therapeutic actions of SSRIs, many of which act as 5-HT_{2B} agonists.[231] In addition, the activation of these receptors and the inhibition of SERT have recently been recognised to play a significant role in the pathogenesis of 5-HT cardiac issues, such as valvulopathy, which has raised concerns about the off target effects of 5-HT_{2B} receptor engagement.[234] Furthermore, the crystal structure of the 5-HT_{2B} receptor in complex with LSD has been resolved by Roth *et al.* revealing a wealth of structural insight into the ligand-receptor interactions and conformational rearrangements induced upon binding of LSD to the orthosteric site.[235]

All ligands within the series showed affinity in the 5-HT_{2B} receptor primary assay (with the exception of **90**, **88**, **67** and **68**). A highly unexpected result was obtained when these ligands progressed to the secondary assay to measure their 5-HT_{2B} affinity.

The radiolabelled 5-HT_2 antagonist **[^{3}H]-LSD** was employed as the 'hot' ligand and the 5-$HT_{2B/C}$ agonist SB206553 was the reference ligand used in the secondary assay. The most striking discovery from screening at the 5-HT_{2B} receptor was that three members of the series (**22**, **23** and **91**) displayed affinity of <100 nM, with two of them (**22** and **23**) exhibiting better 5-HT_{2B} receptor affinity than the reference ligand SB206553 which has a K_i value of 54 nM (Fig. 3.7.20).

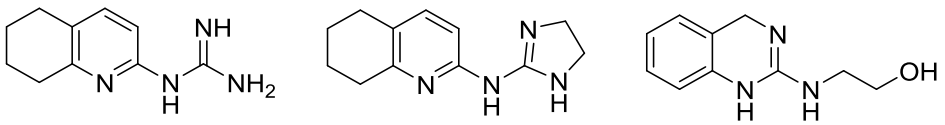

22
33.6 nM

23
40 nM

91
76 nM

Figure 3.7.20. Structures and 5-HT_{2B} receptor affinity of **22**, **23** and **91**.

These unexpected results warrant further investigation and subsequent comparison with α_2–AR results obtained may require these ligands to be reclassified as 5-HT_2 ligands.

3.7.5.2.3. 5-HT_{2C} Receptors

The 5-HT_{2C} receptors have recently been identified as promising targets for the treatment of neuropsychiatric disorders like schizophrenia with the potential for fewer side effects and enhanced efficacy compared with antipsychotic drugs.[236]

The agonists of these receptors have also been shown to modify schizophrenia-like behaviours in mice whereas inhibition of 5-HT_{2A} and 5-HT_{2C} receptors has also shown potential to improve cognitive deficits and working memory in patients treated with current antipschotic drugs.[217,237] In the assays performed for this subtype, the radiolabelled 5-HT_2 antagonist **[^{3}H]-mesulergine** was employed as the 'hot' ligand and the 5-HT_2 antagonist ritanserin was the reference ligand used in the competition binding assay.

A similar pattern of affinity discovered during the 5-HT_{2B} receptor screening was observed for the 5-HT_{2C} receptor assays. Both **22** and **23** displayed significant affinity for the 5-HT_{2C} receptor (<100 nM), whilst five of the other ligands (**34**, **64**, **66**, **67** and **91**) also displayed considerable affinity between 100 and 250 nM (Fig. 3.7.21).

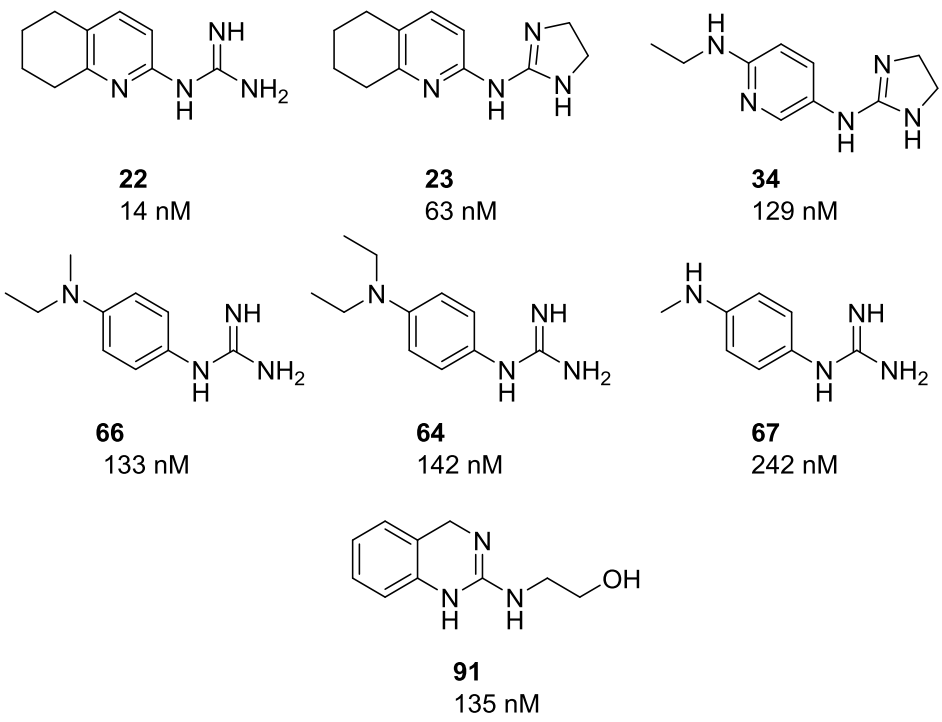

Figure 3.7.21. Structures of 5-HT_{2C} receptor ligands with affinity < 250 nM.

3.7.5.3. 5-HT3 Receptors

None of the compounds in this series exhibited affinity for the 5-HT_3 receptor in the primary assay (% inhibition) using the radiolabelled selective 5-HT_3 antagonist **[^{3}H]-GR65630** as the competitive ligand. Therefore, none of these ligands required analysis in the secondary assay.

3.7.5.4. Summary of the major results from the 5-HT receptors screening

The most striking result found in the affinity screening at the 5-HT_1 and 5-HT_2 receptors was the unprecedented affinity of the guanidine **22** for all three 5-HT_2 receptor subtypes (5-HT_{2A} K_i = 960 nM, 5-HT_{2B} receptor K_i = 33.6 nM and 5-HT_{2C} receptor K_i = 14 nM). The 2-aminoimidazoline analogue of **22**, compound **23**, also exhibited affinity of less than 100 nM for both the 5-HT_{2B} and 5-HT_{2C} receptors (5-HT_{2B} receptor K_i = 40 nM and 5-HT_{2C} receptor K_i = 63 nM).

Another interesting result is the promiscuity of binding exhibited by **91** which was expanded further from the neuroreceptors studied in previous sections as it also displayed affinity for both the 5-HT_{1A} and 5-HT_{1D} subtypes (K_i = 160 nM and 1341 nM, respectively) and all three 5-HT_2 receptor subtypes (5-HT_{2A} K_i = 1777 nM, 5-HT_{2B} K_i = 76 nM and 5-HT_{2C} K_i = 135 nM).

3.7.6. Adrenergic Receptors (ARs)

The primary objective of screening at the different AR subtypes is to determine whether any of the ligands present with preferential binding to the α_{2C}- and α_{2A}-AR subtype. The focus has been placed on these two α_2–AR subtypes as they are the most pertinent and abundant targets in the CNS for this work, as such the affinity for the α_{2B}-AR will not be measured for this series of compounds. The ligands will however be examined for affinity at the three α_1–AR subtypes and the β-ARs; since the focus of this screening process is to identify ligands which can discriminate and selectively engage specific α_2–AR subtypes, any affinity for other adrenergic receptors would be a disadvantage and may disfavour a ligand from progression.

3.7.6.1. α_1– Adrenoceptors

The majority of compounds in the series did not show any affinity for the three α_1–AR subtypes (α_{1A}, α_{1B} and α_{1D}) except **39**, **64**, **66**, **68** and **91**. Prazosin was utilized as both the radioligand and reference ligand for secondary binding assays to measure affinity for the three α_1–AR subtypes. Compounds **39** and **91** showed affinity for the α_{1A}-AR (K_i = 847 nM and 298 nM, respectively) and α_{1B}-AR (K_i = 1060 nM and 1775 nM, respectively).

The other ligands which exhibited relatively poor affinity for the α_{1A}-AR were **64**, **66** and **68** (K_i = 1128 nM, 1981 nM and 2653 nM, respectively). Compound **91** was the only member of the series to exhibit affinity for the α_{1D}–AR (K_i = 102 nM).

3.7.6.2. α_2–Adrenoceptors

All of the ligands in the screening series have originally been developed as potential antidepressants and have been shown to display affinity for α_2–ARs in human PFC tissue by means of competition binding assays using **[^{3}H]-RX821002** as outlined in section 1.7.[132,142,196] Despite being the most physiologically relevant assay environment for these ligands, human PFC is highly heterogeneous which does not facilitate determination of subtype specificity using **[^{3}H]-RX821002** as it is relatively non-selective between the three α_2–AR subtypes.[238]

Therefore, examination of preferential binding at a given α_2–AR subtype requires a tissue which has been transfected with the corresponding gene and therefore stably expresses only a single recombinant human α_2–ARs subtype. As such, this series of ligands has been screened at the PDSP for affinity using recombinant cell lines which selectively express either the α_{2A}–AR or α_{2C}–AR subtype. Then, the radiolabelled α_2–AR antagonist **[^{3}H]-Rauwolscine** was utilised as the 'hot' ligand and the nonselective α_2–AR partial agonist oxymetazoline was used as the reference ligand. **[^{3}H]-Rauwolscine** displays a higher affinity for the α_{2C}-AR subtype than for any of the other subtypes (α_{2C}-AR K_i = 0.6 nM, α_{2A}-AR K_i = 3.5 nM and α_{2B}-AR K_i = 4.6 nM).[239,240]

3.7.6.2.1. α_{2A}–Adrenoceptor subtype

The results obtained from screening at the α_{2A}–AR indicated that all but six ligands in the series exhibit significant affinity for the α_{2A}–AR. These six ligands (compounds **34**, **22**, **65**, **64**, **67** and **36**) became the subset with potential for further development providing that they can exhibit affinity for the α_{2C}–AR subtype (see section 3.7.6.2.2). **91** and **63b** exhibited the highest α_{2A}–AR affinities (K_i = 24 nM and 32 nM, respectively) with **66**, **68**, **69** and **28** also displaying excellent affinity values <100 nM (K_i =63 nM, 55 nM, 48 nM and 50 nM, respectively), whereas the pyridino-2-aminoimidazoline derivatives **23**, **88**, **89** and **90** all exhibited affinities of >200 nM.

Overall, these ligands displayed affinities for the α_{2A}–AR which were similar or slightly higher than the affinity values previously measured in human PFC tissue.[132,142,191] This would suggest that the binding of these ligands to the α_{2A}–AR in human PFC tissue is the dominant factor contributing to the observed affinity measurement during the competition binding assays using **[^{3}H]-RX821002**.

3.7.6.2.2. α_{2C}–ARs subtype

All the compounds in the series except for two (**88** and **63**) display affinity for the α_{2C}–AR subtype including all the compounds that did not display affinity for the α_{2A}–AR (**22**, **34**, **36**, **64**, **65** and **67**). All of the ligands that did not display affinity for the α_{2A}–AR (**34**, **22**, **65**, **64**, **67** and **36**) exhibited affinity for the α_{2C}–AR subtype. Moreover the majority of the ligands which bound to the α_{2A}–AR subtype also displayed affinity for the α_{2C}–AR except for **88** and **63**. The importance of these results will be discussed in greater detail within the context of the overall screening results in section 3.7.6.4.

3.7.6.3. β–Adrenoceptors

Fortunately, none of the ligands in this series displayed affinity for the β_1–AR or the β_3–AR and the only compounds to display affinity for the β_2–AR were **39** and **91** which were subsequently analysed in the secondary assay in which **[^{3}H]-CGP12177** was utilized as the β_2–AR radioligand and the nonselective β–AR agonist alprenolol was reference ligand affording K_i values of 2463 nM and 2264 nM, respectively.

3.7.6.4. Summary of major results exploring adrenergic receptors

Screening for affinity at the chosen ARs has led us to uncover a subset of six ligands (**22**, **34**, **36**, **64**, **65** and **67**) which were shown to bind the α_{2C}-AR but not the α_{2A}-AR subtype (Fig. 3.7.22). These ligands will now be regarded as a collection of *hit* compounds upon which new derivatives will be based on to enhance α_{2C}-AR affinity and antagonist activity.

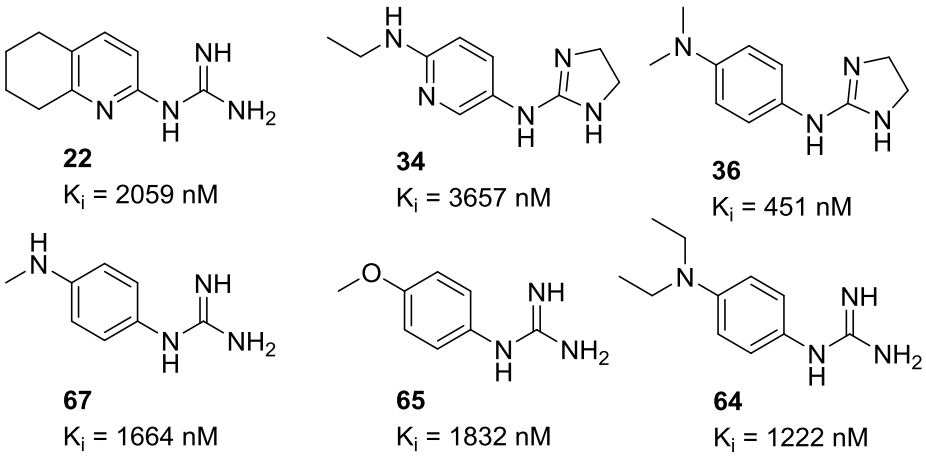

Figure 3.7.22. Structures and affinity values of ligands exhibiting preferential binding to the α_{2C}-AR.

Three of the ligands within this subset (**22**, **34** and **36**), have been previously shown to display antagonist activity[132,142] but displayed relatively low α_{2C}-AR affinity and were shown to exhibit greater affinity at other monoaminergic receptors (5-HT_{2B} / 5-HT_{2C}). However, there is scope to enhance and refine the pharmacological properties of these ligands during the optimization process which will be discussed further in Chapter 4.

Compounds **39** and **91** were the only two ligands to show affinity for the β_2–AR (K_i of 2463 nM and 2264 nM, respectively). These ligands, particularly **91**, also displayed good affinity for the α_{1A}-AR, α_{1B}-AR, α_{2C}-AR and α_{2A}-AR subtypes. These results provide additional evidence of their indiscriminate binding to a wide range of CNS targets and could give an indication of structures to avoid when attempting to design selective ligands.

3.7.6.5. Revising approaches for converting α_2–AR agonists to antagonists

Two approaches have been developed and successfully employed within the Rozas group to enhance α_2–AR antagonist activity of ligands and convert high affinity agonists to antagonists. Firstly, the addition of a substituent to the cationic moiety to form 1,3-disubstituted aryl guanidines led to reduced binding affinity, but also consistently conferred antagonist activity. This approach led to the antagonist **39** (Fig. 3.7.23).

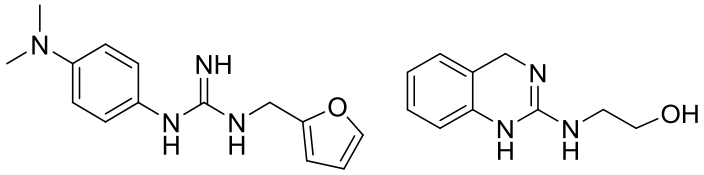

39 Antagonist
pK_i 6.67

91 Antagonist
pK_i 6.26

Figure 3.7.135. Structures of α_2–AR antagonist **39** and 2-amino-1,4-dihydroquinazoline based α_2–AR antagonist **91**.

The second approach to promote antagonism was investigated by Dr. Brendan Kelly who discovered that conformational restriction of the cationic moiety coupled an additional substituent on the exocyclic amino group favoured antagonism, as shown by the a series of substituted 2-amino-1,4-dihydroquinazolines, with **91** (Fig. 3.7.23) displaying the highest affinity.

Both **39** and **91** were found to bind to both the α_{2A}-AR (K_i = 180 nM and 24 nM, respectively) and the α_{2C}–AR with high affinity (K_i = 511 nM and 25 nM, respectively); however, both ligands also bind to α_{1A}-AR (K_i = 847 nM and 298 nM, respectively), α_{1B}-AR (K_i = 1060 nM and 1775 nM, respectively) and β_2-AR (K_i = 2463 nM and 2264 nM respectively). In addition **91** displays high α_{1D}-AR affinity (K_i = 108 nM) as well as good affinity for the dopamine D3 and D4 receptors (K_i = 557 nM and 88 nM respectively).

Moreover, these two compounds also bind to the histamine H2 receptor (1719 nM and 58 nM respectively) and σ_1R (225 nM and 269 nM respectively) with **91** also binding the σ_2R (178 nM). The complex polypharmacology of **39** and **91** is summarised in Fig. 3.7.24.

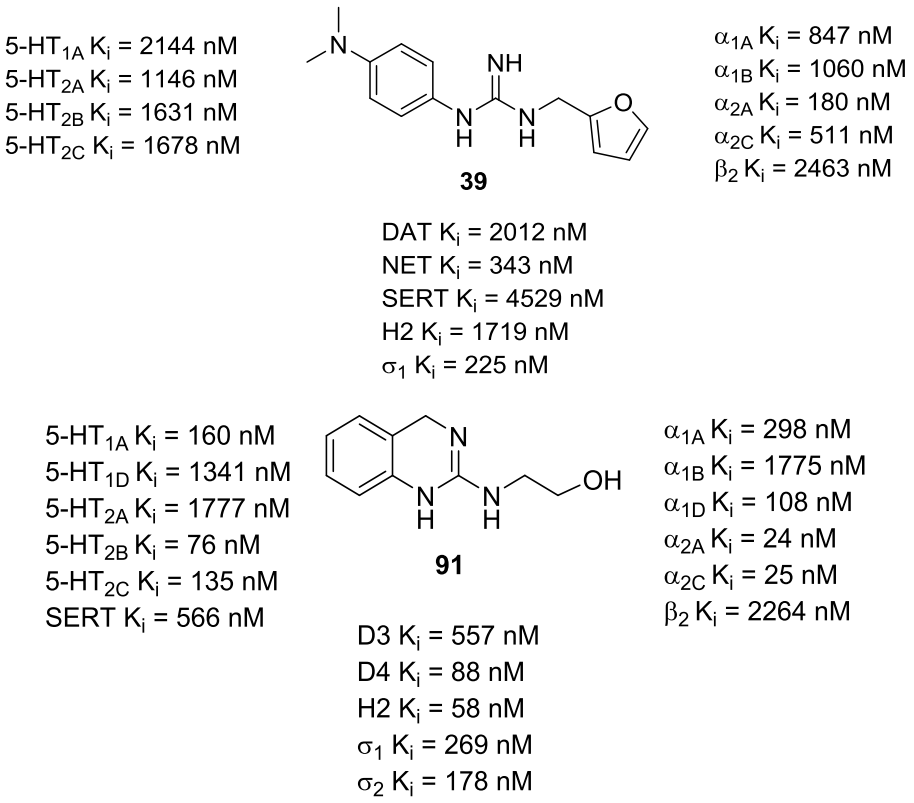

Figure 3.7.24. Complex polypharmacological profile of compounds **39** and **91**.

The complex pharmacology of **91** may stem from the 2-amino-3,4-dihydroquinazoline core. Studies by Dukat *et al.* identified 2-amino-6-chloro-3,4-dihydroquinazoline hydrochloride (**92**), a positional isomer of **93**, as a novel 5-HT$_3$ receptor antagonist.[241] When examined for selectivity, **92** lacked affinity (K_i >10,000 nM) for most of >40 targets including GPCRs, ligand-gated ion channel receptors, transporters; however, **92** displayed affinity for many 5-HT receptors (5-HT$_{1D}$, 5-HT$_{2A}$, 5-HT$_{2B}$, 5-HT$_{2C}$, 5-HT$_{5A}$ and 5-HT$_7$), the three α_2-AR subtypes and low affinity for the σ_1 and σ_1 receptors (Fig. 3.7.25). *In vivo* studies in a preclinical antidepressant model (mouse TST) showed **92** (ED_{50} = 0.23 mg/kg) to be as efficacious as two tricyclic antidepresants (imipramine and desipramine) and the SSRI fluoxetine at commonly employed doses.[242,243]

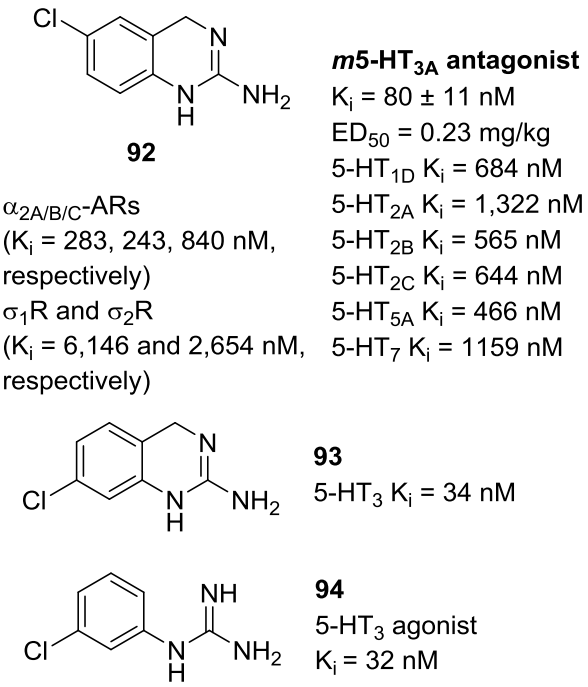

Figure 3.7.25. Structures and associated affinity values for compounds **92**, **93** and **94**.

A related study of cyclic guanidines conducted by Peter *et al.* involved the identification and optimization of a series of 2-amino-1,4-dihydroquinazolines as dual 5-HT_{5A}/5-HT_7 receptor ligands.[244] In general, 4-unsubstituted dihydroquinazolinylamines showed good affinity for 5-HT_{5A}, but extensive SAR studies identified compounds **95** and **96** as potent and 5-HT_{5A}/5-HT_7 selective antagonists with additional optimization leading to enhanced pharmacokinetic (brain penetration) and physicochemical properties (Fig. 3.7.26).[245]

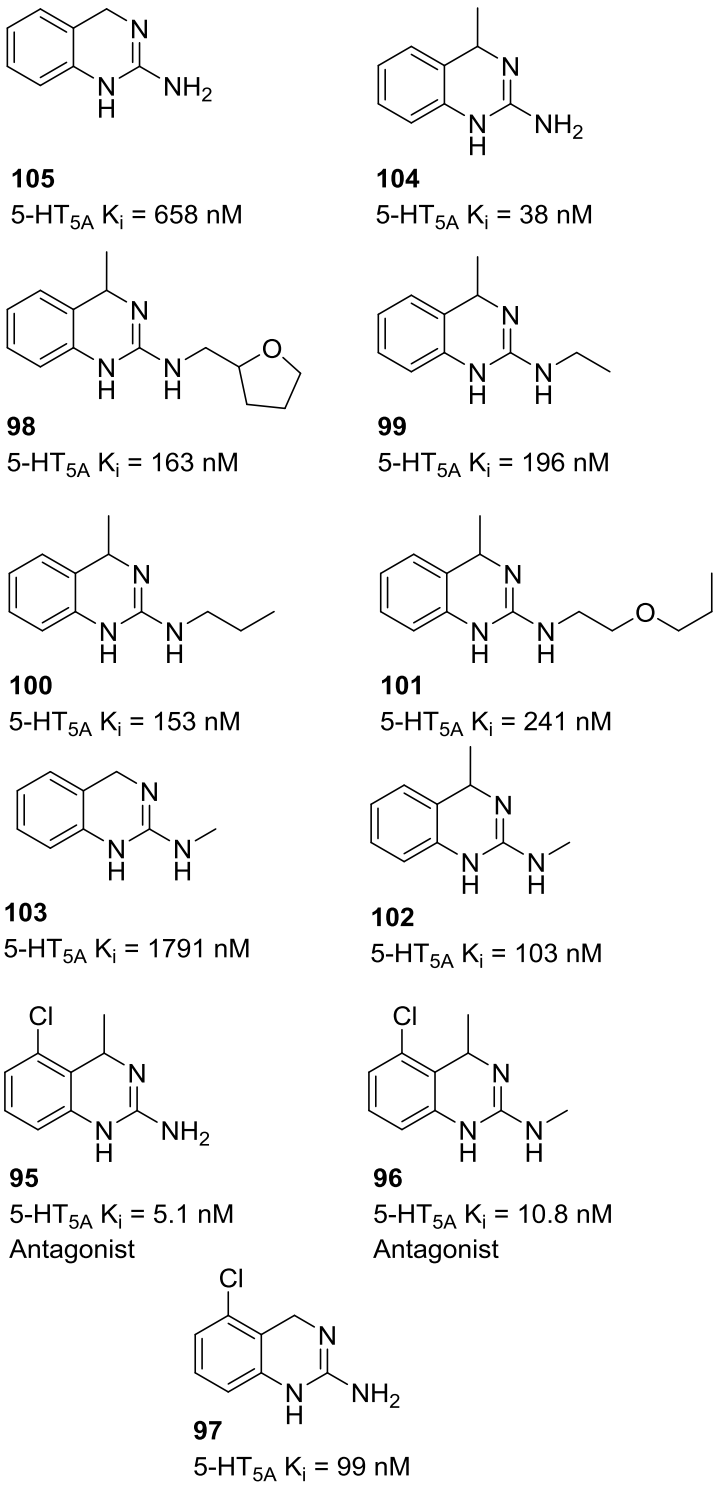

Figure 3.7.26. Structures and associated 5-HT_{5A} affinity values for series of 2-amino-1,4-dihydroquinazolines.

These results, particularly the lack of adrenergic selectivity, have direct negative implications on the utility of **39** and **91** for future development as α_2-AR subtype selective ligands.

Nonetheless, compounds **39** and **91** may be suitable candidates for further investigation and development as novel antidepressants with defined polypharmacology. Further investigation would be required to establish the potential utility of **39** and **91** as muti-target drugs. Overall, the beneficial effects imparted by the 1,3-disubstituted guanidines and 2-amino-1,4-dihydroquinazolines scaffolds in terms of α_2-AR antagonism are outweighed by the indiscriminate binding of multiple receptors and as such further development of these families would not be a suitable strategy when in search of subtype selective ligands.

3.8. Conclusions

The screening process has allowed for the identification of a number of ligands exhibiting unique pharmacological profiles at a variety of previously unexplored targets. These results have also uncovered a collection of affinity trends which exist within groups of structurally related guanidine and 2-aminoimidazoline derivatives.

Careful analysis and consideration of the results obtained led us to choose five *hit* compounds (**22**, **34**, **36**, **65** and **67**) which exhibited unique and desirable pharmacological properties (Fig. 3.8.1). A cross section of these compounds will be used as templates upon which further synthetic development will be based with the aim of refining and improving their pharmacological profiles.

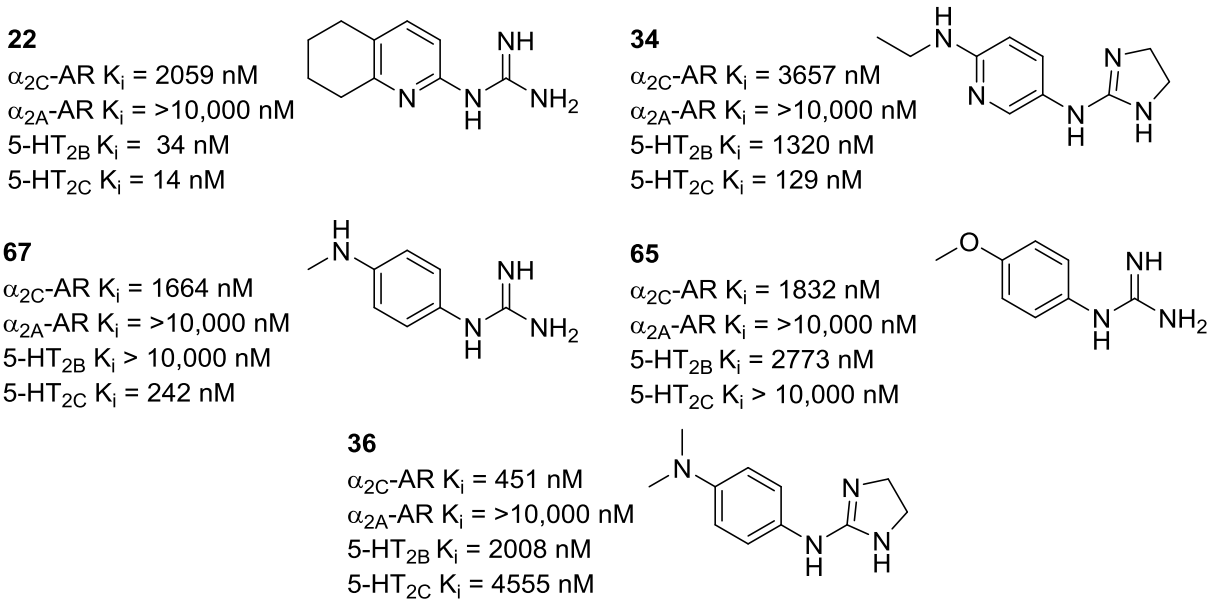

Figure 3.8.1 Structures and associated affinity values of ligands exhibiting preferential binding to the α_{2C}-AR.

The most unprecedented results were those obtained for compounds **22** and **23**. These two ligands which had previously been regarded as α_2–AR antagonists were found to display affinity for a variety of other monoaminergic receptors, most notably 5-HT receptors to which they exhibited stronger binding than α_2–AR. Both of these ligands displayed significantly better affinity for multiple 5-HT receptor subtypes compared to the α_{2A}–AR and α_{2C}–AR adrenoceptor subtypes. Therefore, a reclassification of the primary target for **22** and **23** is needed and they should be more accurately described as 5-HT_{2B}/5-HT_{2C} ligands, with the α_2–AR now considered a secondary target.

The in-depth analysis of α_2-AR engagement will help in the formulation of hypothesis to rationalise the impact of small structural changes on α_2-AR ligand affinity and correlate these with observed activity. The detailed receptor profiles constructed for each of the ligands in this series based on the results of this screening process will be utilized to prioritize and inform the design of future derivatives and facilitate a more focused synthetic effort.

Chapter Four

Design and synthesis of (hetero)aryl cyclic and acyclic guanidine derivatives: Towards preferential α_{2C} -AR engagement

4.1. Introduction

The receptor binding profiles obtained from the screening process have helped to identify five candidates which exhibit preferential binding to the α_{2C}-AR subtype (Fig. 4.1.1). Each of these lead compounds will be examined in turn and a rationale will be proposed for the development of structural analogues based on each template. The aim of this optimization process is to accentuate the α_{2C}-selective binding and antagonist properties of this series of compounds whilst minimizing or modifying each compound off target profile.

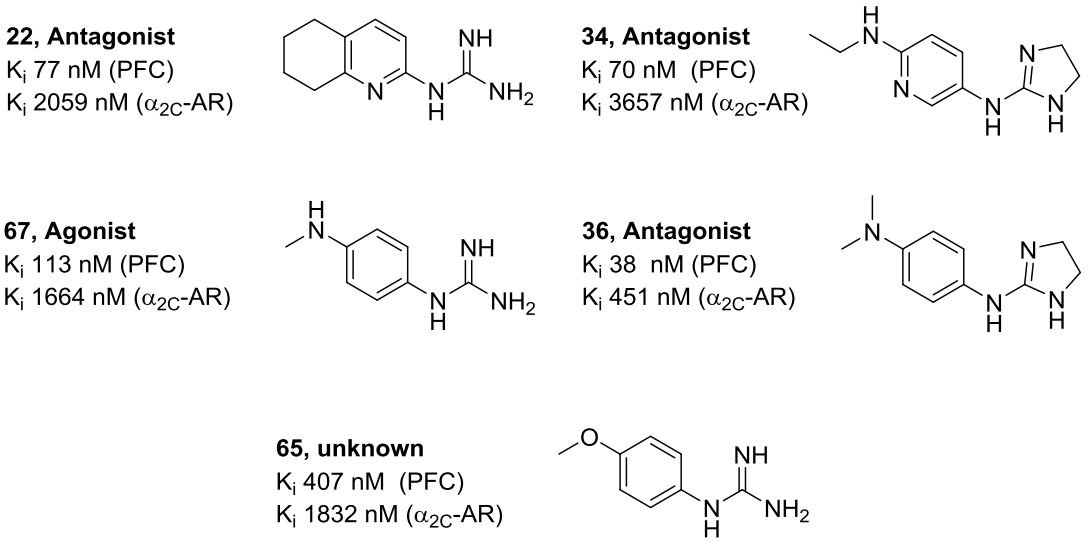

Figure 4.1.1 Structures of α_2-AR ligands exhibiting preferential binding to the α_{2C}-AR.

Previously, three of these hit compounds had been shown to display antagonist activity in [^{35}S]GTPγS binding experiments using human PFC tissue (**34**, **22**, and **36**).[131,132] These compounds were subsequently tested in [^{35}S]GTPγS binding experiments against UK14304 (α_2-AR agonist) to confirm that the observed antagonist activity was mediated through the α_2-AR. Compounds **34** and **22** (10^{-5} M) only induced a small rightward shift (<10-fold) in the EC_{50} value for UK14304; however, **36** produced a large rightwards shift (Table 4.1.1). This suggests that **34** and **22** possess only weak antagonistic effect at the α_2-AR, whereas **36** acts as a potent antagonist at this receptor.[129]

Table 4.1.1. EC_{50} values obtained from the concentration-response curves for UK14304 stimulation of [^{35}S]GTPγS binding (10^{-12} - 10^{-3} M, 10 concentrations) in the absence or presence of **39**, **22**, and **36** (10^{-5} M).[132]

Experiment	EC_{50} value (μM)
UK14304	0.906 ± 0.03
UK14304 + 34	6.71 ± 0.58
UK14304 + 22	2.71 ± 0.27
UK14304 + 36	355 ± 18.2

The results shown in Table 4.1.1 are in agreement with the α_{2C}-AR K_i affinity values measured for these compounds: 3657 nM (**34**), 2059 nM (**22**), and 451 nM (**36**). Regarding the other two candidate molecules (**65** and **67**), only **67** had been previously assessed for activity confirming it as an agonist.[131]

4.2. Structural analogues of 2-aminoimidazoline antagonists 34 and 36

4.2.1. Potential factors in the measurement of affinities in different tissues

Prior to discussing the optimization process, it is first necessary to address the large differences between the affinity values obtained for these two hit compounds (Fig. 4.2.1). There are many contributing factors which could potentially influence the binding affinity measurements. The most obvious difference between these values are the different tissues and competitive radioligands used in these experiments.

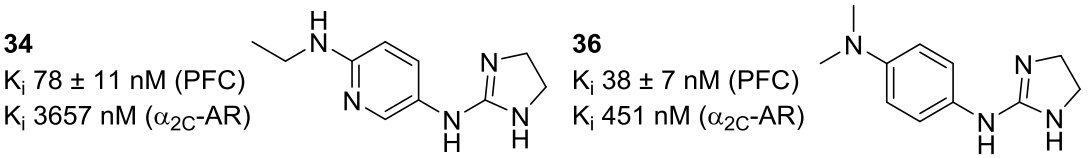

Figure 4.2.1. Structures of **34** and **36**.

The affinity values measured in human PFC tissue utilize **[^{3}H]RX821002** whereas those obtained by the PDSP were conducted using membranes from transgenic CHO cell selectively expressing recombinant human α_2-AR subtypes, using **[^{3}H]rauwolscine** as radioligand. These two factors alone could dramatically influence the values observed for the α_2-AR affinity for these compounds.

The use of different buffers has also been reported to influence the binding of these two radioligands at the different α_2-AR subtypes, with glycylglycine buffers giving higher binding affinities for **[^{3}H]rauwolscine** and **[^{3}H]RX821002** relative to Tris buffer.[246] This is most likely not an influential factor in this instance as both procedures use the same Tris buffer. A number of studies have compared each of these radioligands in kinetic, saturation and competitive binding assays using recombinant human α_2-AR subtypes for their suitability of use in screening for new subtype-selective ligands. These studies validated the use of both **[^{3}H]rauwolscine** and **[^{3}H]RX821002** as a radioligand in subtype-selectivity assays using Tris buffer.[240,247]

In the affinity measurements derived from competition binding experiments in human PFC tissue, **[^{3}H]RX821002** was used at a constant concentration of 2 nM. A potential explanation for this discrepancy that had not previously been considered could be that both the radioligand and the test ligands can bind at alternative non-adrenergic sites. In this sense, a study conducted by Nicolas *et al.* which examined the activity of different α_2-AR ligands in competition binding experiments using recombinant human α_{2A}-AR and 5-HT_{1A} receptors expressed in CHO cells.[222]

Thus, the differences in the reported pK_i values of several α_2-AR antagonists including (±)-idazoxan, yohimbine and RX821002 indicated that these ligands exhibit a preference of only 3.6-, 10- and 11-fold for the α_{2A}-AR versus 5-HT_{1A} receptors, respectively. In this study, RX821002 displayed a K_i 2 nM for α_{2A}-AR and a K_i of 22 nM for the human 5-HT_{1A} receptor where it was also found to act as an antagonist of 5-HT-stimulated [^{35}S]GTPγS binding.[222]

The screening of both **34** and **36** revealed that both of these ligands exhibited substantial affinity for the 5-HT_{1A}, 5-HT_{2B} and 5-HT_{2C} receptors. Therefore, the **[^{3}H]-RX821002** competition binding assays conducted in human PFC tissue, which is known to contain a large number of 5-HT_{1A} receptors,[221] may have been influenced by the simultaneous binding of both the radioligand and test ligands at α_2-ARs and 5-HT_{1A} receptors that may have contributed to the confounding affinity measurements and observed discrepancies. In fact, a biphasic curve was originally obtained for **34** during the **[^{3}H]-RX821002** competition binding assays suggesting competitive binding occurring at a secondary target.[248]

These results emphasise the importance of investigating new methods to help improve the α_2-AR binding affinity and antagonist potency of **34** whilst retaining preferential binding at the α_{2C}-AR. The substantial affinity for 5-HT_{1A}, 5-HT_{2B} and 5-HT_{2C} receptors exhibited by **34** will also be discussed in terms of potential benefits of 5-HT receptor binding to contribute to different therapeutic applications later in this chapter.

4.2.2. Optimization strategies

Analysis of the screening results obtained for the ligands sharing similar structural characteristics with **34** (**28** and **88**, Fig. 4.2.2) highlights the necessity to retain both the pyridine ring and the *N*-ethyl group in order to maintain α_{2C}–AR preferential binding. Comparison of the structures suggests that the pydrin-3-yl 2-aminoimidazoline core present in **28** and the *N*-ethylamino substituent in the agonist **28** are both crucial to enhance the α_{2C}-selective antagonism of **34**. Hence, the aromatic portion of **34** will be maintained with modifications introduced at the cationic moiety. The pydrin-2-yl derivative of **34** had previously displayed poor affinity as a α_2-AR ligand during earlier studies within the Rozas group and, therefore, does not merit further investigation.[132]

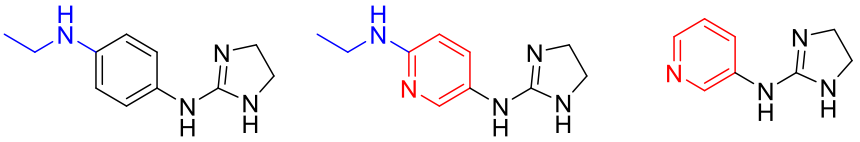

28
K_i 175 ± 36 nM (PFC)
K_i 586 nM (α_{2C}-AR)
K_i 50 nM (α_{2A}-AR)

34
K_i 78 ± 11 nM (PFC)
K_i 3657 nM (α_{2C}-AR)

88
K_i 5000 nM (PFC)
K_i >10,000 nM (α_{2C}-AR)
K_i 1776 nM (α_{2A}-AR)

Figure 4.2.2. Structures of **28**, **34** and **88**.

Two optimization strategies have been proposed with the aim of improving the pharmacological profile of **34** (3659 nM), **67** (1664 nM) and **36** (451 nM) as α_{2C}-selective antagonists. First, the investigation of the impact of ring expansion, from 2-aminoimidazoline to 2-amino-1,4,5,6-tetrahydropyrimidine, on the receptor binding profiles of these ligands. This will require synthesis and pharmacological evaluation of each 2-amino-1,4,5,6-tetrahydropyrimidine analogues (**106**, **107** and **108**) (Fig. 4.2.3), as outlined in Section 2.4.1. An investigation of potential synthetic routes towards the preparation of these derivatives will be discussed in section 4.3.

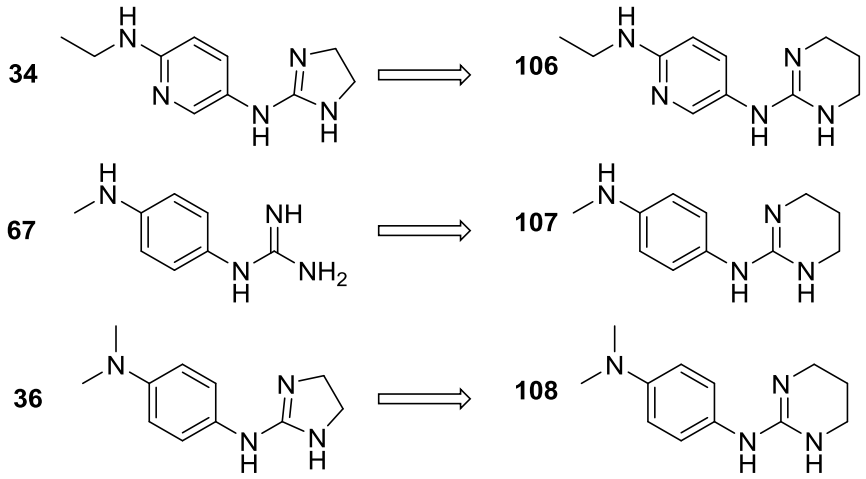

Figure 4.2.3. Structures of **34**, **67** and **36** and proposed ring expanded analogues **106**, **107** and **108**.

The second optimization strategy involves modifying the phenyl core, based upon a earlier approach involving bioisosteric replacement with a ring equivalent, specifically a pyridine ring.[132] This has previously proved a successful strategy to convert α_2-AR agonists to antagonists, as discussed in section 1.7. Despite the effective enhancement of antagonism achieved by bioisosteric replacement with a pyridine ring, a concomitant reduction in affinity is also routinely observed as illustrated by conversion of agonist **28** into antagonist **34**.[132] This strategy will be explored in an effort to optimize **36**.

Preparation of the pyridine-2-yl analogue of **36** was deemed redundant as **36** already exhibited excellent α_{2C}-selective and strong α_2-AR antagonism. Alternatively, structural modifications will centre around **35** (Fig. 4.2.4), the guanidine analogue of **36**, previously determined to act as a high affinity agonist in human PFC tissue (K_i = 87 ± 17 nM).[142] Analysis of structural analogues **67** and **68** suggests that alteration of the cationic moiety with retention of the aromatic portion could serve to enhance preferential α_2-AR recognition (Fig. 4.2.4).

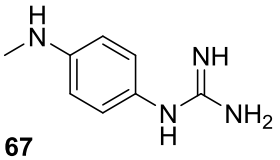

67
Agonist,
K_i 113 nM (α_2-AR, PFC)
K_i 1664 nM (α_{2C}-AR)
K_i > 10,000 nM (α_{2A}-AR)

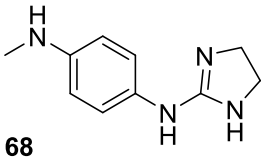

68
Agonist,
K_i 53 nM (α_2-AR, PFC)
K_i 372 nM (α_{2C}-AR)
K_i 55 nM (α_{2A}-AR)

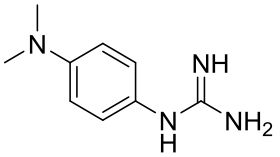

35
Agonist,
K_i 87 nM (α_2-AR, PFC)

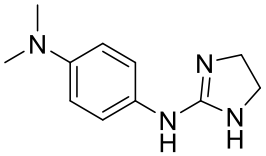

36
Antagonist,
K_i 38 nM (α_2-AR, PFC)
K_i 451 nM (α_{2C}-AR)
K_i > 10,000 nM (α_{2A}-AR)

Figure 4.2.4. Structures and associated affinities (K_i , nM) of **67**, **68**, **35** and **36**.

Previous attempts to optimize the activity of **35** and **36** through modification of the cationic moiety gave mixed results. Firstly, substitution of the guanidine moiety in **35** to give 1,3-disubstituted guanidine **39** proved effective to convert the original agonist into an antagonist.[141] Subsequently, different strategies were employed within the group in an attempt to improve the diminished binding affinity of **39** by preparing substituted 2-aminoimidazolines (**109** and **38**) and conformationally restricted guanidine derivatives such as **37** (Fig. 4.2.5).[141,197]

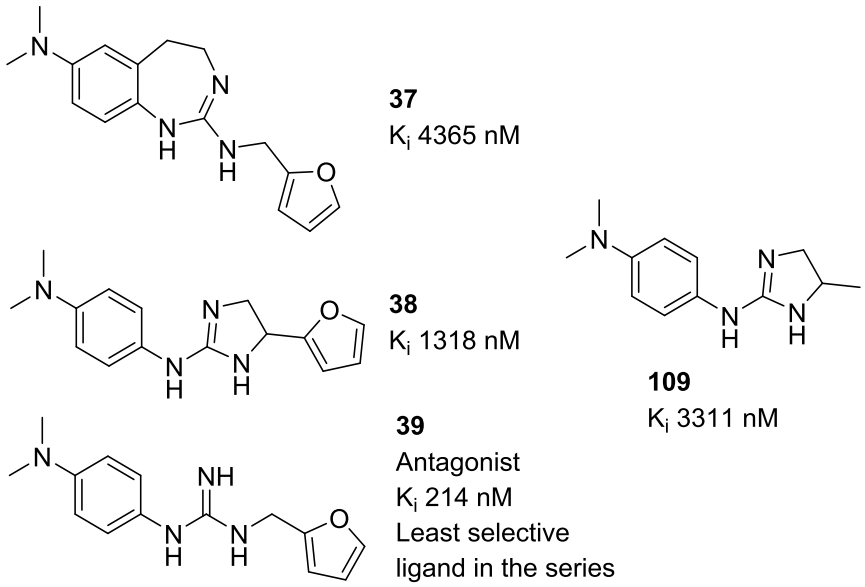

Figure 4.2.5. Structures and associated α_2-AR affinities in PFC (K_i, nM) of **37**, **38**, **39** and **109**.

Unfortunately, all of these derivatives displayed significantly reduced α_2-AR affinities compared with **36** and resulted in these approaches being abandoned. Furthermore, screening of **39** revealed a complex polypharmacological profile with significant binding affinities for a diverse range of targets, including monoamine transporters, thereby highlighting the unsuitability of this ligand, as discussed in section 3.7.6.5.

These results are in line with literature reports concerning modification of the cationic moiety of the known α_2-AR agonists clonidine and **UK14,304**.[249] Munk *et al.* reported the preparation of 11 analogues of **UK14,304**, which showed the dramatic reduction in affinity that resulted from converting the 2-aminoimidazoline moiety (**UK14,304**, K_i = 2.4 ± 0.2 nM) into a 1,2-dimethylguanidine (**110**, K_i = 5300 ± 1000 nM); however, the guanidine analogue gave significantly better affinity (**111**, K_i = 41 ± 9 nM) (Fig. 4.2.6).

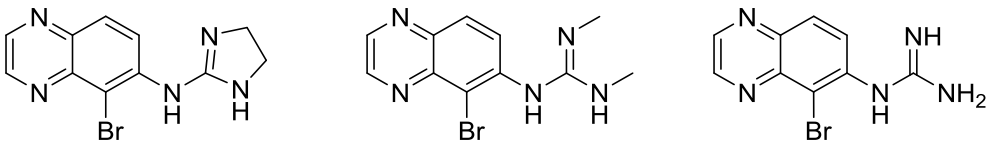

UK14,304
α_2 agonist
K_i 2.4 ± 0.2 nM

110
α_2 agonist
K_i 5300 ± 1000 nM

111
α_2 agonist
K_i 41 ± 9 nM

Figure 4.2.6. Structures of **UK14,304** and related analogues **110** and **111** with α_2-AR affinities (K_i , nM).

Similarly, Schann *et al.* showed that methylation of the imidazoline ring led to a loss of α_2-AR affinity in α_2-AR agonist clonidine and I_1 imidazoline receptor (I_1R) agonist **112** as illustrated in Fig. 4.2.7.[250] Clonidine and **112** were screened alongside their methylated analogues **113** and **114** in competition binding assays using CHO cell membranes transfected with α_{2A}-, α_{2B}- and α_{2C}-ARs subtypes against 0.8, 1 or 2 nM of **[3H]RX821002**, respectively. Consideration of these findings altogether reveals that substitution of the 2-aminoimidazoline moiety and/or conversion to a substituted guanidine has a more detrimental impact for the α_2-AR binding affinity of these molecules than replacement of the cationic moiety with an unsubstituted guanidine. This would suggest that there is a lack of steric tolerance at this position within the orthosteric binding pocket and a more conservative structural modification may be beneficial for α_2-AR binding.

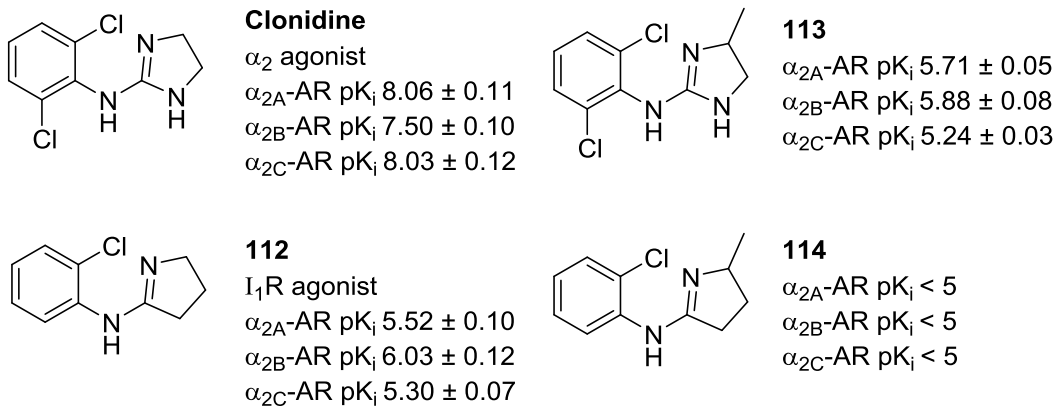

Clonidine
α_2 agonist
α_{2A}-AR pK_i 8.06 ± 0.11
α_{2B}-AR pK_i 7.50 ± 0.10
α_{2C}-AR pK_i 8.03 ± 0.12

113
α_{2A}-AR pK_i 5.71 ± 0.05
α_{2B}-AR pK_i 5.88 ± 0.08
α_{2C}-AR pK_i 5.24 ± 0.03

112
I_1R agonist
α_{2A}-AR pK_i 5.52 ± 0.10
α_{2B}-AR pK_i 6.03 ± 0.12
α_{2C}-AR pK_i 5.30 ± 0.07

114
α_{2A}-AR pK_i < 5
α_{2B}-AR pK_i < 5
α_{2C}-AR pK_i < 5

Figure 4.2.7. Structures of clonidine and **112** with methylated analogues **113** and **114** (α_2-AR affinities expressed as pK_i).[250]

4.2.3. Synthesis of 35 and related derivatives

The original screening series did not include compound **35**; therefore, it was prepared and will be submitted for screening at the PDSP alongside new derivatives from the optimised series for comparison and to complete the homologous series. As such, the preparation of **35** involved guanylation of *N*,*N*-dimethyl-1,4-phenylenediamine (**115**) using a solution of 1,3-bis(*tert*-butoxycarbonyl)-2-methyl-2-pseudothiourea (**85**) in CH_2Cl_2 the presence of $HgCl_2$ and NEt_3 to give the protected derivative **116** (Scheme 4.2.1).[195] This reaction gave **116** in a surprisingly low isolated yield of 20% after purification by flash chromatography.

Scheme 4.2.1. Synthesis of **116** with formation of **117** as the major product.

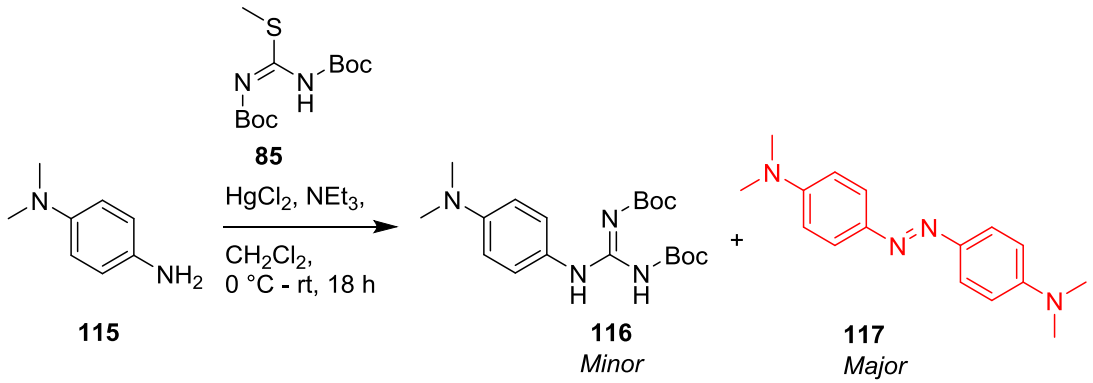

Investigation of the remaining products isolated from the reaction mixture indicated that most of the 1,3-bis-(*tert*-butoxycarbonyl)-2-methyl-2-pseudothiourea had not been consumed after 24 h despite being the limiting reagent in the reaction. A red crystalline side-product was also isolated in a significant quantity and was identified as 4,4′-(diazene-1,2-diyl)-bis-(*N*,*N*-dimethylaniline) (**117**).

The identity of **117** was confirmed by HRMS, melting point, ^{1}H, and ^{13}C NMR analysis. All of the data obtained for this side product matched the characterisation data reported in the literature..[251] Thin plate-like crystals were grown by slow evaporation of a saturated chloroform solution and were subsequently submitted to Dr. Brendan Twamley for crystallographic analysis. The crystal structure of this material indicates a *trans* configuration around the azo group, confirming that the crystals were composed of (*E*)-4,4-(diazene-1,2-diyl)bis(N,N-dimethylaniline) (Fig. 4.2.8).

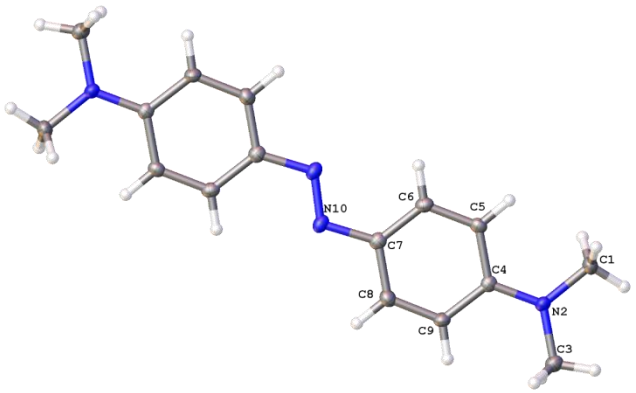

Figure 4.2.8. Symmetry generated molecule of **117** with atomic displacement shown at 50% probability with only symmetry unique atoms labelled for clarity.

This unusual observation prompted investigation of the literature concerning the synthesis of azobenzene derivatives which identified a number of different conditions for the oxidative dimerization of (hetero)aromatic amines to form (hetero)aromatic azo compounds.[251–254]

Two reports in particular described conditions for the oxidative dimerization of anilines which resembled the reaction conditions used in the synthesis of **117**. Orito *et al.* reported the preparation of azobenzenes by reacting a number of substituted anilines and benzyl amines with Hg(II)O and I_2 (1.5 molar equivalents of each) in CH_2Cl_2 (0.2 M) at rt for 1 h (Scheme 4.2.2A).[255] This reaction was thought to proceed *via* a radical mechanism with formation H_2O and HgI_2 as side products.

Scheme 4.2.2. Syntheses of azobenzene derivatives by oxidative dimerization: A. Method reported by Orito *et al.*[255] B. Method reported by Lin *et al.*[251]

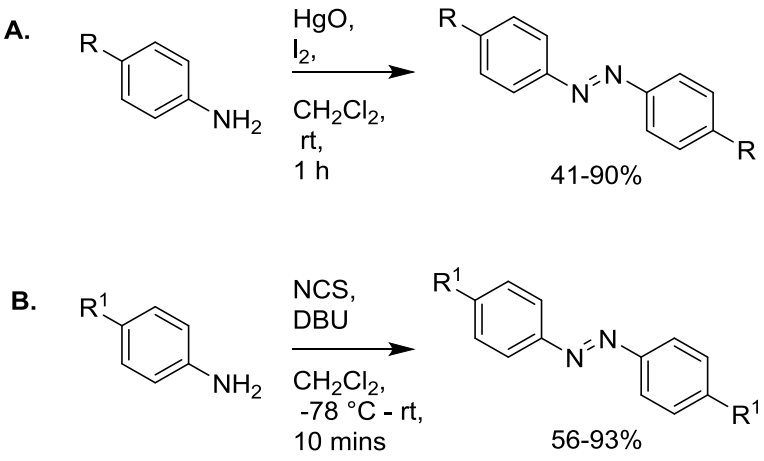

Lin *et al.* also reported the synthesis of a range of substituted azobenzenes by treating anilines with *N*-chlorosuccinimide and 1,8-diazabicyclo-[5.4.0]undec-7-ene (DBU) (2 molar equivalents of each) in CH_2Cl_2 (Scheme 4.2.2B).[256] The reaction was thought to proceed through the formation of an organic oxidant (chlorinated DBU through reaction of DBU with *N*-chlorosuccinimide), which was proposed to participate in two key chlorination/oxidation steps leading to azobenzene formation. This reaction was reported to be completed within 2-10 mins as it was allowed to warm up to rt (-78 °C – rt) and furnished 17 different azobenzenes in good to excellent yield (56-93%).

In an attempt to discern which reagents were responsible for the formation of **117** a number of control reactions were performed. Firstly, the conditions for the synthesis of **117** were replicated apart from the addition of $HgCl_2$. There was no reaction observed with only the two starting materials, **115** and **85**, present by TLC after 24 h (Table 4.2.1, Entry 1). Likewise, no reaction was observed when **115** was stirred in CH_2Cl_2 and NEt_3 for 24 h (Table 4.2.1, Entry 2).

Table 4.2.1. Control experiments to probe reaction conditions for oxidative dimerization of **115** to azobenzene **117.**

Entry	***85***	*$HgCl_2$*	*NEt_3*	*Formation of **117***
1	Yes	No	Yes	No reaction
2	No	No	Yes	No reaction
3	No	Yes	Yes	40-60%

However, **117** was formed upon reaction of 1.1 equivalents of $HgCl_2$ with **115** in CH_2Cl_2 and NEt_3, confirming that $HgCl_2$ was required for oxidative dimerization to occur (Table 4.2.1, Entry 3). The scope and general applicability of these conditions for the preparation of azobenzene derivatives is currently under investigation in the Rozas lab.

Despite this side reaction, a sufficient amount of **116** was obtained for characterization and to proceed to the deprotection and isolation of the desired hydrochloride salt of **35**. Compound **116** was characterised by ^1H NMR, HRMS and melting point analysis, all of which matched literature data.[191] Subsequently, **35** was obtained in an excellent yield of 95% from **116** utilizing the TFA deprotection method as previously discussed in section 3.3 (Scheme 4.2.3).[178]

Scheme 4.2.3. Deprotection of **116** to furnish the dihydrochloride salt **35**.

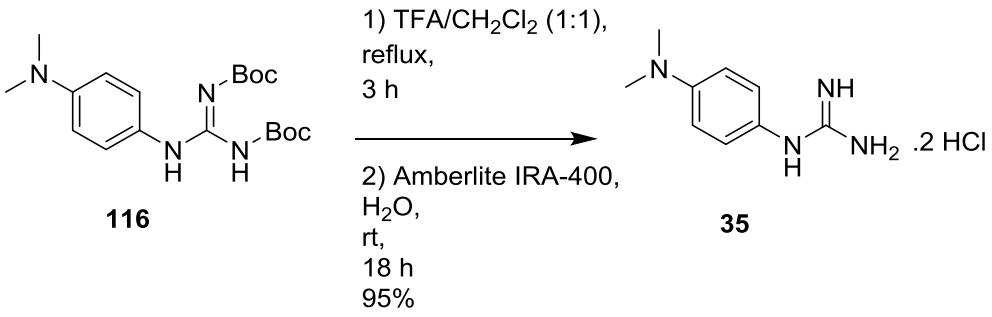

Compound **35** was characterised by ^{1}H and ^{19}F NMR, HRMS, melting point and HPLC analysis which all matched previously published data and confirmed sufficient purity for pharmacological testing (99.8%, t_R = 9.72 min).[191]

The analogue of **35** proposed to expand upon the benzene/pyridine replacement strategy was the pydrin-2-yl guanidine derivative, **118**. The synthetic route envisaged to prepare **118** would be analogous to the route used to synthesise **35**. This route requires the preparation of 2-amino-5-dimethylaminopyridine (**119**) which was prepared according to literature procedures (Scheme 4.2.4).[257]

Scheme 4.2.4. Synthesis of **120**.

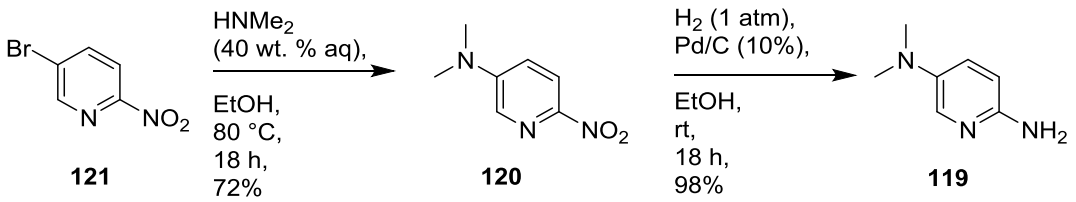

First, **120** was synthesised *via* a nucleophilic aromatic substitution reaction (S_NAr) between dimethylamine and 5-bromo-2-nitropyridine (**121**) (Scheme 4.2.4). A recent mechanistic study of S_NAr reactions of 2-bromopyridines, using computational analysis and kinetic isotope effect studies, suggested that these reactions actually occur in a concerted manner rather than the generally accepted stepwise mechanism involving addition-elimination mechanism with formation of a discrete non-aromatic Meisenheimer complex.[258]

Reaction of dimethylamine and **121** in ethanol under reflux for 18 h provided **120** as a precipitate formed upon cooling of the reaction mixture. This was filtered and washed with cold EtOH to afford **120** in a 72% yield. Catalytic hydrogenation over 10% Pd/C with H_2 (1 atm.) followed by removal of Pd/C by filtration through a Celite pad, rinsing with ethanol and concentration of the filtrate *in vacuo* furnished **119** as a purple oil in an excellent yield of 98%. This 1,4-diaminopyridine derivative also proved unstable to storage and prone to oxidative transformations, as previously discussed in section 3.3.; therefore, it was reacted immediately.[193]

Thus, **120** was subject to the same reaction conditions used in the preparation of **116** to give **122** in a 37% yield (Scheme 4.2.5). TLC analysis of the reaction mixture showed a number of highly polar coloured side products, potentially the result of oxidative dimerization as previously observed. Unfortunately, these could not be identified as they were unstable to isolation by flash chromatography. Upon isolation and purification, the identity of **122** was confirmed by ^{1}H and ^{13}C NMR, HRMS, IR and melting point analysis.

Scheme 4.2.5. Synthesis of **122**.

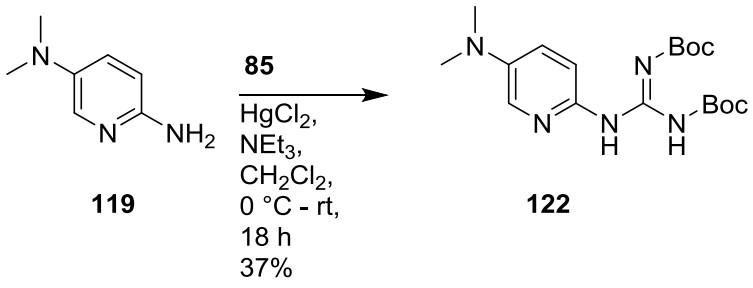

Deprotection of **122** was initially attempted using the standard deprotection conditions of a 1:1 mixture of CH_2Cl_2 and TFA (Scheme 4.2.6). This mixture was allowed to stir overnight before excess solvent was removed *in vacuo*. ^{1}H NMR analysis of the reaction mixture in DMSO-d_6 indicated that the deprotection was not fully successful as a signal corresponding to the Boc *tert*-butyl group were still present.

Scheme 4.2.6. Partial deprotection of **123** to **124** and **125**.

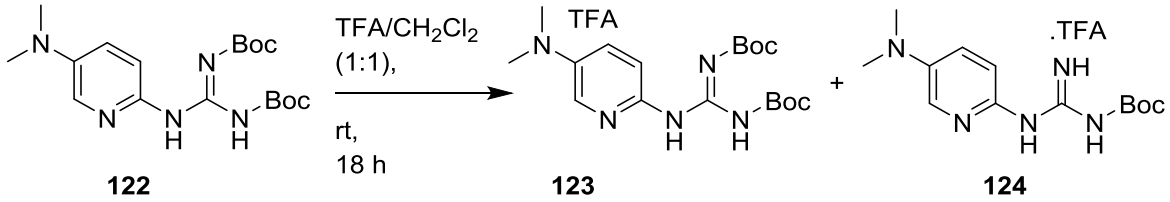

This DMSO-d_6 NMR sample was transferred to sample tube for storage using a deionised H_2O and MeOH mixture and slow evaporation of methanol led to the formation of small cubic crystals. These crystal were isolated, washed with H_2O and submitted for crystallographic analysis to Dr. Brendan Twamley who successfully resolved this sample uncovering an unexpected structure (**124**, Fig. 4.2.9). The crystal structure shows *mono*-Boc-protected **122** coordinated through bidentate parallel hydrogen bonding with a trifluoroacetate anion.

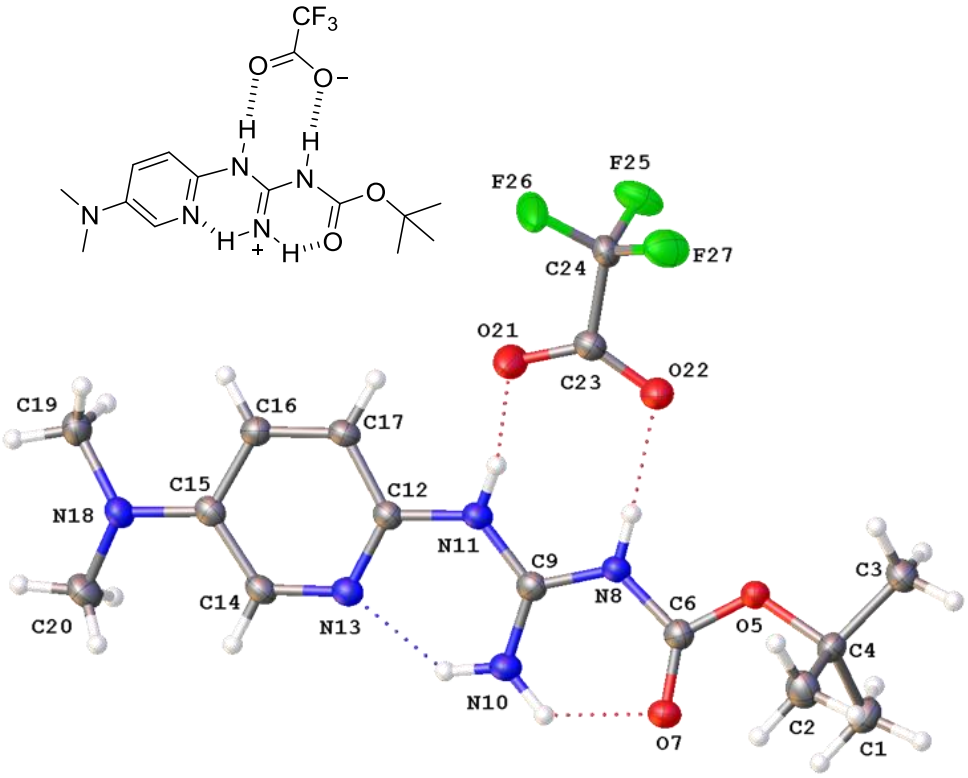

Figure 4.2.9. Crystal structure of **124** with hydrogen bonding indicated by dotted lines.

The IMHB interactions occur between the two N-H protons of the guanidinium with the CO group of the *tert*-butyl carbamate on one side and the pyridinic nitrogen on the other (Fig. 4.2.9). Research previously conducted in our group demonstrated the conformational preference exhibited by a number of different *N*-(pyridin-2-yl)guanidinium cations due to a stabilizing intramolecular hydrogen bond (IMHB) between the pyridine N1 atom and the guanidinium protons.[195] The crystal structure of *N*-(5-methylpyridin-2-yl)guanidinium chloride (**125**) and *N*-(5,6,7,8-tetrahydroquinolin-2-yl)guanidinium chloride (**22**) were resolved as part of that study showing IMHB interactions similar to those observed in sample **124** (Fig. 4.2.10).[195,259]

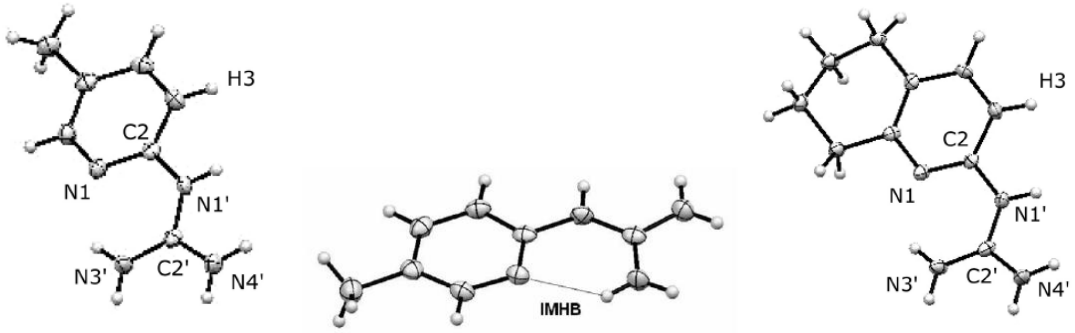

Figure 4.2.10. X-ray crystal structure of **125** (*left and middle)* and **22** (*right*) illustrating the IMHB.[259]

Furthermore, a structural study of *N,N'*-bis-aryl-*N''*-acylguanidines previously conducted in our group identified conformational preference in a related molecule **126** (Fig. 4.2.11). This molecule was shown to exist as two distinct tautomers (**126A** and **126B**) by means of low temperature ^{1}H and ^{13}C NMR analysis and theoretical DFT, NBO and GIAO calculations, with **126A** proving to be the major tautomer. The bulky phenyl substituent in **126** may prevent this compound from adopting a similar pattern of IMHB interactions between the amino protons and both the pyridinic nitrogen and Boc carbonyl group, as in **124**.

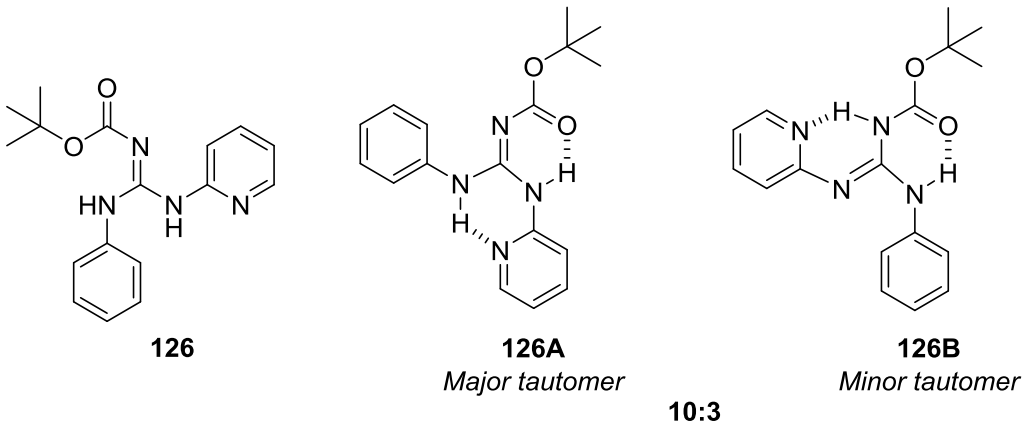

Figure 4.2.11. Structure of **126** with two distinct tautomers (**126A** and **126B**) with different IMHBs.

There are limited reported methodologies for direct preparation of *N*-aryl-*N'*-Boc protected guanidines such as **126**; however, two methods have been reported involving the synthesis of orthogonally protected 1*H*-pyrazole-1-carboxamidines as guanylating agents.

Mourabit *et al.* reported the preparation of compound **127** by Cbz protection of *N*-Boc-1*H*-pyrazole-1-carboxamidine **128** (Fig. 4.2.12). However, as **127** proved unstable to purification, they investigated the reaction of **128** with a variety of alkyl amines which gave *N*-alkyl-*N'*-Boc protected guanidines in good yields. Reaction of **128** with aniline, 3- and 4-methoxyaniline gave low to moderate yields.[260] Moreover, during the total synthesis of araiosamines, Baran *et al.* required a powerful guanidinylation reagent to react with hindered or electron deficient amines to facilitate the installation of mono-*N*-Boc protected guanidines on primary and secondary amines which led to the development of *N*-Boc-*N'*-trifluoroacetylguanylpyrazole (**129**, Fig 4.2.12).

This reagent proved to be highly reactive giving the desired *N*-aryl-*N'*-Boc protected guanidines with a variety of amine substrates including 2-aminopyridine and 4-nitroaniline (77% and 80% yield, respectively). This result was attributed to the enhanced electrophilic character imparted on the carboximidamide due to highly electron-withdrawing nature of the trifluoroacetyl group. [261]

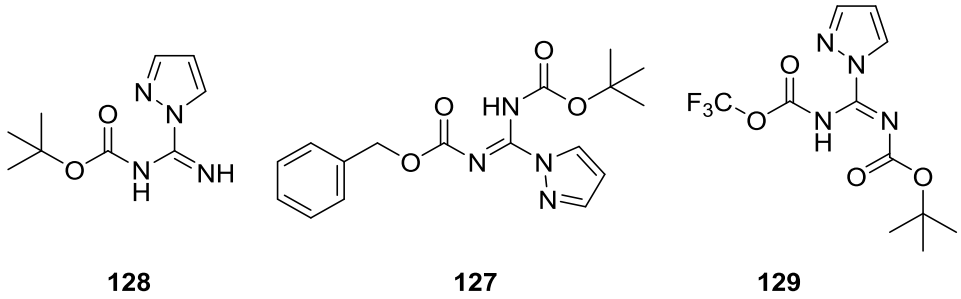

Figure 4.2.12. Structure of guanidinylation reagents **127**, **128** and **129**.

A similar IMHB motif is also seen in an oxoanion receptor reported by Moyer *et al.* which forms a persistent planar pseudo-bicyclic conformation upon coordination with anions such as sulfate and nitrate. This *N*,*N*'-*bis*(2-pyridyl)guanidinium cation (**130**) was also found to feature IMHBs between the pyridinic nitrogens and the guanidinium protons in the solid state (Fig. 4.2.13).[262]

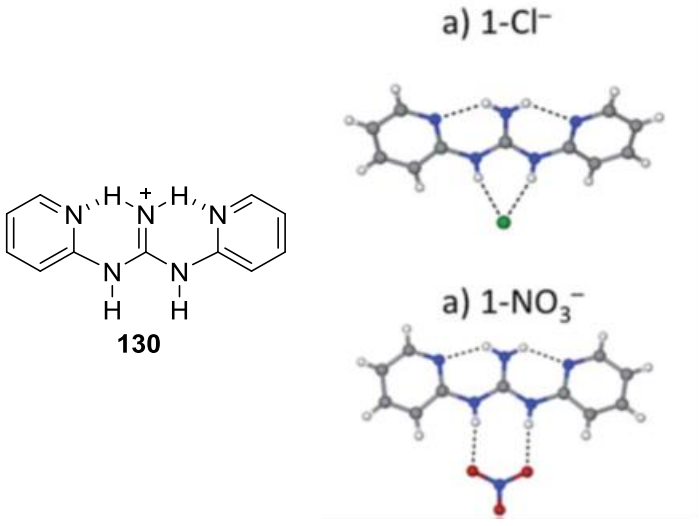

Figure 4.2.13. Dual IMHB structure of **130** (left) and X-ray crystal structure of **130** in 1 : 1 anion–ligand complexes with chloride (a) and nitrate (b) illustrating dual IMHB (*right*); taken from Moyer *et al.*.[262]

Taking all the data found in the literature into consideration, it was postulated that the formation and stability of the **124** complex may slow the Boc deprotection reaction and prevent complete deprotection at ambient temperature. Therefore, more rigorous deprotection conditions were employed to force the deprotection reaction to completion. Thus, quantitative deprotection of **122** was achieved in 3 h by heating in a 1:1 mixture of CH_2Cl_2 and TFA under reflux followed by removal of excess solvent *in vacuo* to furnish trifluoroacetate salt **131** in > 99% yield. Anion exchange resin was subsequently utilized to covert the trifluoroacetate salt **131** to the dihydrochloride salt **118** (98% yield) as previously described(Scheme 4.2.7).[195] This process is typically employed to increase the aqueous solubility of compounds; however, in the case of **131**, which was highly water soluble, it was converted to the hydrochloride salt to maintain consistency with **35**.

Scheme 4.2.7. Deprotection of **122** to final hydrochloride salt **118**.

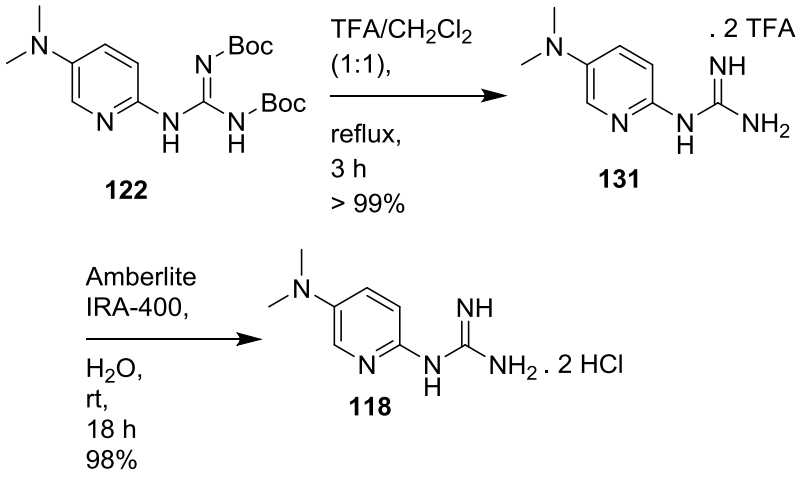

Full characterisation of **118** was conducted using ^{1}H, ^{19}F and ^{13}C NMR, HRMS, IR, melting point alongside HPLC analysis which confirmed sufficient purity for pharmacological testing (99.1%, t_R = 17.5 min).

4.3. Synthesis of 2-arylamino-1, 4, 5, 6-tetrahydropyrimidine derivatives

4.3.1. Literature methods

The next family of derivatives to be investigated were the 2-amino-1,4,5,6-tetrahydropyrimidine analogues. There is limited precedent in the literature for the preparation of 2-arylamino-1,4,5,6-tetrahydropyrimidines, with reports of procedures featuring highly specific examples with low-yields or limit scope. Thus, Chern *et al*. reported a one-pot procedure which utilizes *in situ* formation of 2-chlorotetrahydropyrimidine from tetrahydropyrimidin-2-one using dimethyl chlorophosphate and NEt_3; this is then followed by addition of an aniline which displaces chloride by nucleophilic attack to form the C-N bond.[263] Another method was developed by Katritzky *et al.* for the preparation of 1,2,3-trisubstitued guanidines, including some 2-arylamino-1,4,5,6-tetrahydropyrimidines, which involved the synthesis of (bis-benzotriazol-1-yl-methylene)amines and subsequent cyclization of these intermediates with alkyl diamines.[264] Additionally, Xie *et al.* reported a titanacarborane monoamide catalyzed synthesis of cyclic guanidines from alkyl diamines and carbodiimides.[265]

These routes are limited in terms of scope as each requires either the multistep preparation of the aryl component, (bis-benzotriazol-1-yl-methylene) amines or substituted carbodiimides, or the nontrivial preparation of a complex catalyst. These factors limit the versatility and applicability of these protocols for the synthesis of the intended derivatives; therefore, initial focus was placed on investigating the suitability of methods previously developed and employed within the Rozas group.[266]

4.3.2. Investigation of 2-arylaminopyrimidine route

Shaw *et al.* developed a high-yielding synthetic method utilizing 2-arylaminopyrimidines, which are subsequently reduced to the corresponding 2-arylamino-1,4,5,6-tetrahydropyrimidines (scheme 4.3.1). This approach presents a number of benefits compared with alternative procedures including utilization of commercially available or previously synthesised substituted anilines and formation of the final hydrochloride salt in a simultaneous hydrogenation/protonation step. Hence, this route warranted further investigation.

Scheme 4.3.1. Synthesis of 2-arylamino-1,4,5,6-tetrahydropyrimidines from 2-arylaminopyrimidines as reported by Shaw *et al*.

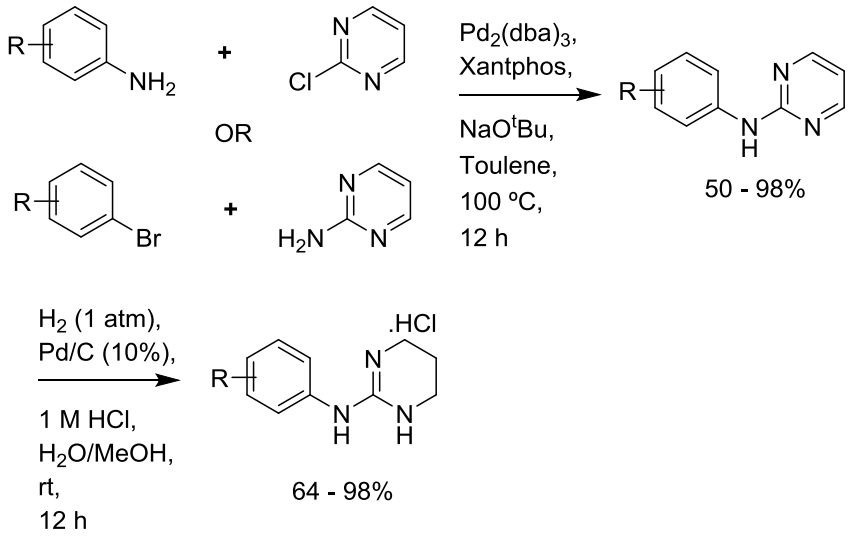

Similar conditions were used to prepare the intermediate 2-arylaminopyrimidine, **132**, in a 60% yield using a Buchwald-Hartwig coupling of **115** and 2-chloropyrimidine **133** (scheme 4.3.2). Unfortunately, application of the reported hydrogenation conditions led to complete degradation of **132** after 12h with no discernible signals in the ^{1}H NMR spectrum.

Scheme 4.3.2. Synthesis 2-arylaminopyrimidines using Buchwald-Hartwig coupling of **133** and **115**.

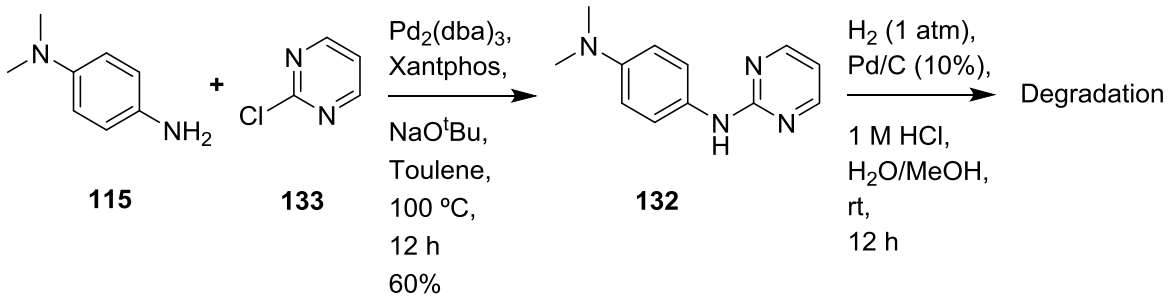

The failure of these conditions prompted exploration of alternative methodologies reported by Rozas *et al.* and others for the preparation of 2-arylamino-1,4,5,6- tetra hydropyrimidines using *N,N'*-di-*tert*-butoxycarbonyl-1,2,3,4-tetrahydropyrimidine-2-thione (**134**) in a $HgCl_2$ mediated guanylation reaction.[213,267] Investigation and attempted optimization of potential synthetic routes towards the preparation of proposed derivatives is discussed in section 4.3.3.

4.3.3. Mercury (II) chloride mediated guanylation using compound 134

Matsumura *et al.* originally reported *N,N'*-di-*tert*-butoxycarbonyl-1,2,3,4-tetrahydropyrimidine-2-thione (**134**) as a alkoxycarbonyl group transfer reagent for the synthesis of carbamate protected alkylamines.[268] Preparation of **134** is analogous to the synthesis of **61** and involves Boc protection of 3,4,5,6-tetrahydro-2-pyrimidinethiol (**135**).[213] Deprotonation of **135** using excess NaH quantitatively forms the corresponding anionic species which reacts upon addition of Boc_2O at 0 °C to afford **134** in a 72% yield after recrystallization from hexanes/EtOAc (Scheme 4.3.3.A).[269]

Recently, compound **134** has been utilized in $HgCl_2$ mediated guanylation of aryl and alkyl amines during the synthesis 2-aryl/alkyl amino-1,4,5,6-tetrahydropyrimidines (Scheme 4.3.3.B).[213,269]

Scheme 4.3.3. A. Preparation of **134** from **135**. B. $HgCl_2$ mediated guanidinylation **134**.[213,269]

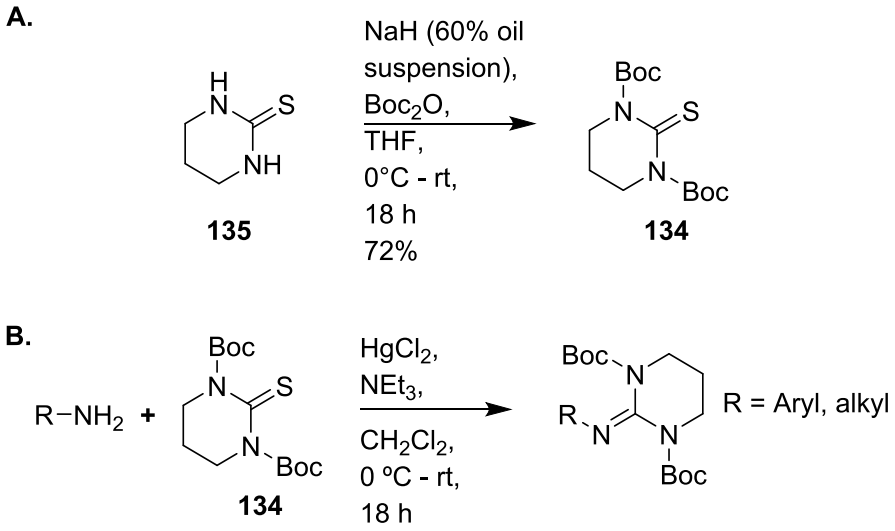

In our group, Dr. Patrick O'Sullivan had employed this reaction for the synthesis of minor groove binder derivative **136** in a 17% yield,[267] whereas Pockes *et al.* utilized **134** in the preparation of histamine H2 receptor agonists such as **137** in a 79% yield (Fig. 4.3.1).[213]

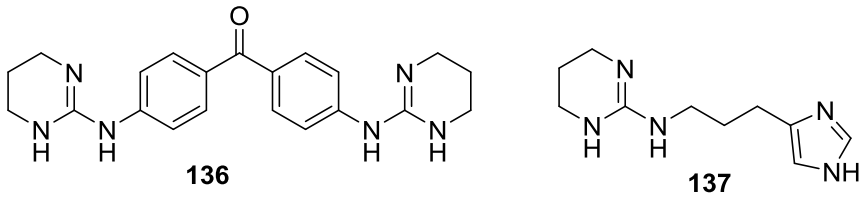

Figure 4.3.1. Structures of amino-1,4,5,6-tetrahydropyrimidines derivatives; minor groove binder **136** (left) and histamine H2 receptor agonists **137** (*right*).

The generality and versatility of this method prompted investigation of this route in the preparation of the proposed 2-arylamino-1,4,5,6-tetrahydropyrimidine derivatives (Fig. 4.3.2).

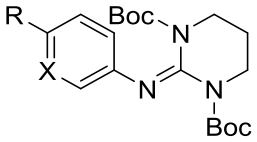

138: X= CH, R= -N(Boc)Me
139: X= N, R= -NHEt
140: X=CH, R= -NHEt
141: X=CH, R= -N(Me)$_2$

Figure 4.3.2. Structures of proposed Boc 2-arylimino-1,4,5,6-tetrahydropyrimidines derivatives.

An alternative synthetic route reported by Martini *et al.* was utilized in this work to prepare a protected version of diamine **70** on gram scale, which also facilitated the desired protecting group strategy to favour reaction at the primary amine (Scheme 4.3.4).[270] Compound **142** was also more stable to both the reaction conditions and storage over longer period than the deprotected compound **70** which was found to degrade overtime.

Scheme 4.3.4. Synthetic route to **142** as reported by Martini *et al.*

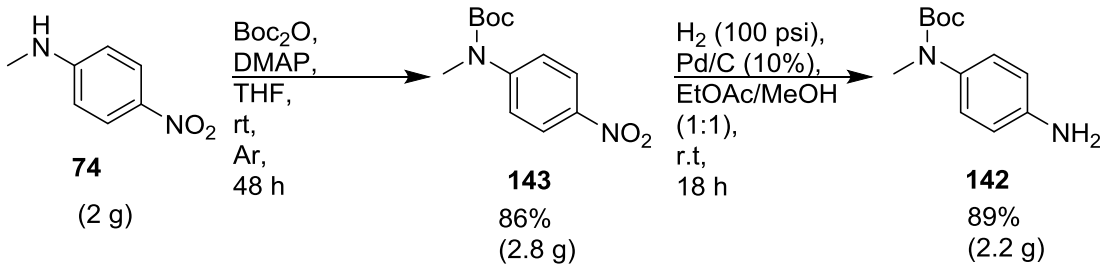

The first three derivatives to be prepared using this procedure were based on *hit* compounds **36**, **28** and **68**. Reaction of the corresponding substituted *p*-phenyl diamines with compound **134** in the presence of $HgCl_2$ in CH_2Cl_2 and NEt_3 for 18 h followed by the standard guanylation reaction, work-up and flash chromatography, furnished **138**, **140** and **141** in 25%, 83% and 77%, yield, respectively. These derivatives were stable to silica gel flash chromatography unlike the corresponding Boc-protected 2-iminoimidazolidine derivatives which exhibit degradation on silica. This would suggest that the ring strain of the 5-membered ring system is a major contributor to the instability of these derivatives.

Scheme 4.3.5. $HgCl_2$ mediated guanidinylation of **115**, **142** and **75**.

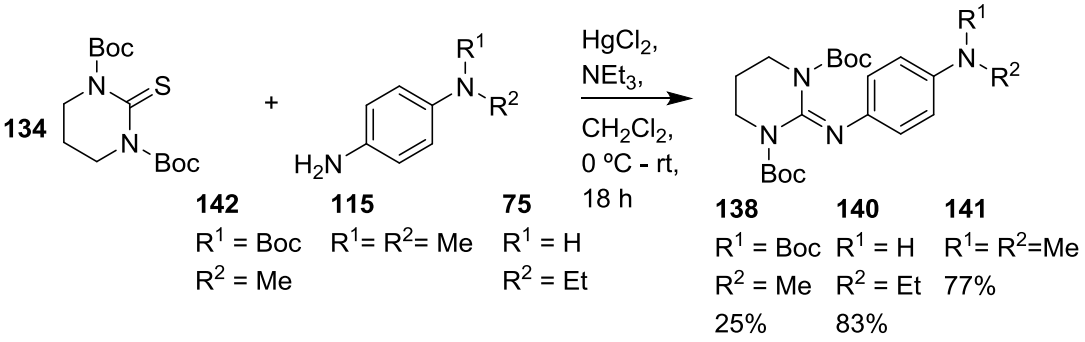

Subsequently, these derivatives were characterised by ^1H and ^{13}C NMR, HRMS, IR and melting point analysis. Analysis of the ^1H NMR spectrum of **140** in $CDCl_3$ (Fig. 4.3.3) shows that the two Boc peaks are inequivalent and the two CH_2 groups adjacent to the Boc protected N atoms are poorly resolved and appear as a broad singlet at 3.68 ppm.

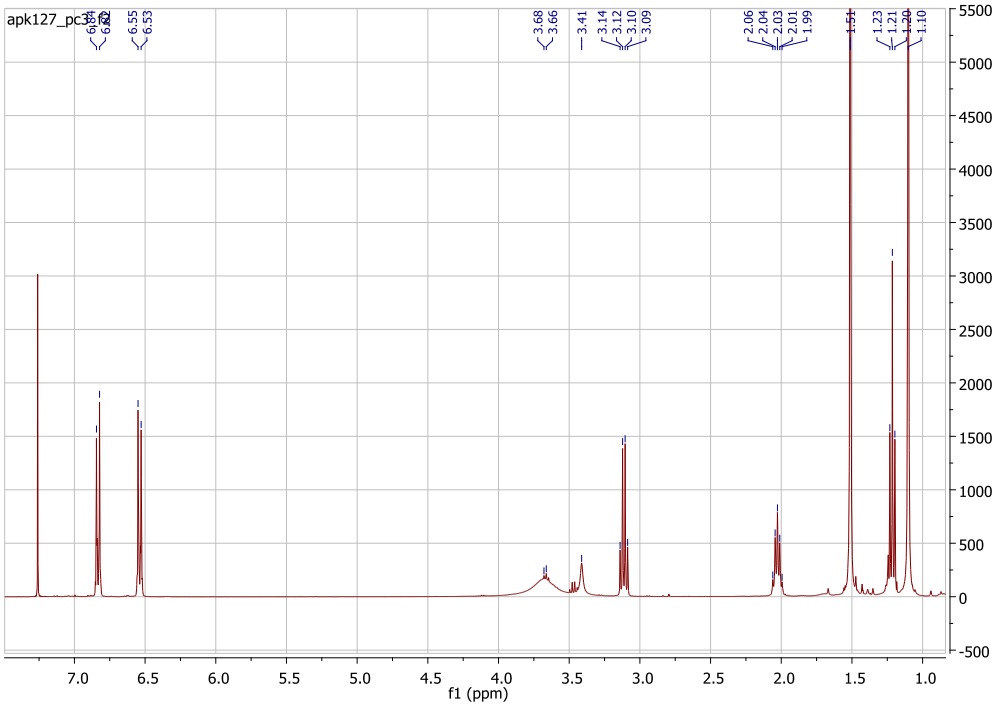

Figure 4.3.3. ^{1}H NMR spectrum of bis-Boc protected 2-arylimino-1,4,5,6-tetrahydropyrimidines **140**.

This patterns is consistent among the three bis-Boc protected 2-arylimino-1,4,5,6-tetrahydropyrimidine derivatives and is suggestive of tautomerization which may facilitate slow rotation around the imine N-C_{Ph} bond (Fig. 4.3.4).

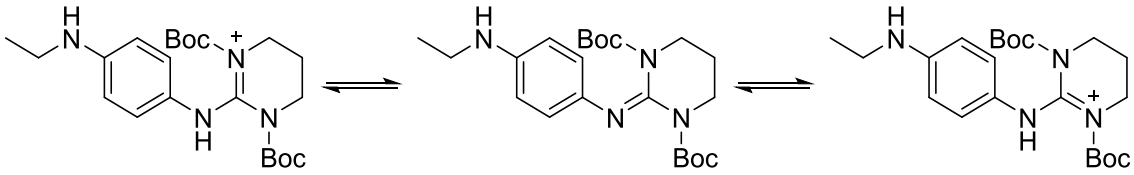

Figure 4.3.4. bis-Boc protected 2-arylimino-1,4,5,6-tetrahydropyrimidines **140**.

The next derivative to be synthesised was **139** which required the preparation of another batch of **77**. The synthesis of this key intermediate originally followed the route discussed in section 3.4.1; however, an alternative route was investigated during its synthesis. This alternative route began with an S_NAr reaction between 2-chloro-5-nitropyridine and ethylamine (Scheme 4.3.6).

An excess of ethylamine (70 wt. % aq.) was used as this reagent plays a dual role as both the nucleophile and base. The reaction was complete after 18h stirring at rt as adjudged by consumption of 2-chloro-5-nitropyridine using TLC analysis. Removal of solvents *in vacuo* followed by an aqueous workup to remove excess ethylamine/ethylamine hydrochloride afforded analytically pure **144** in an excellent yield of 92%. This intermediate was subsequently reduced by catalytic hydrogenation over palladium on carbon (10% w/w) to afford **77** in a 98% yield.

77 was immediately employed in the $HgCl_2$ mediated guanylation with **134** (Scheme 4.3.6). TLC analysis of the reaction mixture after 18 h indicated a complex reaction mixture which suggested that **77** may have degraded under the reaction conditions and/or a number of side products may have formed. Purification by flash chromatography following the usual guanylation work-up procedure afforded the desired product **139** in a yield of 27%.

Scheme 4.3.6. Alternative route to **77** utilized in the synthesis of **139**.

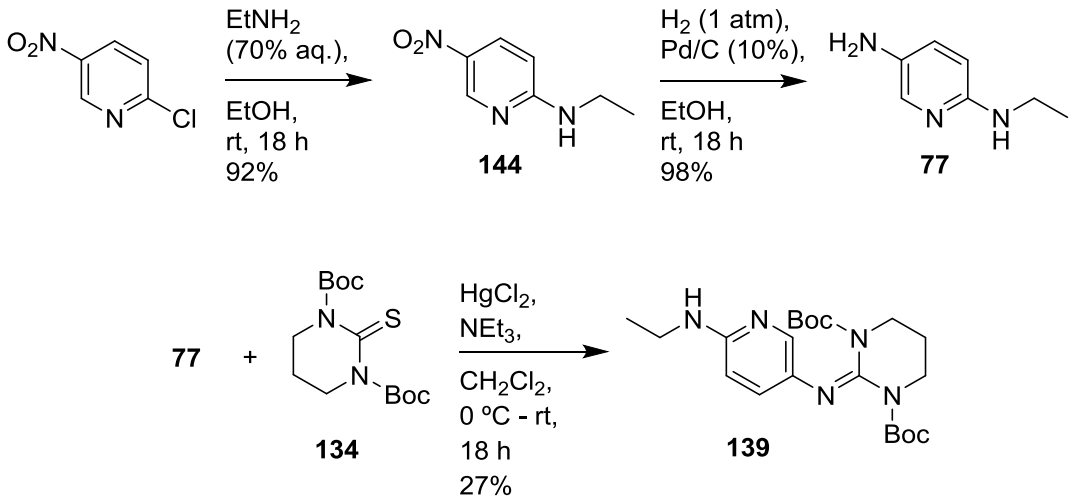

Issues arose, however, when the same procedure was applied in the synthesis of **145** and **146** (Fig. 4.3.5), which were envisaged as precursors of ring expanded analogues of **23**.

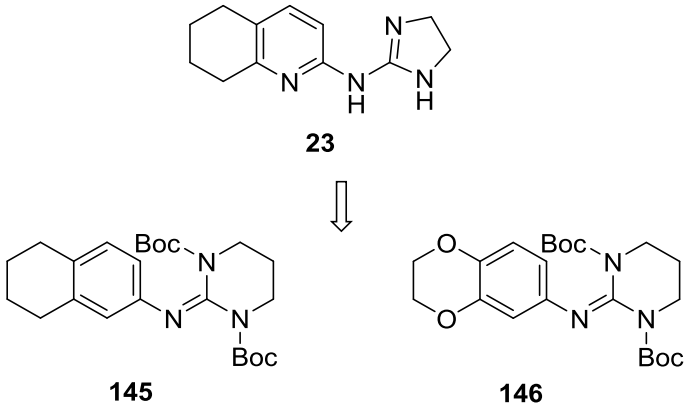

Figure 4.3.5. Structures of bis-Boc protected 2-arylimino-1,4,5,6-tetrahydropyrimidines **145** and **145** as ring expansion derivatives of **23.**

Application of the aforementioned reaction conditions employing commercially available amines 5,6,7,8-tetrahydro-2-naphthylamine (**147**) and 1,4-benzodioxan-6-amine (**148**) initially appeared to be successful with TLC analysis indicating complete consumption of **134**. The issue arose upon isolation of the desired products **145** and **146** which both had very similar R_f values to the starting amines **147** and **148** in various solvent systems.

Iterative rounds of chromatographic purification were performed in an effort to separate the products from the amines, but unfortunately this was not successful with only insufficient quantities of **145** and **146** isolated which were only suitable for used for characterisation. Analysis of the ^{1}H NMR spectrum of the mixed fractions obtained from the reaction with **148** indicated a 4:1 ratio of **146** to **148**.

Scheme 4.3.7. Synthesis of **146** from **148**.

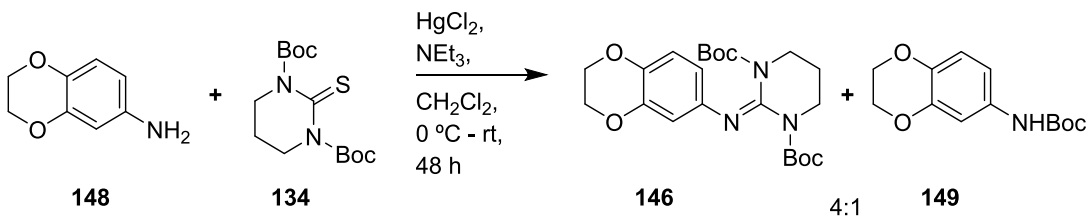

Liquid-liquid extraction was attempted to wash out the contaminating starting material using diethyl ether and 1M HCl (aq.). This was successful in separating one previously unidentified component of the mixture which remained in the ether layer and was identified as **149** (Scheme 4.3.7).[271]

Despite previous reports of **134** acting as an effective alkoxycarbonyl group transfer reagent for primary and secondary alkyl/benzyl amines by Matsumura *et al.*, conditions required for efficient alkoxycarbonyl group transfer involved heating to reflux for several hours in anhydrous 1,4-dioxane under argon.[268] The mild conditions employed in the reaction of **148** with **134** hardly seemed sufficient to promote alkoxycarbonyl group transfer to this poorly nucleophilic aniline; however, similar side reactions have been observed previously in our group by Dr. Patrick O'Sullivan.[267]

A similar situation took place during the guanylation of **147** with **134** resulting in an inseparable mixture of **145** and **150** (Scheme 4.3.8). These results indicated that successful reaction of **134** to give the desired 2-arylamino-1,4,5,6-tetrahydropyrimidine derivatives was highly dependent on the substitution pattern and nucleophilic nature of the corresponding aniline precursor.

This prompted investigation of more versatile and selective reagents than **134** as well as alternative synthetic routes towards the preparation of 2-arylamino-1,4,5,6-tetrahydropyrimidine derivatives such as **145** and **146**. The results of this investigation are discussed in detail in Chapter 5.

Scheme 4.3.8. $HgCl_2$ mediated guanidinylation of **147** with **134**.

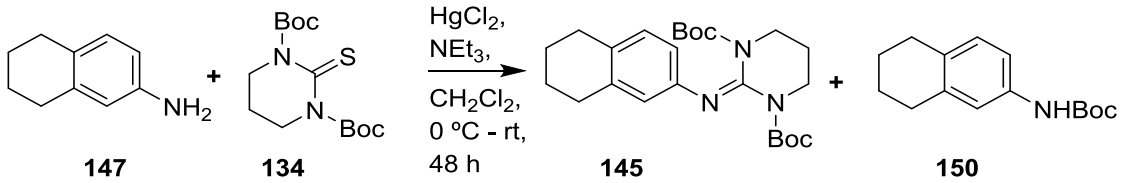

147 **134** **145** **150**

The final deprotection of the bis-Boc protected 2-arylimino-1,4,5,6-tetrahydro pyrimidines derivatives **138**, **139** and **141**, chosen as priority derivatives for testing, utilized excess HCl. Deprotection of **140** will be conducted later together with the **145** and **146** or derivatives thereof. Each of the protected precursors (**138**, **139** and **141**) were dissolved in excess HCl (1 M aq or 1.25 M methanol) and were heated for 1 h at 70 °C (Scheme 4.3.9). The aqueous solutions were then washed with $CHCl_3$ and concentrated *in vacuo* to afford the desired hydrochloride salts in quantitative yield (>98%). Full characterisation of these hydrochloride salts was conducted using ^{1}H and ^{13}C NMR, HRMS, IR and melting point analysis alongside HPLC which confirmed sufficient purity for pharmacological testing (< 95%).

Scheme 4.3.9. Deprotection of Boc protected 2-arylimino-1,4,5,6-tetrahydropyrimidines derivatives.

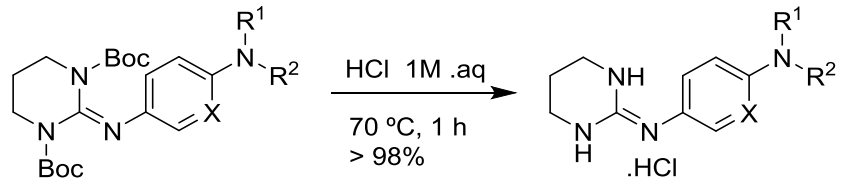

141: $R^1 = R^2 = Me$; X = CH
138: R^1 = Boc; R^2 = Me; X = CH
139: R^1 = H; R^2 = Et; X = N

106: R^1 = H; R^2 = Et; X = N
107: R^1 = H; R^2 = Me; X = CH
108: $R^1 = R^2$ = Me; X = CH

Each of these novel tetrahydropyrimidine hydrochloride salts (**106**, **107**, and **108**) were submitted for pharmacological screening in human PFC tissue to determine their affinity for α_2-ARs in collaboration with the pharmacological laboratory of Prof. Luis Callado at UPV/EHU. The affinities of **106**, **107** and **108** for α_2-ARs measured using human PFC tissue are shown below in Fig. 4.3.6.

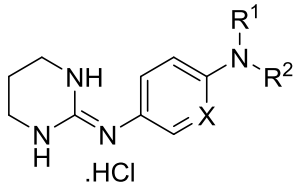

106: R^1 = H; R^2 = Et; X = N
pK_i 4.09 ± 0.19
107: R^1 = H; R^2 = Me; X = CH
pK_i 4.94 ± 0.10
108: $R^1 = R^2$ = Me; X = CH
pK_i 4.99 ± 0.08

Figure 4.3.6. α_2-AR affinity values (pK_i) for **106**, **107** and **108** measured in human PFC tissue.

4.4. Structural analogues of aryl guanidine ligands (67 and 22)

4.4.1. Design and synthesis of hybrid derivatives

21 was one of the original *lead* compounds discovered throughout the course of antidepressant research conducted within the Rozas group. This compound was shown to be a potent antagonist both *in vitro* and *in vivo* as well during behavioural animal model studies in which it exhibited antidepressant-like effects in both the FST and TST stress tests.[133,140] This *lead* compound was the basis of many extensive SAR and optimization studies which led to the design and discovery of **22** and **23** as α_2-AR antagonists (Fig. 4.4.1).

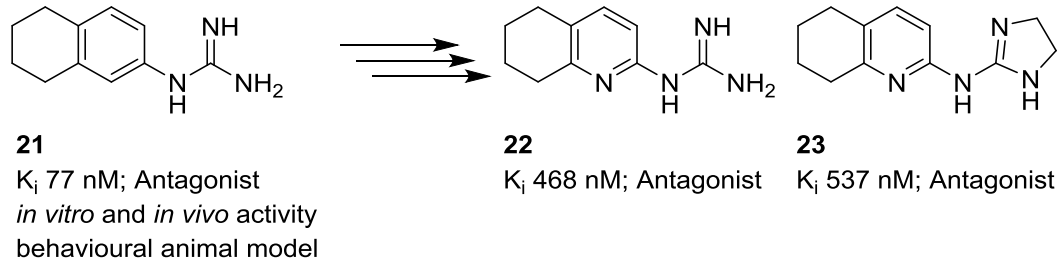

Figure 4.4.1. Structures of **21** and derivatives **22** and **23**.

Therefore, **21** was chosen as a template for the design of a hybrid of **67**. The design of this hybrid analogue (**151**) tried to combine the secondary amino substituent of **67** (α_{2C}-AR selective) into the cyclohexyl moiety of **21 (**potent α_2-AR antagonist) whilst retaining the arrangement of the guanidine substituent relative to the amino group (Fig. 4.4.2).

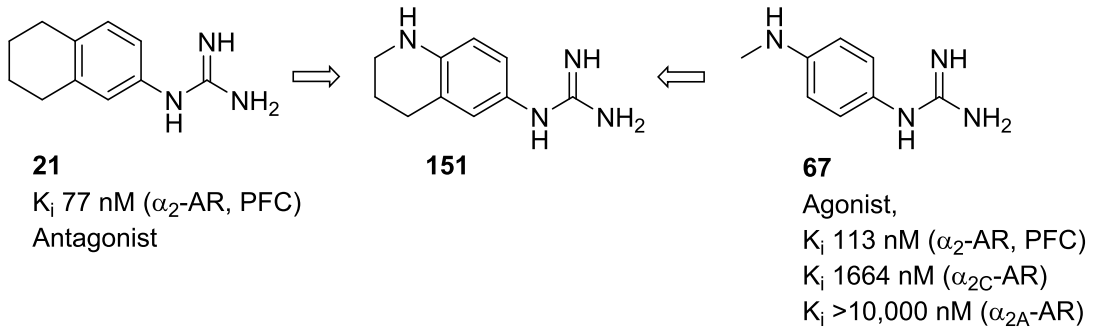

Figure 4.4.2. Structure of proposed hybrid analogue **151** based on **21** and **67**.

A related derivative, **152**, was previously synthesised within the group by Dr. Julian Shaw but exhibited poor α_2-AR affinity in human PFC tissue (Fig. 4.4.3). This result suggests that the six-membered ring substituent may be required to facilitate adequate affinity.

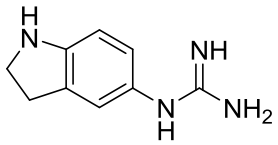

152

K_i 12,883 nM (α_2-AR, PFC)

Figure 4.4.3. Structure of analogue **152**.

The proposed synthetic route to **151** (Scheme 4.4.1) was envisaged to use 6-aminoquinoline (**153**) as the starting material for the preparation of intermediate 1,2,3,4-tetrahydroquinolin-6-amine (**154**). A recent paper by Wu *et al.* reported a facile and efficient metal-free transfer hydrogenation protocol in H_2O mediated by diboronic acid applied to hydrogenate of a variety of N-heterocycles, including **153**.[272] This protocol was utilized to hydrogenate **153** which gave **154** in an excellent yield of 95% after purification by flash chromatography. The standard guanylation conditions were employed for the reaction of **154** with **85**; however, TLC analysis of the reaction mixture after 18 h indicated that a number of components of various polarity were present and some **85** remained unreacted.

Scheme 4.4.1. Proposed synthetic route to **151** from **153**.

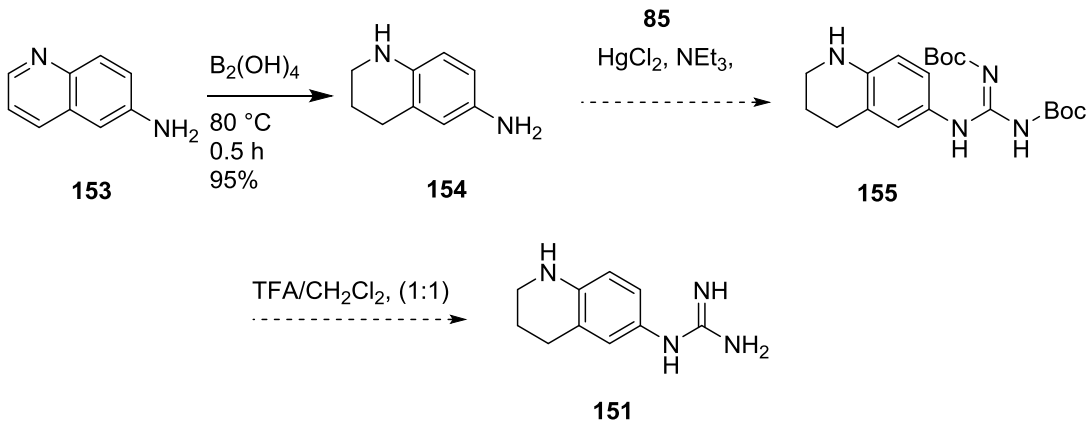

Standard workup to remove mercury side-products was followed by isolation of the major components of the reaction mixture by flash chromatography. Other than unreacted **85**, two other compounds were successfully separated from the reaction mixture neither of which were the desired product **155**. These two compounds, **156** and **157**, were subsequently identified and characterised by HRMS, ^{1}H, ^{13}C and ^{15}N analysis (Scheme 4.4.2). These observed products appear to have formed as the result of oxidative dehydrogenation of **154** prior to guanylation or subsequent dehydrogenation of the desired product **155** which was not isolated from the reaction mixture.

Scheme 4.4.2. Products of the guanylation reaction of **154** and **85** to give **156** and **157**.

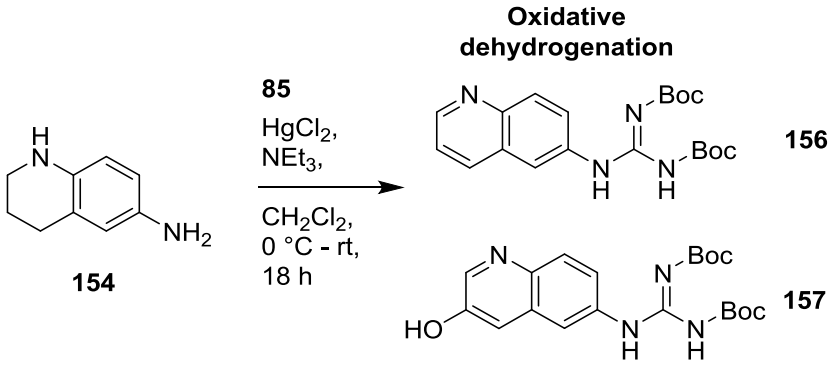

A brief search of the literature in an attempt to rationalise this unusual observation uncovered numerous papers which reported the development of various methods for the aerobic oxidative dehydrogenation of N-heterocycles, including oxidative dehydrogenation of substituted 1,2,3,4-tetrahydroquinolines (Scheme 4.4.3).

Scheme 4.4.3. Oxidative dehydrogenation of 1,2,3,4-tetrahydroquinolines to quinolines, taken from Balaraman *et al.*.[273]

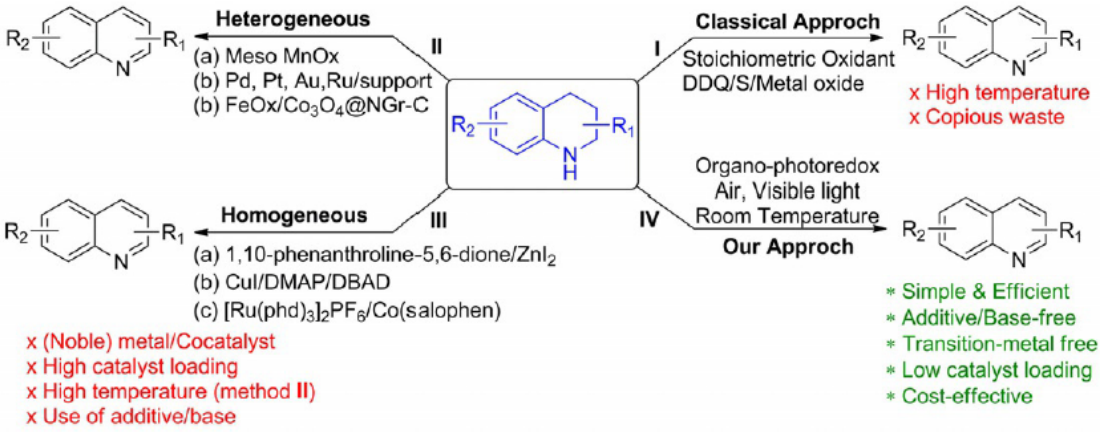

A number of catalytic procedures have recently been developed for the aerobic oxidative dehydrogenation of N-heterocycles which utilize a variety of catalyst system.

These include visible light (organo)-photoredox catalysts such as rose bengal and the tris-(bipyridine)-ruthenium(II) chloride ruthenium complex ($[Ru\text{-}(bpy)_3]Cl_2 \cdot 6H_2O$), oxovanadium(V) catalysts and metal-free carbocatalyst such as graphene oxide.[273–277]

Some of these procedures require heating to reflux in air for extended periods to facilitate efficient dehydrogenation whereas the visible-light promoted reactions all proceed efficiently under ambient conditions. The mechanism of the photoreactions are proposed to consist of amine oxidation through single electron transfer to give an amine radical cation **A** which is subsequently oxidized by a superoxide radical ion ($O_2^{\bullet-}$) forming imine **B** and hydrogen peroxide. Isomerisation of **B** followed by a second dehydrogenation step is proposed to give the corresponding quinoline (Scheme 4.4.4).[273]

Scheme 4.4.4. Proposed photoreaction mechanism for oxidative dehydrogenation of 1,2,3,4-tetrahydroquinolines to quinolines, modified from Badu-Tawiah *et al.*.[273,275]

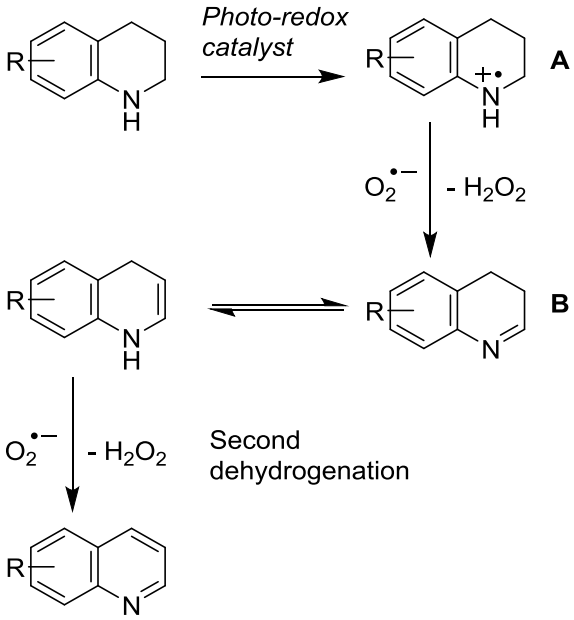

Alternatively, other methods involving the use of stoichiometric organic oxidant like dialkyl azodicarboxylates, such as diethyl azodicarboxylate (DEAD), were also reported to proceed efficiently under ambient conditions.[274]

A series of control experiments were performed to examine the conditions required to favour the oxidative dehydrogenation of **154** (Table 4.4.2).

Table 4.4.2. Control experiments to probe reaction conditions for oxidative dehydrogenation of **6-ATHQ** to **6AQ**.

Entry	*$HgCl_2$*	*NEt_3*	*Product*
1	Yes	No	No reaction
2	No	Yes	No reaction
3	Yes	Yes	**153**

Furthermore, **154** also proved to be inherently unstable as extended exposure to air at ambient temperatures led to degradation of this off-white solid to a dark purple oil. This may be the result of similar oxidative transformations previously discussed in relation to **75** in section 3.3.[193]

Thus, $HgCl_2$ was likely responsible for promoting the oxidative dehydrogenation of **154**; however, the mechanism by which this oxidation occurs is currently under investigation in the Rozas group. There is some precedent in the literature for $HgCl_2$ mediated oxidation reactions. Eder's reaction is the photochemical reaction between $HgCl_2$ and ammonium oxalate in which $HgCl_2$ is reduced to mercury(I) chloride (Hg_2Cl_2) and ammonium chloride and carbon dioxide are formed.[278] In the 1950s, Leonard and Cook published a number of papers detailing the oxidation of substituted pyrrolidines and piperidines using stoichiometric mercuric acetate ($Hg(OAc)_2$) in boiling aqueous acetic acid (5%).[279,280]

The oxidative instability of **154** raised concerns for the potential instability of proposed derivative **151**. This prompted exploration of the literature for compounds which contained a similar scaffold as that proposed for **151**. Munk *et al.* reported the synthesis of related derivatives (Fig. 4.4.4),[281] a series of 1,2,3,4-tetrahydroquinoxaline analogues of **UK14,304**, such as **158**, which involved hydrogenation of the corresponding quinoxaline derivatives; however, these 1,2,3,4-tetrahydroquinoxaline analogues proved unstable as free bases and were converted to dihydrochloride salts to facilitate purification by recrystallization.

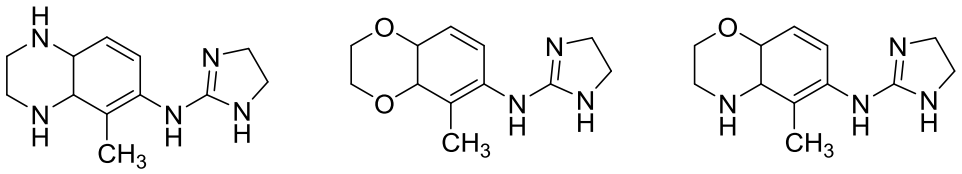

158
α_2 agonist
K_i 9.6 ± 1.2 nM

159
α_2 agonist
K_i 0.25 ± 0.06 nM

160
α_2 agonist
K_i 1.2 ± 0.2 nM

Figure 4.4.4. Structures of derivatives **AGN192172**, **BDIOX** and **AGN193080**.[249]

Evaluation of **158** showed that it possessed potent α_2-AR selective agonist activity *vs.* α_1-ARs but proved to be oxidatively unstable even as the hydrochloride salt. These results prompted Munk *et al.* to redesign this promising candidate with the aim of improving stability by incorporating the structural characteristics of **159**, another potent lead compound (Fig. 4.4.4).[249] This involved replacement of the *p*-amino group by an oxygen atom giving the benzoxazine based derivative **160** which displayed greatly enhanced oxidative stability and α_2-AR agonist potency relative to **158**.[249]

The oxidative instability exhibited by **158** seemed to originate from the 1,4-diamino phenyl arrangement within the aromatic core as replacement of this amine substituent with an oxygen atom to give **160** greatly improved the oxidative stability. Overall, consideration of these results coupled with the unexpected oxidative dehydrogenation observed prompted us to defer preparation of hybrid **151** due to the likelihood of instability. Subsequently, an alternative family (derivatives of **22**) were proposed to investigate the potential of quinoline core based guanidines.

4.4.2. Design and synthesis of quinoline derivatives

The unexpected formation of the two compounds discussed in section 4.4.1., **156** and **157**, provided motivation to evaluate the quinoline core as a basis for the development of potential α_2-AR ligands. Quinolines, naphthalenes and quinazolines have been utilized as core structures in a variety of α_2-AR ligands including naphazoline (**162**), JP-1302 derivative (**161**) and **UK14,304** (Fig. 4.4.5).[145]

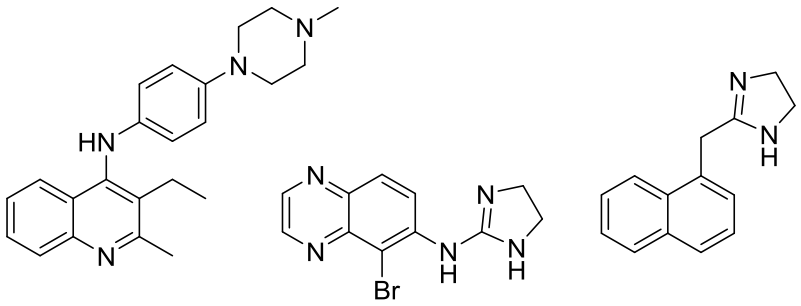

161 **UK14,304** **162**

Figure 4.4.5. Structures of ligands containing quinoline, quinazoline and naphthalene cores.

Chapleo *et al*. reported the synthesis of some phthalazinyl- and quinoxalinyl guanidines (**163**, **164**, **165** and **166**, Fig. 4.4.6), which were shown to display α-AR antagonist activity.[282]

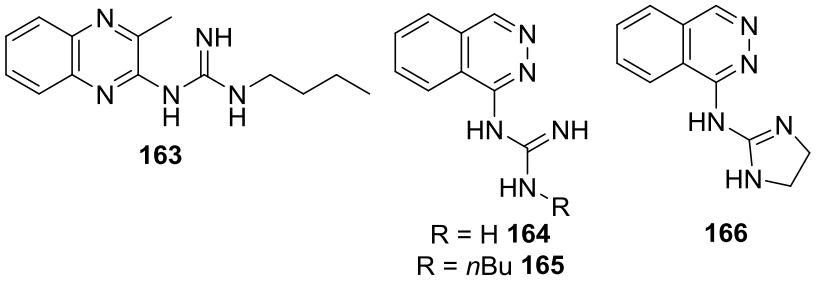

Figure 4.4.6. Structures of Chapleo *et al.* phthalazinyl- and quinoxalinyl guanidines α-AR antagonists.

These findings inspired the design of a family of quinolyl guanidines (see Fig. 4.4.7), which can be considered analogues of **22**, with structural modifications introduced to explore the impact of unsaturation and regioisomerism. The key variation within the family is the relative orientation of the heterocyclic N atom with respect to the guanidine moiety which will allow us probe the importance of planarity induced by IMHB interactions in potential α_2-AR ligands.[195]

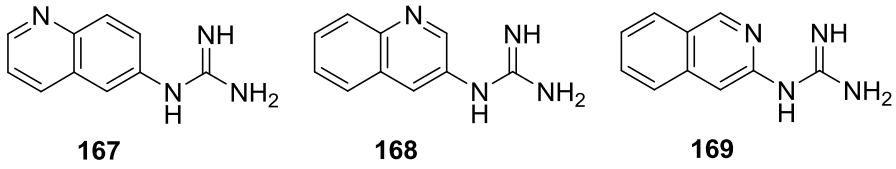

Figure 4.4.7. Structures of proposed quinolyl guanidine derivatives **167**-**169**.

The 2-quinolyl guanidine (**170**), quinoline analogue of **22**, has been intentionally excluded from this series as it has been reported to exhibit significant affinity for a range of other targets such as acid sensing ion channels (ASICs).[283,284]

The proposed synthesis devised for this family involved guanylation of the corresponding amino-quinolines or isoquinoline (**170**, **171** and **172**) with **85** in the presence of $HgCl_2$. The preparation of **169** had been previously reported utilizing this route and thus this approach was applied to synthesise of this family affording **173** and **156** in 70% and 82% yield, respectively (Scheme 4.4.5).[285,286] These compounds were characterised by HRMS, ^{1}H, ^{13}C NMR and melting point analysis which matched the data obtained for **156** that had been characterised earlier. **174** was obtained in a 60% yield, with HRMS and ^{1}H analysis matching the previously published characterisation data.[286]

Scheme 4.4.5. Synthesis of **156**, **173** and **174**.

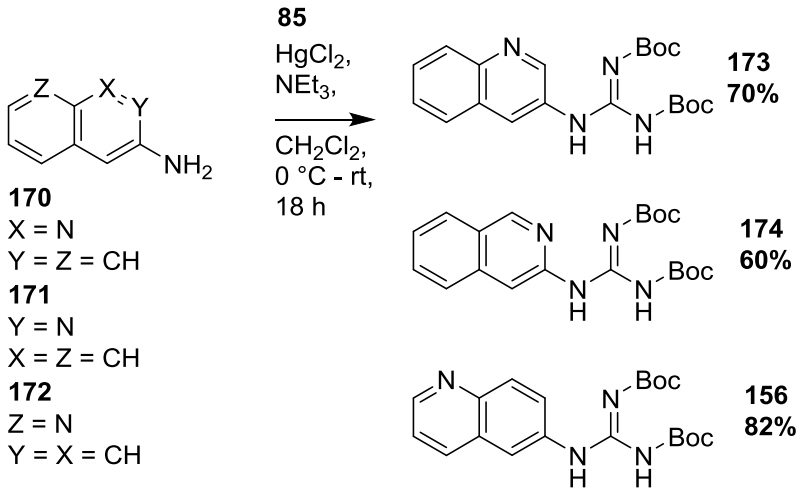

Deprotection of these derivatives using the previously employed TFA method, furnished the corresponding trifluoroacetate salts **167**, **168** and **169** in quantitative yield (Scheme 4.4.6).

Scheme 4.4.6. Deprotection of **173**, **174** and **156**.

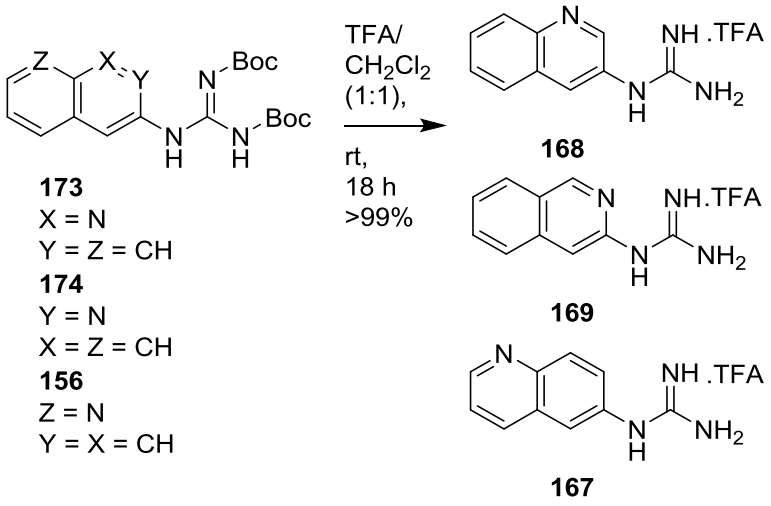

Full characterisation of **167** and **168** was conducted using ^{1}H, ^{19}F and ^{13}C NMR, HRMS, IR, melting point alongside HPLC analysis, which confirmed sufficient purity for pharmacological testing (>95%). Characterisation of **169** matched with previously published characterisation data.[286] These salts all proved to be highly water soluble and were subsequently submitted for pharmacological evaluation in human PFC tissue as trifluoroacetate salts.

4.5. Conclusions

All of the derivatives which have been successfully synthesised within this chapter have been confirmed by HPLC analysis to be of sufficient purity to process to testing (>95%) and are currently undergoing pharmacological evaluation in human PFC tissue to determine their affinity for α_2-ARs in collaboration with the pharmacological laboratory of Prof. Luis Callado at UPV/EHU and we are awaiting the results. The proposed derivatives which could not be prepared using the routes outlined above will be prepared utilizing alternative routes detailed in Chapter 5.

Chapter Five

Investigation and optimization of cyclic guanidine synthesis

5.1. Introduction

5.1.1. Aims and Rationale

A main aim of this work is to investigate the effects that structural variation has on the engagement of mono-aryl *lead* compounds with α_2-ARs, primarily focusing on α_2-AR affinity and activity. The specific structural modifications envisaged involve ring expansion of the 2-aminoimidazoline cationic moiety to a 2-amino-1,4,5,6-tetrahydropyrimidine moiety. A ring expanded series has been synthesised (Section 4.3.2) based upon a set of *hit* compounds identified during the screening process discussed in Chapter 3 (Fig. 5.1.1).

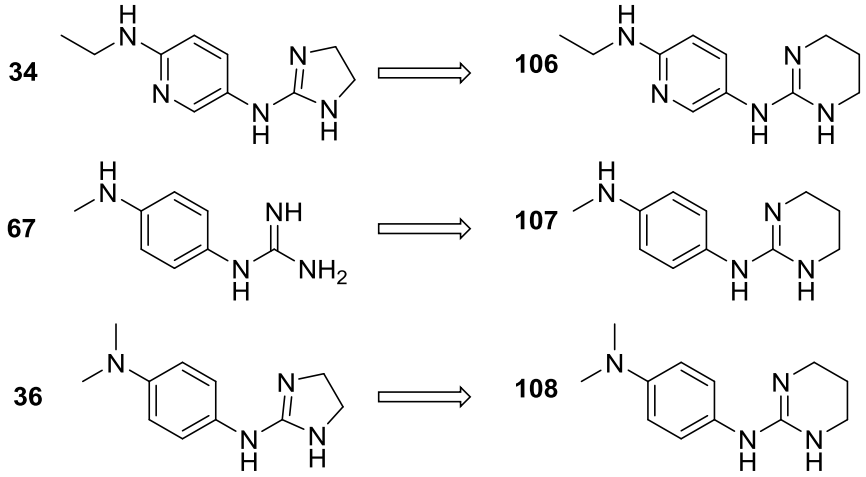

Figure 5.1.1. Structure of ring expanded series **106**, **107** and **108** synthesised in Chapter 4 based on *hit* compounds **34**, **67** and **36**.

Expanding upon this work we envisaged the preparation of a series of guanidine-like derivatives modified at the cyclic cationic moiety with the addition of substituents (R^2 and/or R^3) on the endocyclic N atoms (Figure 5.1.2). The rationale behind the proposed substituted derivatives stems from the SAR studies of α_2-AR mono-aryl *lead* compounds previously conducted within the Rozas group.[132,135,139]

Substitution of the guanidine moiety to 1,3-disubstituted guanidine derivatives and conformational restriction of the cationic moiety have been extensively investigated;[132,139,196] however, the addition of substituents on the endocyclic N atoms of 2-aminoimidazoline derivatives has not yet been explored.

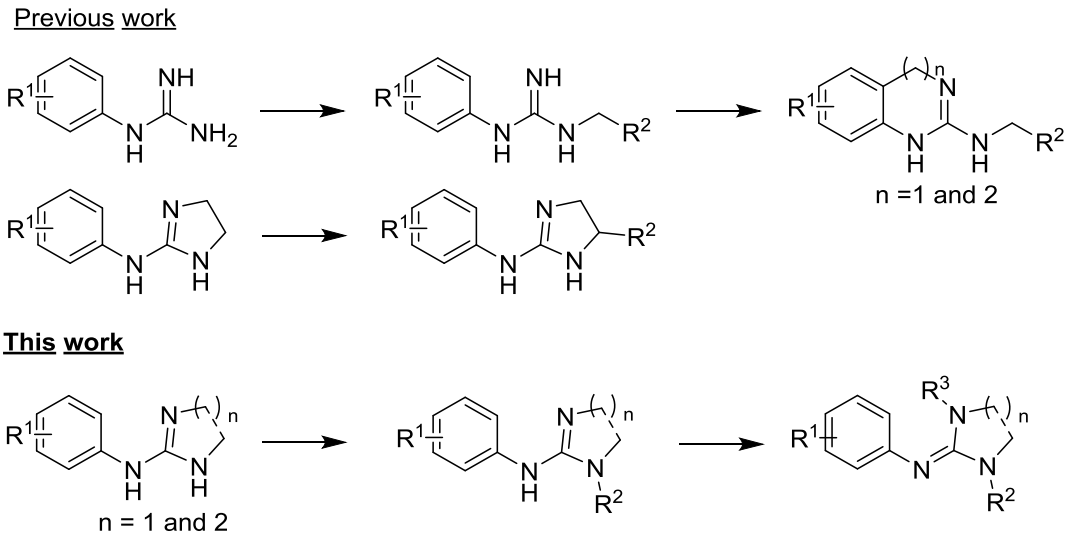

Figure 5.1.2. Previous work based on structural modification of mono-aryl *lead* compounds and outline of the proposed structures for this work.

Similar strategies have been reported in the literature during the optimization of ligands designed for other targets and proved successful. A series of SAR studies conducted by Dukat *et al.* utilized a similar approach which led to the discovery of **94**, a high affinity agonists at the 5-HT_3 receptor (K_i = 32 nM).[243] This investigation revealed that minor structural modifications of **94** were detrimental for 5-HT_3 affinity as the addition of a methyl substituent to give **175** reduced the affinity to 450 nM (Fig. 5.1.3). Additional substitution at the guanidine moiety (**176** and **177**) gave compounds which completely lacked affinity for the 5-HT_3 receptor (K_i > 10,000 nM).[243]

More recent studies by Dukat *et al.* focused on elucidating the most pharmacologically relevant conformations of aryl guanidines and led to the synthesis of conformationally-constrained analogues **178** and **93**, the only derivatives which retained affinity for the 5-HT_3 receptor (K_i = 725 nM and 34 nM, respectively).[241] These studies illustrate the dramatic effect that minor structural changes have on the affinities displayed by a series of structurally similar ligands for a given target.

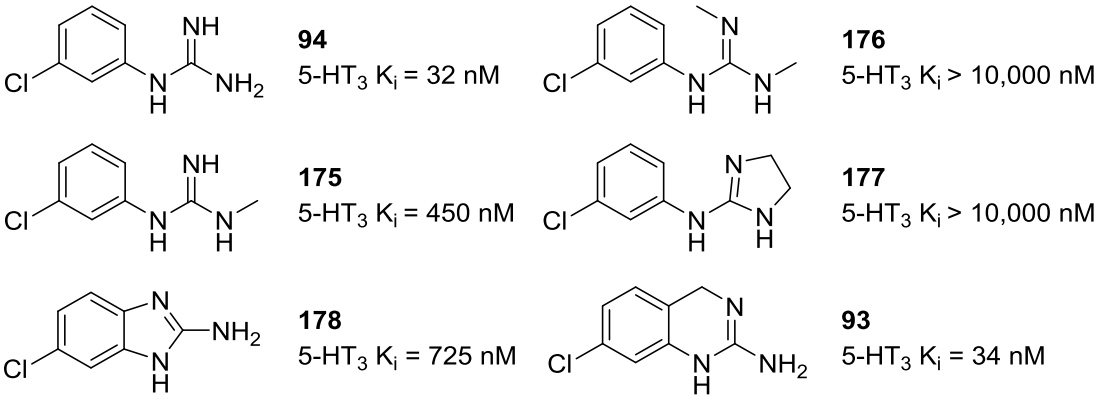

Figure 5.1.3. Structures of **94** and related analogues.

Investigation of the impact of substitution on the physiochemical and pharmacological properties of mono-aryl *lead* compounds will improve our understanding of the key ligand-receptor interactions that influence affinity, activity and subtype selectivity at the α_2-AR. The substituted derivatives proposed in this work will initially consist of small alkyl substituents (methyl/ethyl) to examine the effect of substitution on α_2-AR engagement with the potential for additional substituents to be investigated based on the pharmacological results to be obtained.

5.2. Synthesis of the proposed derivatives

Review of the literature discovered a series of reports outlining the design and synthesis of phenylthiourea based derivatives .[287,288] These probes are generally prepared by reacting an *N*-substituted-1,2-diamino ethane with phenyl isothiocyanate (**179**) to give an *N*-[2-(*N*-substituted)aminoethyl]-*N*'-phenylthiourea (such as **181**, Fig. 5.2.1) that undergo intramolecular guanylation upon detection of Hg^{2+} ions and form 1-substituted-2-phenylaminoimidazoline conjugates (such as **182**, Fig. 5.2.1) which exhibit altered fluorescent properties. A representative synthesis and intramolecular guanylation of the courmarin-thiourea conjugate (**181**) reported by Shiraishi *et al.* is shown in Scheme 5.2.1.[186]

Similarly, Sequeira Aguiar and coworkers have reported an efficient method for the synthesis of cyclic guanidinium salts by the potassium dichloroiodate ($KICl_2$) mediated desulfurization of 1,3-disubstituted thioureas.[289]

Scheme 5.2.1. Synthesis and intramolecular guanylation of the courmarin-thiourea conjugate reported by Shiraishi *et al.*.[186]

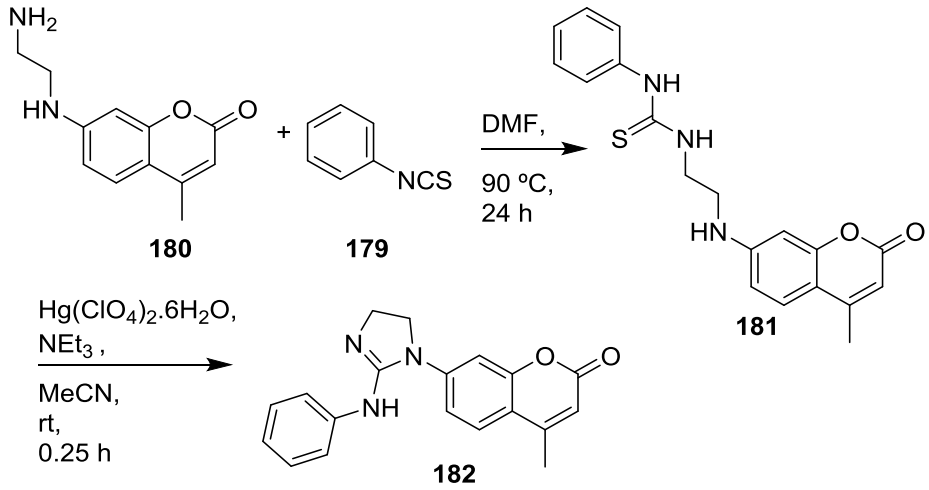

Carley *et al*. employed a different approach utilizing **179** to synthesise an intermediate 1,3-disubstituedthiourea (**185**) during the synthesis of a pyrrolidine based 1-substituted-2-arylamino-1,4,5,6-tetrahydropyrimidine organocatalyst (**183**).[290] A one-pot, two steps cascade involving sequential *S*-methylation (**186**), Boc deprotection (**187**) and base mediated intramolecular guanylation furnished the 1-substituted-2-phenylamino-1,4,5,6-tetrahydropyrimidine (**183**) as the hydroiodide salt in a 98% overall yield (Scheme 5.2.2).

Scheme 5.2.2. Synthesis of 1-substituted-2-phenylamino-1,4,5,6-tetrahydropyrimidines using **179**.[290]

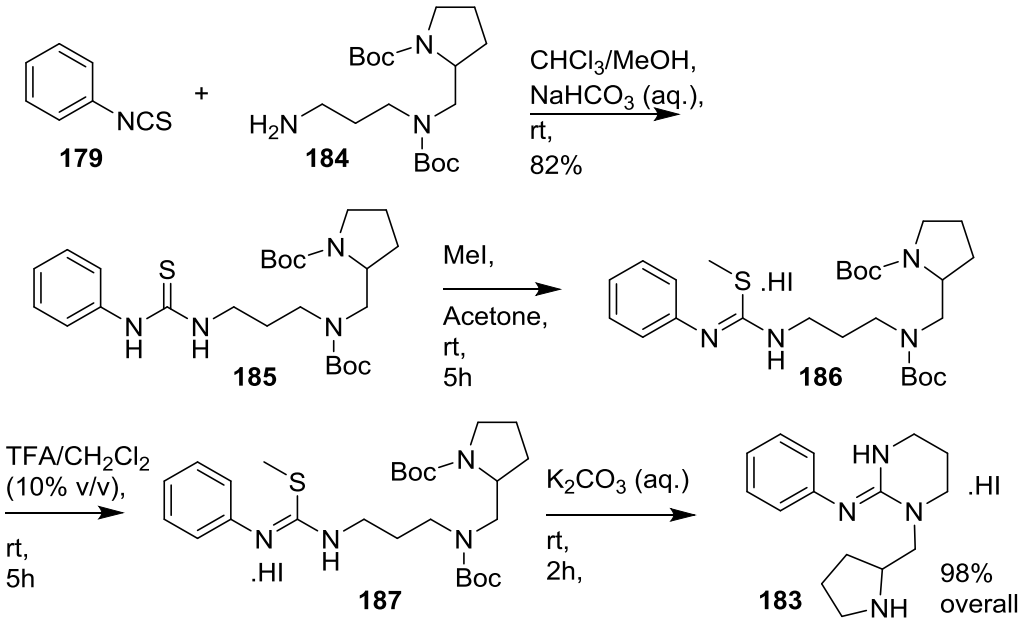

All these previous synthetic approaches inspired the design for the preparation of the proposed derivatives outlined in Figure 5.2.1. Thus, a related synthetic route will be investigated for the preparation and optimization of the proposed substituted cyclic guanidine derivatives. This route will initially focus on the preparation of derivatives based on **21**, one of the most extensively studied *lead* compound within the Rozas group.[140,196]

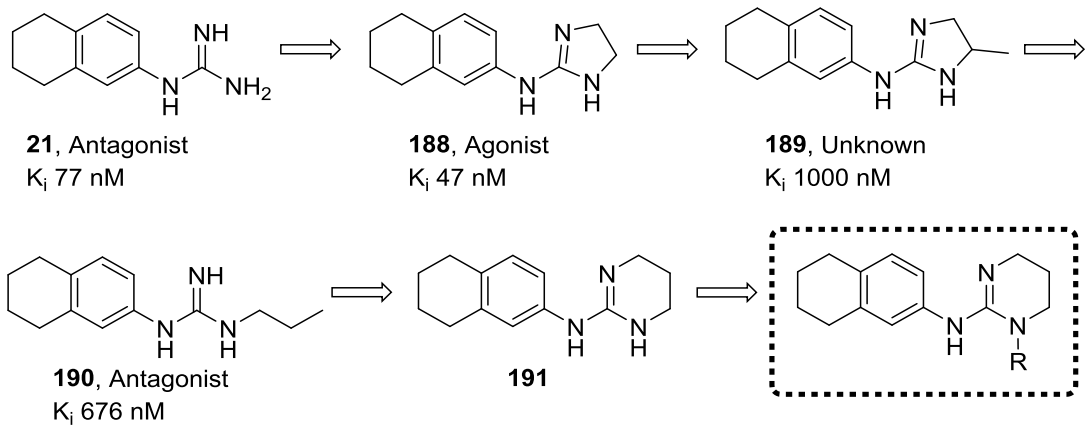

Figure 5.2.1. Structures of **21** and derivatives as rationale for the preparation of guanidine-like derivatives modified at the cyclic cationic moiety.

5.3. Investigation of alternative guanylation method

5.3.1. Synthesis of 2-arylamino-1,4,5,6-tetrahydropyrimidine derivatives

The issues encountered during the attempted synthesis of 2-arylamino-1,4,5,6-tetrahydropyrimidine derivatives such as **145** (section 4.3.3.) prompted the investigation of an alternative guanylating approach. The reaction of **134** with poorly nucleophilic amines such as **147** were hampered by the competing alkoxycarbonyl group transfer reaction which led to an inseparable mixture of products **145** and **150** (scheme 5.3.1).

Scheme 5.3.1. $HgCl_2$ mediated guanylation of **147** with **134**.

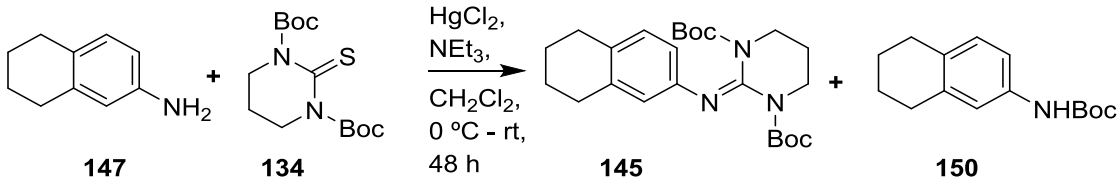

Therefore, an alternative derivative of **134** was prepared which could help to avoid the alkoxycarbonyl group transfer reaction and may also prove more reactive to guanylation with poorly nucleophilic amines. This reagent, the *N*,-Boc protected 2-(methylthio)hexahydropyrimidine (**192**) was prepared by methylation of **135** using methyl iodide which gave **193** as the hydroiodide salt in a 97% yield.[291] This was then Boc protected using Boc_2O and NEt_3 to afford **192** in an isolated yield of 58% (Scheme 5.3.2).

Scheme 5.3.2. Synthesis of **192** from **135**.

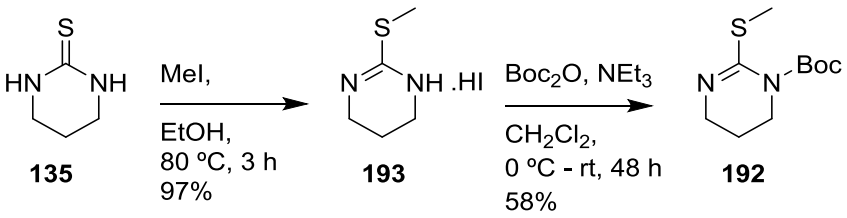

The guanylation reaction of **147** was then repeated using two equivalents of **192** instead of **134** (Scheme 5.3.3).

Scheme 5.3.3. $HgCl_2$ mediated guanidinylation of **147** with **192**.

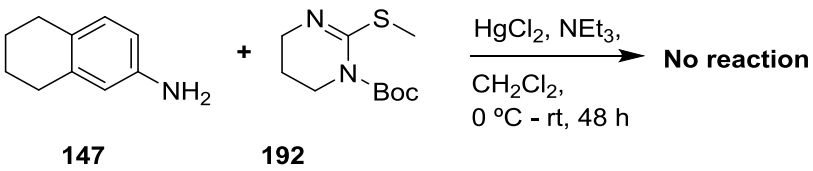

147 **192**

This approach proved unsuccessful with **192** displaying no reactivity towards **145** under mercury promoted guanylation conditions. As such further development of this route was abandoned and priority was diverted to the investigation of an alternative strategy toward the synthesis of 2-arylamino-1,4,5,6-tetrahydropyrimidine derivatives from poorly nucleophilic amines utilizing aryl isothiocyanates.

5.3.2. Utilization of aryl isothiocyanates to prepare cyclic guanidines

Aryl isothiocyanates are widely used in the synthesis of cyclic guanidine derivatives as discussed in section 3.3.2 for the preparation of 2-arylaminoimidazolines.[185] This approach can also be applied in an analogous fashion to the synthesis of 2-arylamino-1,4,5,6-tetrahydropyrimidine using 1,3-diaminopropane (**194**) instead of ethylene diamine (**195**) to give *N*-aryl-*N'*-(3-aminopropyl)thiourea derivatives (Scheme 5.3.4.A). This 1,3-disubstituted thiourea can be isolated or reacted *in situ* to form an intermediate carbodiimide by using an appropriate thiourea activating agent such as $HgCl_2$ (Scheme 5.3.4.B). The intermediate carbodiimide can then be trapped by an intramolecular cyclization reaction with the terminal amino group to furnish the 2-arylamino-1,4,5,6-tetrahydropyrimidine (Scheme 5.3.4.C).

One main advantage of this route is the modular nature of the reactants which facilitates the reaction of a range of substituted aryl isothiocyanates with a variety of different diamines which can be exploited in a combinatorial fashion to produce a diverse range of 2-arylamino-1,4,5,6-tetrahydropyrimidines from common starting materials.

Scheme 5.3.4. General route to 2-arylamino-1,4,5,6-tetrahydropyrimidine using **194** and aryl isothiocyanates.

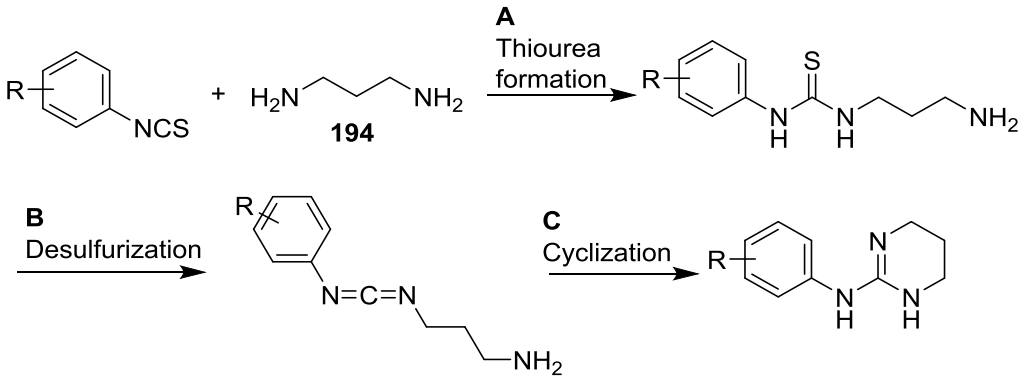

The reactions require two components to form 1,3-disubstituted thioureas, appropriately substituted aryl isothiocyanates (which must be prepared) and the corresponding diamines.

5.3.3. Preparation of 1,3-disubstituted thioureas using phenylisothiocyanate

First, the use of **179** was investigated as a model substrate to help identify optimal reaction conditions. Therefore, **179** was added to solutions of both **194** and **195** in CH_2Cl_2, in the presence of NEt_3, which after recrystallization gave *N*-(3-aminopropyl)-*N*'-phenylthiourea **196** (29%) and *N*-(2-aminoethyl)-*N*'-phenylthiourea **197** (46%), respectively (Scheme 5.3.5).[292]

Scheme 5.3.5. Reaction of **179** with **195** and **194**.

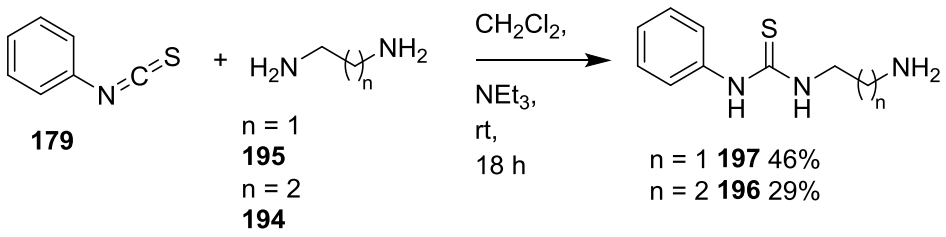

With the required thioureas in hand, the next step was to select a desulfurization strategy. A range of reagents have been reported to facilitate the desulfurization of 1,3-disubstituted thioureas including triphenylphosphine with iodine in the presence of triethylamine ($Ph_3P/I_2/NEt_3$),[293] $KICl_2$,[289] *o*-iodoxybenzoic acid (IBX)/NEt_3,[294] BOP/DBU,[295] cyanuric chloride,[296] and $Hg(OAc)_2/HgCl_2/NEt_3$.[297] Each of these methods has associated advantages and disadvantages including low yields, laborious isolation procedures or the use of toxic or expensive reagents. Therefore, two of these methods (IBX/NEt_3 in MeCN and $HgCl_2/NEt_3$) were explored for the sequential desulfurization and intramolecular cyclisation/guanylation of **197** (Scheme 5.3.6). This thiourea was utilized as a model substrate as the desired product (2-phenylaminoimidazoline, **198**) is a widely reported and known product with previously published characterisation data that facilitates rapid identification.

Scheme 5.3.6. Test reaction of **197** desulfurization/cyclization using two different methods; A. IBX/NEt_3. [298] B. $HgCl_2/NEt_3$.

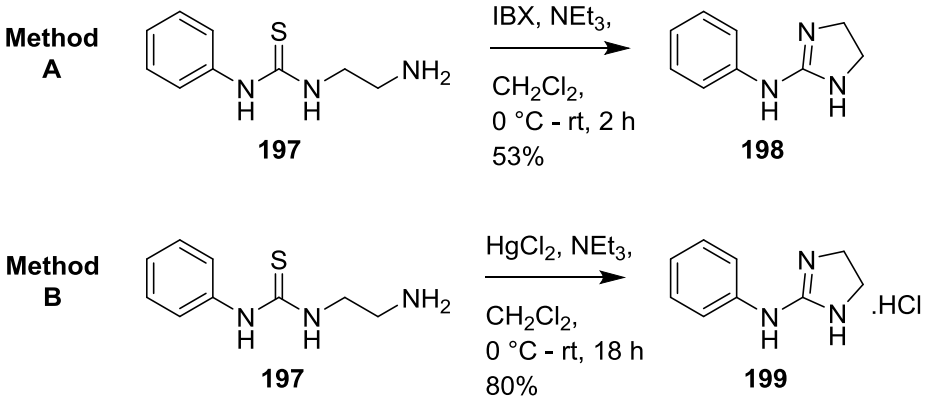

The results obtained from these test reactions indicated that both desulfurization methodologies were effective and furnish the desired product. The principal differences between them is that method A provides the 2-phenylaminoimidazoline free base which must be isolated by flash column chromatography and subsequently protonated, whereas method B produces the 2-phenylaminoimidazolinium hydrochloride salt (**199**) directly which allows for rapid isolation and purification using an aqueous workup and recrystallization.

The direct formation of the cyclic guanidine hydrochloride salt is advantageous for the purposes of this work as the compounds are typically more water soluble in this salt form which facilitates pharmacological testing. Therefore, method B was chosen as the most suitable desulfurization methodology and was applied in the conversion of 1, 3-disubstituted thioureas to their corresponding cyclic guanidines derivatives.

Since there are a variety of commercially available alkyl diamines (including the diamines required for the preparation of the proposed 1,3-disubstituted thioureas) this component did not need to be synthesised. Then, the next step was to prepare the corresponding aryl isothiocyanates required for the synthesis of proposed 1,3-disubstituted thioureas.

5.3.4. Preparation of aryl isothiocyanates

Numerous synthetic methods have been developed to convert amines into the corresponding aryl isothiocyanate analogue, most commonly using triphosgene. This highly toxic reagent poses significant risk and is often incompatible with many functional groups which strongly hinders its utility.[299]

An alternative two step approach requires initial conversion of the amine to a dithiocarbamic acid salt by treatment with carbon disulfide (CS_2) in the presence of NEt_3. This is then followed by a reagent-promoted desulfurization of dithiocarbamic acid salts into the corresponding isothiocyanates (Scheme 5.3.7). Common reagents used for the desulfurization of dithiocarbamic acid salts include I_2/sodium bicarbonate,[300] copper(II) sulfate hexahydrate,[301] triphosgene,[302] and Boc_2O.[303]

Scheme 5.3.7. Method for the conversion of amines to isothiocyanates.

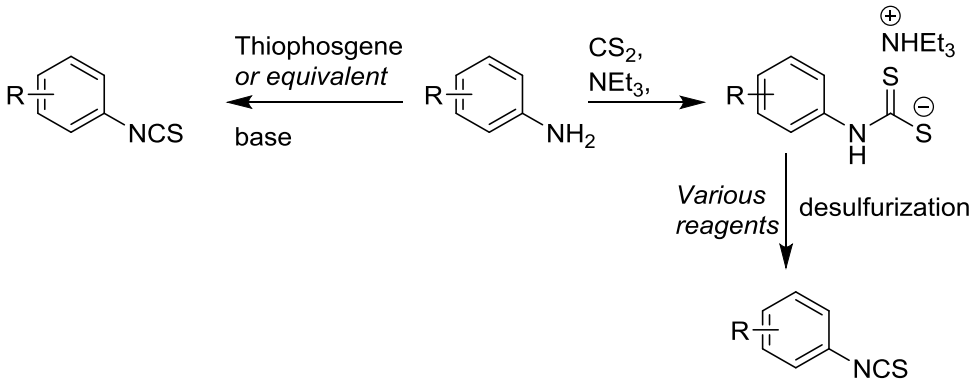

The synthesis of dithiocarbamic acid salts from aryl amines can be difficult as if the amines are poorly nucleophilic this often requires extended reaction times and use of excess reagents (CS_2 and NEt_3).[299] As such, a selection of these methods was screened for the preparation of **200** from **147**. The procedures reported for each desulfurization reagent (triphosgene and Boc_2O) were followed and both methods, which employed a one-pot, two-step cascade reaction, yielded the **200** in 59% and 87% yields, respectively (Scheme 5.3.8).[300,303]

Scheme 5.3.8. Methods employed in the synthesis of **200** from **147**.[302,303]

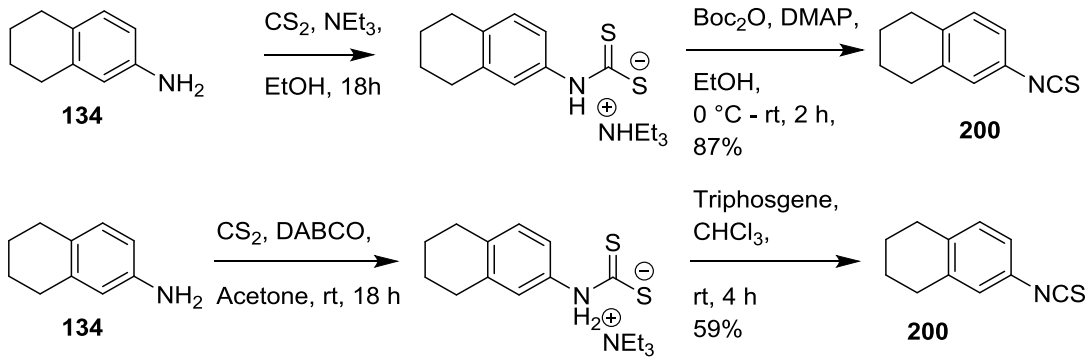

A third method which utilized direct reaction of **147** with the 'thiocarbonyl transfer' reagent 1,1′-thiocarbonyldiimidazole (**201**) was found to be the most efficient (and less dangerous) as it furnished **200** in an excellent yield of 93% (Scheme 5.3.8).[304]

Scheme 5.3.8. Synthesis of **200** using **201**.

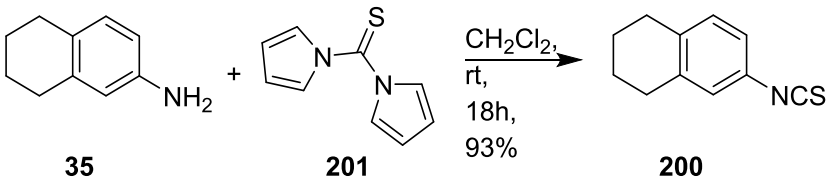

This approach proved to be the most general and efficient one-pot protocol using very mild conditions and was employed in the preparation of all the proposed aryl isothiocyanates from their corresponding anilines (Fig. 5.3.1).

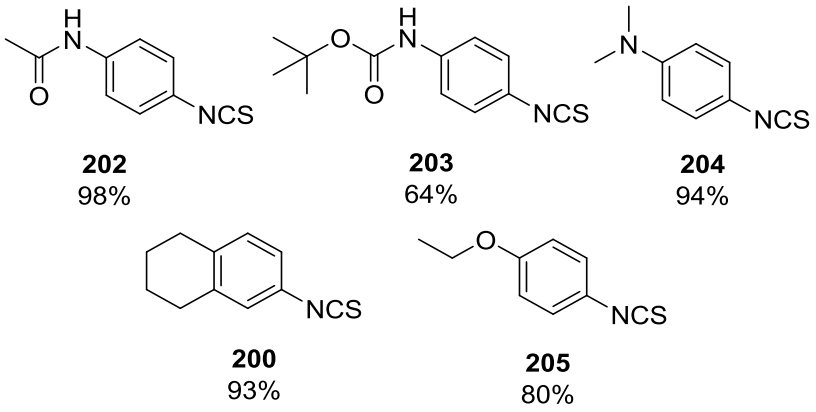

Figure 5.3.1. Series of proposed aryl isothiocyanates prepared from reaction of the corresponding amines with **201**.

The isothiocyanate **206** could not be prepared by this approach; alternatively, it was prepared following a method reported by Nakamura *et al.*, which involved the reaction **148** with tetramethylthiuram disulfide (**207**) in ethanol, heating under reflux to form an intermediate *N*,*N*-dimethyl-*N'*-aryl thiourea (**208**) that was then converted *in situ* to **206** (in a 40% yield) by the addition of HCl (Scheme 5.3.9).[305]

Scheme 5.3.9. Synthesis of **206** from **148** with **207**.

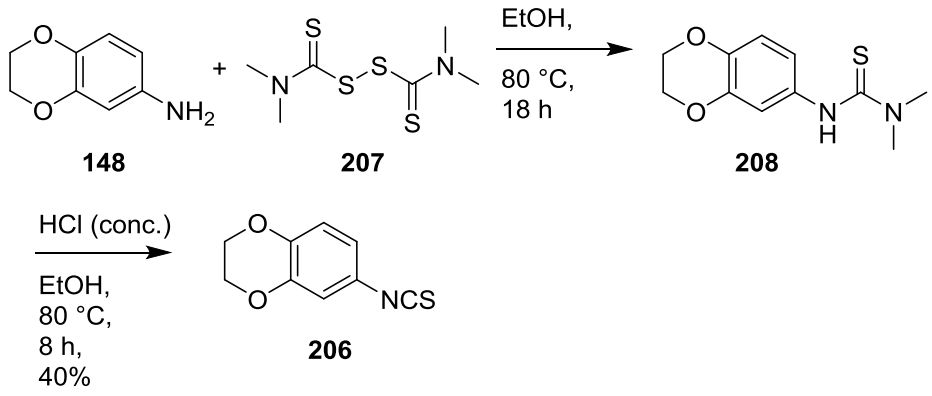

A general and efficient protocol for the preparation of required isothiocyanates was identified and was used to synthesise these material in sufficient quantify. The next step involved reacting this isothiocyanates with the corresponding diamines in order to prepare the 1, 3-disubstituted thiourea intermediates.

5.3.5. Synthesis of diamine-derived 1, 3-disubstituted thioureas

The first derivative to be prepared utilizing the isothiocyanate method was **209**. This involved the synthesis of the intermediate diamine-derived 1,3-disubstituted thiourea **210** from **200** and **194** in a 53% yield (Scheme 5.3.10). The sequential desulfurization and intramolecular guanylation of **210** was effected using $HgCl_2$ and NEt_3 in CH_2Cl_2 to furnish the cyclic guanidinium hydrochloride salt **209**. Purification of this material proved challenging as it had limited solubility in water which prevents the previously employed aqueous extraction/crystallization method.

Instead, the crude reaction mixture was basified to pH 14 using NaOH (1M aq.) followed by extraction with diethyl ether (Et_2O) to isolate the free base cyclic guanidine which was subsequently protonated using a solution of HCl in Et_2O (1.25 M) to give **209** in an 80% yield.

Scheme 5.3.10. Synthesis of **210** from **200** and **194**.

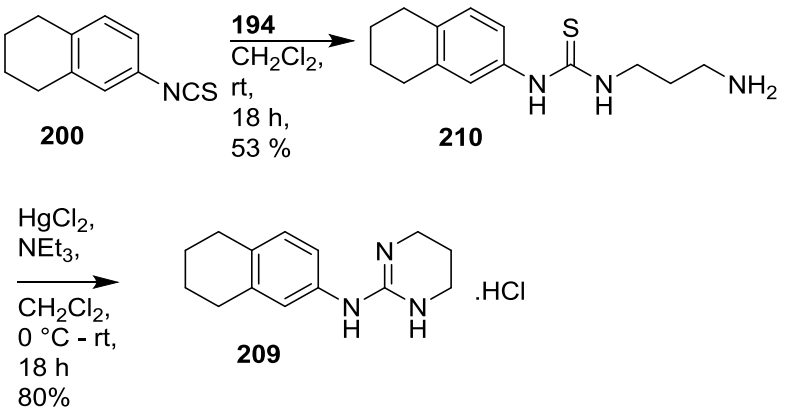

These conditions were then applied utilizing the various isothiocyanates prepared in section 5.3.4. These reactions employed *tert*-Butyl *N*-(3-aminopropyl) carbamate (**211**) inspired by the route reported by Carley *et al.* This alterative diamine component would eliminate the use of excess **194** and may also serve to reduce the polarity of the corresponding 1,3-disubstituted thioureas facilitating more straightforward purification. The reaction of **211** with **205** and **203** afforded the corresponding thioureas **212** and **213** in 77% and 41% yields, respectively (Scheme 5.3.11).

Scheme 5.3.11. Synthesis of **212** and **213** from the reaction of **211** with **205** and **203** respectively.

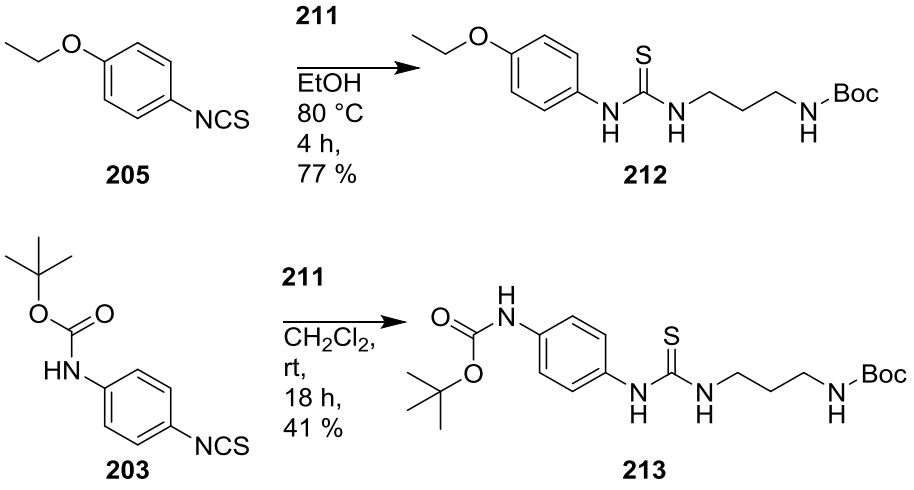

These 1, 3-disubstituted thiourea derivatives were subject to standard guanylation conditions ($HgCl_2$ and NEt_3 in CH_2Cl_2) to investigate whether the intramolecular reaction would be possible with these protected derivatives (Scheme 5.3.12). Even though the thiourea precursors were consumed, the attempted isolation of the resulting product led to degradation. It was surmised that the $HgCl_2$ mediated desulfurization occurred with consumption of the thiourea and generation of the carbodimide intermediate; however, the Boc-protected terminal amine was insufficiently nucleophilic for the intramolecular guanylation to occur. Attempted isolation of the observed product, likely the carbodiimide intermediate, resulted in degradation probably due to the instability of these highly reactive intermediates. The desired mono-Boc protected products of this reaction would be expected to be stable to chromatographic purification as related acyclic derivatives previously prepared in the Rozas group were successfully isolated using column chromatography.[188]

Scheme 5.3.12. Test desulfurization/cyclization reactions of **212** and **213** using $HgCl_2/NEt_3$.

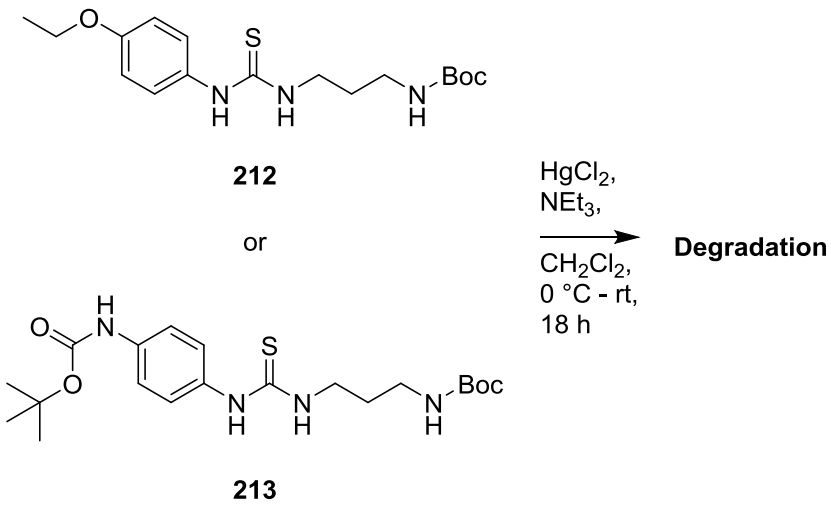

Boc deprotection of both **212** and **213** was also attempted using TFA in CH_2Cl_2 (10%, v/v) as reported by Carley *et al.*[290] Unfortunately, the resulting trifluoroacetate salts proved to be highly water soluble and attempts to isolate them using a basic workup also resulted in degradation and loss of material. Therefore, this approach was deemed unsuitable and further development halted. The remaining derivative was prepared by the previously successful route without the use of protected diamines.

5.4. Synthesis of substituted cyclic guanidines using *N*-substituted diamines

Preparation of the substituted derivatives was first investigated by reacting **179** with commercially available *N*-substituted 1,3-diaminopropanes and 1,2-diaminoethanes (Scheme 5.4.1). This procedure was optimized to eliminate the use of NEt_3 and facilitate isolation by recrystallization. This procedure involved the dropwise addition of a solution of **179** in CH_2Cl_2 to a concentrated solution of the corresponding diamine followed by stirring overnight at room temperature. The resulting reaction mixture was then concentrated *in vacuo* and recrystallized from excess Et_2O to afford the corresponding 1,3-disubstituted thiourea.

This route was successfully utilized in the preparation of a series of novel 1,3-disubstituted thioureas (**218**, **219**, **220** and **221**) in a range of isolated yields (34-56%) after recrystallization (Scheme 5.4.1) and each compound was fully characterised by ^{1}H and ^{13}C NMR, HRMS, IR and melting point analysis.

Scheme 5.4.1. Reaction of **179** with *N*-substituted 1,2-diaminoethanes and 1,3-diaminopropanes.

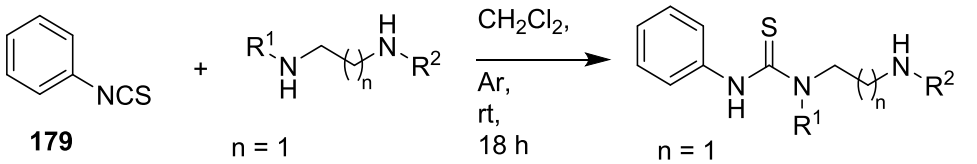

n = 1
214 R^1 = Me R^2 = H
215 R^1 = R^2 = Me
n = 2
216 R^1 = Me R^2 = H
217 R^1 = R^2 = Me

n = 1
218 R^1 = Me R^2 = H (47%)
219 R^1 = R^2 = Me (56%)
n = 2
220 R^1 = Me R^2 = H (53%)
221 R^1 = R^2 = Me (37%)

The sequential desulfurization and intramolecular guanylation of these derivatives was effected using $HgCl_2$ and NEt_3 in CH_2Cl_2 to furnish the corresponding cyclic guanidine products (Scheme 5.4.2).

Scheme 5.4.2. Intramolecular guanylation of *N*-substituted 1,3-disubstituted thioureas (**218**, **219**, **220** and **221**) to give cyclic guanidines (**222**, **223**, **224** and **225**).

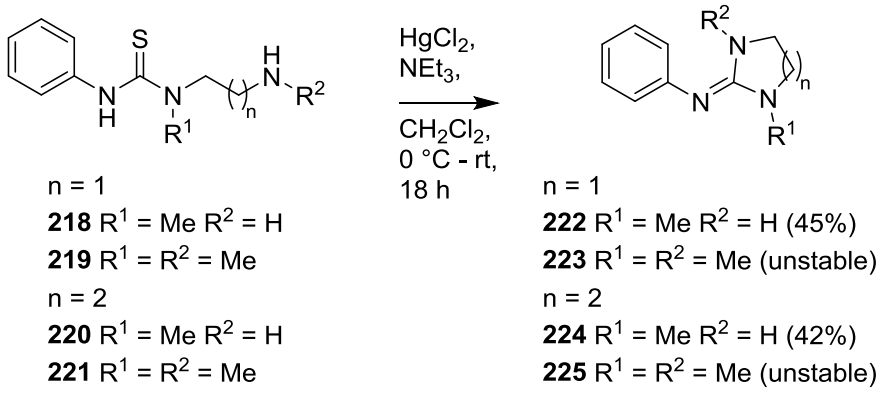

Purification of these cyclic derivatives was not straightforward due to their poor aqueous solubility. Therefore, the crude reaction mixture was basified and free-base cyclic guanidine derivatives were isolated by extraction with Et_2O. Unfortunately, this isolation procedure led to degradation of **223** and **225** which appeared to be unstable under basic conditions. The molecular ion (M+H) for both of these products were identified by HRMS which suggested the intramolecular guanylation had occurred; however, NMR analysis showed each had appeared to degrade into a complex mixture after workup.

This raised concerns about potential instability of proposed the *N*-*N'*-di-substituted cyclic derivatives. Compounds **222** and **225** were successfully isolated and fully characterised by ^{1}H and ^{13}C NMR, HRMS and IR analysis. These derivatives were stored as free-bases and will be converted to the hydrochloride salts using a solution of HCl in Et_2O (1.25 M) prior to submission for their pharmacological evaluation.

This optimized procedure was shown to be partly successful in the synthesis of this series of phenyl substituted cyclic guanidines. Therefore it was investigated further and applied to the preparation of the proposed **147** 2-arylamino-1,4,5,6-tetrahydropyrimidine derivatives (Scheme 5.4.3.).

Scheme 5.4.3. Reaction of **200** with *N*-substituted 1,3-diaminopropanes **220**, **221** and **226**.

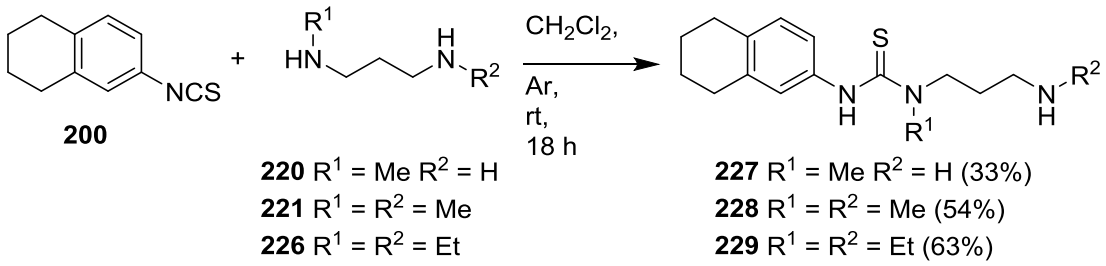

However, in this case it was not possible to isolate the 1,3-disubstituted thioureas by recrystallization as with previous derivatives and, hence, column chromatography was required to purify these thioureas yielding **227**, **228** and **229** in 33%, 54% and 63%, respectively. This procedure was also applied to the synthesis of 2-arylamino-1,4,5,6-tetrahydropyrimidine derivatives using **202** as the starting isothiocyanate (Scheme 5.4.4).

Scheme 5.4.4. Reaction of **202** with *N*-substituted 1,3-diaminopropanes **220**, **221** and **226**.

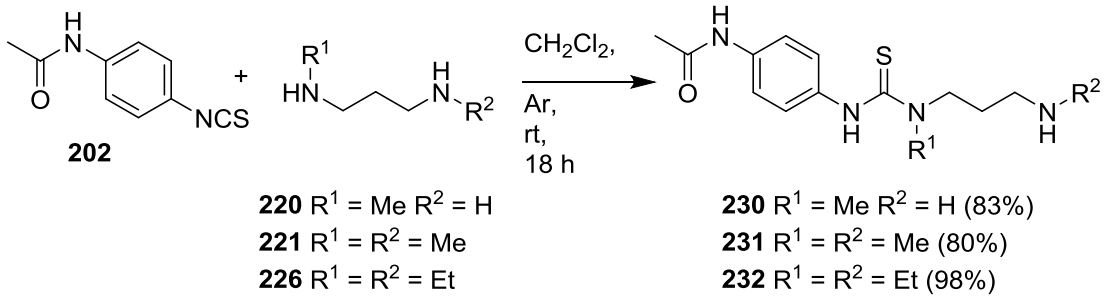

This approach afforded **230**, **231** and **232** in yields of 83%, 80% and 98%, respectively. Each of these intermediates was characterised by ^{1}H and ^{13}C NMR, HRMS and IR analysis. In order to investigate the stability of these *N*-*N'*-di-substituted cyclic derivatives, two representative diamine-derived thioureas (**229** and **231**) from each series were subject to intramolecular guanylation using $HgCl_2$ and NEt_3 in CH_2Cl_2 to yield the cyclic guanidine products **234** and **235** as hydrochloride salts in 37% and 68%, respectively (Scheme 5.4.5).

Isolation and purification of these derivatives utilized flash column chromatography on neutral alumina instead of the basic workup previously employed. The successful isolation of these products would suggest *N-N'*-di-substituted cyclic derivatives are unstable to aqueous base. Different analytical tools such as ^{1}H and ^{13}C NMR, HRMS, IR, melting point and HPLC analysis were used to characterise each of these derivatives and assess their purity. The remaining derivatives will undergo intramolecular guanylation and purification by flash column chromatography on neutral alumina immediately prior to submission for pharmacological analysis to avoid decomposition of these potentially labile salts during storage.

Scheme 5.4.5. Intramolecular guanylation of **229** and **231** to furnish 2-arylamino-1,4,5,6-tetrahydropyrimidine hydrochloride salts **234** and **235**.

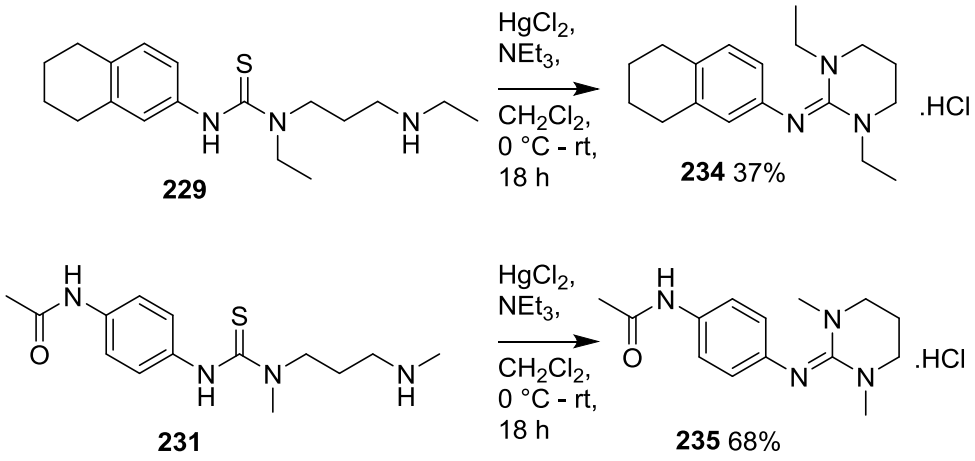

5.5. Conclusion

An alternative guanylating reagent **134** which was envisaged for the preparation of 2-arylamino-1,4,5,6-tetrahydropyrimidines was synthesised; however, it proved unreactive under standard guanylation conditions ($HgCl_2$ and NEt_3 in CH_2Cl_2). The development and optimization of an alternative synthetic route utilising aryl isothiocyanates (derived from their corresponding amines) towards the preparation of substituted and unsubstituted 2-arylamino-1,4,5,6-tetrahydropyrimidines and 2-aminoimidazolines was accomplished.

A general and efficient protocol was identified and applied to the preparation of the proposed isothiocyanates. These isothiocyanates were then successfully utilized in the synthesis of a range of novel diamine-derived 1,3-disubstitued thioureas.

This route proved to be a viable alternative which allowed for the preparation of **209**, which is currently undergoing pharmacological evaluation together with the other unsubstituted 2-arylamino-1,4,5,6-tetrahydropyrimidine derivatives described in section 4.4.3. The rest of the 1,3-disubstitued thioureas prepared will undergo intramolecular guanylation using the established method prior to submission for pharmacological testing.

Chapter Six

Synthesis and pharmacological evaluation of acridine-9-carboxamides

6.1. Introduction

A number of novel α_2-AR antagonists, which exhibit high and selective affinity for α_{2C}-AR, have recently been investigated as therapeutic agents for psychiatric and neurological disorders such as 4-(6,7-dimethoxy-1,2,3,4-tetrahydroisoquinolin-2-yl)methyl-2-aryl-7-methoxy-benzofuran (MBF, **236**); α_{2C}-AR K_i = 20 nM, α_{2A}-AR K_i = 1700 nM, α_{2B}-AR K_i = 750 nM) and acridin-9-yl-[4-(4-methylpiperazin-1-yl)phenyl]amine (JP-1302, **17**); α_{2C}-AR K_i = 28 nM, α_{2A}-AR K_i = 3500 nM α_{2B}-AR K_i = 1500 nM and α_{2D}-AR K_i = 1700 nM) (Fig. 6.1.1). These compounds have been evaluated in vivo and have been shown to exhibit antidepressant and antipsychotic effects.[122,123,306]

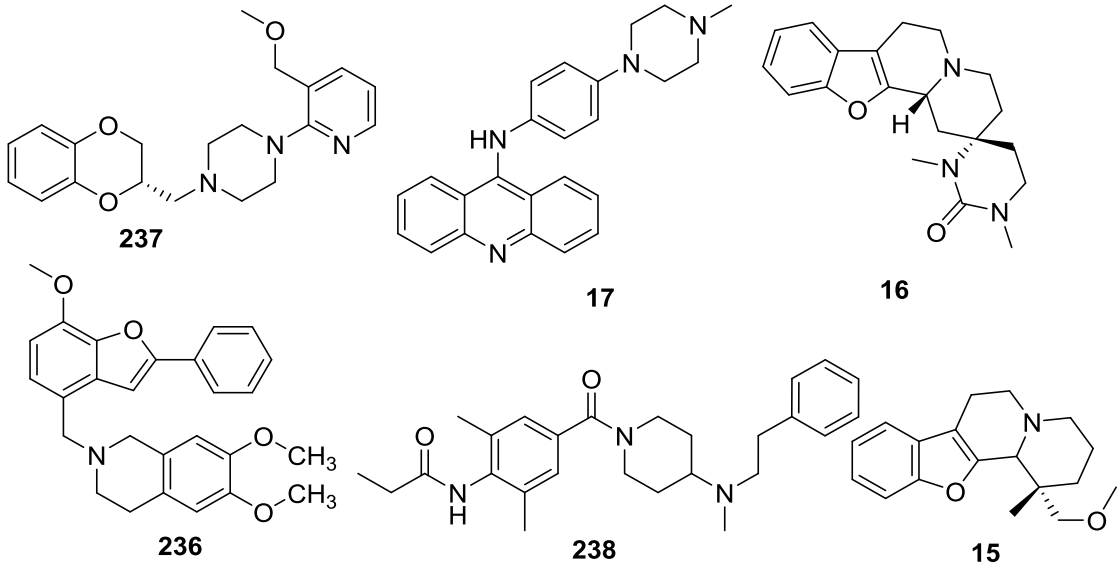

Figure 6.1.1. Structures of α_{2C}-AR selective antagonists **237**, **15**, **238**, **17**, **16** and **236**.

Compounds ORM-13070 (**237**) and **15** (Fig. 6.1.1), both developed and manufactured by Orion Pharma (Orion Corporation, Finland), are also highly selective α_{2C}-AR antagonists under investigation for promising therapeutic applications.[120,307] Moreover, OPC-28326 (**238**, Fig. 6.1.1) which was initially reported as a femoral vasodilator, was later found to act as a selective antagonist at the α_{2C}-AR (α_{2C}-AR K_i = 55 nM, α_{2A}-AR K_i = 2040 nM and α_{2B}-AR K_i = 285 nM).[308–310]

A study was conducted by Kawamura *et al.* to evaluate the in vivo brain penetration of **17** and **236** in mice and their potential influence on efflux transporters such as P-glycoprotein (P-gp) and breast cancer resistance protein (BCRP).[311,312] This study required PET tracer analogues of **17** and **236**, which were synthesized by ^{11}C-methylation of their desmethylated precursors using either ^{11}C-methyl triflate or ^{11}C-methyl iodide and *tetra*-butylammonium hydroxide (TBAOH) respectively (Scheme 6.1.1).

Despite showing high α_{2C}-AR selectivity, **[^{11}C]-236** and **[^{11}C]-17** proved inadequate as PET probes in mice for evaluation of brain α_{2C}-AR function as they either do not readily enter the brain or are rapidly expelled from the CNS by drug efflux transporters. P-gp and BCRP were shown to be responsible as there was an increase of brain radioactivity levels in P-gp/BCRP knock-out mice after injection of **[^{11}C]-236** and **[^{11}C]-17** compared to wild-type mice.[312] Furthermore, **[^{11}C]-17** was shown to bind non-specifically and irreversibly throughout the brains of P-gp/BCRP knock-out mice, confirming that it is inadequate for use as a PET probe in the study α_{2C}-AR brain function[312]

A PET tracer analogue of **237** was also developed utilizing ^{11}C-methylation of *O*-desmethyl **237** using ^{11}C-methyl triflate (Scheme 6.1.1).[311] This compound (**[^{11}C]-237**) was then validated as a highly selective PET ligand for α_{2C}-ARs in vivo imaging through animal studies which evaluated its utility in the brains of rats and knock-out mice.[311] Extensive investigation was carried out to validate the use of **[^{11}C]-237** in humans, involving examination of radiometabolism, pharmacokinetics, whole-body distribution and radiation dose in healthy men with promising results.[313]

This study not only proved that **[^{11}C]-237** was suitable to monitor α_{2C}-AR occupancy in the human brain, but also uncovered its potential as a tool to monitor changes in the extracellular (synaptic) concentration of endogenous NA.[314]

Scheme 6.1.1. Radiosynthesis of ^{11}C-labeled **237**, **17** and **236** from the corresponding desmethyl precursors.

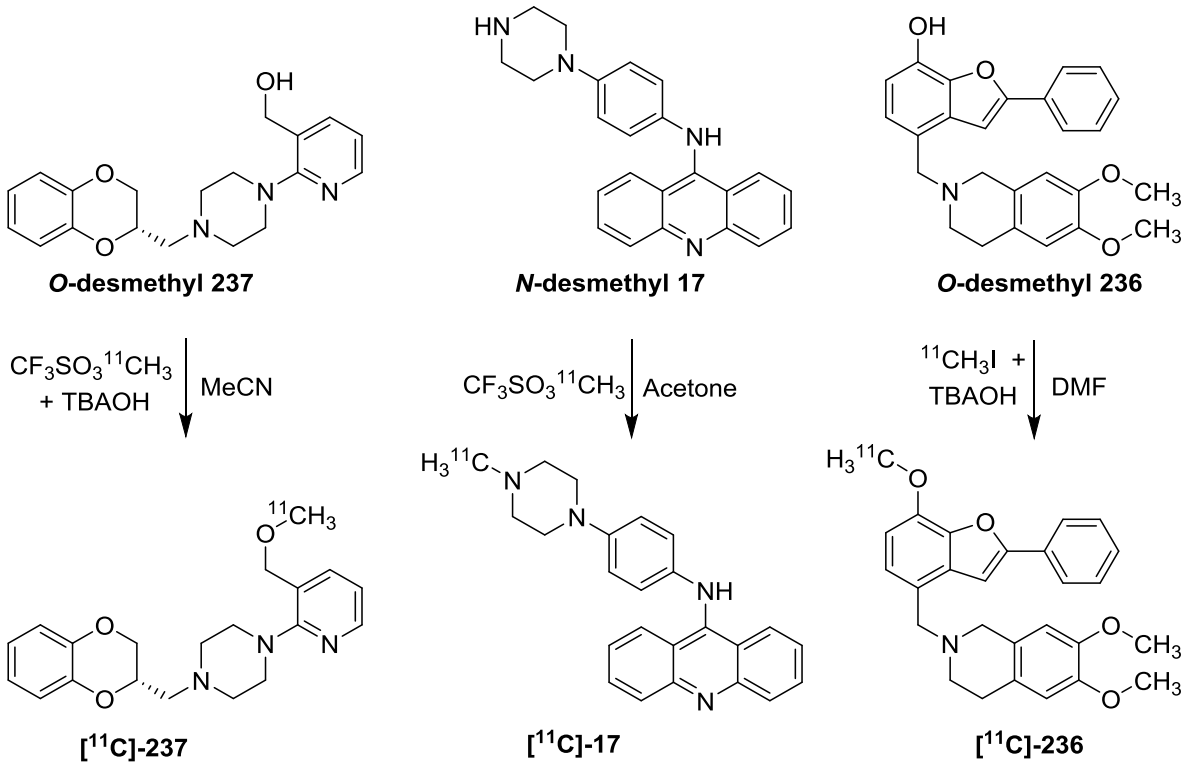

This PET study provided experimental support for the suitability of **[^{11}C]-237** for in vivo imaging of noradrenergic transmission in the human brain, highlights the enormous utility of this compound as a tool to detect whether novel or existing CNS drugs elevate synaptic NA levels in vivo in humans. This will also aid the investigation of neurological and psychiatric conditions, such as MDD and SZ, which involve noradrenergic disturbances by means of PET experiments.[315–317]

Silver *et al.* conducted an extensive SAR study of **17**, which was initially discovered as one of two hit compounds alongside the *N*-ethyl analogue **239**, in a high-throughput screening campaign (Fig. 6.1.2).[318] Each of these hit compounds displayed both significant subtype selectivity (50-100 fold) and excellent affinity for the α_{2C}-AR (K_i = 28 and 37 nM, respectively); however, it was suggested that these acridine-based structures (a well-known class of DNA intercalators) may also exhibit genotoxic properties.

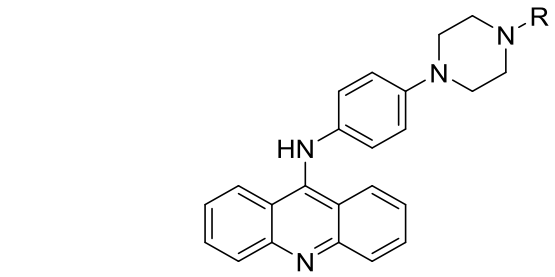

R = Me **17**
α_{2C}-AR K_i = 28 ± 2 nM
α_{2A}-AR K_i = 3200 ± 100 nM

R = Et **239**
α_{2C}-AR K_i = 37 ± 5 nM
α_{2A}-AR K_i = 3600 ± 300 nM

Figure 6.1.2. Structures of hit compounds **17** and **239**.

This concern was well founded as **17** was found to exhibit mutagenic activity in the Ames test. This test is a bacterial reverse mutation assay which measures mutagenicity of chemical compounds on DNA, based on the principle of reverse mutation in a variety of mutated bacterial strains such as *Salmonella* and *Escherichia coli*.[319]

The replacement of the acridine core was prioritised and inspired the synthesis of derivatives of **17** based on substituted 4-aminoquinoline, tetrahydroquinoline (**240**, α_{2C}-AR K_i = 110 ± 10 nM) and 3,5-lutidine cores (**241**) (Fig. 6.1.3). Unsubstituted 4-aminoquinoline derivatives (**242**, α_{2C}-AR K_i = 1700 ± 600 nM) and **241** (α_{2C}-AR K_i > 5000 nM) led to a complete loss of subtype selectivity; however, introduction of small alkyl substituents in the 2- and 3-positions (R^1 = R^2 = Me, **243** and R^1 = Me, R^2 = Et, **244**) restored the same high and selective affinity for the α_{2C}-AR (α_{2C}-AR K_i = 35 ± 3 nM and α_{2C}-AR K_i = 25 ± 3 nM, respectively) as the acridine hit compounds (Fig. 6.1.3).

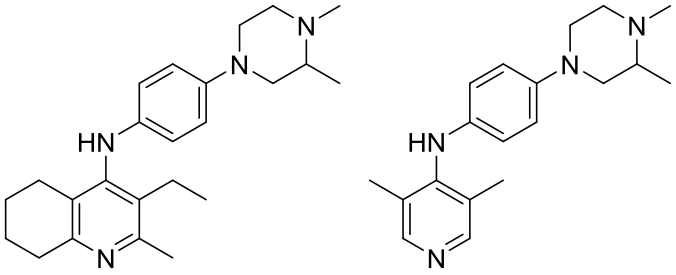

240
α_{2C}-AR K_i = 110 ± 10 nM
α_{2A}-AR K_i = 630 ± 125 nM

241
α_{2C}-AR K_i > 5000 nM
α_{2A}-AR K_i = 3600 ± 100 nM

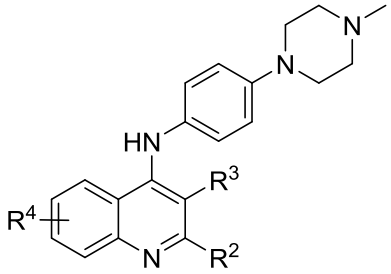

R^2=R^3=R^4= H **242**
α_{2C}-AR K_i = 1700 ± 6000 nM
α_{2A}-AR K_i = 720 ± 60 nM

R^2=R^3= Me, R^4=H **243**
α_{2C}-AR K_i = 35 ± 3 nM
α_{2A}-AR K_i = 2210 ± 20 nM

R^2= Me, R^3= Et, R^4=H **244**
α_{2C}-AR K_i = 25 ± 3 nM
α_{2A}-AR K_i = 1100 ± 100 nM

Figure 6.1.3. Key structures from the SAR study of **17**.

Replacement of the piperazine moiety proved challenging, with 1,4-diazepanes being the only suitable alternative; however, substitution of the 3-position on the piperazine ring exerted a beneficial stereospecific effect on both affinity and potency at the α_{2C}-AR (**240**). The results of this study established a robust SAR and identified a number of 4-aminoquinoline derivatives with good antagonist potencies against the α_{2C}-AR which also displayed excellent subtype selectivity.[318]

As previously discussed, many homology models of the α_2-ARs have been constructed due to the lack of a resolved crystal structure.[132,146–149] One such study by Ostopovici-Halip *et al.* involved the generation of homology models for the different α_2-AR subtypes, using the crystal structure of β_2-AR as a template.

These models were then used in ligand docking experiments with reported α_2-AR subtype selective ligands. Molecular docking of **17** was performed at the binding sites of the three α_2-AR subtypes, as determined by mutagenesis data and the location of the co-crystallised inverse agonist carazolol in the β_2-AR crystal structure, giving different binding modes for each α_2-ARs binding sites (Fig. 6.1.4). These differences were attributed largely to variation of the amino acid at position 8 (AAV8).[147]

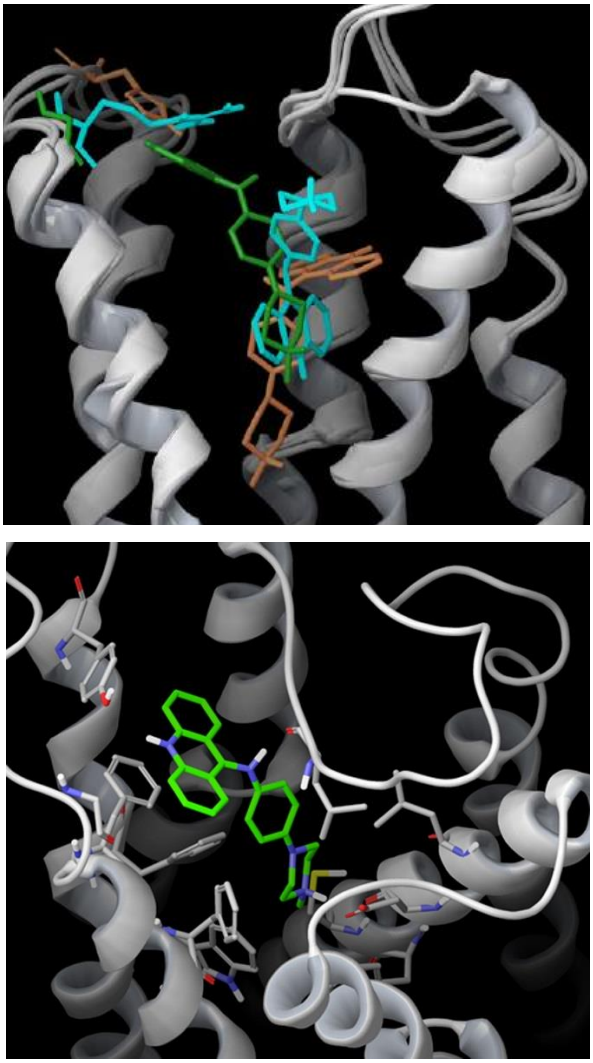

Figure 6.1.4. *Top*: **17** docked in the α_{2A}-AR (blue), α_{2B}-AR (orange) and α_{2C}-AR (green) binding sites. *Bottom*: Specific amino acid residues which can interact with **17** docked in the α_{2C}-AR.

The α_{2C}-AR has a glycine (Gly) residue at position AAV8 which facilitates positioning of the acridine ring of **17** in an extracellular hydrophobic pocket.

The models of the α_{2A}-AR and α_{2B}-AR show that the AAV8 position is occupied by amino acids with larger basic side chains (*i.e.* histidine –His- and arginine –Arg-, respectively) which would prevent the acridine group from adopting the same orientation as at the α_{2C}-AR.

Other amino acids proposed to stabilize binding of **17** in the α_{2C}-AR binding site included phenylalanine (Phe) 7.35 and tyrosines (Tyr) 6.55 and 6.58 which form hydrophobic and π-π stacking interactions with the acridine system.

Electrostatic interactions between aspartate (Asp) 3.32 and the protonated piperazine N atom as well as hydrogen bonding between Tyr 6.58 and the acridine N atom also characterized the binding mode in the α_{2C}-AR binding site.[147]

6.2. Exploring new scaffolds for α_2-AR subtype selectivity

These docking and SAR studies have identified the acridine core as a crucial component for α_{2C}-AR binding. This prompted us to explore the potential of a series of acridine-9-carboxamides as α_2-AR ligands. Structural similarity to **17** led us to investigate this new scaffold by utilizing a small 'in-house' library of acridine-9-carboxamide analogues originally designed as novel dual DNA binding molecules comprising of a minor groove binder (diphenyl guanidine moiety) linked to a well-known intercalator (acridine), as shown in Fig. 6.2.1-A. Over the past 15 years the Rozas group has developed many potent minor groove binders of the general structure shown in Fig. 6.2.1-B.[180,320]

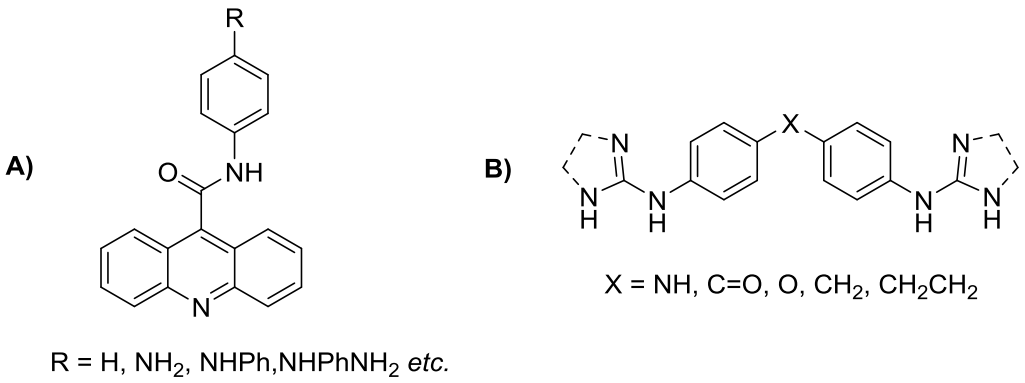

Figure 6.2.1. A) General structure of acridine-9-carboxamide analogues. B) General structure of Rozas diaromatic minor groove binders.

There is a limited number of papers available concerning the synthesis and biological evaluation of acridine-9-carboxamides. Bouyer *et al.* reported the preparation and cytotoxicity study of a series of novel acridine-based platinum (II) complexes (Fig. 6.2.2).[321] Intriguingly, the non platinated acridine-9-carboxamide derivatives where X = NH were completely inactive whilst the platinated complexes displayed significantly lower cytotoxicity in HCT116 (human colorectal carcinoma) and HT-29 (human colon adenocarcinoma) cancer cell lines compared to their acridine-9-carboxylate counterparts with X = O.

Acridine-4-carboxamide and acridine-2-carboxamide tethered Pt(II) complexes have also been reported showing significant in vitro cytotoxicity in P388 leukaemia cells.[322] This distinction between the ester and amide functionality would suggest that the acridine-9-carboxamide core imparts significantly lower cytotoxicity, thereby favouring its utility as a core scaffold in GPCR-based drug discovery, where cytotoxicity is undesirable.

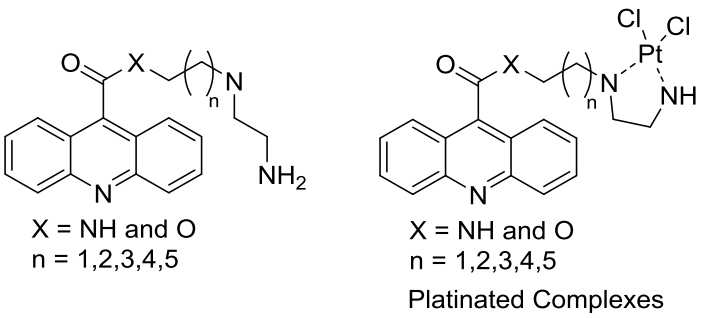

Figure 6.2.2. General structures of non-platinated and platinum (II) complexes of acridine-based tethered (ethane-1,2-diamine) ligands.

The ‘in-house’ library of acridine-9-carboxamides analogues was prepared by previous members of the Rozas group Dr. Alessandra Cordeiro and Dr. Padraic S. Nagle in an attempt to enhance the DNA binding of known minor groove binders developed within the group. This ’in-house’ library was evaluated using biophysical measurements (thermal denaturation studies using salmon testes DNA) and were shown to be poor DNA binders ($\Delta T_m \sim 2$ °C).[323]

These results showed that this design did not enhance the minor groove binding ability of the diphenyl guanidines; instead, this modification abolished the intercalation ability of the acridine core (acridine-9-carboxylic acid $\Delta T_m = 4$ °C). However, the lack of DNA binding and shared structural similarities with **17** supports the suitability of these candidates for screening as potential α_2-AR ligands.

6.2.1. Prior synthesis of acridine-9-carboxamide 'in-house' library

Drs. Cordeiro and Nagle synthesised this library using the synthetic route shown in Scheme 6.2.1 involving the *in situ* generation of acridine-9-carboxylic acid chloride (**245**) by reaction of thionyl chloride and acridine-9-carboxylic acid (**246**).

Scheme 6.2.1. General synthetic route to acridine-9-carboxamides.

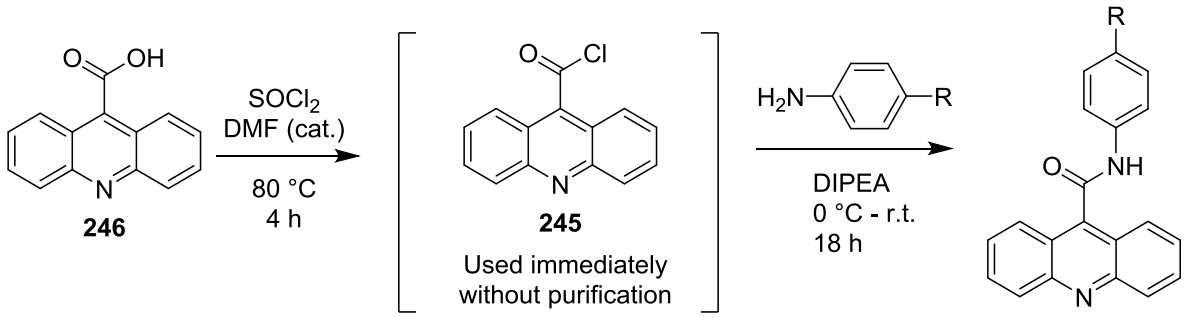

This reaction is one of many methods of preparing acyl chlorides and a detailed reaction mechanism for this is shown in Scheme 6.2.2. Direct reaction of thionyl chloride alone with a carboxylic acid, as in Scheme 6.2.2-A, generates the acyl chloride along with volatile gaseous side products like hydrogen chloride (HCl) and sulfur dioxide (SO_2); however, the addition of catalytic DMF allows for the *in situ* formation of the Vilsmeier reagent (**247**) by the mechanism shown in Scheme 6.2.2-B.

Scheme 6.2.2. A) Mechanism of acyl chloride formation B) Generation of **247** *in situ*.

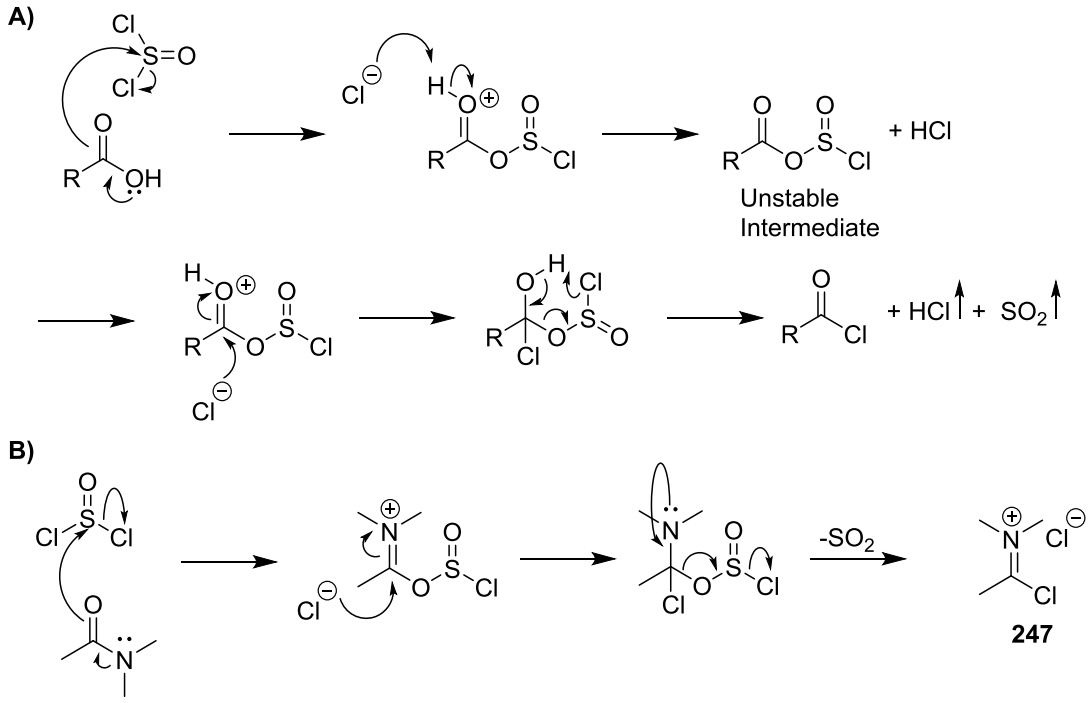

The Vilsmeier reagent then reacts with the carboxylic acid to form the corresponding acyl chloride **245** and regenerates DMF (Scheme 6.2.3), which can then react again with another equivalent of thionyl chloride and continue to form **247** as shown in Scheme 6.2.2. The acid chloride **245** (obtained after removal of volatile reagents *in vacuo*) was then reacted without additional purification by the immediate dropwise addition of a solution of the appropriate aniline in anhydrous MeCN in the presence of a base (NEt_3 or DIEPA) at 0 °C as shown in Scheme 6.2.1.

Scheme 6.2.3. Reaction of **246** with **247** to form **245**.

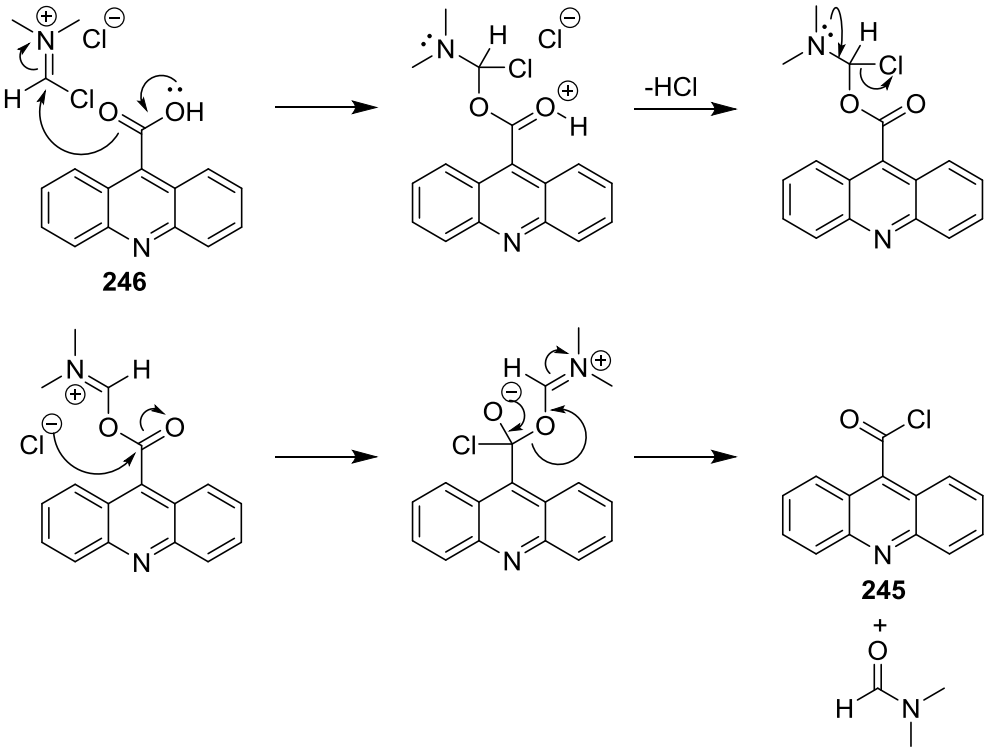

The reaction was then stirred for 1 hour at 0 °C before being warmed to room temperature and stirred for an additional 18 hours to furnish the desired acridine-9-carboxamide as a precipitate. Filtration and washing with MeCN, followed by purification on silica gel column chromatography (eluent: EtOAc/Hexanes) gave the corresponding pure products as solids in yields of 30-80%. The identity of these products was subsequently confirmed by ^{1}H and ^{13}C NMR, HRMS and melting point.

A subset of compounds (**248**-**257**) was chosen for screening at the α_2-AR to determine whether they display affinity and/or selectivity at the different α_2-AR subtypes and explore the structural features that can contribute to selective receptor engagement.

Thus, compounds **248** and **249** were selected in order to examine the potential difference in affinity and/or selectivity between Boc protected **248** and the de-protected hydrochloride salt **249**. The screening was conducted in collaboration with the pharmacological laboratory of Prof. Luis Callado at UPV/EHU (Bilbao, Spain).

The aim was to investigate potential utility of the acridine-9-carboxamide scaffold as core structure in the development of α_2-AR subtype selective ligands.

The chosen collection of compounds submitted for screening at the α_2-ARs is shown in Fig. 6.2.4. Affinity values were determined by competition binding assays conducted using cellular membranes from transgenic CHO cells selectively expressing either human α_{2A}-ARs or α_{2C}-ARs.

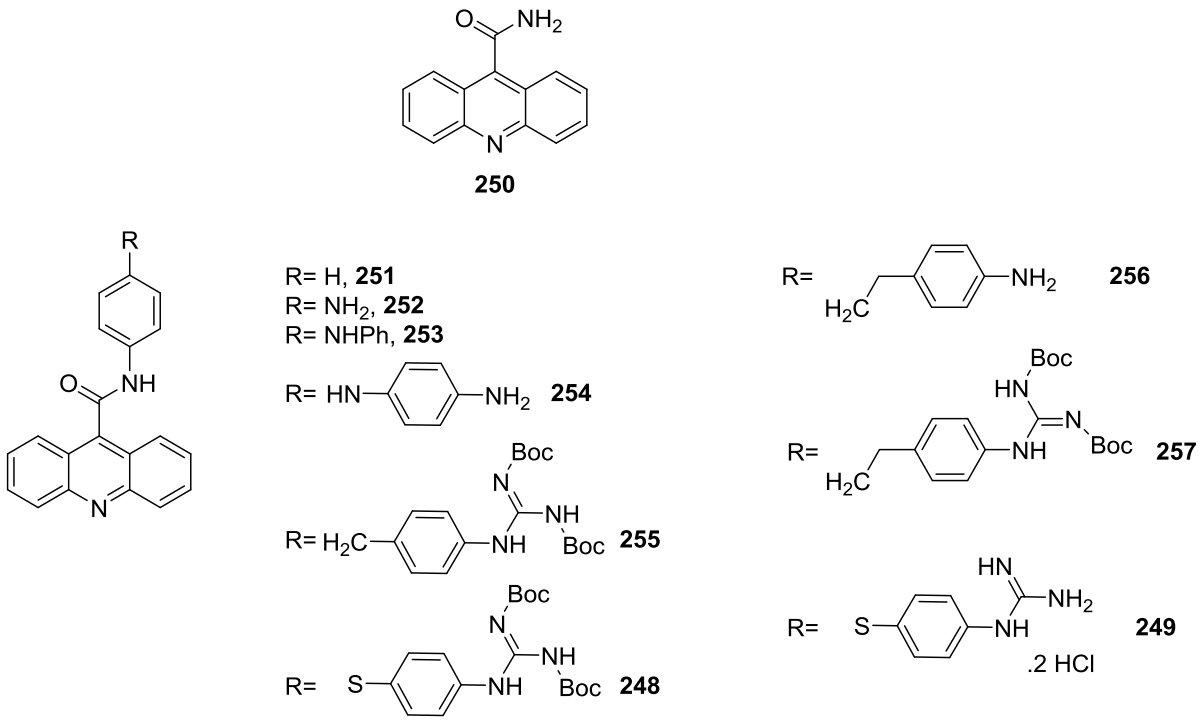

Figure 6.2.3. 'In-house' library of acridine-9-carboxamide derivatives **248** – **257** chosen for screening as α_2-AR ligands.

6.3. Pharmacological screening and structure-selectivity relationship

In order to evaluate α_2-AR engagement by the acridine-9-carboxamide derivatives (**248** – 2**57**), these compounds were subject to competition-binding assays in transgenic CHO cells and human PFC tissue using **[^{3}H]-RX821002** and **[^{3}H]-16** as radioligands. Cellular membranes of CHO cells selectively expressing human α_{2A}-AR or α_{2C}-ARs were purchased from Perkin Elmer (ES-030-M400UA and ES-032-M400UA, respectively). The protocols for each assay (transgenic CHO cell or Human PFC tissue) are detailed in the pharmacological methods section of Chapter 9. As mentioned, tritiated α_2-AR subtype selective antagonists **[^{3}H]-RX821002** (α_{2A}-AR) and **[^{3}H]-16** (α_{2C}-AR) were used as the radioligands (Fig. 6.3.1).

This subtype selective screening was conducted in parallel with competition radioligand binding assays in human PFC membrane preparations (α_2-AR) using **[^{3}H]-RX821002** for comparison.

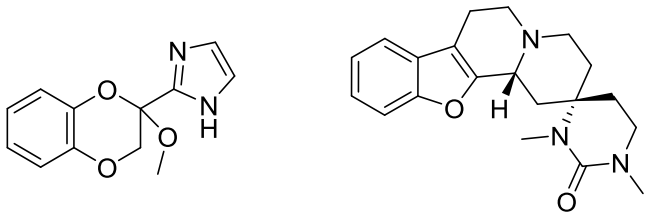

Figure 6.3.1. Structures of α_2-AR subtype selective radioligands **[^{3}H]-RX821002** (α_{2A}-AR) and **[^{3}H]-MK-912** (α_{2C}-AR).

The binding affinities (expressed as K_i nM values) in human PFC tissue at the α_{2A}- and α_{2C}-AR subtypes are shown in Table 6.3.1. These affinity values were measured under different conditions with different competitive radioligands (transgenic CHO vs. PFC membrane preparations); therefore the K_i values should not be directly compared unless the same radioligand has been used.

Firstly, the affinity values for all compounds within the series for the α_2-AR in human PFC tissue is very low, with **249** displaying the highest K_i (5360 ±2960 nM). All studies regarding α_2-AR ligands conducted to date within the Rozas group have utilized binding affinities measured in human PFC tissue to guide compound prioritization and aid *lead* identification.

Typically, any compounds displaying K_i values of $>10^3$ nM would be considered low priority, thus impeding their progression to more detailed pharmacological analysis. Nonetheless, examination of the affinity values measured using CHO cells selectively expressing human α_{2A}-AR or α_{2C}-ARs with consideration of structural similarities presented within the series, unveils a partial structure-selectivity relationship (SSR), albeit with low affinities (Table 6.3.1).

Table 6.3.1. Affinity values expressed as K_i ±SD (nM, i.e. $\times 10^{-9}$) for **248** – **257** at the human α_{2A}- and α_{2C}-AR subtypes in CHO cells and human PFC tissue measured *via* competition-binding assays with **[^{3}H]-16** and **[^{3}H]-RX821002.**

Compound	[^{3}H]-16 α_{2C}-AR CHO cells	[^{3}H]-RX821002 α_{2A}-AR CHO cells	[^{3}H]-RX821002 α_2-AR human PFC
RX821002	*nd*	2.75 ±0.97	1.21 ±0.27
16	0.22 ±0.03	15.25 ±8	*nd*
250	>10^6	>10^6	>10^6
251	822.69 ±691	>10^6	>10^6
256	105.09 ±73	43.51 ±27	10,589.95 ±6788
257	579.68 ±291	74.92 ±43	58,725.88 ±20707
254	12,555.37 ±4427	122.62 ±77	136,076.83 ±33748
253	4778.15 ±976	>10^6	36,844.43 ±9929
254	>10^6	23,397.69 ±6802	48,018.94 ±10865.42
255	9511.58 ±4614	16,953.50 ±3464	30,123.73 ±13528
248	567.26 ±141	14.87 ±5	21,500.86 ±8011
249	9434.44 ±6414	71.68 ±24	5358.24 ±2959

nd –not determined.

Analysis and comparison of these affinity values reveals a number of interesting observations. Firstly, compound **250** shows no affinity for the α_2-AR across all three assays (K_i >10^6 nM); however, **251**, displays significant affinity for the α_{2C}-subtype (K_i 822.69 nM) compared to α_{2A}-AR (K_i >10^6 nM), which suggests that addition of a phenyl substituent even though it does not enhance affinity for α_2-ARs (K_i >10^6 nM), it does increase selectivity for α_{2C}-AR. Compound **256**, which showed weak affinity for α_2-AR in PFC (K_i around 10^4 nM), displayed the highest affinity (K_i 43.51 nM) at the α_{2A}-subtype. However, no selectivity is evident as is displays similar affinity for the α_{2C}-subtype (K_i 105.09 nM).

Compounds **248** and **249** both display good affinity at the α_{2A}-subtype (K_i 14.87 and 71.68 nM, respectively), whilst the guanidinium salt **249** displayed the highest α_2-AR affinity in PFC tissue of the whole series (K_i 5358.24 nM), but exhibited relatively low affinity for α_{2C}-subtype (K_i 9434.44 nM).

Comparison of compounds **252**, **253** and **254** illustrates the impact of introducing an amino substituent at the 4-position of the terminal phenyl ring. Compound **252** exhibited substantial affinity for the α_{2A}-subtype (K_i 122.62 nM), whereas the addition of a second phenyl substituent, as in **253**, favoured binding to the α_{2C}-subtype and also increased α_2-AR affinity in the PFC tissue assay (K_i 12,555.37 and 136,076.83 nM, respectively). This is the only compound of the series which exhibited affinity for the α_2-AR in both PFC tissue and α_{2C}-subtype CHO cells assay without any measureable affinity for the α_{2A}-subtype. The addition of an amino group in the 4-position of the phenyl ring of **253** gives **254** and this additional amino-substituent subsequently enhances binding affinity for the α_{2A}-subtype (K_i 23397.69 nM) and decreases affinity for the α_{2C}-AR (K_i $>10^6$ nM).

Binding assays using **[^{3}H]-RX821002** have been conducted in both PFC and caudate tissues from controls and tissues from suicide victims with depression or other psychiatric disorders, showing that proportions of the α_2-ARs in the caudate were 86-91% α_{2A}-subtype and 9-14% α_{2C}-subtype.[324]

Human PFC is known to express higher levels of the α_{2A}-subtype than the α_{2C}-subtype, therefore, testing in this tissue, despite its superior physiological relevance compared to transgenic CHO cell tissue, comes with an inherent influence on the affinity measurements as they are derived from competitive binding of the test compounds at the most predominant α_2-subtype in a given tissue.[324] In order to probe and expand upon the SSR displayed by some members of this series (i.e. **251**, **256** and **253**), a set of novel acridine-9-carboxamide derivatives were designed and synthesised to investigate the effect of substitution at the 4-position on the phenyl ring in **251**.

Moreover, in order to gain a better understanding of the impact that substitution on the terminal amino group of **252** has on subtype specific binding, a set of alkyl, secondary, tertiary and cyclic amine (piperidine) substituted analogues **258**-**261** have also been proposed (Scheme 6.3.1). The aim was to examine whether addition of substituents to the amine or introduction of the second phenyl substituent was responsible for the enhanced affinity of **253** for the α_{2C}- *vs.* α_{2A}-AR.

Scheme 6.3.1 Structures and retrosynthesis of proposed derivatives **258**-**261**.

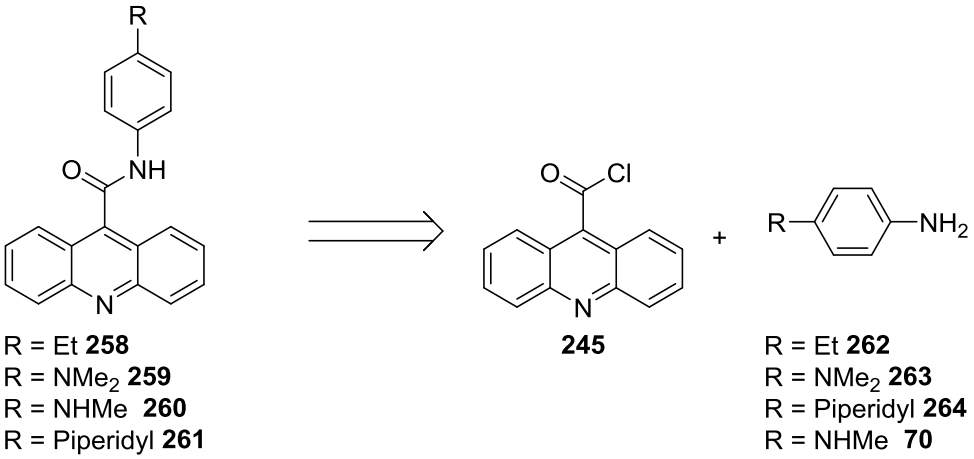

6.4. Synthesis of proposed derivatives

The synthesis of **258**-**261** would require the relevant anilines to couple with **245** forming the required acridine-4-carboxamides as described in Section 6.2.1. Anilines **262**, **263** and **264** are all commercially available; however, aniline **70** is not and therefore the *N*-Boc protected analogue **142** was synthesised as outlined in section 4.3.3.

The procedure shown in Scheme 6.4.1 was utilized to prepare **258** and **259** which were obtained in 52% and 83% yield, respectively. Compounds **258** and **259** were highly insoluble in water thereby facilitating their isolation and removal of by products by aqueous workup affording pure products as shown by ^{1}H NMR analysis. Additional analysis conducted by HPLC identified small amounts of unknown impurities present in both **258** and **259** (7% and 6%, respectively).

Additional purification of these products including trituration with CH_2Cl_2 and EtOAc, washing with water and aqueous acid (1M HCl) failed to remove these impurities sufficiently to achieve the >95% purity required for pharmacological testing; therefore, an alternative synthetic procedure was investigated.

Scheme 6.4.1. Synthetic route utilized to prepare **258** and **259**.

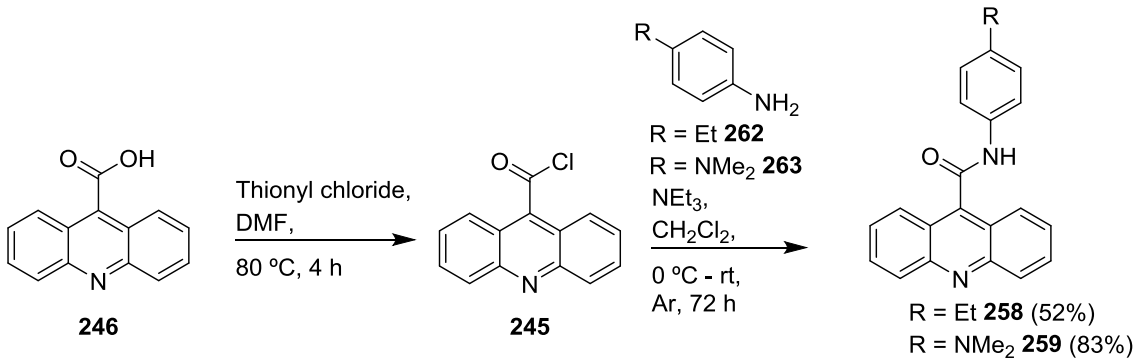

An alternative method for the preparation of amides is the carbodiimide mediated coupling of amines with carboxylic acids. A number of commercially available carbodiimides, such as *N,N'*-dicyclohexylcarbodiimide (DCC), *N*-(3-dimethylaminopropyl)-*N'*-ethylcarbodiimide hydrochloride (EDC.HCl) and *N,N'*-diisopropyl carbodiimide (DIC) have been reported to effectively couple a wide range of amines and carboxylic acids.[325,326]

A general mechanism for the EDC.HCl mediated coupling reaction is shown in Scheme 6.4.2. This reaction produces water soluble side products (**265**) which, together with the solvent and excess reagents, are easily removed by aqueous workup.

Scheme 6.4.2. General mechanism EDC.HCl mediated reaction coupling reaction with **246**.[327]

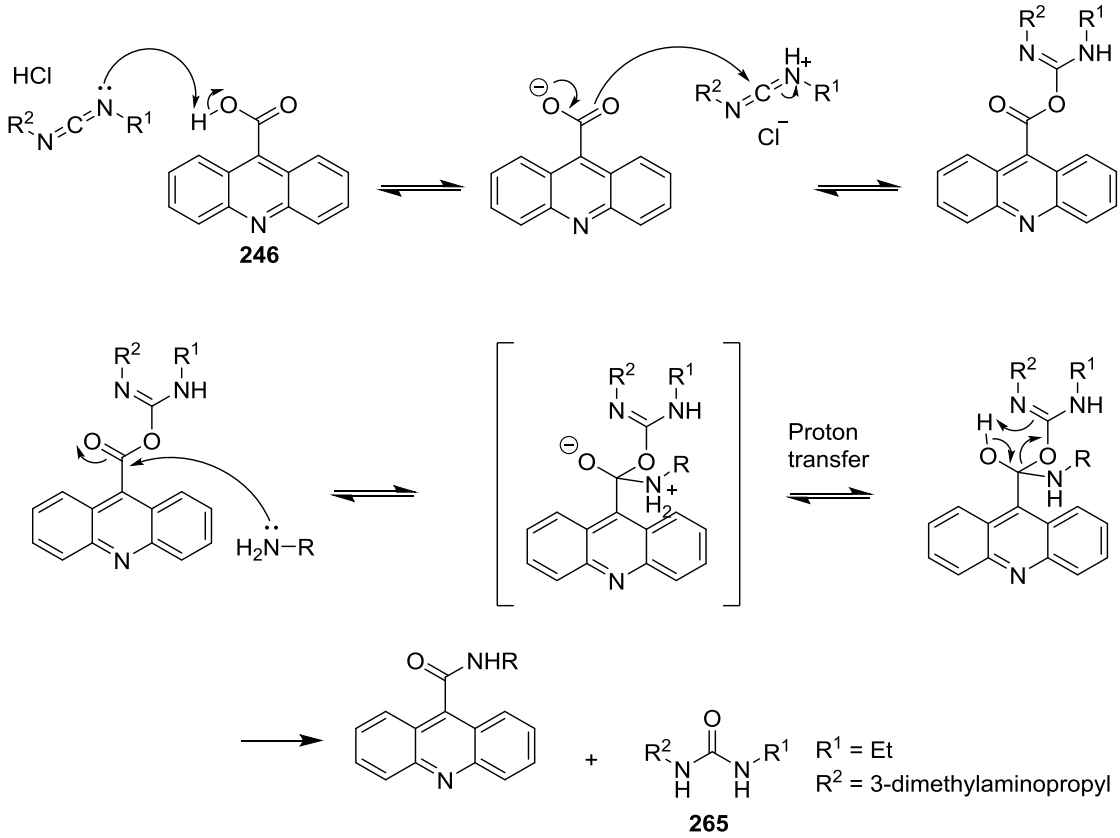

This EDC.HCl mediated amide coupling reaction was investigated as an alternative synthetic route utilized to prepare **266** and **261**, as shown in Scheme 6.4.3. Compound **246** and EDC.HCl were dissolved in anhydrous DMF and cooled to 0 °C under Ar before a solution of **142** or **164** in DMF was added *via* syringe before being allowed to warm to room temperature and stir for 48-72 h. Isolation of the products involved precipitation by sequential addition of EtOAc then H_2O to the reaction mixture, filtering and washing the precipitated product with water using a sinter funnel and Buchner flask before suction drying in air to afford **266** and **261** in high yields of 86% and 84% respectively. These products were subsequently characterised by ^{1}H and ^{13}C NMR, HRMS, IR and melting point analysis.

Scheme 6.4.3. Alternative synthetic route utilized to prepare **261** and **266**.

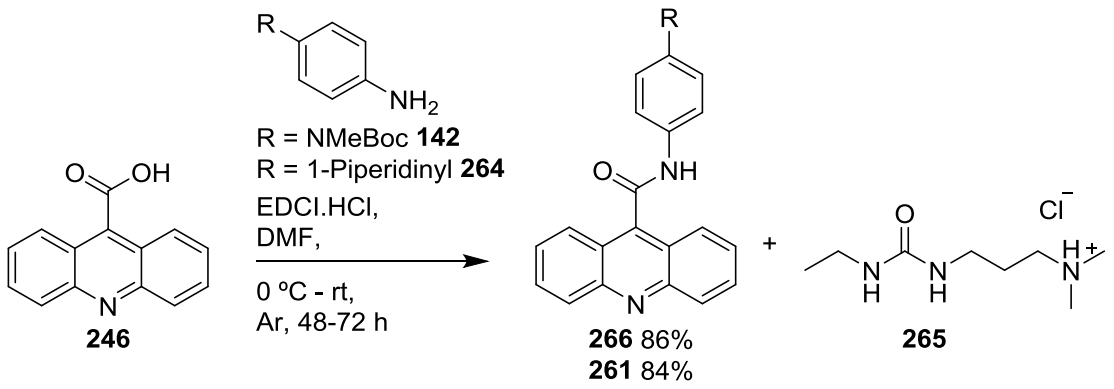

Subsequently, the improved EDC.HCl coupling of the requisite anilines and **246** was applied to prepare **258** and **259**. This alternative procedure afforded analytically pure **258** and **259** after precipitation, filtration and washing with H_2O and EtOAc in 70% and 75% yield respectively (Scheme 6.4.4).

Scheme 6.4.4. Synthesis of acridine-9-carboxamide derivatives *via* EDC.HCl coupling with **246**.

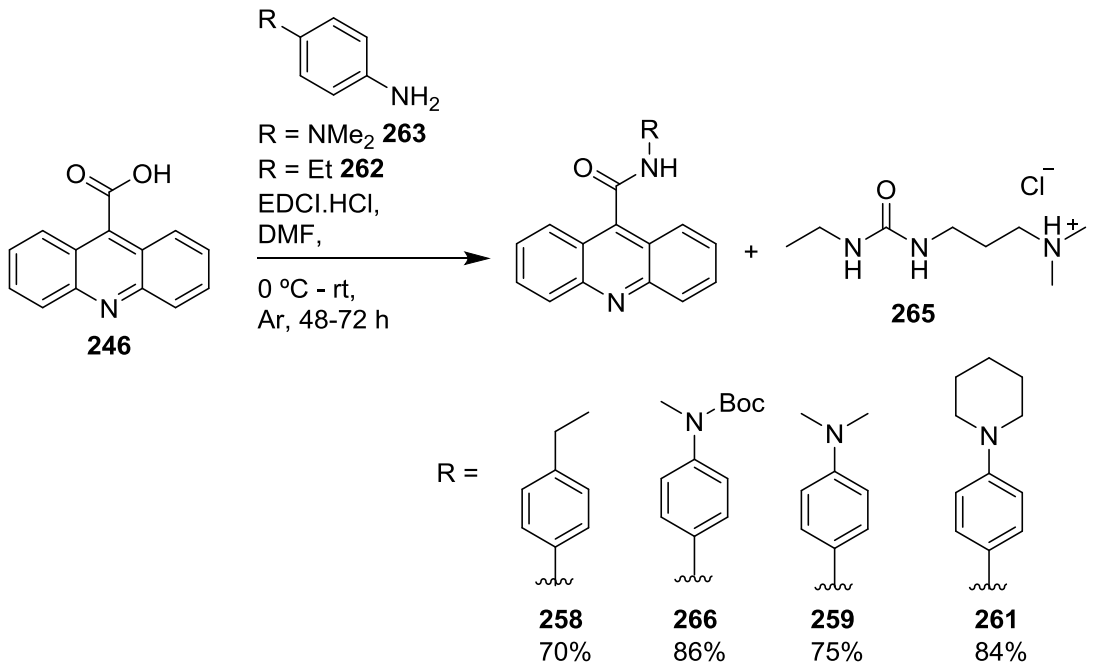

Deprotection conditions previously utilized for the removal of Boc groups from **248** were tested to deprotect **265** to furnish **260**. Unfortunately, stirring **262** in TFA/CH_2Cl_2 at room temperature for 18 hours failed to remove the Boc group and only formed the protonated trifluoroacetate salt of **265**. Fortunately, dissolving **265** in a methanolic HCl solution (10 mL, 1.25 M) and heating under reflux deprotected the Boc group and protonated the acridine ring to afford **260** as a *di*-hydrochloride salt in quantitative yield (Scheme 6.4.5).

Scheme 6.4.5. Conditions for the attempted deprotection of **265**.

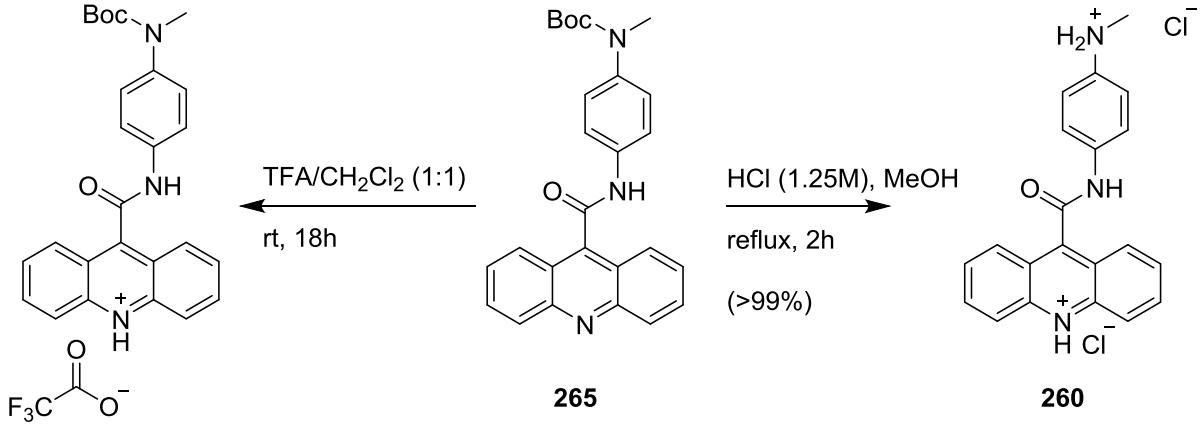

This method was also applied to improve the aqueous solubility of **258**, **259** and **261** yielding the corresponding *mono*- or *di*-hydrochloride salts, **266**, **267** and **268** in quantitative yield (Scheme 6.4.6). These salts were subsequently characterised by ^{1}H and ^{13}C NMR, HRMS, HPLC and melting point analysis and shown to >98% pure by HPLC analysis. **260**, **266**, **267** and **268** were submitted for competition-binding assays in transgenic CHO cells as discussed in section 6.3; however, unforeseen circumstances prevented these and future compounds from being analysed using this assay.

Scheme 6.4.6. Protonation of **258**, **259** and **261** yielding **266**-**268**.

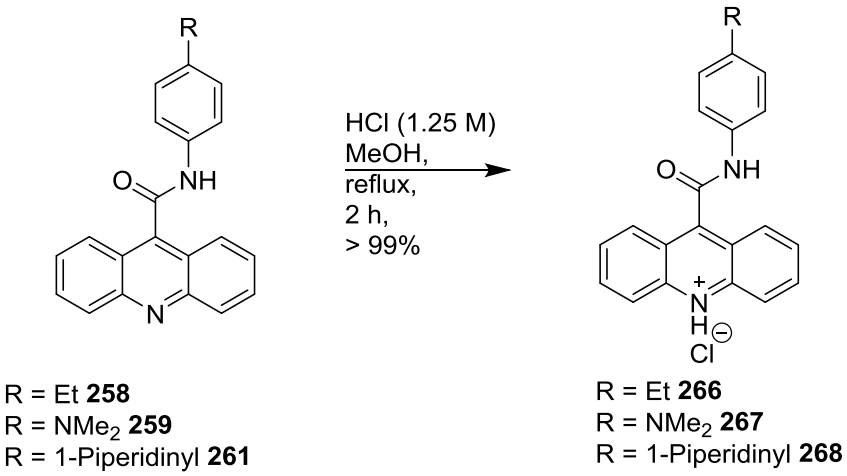

R = Et **258**
R = NMe_2 **259**
R = 1-Piperidinyl **261**

R = Et **266**
R = NMe_2 **267**
R = 1-Piperidinyl **268**

6.5. Conclusions

Unfortunately, financial issues encountered by our collaborators meant they were no longer able to conduct the CHO cell α_{2A}-AR or α_{2C}-AR selectivity assays as the running costs became prohibitive. This resulted in our inability to complete the subtype selectivity screening of the new derivatives **260**, **266**, **267** and **268**. However, the α_2-AR affinity and activity of these novel derivatives were evaluated by competition-binding assay in human PFC tissue using **[^{3}H]-RX821002** as the radioligand in collaboration with the pharmacological laboratory of Prof. Luis Callado at UPV/EHU (Bilbao, Spain). The following affinity values were obtained for **260** (pK_i = 3.53 ± 1.55), **266** (pK_i = 5.09 ± 0.16) and **268** (pK_i = 3.94 ± 0.10). These poor affinity values coupled with extremely poor aqueous solubility led us to terminate synthesis of additional derivatives within this series.

Chapter Seven

Pharmacological Evaluation in Human Platelets

7.1. Introduction

The pharmacological characterization of *hit* compounds is a vital process to predict cytotoxicity and secondary targets that may cause potential side effects *in vivo*. There are a number of established methods to evaluate a compound's pharmacology (absorption, distribution, metabolism, excretion and toxicity; ADMET)[328,329] and physiochemical properties.[330]

There are also many different animal models for neuropsychiatric disorders. Rats are commonly utilized as neuropsychiatric models when performing *in vivo* studies such as the Morris water maze navigation test, Porsolt's forced swimming test and prepulse inhibition (PPI) of startle reflex.[331] The importance of performing pharmacological evaluations in the tissue where the drug candidate is ultimately targeted towards (*e.g.* human PFC tissue) is evident as this is the most physiologically relevant environment to evaluate the performance of a drug candidate and will provide a more accurate representation of how the drug will perform *in vivo*.[332]

The four hit compounds **34**, **22**, **23** and **65**, identified by the screening process discussed in Chapter 3, were shown to preferentially bind to the α_{2C}-AR *vs* α_{2A}-AR (Fig. 7.1.1). The unique polypharmacological profiles of these compounds and considering their relation to Rozas' previously identified potential antidepressant agents,[132,133] each of these compounds was submitted for further pharmacological investigation to determine whether they exhibit cytotoxicity effects or affect human platelet function.[333]

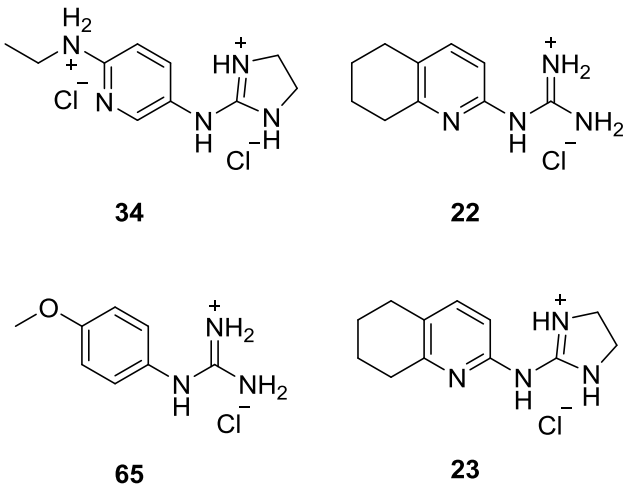

Figure 7.1.1. Structures of hit compounds **34**, **22**, **23** and **65**.

A number of drugs, such as acetylsalicylic acid (Aspirin), are known to impair platelet function and are utilized therapeutically as antiplatelet drugs to prevent and treat thrombotic and thromboembolic events.[334] Platelet dysfunction is also commonly observed as an undesirable side-effect of drugs such as antidepressants (SSRIs), antihistamines, antibiotics, antipsychotic drugs and chemotherapeutic agents.[335] Drug-induced thrombosis or thrombocytopenia can also occur.[336]

The aim of this chapter is to investigate the effects of **34**, **22**, **23** and **65** on platelets viability and on platelet function in collaboration with Prof. Maria Santos-Martinez and her PhD candidate Nadhim Kamil Hante in the School of Pharmacy and Pharmaceutical Sciences at Trinity College Dublin. Evaluation of the effects of drugs on human platelets function is an important process which can provide an early indication of potential side-effects and inform future drug development efforts.

7.2. Blood Collection and Platelet Preparation

This study was approved by The School of Pharmacy and Pharmaceutical Sciences Research Ethics Committee (2015-06-01). Blood was donated by healthy volunteers who had not taken any drugs known to affect platelet function in the previous two weeks. Whole blood was withdrawn using a butterfly needle and at a steady pace to prevent platelet activation, mixed with sodium citrate (3.15% w/v) and centrifuged (Eppendorf 5804, Fisher Scientific, Ireland) to obtain platelet rich plasma (PRP) and platelet poor plasma (PPP) by differential centrifugation.

For the preparation of washed platelets (WP), PRP was centrifuged in the presence of prostacyclin to avoid platelet activation and the platelet pellet re-suspended in Tyrode's salt solution (SIGMA, Ireland). Platelet's concentration in PRP and WP was measured using a Beckman Coulter Z1 Series Coulter Counter (Labplan, Ireland) and adjusted to 250,000 platelets μL^{-1} using Tyrode's salt solution before every experiment.

7.3. Effects on Platelet Function: Light Transmission Aggregometry and Optical Microscopy

Light transmission aggregometry (LTA) is considered the historical gold standard for testing platelet function. LTA measures changes in light transmission of a stirred platelet suspension in a cuvette in the presence of a platelet agonist added to induce platelet aggregation.[337] A PAP-8 Platelet Aggregation Profiler (Biodata Corporation, Ireland) was used to determine whether **34**, **22**, **23** and **65** incubated with PRP at various concentrations exhibit pro- or anti-aggregatory effects in human platelets. All experiments were performed from at least three different healthy donors. Normal platelet function was confirmed for each donor prior experiments by recording the response of platelets to the addition of collagen by LTA.[338] All data from experiments were analysed using GraphPad Prism 5 software (GraphPad Software, La Jolla, CA, USA) and presented as mean and standard deviation. One-way analyses of variance and Dunnett's or Tukey-Kramer's multiple comparisons post tests were performed as appropriate. Statistical significance was considered where $P < 0.05$.

A graphical schematic which illustrates the basic concepts of LTA is depicted in Fig.7.3.1.[339]The aggregometer is calibrated for 100% light transmission using a cuvette containing platelet poor plasma (PPP) and 0% light transmittance is equated to that a cuvette with PRP of resting (inactivated) platelets (baseline A, Fig. 7.3.1). Platelet activation induced by the addition of an agonist leads to a temporary decrease in light transmission due to an increase in platelet's size (B, Fig.7.3.1). When platelets form aggregates there is an increase in light transmission which is recorded by the aggregometer and calculated as a percentage of aggregation (C, Fig.7.3.1). The effect of an agonist of stirred platelets is always used as an internal control and for comparison when appropriated.

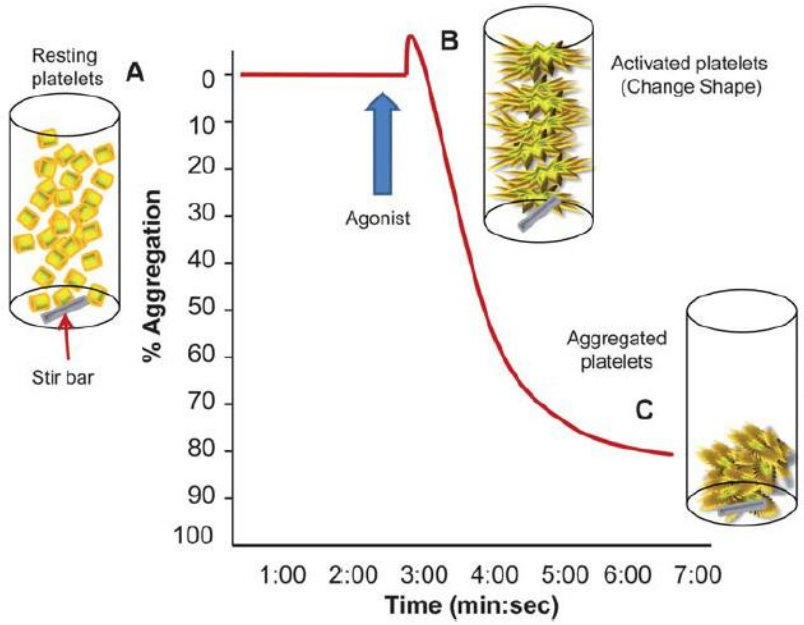

Figure 7.3.1. Illustration of the processes involved in LTA: achieving 0% light transmission or baseline (A), activating platelets with an agonist, (from B to C) and forming platelet aggregates (C).[339]

The effect of each of the test compounds on platelets was also confirmed by optical microscopy. Platelets suspensions incubated with the compounds in the presence or absence of collagen were fixed using a 2% final concentration of paraformaldehyde for 30 minutes at 37°C in the aggregometer. Platelets samples were then taken and spun using a Cytospin 4 cytocentrifuge (ThermoShandon, Ireland) at 1500 rpm for 30 minutes onto glass microscope slides. The resulting samples were visualized using an Olympus BX51M reflection epifluorescence microscope (Mason Technology, Ireland) and photomicrographs captured using a digital camera and the Olympus Cellsense software provided with the microscope.

7.4. Investigation of the potential pro-aggregatory effect of 34, 22, 23 and 65

The test compounds **34**, **22**, **23** and **65** were first investigated to determine if they could induce platelet aggregation. This involved the addition of the compounds (5 µM, 10 µM, 40 µM, 80 µM, 250 µM and 500 µM) to stirred platelets in PRP in the absence of an agonist. LTA analysis determines whether the compounds alone are able to induce platelet aggregation, which would lead to an observed increase in the percentage of aggregation. Therefore, it can be concluded that compounds do not induce aggregation provided baseline transmission (0% aggregation) is maintained over all concentrations for the duration of the experiment.

None of the compounds were found to induce platelet aggregation at the concentrations tested (5 µM, 10 µM, 40 µM, 80 µM, 250 µM and 500 µM) in PRP (n = 3). The statistical analysis and a representative example of the plot obtained from the aggregometer for **65** are shown below in Fig. 7.4.1.

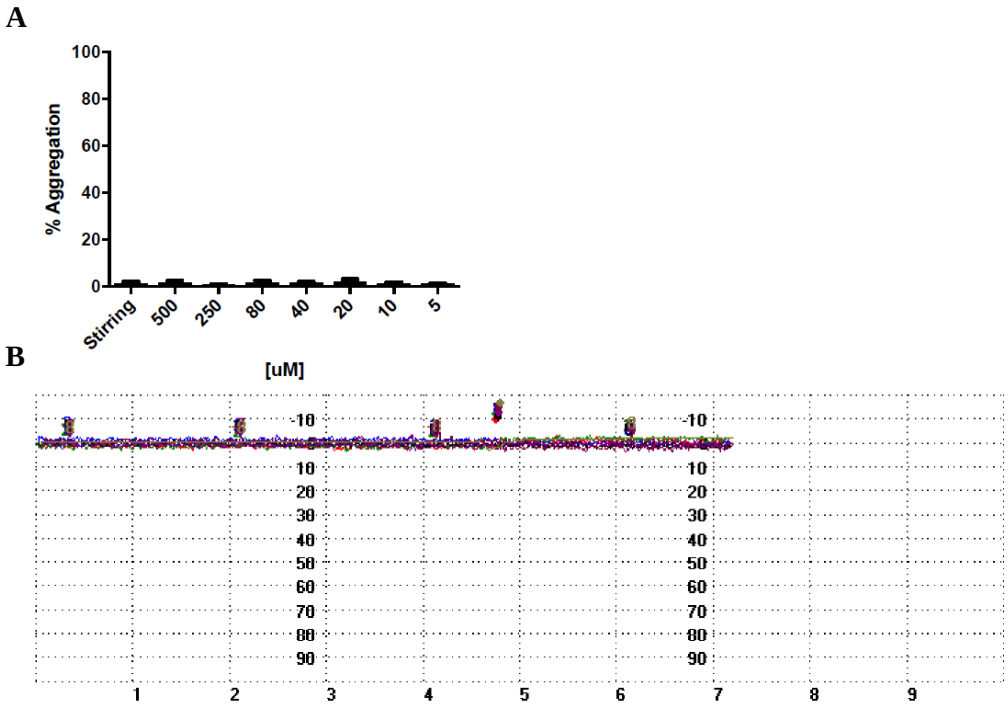

Figure 7.4.1. A) Statistical analysis of the effect of **65** at tested concentrations. (n=3) obtained during LTA analysis of PRP. Stirring platelets in the absence of the compounds are used as control for comparison. B) Representative LTA traces of **65** incubated at various concentrations with PRP showing straight lines and therefore, the absence of platelet aggregation

Next, the test compounds were investigated for their potential antiplatelet activity at the same concentrations as before but with the addition of collagen (2 μg mL^{-1}) as an agonist to induce platelet aggregation using LTA.

7.5. Investigation of the potential anti-aggregatory effect of 65 and 34

The two ligands with the most selective receptor profiles of the screening series, **65** and **34**, both exhibited binding at α_{2C}-AR but did not bind to the α_{2A} or α_{2B} subtypes. These ligands were the first to be analysed for their potential effects on human platelet aggregation induced by collagen. The results obtained from LTA analysis of **65** and **34** are summarised below in Fig. 7.5.1 and Fig. 7.5.2, respectively.

A

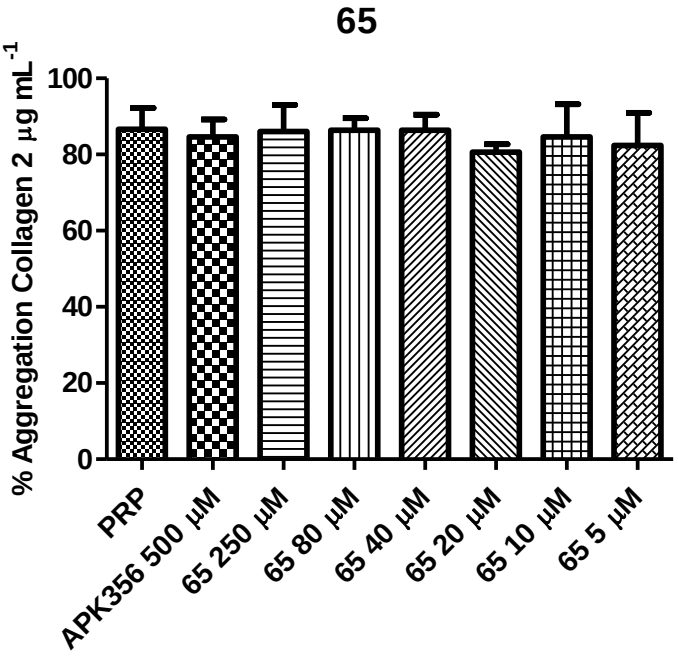

B

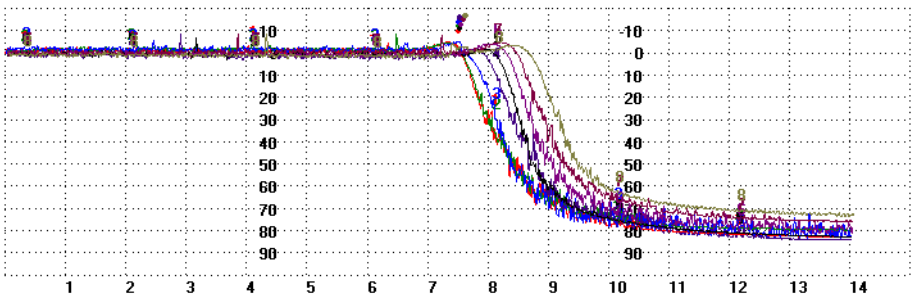

Figure 7.5.1. (A) Statistical analysis of the effect of **65** on platelet aggregation induced by collagen in PRP. Bars represent mean ± Standard Deviation. One-way analysis of variance (ANOVA) and Tukey post-test (n = 3).

(B) Representative LTA traces of **65**. The red line corresponds to the effect of collagen on PRP in the presence of the vehicle. Coloured lines show different percentages of aggregation at corresponding concentrations (5 µM, 10 µM, 40 µM, 80 µM, 250 µM and 500 µM) after the addition of collagen (2 µg mL^{-1}) demonstrating the absence of anti-aggregatory effect

A

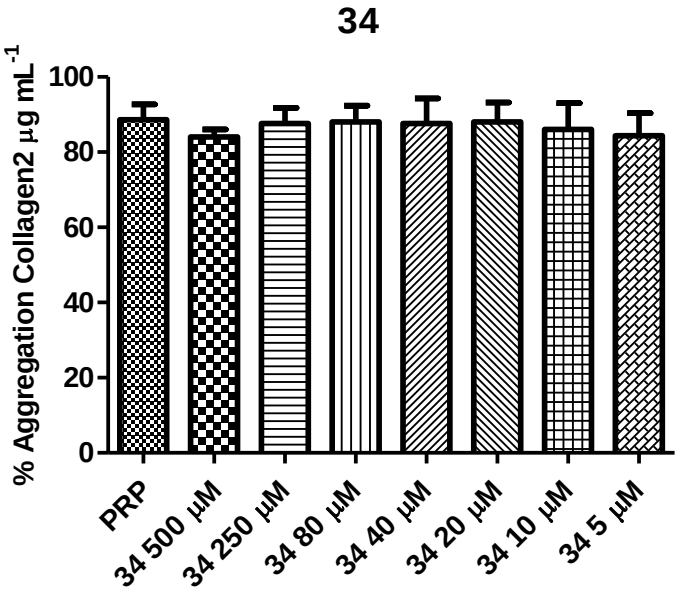

B

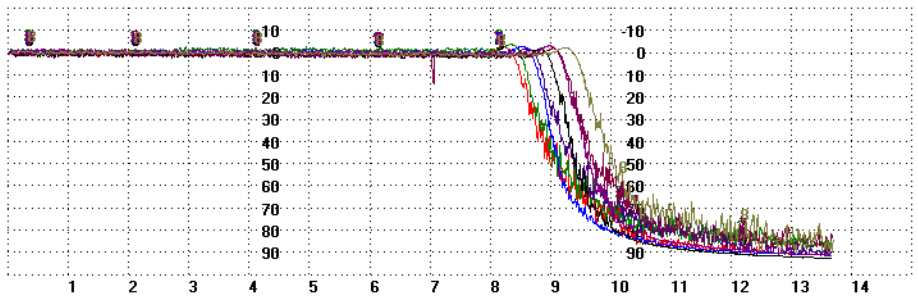

Figure 7.5.2. (A) Statistical analysis of the effect of **34** on platelet aggregation induced by collagen in PRP. Bars represent mean ± Standard Deviation. One-way analysis of variance (ANOVA) and Tukey post-test (n = 3).

(B) Representative LTA traces of **34**. The red line corresponds to the effect of collagen on PRP in the presence of the vehicle. Coloured lines show different percentages of aggregation at corresponding concentrations (5 µM, 10 µM, 40 µM, 80 µM, 250 µM and 500 µM).

Optical microscopy was also used to visualize platelets aggregates in the presence of **65** and **34** (500 µM) and collagen (2 µg mL^{-1}). In each case large aggregates, shown in black, are clearly visible which confirms **65** and **34** do not display antiplatelet activity in the concentration range tested (Fig. 7.5.3 and 7.5.4, respectively).

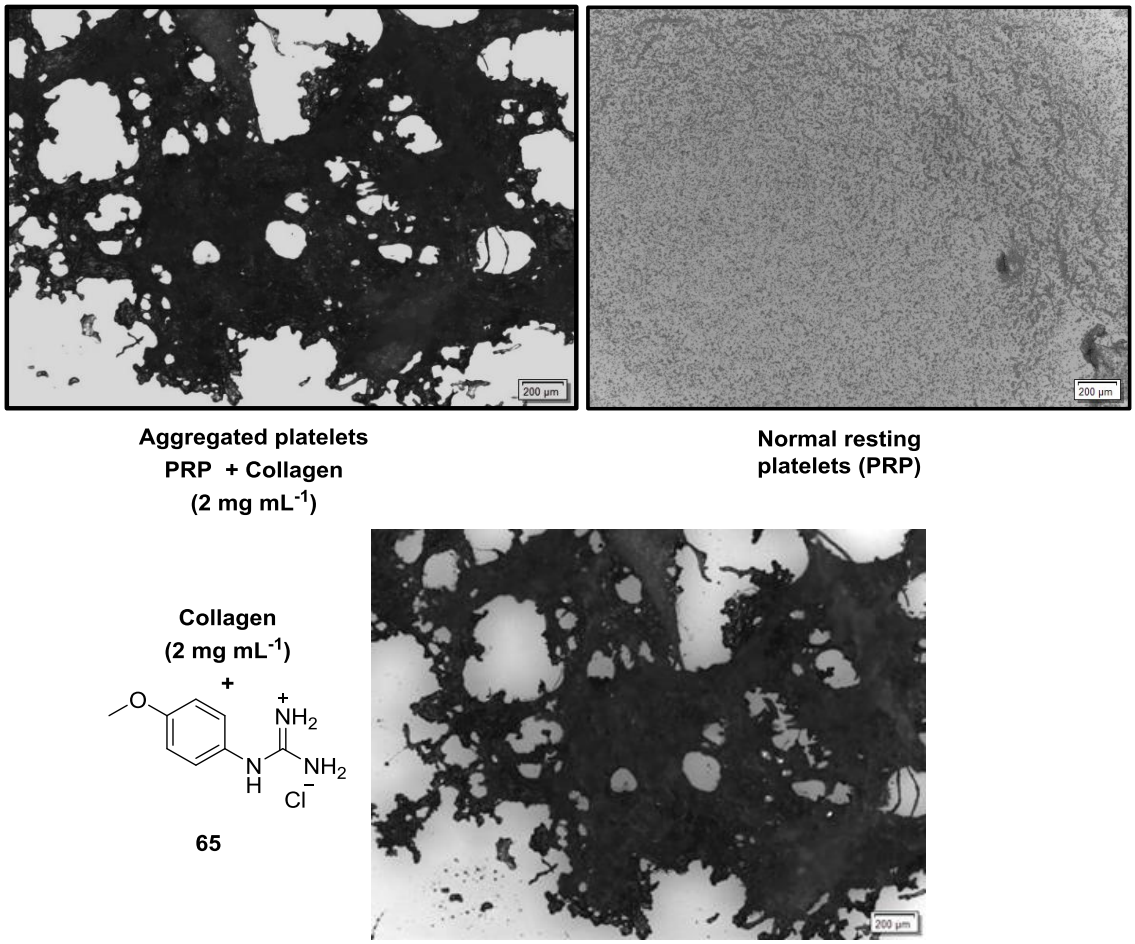

Figure 7.5.3. Photomicrographic analysis of platelet samples. Non-aggregated (resting) platelets in PRP (*top right*) and aggregated platelets (*top left*) compared with PRP in the presence of **65** (500 µM) with collagen (2 µg mL^{-1}) (*bottom*). Large aggregates are shown in black.

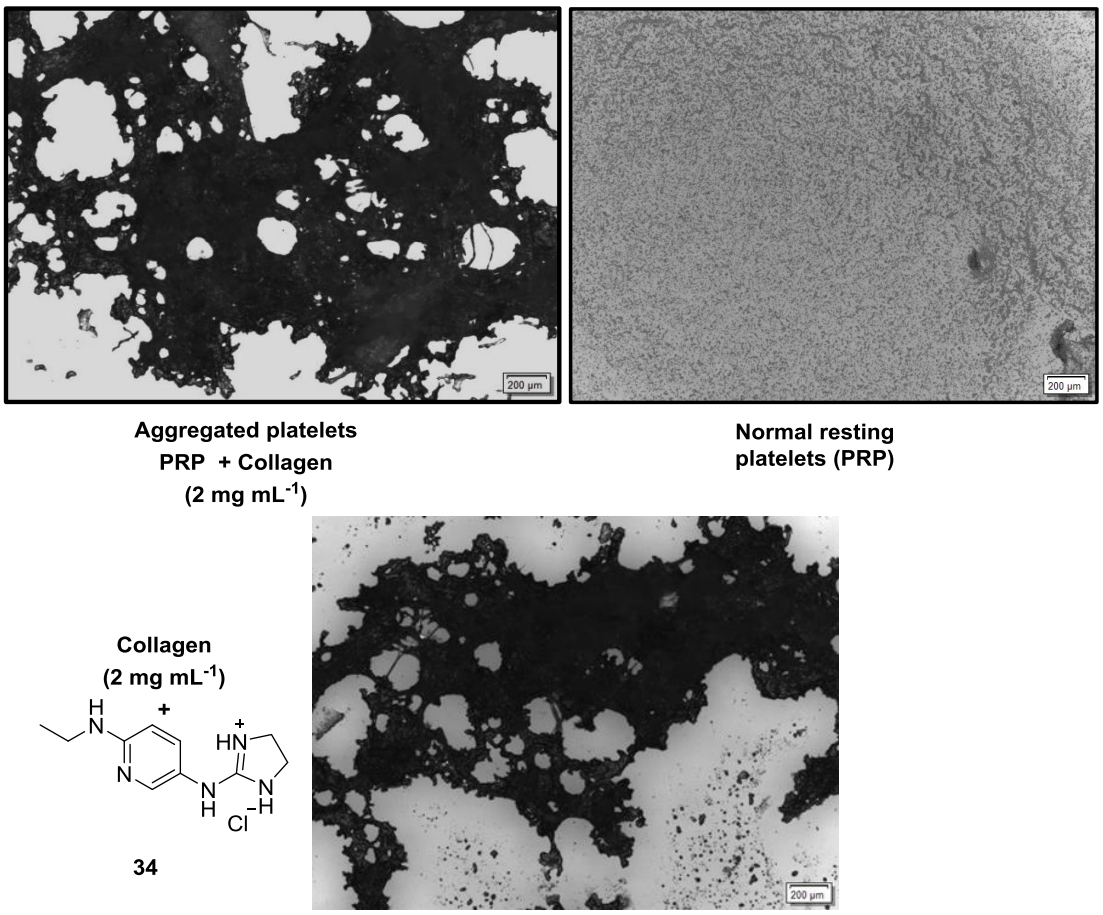

Figure 7.5.4. Photomicrographic analysis of platelets by optical microscopy. Non-aggregated (resting) platelets in PRP (*top right*) and aggregated platelets (*top left*) compared with PRP in the presence of **34** (500 µM) with collagen (2 µg mL^{-1}) (*bottom*). Large aggregates are shown in black.

These results indicate that **65** and **34** neither induce aggregation nor inhibit collagen induced platelet aggregation in samples of PRP over the range of concentrations tested (5 - 500 µM). This is a positive result as any secondary effects, such as affecting platelet function, would be considered undesirable and may stunt the development and future utility of these potential drug candidates.

7.6. Investigation of the potential anti-aggregatory effect of 22 and 23

The next two ligands to be investigated for their effects on platelet aggregation induced by collagen were **22** and **23**. These structurally related compounds were found to display unique receptor binding profiles which included relatively high affinity values (K_i less than 270 nM) for serotonin (5-HT_{2B} and 5-HT_{2C}), histamine (H2) and sigma 1 (σ_1) receptors. Both of these compounds were also shown to bind at α_{2B}-AR (K_i 741 nM and 1664 nM, respectively) and α_{2C}-AR (K_i 2059 nM and 2339 nM, respectively) subtypes with reasonable affinity, with **23** also exhibiting good affinity for the α_{2A}-AR (K_i = 635 nM). The high affinity that **22** and **23** shown for the histamine H2 receptor motivated their further investigation. Histamine H1 receptor antagonists, more commonly known as antihistamines, are well known to exert antiplatelet effects.[340]

Famotidine (**8**), Ranitidine and Cimetidine, are all histamine H2 receptor antagonists used therapeutically to inhibit stomach acid secretion in the treatment of gastroesophageal reflux and peptic ulcer disease, have also been reported to inhibit collagen and ADP induced platelet aggregation of PRP at concentrations of 1.4-1.5 mM.[341] **8** (H2 receptor antagonist) and tiotidine (H2 receptor inverse agonist) are both guanidino-2-thiazole derivatives (Fig. 7.6.1).

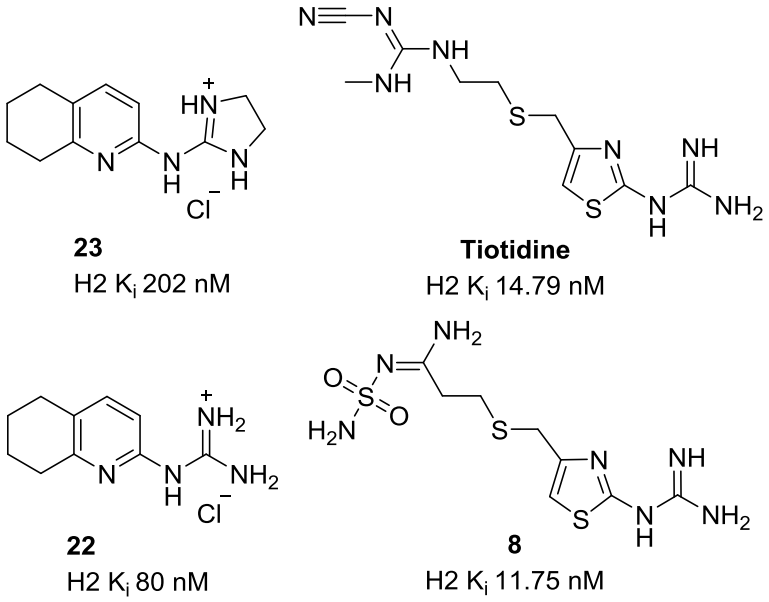

Figure 7.6.1. Structures of hit compounds **22** and **23** with histamine H2 ligands tiotidine and **8**.[211,342]

Interestingly, histamine H2 antagonists such as **8** have been recently investigated in a placebo-controlled, randomized clinical trial as an adjunct treatment of resistant schizophrenia giving promising results. Moreover, the gold standard antipsychotic drug clozapine has also been identified as a full inverse agonist at the H2 receptor.[41] Compounds **22** and **23** which are 2-guanidino and 2-(2-aminoimidazolino) derivatives of pyridine, respectively, share structural homology with the guanidino-2-thiazole core of **8**. Thus, a heteroaromatic core substituted at the 2-positon with a cationic moiety could be considered a potential pharmacophoric feature for histamine H2 antagonism.[211,341] Therefore, these compounds **22** and **23** were investigated for their potential antiplatelet activity to test their potential H2 antagonism. The results obtained from LTA analysis of **22** and **23** are summarised in Figs. 7.6.2 and 7.6.3, respectively.

A

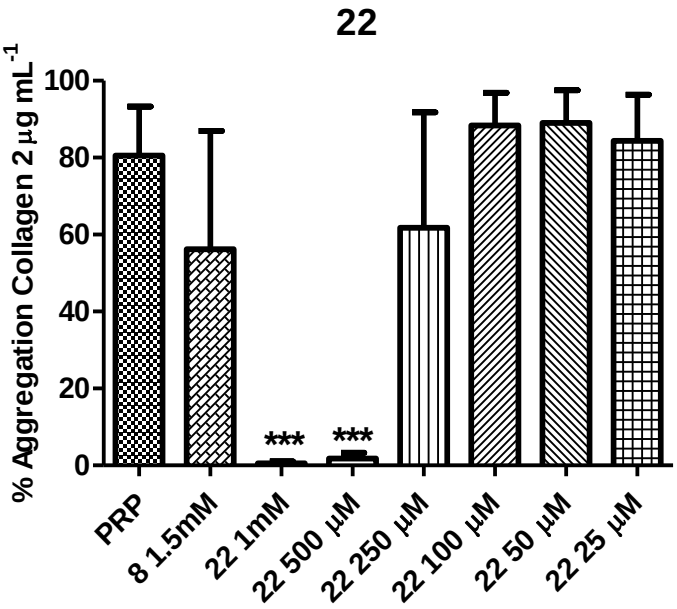

B

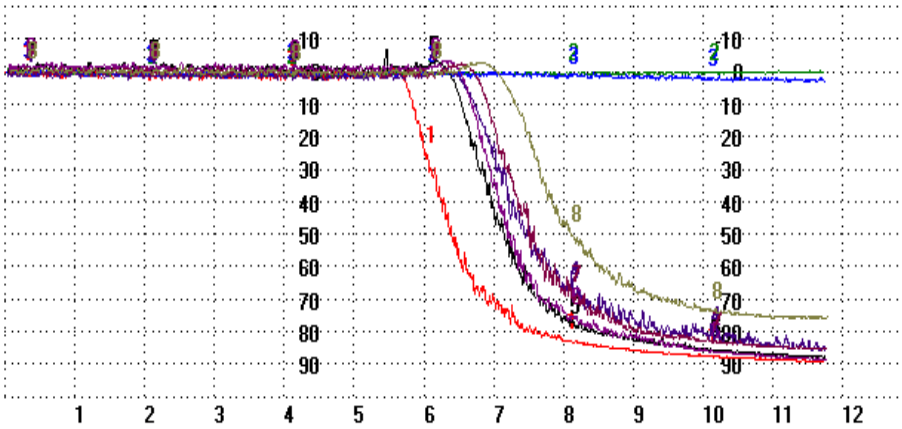

Figure 7.6.2. (A) Statistical analysis of the effect of **22** on platelet aggregation in PRP after the addition of collagen (2 µg mL^{-1}). Bars represent mean ± Standard Deviation. One-way analysis of variance (ANOVA), Tukey post-test (n = 3) followed by Dunnett's test. ***P<0.001 vs control (PRP + Collagen).

(B) Representative LTA traces of the effect of **22** in PRP after the addition of collagen (2 µg/mL). Coloured line traces show different percentages of aggregation at corresponding concentrations of **22** (25 µM, 50 µM, 100 µM, 250 µM, 500 µM and 1 mM) with collagen (2 µg mL^{-1}). Trace 1 (red) – PRP + collagen (2 µg mL^{-1}) only. Trace 2 (green) – 1 mM **22** + PRP + collagen (2 µg mL^{-1}). Trace 3 (blue) –500 µM **22** + PRP + collagen (2 µg mL^{-1}). Trace 4 (purple) – 250 µM **22** + PRP + collagen (2 µg mL^{-1}).

A

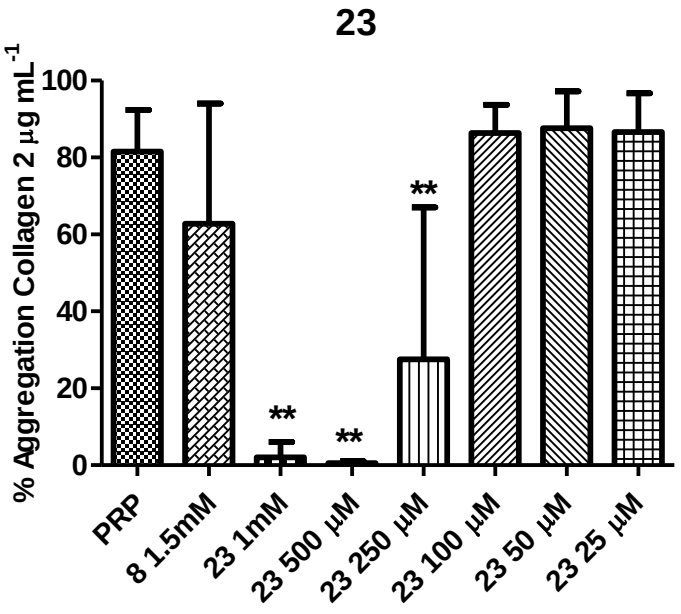

B

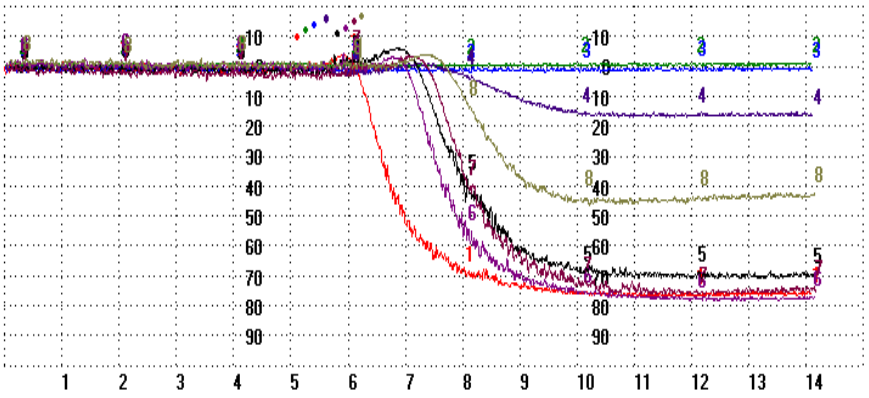

Figure 7.6.3. (A) Statistical analysis of the effect of **23** on % of aggregation in PRP after the addition of collagen (2 µg mL^{-1}). Bars represent mean ± Standard Deviation. One-way analysis of variance (ANOVA), Tukey post-test (n = 3) followed by Dunnett's test. **P<0.01; vs control (PRP + Collagen).

(B) Representative LTA traces of the effect of **23** in PRP after the addition of collagen (2 µg/mL). Coloured line traces show different percentages of aggregation at corresponding concentrations of **23** (25 µM, 50 µM, 100 µM, 250 µM, 500 µM and 1 mM) with collagen (2 µg mL^{-1}). Trace 1 (red) – PRP + collagen (2 µg mL^{-1}) only. Trace 2 (green) – 1 mM **23** + PRP + collagen (µg mL^{-1}). Trace 3 (blue) –500 µM **23** + PRP + collagen (2 µg mL^{-1}). Trace 4 (purple) – 250 µM **23** + PRP + collagen (2 µg mL^{-1}).

Optical microscopy confirmed the antiaggregatory activity of both **22** and **23** at 1 mM for aggregation induced by collagen (2 μg mL^{-1}) (Fig. 7.6.4 and Fig. 7.6.5, respectively).

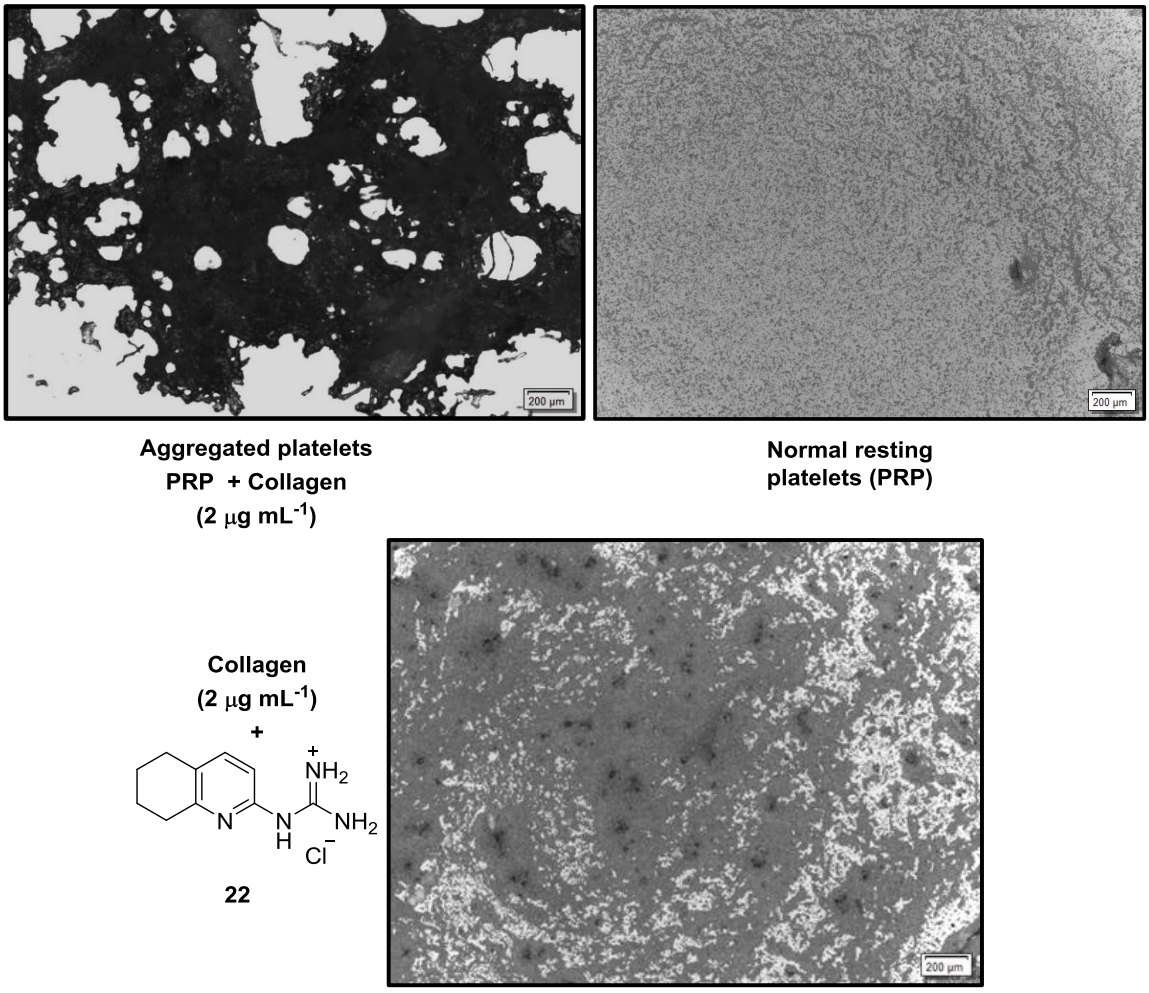

Figure 7.6.4. Photomicrographic analysis of platelet samples. Normal, non-aggregated (resting) platelets in PRP (*top right*) and aggregated platelets (*top left*) compared with PRP in the presence of **22** (500 μM) and collagen (2 μg mL^{-1}) (*bottom*). Large aggregates are shown in black.

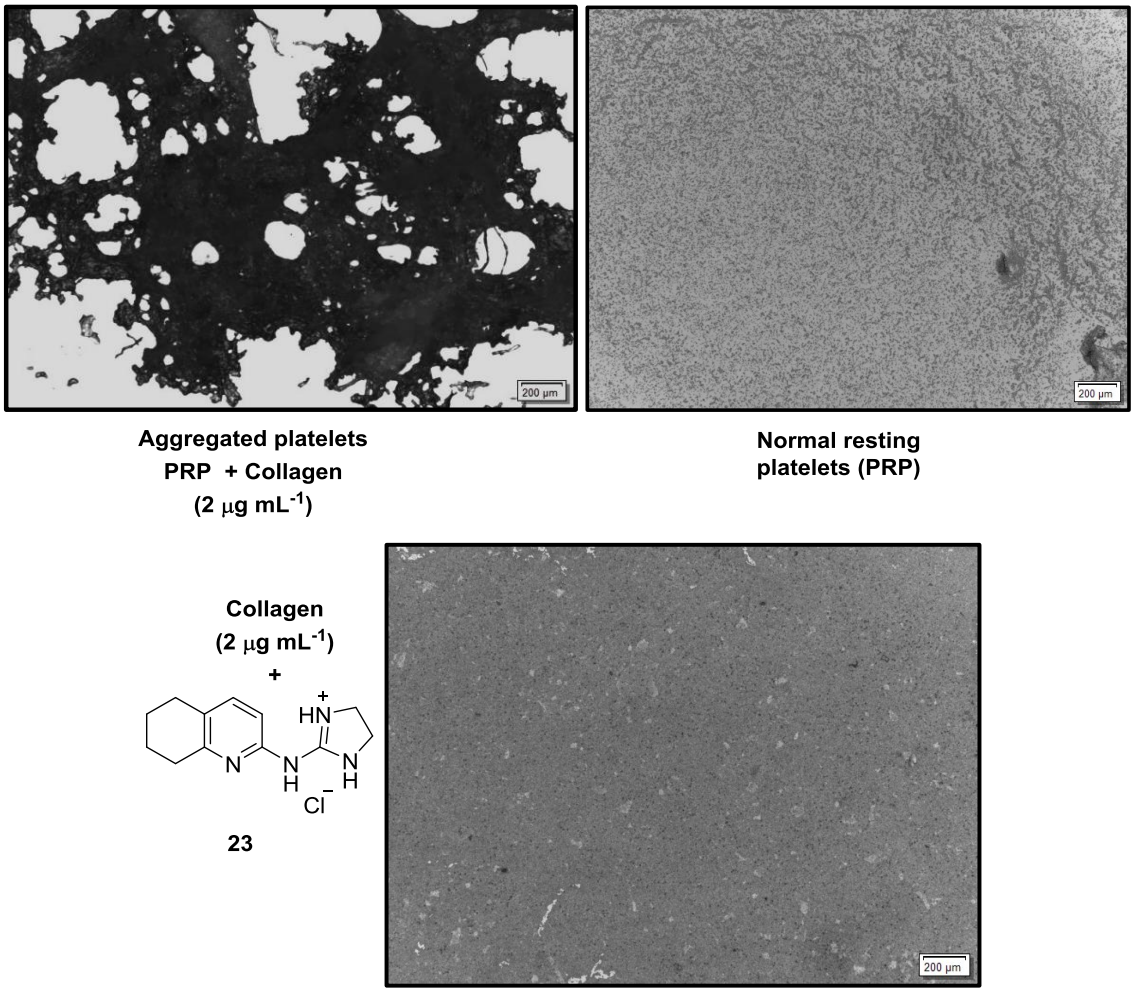

Figure 7.6.5. Photomicrographic analysis of platelet samples. Non-aggregated (resting) platelets in PRP (*top right*) and aggregated platelets (*top left*) compared with PRP in the presence of **23** (500 μM) and collagen (2 μg mL^{-1}) (*bottom*). Large aggregates are shown in black.

It was deemed necessary to probe whether these compounds may be interacting with plasma proteins or collagen, the platelet agonist, leading to a denaturation event thereby preventing the effect of collagen on platelets and therefore the induction of platelet aggregation. A control experiment was designed to infer whether **22** and **23** were inhibiting aggregation through this mechanism. Guanidine hydrochloride is frequently used as denaturation reagent for proteins and has been reported to denature both collagen and human serum albumin.[343–345] Consequently, an experiment was conducted using LTA analysis in the presence of **guanidine hydrochloride** (250 μM, 500 μM and 1 mM) with collagen (2 μg mL^{-1}). The results of this experiment are shown below in Fig. 7.6.6.

A

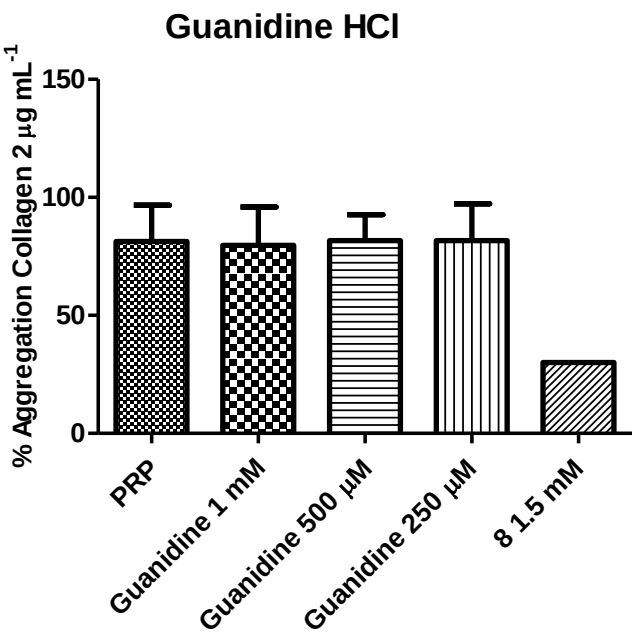

B

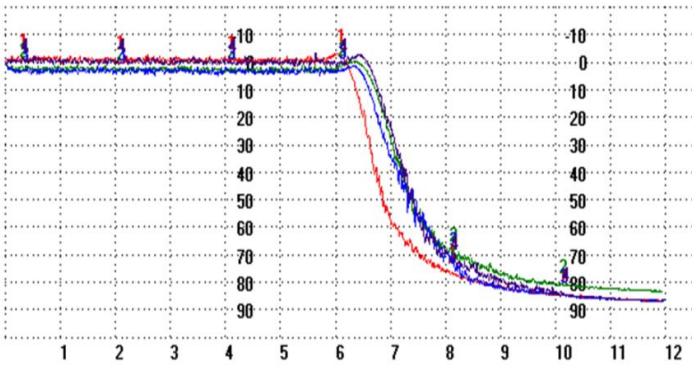

Figure 7.6.6. (A) Statistical analysis of the effect of **Guanidine hydrochloride** on platelet aggregation induced by collagen (2 µg mL^{-1}). Bars represent mean ± Standard Deviation. One-way analysis of variance (ANOVA), Tukey post-test (n = 3). (B) Representative LTA aggregation plot of **Guanidine hydrochloride** using collagen (2 µg mL^{-1}). Coloured line traces show similar percentages of aggregation at corresponding concentrations of **Guanidine hydrochloride** (250 µM, 500 µM and 1 mM) with collagen (2 µg mL^{-1}). Trace 1 (red) – PRP + collagen (2 µg mL^{-1}) only. Trace 2 (green) – 1 mM **Guanidine hydrochloride** + PRP + collagen (2 µg mL^{-1}). Trace 3 (blue) –500 µM **Guanidine hydrochloride** + PRP + collagen (2 µg mL^{-1}). Trace 4 (purple) – 250 µM **Guanidine hydrochloride** + PRP + collagen (2 µg mL^{-1}).

Optical microscopy also confirmed that **guanidine hydrochloride** has no antiplatelet activity, as large black aggregates (Fig. 7.6.7) were observed in PRP samples in the presence of **guanidine hydrochloride** (1 mM) upon addition of collagen (2 µg mL^{-1}). These results indicate that the observed antiplatelet activity of **22** and **23** is most likely the result of direct interaction with the platelets as **guanidine hydrochloride**, known to denature collagen and other plasma proteins, had no impact on collagen induced platelet aggregation.

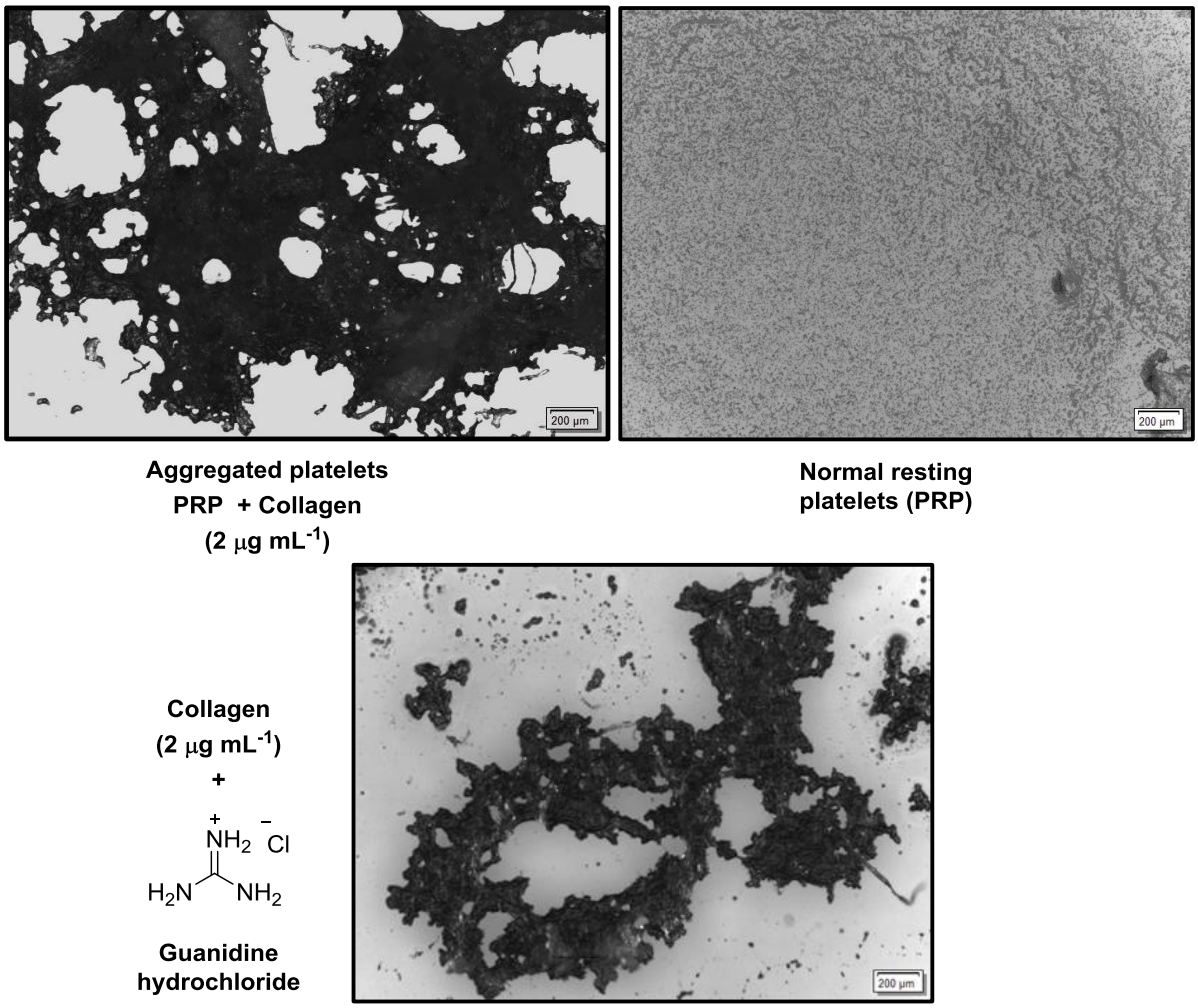

Figure 7.6.7. Photomicrographic analysis of platelet samples. Normal non-aggregated (resting) platelets in PRP (*top right*) and aggregated platelets (*top left*) compared with PRP in the presence of **Guanidine hydrochloride** (1 mM) with collagen (2 µg mL^{-1}) (*bottom*). Large aggregates are shown in black.

ADP is released from platelets and endothelial cells to induce platelet aggregation by acting at the $P2Y_1$ and $P2Y1_2$ nucleotide receptors on the surface of the platelets (Fig. 7.6.8).[346] A second set of LTA experiments were performed using ADP (10 µM) as an alternative agonist in order to confirm the antiplatelet activity observed for **22** and **23** and to corroborate that the effect of the compounds on platelet aggregation in previous experiments was not due to their interactions with collagen.

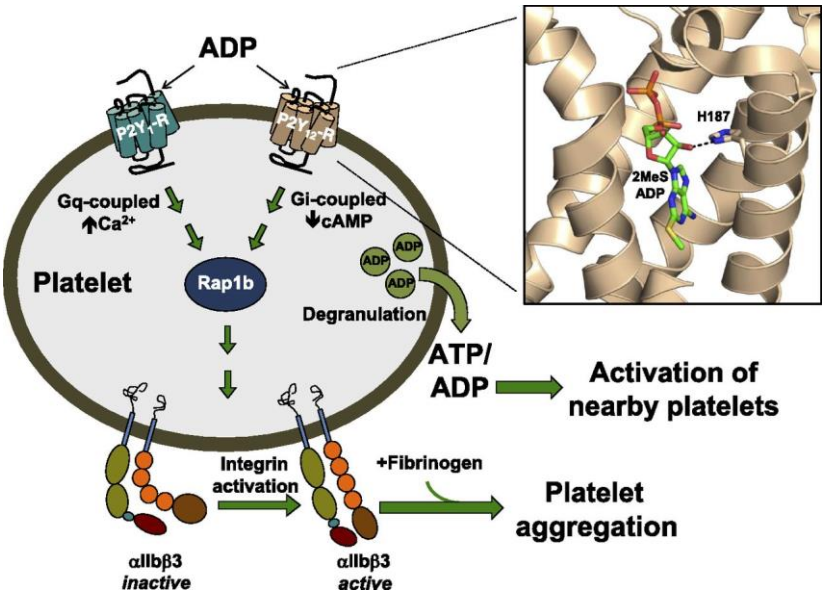

Figure 7.6.8. Schematic of ADP induced platelet aggregation *via* activation of $P2Y_1$ and $P2Y1_2$ receptors.[347]

The results obtained from the LTA analysis of **22** and **23** using ADP (10 µM) as an alternative agonist to induce platelet aggregation are summarised in Fig. 7.6.9.

A

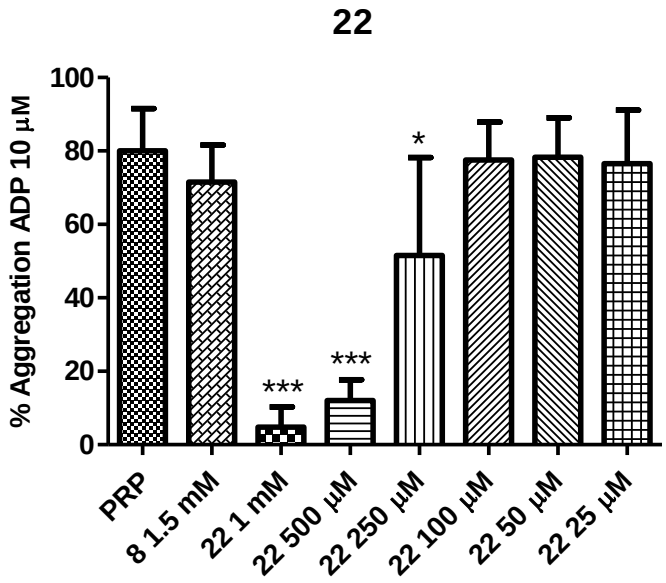

B

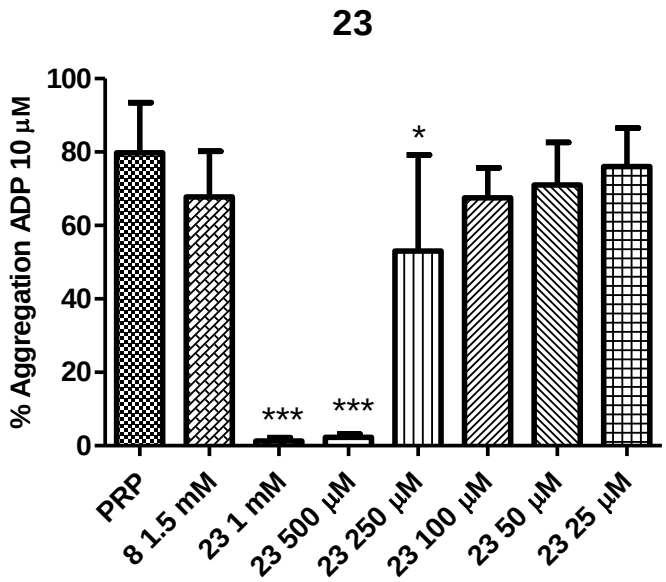

Figure 7.6.9. Statistical analysis of the effect of (A) **22** and (B) **23** on platelet aggregation induced by ADP (10 µM). Bars represent mean ± standard deviation. One-way analysis of variance (ANOVA), Tukey post-test (n = 3) followed by Dunnett's test. *P<0.05; ***P<0.001 vs control (PRP+ADP).

Finally, a control experiment using **guanidine hydrochloride** (250, 500 µM and 1 mM) using ADP (10 µM) as the agonist to induce aggregation was conducted for the purpose of comparison and completeness. **Guanidine hydrochloride** was again found to have no effect on platelet aggregation using this time ADP as the agonist, as shown in Fig. 7.6.10.

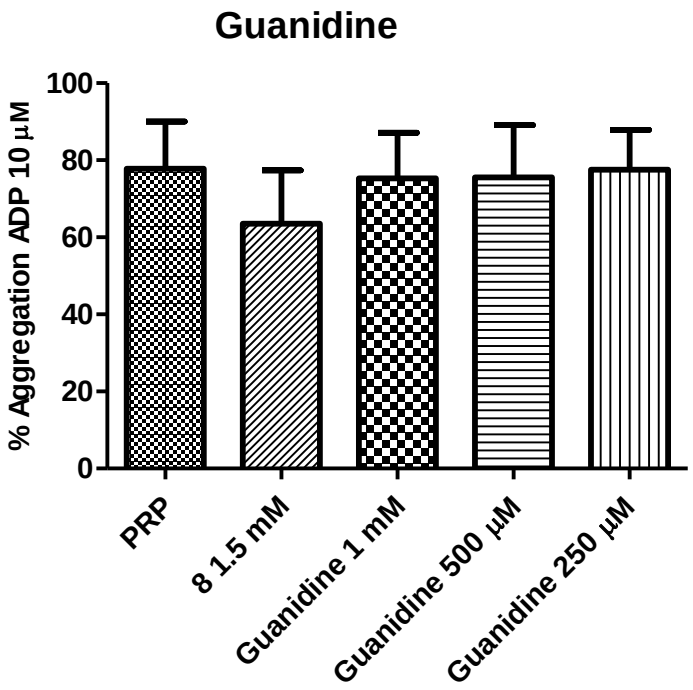

Figure 7.6.10. Statistical analysis of the effect of **Guanidine hydrochloride** on platelet aggregation induced by ADP (10 µM). Bars represent mean ± standard deviation. One-way analysis of variance (ANOVA), Tukey post-test (n = 3).

Altogether, these results indicate that compounds **22** and **23** both display strong antiplatelet activity regardless of the agonist used to induce aggregation, with **23** being the more potent inhibitor showing significant inhibition of aggregation at 250 µM. Comparison of the structures of **22** and **23** prompted the investigation of whether intramolecular hydrogen bonding (IMHB) between the cationic moiety and the pyridine nitrogen may be contributing to the antiplatelet activity of these compounds.

7.7. Investigating the impact of planarity on platelet function

Previous work within our group discovered that pyridin-2-yl guanidine and 2-aminoimidazoline derivatives are capable of adopting a coplanar arrangement due to an IMHB. This IMHB is formed between the pyridine nitrogen lone-pair and a proton from either the guanidinium or 2- aminoimidazolinium (*syn*-conformation, Fig.7.7.1).

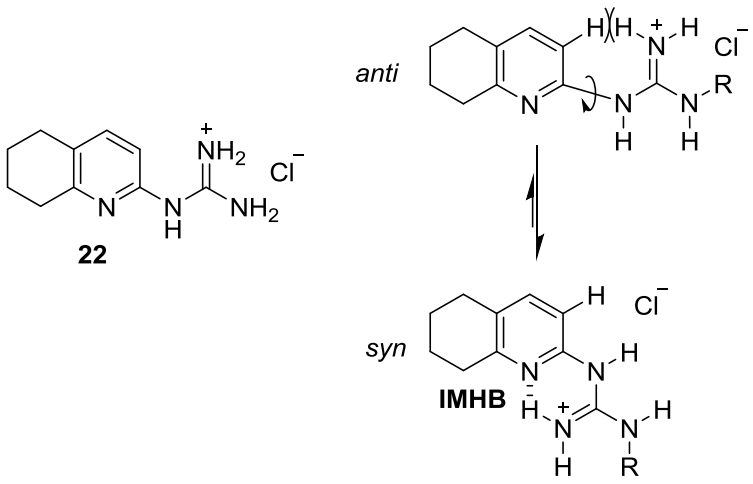

Figure 7.7.1. Structure and *syn*- and *anti*- conformations of **22**. The conformational preference induced by an IMHB is depicted in the *syn*-conformation.

This conformational preference is favoured relative to the *anti*-conformation (Fig. 7.7.1) where repulsion between aromatic protons from the pyridine ring and cationic NH protons forces the cationic moiety out of plane. This effect has been extensively studied within our group using computational, crystallographic and spectroscopic techniques which together provide sufficient evidence to support the claim that this conformational preference persists in an aqueous environment.[348]Hence, two additional compounds previously reported by Rozas *et al.* as α_2-AR ligands, **269** (α_2-AR agonist) and **270** (α_2-AR antagonist) were chosen and prepared from **271** and **272** in 95% and 80%, respectively, as outlined in Scheme 7.7.1.[132]

Scheme 7.7.1. Synthesis of **269** and **270**.

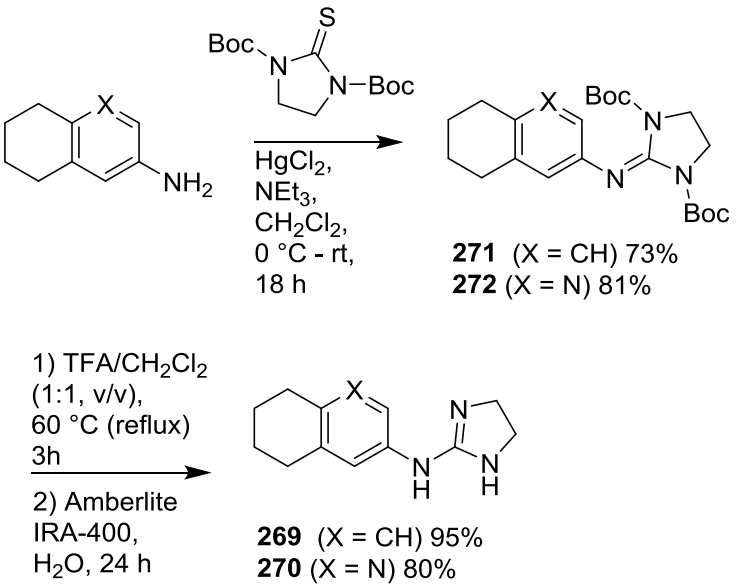

These compounds are bioisosteric analogues of **23** and were chosen as they are not capable of forming IMHB. Evaluating the effect of **269** and **270** on platelet function would allow us to explore the potential influence of IMHB, and hence planarity, on the antiplatelet activity of these structurally similar compounds.

7.7.1. Evaluating the effect of 269 and 270 on platelet function

Thus, compounds **269** and **270** were evaluated for their effect on platelet function using LTA analysis as discussed in Section 7.3. Since neither of these compounds was found to induce platelet aggregation upon addition to PRP, they were progressed to further evaluation for potential antiplatelet activity. The results obtained from LTA analysis of **270** using collagen (2 µg mL^{-1}) to induce platelet aggregation, summarised in Fig. 7.7.2, indicate that **270** displays no antiplatelet activity in PRP within the range of concentrations tested (25, 50, 100, 250 and 500 µM). This would suggest that the planarity induced by the IMHB may play an important role in the inhibition of platelet aggregation.

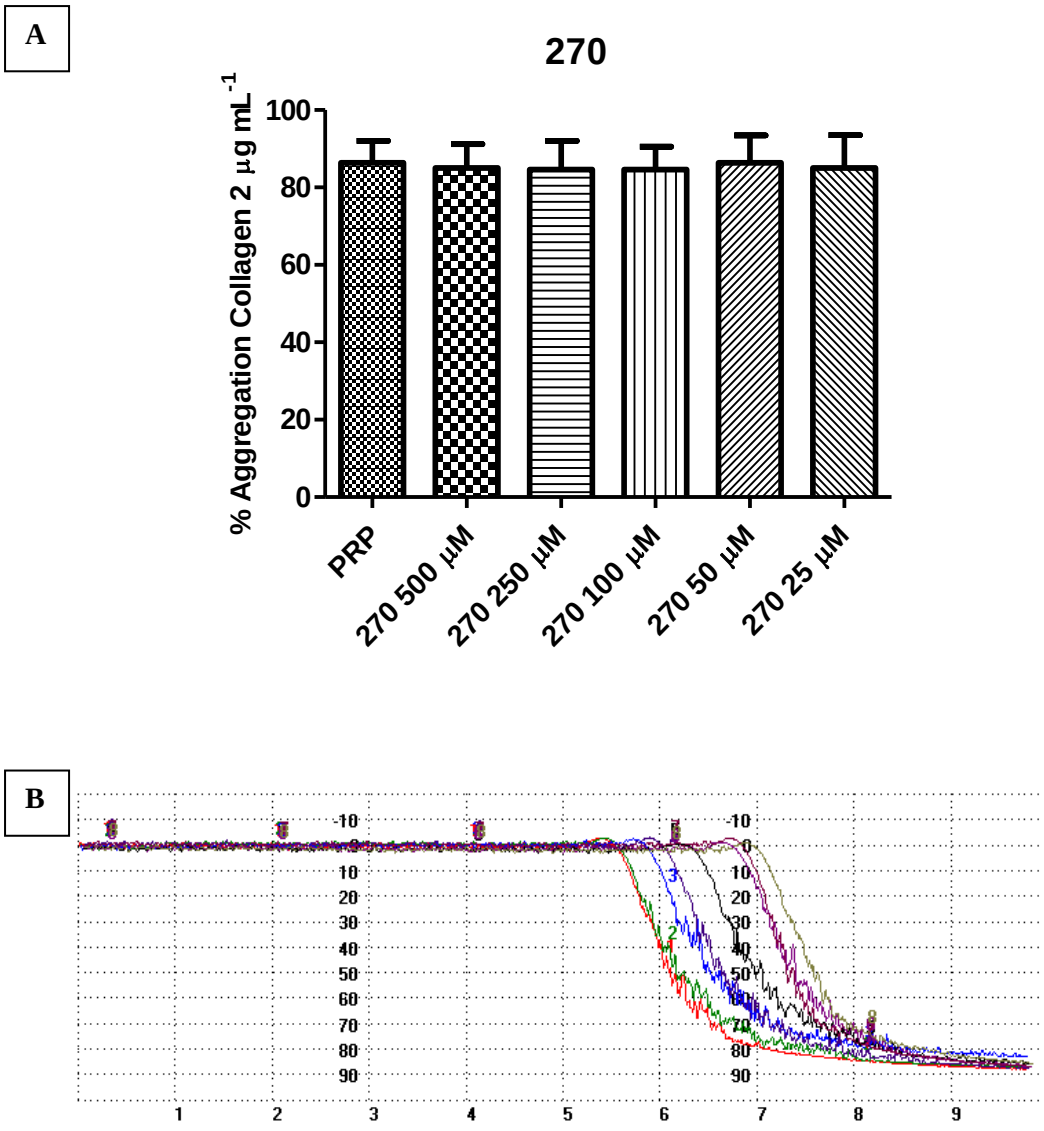

Figure 7.7.2. (A) Statistical analysis of the effect of **270** on platelet aggregation induced by collagen (2 µg mL^{-1}). Bars represent mean ± standard deviation. One-way analysis of variance (ANOVA), Tukey post-test (n = 3).

(B) Representative aggregation plot of **270** using collagen (2 µg mL^{-1}). Coloured line traces show different percentages of aggregation at corresponding concentrations of **270** (25, 50, 100, 250 and 500 µM) with collagen (2 µg mL^{-1}). Trace 1 (red) – PRP + collagen (2 µg mL^{-1}) only. Trace 2 (green) – 500 µM **270** + PRP + collagen (2 µg mL^{-1}). Trace 3 (blue) – 250 µM **270** + PRP + collagen (2 µg mL^{-1}). Trace 4 (purple) – 100 µM **270** + PRP + collagen (2 µg mL^{-1}).

Optical microscopy was again used to visualize platelets the presence of **270** (500 µM) and collagen (2 µg mL^{-1}). Big platelet aggregates (black) were clearly visible confirming that **270** (500 µM) does not display antiplatelet activity (Fig. 7.7.3).

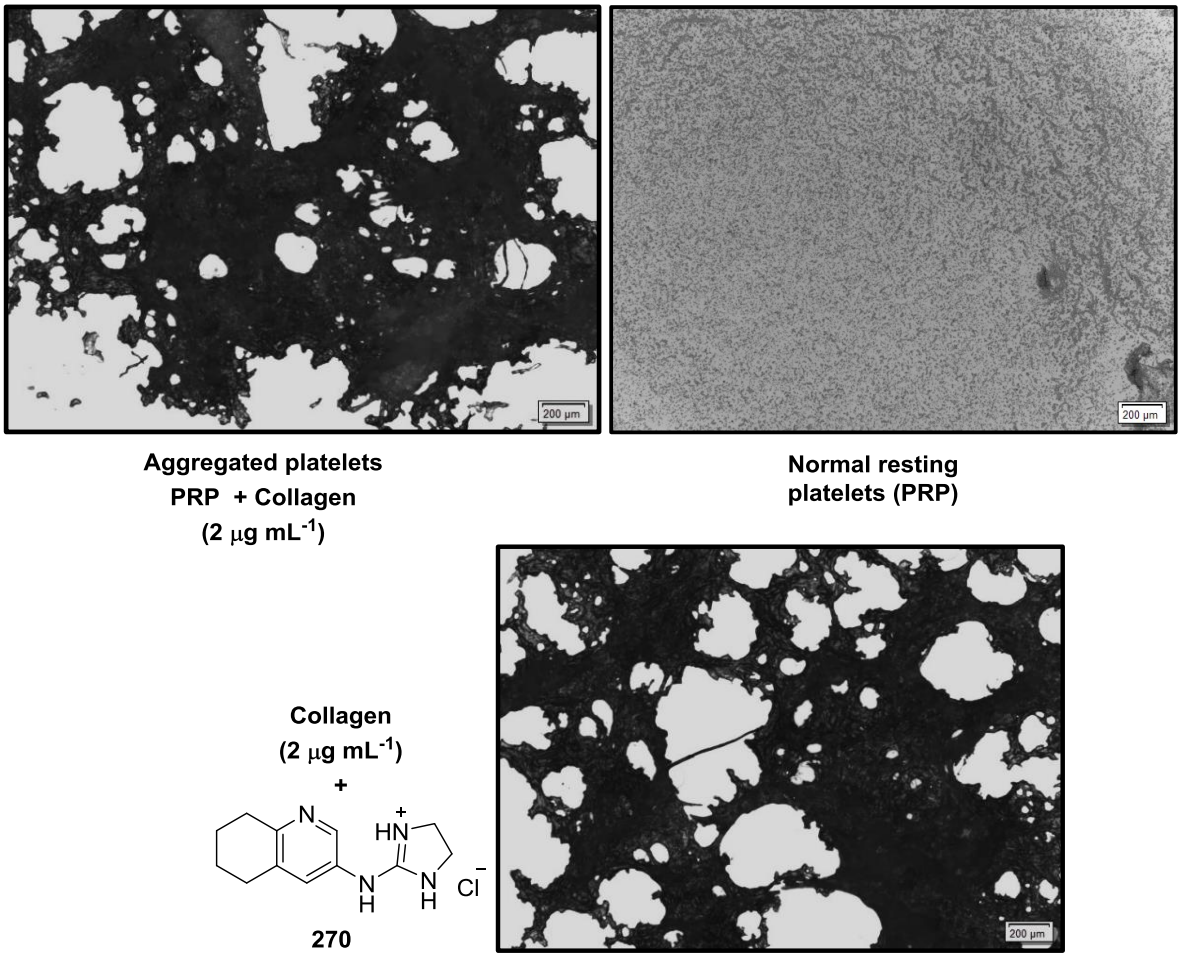

Figure 7.7.3. Photomicrographic analysis of platelet samples. Non-aggregated (resting) platelets in PRP (*top right*) and aggregated platelets (*top left*) compared with PRP incubated with **270** (500 µM) and after the addition of collagen (2 µg mL^{-1}) as agonist agent (*bottom*). Large aggregates are shown in black.

The results obtained from LTA analysis of **269** (25, 50, 100, 250, 500 µM and 1 mM) using collagen (2 µg mL^{-1}) as an agonist to induce platelet aggregation are summarised in Fig. 7.7.4. Unexpectedly, **269** exhibited potent antiplatelet activity at 250, 500 µM and 1 mM in collagen-induced PRP aggregation (2 µg mL^{-1}).

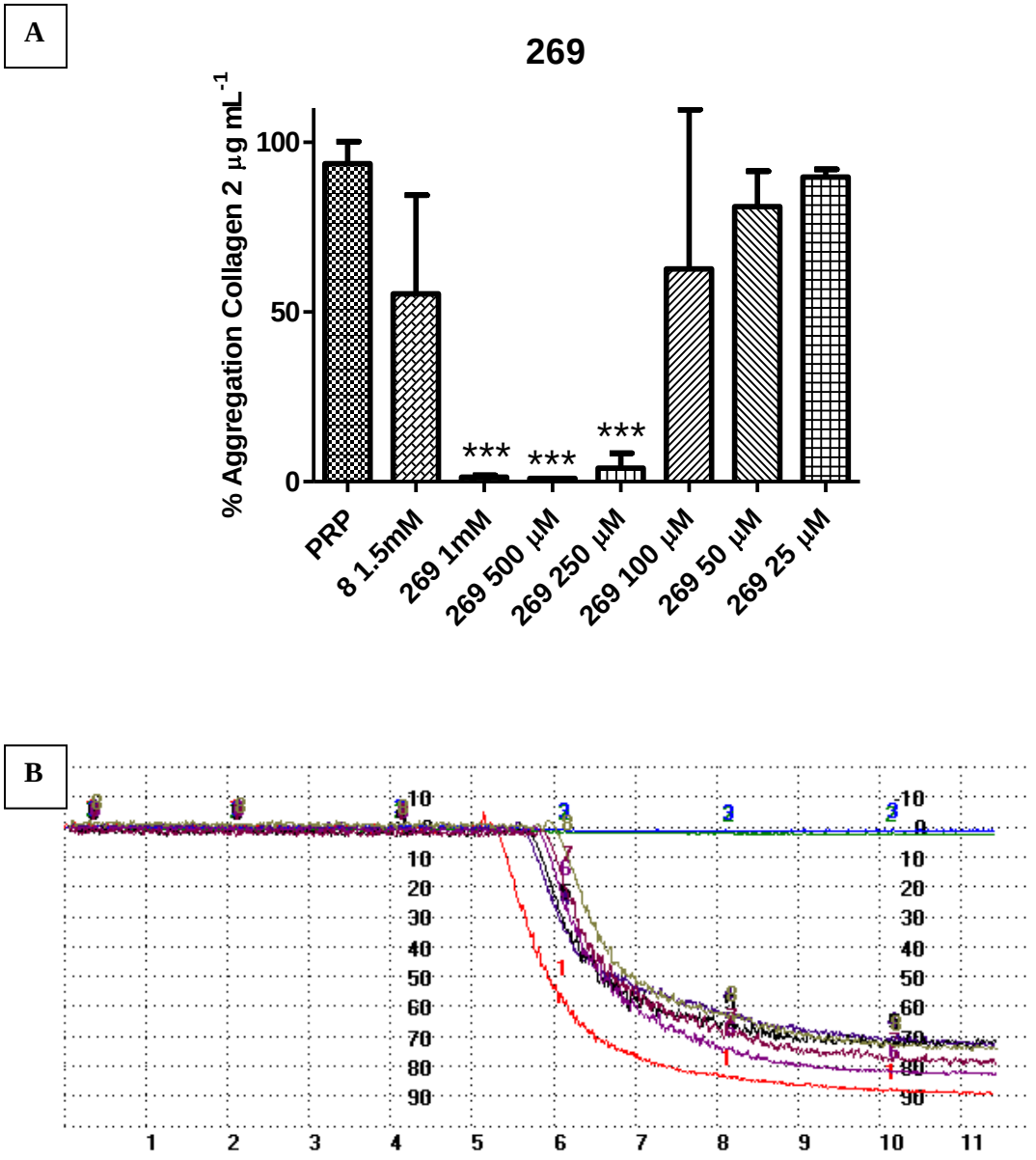

Figure 7.7.4. (A) Statistical analysis of the effect of **269** on platelet aggregation induced by collagen (2 µg mL^{-1}). Bars represent mean ± standard deviation. One-way analysis of variance (ANOVA), Tukey post-test (n = 3) followed by Dunnett's test. ***P<0.001 vs control (PRP + Collagen).

(B) Representative aggregation plot of **269** using collagen (2 µg mL^{-1}). Coloured line traces show different percentages of aggregation at corresponding concentrations of **269** (25, 50, 100, 250, 500 µM and 1 mM) with collagen (2 µg mL^{-1}). Trace 1 (red) – PRP + collagen (2 µg mL^{-1}) only. Trace 2 (green) – 1 mM **269** + PRP + collagen (2 µg mL^{-1}). Trace 3 (blue) – 500 µM **269** + PRP + collagen (2 µg mL^{-1}). Trace 4 (purple) – 250 µM **269** + PRP + collagen (2 µg mL^{-1}).

Optical microscopy was used to visualize a sample of PRP and collagen (2 μg mL^{-1}) in the presence of **269** (1 mM) confirming that no aggregates were formed (Fig. 7.7.5).

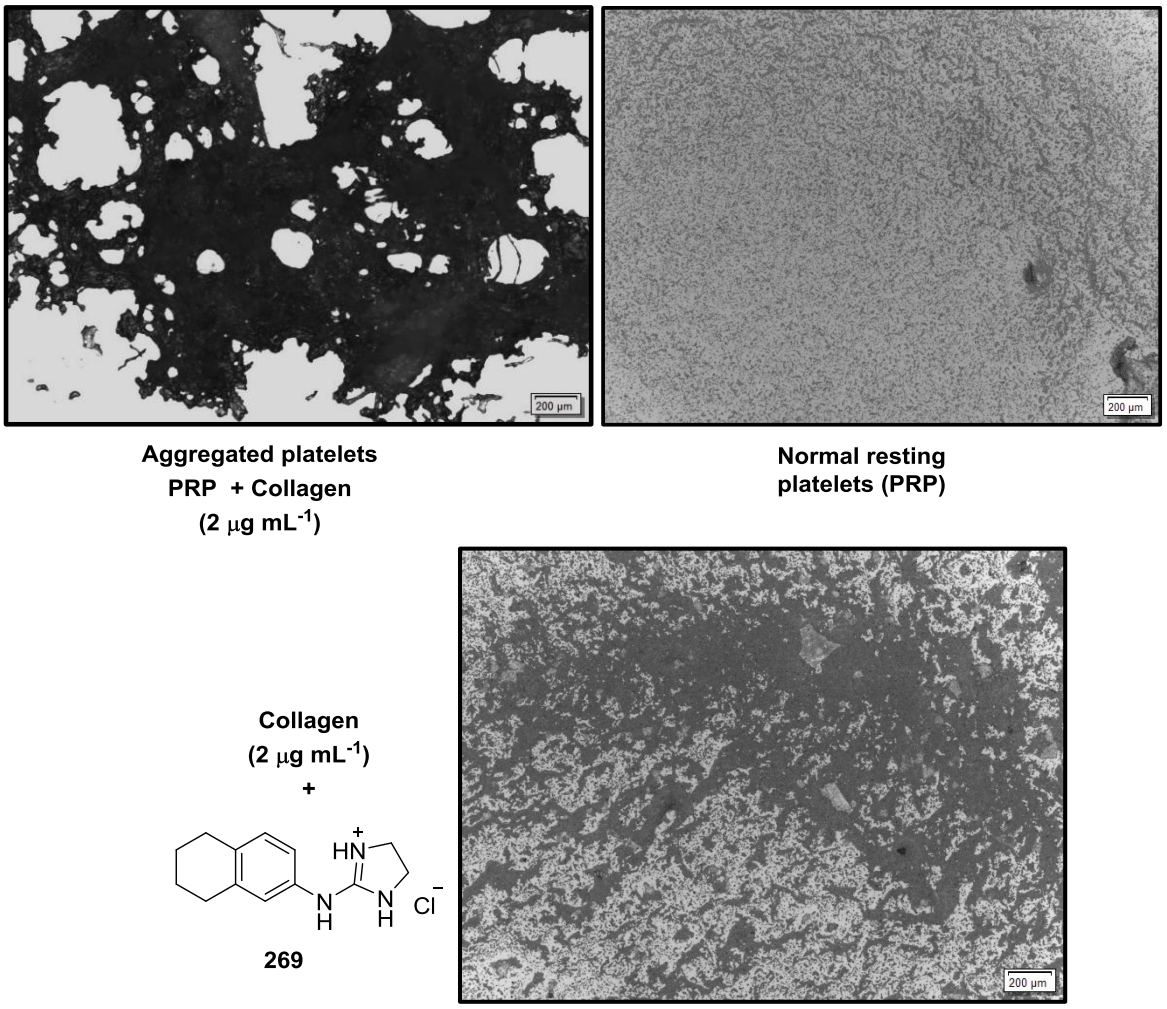

Figure 7.7.5. Photomicrographic analysis of platelet samples. Non-aggregated (resting) platelets in PRP (*top right*) and aggregated platelets (*top left*) compared with PRP in the presence of **269** (500 μM) with collagen (2 μg mL^{-1}) (*bottom*). Large aggregates are shown in black.

Additionally, LTA analysis using ADP (10 μM) as an alternative agonist was performed with **269** (25, 50, 100, 250, 500 μM and 1 mM) in order to corroborate the antiplatelet activity observed and allow for comparison with the results obtained for **22** and **23** (Fig. 7.7.6).

The results achieved are comparable to those obtained for **22** and **23** confirming that all three of these compounds exhibit potent antiplatelet activity at 500 µM in PRP regardless of which agonist is used to induce platelet aggregation.

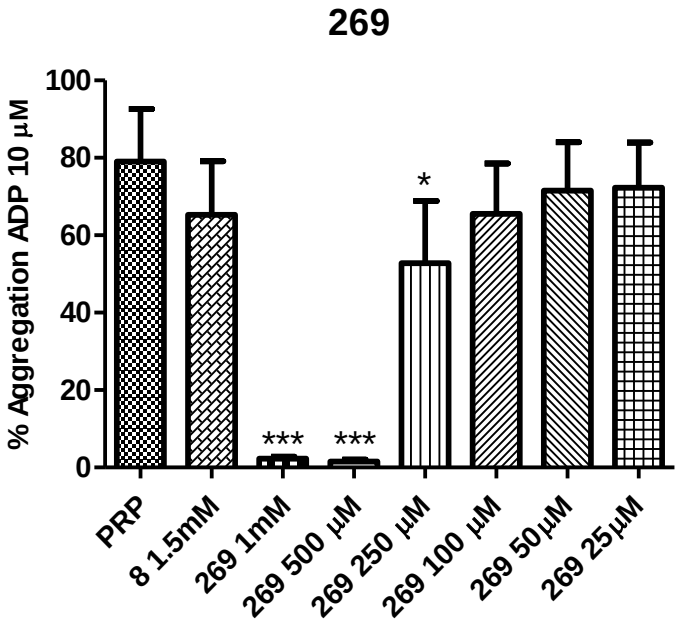

Figure 7.7.6. Statistical analysis of the effect of **269** on platelet aggregation induced by ADP (10 µM). Bars represent mean ± standard deviation. One-way analysis of variance (ANOVA), Tukey post-test (n = 3) followed by Dunnett's test. *P<0.05; ***P<0.001 vs. control (PRP +ADP).

Overall, the antiplatelet activity of **269** suggests that planarity induced by IMHB is not required to inhibit platelet aggregation. Furthermore, **269** exhibits the most potent antiplatelet effect at 250 µM, despite being an agonist at α_2-ARs. These results indicate that antagonism of platelet α_2-ARs may not be solely responsible for the antiaggregatory effects exhibited by this series of compounds and that an alternative target may also be involved.

Platelets are known to express two of the three α_2-AR on their surface, α_{2A}-and α_{2B}-ARs[349,350]. In human platelets, adrenaline/noradrenaline-induced platelet aggregation is mediated by these α_2-ARs.[350] Studies have shown that potent α_2-AR agonists such as clonidine and **UK-14,304** potentiate platelet aggregation whereas α_2-AR antagonists (*e.g.* idazoxan and **ARC 239**) can inhibit adrenaline/noradrenaline-induced platelet aggregation.[351,352]

The receptor profiles for the α_2-AR antagonists **22** and **23**, discussed in Chapter 4, showed that both of these ligands exhibited affinity for the α_{2B}-AR subtype whilst **23** also binds to the α_{2A}-AR (K_i = 635 nM). At present, it is unclear whether antagonism at α_2-ARs or other platelet cell surface receptors contributes to the antiplatelet activity of these ligands. Additional detailed pharmacological studies would be required to establish whether this series acts *via* a common pathway and identify the mechanism involved.

7.8. Platelet toxicity

The CytoTox-ONE Homogeneous Membrane Integrity Assay (Promega) was used to assess the potential cytotoxicity of the three antiplatelet compounds **22**, **23** and **269** in human platelets. This fluorometric cytotoxicity assay is a coupled enzymatic assay which measures the release of lactate dehydrogenase (LDH), a cytosolic enzyme, from damaged cells. The LDH activity is measured by the enzymatic conversion of lactate to pyruvate forming NADH, which is subsequently utilized by a second enzyme, diaphorase, present in the medium to convert resazurin into fluorescent resorufin (Fig. 7.8.1). This generation of resorufin is proportional to the amount of LDH released.[353]

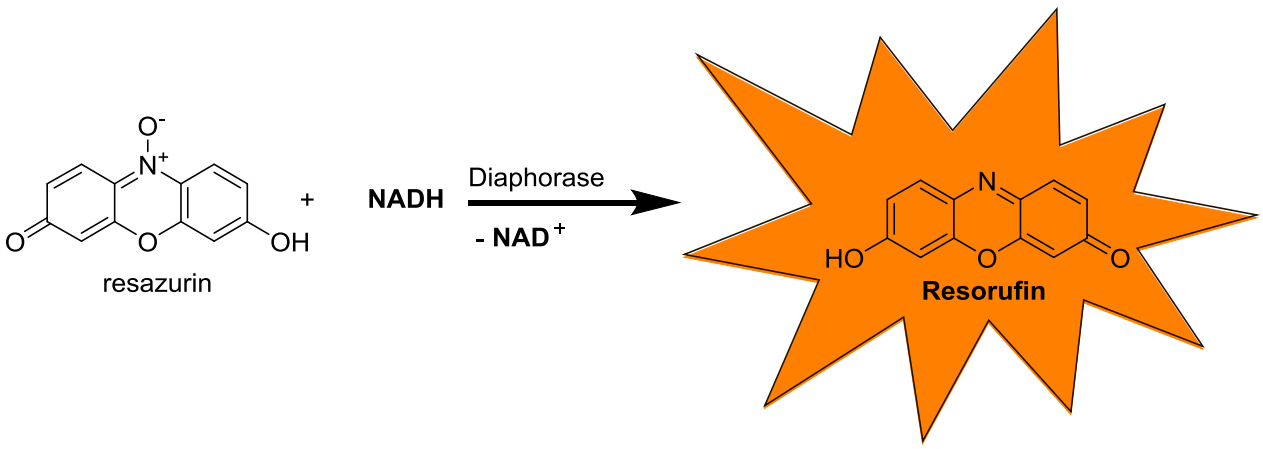

Figure 7.8.1. Enzymatic conversion of resazurin to fluorescent resorufin by diaphorase.

All three compounds showing antiplatelet activity (**22**, **23** and **269**) were incubated with washed platelets (WP) from three different donors at two different concentrations (500 µM and 1 mM). Platelet samples from the same donors were lysed and taken as 100% cytotoxicity for comparison. The effect of the vehicle (DMSO) was also measured for comparison and a sample of untreated washed platelets was used as a control. The results obtained are presented in Fig. 7.8.2.

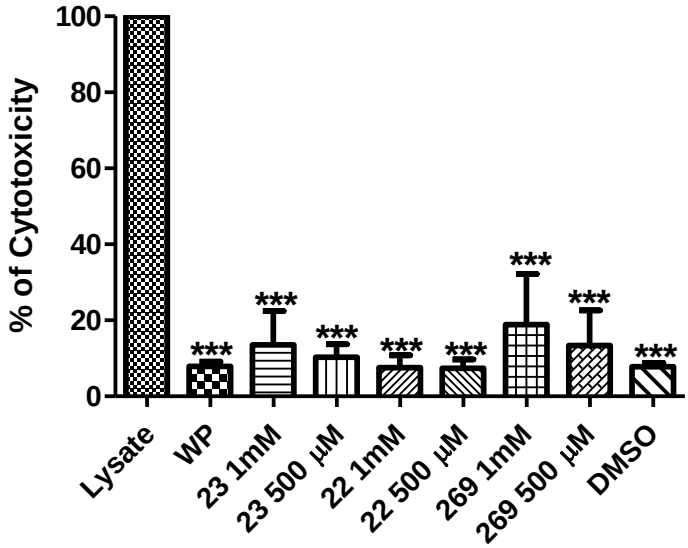

Figure 7.8.2. Statistical analysis of the cytotoxic effect of **22**, **23** and **269** in human platelets (500 µM and 1 mM). Bars represent mean ± standard deviation. One-way analysis of variance (ANOVA), Tukey post-test (n = 3) ***P <0.001 *vs.* lysate. The effect of the vehicle (DMSO) on platelet function was also tested (n = 3) to confirm that the vehicle was not interfering with the observed results.

These results demonstrated that these compounds are not toxic to platelets at high concentrations and confirm that the observed antiaggregatory effects are not the result of an increase in the light transmittance in the LTA due to platelets lysis.

7.9. Effect of 22, 23 and 269 on platelet activation: Flow Cytometry

Flow cytometry is a highly sensitive technique which allows the simultaneous and specific detection of multiple surface antigens at a single cell level. Flow cytometry can be utilized to study platelet activation by measuring the extent of expression of platelet surface specific antigens/receptors.[354] This method involves the use of monoclonal antibodies conjugated to fluorescent dyes which bind to specific platelet receptors. The fluorescence is then measured to facilitate detection, identification and quantification of the platelet receptors under study.[337]

The two most predominant and widely used platelet activation markers are P-selectin and activated GPIIb/IIIa. P-selectin is the largest member of the glycoprotein family of selectins located in the α-granule membrane and it is translocated to the plasma membrane after platelet activation. Glycoprotein IIb/IIIa (GPIIb/IIIa) is the most abundant platelet receptor which facilitates binding of platelets to Von Willebrand factor and enables platelet cross-linking by binding fibrinogen.[355] PAC-1 is the specific antibody for the activated form of GPIIb/IIIa.[356]

Thus, a number of experiments were conducted using flow cytometry to evaluate the effect of **22**, **23** and **269** on PAC-1 and P-selectin expression. Fluorescein isothiocyanate (FITC) was the fluorochrome used for measuring PAC1 expression and phycoerythrin (PE) for labelling P Selectin (BD Biosciences, Ireland) in platelets from three healthy donors. Platelet samples were incubated with two different concentrations of each of the test compounds (500 µM and 1 mM) and then collagen (2 µg/mL) added to induce platelet aggregation. Aliquots from each sample were collected from the LTA and incubated with saturated concentrations of the antibodies, diluted and subsequently analysed using flow cytometry.

The results obtain for these experiments to measure the effect of **22**, **23** and **269** (500 µM and 1 mM) on platelet activation using PAC1 expression are shown below in Fig.7.9.1.

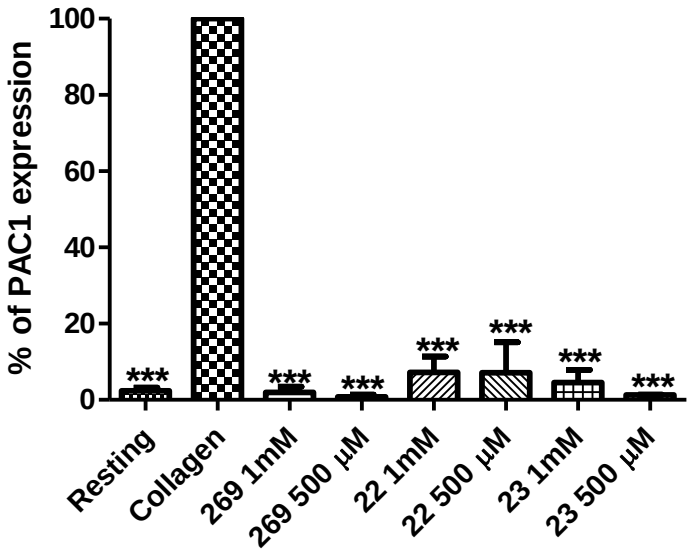

Figure 7.9.1. Statistical analysis of the PAC1 expression on platelets incubated **269**, **22** and **23** (1 mM and 500 µM) after induction of platelet aggregation by collagen. Bars represent mean ± Standard Deviation. One-way analysis of variance (ANOVA), Tukey post-test (n = 3) ***P<0.001 *vs.* aggregated platelets (collagen).

Representative plots from flow cytometry experiments analysing the expression of PAC1 on platelets incubated with the **22**, **23** and **269** (500 µM and 1 mM) and stimulated with collagen, including a sample of inactivated platelets and untreated collagen activated platelets as controls, are shown below in Fig. 7.9.2.

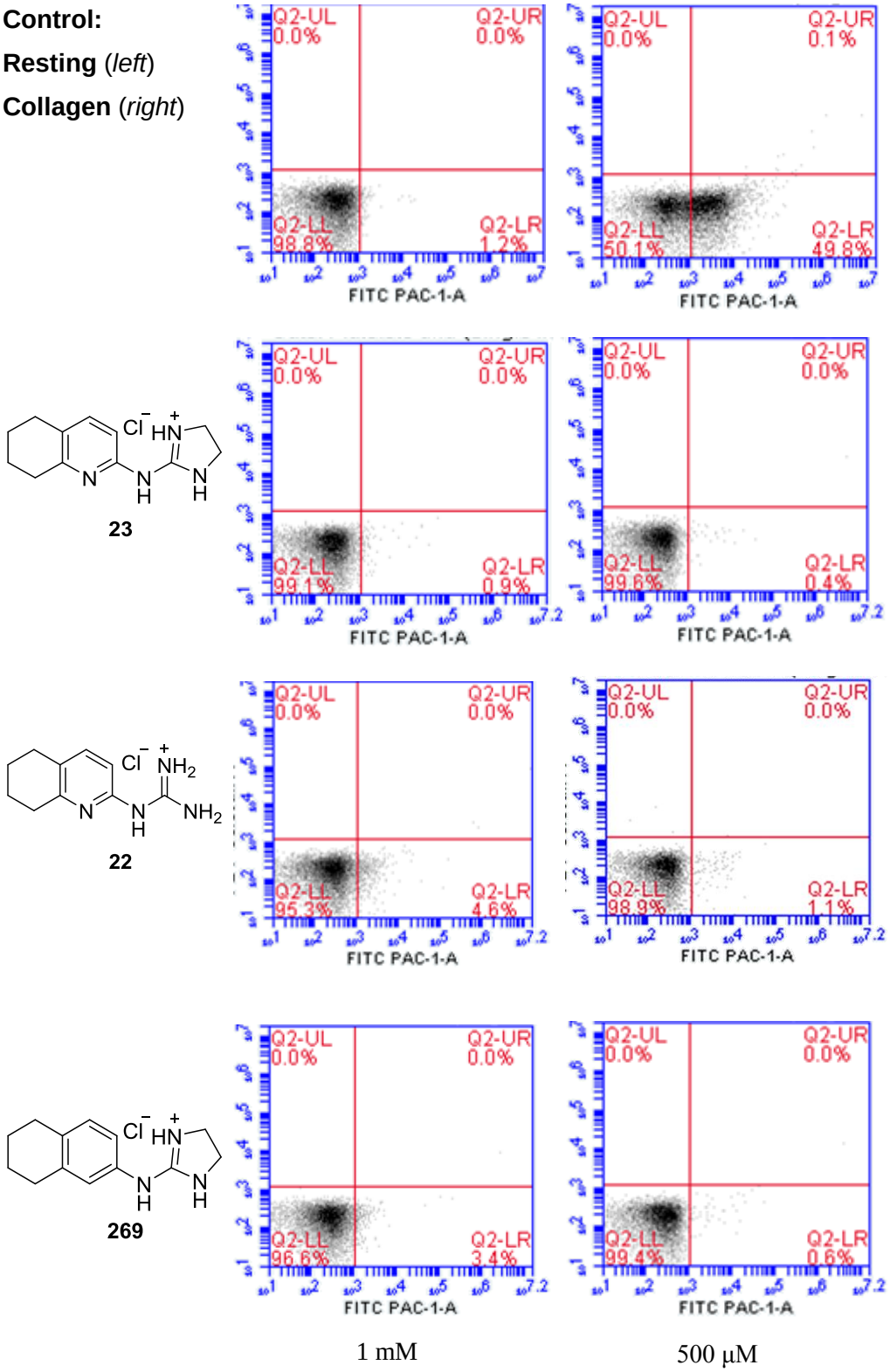

Figure 7.9.2. Representative plots from the analysis of PAC-1 expression with **22**, **23** and **269** (1 mM and 500 µM) on platelets byFlow Cytometry. Q2-LL represents inactivated platelets population. Q2-LR represents activated platelets population.

Similarly, the results obtain for the flow cytometry experiments to measure the effect of **22**, **23** and **269** (500 µM and 1 mM) on platelet activation using P-selectin expression are summarised in Figs. 7.9.3 and 7.9.4.

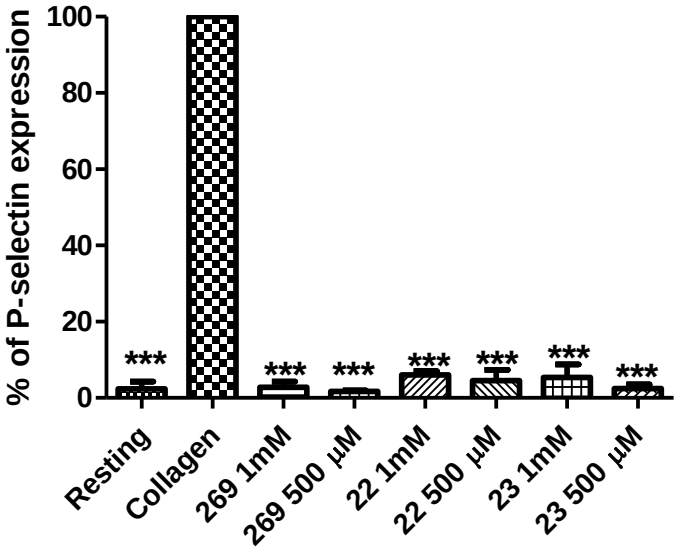

Figure 7.9.3. Statistical analysis of the P-selectin expression on platelets incubated with **269**, **22** and **23** (1 mM and 500 µM) and stimulated with collagen. Bars represent mean ± Standard Deviation. One-way analysis of variance (ANOVA), Tukey post-test (n = 3) ***P<0.001 *vs.* control (platelets activated with collagen).

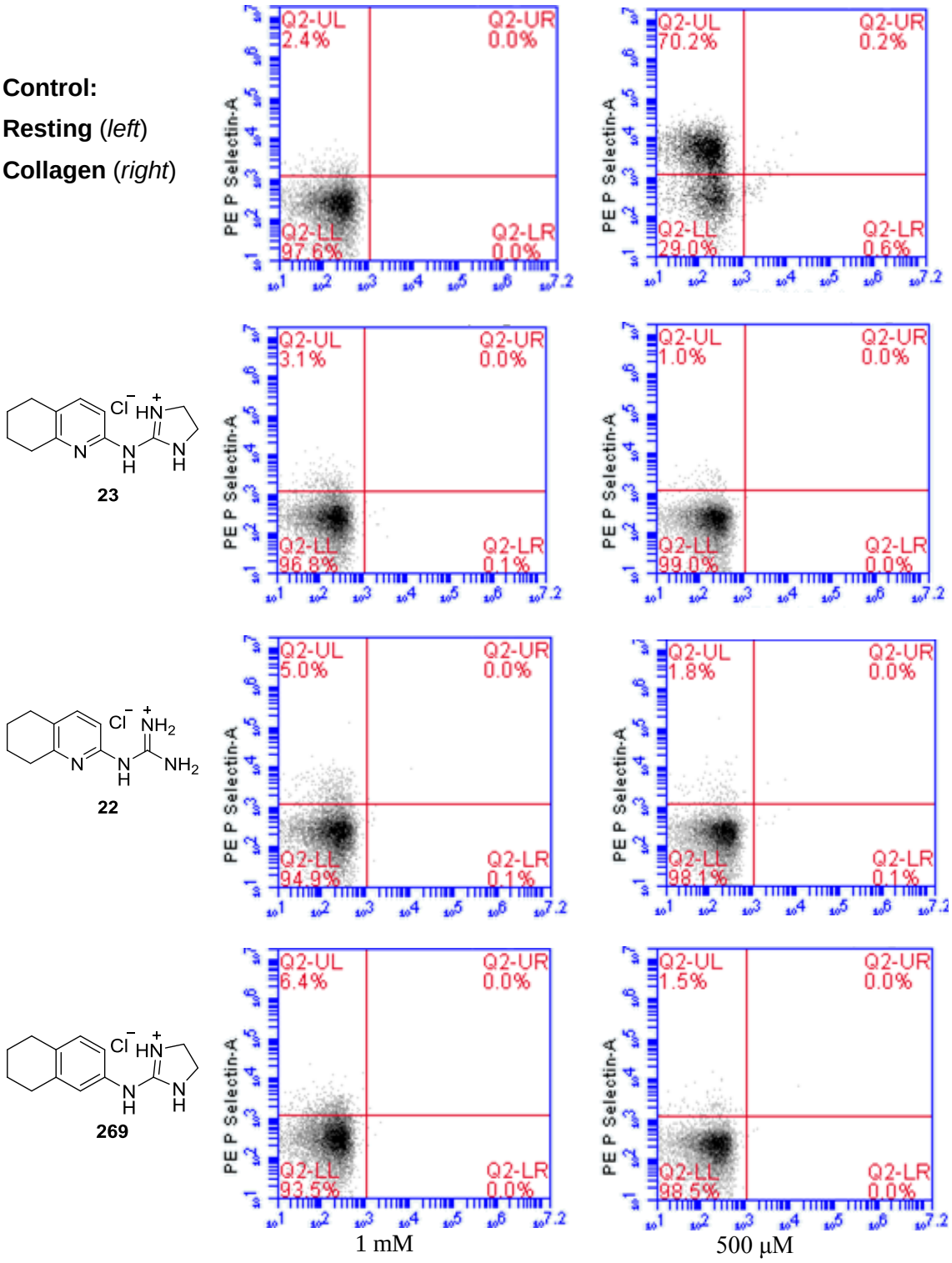

Figure 7.9.4. Representative plots from the analysis of P-selectin expression with **22**, **23** and **269** (1 mM and 500 µM) on platelets by Flow Cytometry. Q2-LL represents inactivated platelets population. Q2-UL represents activated platelets population.

In summary, these results provide comprehensive evidence that compounds **22**, **23** and **269** are capable of inhibiting the expression of both PAC-1 and P-selectin at the concentrations analysed (500 µM and 1 mM) without exhibiting cytotoxicity. This data suggests that the antiplatelet effects observed for these compounds involve a pathway which can inhibit activation and ultimately sustain the platelets in a resting inactivated state despite the presence of a platelet agonist, collagen.

7.10. Conclusion

The effect of compounds **34**, **22**, **23** and **65** on platelets viability and platelet function were investigated in collaboration with the School of Pharmacy and Pharmaceutical Sciences at Trinity College Dublin. This study revealed that **34** and **65** displayed no effect of platelet function; whereas, **22** and **23** both exhibited potent antiplatelet activity. In addition, investigation of a related derivative, compound **269**, suggested that IMHB was not necessary for this class of to exhibit antiaggregatory effects. Compound **269** was shown to display the most potent antiplatelet activity of the series, even though this compound is known to act as an agonist at α_2-ARs.[130]

The antiplatelet activity of these three compounds was confirmed by LTA analysis using two different agonists (collagen and ADP) to induce platelet aggregation. LDH cytotoxicity assay was utilized to evaluated potential cytotoxic effects of **22**, **23** and **269** in human platelets (500 µM and 1 mM). The results demonstrated that these compounds are not toxic to platelets at high concentrations.

Furthermore, flow cytometry studies in human platelets were conducted using **22**, **23** and **269** (500 µM and 1 mM). These studies revealed that these compounds inhibit the expression of two platelet activation markers (P-selectin expression and expression of PAC1) at both (500 µM and 1 mM) relative to control samples of resting platelets and activated platelets induced by collagen. This would indicate that these compounds can inhibit agonist induced activation of platelets and sustain the platelets in a resting inactivated state. Elucidation of the precise molecular mechanism/pathway through which these compounds exert the observed antiplatelet effects would require extensive pharmacological and biochemical investigation beyond the remit of this present work.

Chapter Eight

Conclusions and future work

8.1. Conclusions

The ultimate aim of this work was to refine and improve our understanding of the SARs concerning some of the most promising *hit* and *lead* α_2-AR ligands developed within our group. During this project a comprehensive pharmacological screening process was conducted at the NIMH PDSP (UNC Chapel Hill) involving a representative series of compounds which successfully uncovered a wealth of useful information. This process proved highly beneficial as it allowed for the affinities at a specific set of CNS targets to be measured and highlighted those compounds with potential to be developed as novel therapies for numerous neuropsychiatric disorders such as schizophrenia and MDD.

The highly valuable results obtained from this process revealed a number of unexpected trends and most importantly helped to identify a subset of compounds which exhibited preferential binding to the α_{2C}-AR, a primary objective of this work. As a results these compounds have been designated as *hit* compounds and form the basis for the development of novel treatments for schizophrenia. Other members of the series, which had previously been considered *lead* α_2-AR antagonists, were shown to display indiscriminate binding at numerous CNS targets and as such have been deemed unsuitable for further development.

This newly prioritised set of *hit* compounds have been utilized as template structures, helping to refine the design of proposed compounds and to focus the synthetic effort towards the successful preparation and characterisation of several promising derivatives. All final compounds prepared throughout the course of this work were fully characterised and their purity was determined by HPLC, with a minimum purity of 95% required for pharmacological testing. These novel derivatives will undergo preliminary pharmacological evaluation in human PFC brain tissue to determine their binding affinity for the α_2-AR in collaboration with the pharmacological laboratory of Prof. Luis Callado at UPV/EHU.

Hit candidates found to exhibit optimal affinity and selectivity profiles, specifically antagonists with α_2-subtype selectivity, will be submitted to the NIMH PDSP to undergo more extensive pharmacological investigation.

8.1.1. Screening results

The screening process helped us to identify which structures gave the most promising results for further development and provided justification for the exclusion of others which showed indiscriminate binding as discussed in Chapter 3. Extensive analysis of the data obtained from the screening has allowed identifying pharmacological profiles for the most promising members of the studied series. Comparison of these pharmacological profiles has helped to uncover some unprecedented findings concerning some pertinent CNS targets and a thorough review of the literature helped to rationalise the key observations.

This comprehensive evaluation of receptor engagement has altered our understanding of the pharmacological behaviour of some of the compounds studied. Thus, primary targets previously attributed to some *lead* compounds had to be redefined and this has prompted the revaluation of our current strategies searching for α_2-AR antagonist activity as detailed in section 3.7.6.5.[200,357,358] For example, a reclassification of the primary targets for **22** and **23** was required, as they are more accurately described as 5-HT_{2B}/5-HT_{2C} ligands with the α_2–AR now being considered their secondary target.

In-depth analysis of α_2-AR engagement of the screened series has aided the formulation of a hypothesis that relates the impact of small structural changes on the affinity for a given target, such as α_2-AR, sigma receptors and the histamine H2 receptors and may also correlate with the observed activity. Overall, the results derived from the screening process have served to revolutionise our interpretation of existing results and allows for the consolidation of various SARs which had been established for these ligands.

8.1.2. Synthesis

Careful consideration of key findings from the screening process facilitated the selection of five *hit* compounds (**34**, **22**, **67**, **65** and **36**) as detailed in section 3.8. Some of these compounds were chosen as templates for further synthetic development involving new cyclic and acyclic guanidine derivatives with the potential for optimized affinity, selectivity and receptor binding profile. These new compounds will contribute to the formulation of more definitive SARs. A major component of this work was to investigate the effects of structural variation on the α_2-ARs engagement of some *mono*-aryl *hit* compounds with the potential for further investigation of subtype selectivity.

A variety of synthetic routes to access new cyclic and acyclic guanidine derivatives were examined. The ultimate aim was to identify a robust and versatile synthetic route of modular design utilizing readily available starting materials. The impact on the α_2-AR profiles of ring expansion, from 2-arylaminoimidazolines to 2-arylamino-1,4,5,6-tetrahydropyrimidines, has been investigated with the synthesis and characterisation of novel derivatives being successfully completed as detailed in section 4.3.3. These analogues will serve as a representative series, preliminary evaluation of which will help to identify the potential utility of ring expansion. Synthesis of derivatives with substituents on the nitrogen atoms of both 2-arylaminoimidazolines and 2-arylamino-1,4,5,6-tetrahydropyrimidines rings has also been investigated.

An alternative guanylating reagent **134** was prepared and tested in the synthesis of 2-arylamino-1,4,5,6-tetrahydropyrimidines, but unfortunately proved unreactive under standard guanylation conditions. An alternative route utilizing aryl isothiocyanates was then investigated and successfully applied in the preparation of substituted and unsubstituted 2-arylamino-1,4,5,6-tetrahydropyrimidines and 2-aminoimidazolines. An efficient protocol was also identified and applied to the preparation of the required isothiocyanates and this route proved to be a viable alternative which allowed for the preparation of **209**.

Another goal of this work was to investigate a variety of core scaffolds for their potential to enhance α_2-AR engagement, with specific emphasis on subtype selectivity. In particular, compounds sharing common core structures with previously reported α_{2C}-selective derivatives were studied.

Accordingly, the affinity of a small 'in-house' library of acridine-9-carboxamide derivatives was evaluated for subtype selectivity at the α_{2A}- and α_{2C}-AR subtypes, using a transgenic CHO cell-based subtype selectivity assay. Evaluation of subtype selectivity data of these compounds revealed selectivity trends, which informed the design of new derivatives incorporating the common structural components shown to enhance affinity and selectivity for the α_{2C}-AR. These novel derivatives (**260**, **266**, **267** and **268**) have been successfully synthesised and characterised; however, financial issues affecting our collaborators prohibited α_2-AR subtype selectivity studies of these compounds.

Nonetheless, these derivatives have been submitted for evaluation of their activity using competition radioligand binding assays and [^{35}S]GTPγS binding functional assays performed in human PFC brain tissue at the pharmacological laboratory of Prof. Luis Callado at UPV/EHU.

8.1.3. Platelets study

The effect of compounds **34**, **22**, **23** and **65** on platelets viability and platelet function was investigated in collaboration with the School of Pharmacy and Pharmaceutical Sciences at Trinity College Dublin. This study revealed that **34** and **65** displayed no effect on platelet function, whereas **22** and **23** exhibited potent antiplatelet activity. In addition, investigation of a related derivative, compound **269**, suggested that IMHB was not necessary for these compounds to exhibit antiaggregatory effects and was shown to display the most potent antiplatelet activity of the series, even though this compound is known to act as an agonist at α_2-ARs.[130] The antiplatelet activity of these three compounds was confirmed by LTA analysis using two different agonists (collagen and ADP) to induce platelet aggregation.

The LDH cytotoxicity assay was utilized to evaluate potential cytotoxic effects of **22**, **23** and **269** in human platelets and the results demonstrated that these compounds are not toxic to platelets at high concentrations. Flow cytometry studies in human platelets were also conducted using **22**, **23** and **269**, revealing that these compounds inhibit the expression of two platelet activation markers (P-selectin and PAC1) at both 500 μM and 1 mM concentrations relative to controls. This data indicates that these compounds inhibit agonist induced activation of platelets and sustain the platelets in a resting inactivated state.

Elucidation of the precise molecular mechanism/pathway through which these compounds exert the observed antiplatelet effects would require extensive pharmacological and biochemical investigation beyond the remit of this present work.

Summarising, this work constitutes a strong foundation for future expansion and development of novel α_2-AR subtype selective ligands. The extensive receptor profiles here compiled will serve as a set of guidelines to assist the design of new compounds aimed at targeting a specific subset of CNS targets with improved affinity and specificity. The new compounds prepared throughout the course of this work will establish some core structural features necessary to impart optimal pharmacological properties required for the envisaged therapeutic application, whether it is the treatment of schizophrenia or MMD.

8.2. Future work

The comprehensive pharmacological evaluation of existing *lead* α_2-AR antagonists carried out in this work has identified the bioisosteric replacement of the aryl component with a heteroaryl ring equivalent as the most suitable and promising optimization strategy in the development of novel α_2-AR subtype selective ligands. However, further investigation is required to gain a more complete understanding of the pharmacological consequences of this strategy concerning α_2-AR engagement and the potential impact regarding other pertinent CNS targets (*i.e.* 5-HT receptors).

Current data suggests that whilst pyridine-benzene replacement does promote α_2-AR antagonism, it also appears to dramatically influence the primary binding profiles of some of these ligands. The pharmacological implications of this replacement are clearly exemplified by comparison of the data obtained for compounds **28** and **34** (Fig. 8.2.1). Thus, replacement of the benzene ring of **28** with pyridine imparted **34** with preferential binding to the α_{2C}-AR but no significant binding at the α_{2A}-AR. However, this modification also endowed **34** with significantly higher affinity for two 5-HT receptors relative to **28**, particularly the 5-HT_{2C} receptor.

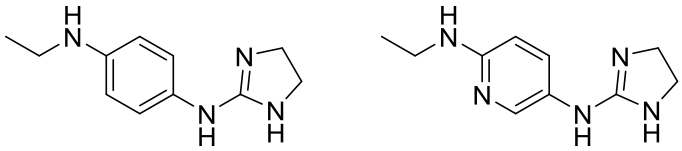

28
α_2-AR (PFC) K_i = 175 nM
α_{2C}-AR K_i = 586 nM
α_{2A}-AR K_i = 50 nM
5-HT_{2B} K_i = 2620 nM
5-HT_{2C} K_i = >10,000 nM

34
α_2-AR (PFC) K_i = 70 nM
α_{2C}-AR K_i = 3657 nM
α_{2A}-AR K_i = >10,000 nM
5-HT_{2B} K_i = 1320 nM
5-HT_{2C} K_i = 129 nM

Figure 8.2.1. Illustration of the pharmacological implications of pyridine-benzene replacement of **28** and **34**.

Additional pharmacological characterisation of pyridine-benzene replacement analogue pairs such as **28** and **34** would help to elucidate the extent of the mentioned pharmacological implications and, perhaps, to establish new SARs for these derivatives. The recently resolved crystal structure of the LSD/5-HT_{2B} complex may also prove useful in rationalising this trend.[235]

A number of unprecedented side reactions were encountered during the preparation of some proposed derivatives, with preliminary investigation helping to elucidate some of the factors involved. The oxidative dimerization and oxidative dehydrogenation reactions discussed in Chapter 4 require more detailed investigation to evaluate the substrate scope, utility and potential implications of these side reactions in relation to the preparation of certain aryl guanidine derivatives using $HgCl_2$ and NEt_3.

The impact of ring expansion, as discussed in section 8.1.2, was investigated by the preparation of a representative series of analogues (**106**, **107**, **108** and **209**) which are currently undergoing preliminary pharmacological evaluation. Subsequent comparison of these results with those of the corresponding *lead* analogues from previous studies will establish any potential benefits exhibited by this ring expanded series as summarised in Fig. 8.2.2.

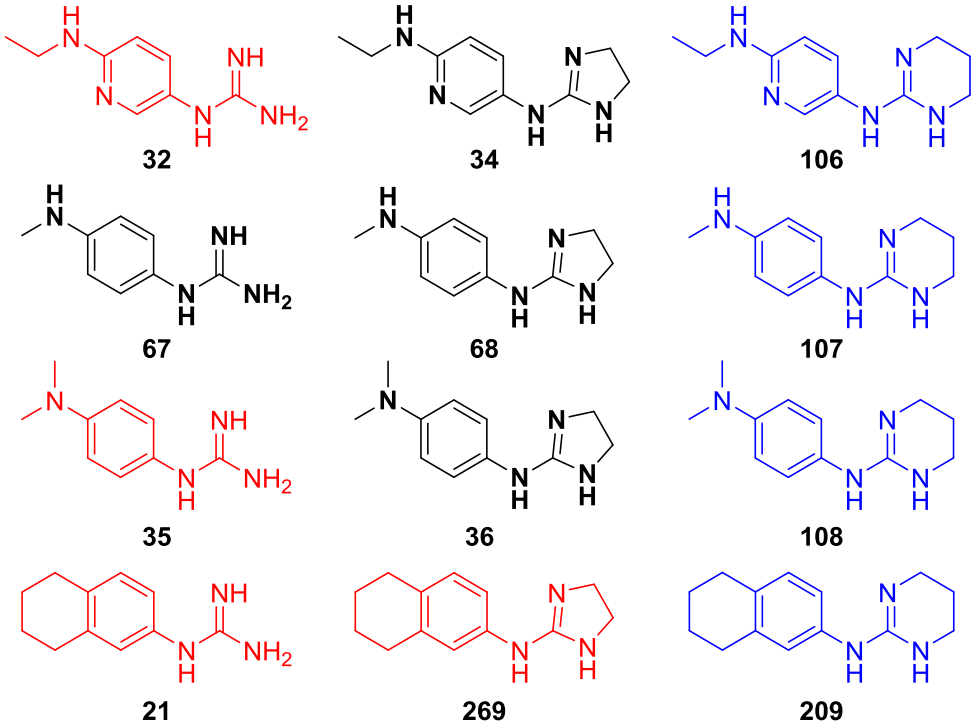

Figure 8.2.2. Summary of representative compounds from the ring expansion series. *Blue:* Novel 2-arylamino-1,4,5,6-tetrahydropyrimidine derivatives. *Black:* Ligands already screened at the PDSP (Chapter 3). *Red:* Other known ligands that require additional pharmacological screening at the PDSP.

Chapter Nine
Experimental

9.1. Materials and Methods

All commercial chemicals used were supplied by Sigma Aldrich, Fluorochem, and Santa Cruz Biotechnology and used without further purification unless otherwise stated. Deuterated solvents for NMR were purchased from Apollo or VWR. Solvents for synthesis purposes were used at GPR grade. Anhydrous CH_2Cl_2, THF, CH_3CN and Et_2O was obtained PureSolv MD-4EN Solvent Purification System. Silica gel 60 (Merck, 230-400 mesh) was used for flash column chromatography. All compounds were subject to purification using silica gel, unless otherwise stated. Analytical thin layer chromatography was carried out with silica gel 60 (fluorescence indicator F254; Merck) and visualised by UV irradiation.

Melting points are uncorrected and were measured with a Stuart SP-10 melting point apparatus. NMR spectra were recorded using Bruker DPX 400 (400.13 MHz for ^{1}H NMR and 100.61 MHz for ^{13}C NMR), Bruker AV 600 (600.13 MHz for ^{1}H NMR and 150.90 MHz for ^{13}C NMR), Bruker AV 400 (400.13 MHz for ^{1}H NMR and 100.61 MHz for ^{13}C NMR) or Agilent MR400 (400.13 MHz for ^{1}H NMR and 100.61 MHz for ^{13}C NMR) instruments. Chemical shifts, δ, are in ppm units downfield from an internal reference.[359] NMR data was processed using MestReNova software. The assignment of the signals was confirmed by 2D spectra (COSY, HMBC, HSQC). MALDI Tof spectra were acquired using a Waters MALDI Q-Tof Premier in positive or negative mode with DCTB (trans-2-[3-(4-tert-butylphenyl)-2-methyl-2-propenylidene]malononitrile) as the MALDI matrix. ESI mass spectra were acquired in positive and negative modes as required, using a Micromass time of flight mass spectrometer (TOF), interfaced to a Waters 2690 HPLC or a Bruker microTOF-Q III spectrometer interfaced to a Dionex UltiMate 3000 LC.

APCI experiments were carried out on a Bruker micrOTOF-Q III spectrometer interfaced to a Dionex UltiMate 3000 LC or direct insertion probe in positive or negative modes. Infrared spectra (IR) spectra were recorded on a Perkin-Elmer Spectrum 100 FT-IR spectrometer, equipped with a Universal ATR sampling accessory.

Purity of final hydrochloride salts was determined using HPLC. Purity was assessed using reverse phase HPLC with a diode-array detector scanning wavelengths from 200 to 950 nm. HLPC analysis was carried out using a Varian ProStar system equipped with a Varian Prostar 335 diode array detector and a manual injector (20 µL). For purity assessment, UV detection was performed at 245 nm and peak purity was confirmed using a purity channel. The stationary phase consisted of an ACE 5 C18-AR column (150 mm × 4.6 mm), and the mobile phase used the following gradient system, eluting at 1 mL/min: aqueous formate buffer (30 mM, pH 3.0) for 10 min, linear ramp to 85% methanol buffered with the same system over 25 min, hold at 85% buffered methanol for 10 min. Minimum requirement for purity was set at 95.0%.

9.2. General procedures

Method A: *General procedure for the synthesis of Boc-protected guanidine derivatives*

Each of the corresponding amines (1.0 eq.) in the CH_2Cl_2 at 0 °C was treated with $HgCl_2$ (1.1 eq.), *N,N'*-di(*tert*-butoxycarbonyl)-thiourea (1.0 eq.) or 1,3-bis(*tert*-butoxycarbonyl)-2-methyl-2-thiopseudourea (1.0 eq.) and NEt_3 (3.1 eq.). The resulting mixture was stirred at 0 °C for 1 h and for the appropriate duration at room temperature until reaction was adjudged complete by TLC analysis. Then the reaction mixture was diluted with EtOAc and filtered through a pad of Celite to remove mercury by-products. The filter cake was rinsed with EtOAc. The organic phase was extracted with water (2 x 30 mL), washed with brine (1 x 30 mL), dried over anhydrous Na_2SO_4, and concentrated under reduced pressure to give a residue that was purified by silica gel column chromatography, eluting with the appropriate solvent system.

Method B: *General procedure for the synthesis of the Boc-protected 2-iminoimidazolidine derivatives.*

Each of the corresponding amines (1.0 eq.) was treated in the CH_2Cl_2 at 0 °C with $HgCl_2$ (1.1 eq,), *N,N'*-di(*tert*-butoxycarbonyl)-imidazolidine-2-thione (1.0 eq.) and NEt_3 (3.1 eq.). The resulting mixture was stirred at 0 °C for 1 h and for the appropriate duration at room temperature until reaction was adjudged complete by TLC analysis. Then the reaction mixture was diluted with EtOAc and filtered through a pad of Celite to remove mercury by-products. The filter cake was rinsed with EtOAc. The organic phase was extracted with water (2 x 30 mL), washed with brine (1 x 30 mL), dried over anhydrous Na_2SO_4, and concentrated under reduced pressure to give a residue that was purified by neutral alumina column flash chromatography, eluting with the appropriate solvent system. The residue obtained after the column was recrystallized from the appropriate solvent when required.

Method C: *Synthesis of N,-N'-di-tert-butoxycarbonyl-2-arylimino-1,4,5,6-tetrahydropyrimidines.*

Each of the corresponding amines (1.0 eq.) was treated in the CH_2Cl_2 at 0 °C with $HgCl_2$ (2.0 eq.), *N,N'*-di(*tert*-butoxycarbonyl)-1,2,3,4-tetrahydropyrimidine-2-thione (1.0 eq.) and NEt_3 (3.5 eq.). The resulting mixture was stirred at 0 °C for 1 h and for the appropriate duration at room temperature until reaction was adjudged complete by TLC analysis. Then the reaction mixture was diluted with EtOAc and filtered through a pad of Celite to remove mercury by-products. The filter cake was rinsed with EtOAc.

The organic phase was extracted with water (2 x 30 mL), washed with brine (1 x 30 mL), dried over anhydrous Na_2SO_4, and concentrated under reduced pressure to give a residue that was purified by silica gel column chromatography, eluting with the appropriate solvent system.

Method D: *Procedure for the synthesis of hydrochloride salts.*

The Boc protected derivative (0.5 mmol) was treated with a solution of 50% TFA in CH_2Cl_2 (excess, 15 mL). After 3-6 h stirring at room temperature, CH_2Cl_2 and TFA were removed under reduced pressure to afford the trifluoroacetate salt. This salt was dissolved in H_2O (10 mL and 1.0 g of activated Amberlite IRA-400 chloride form (excess) was added, and the reaction was stirred overnight. After 24 h the Amberlite was removed by filtration, and the filtrate was washed with CH_2Cl_2 (2 x15 mL). The aqueous phase was concentrated to dryness under vacuum to yield the hydrochloride salt, ^{19}F NMR confirmed the absence of TFA.

Method E: *Synthesis of acridine-9-carboxamides using EDCI.* [360]

A 25 mL RBF was charged with acridine-9-carboxylic acid hydrate **246** (1.0 eq.) and EDCI (1.4 eq.). Anhydrous DMF (5 mL) was then added under Ar followed by a solution of amine (1.1 eq.) in anhydrous DMF (5 mL) added *via* syringe also under Ar. The reaction was then allowed to stir at room temperature under Ar until completion as adjudged by TLC analysis. The reaction mixture was then diluted with EtOAc (5 mL) and water (5 mL) to produce a precipitate which was collected by suction filtration, washed with EtOAc and dried in air to yield the desired product.

Method F: *Preparation of N,N'-di-Boc-thioureas and thiones.*[297]

To a solution of the corresponding thiourea (1.0 eq.) in dry tetrahydrofuran under Ar at approx. 0 °C, sodium hydride (4.5 eq.) as a 60% suspension in mineral oil was added and the reaction allowed to gradually warm to room temperature. The reaction was stirred at room temperature for 45 min to complete formation of the anion and before cooling again to approx. 0 °C prior to addition of di-*tert*-butyl dicarbonate (2.2 eq.). After stirring at room temperature for 8 h, the reaction was quenched by dropwise addition of a saturated aqueous $NaHCO_3$ solution and the mixture was poured onto water and the aqueous layer extracted with EtOAc. The combined organic phases were washed with brine, dried over Na_2SO_4 and concentrated under vacuum to give a residue that was either purified by silica gel column chromatography, eluting with the appropriate solvent system or recrystallized using the appropriate solvent system.

Method G: *Procedure for the synthesis of the hydrochloride salts from 1,3-disubstituted thioureas.*

A solution of the 1,3-disubstituted thiourea derivative (1 eq.) in CH_2Cl_2 at 0 °C was treated with $HgCl_2$ (1.1 eq.) and NEt_3 (3.1 eq.). The resulting mixture was stirred at 0 °C for 1 h and for the appropriate duration at room temperature until the reaction was adjudged complete by TLC analysis. Then the reaction mixture was diluted with MeOH and filtered through a pad of Celite to remove mercury by-products. The filter cake was rinsed with MeOH and the filtrate was concentrated under reduced pressure. The residue obtained was dissolved in water (10 mL) and washed with $CHCl_3$ (2 x 30 mL). The aqueous phase was concentrated under reduced pressure to give a residue which was purified by recrystallization/trituration or by neutral alumina column flash chromatography, eluting with the appropriate solvent system.

Method H: *Procedure for nitro reduction using Palladium on Carbon (Pd/C).*

A degassed (bubbled with N_2) solution of the appropriate nitro derivative (1 eq.) in the specified solvent was treated with 10% Pd/C (10 mol%) and the reaction mixture was stirred at room temperature under a hydrogen atmosphere (1.0 atm) at room temperature for 24 h or until the reaction was adjudged complete by TLC analysis.

The reaction mixture was diluted with the reaction solvent and filtered through a pad of Celite to remove the catalyst. The filter cake was rinsed with the reaction solvent and the filtrate was concentrated under reduced pressure to give a residue, which if required was purified by silica gel column chromatography, eluting with the appropriate solvent system or recrystallized.

Method I: *Synthesis of aryl isothiocyanates from aryl amines using 1,1'-thiocarbonyldiimidazole.*

A 50 mL 2-necked RBF was charged with the appropriate amine (1 eq.) and a stirring bar, sealed with septa, evacuated and placed under Ar atmosphere. Anhydrous CH_2Cl_2 or MeCN (~ 10 mL per mmol of amine) was added via syringe followed by1,1'-thiocarbonyldiimidazole (1.1 eq.) and reaction stirred at room temperature for 18h. Once reaction was complete as adjudged by TLC, the reaction mixture was concentrated under reduced pressure to give a residue that was purified by silica gel column chromatography, eluting with the appropriate solvent system.

9.3. Synthesis and Characterisation

N,N'-di-(*tert*-butoxycarbonyl)imidazolidine-2-thione (61)[128]

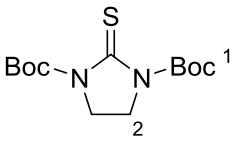

Following Method F, a solution of 2-imidazolidinethione (4.21 g, 41.21 mmol) in dry THF (40 mL) under Ar at approx. 0 °C cooling with an ice/water bath was treated with NaH (4.5 eq., 7.42 g, 185.44 mmol) as a 60% suspension in mineral oil. After 5 min, the ice/water bath was removed and the reaction was stirred for 10 min at room temperature. The mixture was cooled to approx. 0 °C and di-*tert*-butyldicarbonate (2.2 eq., 19.79 g, 90.66 mmol) was added. After 30 min, the ice/water bath was removed and the reaction mixture was stirred at room temperature for 18 h. The reaction was quenched by the drop-wise addition of saturated $NaHCO_3$ solution (25 mL), diluted with EtOAc (50 mL) and filtered through a bed of Celite. The filtrate was extracted with EtOAc (3 × 40 mL) and the combined organic phases were washed with brine (20 mL) and H_2O (20 mL), dried over $MgSO_4$, filtered and concentrated under vacuum affording **61** an orange crystalline solid (89%, 11.09 g, 36.68 mmol).

Yield: 89 % (11.09 g, 36.68 mmol).

M.P.: 116-118 °C (Lit. 117-119 °C).[128]

δ_H (400 MHz, $CDCl_3$) : 1.56 (s, 18H, $(CH_3)_3$-1), 3.92 (s, 4H, CH_2-2).

(*N*,*N*-di-*tert*-butoxycarbonyl)-thiourea (52)[361]

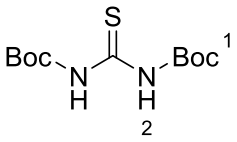

Following Method F, a solution of thiourea (4.00 g, 52.55 mol) in anhydrous THF (525 mL) at 0 ºC under Ar was treated with NaH (5.68 g, 0.236 mol) as a 60% suspension in mineral oil. The reaction was stirred in an ice/water bath for 5 min at approx. 0 ºC before being allowed to warm and stir for at room temperature 15 min. The reaction mixture was again cooled to approx. 0 ºC in an ice/water bath before di-*tert*-butyl dicarbonate (25.23 g, 0.116 mol) was added neat. After 30 min, the ice/water bath was removed and the reaction mixture was stirred overnight at room temperature.

The reaction mixture was quenched drop wise with a saturated $NaHCO_3$ solution (30 mL) to form an intense yellow solution and white cream. The mixture was poured into 200 mL of water and the aqueous layer was extracted with EtOAc (6 x 75 mL). The combined organic phases were washed with brine (1 x 50 mL), dried over $MgSO_4$, filtered and concentrated *in vacuo* affording an off-white powder. Recrystallization from boiling hexane affording **52** as a white solid (62%, 9.02 g, 32.66 mmol).

Yield: 62% (9.02 g, 32.66 mmol).

M.P: 118-120 °C (Lit. 120-122 °C).[361]

δ_H (400 MHz, $CDCl_3$): 1.52 (s, 18H, $(CH_3)_3$-1), 10.2 (broad s, 2H, NH-2).

4-*N*-Ethylaminoaniline (75)[131]

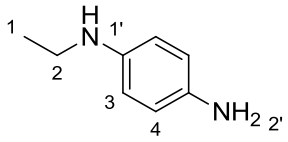

$LiAlH_4$ (0.89 g, 23.3 mmol) was suspended in anhydrous 1,4-dioxane (60 mL) under Ar in a 250 mL three necked RBF fitted with a reflux condenser and then cooled to approx. 0 °C in an ice/water bath *N*-acetyl-*p*-phenylenediamine (**76**, 1.02 g, 6.66 mmol) was added under Ar at approx. 0 °C portion-wise over 10 min. The ice/water bath was then removed and the reaction heated to 70 °C under reflux. Once the reaction was adjudged complete by TLC, it is cooled to approx. 0 °C before being quenched by dropwise the addition of aqueous 1M NaOH (~20 mL) followed by H_2O (~10 mL). The reaction mixture was filtered through a pad of Celite to remove the precipitate. The Celite pad was washed with $CHCl_3$ and the filtrate was extracted with isopropyl alcohol/$CHCl_3$ (2:8) (5 × 25 mL), dried over $MgSO_4$, filtered and concentrated *in vacuo* to give a residue which was purified silica gel column chromatography with gradient elution (100% Et_2O to 1:4 acetone/Et_2O) affording **75** as a red oil (56%, 0.51 g, 3.70 mmol).

Yield: 56% (0.51 g, 3.70 mmol).

δ_H (400 MHz, $CDCl_3$): 1.24 (t, 3H, *J* 7.0 Hz, CH_3-1), 3.08 (m, 2H, CH_2-2), 3.18 (bs, 3H, NH-1' and NH_2-2'), 6.5 (d, 2H, *J* 8.5 Hz, CH-3), 6.59 (d, 2H, *J* 8.5 Hz, CH-4).

ν_{max} (ATR)/cm^{-1}: 3356 (N-H), 1580 (C-C), 1248 (C-N).

HRMS: (m/z ESI^+) Found: 137.1073 $(M+H)^+$ $C_8H_{13}N_2$ Requires: 137.1079

4-*N*-Methylaminoaniline (70)[131]

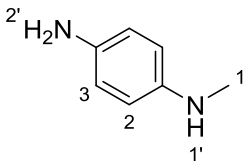

Following method H, a degassed solution of **74** (1.00 g, 6.57 mmol) in EtOAc (20 mL) was treated with 10% Pd/C (10 mol%, 0.69 g, 0.66 mmol) and the reaction mixture was stirred at room temperature for 18 h under H_2 (1 atm). The reaction mixture was diluted with EtOAc (20 mL) EtOAc and filtered through a pad of Celite to remove the Pd/C. The filter cake was rinsed with EtOAc and filtrate was concentrated *in vacuo* to afford **70** as a red oil (95%, 0.76 g, 6.24 mmol).

Yield: 95% (0.763 g, 6.24 mmol).

δ_H (400 MHz, $CDCl_3$): 2.79 (s, 3H, CH_3-1), 3.27 (bs, 3H, NH-1' and NH_2-2'), 6.54 (d, 2H, *J* 8.4 Hz, CH-2), 6.64 (d, 2H, *J* 8.4 Hz, CH-2).

ν_{max} (ATR)/cm^{-1}: 3340 (N-H), 3098 (C-H), 1667(C-H).

1-[2,3-Di(*tert*-butoxycarbonyl)guanidino]-4-methoxybenzene (B65)[191]

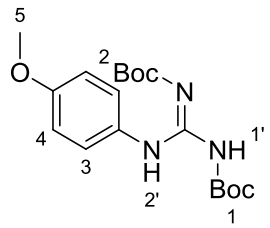

Following method A, a solution of 4-methoxyaniline (0.37 g, 3.0 mmol) in CH_2Cl_2 (5 mL) at 0 °C was treated with $HgCl_2$ (0.89 g, 3.3 mmol), **52** (0.83 g, 3.0 mmol) and NEt_3 (1.3 mL, 9.3 mmol). The resulting mixture was stirred at 0 °C for 1 h and 18 h at room temperature. The usual workup followed by silica gel column chromatography afforded **B65** as a white solid (80%, 0.88 g, 2.4 mmol).

Yield: 80% (0.88 g, 2.4 mmol).

M.P: 180-182 °C (Lit. 181-183 °C).[191]

δ_H (400 MHz, $CDCl_3$): 1.52 (s, 9H, $(CH_3)_3$-1), 1.56 (s, 9H, $(CH_3)_3$-2), 3.85 (s, 3H, CH_3-5), 6.90 (d, 2H, *J* 8.0 Hz, CH-4), 7.50 (d, 2H, *J* 8.0 Hz, CH-3), 10.18 (bs, 1 H, NH-1'), 11.70 (bs, 1 H, NH-2').

_N_-(4-[2,3-Di(*tert*-butoxycarbonyl)guanidino]phenyl)-piperidine (B63)[191]

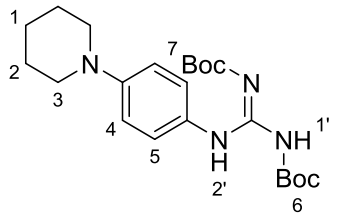

Following method A, a solution of *N*-(4-aminophenyl)-piperidine (0.53 g, 3.0 mmol) in CH_2Cl_2 (5 mL) at 0 °C was treated with $HgCl_2$ (0.89 g, 3.3 mmol), **52** (0.83 g, 3.0 mmol) and NEt_3 (1.3 mL, 9.3 mmol). The resulting mixture was stirred at 0 °C for 1 h and 18 h at room temperature. The usual workup followed by silica gel column chromatography afforded **B63** as a white solid (60%, 0.75 g, 1.8 mmol).

Yield: 60% (0.75 g, 1.8 mmol).

M.P: 160-162 °C (Lit. 160-162 °C).[191]

δ_H (400 MHz, $CDCl_3$): 1.56 (m, 20H, $(CH_3)_3$-6, $(CH_3)_3$-7 and CH_2-1), 1.69 (m, 4H, CH_2-2), 3.11 (m, 4H, CH_2-3), 6.89 (d, 2H, *J* 9.0 Hz, CH-4), 7.40 (d, 2H, *J* 9.0 Hz, CH-5), 10.07 (bs, 1H, NH-1'), 11.87 (bs, 1H, NH-2').

1-[2,3-di(tert-butoxycarbonyl)guanidino]-4-(N,N-diethyl)benzene (B64)[191]

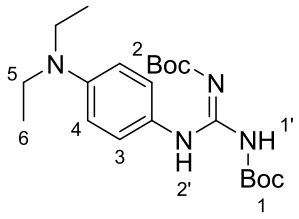

Following method A, a solution of *N*,*N*-diethyl-*p*-phenylenediamine (0.83 g, 3.0 mmol) in CH_2Cl_2 (5 mL) at 0 °C was treated with $HgCl_2$ (0.89 g, 3.3 mmol), **52** (0.83 g, 3.0 mmol) and NEt_3 (1.3 mL, 9.3 mmol). The resulting mixture was stirred at 0 °C for 1 h and then for 18 h at room temperature. The usual workup followed by silica gel column chromatography afforded **B64** as a white solid (71%, 0.87 g, 2.13 mmol).

Yield: 71% (0.87 g, 2.13 mmol).

M.P: 144-146 °C (Lit. 146-148 °C).[191]

δ_H (400 MHz, $CDCl_3$): 1.16 (t, 6H, *J* 7.0 Hz, CH_3-6), 1.51 (s, 9H, $(CH_3)_3$-1), 1.55 (s, 9H, $(CH_3)_3$-2), 3.33 (q, 4H, *J* 7.0 Hz, CH_2-5), 6.66 (d, 2H, *J* 8.0 Hz, CH-4), 7.40 (d, 2H, *J* 8.0 Hz, CH-3), 10.10 (bs, 1H, NH-1'), 11.67 (bs, 1H, NH-2').

1-[2,3-di(*tert*-butoxycarbonyl)guanidino]-4-(*N*-ethyl-*N*-methyl)benzene (B66) [131]

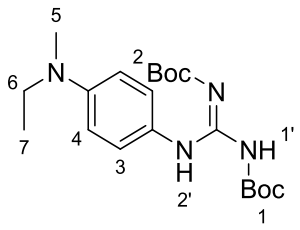

Following method A, a solution of *N*-ethyl-*N*-methyl-benzene-1,4-diamine (0.45 g, 3.0 mmol) in CH_2Cl_2 (5 mL) at 0 °C was treated with $HgCl_2$ (0.89 g, 3.3 mmol), **52** (0.83 g, 3.0 mmol) and NEt_3 (1.3 mL, 9.3 mmol). The resulting mixture was stirred at 0 °C for 1 h and 18 h at room temperature. Usual work up followed by silica gel column chromatography afforded **B66** as a white solid (60%, 0.71 g, 1.8 mmol).

Yield: 60% (0.71 g, 1.8 mmol).

M.P: 118-120 °C (Lit. 120-122 □C). [131]

δ_H (400 MHz, $CDCl_3$): 1.1 (t, 3H, *J* 7.0 Hz, CH_3-7), 1.50 (s, 9H, $(CH_3)_3$-1), 1.54 (s, 9H, $(CH_3)_3$-2), 2.89 (s, 3H, CH_3-5), 3.38 (q, 2H, *J* 7.0 Hz, CH_2-6), 6.68 (d, 2H, *J* 9.0 Hz, CH-4), 7.41 (d, 2H, *J* 9.0 Hz, CH-3), 10.10 (bs, 1H, NH-1`), 11.68 (bs, 1H, NH-2').

1-[2,3-di(*tert*-butoxycarbonyl)guanidino]-4-(*N*-methyl)benzene (B67) [131]

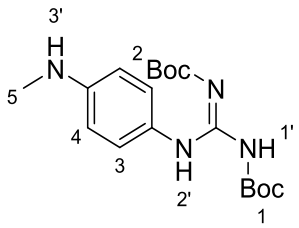

Following method A, a solution of **70** (0.37 g, 3.0 mmol) in CH_2Cl_2 (5 mL) at 0 °C was treated with $HgCl_2$ (0.89 g, 3.3 mmol), **52** (0.83 g, 3.0 mmol) and NEt_3 (1.3 mL, 9.3 mmol). The resulting mixture was stirred at 0 °C for 1 h and 18 h at room temperature. Usual work up followed by silica gel column chromatography afforded **B67** as a white solid (70%, 0.77 g, 2.1 mmol).

Yield: 70% (0.77 g, 2.1 mmol).

M.P: 104-106 °C (Lit. 104-106 °C). [131]

δ_H (400 MHz, $CDCl_3$): 1.48 (s, 9H, $(CH_3)_3$-1), 1.52 (s, 9H, $(CH_3)_3$-2), 2.76 (s, 3H, CH_3-5), 3.80 (bs, 1H, NH-3'), 6.52 (d, 2H, *J* 8.5 Hz, CH-4), 7.33 (d, 2H, *J* 8.5 Hz, CH-3), 10.05 (bs, 1H, NH-1'), 11.68 (bs, 1H, NH-2').

1-Guanidino-4-(*N*,*N*-diethyl)benzene dihydrochloride (64)[191]

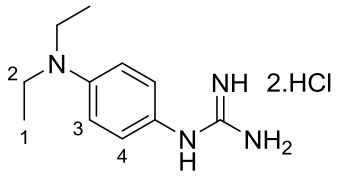

Following method D, **B64** (0.41 g, 1.0 mmol) was treated with a solution of 50% TFA in CH_2Cl_2 (20 mL) for 3 h stirring at room temperature. Solvents were removed under reduced pressure to afford the trifluoroacetate salt.
This salt was dissolved in H_2O (20 mL) and treated with Amberlite IRA 400 chloride form (1.0 g) for 24 h. The resin was removed by filtration and the aqueous solution was washed with CH_2Cl_2 (2 x 10 mL). Evaporation of the water afforded the pure hydrochloride salt **64** as a white solid (90%, 0.25 g, 0.90 mmol).

Yield: 90% (0.25 g, 0.90 mmol).

M.P: 236-238 °C (Lit. 238-240 °C).[191]

δ_H (400 MHz, D_2O): 1.16 (t, 6H, *J* 7.5 Hz, CH_3-1), 3.69 (q, 4H, *J* 7.5 Hz, CH_2-2), 7.59 (d, 2H, *J* 8.9 Hz, CH-3), 7.65 (d, 2H, *J* 8.9 Hz, CH-4).

HPLC: 99.9% (t_R = 6.2 min)

_N_-(4-Guanidinophenyl)piperidine dihydrochloride (63)[191]

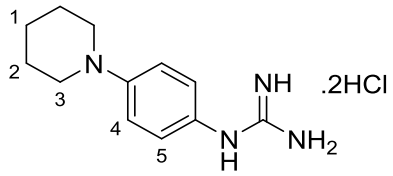

Following method D, **B63** (0.42 g, 1.0 mmol) was treated with a solution of 50% TFA in CH_2Cl_2 (20 mL) for 3 h stirring at room temperature. Solvents were removed under reduced pressure to afford the trifluoroacetate salt. This salt was dissolved in H_2O (20 mL) and treated with Amberlite IRA 400 chloride form (1.0 g) for 24 h. The resin was removed by filtration and the aqueous solution was washed with CH_2Cl_2 (2 x 10 mL). Evaporation of the water afforded the pure hydrochloride salt **63** as a white solid (90%, 0.27 g, 0.92 mmol).

Yield: 92% (0.27 g, 0.92 mmol)

M.P: 122-124 °C (Lit. 124-126 °C).[191]

δ_H (400 MHz, D_2O): 1.80 (m, 2H, CH_2,-1), 2.04 (m, 4H, CH_2-2), 3.66 (m, 4H, CH_2-3), 7.54 (d, 2H, *J* 9.0 Hz, CH-4), 7.71 (d, 2H, *J* 9.0 Hz, CH-5).

HPLC: 97.3% (t_R = 15.35 min)

***N*-[4-(Ethyl-methyl-amino)-phenyl]-Guanidine dihydrochloride (66)**[131]

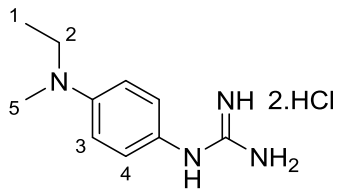

Following method D, **B66** (0.39 g, 1.0 mmol) was treated with a solution of 50% TFA in CH_2Cl_2 (20 mL) for 3 h stirring at room temperature. Solvents were removed under reduced pressure to afford the trifluoroacetate salt. This salt was dissolved in H_2O (20 mL) and treated with Amberlite IRA 400 chloride form (1.0 g) for 24 h. The resin was removed by filtration and the aqueous solution was washed with CH_2Cl_2 (2 x 10 mL). Evaporation of the water afforded the pure hydrochloride salt **66** as a white solid (88%, 0.23 g, 0.88 mmol).

Yield: 88% (0.23 g, 0.88 mmol)

M.P: >150 °C (decomp.) (Lit. >150 °C).[131]

δ_H (400 MHz, D_2O): 1.20 (t, 3H, *J* 7.0 Hz, CH_3-1), 3.29 (s, 3H, CH_3-5), 3.67 (q, 2H, *J* 7.0 Hz, CH_2-2), 7.55 (d, 2H, *J* 9.0 Hz, CH-3), 7.66 (d, 2H, *J* 9.0 Hz, CH-4).

HPLC: 96% (t_R = 11.1 min)

***N*-(4-Methylamino-phenyl)-guanidine dihydrochloride (67)**[131]

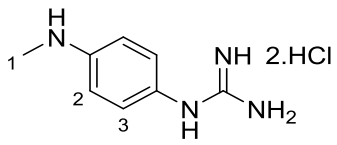

Following method D, **B67** (0.36 g, 1.0 mmol) was treated with a solution of 50% TFA in CH_2Cl_2 (20 mL) for 3 h stirring at room temperature. Solvents were removed under reduced pressure to afford the trifluoroacetate salt. This salt was dissolved in H_2O (20 mL) and treated with Amberlite IRA 400 chloride form (1.0 g) for 24 h. The resin was removed by filtration and the aqueous solution was washed with CH_2Cl_2 (2 x 10 mL). Evaporation of the water afforded the pure hydrochloride salt **67** as a red solid (92%, 0.22 g, 0.92 mmol).

Yield: 92% (0.22 g, 0.92 mmol).

M.P: 72-74 °C (Lit. 74-76 °C).[131]

δ_H (400 MHz, D_2O): 3.12 (s, 3H, CH_3-1), 7.52 (d, 2H, *J* 9.0 Hz, CH-3), 7.58 (d, 2H, *J* 9.0 Hz, CH-4).

HPLC: 97.6% (t_R = 5.3 min).

1-Guanidino-4-methoxybenzene hydrochloride (65)[191]

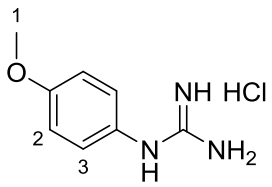

Following method D, **B65** (0.37 g, 1.0 mmol) was treated with a solution of 50% TFA in CH_2Cl_2 (20 mL) for 3 h stirring at room temperature. Solvents were removed under reduced pressure to afford the trifluoroacetate salt. This salt was dissolved in H_2O (20 mL) and treated with Amberlite IRA 400 chloride form (1.0 g) for 24 h. The resin was removed by filtration and the aqueous solution was washed with CH_2Cl_2 (2 x 10 mL). Evaporation of the water afforded the pure hydrochloride salt **65** as a white solid (94%, 0.19 g, 0.94 mmol).

Yield: 94% (0.19 g, 0.94 mmol).

M.P: 138-142 °C (Lit. 139-141 °C).[191]

δ_H (400 MHz, D_2O): 3.87 (s, 3H, CH_3-1), 7.08 (d, 2H, *J* 8.8 Hz, CH-2), 7.30 (d, 2H, *J* 8.8 Hz, CH-3).

HPLC: 99% (t_R =17.56 min)

2-(4-Ethylamino-phenylimino)-imidazolidine-1,3-dicarboxylic acid di-*tert*-butyl ester (B28)[131]

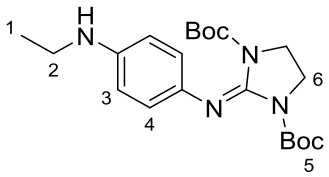

Following method B, a solution of **75** (0.41 g, 3.0 mmol) in CH_2Cl_2 (5 mL) at 0 °C was treated with $HgCl_2$ (0.896 g, 3.3 mmol), **61** (0.907 g, 3.0 mmol) and NEt_3 (1.3 mL, 9.3 mmol). The resulting mixture was stirred at 0 °C for 1 h and 18 h at room temperature. Standard work up followed by neutral alumina column flash chromatography afforded **B28** as a white solid (50%, 0.61 g, 1.5 mmol).

Yield: 50% (0.61 g, 1.5 mmol).

M.P.: 124-126 ºC (Lit. 124-126 ºC).[131]

δ_H (400 MHz, $CDCl_3$): 1.21 (t, 3H, *J* 7.0 Hz, CH_3-1), 1.32 (s, 18H, $(CH_3)_3$ -5), 3.10 (q, 2H, *J* 7.0 Hz, CH_2-2), 3.30 (bs, 1H, NH). 3.80 (s, 4H, CH_2-6), 6.52 (d, 2H, *J* 8.8 Hz, CH-3), 6.88 (d, 2H, *J* 8.8 Hz, CH-4).

2-(4-methylamino-phenylimino)-imidazolidine-1,3-dicarboxylic acid di-*tert*-butyl ester (B68)[131]

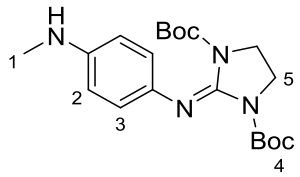

Following method B, a solution of **70** (0.37 g, 3.0 mmol) in CH_2Cl_2 (5 mL) at 0 °C was treated with $HgCl_2$ (0.89 g, 3.3 mmol), **61** (0.91 g, 3.0 mmol) and NEt_3 (1.3 mL, 9.3 mmol). The resulting mixture was stirred at 0 °C for 1 h and 18 h at room temperature. Standard work up followed by neutral alumina column flash chromatography afforded **B68** as a yellow solid (55%, 0.64 g, 1.65 mmol).

Yield: 55% (0.64 g, 1.65 mmol).

M.P.: 52-54 ºC (Lit. 54-56 ºC).[131]

δ_H (400 MHz, $CDCl_3$): 1.30 (s, 18H, $(CH_3)_3$ -5), 2.75 (s, 3H, CH_3-1), 3.30 (bs, 1H, NH), 3.76 (s, 4H, CH_2-5), 6.49 (d, 2H, *J* 8.0 Hz, CH-2), 6.86 (d, 2H, *J* 8.0 Hz, CH-3).

2-(4-*N*,*N*-diethylamino-phenylimino)-imidazolidine-1,3-dicarboxylic acid di-*tert*-butyl ester (B69)[191]

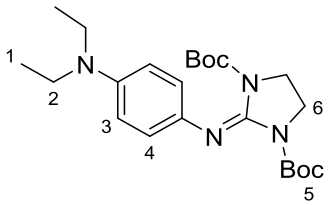

Following method B, a solution of *N*,*N*-diethyl-*p*-phenylenediamine (0.49 g, 3.0 mmol) in CH_2Cl_2 (5 mL) at 0 °C was treated with $HgCl_2$ (0.89 g, 3.3 mmol), **61** (0.91 g, 3.0 mmol) and NEt_3 (1.3 mL, 9.3 mmol). The resulting mixture was stirred at 0 °C for 1 h and 18 h at room temperature. Usual work up followed by neutral alumina column flash chromatography afforded **B69** as a white solid (75%, 0.97 g, 2.25 mmol).

Yield: 75% (0.97 g, 2.25 mmol).

M.P.: 88-90 ºC (Lit. 88-90 ºC).[191]

δ_H (400 MHz, $CDCl_3$): 1.08 (t, 6H, *J* 7.0 Hz, CH_3-1), 1.32 (s, 18H, $(CH_3)_3$ -5), 3.28 (q, 4H, *J* 7 Hz, CH_2-2), 3.80 (s, 4H, CH_2-6), 6.65 (m, 2H, CH-3), 6.92 (d, 2H, *J* 9 Hz, CH-4).

2-(4-*N*,*N*-dimethylamino-phenylimino)-imidazolidine-1,3-dicarboxylic acid di-*tert*-butyl ester (B36).[191]

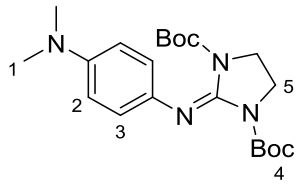

Following method B, a solution of *N*,*N*-dimethyl-*p*-phenylenediamine (0.409 g, 3.0 mmol) in CH_2Cl_2 (5 mL) at 0 °C was treated with $HgCl_2$ (0.896 g, 3.3 mmol), **61** (0.907 g, 3.0 mmol) and NEt_3 (1.3 mL, 9.3 mmol). The resulting mixture was stirred at 0 °C for 1 h and 18 h at room temperature. Usual work up followed by neutral alumina column flash chromatography afforded **B36** as a white solid (60%, 0.73 g, 1.8 mmol).

Yield: 60% (0.73 g, 1.8 mmol).

M.P.: 122-124 ºC (Lit. 124-126 ºC).[191]

δ_H (400 MHz, $CDCl_3$): 1.34 (s, 18H, $(CH_3)_3$-4), 2.88 (s, 6H, CH_3-1), 3.83 (s, 4H, CH_2-5), 6.73 (d, 2H, *J* 8.6 Hz, CH-2), 6.96 (d, 2H, *J* 8.6 Hz, CH-3).

2-(4-piperidin-1-yl-phenylimino)-imidazolidine-1,3-dicarboxylic acid di-*tert*-butyl ester (B63b).[191]

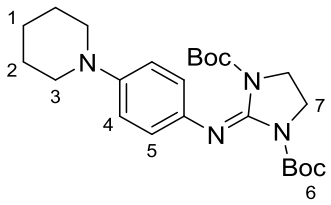

Following method B, a solution of *N*-(4-aminophenyl)-piperidine (0.53 g, 3.0 mmol) in CH_2Cl_2 (5 mL) at 0 °C was treated with $HgCl_2$ (0.89 g, 3.3 mmol), **61** (0.91 g, 3.0 mmol) and NEt_3 (1.3 mL, 9.3 mmol). The resulting mixture was stirred at 0 °C for 1 h and 18 h at room temperature. Usual work up followed by neutral alumina column flash chromatography afforded **B63b** as a white solid (80%, 1.07 g, 2.4 mmol).

Yield: 80% (1.07 g, 2.4 mmol).

M.P.: 116-118 ºC (Lit. 116-118 ºC).[191]

δ_H (400 MHz, $CDCl_3$): 1.33 (s, 18H, $(CH_3)_3$-5), 1.56 (m, 2H, CH_2-1), 1.70 (m, 4H, CH_2-2), 3.05 (m, 4H, CH_2-3), 3.81 (s, 4H, CH_2-7), 6.87 (d, 2H, *J* 8.6 Hz, CH-4), 6.94 (d, 2H, *J* 8.6 Hz, CH-5).

***N*-[4-(2-Imidazolidinylimino)phenyl]-piperidine (63b)**[191]

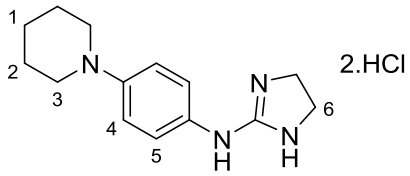

Following method D, **B67** (0.31 g, 0.70 mmol) was treated with a solution of 50% TFA in CH_2Cl_2 (20 mL) for 3 h stirring at room temperature. Solvents were removed under reduced pressure to afford the trifluoroacetate salt. This salt was dissolved in H_2O (20 mL) and treated with Amberlite IRA 400 chloride form (1.0 g) for 24 h. The resin was removed by filtration and the aqueous solution was washed with CH_2Cl_2 (2 x 10 mL). Evaporation of the water afforded the pure hydrochloride salt **63b** as a white solid (92%, 0.21 g, 0.65 mmol).

Yield: 92% (0.21 g, 0.65 mmol).

M.P: 106-108 °C (Lit. 108-110 °C).[191]

δ_H (400 MHz, D_2O): 1.79 (m, 2H, CH_2, H-1), 2.05 (m, 4H, CH_2-2), 3.67 (m, 4H, CH_2-3), 3.81 (s, 4H, CH_2-6), 7.52 (d, 2H, *J* 9.0 Hz, CH-4), 7.72 (d, 2H, *J* 9.0 Hz, CH-5).

HPLC: 99.5% (t_R = 17.1 min)

1-(2-Imidazolidinylimino)-4-(*N*,*N*-dimethyl)benzene dihydrochloride (36)[191]

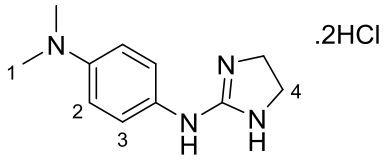

Following method D, **B36** (0.40 g, 1.0 mmol) was treated with a solution of 50% TFA in CH_2Cl_2 (20 mL) for 3 h stirring at room temperature. Solvents were removed under reduced pressure to afford the trifluoroacetate salt. This salt was dissolved in H_2O (20 mL) and treated with Amberlite IRA 400 chloride form (1.0 g) for 24 h. The resin was removed by filtration and the aqueous solution was washed with CH_2Cl_2 (2 x 10 mL). Evaporation of the water afforded the pure hydrochloride salt **36** as a white solid (86%, 0.24 g, 0.86 mmol).

Yield: 86% (0.24 g, 0.86 mmol).

M.P: 234-236 °C (Lit. 236-238 °C).[191]

δ_H (400 MHz, D_2O): 3.32 (s, 6H, CH_3-1), 3.81 (s, 4H, CH_2-4), 7.52 (d, 2H, *J* 8.9 Hz, CH-2), 7.70 (d, 2H, *J* 8.9 Hz, CH-3).

HPLC: 99.3% (t_R = 15.9 min)

1-(2-Imidazolidinylimino)-4-(*N*-ethyl)benzene dihydrochloride (68)[131]

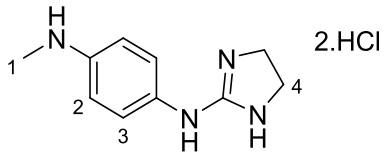

Following method D, **B68** (0.39 g, 1.0 mmol) was treated with a solution of 50% TFA in CH_2Cl_2 (20 mL) for 3 h stirring at room temperature. Solvents were removed under reduced pressure to afford the trifluoroacetate salt. This salt was dissolved in H_2O (20 mL) and treated with Amberlite IRA 400 chloride form (1.0 g) for 24 h. Then, the resin was removed by filtration and the aqueous solution was washed with CH_2Cl_2 (2 x 10 mL). Evaporation of the water afforded the pure hydrochloride salt **68** as a red solid (80%, 0.21 g, 0.80 mmol).

Yield: 80% (0.21 g, 0.80 mmol).

M.P: 228-230 °C (Lit. 230-232 °C).[131]

δ_H (400 MHz, D_2O): 3.12 (s, 3H, CH_3-1), 3.80 (s, 4H, CH_2-4), 7.49 (d, 2H, *J* 8.8 Hz, CH-2), 7.58 (d, 2H, *J* 8.8 Hz, CH-3).

HPLC: 98.7% (t_R = 5.9 min)

1-(2-Imidazolidinylimino)-4-(*N*,*N*-diethyl)benzene dihydrochloride (69)[191]

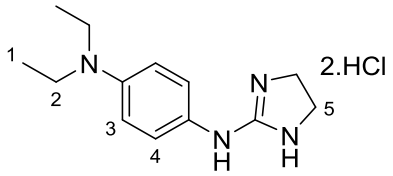

Following method D, **B69** (0.43 g, 1.0 mmol) was treated with a solution of 50% TFA in CH_2Cl_2 (20 mL) for 3 h stirring at room temperature. Solvents were removed under reduced pressure to afford the trifluoroacetate salt. This salt was dissolved in H_2O (20 mL) and treated with Amberlite IRA 400 chloride form (1.0 g) for 24 h. The resin was removed by filtration and the aqueous solution was washed with CH_2Cl_2 (2 x 10 mL). Evaporation of the water afforded the pure hydrochloride salt **69** as a white solid (88%, 0.27 g, 0.88 mmol).

Yield: 88% (0.27 g, 0.88 mmol).

M.P: 94-96 °C (Lit. 96-98 °C).[191]

δ_H (400 MHz, D_2O): 1.15 (t, 3H, *J* 7.2 Hz, CH_3-1), 3.67 (m, 4H, CH_2-3), 3.82(s, 4H, CH_2-5), 7.55 (d, 2H, *J* 9.0 Hz, CH-3), 7.63 (d, 2H, *J* 8.6 Hz, CH-4).

HPLC: 99.6% (t_R = 10.9 min).

1-(2-Imidazolidinylimino)-4-(*N*-ethyl)benzene dihydrochloride (28)[131]

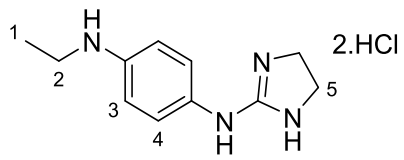

Following method D, **B28** (0.40 g, 1.0 mmol) was treated with a solution of 50% TFA in CH_2Cl_2 (20 mL) for 3 h stirring at room temperature. Solvents were removed under reduced pressure to afford the trifluoroacetate salt. This salt was dissolved in H_2O (20 mL) and treated with Amberlite IRA 400 chloride form (1.0 g) for 24 h. The resin was removed by filtration and the aqueous solution was washed with CH_2Cl_2 (2 x 10 mL). Evaporation of the water afforded the pure hydrochloride salt **28** as a red solid (89%, 0.25 g, 0.89 mmol).

Yield: 89% (0.25 g, 0.89 mmol).

M.P: 196-200 °C (Lit. 198-200 °C).[131]

δ_H (400 MHz, D_2O): 1.33 (t, 3H, *J* 7.3 Hz, CH_3-1), 3.49 (q, 2H, *J* 7.3 Hz, CH_2-2), 3.80 (s, 4H, CH_2-5), 7.48 (d, 2H, *J* 9.0 Hz, CH-3), 7.53 (d, 2H, *J* 8.8 Hz, CH-4).

HPLC: 99.5% (t_R = 16.96min).

***N*-(Pyridin-2-yl)-acetamide (79)**[132]

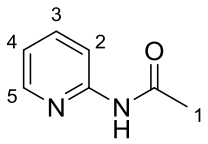

A solution of **78** (4.14 g, 44.0 mmol) anhydrous DMF (25 mL) cooled to approx. 0 °C in an ice/water bath was treated with pyridine (4.40 mL, 54.4 mmol) and acetic anhydride (4.60 mL, 48.40 mmol) drop-wise over 10 min under Ar. The ice/water bath was then removed and the reaction was stirred at rt for 18 h. The reaction mixture was then quenched by addition of saturated $NaHCO_3$ (50 mL, aq.) and the mixture extracted with EtOAc (5 x 50 mL). The organic phase was washed with water (4 x 100 mL) and brine (4 x 100 mL), dried over anhydrous Na_2SO_4, and concentrated under reduced pressure to give an orange oil which was co-evaporated with toluene (5 x 50 mL) affording **79** as an orange solid (91%, 5.45 g, 40.0 mmol).

Yield: 91% (5.45 g, 40.0 mmol).

M.P: 68-70 °C (Lit. 70-71 °C).[132]

δ_H (400 MHz, $CDCl_3$): 2.21 (s, 3H, CH_3-1), 7.04 (m, 1H, CH-4), 7.72 (m, 1H, CH-2), 8.24 (m, 2H, CH-3, CH-5), 8.62 (bs, 1H, NH).

HRMS: (m/z ESI$^+$) Found: 137.0714 $(M+H)^+$ $C_7H_9N_2O$ Requires: 137.0710

2-(*N*-ethylamino)-pyridine (80)[132]

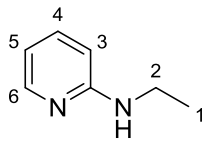

A solution of **79** (0.42 g, 3.1 mmol) in anhydrous THF (30 mL) cooled to approx. 0 °C in an ice/water bath was treated with $LiAlH_4$ (0.56 g, 15.1 mmol) portion-wise over 10 min under Ar. The ice/water bath was then removed and the reaction was stirred at rt until adjudged complete by TLC. The reaction was cooled to approx. 0 °C and quenched by dropwise the addition of aqueous 1M NaOH (~10 mL) followed by H_2O (~5 mL). The reaction mixture was filtered through a pad of Celite to remove the precipitate. The Celite pad was washed with $CHCl_3$ and the filtrate was extracted with isopropyl alcohol/$CHCl_3$ (2:8) (5 × 25 mL), dried over $MgSO_4$, filtered and concentrated *in vacuo* to give a residue which was purified silica gel column chromatography with gradient elution (100% Et_2O to 1:4 acetone/Et_2O) affording **80** as a red liquid (82%, 0.31 g, 2.53 mmol).

Yield: 82% (0.31 g, 2.53 mmol).

δ_H (400 MHz, $CDCl_3$): 1.23 (t, 3H, *J* 7.2 Hz, CH_3-1), 3.26 (m, 2H, CH_2-2), 4.58 (bs, 1H, NH), 6.35 (d, 1H, *J* 8.4 Hz, CH-3), 6.53 (m, 1H, CH-5), 7.39 (m, 1H, CH-4), 8.03 (m, 1H, CH-6).

HRMS: (m/z ESI^+) Found: 123.0911 $(M+H)^+$ $C_7H_{11}N_2$ Requires: 123.1917

2-(*N*-ethylamino)-5-nitropyridine (81)[132]

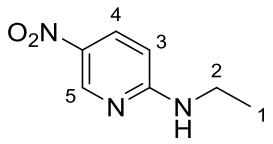

A solution of **80** (0.76 g, 6.23 mmol) in 98% sulfuric acid (12 mL) cooled to approx. 0 °C in an ice/water bath was treated with potassium nitrate (0.70 g, 6.90 mmol) portion-wise over 10 min and stirred at approx. 0 °C for 0.5 h. The ice/water bath was then removed and the reaction was stirred at rt for 5 h. The reaction mixture was then cooled to approx. 0 °C in an ice/water bath and quenched by the drop-wise addition of concentrated ammonium hydroxide to pH 12. The reaction mixture was extracted with EtOAc (5 × 50 mL) and the organic phase washed with water (2 × 20 mL), brine (1 x 20 mL), dried over $MgSO_4$, filtered and concentrated *in vacuo* to give a residue which was purified silica gel column chromatography with gradient elution (3:1 hexane:EtOAc to 1:1 hexane:EtOAc) to afford **81** as a yellow solid (65%, 0.68 g, 4.10 mmol).

Yield: 65% (0.68 g, 4.10 mmol).

M.P: 118-120 °C (Lit. 117-119 °C).[132]

δ_H (400 MHz, $CDCl_3$): 1.31 (t, 3H, *J* 7.2 Hz, CH_3-1), 3.44 (m, 2H, CH_2-2), 5.34 (bs, 1H, NH), 6.35 (d, 1H, *J* 9.3 Hz, CH-3), 8.20 (m, 1H, CH-4), 9.01 (d, 1H, *J* 2.5 Hz, CH-5).

HRMS: (m/z ESI^+) Found: 168.0770 $(M+H)^+$ $C_7H_{10}N_3O_2$ Requires: 168.0773

2-(*N*-ethylamino)-5-aminopyridine (77)[132]

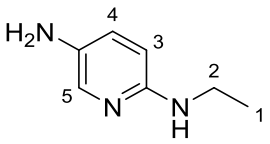

Following method H, a degassed solution of **81** (0.17 g, 1.00 mmol) in EtOAc (12 mL) was added 10% Pd/C (0.025 g, 0.02 mmol) and the reaction mixture was stirred at rt under a H_2 atmosphere (6.0 atm) until the reaction was adjudged complete by TLC analysis after 4 h.

The reaction mixture was diluted with the EtOAc and filtered through a pad of Celite to remove the catalyst. The filter cake was rinsed with MeOH and the filtrate was concentrated under reduced pressure to give a residue which was purified by silica gel column chromatography eluting with 100% Et_2O to afford **77** as a dark red oil (73%, 0.10 g, 0.73 mmol).

Yield: 73% (0.68 g, 4.10 mmol).

δ_H (400 MHz, $CDCl_3$): 1.23 (t, 3H, *J* 7.2 Hz, CH_3-1), 2.64 (bs, 3H, NH, NH_2), 3.23 (q, 2H, *J* 7.2 Hz, CH_2-2), 6.33 (d, 1H, *J* 8.7 Hz, CH-3), 6.98 (dd, 1H, *J* 8.7 Hz, 2.9 Hz, CH-4), 7.65 (d, 1H, *J* 2.7 Hz, CH-5)

HRMS: (m/z ESI^+) Found: 138.1031 $(M+H)^+$ $C_7H_{12}N_3$ Requires: 138.1026

1-(6-(Ethylamino)pyridin-3'-yl)-2,3-di(*tert*-butoxycarbonyl)-2-iminoimidazolidine (82)[132]

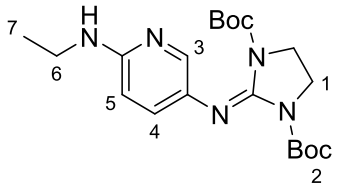

Following method B, a solution of **77** (0.2 g, 1.46 mmol) in CH_2Cl_2 (5 mL) at 0 °C was treated with $HgCl_2$ (0.44 g, 1.6 mmol), **61** (0.44 g, 1.46 mmol) and NEt_3 (0.92 mL, 6.61 mmol). The resulting mixture was stirred at 0 °C for 1 h and 18 h at room temperature. The usual workup followed by neutral alumina column flash chromatography afforded **82** as a white solid (60%, 0.35 g, 0.87 mmol).

Yield: 60% (0.35 g, 0.87 mmol).

M.P: 120-122 °C (Lit 121-123 °C).[132]

δ_H (400 MHz, $CDCl_3$): 0.99 (t, 3H, *J* 7.0 Hz, CH_3-7), 1.14 (s, 18H, $(CH_3)_3$-2), 3.06 (q, 2H, *J* 7.0 Hz, CH_2-6), 3.60 (s, 4H, CH_2-1), 4.48 (bs, 1H, NH), 6.13 (d, 1H, *J* 8.8 Hz, CH-5), 6.98 (dd, 1H, *J* 8.8 Hz, 2.6 Hz, CH-4), 7.65 (d, 1H, *J* 2.6 Hz, CH-3).

1-(6-(Ethylamino)pyridin-3-yl)-2-iminoimidazolidine dihydrochloride (34)

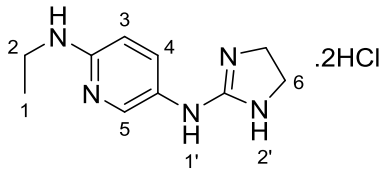

Following method D, **82** (0.35 g, 0.87 mmol) was treated with a solution of 50% TFA in CH_2Cl_2 (20 mL) for 3 h stirring at room temperature. Solvents were removed under reduced pressure to afford the trifluoroacetate salt. This salt was dissolved in H_2O (20 mL) and treated with Amberlite IRA 400 chloride form (1.0 g) for 24 h. The resin was removed by filtration and the aqueous solution was washed with CH_2Cl_2 (2 x 10 mL). Evaporation of the water afforded the pure hydrochloride salt **34** as a white solid (90%, 0.22 g, 0.78 mmol).

Yield: 90% (0.22 g, 0.78 mmol).

M.P: Decomp. >210 °C (Lit. >210 °C).[132]

δ_H (600 MHz, DMSO-d_6): 1.24 (t, 3H, *J* 7.1 Hz, CH_3-1), 3.47 (q, 2H, *J* 7.1 Hz, CH_2-2), 3.65 (s, 4H, CH_2-6), 7.18 (d, 1H, *J* 9.4 Hz, CH-3), 7.78 (d, 1H, *J* 9.4 Hz, CH-4), 7.92 (s, 1H, CH-5), 8.58 (bs, 2H, NH-2'), 10.65 (bs, 2H, NH-1').

HPLC: 96% (t_R = 3.2 min)

2-Amino-5,6,7,8-tetrahydroquinoline (83)[194]

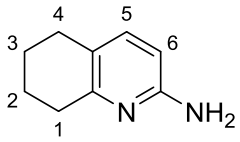

A solution of hydroxylamine hydrochloride (1.80 g, 26.00 mmol) in H_2O (6 mL) cooled to approx. 0 °C in an ice/water bath was treated a solution of **84** (3.0 g, 19.84 mmol) in Et_2O (40 mL) added drop-wise over 10 min. A solution of NaOH (1.17g in 6 mL H_2O, 4.9 M) was then added with stirring at approx. 0 °C drop-wise as to maintain a temperature below 10 °C. The ice/water bath was then removed and the reaction was stirred at rt for 5 h. The reaction mixture was then diluted with Et_2O (40 mL) and the aqueous layer extracted with Et_2O (3 x 20 mL). The organic phase was washed with water (2 x 20 mL), dried over anhydrous Na_2SO_4, and concentrated under reduced pressure to give the oxime intermediate as a crude oil (60%, 1.99 g, 12 mmol) which was immediately reacted in the next step.

The crude oxime intermediate (1.99 g, 12 mmol) was treated with acetic anhydride (1.2 mL, 12.74 mmol) and acetyl chloride (1.24 mL, 17.36 mmol). The reaction mixture was then heated under reflux at 120 °C for 8 h and then cooled to rt and quenched with a solution of NaOH (2.1g, 52.5 mmol) in 10 mL H_2O and subsequently heated under reflux at 120 °C for another 2 h. The reaction mixture was then diluted with EtOAc (40 mL) and the aqueous layer extracted with EtOAc (3 x 20 mL). The organic phase was washed with acetic acid (1M, 2 x 20 mL), dried over anhydrous Na_2SO_4, and concentrated under reduced pressure to give a residue which was purified by silica gel column chromatography with gradient elution (1:1 hexane:EtOAc to 100% EtOAc) to afford **83** as a white solid (31%, 0.55 g, 3.72 mmol).

Yield: 31% (0.55 g, 3.72 mmol).

δ_H (400 MHz, $CDCl_3$): 1.83 (m, 4H, CH_2-2, CH_2-3), 2.69 (t, 2H, *J* 6.2 Hz, CH_2-4), 2.79 (t, 2H, *J* 6.3 Hz, CH_2-1), 6.62 (d, 1H, *J* 8.2 Hz, CH-6) 7.31 (d, 1H, *J* 8.2 Hz, CH-5), 10.37 (bs, 2H, NH_2).

HRMS: (m/z ESI^+) Found: 149.1076 $(M+H)^+$ $C_9H_{13}N_2$ Requires: 149.1073.

1-(5,6,7,8-Tetrahydroquinolin-2-yl)-2,3-di(tert-butoxycarbonyl)guanidine (86)[195]

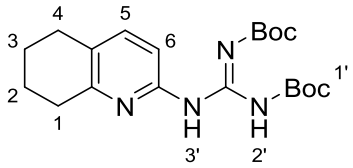

Following method A, a solution of **83** (0.10 g, 0.67 mmol) in CH_2Cl_2 (4 mL) at 0 °C was treated with $HgCl_2$ (0.19 g, 0.71 mmol), **85** (0.21 g, 0.71 mmol) and NEt_3 (0.3 mL, 2.36 mmol). The resulting mixture was stirred at 0 °C for 1 h and 18 h at room temperature. The standard work up followed by silica gel column chromatography afforded **86** as a white solid (80%, 0.21 g, 0.539 mmol).

Yield: 80% (0.21 g, 0.54 mmol).

M.P.: 164-166 ºC (Lit. 164-165 ºC).[195]

δ_H (400 MHz, $CDCl_3$): 1.51 (s, 18H, $(CH_3)_3$ -1'), 1.75 (m, 2H, CH_2-3), 1.83 (m, 2H, CH_2-2), 2.69 (t, 2H, *J* 6.3 Hz CH_2-4), 2.78 (t, 2H, *J* 6.3 Hz, CH_2-1), 7.35 (d, 1H, *J* 8.3 Hz, CH-5), 8.04 (bs, 1H, CH-6), 10.63 (bs, 1H, NH-2'), 11.54 (bs, 1H, NH-3').

1-(5,6,7,8-Tetrahydroquinolin-2'-yl)-2,3-di(*tert*-butoxycarbonyl)-2-iminoimidazolidine (87)

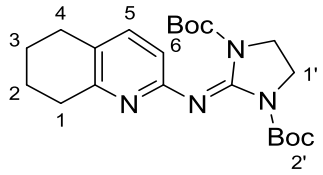

Following method B, a solution of **83** (0.10 g, 0.67 mmol) in CH_2Cl_2 (4 mL) at 0 °C was treated with $HgCl_2$ (0.19 g, 0.71 mmol), **61** (0.22 g, 0.74 mmol) and NEt_3 (0.3 mL, 2.36 mmol). The resulting mixture was stirred at 0 °C for 1 h and 18 h at room temperature. The usual workup followed by neutral alumina column flash chromatography afforded **87** as a yellow oil (71%, 0.20 g, 0.48 mmol).

Yield: 71% (0.20 g, 0.48 mmol).

δ_H (400 MHz, $CDCl_3$): 1.44 (s, 18H, $(CH_3)_3$-2'), 1.75 (m, 4H, CH_2-2, CH_2-3), 2.68 (t, 2H, *J* 6.3 Hz CH_2-4), 2.74 (t, 2H, *J* 6.3 Hz, CH_2-1), 3.82 (s, 4H, CH_2-1'), 6.77 (d, 1H, *J* 8.1 Hz, CH-6), 7.28 (d, 1H, *J* 8.1 Hz, CH-5).

HRMS: (m/z ESI$^+$) Found: 417.2498 $(M+H)^+$ $C_{22}H_{33}N_4O_4$ Requires: 417.2496.

1-(5,6,7,8-Tetrahydroquinolin-2-yl)guanidine hydrochloride (22)[195]

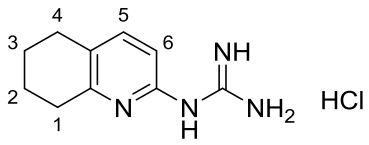

Following method D, **86** (0.21 g, 0.54 mmol) was treated with a solution of 50% TFA in CH_2Cl_2 (10 mL) for 3 h stirring at room temperature. Solvents were removed under reduced pressure to afford the trifluoroacetate salt. This salt was dissolved in H_2O (20 mL) and treated with Amberlite IRA 400 chloride form (1.0 g) for 24 h. The resin was removed by filtration and the aqueous solution was washed with CH_2Cl_2 (2 x 10 mL). Evaporation of the water afforded the pure hydrochloride salt **22** as a brown solid (88%, 0.11 g, 0.47 mmol).

Yield: 88% (0.11 g, 0.47 mmol).

M.P.: 224-226 °C (Lit. 224-228 °C, Decomp.).[195]

δ_H (600 MHz, D2O): 1.8 (m, 4H, CH_2-2, CH_2-2), 2.72 (t, 2H, *J* 6.2 Hz, CH_2-4), 2.79 (t, 2H, *J* 6.4 Hz, CH_2-1), 6.78 (d, 1H, *J* 8.3 Hz, CH-6), 7.54 (d, 1H, *J* 8.3 Hz,CH-5).

HPLC: 98% (t_R = 27.2 min).

1-(5,6,7,8-Tetrahydroquinolin-2-yl)-2-iminoimidazolidine hydrochloride (23)[132]

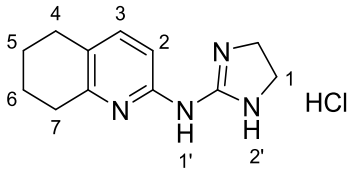

Following method D, **87** (0.20 g, 0.48 mmol) was treated with a solution of 50% TFA in CH_2Cl_2 (10 mL) for 3 h stirring at room temperature. Solvents were removed under reduced pressure to afford the trifluoroacetate salt. This salt was dissolved in H_2O (20 mL) and treated with Amberlite IRA 400 chloride form (1.0 g) for 24 h. The resin was removed by filtration and the aqueous solution was washed with CH_2Cl_2 (2 x 10 mL). Evaporation of the water afforded the pure hydrochloride salt **23** as a white solid (86%, 0.10 g, 0.41 mmol).

Yield: 86% (0.10 g, 0.41 mmol).

M.P.: 208-210 °C (Lit. 208-212 °C).[132]

δ_H (600 MHz, DMSO-d_6) : 1.74 (m, 2H, CH_2-5), 1.81 (m, 2H, CH_2-6), 2.70 (t, 2H, *J* 6.2 Hz, CH_2-4), 3.02 (t, 2H, *J* 6.2 Hz, CH_2-7), 3.73 (s, 4H, CH_2-1), 6.93 (d, 1H, *J* 8.2 Hz, CH-2), 7.55 (d, 1H, *J* 8.2 Hz, CH-3), 8.80 (bs, 2H, NH-2'), 11.89 (bs, 1H, NH-1').

HPLC: 96% (t_R = 21.7 min).

6-[2,3-di(*tert*-butoxycarbonyl)guanidino]-1,2,3,4-tetrahydronaphthalene (B21)[130]

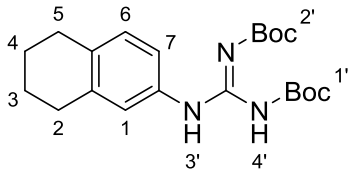

Following method A, a solution of **147** (0.53 g, 3.62 mmol) in CH_2Cl_2 (5 mL) at 0 °C was treated with $HgCl_2$ (1.08 g, 3.98 mmol), **52** (1.00 g, 3.62 mmol) and NEt_3 (1.56 mL, 11.22 mmol). The resulting mixture was stirred at 0 °C for 1 h and 18 h at room temperature. The usual workup followed by silica gel column chromatography afforded **B21** as a white solid (78%, 1.10 g, 2.82 mmol).

Yield: 78% (1.10 g, 2.82 mmol).

M.P: 120-122 °C (Lit. 122-124 °C).[130]

δ_H (400 MHz, $CDCl_3$): 1.52 (s, 9H, $(CH_3)_3$ -1'), 1.56 (s, 9H, $(CH_3)_3$-2'), 1.79 (m, 4H, CH_2-3 and -4), 2.74 (m, 2H, CH_2-5), 2.77 (m, 2H, CH_2-2), 7.03 (d, 1H, *J* 8.0 Hz, CH-6), 7.24 (s, 1H, CH-1), 7.36 (d, 1H, *J* 8.0 Hz, H-7), 10.21 (bs, 1H , NH-4'), 11.67 (bs, 1H , NH-3').

2-(5,6,7,8-tetrahydro-naphthalen-2-ylimino)-imidazolidine-1,3-dicarboxylic acid di-*tert*butyl ester (271)[130]

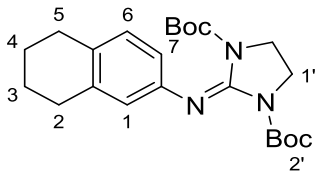

Following method B, a solution of **147** (0.53 g, 3.62 mmol) in CH_2Cl_2 (5 mL) at 0 °C was treated with $HgCl_2$ (1.08 g, 3.98 mmol), **61** (1.09 g, 3.62 mmol) and NEt_3 (1.56 mL, 11.22 mmol). The resulting mixture was stirred at 0 °C for 1 h and 18 h at room temperature. The usual workup followed by neutral alumina column flash chromatography afforded **271** as a white solid (73%, 1.1 g, 2.64 mmol).

Yield: 73% (1.1 g, 2.64 mmol).

M.P: 140-142 (Lit. 140-142 °C).[130]

δ_H (400 MHz, $CDCl_3$): 1.28 (s, 18H, $(CH_3)_3$-2'), 1.72 (m, 4H, CH_2-3 and -4), 2.64 (m, 4H, CH_2-2 and -5), 3.77 (s, 4H, CH_2-1'), 6.65 (s, 1H, CH-1), 6.69 (d, 1H, *J* 8.0 Hz, CH-6), 6.87 (d, 1H, *J* 8.0 Hz, CH-7).

1-[2,3-Di(*tert*-butoxycarbonyl)guanidino]-4-(*N*,*N*-dimethyl)-benzene (116)[191]

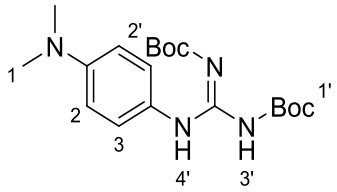

Following method A, a solution of *N*,*N*-dimethyl-*p*-phenylenediamine (0.14 g, 1.0 mmol) in CH_2Cl_2 (5 mL) at 0 °C was treated with $HgCl_2$ (0.30 g, 3.3 mmol), **85** (0.29 g, 1.0 mmol), and NEt_3 (0.5 mL, 3.5 mmol). The resulting mixture was stirred at 0 °C for 1 h and then for 18 h at room temperature. The usual workup followed by silica gel column chromatography afforded **116** as a yellow solid (20%, 0.08 g, 0.2 mmol).

Yield: 20% (0.08 g, 0.2 mmol).

δ_H (400 MHz, $CDCl_3$): 1.51 (s, 9H, $(CH_3)_3$-1'), 1.55 (s, 9H, $(CH_3)_3$-2'), 2.92 (s, 6H, CH_3-1), 6.70 (d, 2H, *J* 8.5 Hz, CH-2), 7.43 (d, 2H, *J* 8.5 Hz, CH-3), 10.11 (bs, 1H, NH-3'), 11.7 (bs, 1H, NH-4')

HRMS: (m/z ESI$^+$) Found: 379.2339 $(M+H)^+$ $C_{19}H_{31}N_4O_4$ Requires: 379.2339.

1-Guanidino-4-(*N*,*N*-dimethyl)benzene dihydrochloride (35)[191]

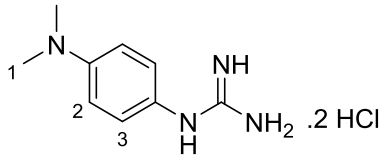

Following method D, **116** (0.08 g, 0.2 mmol) was treated with a solution of 50% TFA in CH_2Cl_2 (5 mL) for 3 h stirring at room temperature. Solvents were removed under reduced pressure to afford the trifluoroacetate salt. This salt was dissolved in H_2O (20 mL) and treated with Amberlite IRA 400 chloride form (1.0 g) for 24 h. Then, the resin was removed by filtration and the aqueous solution was washed with CH_2Cl_2 (2 x 10 mL). Evaporation of the water afforded the pure hydrochloride salt **35** as a red solid (95%, 0.05 g, 0.19 mmol).

Yield: 95% (0.05 g, 0.19 mmol).

M.P: 230−232 °C (Lit. 232−234 °C).[191]

δ_H (400 MHz, D_2O): 3.12 (s, 6H, CH_3-1), 7.53 (d, 2H, *J* 9.1 Hz, CH-2), 7.68 (d, 2H, *J* 9.1 Hz, CH-3).

HRMS: (m/z ESI$^+$) Found: 179.1295 $(M+H)^+$ $C_9H_{15}N_4$ Requires: 179.1291.

HPLC: 99.8% (t_R = 9.7 min).

(*E*)-4,4′-(Diazene-1,2-diyl)bis(*N*,*N*-dimethylaniline) (117)[251]

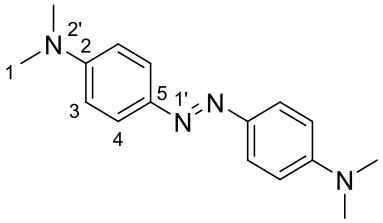

A solution of *N*,*N*-dimethyl-*p*-phenylenediamine (0.136 g, 1.0 mmol) in CH_2Cl_2 (5 mL) at 0 °C was treated with $HgCl_2$ (0.299 g, 3.3 mmol) and NEt_3 (0.5 mL, 3.5 mmol). The resulting mixture was stirred at 0 °C for 1 h and then for 18 h at room temperature. The usual workup followed by silica gel column chromatography eluting with 100% Et_2O afforded **117** as a dark red solid (54%, 0.14 g, 0.54 mmol).

Yield: 54 % (0.14 g, 0.54 mmol).

M.P: 264-266 °C (Lit. 264.7−265.2 °C).[251]

δ_H (400 MHz, $CDCl_3$): δ 3.06 (s, 12H, CH_3-1), 6.76 (d, 4H, *J* 9.0 Hz, CH-4), 7.81 (d, 4H, *J* 9.0 Hz, CH-3).

δ_C (150 MHz, $CDCl_3$) : 40.4 (CH_3-1), 111.8 (CH-4), 124.0 (CH-3), 144.1 (qC-5) , 151.5 (qC-2).

HRMS: (*m/z* ESI^+) Found: 269.17598 (M+H) $C_{16}H_{21}N_4$ Requires: 269.1760.

X-ray structure: See section 9.3.1 for data.

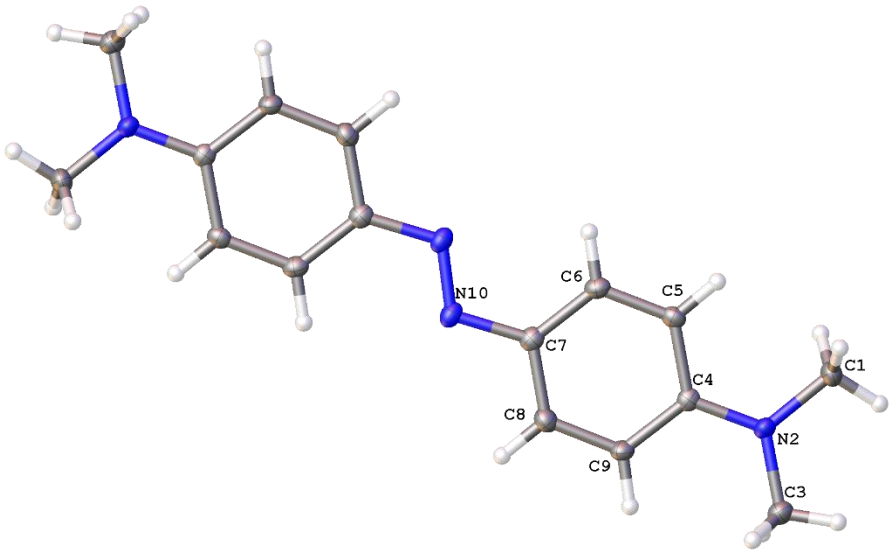

5-Dimethylamino-2-nitropyridine (120)[257]

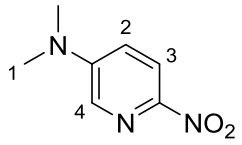

A solution of **121** (3.00 g, 15.00 mmol) in EtOH (30 mL) was treated with a solution of dimethylamine (5.65 mL, 40 wt. %, aq.) and the reaction mixture heated at 80 °C under reflux for 18 h. After cooling to rt the reaction mixture was cooled to approx. 0 °C in an ice/water bath and a precipitated solid formed which was isolated by filtration and washed with cold H_2O and dried under vacuum to afford **120** as a bright yellow solid (72 %, 1.81 g, 10.85 mmol).

Yield: 72 % (1.81 g, 10.85 mmol)

δ_H (400 MHz, $CDCl_3$): 3.16 (s, 6H, CH_3-1), 6.98 (dd, 1H, *J* 9.2 Hz, 2.9 Hz, CH-2), 7.96 (d, 1H, *J* 2.5 Hz, CH-4), 8.17 (d, 1H, *J* 9.2 Hz, CH-3).

M.P.: 200-202 °C (Lit. 199.8-200.5 °C).[257]

HRMS: (*m/z* ESI^+) Found: 168.0766 (M+H) $C_7H_{10}N_6O_2$ Requires: 168.0773.

2-Amino-5-dimethylaminopyridine (119)[362]

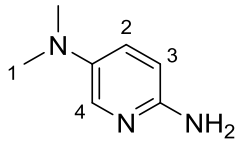

Following method H, a degassed solution **120** (0.64 g, 3.83 mmol) in EtOH (12 mL) was treated with 10% Pd/C (0.203 g, 0.02 mmol) and the reaction mixture was stirred at rt under a H_2 atmosphere (6.0 atm.) until the reaction was adjudged complete by TLC analysis after 16 h. The reaction mixture was diluted with the EtOAc and filtered through a pad of Celite to remove the catalyst. The filter cake was rinsed with EtOAc and the filtrate concentrated under reduced pressure to afford **119** as a dark purple oil (98 %, 0.52 g, 3.79 mmol).

Yield: 98 % (0.52 g, 3.79 mmol).

δ_H (400 MHz, $CDCl_3$): 2.76 (s, 6H, CH_3-1), 4.13 (bs, 2H, NH_2), 6.43 (d, 1H, *J* 8.8 Hz, CH-3), 7.01 (dd, 1H, *J* 8.8 Hz, 3.0 Hz, CH-2), 7.63 (d, 1H, *J* 3.0 Hz, CH-4).

HRMS: (m/z ESI^+) Found: 138.1033 $(M + H)^+$ $C_7H_{12}N_3$ Requires: 138.1031

1,3-di(tert-butyloxycarbonyl)-2-[5-(dimethylamino)pyridine-2-amine]formamidine (122) [363]

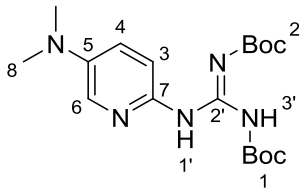

Following method A, a solution of **119** (0.22 g, 1.6 mmol) in CH_2Cl_2 (5 mL) at 0 °C was treated with $HgCl_2$ (0.48 g, 1.76 mmol), **85** (0.46 g, 1.6 mmol), and NEt_3 (0.7 mL, 5.0 mmol). The resulting mixture was stirred at 0 °C for 1 h and then for 18 h at room temperature. The usual workup followed by silica gel column chromatography afforded **122** as a white solid (37%, 0.22 g, 0.60 mmol).

Yield: 37% (0.22 g, 0.60 mmol).

M.P: 128-130 °C

δ_H (600 MHz, $CDCl_3$): 1.51 (s, 9H, $(CH_3)_3$ -1), 1.52 (s, 9H, $(CH_3)_3$ -2), 2.93 (s, 6H, CH_3-8), 7.09 (dd, 1H, *J* 9.1 Hz, 3.2 Hz, H-4), 7.81 (d, 1H, *J* 2.8 Hz, H-6), 8.13 (bs, 1H, H-3), 10.64 (bs, 1H , NH-3'), 11.51 (bs, 1H, NH-1').

δ_C (125 MHz, $CDCl_3$) : 28.2 ($(CH_3)_3$ -1), 28.4 ($(CH_3)_3$ -1), 40.7 (CH_3-8), 79.6 (qC-1), 83.7 (qC-2), 116.8 (CH-3), 121.9 (CH-4), 132.7 (CH-6), 141.1 (qC-5), 144.2 (qC-7), 152.9 (C=O), 153.0 (C=O), 163.6 (qC-2').

ν_{max} (ATR)/cm-1: 3424 (N-H), 1721 (C=O), 1593 (N-H), 1557 (N-H), 1459 (C-C), 1291, (C-N), 1230 (C-N), 1035 (C-N).

HRMS: (m/z ESI^+) Found: 380.2299 $(M + H)^+$ $C_{18}H_{29}N_5O_4$ Requires: 380.2292.

1,(tert-butyloxycarbonyl)-2-[5-(dimethylamino)pyridine-2-amine]formamidine trifluoroacetate (124)

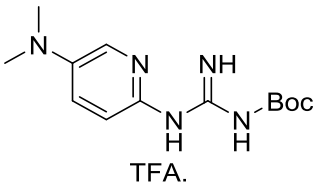

HRMS: (m/z ESI$^+$) Found: 280.1767 $(M + H)^+$ $C_{13}H_{22}N_5O_2$ Requires: 280.1768.

X-ray structure: See section 9.3.2 for data.

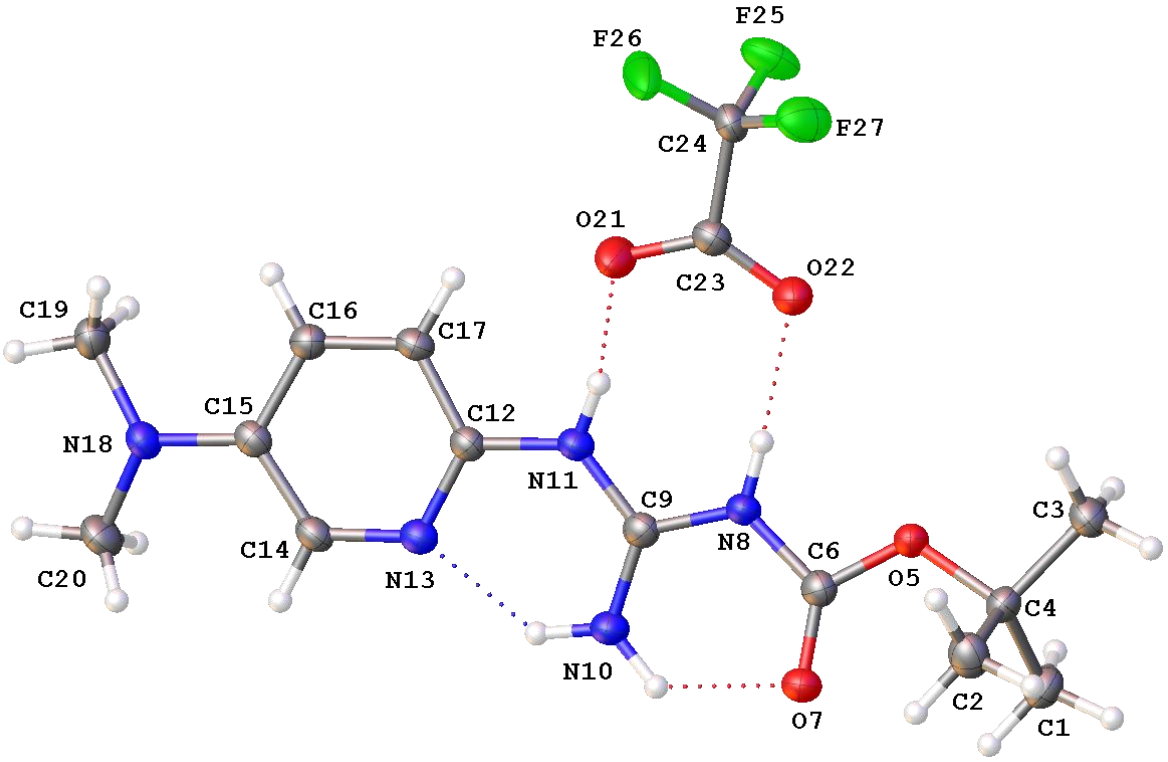

1-(5-(dimethylamino)pyridin-2-yl)guanidine dihydrochloride (118)[363]

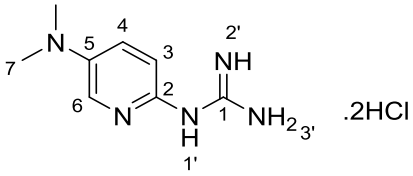

Following method D, **122** (0.22 g, 0.60 mmol) was treated with a solution of 50% TFA in CH_2Cl_2 (10 mL) for 3 h stirring at room temperature. Solvents were removed under reduced pressure to afford the trifluoroacetate salt. This salt was dissolved in H_2O (20 mL) and treated with Amberlite IRA 400 chloride form (1.0 g) for 24 h. Then, the resin was removed by filtration and the aqueous solution was washed with CH_2Cl_2 (2 x 10 mL). Evaporation of the water afforded the pure hydrochloride salt **118** as a white solid (98%, 0.15 g, 0.59 mmol).

Yield: 98% (0.15 g, 0.59 mmol)

M.P: 208-210 °C

δ_H (600 MHz, DMSO-d_6): 2.90 (s, 6H, CH_3-7), 6.94 (d, 1H, *J* 9.0 Hz, CH-4), 7.34 (dd, 1H, *J* 9.0 Hz, 3.2 Hz, CH-3), 7.77 (d, 1H, *J* 3.1 Hz, CH-6), 8.07 (bs, 3H, NH_2-3' and NH-2'), 10.60 (bs, 1H, NH-1').

δ_C (150 MHz, DMSO-d_6): 40.0 (CH_3-7), 113.8 (CH-3), 123.7 (CH-4), 129.9 (CH-6), 141.8 (qC-2), 143.5 (qC-5), 154.8 (qC-1).

νmax (ATR/cm^{-1}): 3274 (N-H), 1625 (C=C), 1293 (C-N), 1260 (C-N),1164 (C-N), 1002 (C-H).

HRMS: (m/z ESI^+) Found: 180.1247 $(M + H)^+$ $C_8H_{13}N_5$ Requires: 180.1243.

HPLC: 99.1 % (t_R = 22.4 min).

1,2,3,4-Tetrahydroquinolin-6-amine (154)[272]

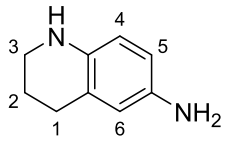

A solution of **153** (0.14 g, 1 mmol) in deionized water (20 mL) was treated with diboronic acid (0.9 g, 10 mmol) and the reaction mixture heated at 80 °C under reflux for 0.5 h. After cooling to rt the reaction mixture was diluted with EtOAc (20 mL) and the aqueous layer extracted with EtOAc (3 x 20 mL). The organic phase was washed with brine (1 x 20 mL), dried over anhydrous Na_2SO_4, and concentrated under reduced pressure to give a residue which was purified by silica gel column chromatography with gradient elution (10:1 EtOAc/petroleum ether) to afford **154** as an off white solid (95%, 0.14 g, 0.95 mmol).

Yield: 95% (0.14 g, 0.95 mmol).

M.P.: 96-98 °C (Lit. 95-97 °C).[272]

δ_H (400 MHz, $CDCl_3$): 1.90 (m, 2H, CH_2-2), 2.69 (m, 2H, CH_2-1), 3.28 (m, 4H, CH_2-3 and NH_2) 6.39 (m, 3H, CH-4, CH-5 and CH-6).

1-(3-hydroxyquinolin-6-yl)-2,3-di(*tert*-butoxycarbonyl)guanidine (157)

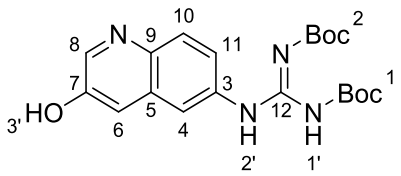

Following method A, a solution of **154** (0.10 g, 0.68 mmol) in CH_2Cl_2 (5 mL) at 0 °C was treated with $HgCl_2$ (0.20 g, 0.74 mmol), **85** (0.197 g, 0.68 mmol), and NEt_3 (0.3 mL, 2.1 mmol). The resulting mixture was stirred at 0 °C for 1 h and then for 18 h at room temperature. The usual workup followed by silica gel column chromatography afforded **157** as an off-white solid (29%, 0.08 g, 0.2 mmol) and **156** as a white solid (45%, 0.12g, 0.31 mmol).

Yield: 29% (0.08 g, 0.2 mmol).

M.P.: > 300 °C (Decomp.)

δ_H (600 MHz, $CDCl_3$): 1.46 (s, 9H,$(CH_3)_3$-1), 1.57 (s, 9H,$(CH_3)_3$-2), 7.12 (d, 1H, *J* 2.5 Hz, CH-6), 7.41 (dd, 1H, *J* 9.0 Hz, 2.3 Hz, CH-11), 7.77 (d, 1H, *J* 2.0 Hz, CH-4), 7.89 (d, 1H, *J* 9.0 Hz, CH-10), 8.37 (d, 1H, *J* 2.5 Hz, CH-8), 9.08 (bs, 1H, OH-3'), 10.40 (bs, 1H, NH-2'), 11.70 (bs, 1H, NH-1').

δ_C (150 MHz, $CDCl_3$) : 28.1 ($(CH_3)_3$-1), 28.1 ($(CH_3)_3$-2), 80.2 ($C(CH_3)_3$-1), 84.2 ($C(CH_3)_3$-2), 116.3 (CH-6), 120.3 (CH-4), 123.2 (CH-11), 129.4 (qC-5), 129.6 (CH-10), 134.0 (qC-3), 140.7 (qC-9), 143.4 (CH-8), 150.9 (qC-7), 153.1 (C=O-2), 155.1 (C=O-1), 163.1 (qC-12).

ν_{max} (ATR)/cm^{-1} : 3599 (OH), 3386 (N-H), 2898 (CH), 1740 (C=O), 1646 (C=N), 1222 (C-O).

HRMS: (m/z ESI^+) Found: 403.1967 $(M+H)^+$ $C_{20}H_{27}N_4O_5$ Requires: 403.1975

1-(quinolin-6-yl)-2,3-di(*tert*-butoxycarbonyl)guanidine (156)

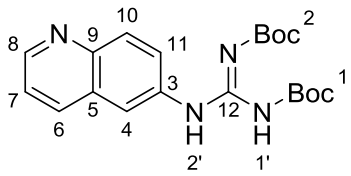

Following method A, a solution of **153** (0.14 g, 1.0 mmol) in CH_2Cl_2 (5 mL) at 0 °C was treated with $HgCl_2$ (0.20 g, 0.74 mmol), **85** (0.197 g, 0.68 mmol), and NEt_3 (0.3 mL, 2.1 mmol). The resulting mixture was stirred at 0 °C for 1 h and then for 18 h at room temperature. The usual workup followed by silica gel column chromatography afforded **157** as a white solid (82%, 0.22 g, 0.56 mmol).

Yield: 82% (0.22 g, 0.56 mmol).

M.P.: > 300 °C (Decomp.)

δ_H (600 MHz, $CDCl_3$): 1.55 (s, 9H,$(CH_3)_3$-1), 1.58 (s, 9H,$(CH_3)_3$-2), 7.38 (dd, 1H, *J* 8.3 Hz, 4.2 Hz, CH-7), 7.81 (dd, 1H, *J* 9.0 Hz, 2.3 Hz, CH-11), 8.06 (d, 1H, *J* 9.0 Hz, CH-10), 8.16 (d, 1H, *J* 8.3 Hz, CH-6), 8.33 (d, 1H, *J* 2.2 Hz, CH-4), 8.85 (m, 1H, CH-8), 10.63 (bs, 1H, NH-2'), 11.70 (bs, 1H, NH-1').

δ_C (150 MHz, $CDCl_3$) : 28.08 ($(CH_3)_3$-2), 28.18 ($(CH_3)_3$-1), 79.9 ($C(CH_3)_3$-1), 84.0 ($C(CH_3)_3$-2), 118.6 (CH-4), 121.5 (CH-7), 125.3 (CH-11), 128.6 (qC-5), 130.1 (CH-10), 135.0 (qC-3), 136.0 (CH-6), 145.9(qC-9), 149.7 (CH-8), 153.4 (C=O-2), 153.6 (C=O-1), 163.0 (qC-12).

ν_{max} (ATR)/cm^{-1} : 3253 (N-H), 2866 (CH), 1713 (C=O), 1646 (C=N), 1602(C=C).

HRMS: (m/z ESI^+) Found: 387.2011 $(M+H)^+$ $C_{20}H_{27}N_4O_4$ Requires: 387.2026

1-(quinolin-3-yl)-2,3-di(*tert*-butoxycarbonyl)guanidine (173)

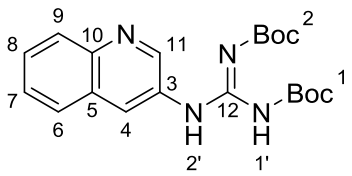

Following method A, a solution of **170** (0.14 g, 1.0 mmol) in CH_2Cl_2 (5 mL) at 0 °C was treated with $HgCl_2$ (0.20 g, 0.74 mmol), **85** (0.29 g, 0.68 mmol), and NEt_3 (0.3 mL, 2.1 mmol). The resulting mixture was stirred at 0 °C for 1 h and then for 18 h at room temperature. The usual workup followed by silica gel column chromatography afforded **173** as a white solid (70%, 0.18 g, 0.476 mmol).

Yield: 70% (0.18 g, 0.476 mmol).

M.P.: 238-240 °C

δ_H (600 MHz, $CDCl_3$): 1.53 (s, 9H,$(CH_3)_3$-1), 1.57 (s, 9H,$(CH_3)_3$-2), 7.52 (m,1 H, CH-7), 7.64 (m, 1H, CH-8), 7.83 (d, 1H, *J* 8.1 Hz, CH-6), 8.04 (d, 1H, *J* 8.4 Hz, CH-9), 8.69 (d, 1H, *J* 2.1 Hz, CH-4), 8.92 (d, 1H, *J* 2.5 Hz, CH-11), 10.62 (bs, 1H, NH-1'), 11.65 (bs, 1H, NH-2').

δ_C (150 MHz, $CDCl_3$): 28.2 ($(CH_3)_3$-2), 28.3 ($(CH_3)_3$-1), 80.2 ($C(CH_3)_3$-1), 84.4 ($C(CH_3)_3$-2), 126.6 (CH-4), 127.2 (CH-7), 128.1 (CH-6), 128.2 (qC-5), 128.6 (CH-8), 129.2 (CH-9), 130.8 (qC-3), 145.6 (C=O-1), 146.1 (C-11), 153.5 (qC-10), 154.0 (C=O-2), 163.5 (qC-12).

ν_{max} (ATR)/cm^{-1} : 3248 (N-H), 2980 (N-H), 2931 (CH), 1727 (C=O), 1626 (C=N), 1390 (C=C).

HRMS: (m/z ESI^+) Found: 387.2035 $(M+H)^+$ $C_{20}H_{27}N_4O_4$ Requires: 387.2026.

1-(isoquinolin-3-yl)-2,3-di(*tert*-butoxycarbonyl)guanidine (174)[283]

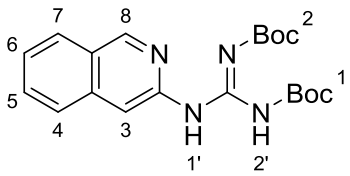

Following method A, a solution of **171** (0.14 g, 1.0 mmol) in CH_2Cl_2 (5 mL) at 0 °C was treated with $HgCl_2$ (0.20 g, 0.74 mmol), **85** (0.197 g, 0.68 mmol), and NEt_3 (0.3 mL, 2.1 mmol). The resulting mixture was stirred at 0 °C for 1 h and then for 18 h at room temperature. The usual workup followed by silica gel column chromatography afforded **174** as a white solid (60%, 0.16 g, 0.41 mmol).

Yield: 60% (0.16 g, 0.41 mmol).

δ_H (600 MHz, $CDCl_3$): 1.55 (s, 9H,$(CH_3)_3$-1), 1.56 (s, 9H,$(CH_3)_3$-2), 7.47 (t, 1H, *J* 7.7 Hz, CH-4), 7.63 (dd, 1H, *J* 11.4 Hz, 4.5 Hz, CH-7), 7.88 (m, 2H, CH-5 and CH-6), 8.71 (s, 1H, CH-3), 8.99 (s, 1H, CH-8), 11.05 (bs, 1H, NH-2'), 11.58 (bs, 1H, NH-1').

HRMS: (m/z ESI^+)

Found: 409.1860 $(M+Na)^+$ $C_{20}H_{26}N_4O_4Na$ Requires: 409. 1846

Found: 387.2022 $(M+H)^+$ $C_{20}H_{27}N_4O_4$ Requires: 387.2026

1-(Quinolin-6-yl)guanidinium *bis*-trifluoroacetate (167)[174]

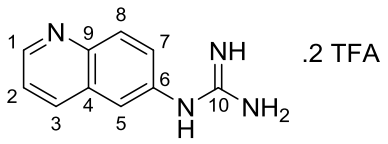

Following method D, **156** (0.22 g, 0.56 mmol) was treated with a solution of 50% TFA in CH_2Cl_2 (10 mL) for 3 h stirring at room temperature. Solvents were removed under reduced pressure to afford the trifluoroacetate salt **167** as a colourless gum in quantitative yield (<99%, 0.23 g, 0.56 mmol).

Yield: >99% (0.23 g, 0.56 mmol).

δ_H (600 MHz, D_2O): 7.94 (m, 2H, CH-2, CH-7), 8.09 (d, 1H, *J* 2.0 Hz, CH-5), 8.22 (d, 1H, *J* 9.1 Hz, CH-3), 8.88 (d, 1H, *J* 8.4 Hz, CH-8), 9.03 (d, 1H, *J* 4.0 Hz, CH-1).

δ_C (150 MHz, D_2O): 122.5 (CH-2), 123.1 (CH-5), 124.3 (CH-3), 129.3 (qC-4), 130.7 (CH-7), 135.3 (qC-6), 138.2 (qC-9), 144.5 (CH-8), 145.9 (CH-1), 156.1 (qC-10).

ν_{max} (ATR)/cm^{-1} : 3222 (N-H), 1607 (C=C), 1252 (C-N), 1175 (C-H).

HRMS: (m/z ESI^+) Found: 187.0979 $(M+H)^+$ $C_{10}H_{11}N_4$ Requires: 187.0978

HPLC: 96% (t_R = 7.2 min)

1-(Quinolin-3-yl)guanidinium trifluoroacetate (168)[364]

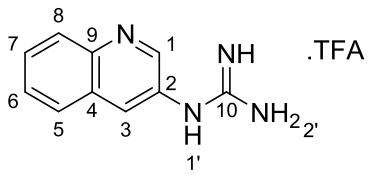

Following method D, **173** (0.18 g, 0.48 mmol) was treated with a solution of 50% TFA in CH_2Cl_2 (10 mL) for 3 h stirring at room temperature. Solvents were removed under reduced pressure to afford the trifluoroacetate salt **168** as a colourless gum in quantitative yield (>99%, 0.14 g, 0.48 mmol)

Yield: >99% (0.14 g, 0.48 mmol).

δ_H (600 MHz, DMSO-d_6) : 7.66 (m, 3H, CH-7 and NH_2-2'), 7.79 (t, 1H, *J* 7.6 Hz, CH-6), 8.02 (d, 1H, *J* 8.1 Hz, CH-5), 8.05 (d, 1H, *J* 8.4 Hz, CH-8), 8.27 (d, 1H, *J* 2.1 Hz, CH-1), 8.79 (d, 1H, *J* 2.3 Hz, CH-3), 9.97 (bs, 1H, NH-1').

δ_C (150 MHz, DMSO-d_6): 127.4 (CH-7), 127.7 (qC), 128.1 (CH-5), 128.7 (CH-8), 129.3 (qC-4), 129.7 (CH-6), 130.9 (CH-1), 145.8 (qC-2), 148.3 (CH-3), 156.3 (qC-10).

ν_{max} (ATR)/cm^{-1} : 3277 (N-H), 2890 (C-H), 1676 (C=N), 1620 (C=C).

HRMS: (m/z ESI^+) Found: 187.0974 $(M+H)^+$ $C_{10}H_{11}N_4$ Requires: 187.0978

HPLC: 99.8% (t_R = 20.2 min)

1-(isoquinolin-3-yl)guanidinium trifluoroacetate (169)[286]

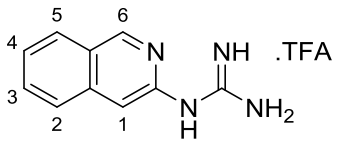

Following method D, **17** (0.16 g, 0.41 mmol) was treated with a solution of 50% TFA in CH_2Cl_2 (10 mL) for 3 h stirring at room temperature. Solvents were removed under reduced pressure to afford the trifluoroacetate salt **169** as a white solid in quantitative yield (>99%, 0.12 g, 0.41 mmol).

Yield: >99% (0.123 g, 0.41 mmol).

δ_H (600 MHz, MeOD): 7.39 (s, 1H, CH-1), 7.61 (t, 1H, *J* 7.6 Hz, CH-4), 7.77 (t, 1H, *J* 7.6 Hz, CH-3), 7.88 (d, 1H, *J* 8.3 Hz, CH-2), 8.09 (d, 1H, *J* 8.3 Hz, CH-5), 9.14 (s, 1H, CH-6).

HRMS: (m/z ESI^+) Found: 187.0974 $(M+H)^+$ $C_{10}H_{11}N_4$ Requires: 187.0978

HPLC: 99.9% (t_R = 25.6 min)

***N,N'*-Di-(*tert*-butoxycarbonyl)-1,2,3,4-tetrahydropyrimidine-2-thione (134)** [268]

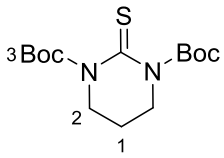

135 (2.05 g, 17.4 mmol) was added to a 500 mL 3-necked RBF charged with a solution of NaH (4.8 g, 103.3 mmol, 60% in mineral oil) in anhydrous THF (200 mL) at 0 ºC under Ar. The reaction was stirred in an ice/water bath for 5 min at approx. 0 ºC before being allowed to warm and stir for 30 min at r.t. The reaction mixture was again cooled to ~ 0 °C in an ice/water bath before di-*tert*-butyl dicarbonate (10.9 g, 49.9 mmol) was added neat. After 30 min, the ice-bath was removed and the reaction mixture was stirred at r.t. overnight. The reaction mixture was quenched drop wise with saturated $NaHCO_3$ solution until effervescence ceased (~10 mL) then deionised water (50 mL) to give a clear intense yellow solution. The mixture was extracted with EtOAc (3 × 75 mL) to give an intensely yellow organic layer and colourless aqueous layer. The combined organic phases were washed with brine (50 mL), dried over anhydrous $MgSO_4$ and concentrated *in vacuo* to give a residue which was recrystallized from boiling hexanes to afford **134** as a yellow solid (72%, 3.94 g, 12.53 mmol).

Yield: 72% (3.94 g, 12.53 mmol)

M.P.: 90-94 °C (Lit. 93-94 °C).[213]

δ_H (400 MHz, $CDCl_3$) : 1.51 (s, 18H, $(CH_3)_3$-3), 1.13 (p, 2H, *J* 6.9 Hz CH_2-1), 3.65 (t, 4H, *J* 6.9 Hz, CH_2-2).

(*N*-Methyl-*N*-*tert*-butylcarbonyl)-4-nitroaniline (143)

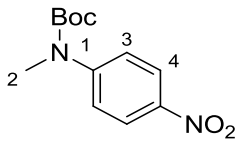

A solution of **74** (2.00 g, 13.14 mmol) in anhydrous THF (12 mL) under Ar at approx. 0 °C cooled in an ice/water bath was treated with di-*tert*-butyl dicarbonate (3.20 g, 14.46 mmol) and a solution of 4-dimethylaminopyridine (0.07 g, 0.57 mmol) in anhydrous THF (12 mL) was added portion-wise over 10 min and the reaction stirred at approx. 0 °C for 0.5 h. The ice/water bath was then removed and the reaction was stirred at rt for 18 h. The reaction mixture was cooled to approx. 0 °C in an ice/water bath, quenched by the drop-wise addition of 1M citric acid (20 mL, aq.) and extracted with EtOAc (3 × 50 mL). The organic phase was washed with water (30 mL) and brine (30 mL), dried over anhydrous $MgSO_4$ and concentrated *in vacuo* affording a residue that was purified by silica gel column chromatography with gradient elution (100% Hexane to 1:9 Hexane/Et_2O) affording **143** as an orange crystalline solid (86%, 2.85 g, 11.31 mmol).

Yield: 86% (2.85 g, 11.31 mmol)

M.P.: 75-77 °C (Lit. 76 -78 °C).[270]

δ_H (400 MHz, $CDCl_3$) : 1.49 (s, 9H, $(CH_3)_3$-1), 3.32 (s, 3H, CH_3-2), 7.45 (m, 2H, CH-3), 8.15 (m, 2H, CH-4).

(*N*-Methyl-*N*-*tert*-butylcarbonyl)-4-aminoaniline (142)[270]

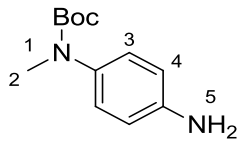

Following method H, a degassed solution of **143** (2.85 g, 11.29 mmol) in EtOAc (12 mL) was treated with Pd 10%/C (0.33 g) and stirred under H_2 (1 atm) for 24 h. Once the reaction was adjudged complete by TLC it was diluted with EtOAc, filtered through celite and concentrated *in vacuo* to give a residue which was purified by silica gel chromatography eluting with 100% EtO_2 affording **142** as an off-white solid (89%, 2.23 g, 10.01 mmol).

Yield: 89% (2.23 g, 10.01 mmol)

M.P.: 68-70 °C (Lit. 69 -71 °C).[270]

δ_H (400 MHz, $CDCl_3$): 1.42 (s, 9 H, $(CH_3)_3$-1), 3.18 (s, 3H, CH_3-2), 3.57 (bs, 2H, NH_2-5), 6.61 (d, 2H, *J* 8.0 Hz, CH-4), 6.98 (d, 2H, *J* 6.9 Hz, CH-3).

1,3-Di-(*tert*-butoxycarbonyl)-2-(4-ethylanilino)imino-1,4,5,6-(2H,3H)-tetrahydropyrimidine (140)

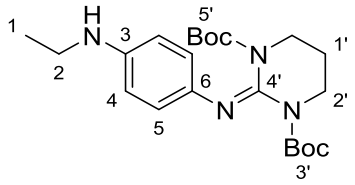

Following method C, A solution of **75** (0.755 g, 2.4 mmol) in DMF (10 mL) cooled to approx. 0 °C in an ice/water bath was treated with $HgCl_2$ (0.65 g, 2.4 mmol) and NEt_3 (0.78 mL, 5.6 mmol) was then added and the solution was stirred at approx. 0 °C for 0.5 h. A solution **134** (0.29 g, 1.6 mmol) in DMF (5 mL) was then added dropwise over 10 min and the resulting mixture stirred at approx. 0 °C for 1 h then at rt for 18 h. Standard workup with additional water (10 x 30 mL) and brine (5 x 30 mL) washes to remove DMF gave a residue which was purified using silica gel chromatography with gradient elution from 9:1 to 1:1 hexanes:EtOAc affording the product as a red crystalline solid (83%, 0.56 g, 1.33 mmol).

Yield: 83% (0.56 g, 1.33 mmol)

M.P.: 83-85 °C

δ_H (400 MHz, $CDCl_3$) : 1.11 (bs, 9H, $(CH_3)_3$-3'), 1.22 (t, 3H, *J* 7.0 Hz, CH_3-1), 1.51 (bs, 9H, $(CH_3)_3$-5'), 2.04 (m, 2H, CH_2-1'), 3.12 (q, 2H, *J* 7.0 Hz, CH_2-2), 3.67 (bs, 4H, CH_2-2'), 6.55 (d, 2H, *J* 8.7 Hz, CH-5), 6.84 (m, 2H, CH-4).

δ_C (100 MHz, $CDCl_3$) : 15.0 (CH_3-1), 23.5 (CH_2-1'), 27.8 (($CH_3)_3$-3'), 28.4 (($CH_3)_3$ -5'), 39.1 (CH_2-2), 42.7 (CH_2-2'), 42.8 (CH_2-2'), 113.4 (CH-5), 123.0 (CH-4), 137.6 (qC-6), 139.1 (q C-4'), 145.5 (qC-3), 151.7 (qC=O, 5'), 153.0 (qC=O, 3').

ν_{max} (ATR)/cm^{-1}: 3365 (N-H), 2969 (C-H), 2931(C-H), 2872 (C-H), 1672 (C=N), 1608 (C=O) 1477 (C-C), 1460 (C-C), 1318(C-N), 1287 (C-N), 1253 (C-N).

HRMS: (m/z ESI^+) Found: 419.2662 $(M+H)^+$ $C_{22}H_{35}N_4O_4$ Requires: 419.2658.

1,3-Di-(*tert*-butoxycarbonyl)-2-(4-dimethylanilino)imino-1,4,5,6-(2H,3H)-tetrahydropyrimidine (141)

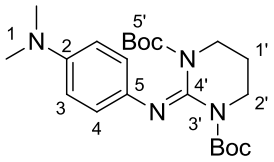

Following method C, a 50 mL RBF was charged with **115** (0.19 g, 1.33 mmol), **134** (0.31 g, 1 mmol) and CH_2Cl_2 (10 mL) before being cooled to approx. 0 °C. NEt_3 (0.5 mL, 3.51 mmol) and $HgCl_2$ (0.299 g, 1.1 mmol) were added at approx. 0 °C and stirred at this temperature for 0.5 h, then allowed to return to rt and stir overnight (18 h). Once reaction was complete (TLC) standard work up and purification using silica gel chromatography eluting with Hexanes/Et_2O (1:1) afforded **141** as a red crystalline solid (77%, 0.32 g, 0.77 mmol).

Yield: 77% (0.32 g, 0.77 mmol)

M.P.: 93-95 °C

δ_H (400 MHz, $CDCl_3$) : 1.06 (9H, bs, $(CH_3)_3$-3'), 1.49 (9H, bs, $(CH_3)_3$-5'), 2.01 (2H, m, CH_2-1'), 2.85 (6H, s, CH_3-1), 3.66 (4H, bs, CH_2-2), 6.66 (2H, m, CH-4), 6.86 (2H, m, CH-3).

δ_C (100 MHz, $CDCl_3$) : 23.4 (CH_2-1'), 27.7 (($CH_3)_3$-3'), 28.3 (($CH_3)_3$-5'), 41.3 (CH_3-1), 42.6 (CH_2-2'), 42.7 (CH_2-2'), 81.7 ($C(CH_3)_3$-3'), 81.9 ($C(CH_3)_3$-5'), 113.6 (CH-4), 122.7 (CH-3), 137.3 (qC-5), 139.3 (C=N-4'), 148.1 (qC-2), 151.6 (qC=O-5'), 152.9 (qC=O, 3').

ν_{max} (ATR)/cm^{-1}: 2975 (C-H), 2931 (C-H), 2872 (C-H), 2804 (C-H), 1694 (C=O), 1660 (C=N), 1513 (C-C), 1479 (C-C), 1346(C-N), 1320 (C-N), 1251 (C-N), 1139 (C-N), 821 (C-H), 799 (N-H).

HRMS: (m/z ESI^+) Found: 419.2663 $(M+H)^+$ $C_{22}H_{35}N_4O_4$ Requires: 419.2658.

1,3-Di-(*tert*-butoxycarbonyl)-2-(*N*-methyl-N' *tert*-butoxycarbonyl-anilino)imino-1,4,5,6-(2H,3H)-tetrahydropyrimidine (138)

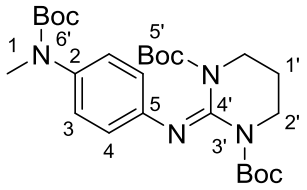

Following method C, a 50 mL RBF was charged with **142** (0.22 g, 1.00 mmol), **134** (0.31 g, 1 mmol) and CH_2Cl_2 (10 mL) before being cooled to approx. 0 °C. NEt_3 (0.44 mL, 3.1 mmol) and $HgCl_2$ (0.30 g, 1.1 mmol) were added at approx. 0 °C and stirred at this temperature for 0.5 h, then allowed to return to rt and stir overnight (18 h). Once reaction was complete (TLC) standard work up and purification using silica gel chromatography eluting with EtOAc/CH_2Cl_2 (1:4) afforded **138** as an amorphous yellow gum (25%, 0.13 g, 0.25 mmol).

Yield: 25% (0.13 g, 0.25 mmol)

δ_H (400 MHz, $CDCl_3$): 1.09 (bs, 9H, $(CH_3)_3$-3'), 1.37 (s, 9H, $(CH_3)_3$-6'), 1.48 (bs, 9H, $(CH_3)_3$-5'), 2.02 (m, 2H, CH_2-1'), 3.14 (s, 6H, CH_3-1), 3.66 (4H, bs, CH_2-2'), 6.84 (d, 2H, *J* 8.7 Hz, CH-4), 7.06 (d, 2H, *J* 8.6 Hz, CH-3).

δ_C (100 MHz, $CDCl_3$): 23.8 (CH_3-1), 27.7 (($CH_3)_3$-3'), 28.2 (($CH_3)_3$-5'), 28.4 (($CH_3)_3$-6'), 37.6 (CH_3-1), 42.1 (CH_2-2'), 80.1 (qC-6'), 82.2 (qC3'/5'), 121.7 (CH-4), 126.0 (CH-3), 139.6 (qC-5), 141.6 (qC-4'), 144.6 (qC-2), 151.3 (C=O3'/5'), 152.6 (C=O3'/5'), 154.9 (C=O-6').

HRMS: (m/z ESI^+) Found: 505.3035 $(M+H)^+$ $C_{26}H_{41}N_4O_6$ Requires: 505.3021

1,3-Di-(*tert*-butoxycarbonyl)-2-(4-*N*-ethylaminopyridin-3-yl)imino-1,4,5,6-(2H,3H)-tetrahydropyrimidine (139)

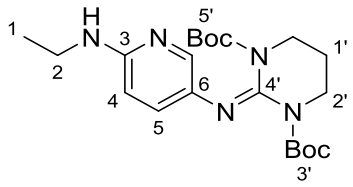

Following method C, a 50 mL RBF was charged with **77** (0.10 g, 0.77 mmol), **134** (0.44 g, 1.4 mmol) and CH_2Cl_2 (10 mL) before being cooled to approx. 0 °C. NEt_3 (0.32 mL, 2.3 mmol) and $HgCl_2$ (0.38 g, 1.4 mmol) were added at approx. 0 °C and stirred at this temperature for 0.5 h, then allowed to return to rt and stir overnight (18 h). Once reaction was complete (TLC) standard work up and purification using silica gel chromatography eluting with EtOAc/CH_2Cl_2 (1:4) afforded **139** as a red oil (27%, 0.09 g, 0.21 mmol).

Yield: 27% (0.09 g, 0.21 mmol)

δ_H (400 MHz, $CDCl_3$): 1.17 (bs, 9H, $(CH_3)_3$-3'), 1.23 (t, 3H *J* 7.2 Hz, CH_3-1), 1.51 (bs, 9H, $(CH_3)_3$-5'), 2.04 (p, 2H, *J* 6.7 Hz, CH_2-1')3.26 (q, 2H, *J* 6.9 Hz, CH_2-2), 3.70 (m, 4H, CH_2-2'), 4.62 (bs, 1H, NH), 6.36 (d, 1H, *J* 8.8 Hz, CH-4), 7.16 (dd, 1H, *J* 8.8, 2.5 Hz, CH-5), 7.80 (bs, 1H, CH-7).

δ_C (100 MHz, $CDCl_3$): 15.0 (CH_2-1), 23.7 (CH_2-1'), 27.9 (($CH_3)_3$-3'), 28.4(($CH_3)_3$-5'), 42.5 (CH_2-2'), 42.4 (CH_2-2'), 82.2 (qC5'), 82.4 (qC3'), 106.3 (CH-4), 131.4 (CH-5), 134.4 (qC6), 141.2 (CH-7), 141.7 (C=O), 151.4 (C=O), 152.8 (qC4'), 155.8 (qC3).

HRMS: (m/z ESI$^+$) Found: 420.2605 $(M+H)^+$ $C_{21}H_{34}N_5O_4$ Requires: 420.2605

1,3-Di-(*tert*-butoxycarbonyl)-2-(5,6,7,8-tetrahydronaphthalen-2-yl)imino-1,4,5,6-(2H,3H)-tetrahydropyrimidine (145)

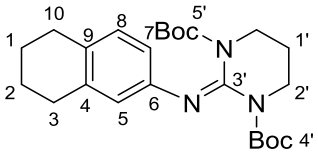

Following method C, a solution of **147** (0.15 g, 1.00 mmol) and **134** (0.16 g, 0.5 mmol) in CH_2Cl_2 (5 mL) was cooled in an ice/water bath and treated with NEt_3 (0.25 mL, 3.5 mmol) and $HgCl_2$ (0.27 g, 1 mmol). The reaction was stirred for 0.5 h at approx. 0°C and then stirred at rt for 48h. After 48 h, complete consumption of **134** adjudged by TLC was observed. Standard work up and multiple rounds of purification using silica gel chromatography afforded **145** as a brown oil (20%, 0.04 g, 0.01 mmol).

Yield: 20% (0.04 g, 0.01 mmol).

δ_H (400 MHz, $CDCl_3$) : 1.09 (bs, 9H, $(CH_3)_3$-4'), 1.51 (bs, 9H, $(CH_3)_3$-5'), 1.74 (m, 4H, CH_2-1 and CH_2-2), 2.04 (p, 2H, *J* 6.7 Hz, CH_2-1'), 2.69 (m, 4H, CH_2-3 and CH_2-10), 3.67 (bs, 4H, CH_2-2'), 6.62 (m, 2H, CH-7 and CH-8), 6.93 (d, 1H, *J* 8.6 Hz, CH-5).

δ_C (100 MHz, $CDCl_3$) : 23.4 (CH_2-1'), 23.6 (CH_2-2), 23.8 (CH_2-1), 27.4 (($CH_3)_3$-4'), 28.2 (($CH_3)_3$-5'), 27.6 (CH_2-3), 28.4 (CH_2-10), 42.4 (CH_2-2') ,42.7 (CH_2-2'), 118.5 (CH-8), 122.2 (CH-7), 129.8 (CH-5), 132.6 (qC-4'), 137.2 (qC-6), 140.8 (qC-3'), 144.6 (qC-5').

ν_{max} (ATR)/cm^{-1}: 2981 (C-H), 2930 (C-H), 1705 (C=O), 1666 (C=N), 1496 (C-C), 1475 (C-C), 1456 (C-C), 1317 (C-N), 1283 (C-N), 1251 (C-N), 908 (C-H).

HRMS: (m/z ESI^+) Found: 430.2692 $[M+H]^+$ $C_{24}H_{36}N_3O_4$ Requires: 430.2706.

1,3-Di-(*tert*-butoxycarbonyl)-2-(2,3-dihydrobenzo[b][1,4]dioxin-6-yl)imino-1,4,5,6-(2H,3H)-tetrahydropyrimidine (146)

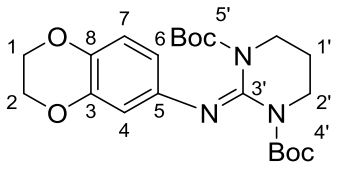

Following method C, a solution of **148** (0.15 g, 1.0 mmol) and **134** (0.31 g, 1.0 mmol) in CH_2Cl_2 (5 mL) was cooled in an ice/water bath and treated with NEt_3 (0.44 mL, 3.1 mmol) and $HgCl_2$ (0.3 g, 1.1 mmol). The reaction was stirred for at approx. 0°C 0.5 h and then stirred at rt for 72h. After 72 h, **134** remained unreacted as adjudged by TLC. Standard work up and purification using silica gel chromatography with gradient elution of 100% hexanes to 1:1 hexanes:EtOAc afforded **146** as a red oil (22%, 0.09 g, 0.22 mmol).

Yield: 22% (0.09 g, 0.22 mmol).

δ_H (400 MHz, $CDCl_3$) : 1.16 (bs, 9H, $(CH_3)_3$-4'), 1.51 (bs, 9H, $(CH_3)_3$-5'), 2.04 (p, 2H, *J* 6.7 Hz, CH_2-1'), 3.67 (bs 4H, , CH_2-2'), 4.21 (m, 4H, CH_2-1 and CH_2-2), 6.45 (m, 2H, CH-6 and CH-7), 6.76 (d, 1H, *J* 8.5 Hz, CH-4).

δ_C (100 MHz, $CDCl_3$) : 23.7 (CH_2-1'), 27.8 (($CH_3)_3$-4'), 28.4 (($CH_3)_3$-5'), 42.4 (CH_2-2'), 42.6 (CH_2-2'), 64.5 (CH_2-1/2), 64.6 (CH_2-1/2), 110.7 (CH-6), 115.1 (CH-7), 117.2 (CH-4), 140.2 (qC-8), 141.0 (qC-5), 141.26 (qC-3'), 143.5 (qC-3), 151.6 (qC-5'), 152.9 (qC-4').

ν_{max} (ATR)/cm^{-1}: 2977 (C-H), 2932 (C-H), 2874 (C-H), 1703 (C=O), 1666 (C=N), 1500 (C-C), 1458(C-C), 1305 (C-N), 1280(C-N), 1254 (C-N), 1135 (C-O), 1067 (C-O), 912 (C-H), 853 (N-H).

HRMS: (m/z ESI^+) Found: 456.2119 $[M+Na]^+$ $C_{22}H_{31}N_3O_6Na$ Requires: 456.2111.

2-(4-*N*-dimethylaminoanilino)-1,4,5,6-tetrahydropyrimidine Hydrochloride (108)

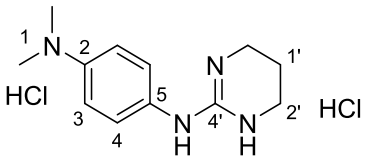

141 (0.32 g, 0.77 mmol) was treated with excess HCl (10 mL, 1M aq.) and heated at 70 °C for 1h. The aqueous layer was then washed with $CHCl_3$ (3 x 10 mL) and the aqueous layer was concentrated under reduced pressure. Removal of excess solvent and HCl *in vacuo* afforded dihydrochloride salt **108** as a red gum in quantitative yield (<99%, 0.22 g, 0.77 mmol).

Yield: >99% (0.22 g, 0.77 mmol).

δ_H (600 MHz, D_2O): 2.01 (p, 2H, *J* 5.8 Hz, CH_2-1') 3.31 (s, 6H, CH_3-1), 3.39 (t, 4H, *J* 5.8 Hz, CH_2-2'), 7.46 (d, 2H, *J* 8.8 Hz, CH-3), 7.67 (d, 2H, *J* 8.8 Hz, CH-4).

δ_C (150 MHz, D_2O): 19.2 (CH_2-1'), 38.4 (CH_2-2'), 46.4 (CH_3-1), 122.05 (CH-4), 126.1 (CH-3), 136.8 (qC-5), 139.8 (qC-2), 152.1 (qC-4').

HRMS: (m/z ESI$^+$) Found: 217.1458 $(M+H)^+$ $C_{12}H_{17}N_4$ Requires: 217.1458

HPLC: 99.0% (t_R = 16.8 min)

2-(4-*N*-methylaminoanilino)-1,4,5,6-tetrahydropyrimidine hydrochloride (107)

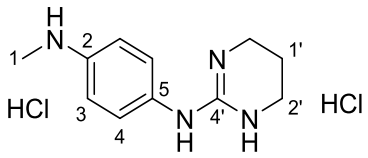

138 (0.13 g, 0.25 mmol) was treated with excess HCl (10 mL, 1.25 M in MeOH) and heated at 70 °C for 1h. Excess solvent was removed *in vacuo* to give a residue which was dissolved in H_2O (10 mL) and washed with $CHCl_3$ (3 x 10 mL). The aqueous layer was then concentrated under reduced pressure. Removal of excess solvent and HCl *in vacuo* afforded dihydrochloride salt **107** as a pink gum in quantitative yield (<99%, 0.07 g, 0.25 mmol).

Yield: >99% (0.07 g, 0.25 mmol).

δ_H (600 MHz, D_2O): 2.00 (m, 2H, CH_2-1') 3.08 (s, 3H, CH_3-1), 3.38 (t, 4H, *J* 5.8 Hz, CH_2-2'), 7.41 (d, 2H, *J* 8.8 Hz, CH-3), 7.49 (d, 2H, *J* 8.8 Hz, CH-4).

δ_C (150 MHz, D_2O): 19.3 (CH_2-1'), 35.9 (CH_3-1), 38.2 (CH_2-2'), 122.7 (CH-4), 126.5 (CH-3), 136.2 (qC-5), 136.8 (qC-2), 152.4 (qC-4').

HRMS: (m/z ESI^+) Found: 205.1449 $(M+H)^+$ $C_{11}H_{17}N_4$ Requires: 205.1448

HPLC: 96% (t_R = 15.1 min)

2-(6-(Ethylamino)pyridin-3′-yl)-1,4,5,6-tetrahydropyrimidine hydrochloride (106)

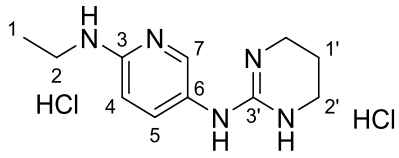

139 (0.09 g, 0.21 mmol) was treated with excess HCl (10 mL, 1M) and heated at 70 °C for 1h. The aqueous layer was then washed with $CHCl_3$ (3 x 10 mL) and the aqueous layer was concentrated under reduced pressure. Removal of excess solvent and HCl *in vacuo* afforded dihydrochloride salt **106** as a red gum in quantitative yield (<99%, 0.06 g, 0.25 mmol).

Yield: >99% (0.06 g, 0.21 mmol).

δ_H (600 MHz, D_2O): 1.29 (t, 3H *J* 7.3 Hz, CH_3-1), 1.96 (m, 2H, CH_2-1’), 3.39 (m, 6H, CH_2-2’ and CH_2-2), 7.05 (d, 1H, *J* 9.7 Hz, CH-4), 7.74 (dd, 1H, *J* 9.7, 2.4 Hz, CH-5), 7.80 (d, 1H, *J* 2.0 Hz, CH-7).

δ_C (150 MHz, D_2O): 12.4 (CH_3-1), 19.1 (CH_2-1’), 37.1 (CH_2-2), 38.3 (CH_2-2’), 115.0 (CH-4), 120.3 (qC-3), 133.4 (CH-7), 142.5 (CH-5), 151.7 (qC-6), 152.7 (qC-4’).

HRMS: (m/z ESI^+) Found: 220.1567 $(M+H)^+$ $C_{11}H_{18}N_5$ Requires: 220.1556

HPLC: 96.1% (t_R = 4.3 min)

2-Methylthio-1,4,5,6-tetrahydropyrimidine hydroiodide (193)[291]

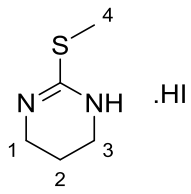

A solution of **135** (0.56 g, 4.82 mmol) in EtOH (5 mL) in a 25 mL RBF fitted with a reflux condenser was treated with iodomethane (0.3 mL, 4.82 mmol) and the reaction mixture heated under reflux for 3 h. The solvent was then removed *in vacuo* to give a residue that was triturated with cold Et_2O and filtered to afford 2-methylthio-1,4,5,6-tetrahydropyrimidine hydroiodide **193** as a white crystalline solid (97 %, 1.21 g, 4.69 mmol).

Yield: 97% (1.21 g, 4.69 mmol).

M.P.: 145-148 °C (Lit. 146-148 °C).[291]

δ_H (400 MHz, DMSO-d_6) : 1.82 (p, 2H, *J* 3.7 Hz, *J* 1.8 Hz, CH_2-2), 2.58 (s, 3H, CH_3-4), 3.38 (t, 4H, *J* 5.8 Hz, CH_2-1 and CH_2-3), 9.54 (bs, 2H, NH).

HRMS: (m/z ESI^+) Found: 130.0565 $(M+H)^+$ $C_5H_{10}N_2S$ Requires: 130.0565.

1-*N*-(*tert*-Butylcarbamate)-2-methylthio-1,4,5,6-tetrahydropyrimidine (192)

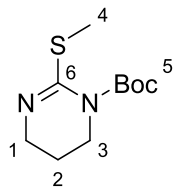

A solution of **193** (0.134 g, 1.01 mmol) in anhydrous CH_2Cl_2 (5 mL) was treated with NEt_3 (0.14 mL, 1.00 mmol) under Ar and reaction cooled on ice/water bath. Di-*tert*-butyl dicarbonate (0.258 g, 1.11 mmol) was then added under Ar and reaction allowed to warm to r.t and stir for 18 h. Upon completion of the reaction by TLC the solvent was removed *in vacuo* and product purified by silica gel chromatography eluting with 100% EtOAc to afford **192** as a colourless oil (58%, 0.14 g, 0.58 mmol).

Yield: 58%% (0.14 g, 0.58 mmol).

δ_H (600 MHz, $CDCl_3$) : 1.45 (s, 9H, $(CH_3)_3$-5), 1.76 (p, 2H, *J* 5.7 Hz, CH_2-2), 2.17 (s, 3H, CH_3-4), 3.44 (t, 2H, *J* 5.9 Hz, CH_2-3), 3.56 (t, 2H, *J* 6.1 Hz, CH_2-1).

δ_C (150 MHz, $CDCl_3$) : 15.7 (CH_3-4), 22.3 (CH_2-2), 28.1 (($CH_3)_3$-5), 44.5 (CH_2-1), 46.6 (CH_2-3), 82.8 (qC$(CH_3)_3$-5), 85.07, 146.70 (qC=O-5), 152.34 (qC-4).

ν_{max} (ATR)/cm^{-1}: 2978 (C-H), 2945 (C-H), 2882 (C-H), 1696 (C=N), 1475 (C=O), 1245 (C-N).

HRMS: (m/z APCI$^+$) Found: 231.1165 $(M+H)^+$ $C_{10}H_{19}N_2O_2S$ Requires: 231.1162.

_N_-(3-Aminoethyl)-_N'_-phenylthiourea (197)[292]

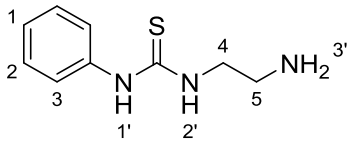

A solution of **195** (1.2 mL, 20.00 mmol) and NEt_3 (3.3 mL, 24.00 mmol) in anhydrous CH_2Cl_2 (60 mL) cooled in an ice/water bath was treated dropwise with **179** (2.9 mL, 24.00 mmol). Once addition was complete, the reaction was stirred at rt for 18 h. Removal of solvent *in vacuo* followed by recrystallization from cold CH_2Cl_2 afforded the desired product **197** as a white crystalline solid (46%, 1.80 g, 9.2 mmol).

Yield: 46% (1.80 g, 9.2 mmol).

M.P.: 134-136 °C (Lit. 135-137 °C).[292]

δ_H (400 MHz, $CDCl_3$) : 2.69 (t, 2H, *J* = 6.1 Hz, CH_2-4), 3.41 (m, 2H, CH_2-5), 7.27 (m, 3H, CH-1 and CH-2), 7.41 (t, 2H, *J* 7.8 Hz, CH-3).

HRMS: (m/z ESI$^-$) Found: 194.0756 $[M-H]^-$ $C_9H_{12}N_3S$ Requires: 194.0752.

***N*-(3-Aminopropyl)-*N'*-phenylthiourea (196)**[292]

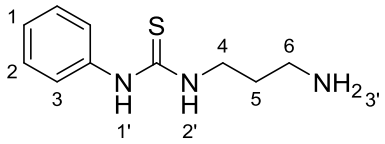

A solution of **194** (1.7 mL, 20.00 mmol) and NEt_3 (3.3 mL, 24.00 mmol) in anhydrous CH_2Cl_2 (60 mL) cooled in an ice/water bath was treated dropwise with **179** (2.9 mL, 24.00 mmol). Once addition was complete, the reaction was stirred at rt for 18 h. Removal of solvent *in vacuo* followed by recrystallization from cold CH_2Cl_2 afforded the desired product **196** as a white crystalline solid (29 %, 1.20 g, 5.7 mmol).

Yield: 29% (1.20 g, 5.7 mmol).

M.P.: 102-104 °C (Lit. 103-105 °C).[292]

δ_H (400 MHz, $CDCl_3$) : 1.33 (bs, 2H, NH-3'), 1.64 (m, 2H, CH_2-5), 2.78 (m, 2H, CH_2-6), 3.73 (m, 2H, CH_2-4), 7.24 (m, 3H, CH-1 and CH-2), 7.37 (t, 2H, *J* 7.7 Hz, CH-3) 7.69 (bs, 1H, NH-1'), 7.90 (bs, 1H, NH_2-2').

HRMS: (m/z ESI$^+$) Found: 208.0910 $[M+H]^+$ $C_{10}H_{14}N_3S$ Requires: 208.0908.

2-(Phenylamino) imidazoline hydrochloride (199)[140]

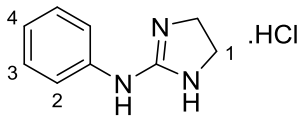

Following method G, a solution of **197** (0.98 g, 5.0 mmol) in CH_2Cl_2 at 0 °C was treated with $HgCl_2$ (1.49 g, 5.5 mmol) and NEt_3 (2.4 mL, 17.5 mmol) and was allowed to stir at rt until the reaction was adjudged complete by TLC analysis. Standard work up and trituration with $CHCl_3$ afforded **199** as a white solid (80%, 0.79 g, 4.00 mmol).

Yield: 80% (0.79 g, 4.00 mmol).

M.P: 210-212 °C (Lit. 211-213 °C).[130]

δ_H (400 MHz, D2O): 3.77 (s, 4H, CH_2-1), 7.32 (m, 2H, H-3), 7.40 (m, 1H, H-4), 7.51 (m, 2H, H-2).

HRMS: (m/z ESI^+) Found: 162.1026 $[M+H]^+$ $C_9H_{12}N_3$ Requires: 162.1031.

2-(Phenylamino) imidazoline (198)

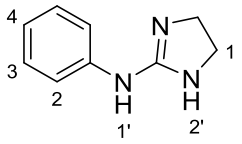

A solution of **197** (0.98 g, 3.02 mmol) in MeCN (10 mL) at 0 °C was treated with a solution of IBX (0.93 g, 3.32 mmol) and NEt_3 (1.26 mL, 9.06 mmol) in MeCN (10 mL) dropwise. The reaction mixture was allowed to stir at rt until the reaction was adjudged complete by TLC analysis. The mixture was diluted with EtOAc (10 mL) and the organic phase washed with water (2 × 20 mL), saturated Na_2CO_3 (1 x 20 mL), dried over $MgSO_4$, filtered and concentrated *in vacuo* to give a residue which was purified silica gel column chromatography with gradient elution (3:1 hexane:EtOAc to 1:1 hexane:EtOAc) to afford **198** as a white solid (53%, 0.26 g, 1.60 mmol).

Yield: 53% (0.26 g, 1.60 mmol).

δ_H (400 MHz, $CDCl_3$) : 3.81 (s, 4H, CH_2-1), 7.29 (m, 3H, CH-3 and CH-4), 7.40 (t, 2H, *J* 8.0 Hz, CH-2), 11.16 (bs, 2H, NH-2').

M.P: 112-116 °C (Lit. 138-139 °C).[263]

6-isothiocyanato-1,2,3,4-tetrahydronaphthalene (200)[365]

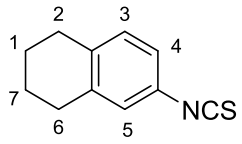

Following method I, **134** (0.15 g, 1.0 mmol) and **201** (0.12 g, 1.1 mmol) were stirred in anhydrous CH_2Cl_2 (10 mL) under Ar for 18 h and concentrated *in vacuo* to give a residue which was purified by silica gel chromatography eluting with 100% Hexanes affording **200** as a colourless oil (93 %, 0.18 g, 0.93 mmol).

Yield: 93% (0.18 g, 0.93 mmol).

δ_H (400 MHz, $CDCl_3$) : 1.78 (dt, 4H, *J* 6.7 Hz, *J* 3.4 Hz, CH_2-1 and CH_2-7). 2.73 (m, 4H, CH_2-2 and CH_2-6), 6.92 (m, 2H, CH-3 and CH-4), 7.02 (m, 1H, CH-5).

ν_{max} (ATR)/cm^{-1}: 2928 (C-H), 2856 (C-H), 2220 (C-H), 2055 (N=C=S), 1605 (C-C), 1492 (C-C), 1448 (C-C), 1292 (C-N).

HRMS: (m/z ESI^+) Found: 189.0608 $(M+H)^+$ $C_{11}H_{11}NS$ Requires: 189.0612

(*N*-*tert*-butoxycarbonyl)--4-isothiocyanatoaniline (203)[366]

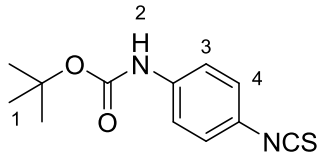

Following method I, (*N*-*tert*-butoxylcarbonyl)-*p*-phenylenediamine (0.31 g, 1.50 mmol) and **201** (0.29 g, 1.65 mmol) were stirred in anhydrous CH_2Cl_2 (15 mL) under Ar for 18 h and concentrated *in vacuo* to give a residue which was purified by silica gel chromatography with gradient elution 100% Hexanes to 1:4 EtOAc:Hexanes affording **203** as an off-white crystalline solid (64 %, 0.24 g, 0.960 mmol).

Yield: 64% (0.24 g, 0.960 mmol).

M.P.: 108-111 °C (Lit. 109-114 °C).[366]

δ_H (400 MHz, $CDCl_3$) : 1.51 (s, 9H, $(CH_3)_3$-1), 6.51 (bs, 1H, NH-2), 7.15 (m, 2H, CH-3), 7.35 (d, 2H, *J* 8.8 Hz, CH-4).

HRMS: (m/z ESI$^-$) Found: 249.0705 $(M-H)^-$ $C_{12}H_{13}N_2O_2S$ Requires: 249.0703

4-isothiocyanato-N,N-dimethylaniline (204)[367]

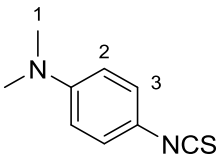

Following method I, **115** (0.19 g, 1.33 mmol) and **201** (0.23 g, 1.43 mmol) were stirred in anhydrous MeCN (10 mL) under Ar for 18 h and concentrated *in vacuo* to give a residue which was purified by silica gel chromatography eluting with 100% Et_2O affording **204** as an orange crystalline solid (94%, 0.225 g, 1.26 mmol).

Yield: 94% (0.225 g, 1.26 mmol).

M.P.: 65-68 °C (Lit. 67-69 °C).[367]

δ_H (400 MHz, $CDCl_3$) : 2.97 (s, 6H, CH_3-1), 6.63 (d, 2H, *J* 8.4 Hz CH-2), 7.12 (d, 2H, *J* 9.1 Hz CH-3).

HRMS: (m/z ESI^-) Found: 249.0705 $(M-H)^-$ $C_{12}H_{13}N_2O_2S$ Requires: 249.0703

1-Ethoxy-4-isothiocyanatobenzene (205)[368]

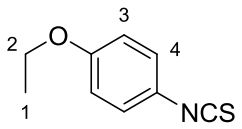

Following method I, 4-ethoxy aniline (1.3 mL, 10.0 mmol) and **201** (1.96 g, 11.0 mmol) were stirred in anhydrous CH_2Cl_2 (100 mL) under Ar for 18 h and concentrated *in vacuo* to give a residue which was purified by silica gel chromatography eluting with 100% Hexanes affording **205** as a white crystalline solid (80 %, 0.29 g, 1.60 mmol).

Yield: 80% (0.286 g, 1.60 mmol).

M.P.: 44-46 °C (Lit. 45-48 °C).[368]

δ_H (400 MHz, $CDCl_3$) : 1.41 (t, 3H, *J* 5.3 Hz, CH_3-1), 3.99 (q, 2H, *J* 7.0 Hz, CH_3-2), 6.81 (m, 2H, CH-3), 7.11 (m, 2H, CH-4).

N-(4-isothiocyanatophenyl)acetamide (202)[369]

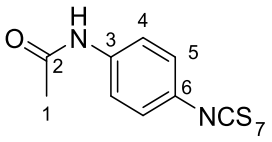

Following method I, **76** (0.67 g, 4.40 mmol) and **201** (0.86 g, 4.84 mmol) were stirred in anhydrous MeCN (40 mL) under Ar for 18 and concentrated *in vacuo* to give a residue which was purified by silica gel chromatography eluting with 100% Et_2O affording white crystalline solid **202** (98%, 0.83g, 4.30 mmol).

Yield: 98% (0.83 g, 4.30 mmol).

M.P.: 185-190 °C

δ_H (400 MHz, $CDCl_3$) : 1.60 (bs, 1H, NH), 2.19 (s, 3H, CH_3-1), 7.18 (d, 2H, *J* 8.6 Hz, CH-5), 7.51 (d, 2H, *J* 8.4 Hz, CH-4).

δ_C (150 MHz, $CDCl_3$): 24.6 (CH_3-1), 120.4 (CH-4), 126.4 (CH-3), 127.0 (qC-6), 135.2 (qC-7), 137.0(qC-1), 168.3 (C=O).

ν_{max} (ATR)/cm^{-1}: 3296 (N-H), 3117 (C-H), 3067 (C-H), 2932 (C-H), 2594 (C-H), 2082 (N=C=S), 1663 (C=O), 1599 (C-N).

HRMS: (m/z ESI^-) Found: 191.0279 $(M-H)^-$ $C_9H_7N_2OS$ Requires: 191.0279.

1,4-Benzodioxan-6-isothiocyanate (206)

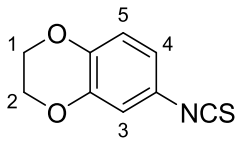

A solution of **148** (1 mL, 8.10 mmol) in EtOH (30 mL) was treated with **207** (2.14g, 8.91 mmol) and the reaction mixture heated at 80 °C under reflux for 18 h. After cooling to rt the reaction mixture was cooled to approx. 0 °C in an ice/water bath and a precipitated solid formed which was isolated by filtration and washed with cold EtOH and dried under vacuum to afford **208** as a crude brown solid (1.0 g). A solution of this solid in EtOH (20 mL) was then treated with conc. HCl (2 mL) and the reaction mixture heated at 80 °C under reflux for 18 h. The reaction mixture was concentrated *in vacuo* to give a residue which was dissolved in CH_2Cl_2 (50 mL) and the organic phase washed with water (2 × 20 mL), brine (1 x 20 mL), dried over $MgSO_4$, filtered and concentrated *in vacuo* to give a residue that was purified by silica gel chromatography eluting with 100% Hexanes affording **206** as a brown solid (40 %, 0.62 g, 3.24 mmol).

Yield: 40 % (0.62 g, 3.24 mmol).

δ_H (400 MHz, $CDCl_3$): 4.28 (s, 4H, CH_2-1), 6.77 (s, 1H, CH-3), 6.82 (d, 1H, *J* 0.4 Hz, CH-5), 6.84 (d, 1H, *J* 0.4 Hz, CH-4).

M.P.: 60-62 °C

1-(3-Aminopropyl)-3-(5,6,7,8-tetrahydronaphthalen-2-yl)thiourea (210)

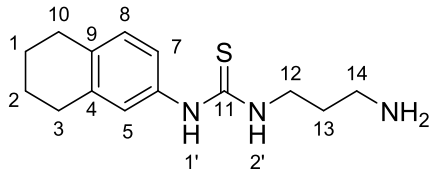

Following method I, **200** (0.10 g, 0.53 mmol) and **194** (0.35 mL, 5.31 mmol) were stirred in anhydrous CH_2Cl_2 (10 mL) under Ar for 18 h and concentrated *in vacuo* to give a residue which was purified by silica gel chromatography eluting with 100% CH_2Cl_2 to MeOH/CH_2Cl_2 (1:4) to afford **210** as a brown oil (53%, 0.073 g, 0.28 mmol).

Yield: 53% (0.073 g, 0.28 mmol).

δ_H (400 MHz, $CDCl_3$) : 1.71 (m, 6H, CH_2-1, CH_2-2 and CH_2-13). 2.69 (m, 4H, CH_2-3 and CH_2-10), 2.78 (m, 2H, CH_2-14), 3.69 (m, 2H, CH_2-12), 6.90 (m, 2H, CH-5 and CH-7), 7.01 (m, 1H, CH-8), 7.19 (bs, 1H, NH-1').

δ_C (150 MHz, $CDCl_3$): 22.9 (CH_2-1), 23.0 (CH_2-2), 29.0 (CH_2-3)., 29.4 (CH_2-10), 29.7(CH_2-13), 39.7 (CH_2-14), 44.0 (CH_2-12), 122.7 (CH-7), 125.9 (CH-5), 130.3 (CH-8),133.7 (qC4), 136.1 (qC9), 138.8 (qC6), 180.7 (C=S-11).

ν_{max} (ATR)/cm^{-1}: 3210 (N-H), 2925 (C-H), 2856 (C-H), 2220 (C-H), 1630 (C-C), 1492 (C-C), 1438 (C-C), 1195 (C=S).

HRMS: (m/z ESI^+) Found: 264.1523 $(M+H)^+$ $C_{14}H_{22}N_3S$ Requires: 264.1529

2-(5,6,7,8-tetrahydronaphthalen-2-yl)-1,4,5,6-tetrahydropyrimidine (209)

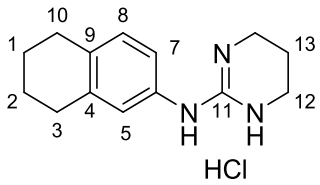

Following method G, a solution of **210** (0.03 g, 0.12 mmol) in CH_2Cl_2 (5 mL) at 0 °C was treated with $HgCl_2$ (0.04 g, 0.14 mmol) and NEt_3 (0.1 mL, 0.42 mmol) and was allowed to stir at rt until the reaction was adjudged complete by TLC analysis. The reaction mixture was then diluted with MeOH and filtered through a pad of Celite. The Celite pad was rinsed with MeOH and the filtrate concentrated under reduced pressure to give a residue which was dissolved in NaOH (10 mL, 1M aq.) and extracted with Et_2O. The organic layer was then acidified by the addition of hydrochloric acid solution (10 mL, 1.25 M in Et_2O). Removal of excess solvent and HCl *in vacuo* afforded **209** as a yellow gum (80%, 0.025 g, 0.10 mmol).
Yield: 80% (0.025 g, 0.10 mmol).

δ_H (400 MHz, D_2O): 1.77 (m, 4H, CH_2-1, CH_2-2). 1.98 (m, 2H, CH_2-13), 2.76 (d, 4H, *J* 4.2 Hz, CH_2-3 and CH_2-10), 3.36 (t, 4H, *J* 5.8 Hz, CH_2-12), 6.99 (m, 2H, CH-5 and CH-7) 7.20 (d, 1H, *J* 7.8 Hz, CH-8).

δ_C (150 MHz, D_2O): 19.4 (CH_2-13), 22.4 (CH_2-1/CH_2-2), 22.5 (CH_2-1/CH_2-2), 28.4 (CH_2-3/CH_2-10), 28.8 (CH_2-3/CH_2-10), 38.3 (CH_2-12), 122.9 (CH-7), 126.2 (CH-5), 130.4 (CH-8), 131.3 (qC6), 137.1 (qC9), 139.3 (qC9), 152.5 (qC11).

HRMS: (m/z ESI^+) Found: 230.1652 $[M+H]^+$ $C_{14}H_{20}N_3$ Requires: 230.1652.

HPLC: 98.1 % (t_R = 27.1 min).

1-methyl-1-(2-aminoethyl)-3-phenylthiourea (218)

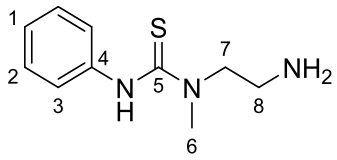

Following method I, **179** and *N*,*N*'-dimethylethylenediamine were stirred in anhydrous CH_2Cl_2 (10 mL) under Ar for 18 h and concentrated *in vacuo* to give a residue which was purified by recrystallization from cold Et_2O to afford **218** as a pale yellow solid (47%, 0.12 g, 0.95 mmol).

Yield: 47% (0.12 g, 0.95 mmol).

δ_H (400 MHz, $CDCl_3$) : 1.72 (s, 2H, NH_2), 3.09 (t, 2H, *J* 6.0 Hz, CH_2-8), 3.14 (s, 3H, CH_3-6), 3.67 (t, 2H, *J* 6.0 Hz, CH_2-7), 7.13 (t, 1H, *J* 8.0 Hz, CH-1), 7.33 (t, 2H, *J* 8.0 Hz, CH-2), 7.42 (d, 2H, *J* 8.0 Hz, CH-3) 11.06 (s, 1H, NH).

δ_C (150 MHz, $CDCl_3$): 40.5 (CH_2-8), 40.6 (CH_3-6), 56.6 (CH_2-7), 123.8 (CH-3), 124.4 (CH-1), 128.5 (CH-2), 140.9 (qC-4), 184.3 (C=S-5).

M.P.: 58-60 °C

HRMS: (m/zESI$^+$) Found: 210.1061 $(M+H)^+$ $C_{10}H_{16}N_3S$ Requires: 210.1059.

***ν*max (ATR)/cm^{-1}** : 3198 (N-H), 3056 (C-H), 1203 (C=S), 853 (C-N).

1-Methyl-1-(2-methylamino)ethyl)-3-phenylthiourea (219)

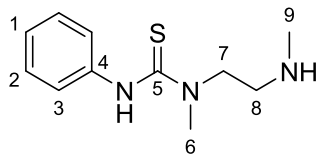

Following method I, **179** and *N*,*N*'-dimethylethylenediamine were stirred in anhydrous CH_2Cl_2 (10 mL) under Ar for 18 h and concentrated *in vacuo* to give a residue which was purified by recrystallization from cold Et_2O to afford **219** as a yellow solid (56%, 0.32 g, 1.41 mmol).

Yield: 56% (0.32 g, 1.41 mmol)

δ_H (400 MHz, $CDCl_3$) : 2.94 (t, 2H, *J* 4.0 Hz, CH_2-8), 3.16 (s, 3H, CH_3-6), 3.39 (s, 3H, CH_3-9), 3.65 (t, 2H, *J* 4.0 Hz, CH_2-7), 7.09 (t, 1H, *J* 8.0 Hz, CH-1), 7.34 (m, 4H, CH-2 and CH-3).

δ_C (150 MHz, $CDCl_3$): 39.7 (CH_3-6), 50.6 (CH_2-7/8), 126.10 (CH-3), 128.6 (CH-2), 140.3 (qC-4), 182.0 (C=S-5).

M.P.: 64-66 °C

HRMS: (m/zESI^+) Found: 224.2887 $(M+H)^+$ $C_{11}H_{17}N_3S$ Requires: 224.1216.

***ν*max (ATR)/cm^{-1}** : 3356 (N-H), 3091 (C-H), 1398 (N-C), 1092 (C=S).

1-(3-aminopropyl)-1-methyl-3-phenylthiourea (220)

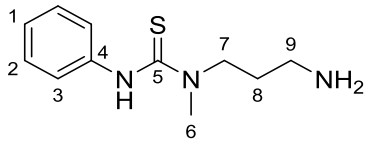

Following method I, **179** and *N*-methyl-1,3-diaminopropane were stirred in anhydrous CH_2Cl_2 (10 mL) under Ar for 18 h and concentrated *in vacuo* to give a residue which was purified by recrystallization from cold Et_2O to afford **220** as a yellow solid (0.31 g, 1.33 mmol, 53%).

Yield: 53% (0.31 g, 1.33 mmol).

δ_H (400 MHz, $CDCl_3$) : 1.50 (bs, 2H, NH_2), 1.80 (p, 2H, *J* 6.0 Hz, CH_2-8), 2.79 (t, 2H, *J* 6.0 Hz, CH_2-9), 3.32 (s, 3H, CH_3-6), 3.72 (t, 2H, *J* 6.0 Hz, CH_2-7), 7.10 (t, 2H, *J* 8.0 Hz, CH-1), 7.29 (t, 2H, *J* 8.0 Hz, CH-3), 7.36 (dd, 2H, *J* 8.0 Hz, 2.0 Hz, CH-2), 10.91 (bs, NH).

δ_C (150 MHz, $CDCl_3$): 28.5 (CH_2-8), 36.4 (CH_3-6), 39.4 (CH_2-9), 48.5 (CH_2-7), 124.4 (CH-1), 124.6 (CH-2), 128.4 (CH-3), 141.4 (qC-4), 183.5 (C=S-5).

M.P.: 72-74 °C.

HRMS: (m/z ESI^-) Found: 222.1065 (M-H) $C_{11,}H_{17}N_3S$ Requires: 222.1065.

***ν*max (ATR)/cm^{-1}** : 3061 (C-H), 2987 (C-H), 1610 (N-H), 1385 (C-N), 1125 (C=S).

1-Methyl-1-(3-(methylamino)propyl)-3-phenylthiourea (221)

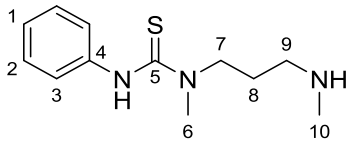

Following method I, **179** and *N*,*N*'-dimethyl-1,3-diaminopropane were stirred in anhydrous CH_2Cl_2 (10 mL) under Ar for 18 h and concentrated *in vacuo* to give a residue which was purified by recrystallization from cold Et_2O to afford **221** as a yellow-orange solid. (0.22 g, 0.92 mmol, 37%).

Yield: 37% (0.22 g, 0.92 mmol).

δ_H (400 MHz, $CDCl_3$) : 1.52 (bs, N-H), 1.87 (p, 2H, *J* 6.0, CH_2, C-8), 2.46 (s, 3H, CH_3-6), 2.68 (t, 2H, *J* 6.0 Hz, CH_2-9), 3.34 (s, 3H, CH_3-10), 3.71 (t, 2H, *J* 6.0 Hz, CH_2-7), 7.12 (bs, Ar-NH), 7.18 (t, 1H, *J* 8.0 Hz, CH-1), 7.27 (m, 2H, CH-3), 7.33 (t, 2H, *J* 8.0 Hz, CH-2).

δ_C (150 MHz, $CDCl_3$): 25.1 (CH_2-8), 38.3 (CH_3-6), 38.3 (CH_3-10), 51.6 (CH_2-9), 54.6 (CH_2-7), 125.6 (CH-3), 125.9 (CH-1), 128.8 (CH-2), 140.0 (qC-4), 182.1 (S=C-5).

M.P.: 62-64 °C.

HRMS: (m/z ESI^-) Found: 236.1232 $(M-H)^-$ $C_{12}H_{19}N_3S$ Requires: 236.1221.

***ν*max (ATR)/cm^{-1}** : 3027 (C-H), 2987 (C-H), 1598 (N-H), 1412 (C-H), 1045 (C=S).

(E)-1-methyl-*N*-phenyltetrahydropyrimidin-2(1*H*)-imine (224)

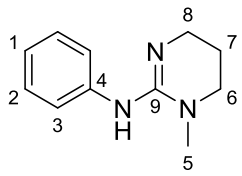

Following method G, a solution of **220** (0.22 g, 1.0 mmol) in CH_2Cl_2 at 0 °C was treated with $HgCl_2$ (0.3 g, 1.1 mmol) and NEt_3 (0.4 mL, 3.3 mmol) and was allowed to stir at rt for 18 h. The reaction was complete once **220** has been consumed adjudged by TLC analysis. Standard work up afforded **224** as a yellow oil 42% (0.08 g, 0.42 mmol).

Yield: 42% (0.08 g, 0.42 mmol)

δ_H (400 MHz, $CDCl_3$) : 1.77 (m, 2H, CH_2-7), 2.58 (bs, 1h, NH), 3.06 (s, 3H, CH_3-5), 3.14 (m, 2H, CH_2-6), 3.54 (m, 2H, CH_2-8), 6.74 (d, 2H, *J* 8.0 Hz, CH-2), 6.98 (t, 1H, *J* 8.0 Hz, CH-1), 7.22 (t, 2H, *J* 8.0 Hz, CH-3).

δ_C (150 MHz, $CDCl_3$): 22.8 (CH_2-7), 35.9 (CH_3-5), 37.5 (CH_2-8), 48.9 (CH_2-6), 118.5 (CH-3), 124.1 (CH-1), 128.4 (CH-2), 147.7 (qC-4), 153.7 (qC-8).

HRMS: (m/z ESI$^+$) Found: 190.1349 $(M+H)^+$ $C_{11}H_{16}N_3$ Requires: 1909.1339.

***v*max (ATR)/cm^{-1}** : 3476 (N-H), 2948 (C-H), 1687 (N=C), 1276 (C-N).

1-methyl-*N*-phenyl-4,5-dihydro-1*H*-imidazol0-2amine (222)

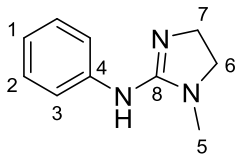

Following method G, a solution of **218** (0.12 g, 0.95 mmol) in CH_2Cl_2 at 0 °C was treated with $HgCl_2$ (0.3 g, 1.1 mmol) and NEt_3 (0.4 mL, 3.3 mmol) and was allowed to stir at rt for 18 h. The reaction was complete once **218** has been consumed adjudged by TLC analysis. Standard work up afforded **222** as a yellow oil (46%, 0.02 g, 0.9 mmol).

Yield: 46% (0.02 g, 0.9 mmol).

δ_H (400 MHz, $CDCl_3$) : 2.81 (bs, 1H, NH), 3.18 (s, 3H, CH_3-5), 3.42 (m, 4H, CH_2-6 and CH_2-7), 6.87 (d, 2H, *J* 8.0 Hz, CH-2), 7.03 (t, 1H, *J* 8.0 Hz, CH-1), 7.25 (t, 2H, *J* 8.0 Hz, CH-3),

δ_C (150 MHz, $CDCl_3$): 39.6 (CH_3-5), 46.8 (CH_2-7), 50.1 (CH_2-6), 122.5 (CH-2), 123.0 (CH-1), 128.7 (CH-3), 148.4 (qC-4), 155.8 (qC-8).

HRMS: (m/z ESI^+) Found: 176.1180 $(M+H)^+$ $C_{10}H_{14}N_3$ Requires: 176.1182.

***ν*max (ATR)/cm^{-1}** : 3289 (N-H), 2895 (C-H), 1667 (N=C), 1314 (C-N).

1-(1-methyl-3-aminopropyl)-3-(5,6,7,8-tetrahydronaphthalen-2-yl)thiourea (227)

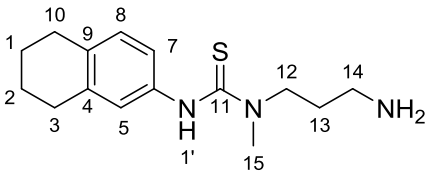

Following method I, **200** (0.91 mmol) and **220** (0.91 mmol) were stirred in anhydrous CH_2Cl_2 (10 mL) under Ar for 18 h and concentrated *in vacuo* to give a residue which was purified by silica gel chromatography eluting with 100% CH_2Cl_2 to MeOH/CH_2Cl_2 (1:4) to afford **227** as a brown gum (33%, 0.08 g, 0.30 mmol).

Yield: 33% (0.08 g, 0.30 mmol).

δ_H (400 MHz, $CDCl_3$): 1.79 (m, 4H, CH_2-1 and CH_2-2), 2.06 (m, 2H, CH_2-13), 2.74 (m, 4H, CH_2-3 and CH_2-10), 3.02 (s, 3H, CH_3-15), 3.42 (t, *J* 6.2 Hz, 2H, CH_2-12), 3.43 (t, *J* 5.9 Hz, 2H, CH_2-14), 6.84 (d, *J* 8.0 Hz, 1H, CH-7), 6.86 (s, 1H, CH-5), 7.03 (d, J 8.0 Hz, 1H, CH-8).

δ_C (150 MHz, $CDCl_3$): 21.8 (CH_2-13), 22.9 (CH_2-1), 23.1 (CH_2-2), 28.9 (CH_2-10), 29.4 (CH_2-3), 38.9 (CH_2-14), 39.7 (CH_3-15), 48.6 (CH_2-12), 120.7 (CH-7), 124.1 (CH-5), 130.2 (CH-8), 134.4 (qC 9), 138.0 (qC 4/6), 153.4 (qC-11).

ν_{max} (ATR)/cm^{-1}: 3211 (NH), 2925(C-H), 2855(C-H), 1287 (C-H), 1198 (C=S).

HRMS: (m/z ESI^-) Found: 276.1541 $(M-H)^-$ $C_{13}H_{22}N_3S$ Requires: 276.1534

1-(1-methyl-3-methylaminopropyl)-3-(5,6,7,8-tetrahydronaphthalen-2-yl)thiourea (228)

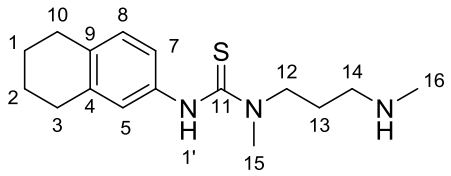

Following method I, **200** (1.0 mmol) and **221** (1.0 mmol) were stirred in anhydrous CH_2Cl_2 (10 mL) under Ar for 18 h and concentrated *in vacuo* to give a residue which was purified by silica gel chromatography eluting with 100% CH_2Cl_2 to MeOH/CH_2Cl_2 (1:4) to afford **228** as a colourless gum (54%, 0.16 g, 0.54 mmol).

Yield: 54% (0.16 g, 0.54 mmol).

δ_H (400 MHz, $CDCl_3$): 1.28 (bs, 3H, CH_3-16), 1.80 (m, 6H, CH_2-1, CH_2-2 and CH_2-13), 2.76 (m, 6H, CH_2-3, CH_2-10 and CH_2-14), 3.28 (s, 3H, CH_3-15), 4.02 (m, 2H, CH_2-12), 6.96 (bs, 1H, CH-5), 7.05 (m, 2H, CH-7 and CH-8), 7.13 (bs, 1H, NH-1').

δ_C (150 MHz, $CDCl_3$): 23.2 (CH_2-13), 23.3 (CH_2-1, CH_2-2), 29.1 (CH_2-3, CH_2-10 and CH_3-16), 29.6 (CH_2-14), 39.5 (CH_3-15), 49.2 (CH_2-12), 123.2 (CH-7), 125.9 (CH-5), 129.3 (CH-8), 134.0 (qC-9), 137.4 (qC-6), 138.7 (qC-4), 184.7 (qC-11).

ν_{max} (ATR)/cm^{-1}: 3016 (N-H), 2971 (C-H), 1738 (C-N) 1366 (C-H), 1092(C=S).

HRMS: (m/z ESI^-) Found: 290.1687 $(M-H)^-$ $C_{10}H_{24}N_3S$ Requires: 290.1691.

1-(1-ethyl-3-ethylaminopropyl)-3-(5,6,7,8-tetrahydronaphthalen-2-yl)thiourea (229)

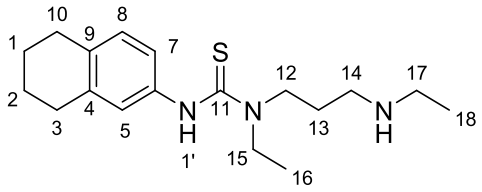

Following method I, **200** (1.0 mmol) and **226** (1.0 mmol) were stirred in anhydrous CH_2Cl_2 (10 mL) under Ar for 18 h and concentrated *in vacuo* to give a residue which was purified by silica gel chromatography eluting with 100% CH_2Cl_2 to MeOH/CH_2Cl_2 (1:4) to afford **229** as a colourless gum (63%, 0.20 g, 0.63 mmol).

Yield: 63% (0.20 g, 0.63 mmol).

δ_H (400 MHz, $CDCl_3$): 1.00 (t, 3H, *J* 8.0 Hz, CH_3-18), 1.30 (t, 3H, *J* 8.0 Hz, CH_3-16), 1.76 (m, 4H, CH_2-1 and CH_2-2), 1.83 (m, 2H, CH_2-13), 2.65 (q, 2H, *J* 4.0 Hz, 6.0 Hz, CH_2-14), 2.72 (m, 6H, CH_2-3, CH_2-10 and CH_2-17), 3.68 (m, 2H, CH_2, C-12), 3.86 (q, *J* = 6 Hz, 2H, CH_2, C-15), 6.89 (bs, 1H, CH-8), 7.01 (m, 2H, CH-5 and CH-7).

δ_C (150 MHz, $CDCl_3$): 12.2 (CH_3-16), 14.8 (CH_3-18), 23.1 (CH_2-2), 27.3 (CH_2-15), 29.0 (CH_2-10) 29.4 (CH_2-3), 43.5 (CH_2-14), 44.3 (CH_2-15), 45.8 (CH_2-12), 123.9 (CH-7), 126.5 (CH-5), 129.2 (CH-10), 134.2 (qC-9), 138.0 (qC-4), 147.6 (qC-6), 183.5 (qC-11).

ν_{max} (ATR)/cm^{-1}: 3241 (C-H), 2925 (C-H), 1333 (C-N), 1233 (C-N), 1119 (C=S).

HRMS: (m/z ESI^+) Found: 320.2167 $(M+H)^+$ $C_{18}H_{29}N_3S$ Requires: 320.2160.

1-(1-methyl-3-aminopropyl)-3-(4-acetylamidoanilino)thiourea (230)

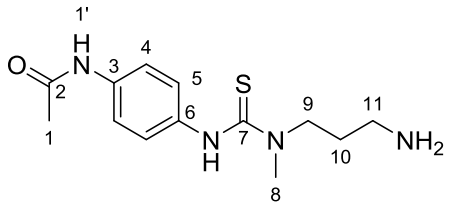

Following method I, **202** (1.0 mmol) and **220** (1.0 mmol) were stirred in anhydrous CH_2Cl_2 (10 mL) under Ar for 18 h and concentrated *in vacuo* to give a residue which was purified by silica gel chromatography eluting with 100% CH_2Cl_2 to MeOH/CH_2Cl_2 (1:4) to afford **230** as a colourless gum (83%, 0.23 g, 0.83 mmol).

Yield: 83% (0.23 g, 0.83 mmol).

δ_H (400 MHz, $CDCl_3$): 1.75 (m, 2H, CH_2-10), 2.02 (s, 3H,CH_3-1), 2.62 (t, 2H, *J* 6.4 Hz, CH_2-11), 3.19 (s, 3H, CH_3-8), 3.74 (m, 2H, CH_2-9), 7.21 (d, 2H, *J* 8.8 Hz, CH-5), 7.45 (d, 2H, *J* 8.8 Hz, CH-4), 9.85 (bs, 1H, NH-1').

δ_C (150 MHz, $CDCl_3$): 23.9 (CH_3-1), 28.25 (CH_2-10), 36.8 (CH_3-11), 38.8 (CH_3-12), 49.2 (CH_2-9), 118.6 (CH-5), 125.4 (CH-4), 135.5 (qC-3), 136.7 (qC-4), 168.0 (C=0-2), 181.8 (qC-7).

ν_{max} (ATR)/cm^{-1}: 3364 (N-H), 3272 (N-H), 3017 (C-H), 2971(C-H), 2921 (C-H), 1741 (C=S), 1670 (C=O), 1229 (C-H), 1146, (C=S).

HRMS: (m/z ESI^+) Found: 281.1443 $(M+H)^+$ $C_{13}H_{20}N_4OS$ Requires 281.1436.

1-(1-methyl-3-methylaminopropyl)-3-(4-acetylamidoanilino)thiourea (231)

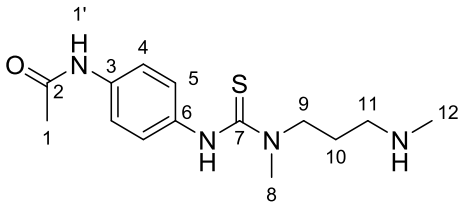

Following method I, **202** (1.0 mmol) and **221** (1.0 mmol) were stirred in anhydrous CH_2Cl_2 (10 mL) under Ar for 18 h and concentrated *in vacuo* to give a residue which was purified by silica gel chromatography eluting with 100% CH_2Cl_2 to MeOH/CH_2Cl_2 (1:4) to afford **231** as amorphous yellow gum (80%, 0.23 g, 0.80 mmol).

Yield: 80% (0.23 g, 0.80 mmol).

δ_H (400 MHz, MeOD): 1.98 (p, 2H, *J* 6.6 Hz, CH_2-10), 2.12 (s, 3H, CH_3-1), 2.51 (m, 5H, CH_3-12 and CH_2-11), 2.79 (m, 2H, CH_2-9), 3.26 (s, 3H, CH_3-8), 7.25 (d, 2H, *J* 8.7 Hz, CH-5), 7.51 (d, 2H, *J* 8.8 Hz, CH-4).

δ_C (150 MHz, MeOD): 22.0 (CH_3-1), 24.7 (CH_2-10), 33.3 (CH_2-11), 36.4 (CH_3-8), 49.8 (CH_2- 9), 119.2 (CH-4), 126.2 (CH-5), 135.6 (qC-3), 136.2 (qC-6), 171.5 (C=O-2), 181.6 (C=S-7).

ν_{max} (ATR)/cm^{-1}: 3249 (N-H), 2931 (C-H), 2787 (C-H), 2471 (C-H), 1685 (C-N), 1617(C=O), 1582 (N-H), 1050 (C=S).

HRMS: (m/z ESI^+) Found: 285.1597 $(M+H)^+$ $C_{14}H_{22}N_4OS$ Requires 295.1593.

1-(1-ethyl-3-ethylaminopropyl)-3-(4-acetylamidoanilino)thiourea (232)

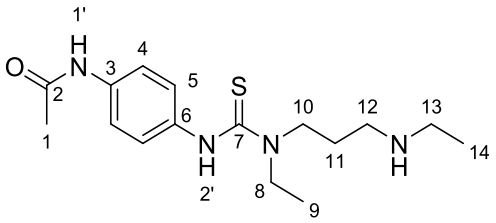

Following method I, **202** (1.0 mmol) and **226** (1.0 mmol) were stirred in anhydrous CH_2Cl_2 (10 mL) under Ar for 18 h and concentrated *in vacuo* to give a residue which was purified by silica gel chromatography eluting with 100% CH_2Cl_2 to MeOH/CH_2Cl_2 (1:4) to afford **232** as amorphous yellow gum (98%, 0.32 g, 0.98 mmol).

Yield: 98% (0.32 g, 0.98 mmol).

δ_H (400 MHz, $CDCl_3$): 1.00 (m, 3H, CH_3-14), 1.31 (t, 3H, *J* 7 Hz, CH_3-9), 1.87 (m, 2H, CH_2-11), 2.14 (s, 3H, CH_3-1), 2.69 (m, 2H, CH_2-13), 2.73 (t, 2H, *J* 5.3 Hz, CH_2-12), 3.71 (bs, 2H, CH_2-10), 3.86 (d, 2H, *J* 5.3 Hz, CH_2-8), 4.58 (bs, 1, NH-2'), 7.20 (d, 2H, *J* 8.5 Hz, CH-5), 7.43 (d, 2H, *J* 8.5 Hz, CH-4), 8.08 (bs, 1H, NH-2').

δ_C (150 MHz, $CDCl_3$): 12.3 (CH_3-9), 14.5 (CH_2-14), 24.7 (CH_3-1), 26.9 (CH_2-11), 44.0 (CH_2-13), 44.4 (CH_2-12), 46.1 (CH_2-8), 46.2 (CH_2-13), 120.3 (CH-4), 127.0 (CH-5), 129.9 (qC-3), 164.5 (qC-7), 168.5 (C=O-2).

ν_{max} (ATR)/cm^{-1}: 3457 (N-H), 3245 (C-H), 2970 (C-H), 1738 (C=S), 1665 (C=O), 1512, 1443 (C-H), 1366 (C-N), 1229 (C-H), 1120 (C=S).

HRMS: (m/z ESI^-) Found: 321.1754 $(M-H)^-$ $C_{16}H_{25}N_4OS$ Requires: 321.1749.

1,3-Diethyl-N-(5,6,7,8-tetrahydronapthalen-2-yl)tetrahydropyrimidin-2(1H)-imine hydrochloride (234)

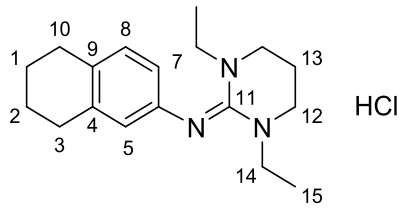

Following method G, a solution of **229** (0.10 g, 0.31 mmol) in CH_2Cl_2 (5 mL) at 0 °C was treated with $HgCl_2$ (0.04 g, 0.14 mmol) and NEt_3 (0.1 mL, 0.42 mmol) and was allowed to stir at rt until the reaction was adjudged complete by TLC analysis. The reaction mixture was then diluted with MeOH and filtered through a pad of Celite. The Celite pad was rinsed with MeOH and the filtrate concentrated under reduced pressure to give a residue purified which was purified by silica gel chromatography eluting with 100% CH_2Cl_2 to MeOH/CH_2Cl_2 (1:4) to afford **234** as a white solid (37%, 0.01 g, 0.01 mmol).

Yield: 37% (0.01 g, 0.01 mmol).

M.P.: 85-89 °C

δ_H (400 MHz, $CDCl_3$): 1.15 (t, 6H, *J* 6.5 Hz, CH_3-15), 1.79 (m, 6H, CH_2-1, CH_2-2 and CH_2-13), 2.06 (m, 8H, CH_2-12 and CH_2-14), 2.73 (m, 4H, CH_2-3 and CH_2-10), 6.79 (m, 1H, CH-5), 6.81 (m, 1H CH-7), 7.01(d, 1H, *J* 7.5 Hz, CH-8).

δ_C (150 MHz, $CDCl_3$): 9.0 (CH_3-15), 12.9 (CH_2-13), 21.5 (CH_2-1, CH_2-2), 29.7 (CH_2-10, CH_2-3), 46.3 (CH_2-14), 47.8 (CH_2-12), 125.3 (CH-7), 128.2 (CH-5), 129.1 (CH-8), 130.1 (qC-9), 133.5 (qC-4), 137.9 (qC-6), 138.8 (qC-11).

HRMS: (m/z ESI$^+$) Found: 286.2205 $(M+H)^+$ $C_{18}H_{28}N_3$ Requires: 286.2278.

HPLC: 98.4% (t_R = 29.5 min)

1,3-Dimethyl-N-(4-acteylamidoaniline)tetrahydropyrimidin-2(1H)-imine hydrochloride (235)

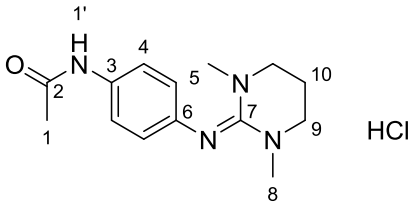

Following method G, a solution of **231** (0.15 g, 0.5 mmol) in CH_2Cl_2 (5 mL) at 0 °C was treated with $HgCl_2$ (0.14 g, 0.51 mmol) and NEt_3 (0.3 mL, 1.26 mmol) and was allowed to stir at rt until the reaction was adjudged complete by TLC analysis. The reaction mixture was then diluted with MeOH and filtered through a pad of Celite. The Celite pad was rinsed with MeOH and the filtrate concentrated under reduced pressure to give a residue purified which was purified by neutral alumina flash chromatography eluting with 100% CH_2Cl_2 to MeOH/CH_2Cl_2 (1:4) to afford **235** as a brown gum (68%, 0.11 g, 0.36 mmol).

Yield: 68% (0.11 g, 0.36 mmol).

δ_H (400 MHz, MeOD): 2.12 (m, 5H, CH_2-1, CH_3-10), 2.97 (s, 6H, CH_3-8), 3.46 (m, 4H, CH_2-9), 7.01 (d, 2H, *J* 8.9 Hz, CH-5), 7.57 (d, 2H, *J* 8.9 Hz, CH-4).

δ_C (150 MHz, MeOD): 22.9 (CH_2-9), 23.9 (CH_3-1), 40.5 (CH_3-8), 49.6 (CH_2-9), 121.6 (CH-5), 122.5 (CH-4), 154.4 (qC-7), 171.6 (C=O-2).

ν_{max} (ATR)/cm^{-1}: 3189 (C-H), 2855 (C-H), 1679 (C=O), 1512 (N-H), 1418 (C-H).

HRMS: (m/z ESI^+) Found: 261.1718 $(M+H)^+$ $C_{14}H_{21}N_4O$ Requires: 261.1715.

HPLC: 99.8% (t_R = 19.8 min)

_N_-(4-(_N_'-tert-butylcarbamate- _N_'-methylamino)phenyl) acridine-9-carboxamide (266)

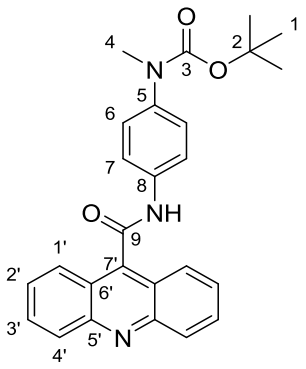

Following method E, a solution of **246** (0.2 g, 0.9 mmol) and EDC.HCl (0.23 g, 1.3 mmol) in anhydrous DMF (2 mL) was treated with a solution of **142** (0.22 g, 1.0 mmol) in DMF (2.5 mL) and allowed to stir at rt under Ar for 72 h. The reaction mixture was then diluted with EtOAc (5 mL) and H_2O (5 mL) forming a precipitate which was collected by suction filtration, washed with EtOAc and dried in air to afford **266** as a cream powder (86%, 0.33 g, 0.77 mmol).

Yield: 86% (0.33 g, 0.77 mmol).

M.P.: > 250 °C (Decomp.)

δ_H (600 MHz, DMSO-d_6) : 1.42(s, 9H, $(CH_3)_3$-1), 3.20 (s, 3H, CH_3-4), 7.33 (d, 2H, *J* 8.8 Hz, CH-7), 7.71 (m, 2H, CH-3'), 7.80 (d, 2H, *J* 8.8 Hz, CH-6), 7.92 (dd, 2H, *J* 8.3 Hz, *J* 7.0 Hz, CH-2'), 8.06 (d, 2H, *J* 8.6 Hz, CH-1'), 8.24 (d, 2H, *J* 8.8 Hz, CH-4'), 11.08 (bs, 1H, NH).

δ_C (150 MHz, DMSO-d_6) : 28.0 $(CH_3)_3$-1), 37.1 (CH_3-4), 79.6 (qC-2) 120.0 (CH-6) 121.7 (qC-7'), 125.4 (CH-1'), 126.0 (CH-7), 127.2 (CH-3'), 129.4 (CH-4'), 130.8 (CH-2'), 135.8 (qC-8), 139.7 (qC-5), 141.4 (qC-5'), 148.3 (qC-6'), 153.8 (C=O-3), 164.7 (qC=O-9).

ν_{max} (ATR)/cm^{-1}: 3415 (N-H), 3056 (C-H), 3015 (C-H), 2980 (C-H), 2890 (C-H), 1700 (C=O), 1651(C=O), 1554 (C-C), 1455 (C-C), 1362 (C-N),1289 (C-N), 1016 (C-N).

HRMS: (m/z ESI^+) Found: 428.1995 $(M+H)^+$ $C_{26}H_{26}N_3O_3$ Requires: 428.1974.

***N*-(4-(piperidin-1-yl)phenyl)acridine-9-carboxamide (261)**

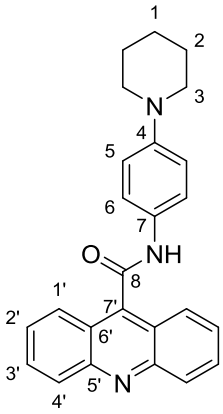

Following method E, a solution of **246** (0.2 g, 0.9 mmol) and EDC.HCl (0.23 g, 1.3 mmol) in anhydrous DMF (2 mL) was treated with a solution of **264** (0.18 g, 1.0 mmol) in DMF (2.5 mL) and allowed to stir at rt under Ar for 72 h. The reaction mixture was then diluted with EtOAc (5 mL) and H_2O (5 mL) forming a precipitate which was collected by suction filtration, washed with EtOAc and dried in air to afford **261** as a yellow powder (84%, 0.29 g, 0.76 mmol).

Yield: 84% (0.29 g, 0.76 mmol).

M.P.: > 250 °C (Decomp.)

δ_H (600 MHz, DMSO-d_6) : 1.55 (m, 2H, CH_2-1), 1.65 (m, 4H, CH_2-2), 3.13 (t, 4H, *J* 5.2 Hz, CH_2-3), 6.99 (d, 2H, *J* 8.9 Hz, CH-6), 7.69 (m, 4H, CH-5 and CH-3'), 7.92 (t, 2H, *J* 7.2 Hz, CH-2'), 8.05 (d, 2H, *J* 8.6 Hz, CH-1'), 8.23 (d, 2H, *J* 5.2 Hz, CH-4'), 10.79 (bs, 1H, NH).

δ_C (150 MHz, DMSO-d_6) : 23.9 (CH_2-1), 25.2 (CH_2-2), 50.0 (CH_2-3), 116.3 (CH-5), 121.0, (CH-6), 121.8 (CH-5'), 125.5 (CH-1'), 127.0 (CH-3'), 129.3 (CH-4'), 130.2 (qC-7), 130.7 (CH-2'), 141.9 (qC-7'), 148.3 (qC-6), 148.8 (qC-4), 164.1 (qC=O-8).

ν_{max} (ATR)/cm^{-1}: 3385 (N-H), 2936 (C-H), 2892 (C-H), 2831 (C-H), 1648 (C=O), 1605 (C=N), 1510 (C-C), 1463 (C-C), 1413 (C-C), 1341 (C-N), 1318 (C-N), 1267 (C-N), 1236 (C-N),

HRMS: (m/z ESI$^+$) Found: 382.1926 $(M+H)^+$ $C_{25}H_{24}N_3O$ Requires: 382.1919.

_N_-(4-(ethyl)phenyl)acridine-9-carboxamide (258)

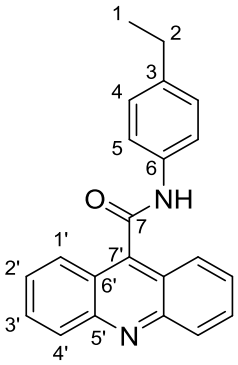

Following method E, a solution of **246** (0.2 g, 0.9 mmol) and EDC.HCl (0.23 g, 1.3 mmol) in anhydrous DMF (2 mL) was treated with a solution of **262** (0.12 mL, 1.0 mmol) in DMF (2.5 mL) and allowed to stir at rt under Ar for 24 h. The reaction mixture was then diluted with EtOAc (5 mL) and H_2O (5 mL) forming a precipitate which was collected by suction filtration, washed with EtOAc and dried in air to afford **258** as a yellow powder (70%, 0.21 g, 0.63 mmol).

Yield: 70% (0.21 g, 0.63 mmol).

M.P.: > 250 °C (Decomp.)

δ_H (600 MHz, DMSO-d_6) : 1.21 (t, 3H, *J* 7.5 Hz, CH_3-1), 2.63 (q, 2H, *J* 7.5 Hz, CH_2-2), 7.27 (d, 2H, *J* 8.3 Hz,CH-5), 7.7 (dd, 2H, *J* 11.3, *J* 4.0 Hz, CH-3'), 7.75 (d, 2H, *J* 8.3 Hz, CH-4), 7.92 (m, 2H, CH-2'), 8.05 (d, 2H, *J* 8.6 Hz, CH-1'), 8.24 (d, 2H, *J* 8.8 Hz, CH-4'), 10.97 (bs, 1H, NH).

δ_C (150 MHz, DMSO-d_6) : 15.8 (CH_3-1), 27.7 (CH_2-2), 120.0 (CH-4), 121.7 (qC-5'), 125.4 (CH-1'), 127.7 (CH-2'), 129.4 (CH-4'), 130.7 (CH-3'), 139.9 (qC-3), 136.3 (qC-6), 141.6 (qC-6'), 148.3 (qC-7'), 164.6 (qC=O-7).

ν_{max} (ATR)/cm^{-1}: 3228 (N-H), 3179 (C-H), 3102 (C-H), 3044 (C-H), 2959 (C-H), 2925 (C-H), 1661 (C=O), 1600 (C=N).

HRMS: (m/z ESI^+) Found: 327.1513 $(M+H)^+$ $C_{22}H_{19}N_2O$ Requires: 327.1497.

N-(4-(dimethylamino)phenyl)acridine-9-carboxamide (259)

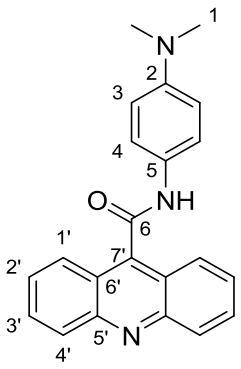

Following method E, a solution of **246** (0.2 g, 0.9 mmol) and EDC.HCl (0.23 g, 1.3 mmol) in anhydrous DMF (2 mL) was treated with a solution of **263** (0.14 g, 1.0 mmol) in DMF (2.5 mL) and allowed to stir at rt under Ar for 24 h. The reaction mixture was then diluted with EtOAc (5 mL) and H_2O (5 mL) forming a precipitate which was collected by suction filtration, washed with EtOAc and dried in air to afford **259** as an orange powder (75%, 0.23 g, 0.68 mmol).

Yield: 75% (0.23 g, 0.68 mmol).

M.P.: > 250 °C (Decomp.)

δ_H (600 MHz, DMSO-d_6) : 2.91 (s, 6H, CH_3-1), 6.80 (d, 2H, *J* 9.0 Hz, CH-3), 7.65 (d, 2H, *J* 9.0 Hz, CH-4), 7.70 (m, 2H, CH-3'), 7.91 (dd, 2H, *J* 11.4 Hz, *J* 3.9 Hz CH-2'), 8.06 (d, 2H, *J* 8.6 Hz, CH-1'), 8.23 (d, 2H, *J* 8.7 Hz, CH-4'), 10.7 (bs, 1H, NH).

δ_C (150 MHz, DMSO-d_6) : 45.6 (CH_3-1), 112.7 (CH-3), 121.7 (CH-4), 121.8 (qC-5), 125.5 (CH-1'), 127.0 (CH-2'), 128.4 (qC-7'), 129.3 (CH-4'), 142.0 (qC-6'), 147.8 (qC-2), 148.28 (qC-5'), 163.9 (qC=O-6).

ν_{max} (ATR)/cm^{-1}: 3260 (N-H), 3064 (C-H), 3026 (C-H), 2977 (C-H), 2936 (C-H), 2852 (C-H), 1645 (C=O), 1605 (C=N), 1550 (C-C), 1518 (C-C), 1441 (C-C).

HRMS: (m/z ESI^+) Found: 342.1603 $(M+H)^+$ $C_{22}H_{20}N_3O$ Requires: 342.1606.

N-(4-(methylamino)phenyl)acridine-9-carboxamide dihydrochloride (260)

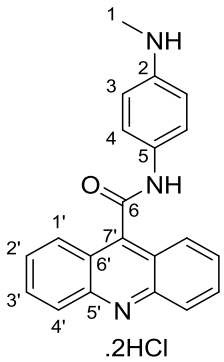

266 (0.05 g, 0.12 mmol) was dissolved in 5 mL of 1.25M HCl/MeOH and stirred under reflux at 80 °C for 4 h. Removal of the solvents and excess HCl *in vacuo* gave **260** as a bright yellow powder in near quantitative yield (>99%, 0.048 g, 0.12 mmol).

Yield: >99% (0.048 g, 0.12 mmol).

M.P.: 290 °C (Decomp.)

δ_H (600 MHz, DMSO-d_6): 1.42 (s, 3H, CH_3-1), 7.34 (d, 2H, *J* 8.6 Hz, CH-4), 7.79 (m, 4H, CH-3 and CH-3'), 8.02 (m, 2H, CH-2'), 8.13 (d, 2H, *J* 8.6 Hz, CH-1'), 8.33 (d, 2H, *J* 8.6 Hz, CH-4'), 11.17 (s, 1H, C=ONH).

δ_C (150 MHz, DMSO-d_6): 28.3 (CH_3-1), 120.0 (CH-3), 121.8 (qC-5), 125.7 (CH-1'), 126.0 (CH-4), 127.6 (CH-3'), 127.9 (CH-4'), 132.6 (CH-2'), 135.6 (qC-2), 139.8 (qC-6'), 147.2 (qC-5') 153.8 (qC-7'), 164.2 (C=O-6).

ν_{max} (ATR)/cm^{-1} : 3354 (N-H), 3218 (N-H), 3053 (C-H), 1618 (C=O), 1555 (C=C), 1436 (C=C), 1243 (C-N).

HRMS: (m/z ESI^+) Found: 328.1447 $(M+H)^+$ $C_{21}H_{18}N_3O$ Requires: 328.1444

HPLC: 99% (t_R = 28.47 min)

N-(4-(dimethylamino)phenyl)acridine-9-carboxamide dihydrochloride (267)

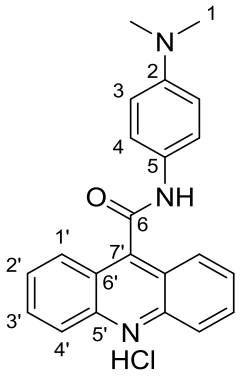

259 (0.06 g, 0.175 mmol) was added to a 5 mL RBF and 1.25 M HCl/MeOH (2 mL) was then added and the reaction stirred at rt for 4 h. Removal of the solvents and excess HCl *in vacuo* gave **267** as a yellow powder in near quantitative yield (>99% 0.073 g, 0.175 mmol).

Yield: >99% (0.073 g, 0.175 mmol).

M.P.: 308-310 °C

δ_H (600 MHz, DMSO-d_6): 3.11 (bs, 6H, CH_3-1), 7.70 (bs, 2H, CH-3), 7.84 (t, 2H, *J* 7.1 Hz, CH-3') 7.94 (m, 2H, CH-4), 8.13 (m, 2H, CH-2') 8.19 (d, 2H, *J* 8.4 Hz, CH-1'), 8.45 (d, 2H, *J* 8.4 Hz, CH-4'), 10.19 (bs, 1H, NMe_2H) 11.46 (bs, 1H, NH).

δ_C (150 MHz, DMSO-d_6): 45.4 (CH_3-1), 121.2 (CH-4), 121.9 (CH-3), 126.0 (CH-1' and CH4'), 128.1 (CH-3'), 133.7 (CH-2'), 144.7 (qC), 144.8 (qC), 144.9 (qC), 163.9 (C=O-6).

ν_{max} (ATR)/cm^{-1}: 3351 (N-H), 3033 (C-H), 1642 (C=O), 1554 (N-H), 1433 (C=C), 1426 (C-C), 1354 (C-N), 1320 (C-N), 1275 (C-N), 1228 (C-N).

HRMS: (m/z ESI^-) Found: 340.1462 $(M-H)^-$ $C_{22}H_{18}N_3O$ Requires: 340.1455

HPLC: 99% (t_R = 31.28 min)

_N_-(4-(ethyl)phenyl)acridine-9-carboxamide hydrochloride (266)

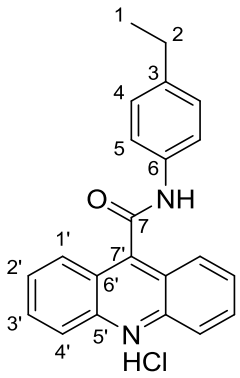

258 (0.10 g, 0.30 mmol) was added to a 25 mL RBF and 10 mL of MeOH was then added. 1.25 M HCl in MeOH (1mL) was subsequently added and stirred at rt for 2 h. Removal of the solvents and excess HCl *in vacuo* gave **266** as a bright yellow powder in a >99% yield (0.11 g, 0.3 mmol).

Yield: >99% (0.11 g, 0.30 mmol).

M.P.: 250 °C (Decomp.)

δ_H (600 MHz, DMSO-d_6): 1.20 (t, 3H, *J* 7.5 Hz, CH_3-1), 2.63 (q, 2H, *J* 7.5 Hz, CH_2-2), 7.29 (d, 2H, *J* 8.1 Hz,CH-4), 7.74 (d, 2H, *J* 8.1 Hz, CH-5), 7.87 (t, 2H, *J* 7.4 Hz, CH-3'), 8.17 (t, 2H, *J* 7.3 Hz, CH-2'), 8.22 (d, 2H, *J* 8.5 Hz, CH-1'), 8.48 (d, 2H, *J* 8.5 Hz, CH-4'), 11.23 (bs, 1H, NH).

δ_C (150 MHz, DMSO-d_6): 15.9 (CH_3-1), 27.8 (CH_2-2), 120.2 (CH-5), 122.0 (qC-5'), 124.6 (CH-4'), 126.2 (CH-1'), 128.3 (CH-4), 134.4 (CH-2'), 136.0 (qC-6), 140.4 (qC-3), 143.9 (CH-3'), 144.0 (qC-7'), 163.2 (qC=O-7).

ν_{max} (ATR)/cm^{-1}: 3390 (N-H), 3052 (C-H), 2971 (C-H), 2873 (C-H), 1619(C=O) 1536 (C-H), 1461 (C-C), 1437 (C-C), 1314 (C-N), 1255 (C-N).

HRMS: (m/z ESI^-) Found: 325.1348 $(M-H)^-$ $C_{22}H_{17}N_2O$ Requires: 325.1346

HPLC: 99% (t_R = 34.9 min)

_N_-(5,6,7,8-Tetrahydronaphthalen-2-yl)-guanidine hydrochloride (21)

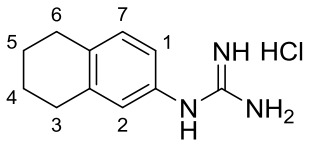

Following method D, **B21** (0.39 g, 1.0 mmol) was treated with a solution of 50% TFA in CH_2Cl_2 (20 mL) for 3 h stirring at room temperature. Solvents were removed under reduced pressure to afford the trifluoroacetate salt. This salt was dissolved in H_2O (20 mL) and treated with Amberlite IRA 400 chloride form (1.0 g) for 24 h. The resin was removed by filtration and the aqueous solution was washed with CH_2Cl_2 (2 x 10 mL). Evaporation of the water afforded the pure hydrochloride salt **21** as a white solid (89%, 0.20 g, 0.89 mmol).

Yield: 89% (0.20 g, 0.89 mmol).

M.P: 38-42°C (Lit. 39-41 °C).[130]

δ_H (400 MHz, D_2O): 1.69 (m, 4H, CH_2-4, CH_2-5), 2.67 (m, 4H, CH_2-3, CH_2-6), 6.94 (m, 2H, CH-2, CH-1), 7.12 (d, 1H, *J* 7.8 Hz, CH-7).

Imidazolidin-2-ylidene-(5,6,7,8-tetrahydronaphthalen-2-yl)amine hydrochloride (269)

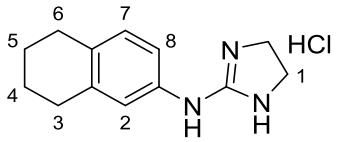

Following method D, **271** (0.42 g, 1.0 mmol) was treated with a solution of 50% TFA in CH_2Cl_2 (20 mL) for 3 h stirring at room temperature. Solvents were removed under reduced pressure to afford the trifluoroacetate salt. This salt was dissolved in H_2O (20 mL) and treated with Amberlite IRA 400 chloride form (1.0 g) for 24 h. Then, the resin was removed by filtration and the aqueous solution was washed with CH_2Cl_2 (2 x 10 mL). Evaporation of the water afforded the pure hydrochloride salt **269** as a white solid (92%, 0.23 g, 0.92 mmol).

Yield: 92% (0.23 g, 0.92 mmol).

M.P: 88-90°C (Lit. 87-89 °C).[130]

δ_H (400 MHz, D_2O): 1.77 (m, 4H, CH_2-4, CH_2-5), 2.76 (m, 4H, CH_2-3, CH_2-6), 3.75 (s, 4H, CH_2-1), 7.01 (m, 2H, CH-2, CH-8), 7.20 (d, 1H, *J* 7.8 Hz, CH-7).

HPLC: 97.3% (t_R = 27.5 min).

9.3. X-ray Crystallography

9.3.1. Structure Report for TCD1126 (117)

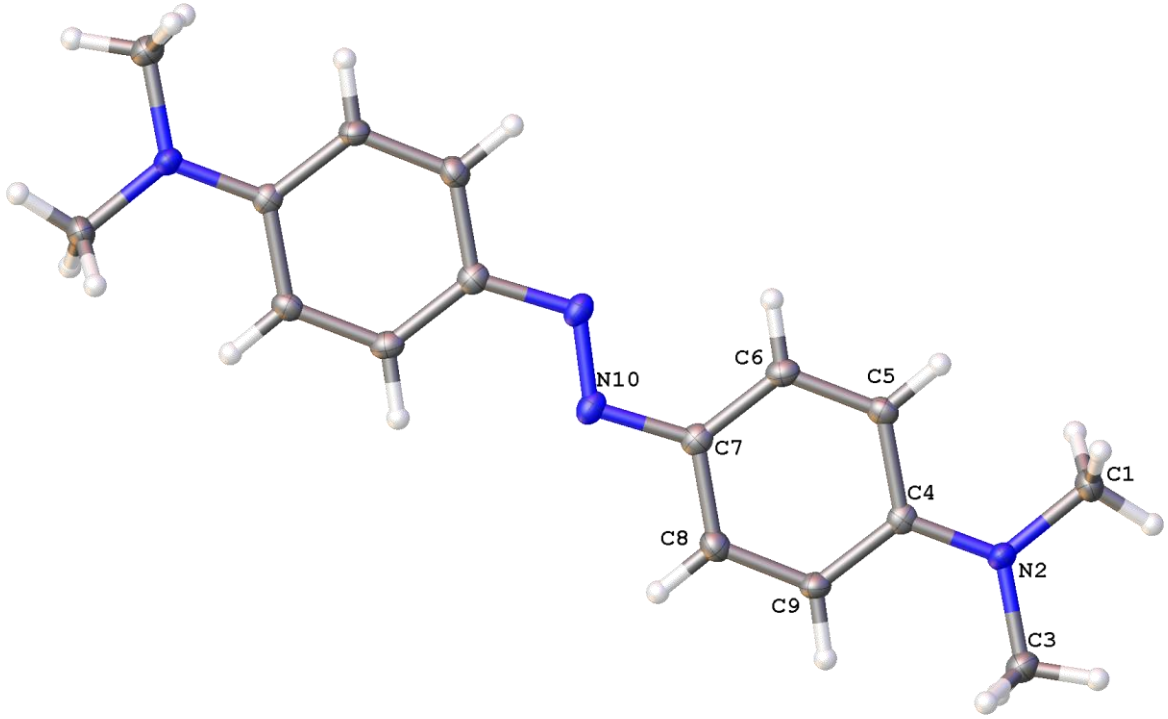

Fig. 1. Symmetry generated molecule of TCD1126_5 with atomic displacement shown at 50% probability. Only symmetry unique atoms labelled for clarity.

21/8/18

Author: Brendan Twamley

Crystal Structure Report for TCD1126_5

A specimen of $C_{16}H_{20}N_4$, approximate dimensions 0.100 mm x 0.120 mm x 0.190 mm, was used for the X-ray crystallographic analysis. The X-ray intensity data were measured at 100(2)K on a Bruker D8 Quest ECO with an Oxford Cryostream 800 low temperature device using a MiTeGen micromount. Bruker APEX software was used to correct for Lorentz and polarization effects.

A total of 1875 frames were collected. The total exposure time was 12.81 hours. The integration of the data using a monoclinic unit cell yielded a total of 2867 reflections to a maximum θ angle of 26.33° (0.80 Å resolution), of which 2867 were independent (average redundancy 1.000, completeness = 98.3%, R_{int} = 5.16%, R_{sig} = 4.35%) and 2233 (77.89%) were greater than 2σ(F^2). The final cell constants of a = 6.1102(11) Å, b = 7.2669(11) Å, c = 15.905(3) Å, β = 93.551(8)°, volume = 704.9(2) $Å^3$, are based upon the refinement of the XYZ-centroids of reflections above 20 σ(I). The calculated minimum and maximum transmission coefficients (based on crystal size) are 0.6232 and 0.7454.

The structure was solved with the XT structure solution program using Intrinsic Phasing and refined with the XL refinement package using Least Squares minimisation with Olex2, using the space group $P2_1/c$, with Z = 2 for the formula unit, $C_{16}H_{20}N_4$. The final anisotropic full-matrix least-squares refinement on F^2 with 94 variables converged at R1 = 5.98%, for the observed data and wR2 = 16.03% for all data. The goodness-of-fit was 1.193. The largest peak in the final difference electron density synthesis was 0.246 $e^-/Å^3$ and the largest hole was -0.288 $e^-/Å^3$ with an RMS deviation of 0.065 $e^-/Å^3$. On the basis of the final model, the calculated density was 1.264 g/cm^3 and F(000), 288 e^-.

Refinement Note: Refined as a 2 component rotational twin with a ratio of 0.481(3). Rotated from first domain by 180.0 degrees about reciprocal axis 1.000 0.000 -0.165 and real axis 1.000 0.000 0.003. Twin law to convert hkl from first to this domain (SHELXL TWIN matrix): 1.001 0.000 0.005 -0.001-1.000 0.000 -0.330 0.000 -1.001

References:

Bruker (2013). SAINT v8.37A, Bruker AXS Inc., Madison, WI, USA.

Bruker (2017). APEX3 v2017.3-0, Bruker AXS Inc., Madison, WI, USA.

Bruker (2016/2). SADABS, Bruker AXS Inc., Madison, Wisconsin, USA.

Dolomanov, O.V., Bourhis, L.J., Gildea, R.J, Howard, J.A.K. & Puschmann, H. (2009), J. Appl. Cryst. 42, 339-341.

Sheldrick, G.M. (2008). Acta Cryst. A64, 112-122.

Sheldrick, G.M. (2015). Acta Cryst. A71, 3-8

9.3.2. Structure Report TCD1071 (124)

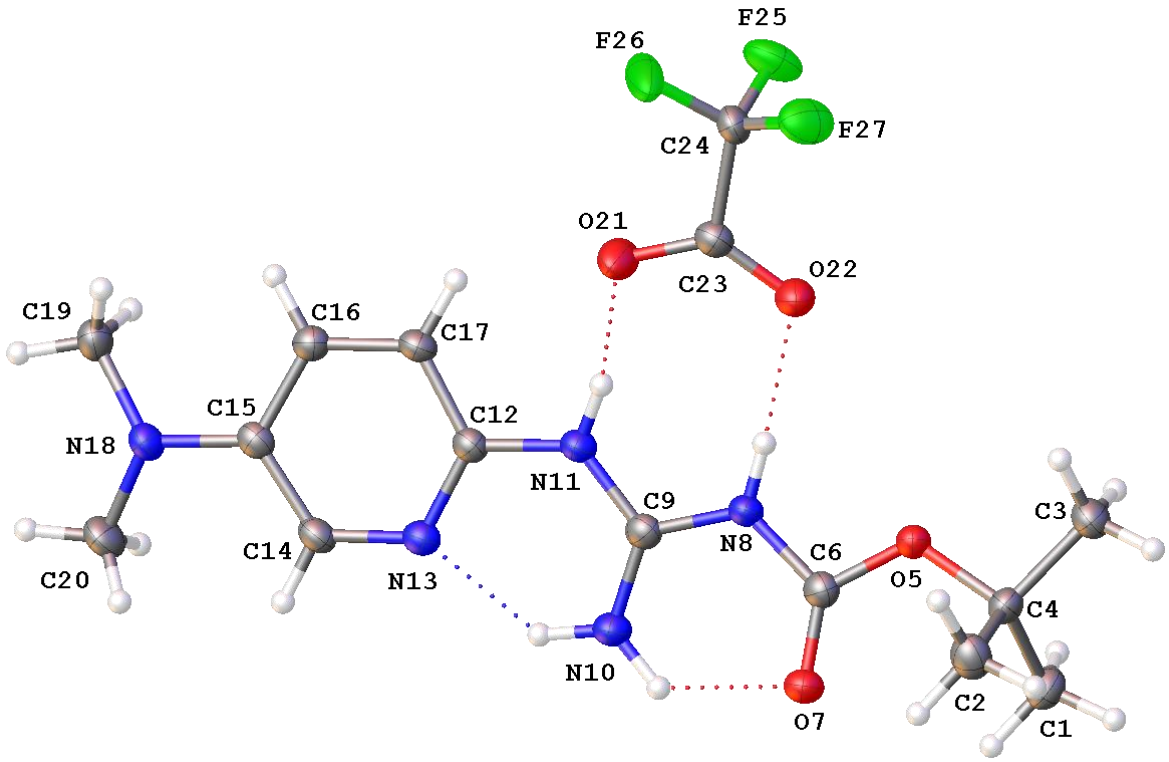

Fig. 1. M structure of TCD1071 with hydrogen bonding indicated by dotted lines..

30/5/18

Author: Brendan Twamley

Crystal Structure Report for TCD1071

A clear colourless plate-like specimen of $C_{15}H_{22}F_3N_5O_4$, approximate dimensions 0.100 mm x 0.230 mm x 0.270 mm, was used for the X-ray crystallographic analysis. The X-ray intensity data were measured at 100(2)K on a Bruker B8 Quest Eco with an Oxford Cryostream low temperature device using a MiTeGen micromount. Bruker APEX software was used to correct for Lorentz and polarization effects.

A total of 1020 frames were collected. The total exposure time was 9.92 hours. The frames were integrated with the Bruker SAINT software package using a narrow-frame algorithm. The integration of the data using a monoclinic unit cell yielded a total of 35431 reflections to a maximum θ angle of 26.97° (0.78 Å resolution), of which 3906 were independent (average redundancy 9.071, completeness = 99.4%, R_{int} = 6.18%, R_{sig} = 3.06%) and 2963(75.86%) were greater than 2σ(F^2). The final cell constants of a = 12.7269(6) Å, b = 10.9268(5) Å, c = 13.2087(6) Å, β = 100.183(2)°, volume = 1807.92(14) $Å^3$, are based upon the refinement of the XYZ-centroids of 9996 reflections above 20 σ(I) with 5.54° < 2θ < 53.79°. Data were corrected for absorption effects using the Multi-Scan method (SADABS). The ratio of minimum to maximum apparent transmission was 0.838. The calculated minimum and maximum transmission coefficients (based on crystal size) are 0.9670 and 0.9880.

The structure was solved with the XT structure solution program using Intrinsic Phasing and refined with the XL refinement package using Least Squares minimisation with Olex2, using the space group $P2_1/n$, with Z = 4 for the formula unit, $C_{15}H_{22}F_3N_5O_4$. The final anisotropic full-matrix least-squares refinement on F^2 with 266 variables converged at R1 = 4.51%, for the observed data and wR2 = 12.21% for all data. The goodness-of-fit was 1.030. The largest peak in the final difference electron density synthesis was 0.285 $e^-/Å^3$ and the largest hole was -0.288 $e^-/Å^3$ with an RMS deviation of 0.056 $e^-/Å^3$. On the basis of the final model, the calculated density was 1.445 g/cm^3 and F(000), 824 e^-.

Refinement Note: Donor (N-H) hydrogens located on the difference map and refined with restraints (DFIX).

References:

Bruker (2016). SAINT v8.38A, Bruker AXS Inc., Madison, WI, USA.

Bruker (2017). APEX3 v2017.3-0, Bruker AXS Inc., Madison, WI, USA.

Bruker (2016/2). SADABS, Bruker AXS Inc., Madison, Wisconsin, USA.

Dolomanov, O.V., Bourhis, L.J., Gildea, R.J, Howard, J.A.K. & Puschmann, H. (2009), J. Appl. Cryst. 42, 339-341.

Sheldrick, G.M. (2008). Acta Cryst. A64, 112-122.

Sheldrick, G.M. (2015). Acta Cryst. A71, 3-8

9.4. Pharmacological methods

9.4.1. Preparation of Membranes for [^{3}H]RX821002 Binding Assays

9.4.1.1. Materials and Methods

[^{3H}]RX821002 (specific activity 55 Ci/mmol) was obtained from GE Healthcare, UK. [^{35}S]GTPγS (1250 Ci/mmol) was purchased from PerkinElmer Life and Analytical Sciences, Inc. RX821002 HCl and UK14304 were purchased from Sigma (St.Louis, USA). [^{3}H]MK912 (specific activity 81 Ci/mmol) were obtained from Perkin Elmer, UK. MK912 hydrate was purchased from Tocris, UK.

9.4.1.2. Preparation of Membranes

Neural membranes (P2 fractions) were prepared from the PFC of human brains obtained at autopsy in the Instituto Vasco de Medicina Legal, Bilbao, Spain. Postmortem human brain samples of each of 12 subjects (~ 300 mg) were homogenized using a using an Ultra-Turrax T8 (IKA Labortechnik, Staufen, Germany) at maximum speed for 10 seconds (4ºC) in 30 volumes of homogenization buffer (1 mM $MgCl_2$, and 5 mM Tris-HCl, pH 7.4) supplemented with 0.25 M sucrose. The crude homogenate was centrifuged for 5 min at 1000 X g (4 ºC) and the supernatant was centrifuged again for 10 min at 40000 X g (4 ºC). The resultant pellet was washed twice in 5 volumes of incubation buffer (50 mM Tris-HCl; pH 7.5) and re-centrifuged in similar conditions. Aliquots of 1.2 mg protein were stored at –70 ºC until assay. Protein content was measured according to the method Bradford using BSA as standard, and was similar in the different brain samples. The day of the experiment the membrane pellets were defrosted (4 ˚C), thawed and re-suspended in incubation buffer reaching a final protein concentration of 0.4 mg/ml approximately. The real final protein content was measured after the experiment according to Bradford's method.

9.4.2. [^{3}H]RX821002 Binding Assays

Specific [^{3}H]RX821002 binding was measured in 0.250 mL aliquots (50 mM Tris-HCl, pH 7.5) of the neural membranes, which were incubated In 96-well plates with [3H]RX821002 (2 nM) for 30 min at 25 °C in the absence or presence of the competing compounds (10^{-12} to 10^{-3} M, 10 concentrations).

Incubations were terminated by diluting the samples with 5 mL of ice-cold Tris incubation buffer (4 °C). Membrane bound [^{3}H]RX821002 was measured by vacuum filtration using a Brandel 30R cell harvester through Whatman GF/C glass filters presoaked with 0.5% polyethylenimine. The filters were rinsed twice with 5 mL of Tris incubation buffer, air dried, transferred to minivials that contained 5 mL of OptiPhase HiSafe II cocktail and counted for radioactivity for 5 min by liquid scintillation spectrometry. Free ligand was separated from bound ligand by rapid filtration under vacuum (1450 FilterMate Harvester, PerkinElmer) through GF/C glass fiber filters (Printed Filtermat A) presoaked with 0.5% polyethylenimine.

The filters were then rinsed three times with 300 µL of ice-cold Tris incubation buffer (4 °C), air dried and counted for radioactivity by liquid scintillation spectrometry using a MicroBeta TriLux counter (PerkinElmer). Specific binding was determined and plotted as a function of the compound concentration. Nonspecific binding was determined in the presence of adrenaline (10^{-5} M).

9.4.2.1. Analysis of binding data

Analysis of competition experiments to obtain the inhibition constant (K_i) were performed by nonlinear regression using the GraphPad Prism® software. All experiments were analysed assuming a one-site model of radioligand binding.

9.4.3. Preparation of Membranes for [^{35}S]GTPγS Binding Assays

Preparation of plasma membranes (P2 fraction) and [^{35}S]GTPγS binding assays were performed as previously described (Gonzalez-Maeso et al.) with minor modifications. Tissue samples of each subject (~200 mg) were homogenized using a Teflon-glass grinder (10 up-and-down strokes at 1,500 rpm) in 30 volumes of homogenization buffer (1 mM EGTA, 3 mM $MgCl_2$, 1 mM DTT, and 50 mM Tris-HCl, pH 7.4) supplemented with 0.25 M sucrose. The crude homogenate was centrifuged for 5 min at 1,000 g at 4 ˚C and the supernatant layer was re-centrifuged for 10 min at 40,000 g (4˚C). The resultant pellet was washed twice in 20 volumes of homogenization buffer and re-centrifuged in similar conditions. Protein content was measured according to the method of Bradford using BSA as standard. Samples were aliquoted in order to have a protein content of 1.2 mg and then centrifuged in a benchtop centrifuge (EBA 12 R, Hettich Instruments, Tuttlingen, Germany) at 14.000 rpm for 15 min at 4 ºC.

The supernatant layer was carefully discarded and the pellets stored at -70 ˚C until assay. On the day of the experiment the membrane pellets were defrosted (4 ˚C), thawed and re-suspended in 12 ml of buffer containing 1 mM EGTA, 3 mM $MgCl_2$, 100 mM NaCl, and 50 mM Tris-HCl, pH 7.4, reaching a final protein concentration of 0.8 mg/ml approximately. The real final protein content was measured after the experiment according to Bradford's method.

9.4.4. [35S]GTPγS Binding Assays

The incubation buffer for measuring [^{35}S]GTPγS binding to brain membranes contained, in a total volume of 250 µL, 1 mM EGTA, 3 mM $MgCl_2$, 100 mM NaCl, 50 mM GDP, 50 mM Tris-HCl at pH 7.4, and 0.5 nM [^{35}S]GTPγS. Protein aliquots were thawed and re-suspended in the same buffer. The incubation was started by addition of the membrane suspension (20 µg of membrane proteins per well) to the previous mixture and was performed at 30 ˚C for 120 min with shaking. In order to evaluate the influence of the compounds on [^{35}S]GTPγS binding, 10 concentrations (10^{-12} to 10^{-3} M) of the different compounds were added to the assay.

All compounds that showed an antagonist activity in the [^{35}S]GTPγS binding assays (no stimulation nor inhibition of the basal binding) were also assayed at a constant concentration (10^{-5} M) for [^{35}S]GTPγS binding in the presence of increasing concentrations of the α_2 receptor agonist UK14304 (10^{-13}-10^{-4} M). These experiments were performed in order to investigate the potential of the compounds to specifically modify the EC_{50} or the E_{max} values in the UK14304 stimulation curve. Incubations were terminated by rapid filtration through Whatman GF/C filters pre-soaked in the same buffer. The filters were then rinsed three times with 300 µL of ice-cold incubation buffer (4 °C), air dried and counted for radioactivity by liquid scintillation spectrometry using a MicroBeta TriLux counter (PerkinElmer). The [^{35}S]GTPγS bound was about 7–14% of the total [^{35}S]GTPγS added. Nonspecific binding (NS) of the radioligand was defined as the remaining [^{35}S]GTPγS binding in the presence of 100 µM unlabelled GTPγS.

9.4.4.1. Mathematical and statistical analysis of the results

The non-specific binding (NS) was subtracted to the net experimental stimulations (NStim).

In order to allow a good interpretation of the data, they are either displayed as relative stimulations over basal values (B) (% over basal). The basal binding of [^{35}S]GTPγS, defined in the absence of agonist, was considered the 100% and the percentage of stimulation (or inhibition) over the basal level was calculated as follows:

Equation 1: % over basal= ((Stim-NS)/B-NS) x 100

The pharmacological parameters of the stimulation or inhibition of the [^{35}S]GTPγS binding, the maximal effect (E_{max}) and the concentration of the drug that determines the half maximal effect (EC_{50}), were obtained by non-linear analysis using GraphPad Prism® software. The points fit to a concentration-response curve, shown in equation 1. The pharmacological parameters E_{max} and EC_{50} are expressed as means ± S.E.M.

9.4.5 [^{3}H]RX821002 and [^{3}H]MK912 binding assays at human α_{2A}-AR/α_{2C}-ARs

9.4.5.1. Cells expressing human α_{2A}-AR or α_{2C}-ARs

Cellular membranes of CHO cells selectively expressing human α_{2A}-AR or α_{2C}-ARs were purchased from Perkin Elmer (ES-030-M400UA and ES-032-M400UA, respectively). According to manufacturer instructions, cells were kept at -80ºC and small aliquots were prepared in order to minimize negative impact of freeze-thawing. The day of the experiments 100 µL of cells were diluted in 50ml of 50 mM Tris-HCl, pH 7.5.

9.4.5.2. [3H]RX821002 Binding Assays in cells expressing human α_{2A}-AR

Specific [^{3}H]RX821002 binding was measured in 0.250 mL aliquots of cellular membranes of cells expressing human α_{2A}-AR (50 mM Tris-HCl, pH 7.5), which were incubated in 96-well plates with [^{3}H]RX821002 (2 nM) for 30 min at 25 °C in the absence or presence of the competing compounds (10^{-12} to 10^{-3} M, 10 concentrations). Incubations were terminated by diluting the samples with 5 mL of ice-cold Tris incubation buffer (4°C). Free ligand was separated from bound ligand by rapid filtration under vacuum (1450 FilterMate Harvester, PerkinElmer) through GF/C glass fibre filters (Printed Filtermat A) pre-soaked with 0.5% polyethylenimine. The filters were then rinsed three times with 300 µL of ice-cold Tris incubation buffer (4 °C), air dried and radioactivity counted by liquid scintillation spectrometry using a MicroBeta TriLux counter (PerkinElmer).

Specific binding was determined and plotted as a function of the compound concentration. Nonspecific binding was determined in the presence of adrenaline (10^{-5} M).

9.4.5.3. [^{3}H]MK912 Binding Assays in cells expressing human α_{2C}-AR

These experiments were carried out as specified above with the exceptions that the radioligand was [^{3}H]MK912 (1 nM), the membranes were from cells expressing human α_{2C}-AR and the incubation was 60 min at 25 °C.

9.4.5.4. Analysis of binding data

Analysis of competition experiments to obtain the inhibition constant (K_i) were performed by nonlinear regression using the GraphPad Prism® software. All experiments were analysed assuming a one-site model of radioligand binding.

References

1 B. K. Kobilka, *Trends Pharmacol Sci*, 2011, **32**, 213–218.

2 D. Bylund, *Pharmacol. Rev.*, 1994, **46**, 121–136.

3 B. Civantos Calzada and A. Aleixandre De Artiñano, *Pharmacol. Res.*, 2001, **44**, 195–208.

4 S. G. F. Rasmussen, B. T. DeVree, Y. Zou, A. C. Kruse, K. Y. Chung, T. S. Kobilka, F. S. Thian, P. S. Chae, E. Pardon, D. Calinski, J. M. Mathiesen, S. T. A. Shah, J. A. Lyons, M. Caffrey, S. H. Gellman, J. Steyaert, G. Skiniotis, W. I. Weis, R. K. Sunahara and B. K. Kobilka, *Nature*, 2011, **477**, 549–555.

5 D. Latek, A. Modzelewska, B. Trzaskowski, P. Krzysztof and S. Filipek, *Acta Biochim Pol*, 2012, **59**, 515–529.

6 A. J. Venkatakrishnan, X. Deupi, G. Lebon, F. M. Heydenreich, T. Flock, T. Miljus, S. Balaji, M. Bouvier, D. B. Veprintsev, C. G. Tate, G. F. X. Schertler and M. M. Babu, *Nature*, 2016, **536**, 484–487.

7 P. Michael W King, *themedicalbiochemistrypage.org*, 2018.

8 X. Deupi and B. Kobilka, *Adv. Protein Chem.*, 2007, **74**, 137–166.

9 M. Jiang and N. S. Bajpayee, *NeuroSignals*, 2009, **17**, 23–41.

10 N. Wettschureck and S. Offermanns, *Physilological Rev.*, 2005, 1159–1204.

11 C. Galés, J. J. J. Van Durm, S. Schaak, S. Pontier, Y. Percherancier, M. Audet, H. Paris and M. Bouvier, *Nat. Struct. Mol. Biol.*, 2006, **13**, 778–786.

12 S. Osawa, N. Dhanasekaran, C. W. Woon and G. L. Johnson, *Cell*, 1990, **63**, 697–706.

13 S. Offermanns, N. Wettschureck, A. Moers, B. Wallenwein and A. F. Parlow, *Mol. Cell. Biol.*, 2005, **25**, 1942–1948.

14 S. Z. Langer, *Trends Pharmacol. Sci.*, 2015, **36**, 196–202.

15 N. Suzuki, N. Hajicek and T. Kozasa, *NeuroSignals*, 2009, **17**, 55–70.

16 M. Galaz-Montoya, S. J. Wright, G. J. Rodriguez, O. Lichtarge and T. G. Wensel, *J. Biol. Chem.*, 2017, **292**, 9967–9974.

17 K. Gyires, Z. S. Zádori, T. Török and P. Mátyus, *Neurochem. Int.*, 2009, **55**, 447–453.

18 D. Wacker, R. C. Stevens and B. L. Roth, *Cell*, 2017, **170**, 414–427.

19 Y. Huang and A. Thathiah, *FEBS Lett.*, 2015, **589**, 1607–1619.

20 K. M. Betke, C. A. Wells and H. E. Hamm, *Prog. Neurobiol.*, 2012, **96**, 304–

321.

21 K. Pytka, K. Podkowa, A. Rapacz, A. Podkowa, E. Zmudzka, A. Olczyk, J. Sapa and B. Filipek, *Pharmacol. Reports*, 2016, **68**, 263–274.

22 L. Cinnamon Bidwell, R. E. Dew and S. H. Kollins, *Curr. Psychiatry Rep.*, 2010, **12**, 366–373.

23 V. Maletic, A. Eramo, K. Gwin, S. J. Offord and R. A. Duffy, *Front. Psychiatry*, 2017, **8**.

24 L. Hein, *Cell Tissue Res.*, 2006, **326**, 541–551.

25 Q. Zhou, Y. Lai, T. Bacaj, M. Zhao, A. Y. Lyubimov, M. Uervirojnangkoorn, O. B. Zeldin, A. S. Brewster, N. K. Sauter, A. E. Cohen, S. M. Soltis, R. Alonso-mori, M. Chollet, H. T. Lemke, R. a Pfuetzner, U. B. Choi, W. I. Weis, J. Diao, A. T. Brunger and T. C. Su, *Nature*, 2015.

26 K. Starke, E. Board, S. Duckles, M. Eichelbaum, D. Ganten, F. Hofmann, C. Page, W. Rosenthal, G. Rubanyi and S. Diego, *Handbook of Experimental Pharmacology*, vol. 184.

27 C. Cottingham and Q. Wang, *Neurosci. Biobehav. Rev.*, 2012, **36**, 2214–25.

28 F. P. Bymaster, R. K. McNamara and P. V Tran, *Expert. Opin. Investig. Drugs*, 2003, **12**, 531–543.

29 C. A. Mejias-Aponte, *Brain Res.*, 2016, **1641**, 258–273.

30 M. P. Castelli, S. Spiga, A. Perra, C. Madeddu, G. Mulas, M. G. Ennas and G. L. Gessa, *Neuroscience*, 2016, **332**, 130–139.

31 O. D. Howes and S. Kapur, *Schizophr. Bull.*, 2009, **35**, 549–562.

32 J.-M. Beaulieu and R. R. Gainetdinov, *Pharmacol. Rev.*, 2011, **63**, 182–217.

33 S. Jafari, F. Fernandez-Enright and X.-F. Huang, *J. Neurochem.*, 2012, **120**, 371–384.

34 A. F. T. Arnsten, *J. Psychopharmacol.*, 1997, **11**, 151–162.

35 P. Devoto and G. Flore, *Curr. Neuropharmacol.*, 2006, **4**, 115–25.

36 A. F. T. Arnsten, *Nat. Neurosci.*, 2015, **18**, 1376–1385.

37 A. F. T. Arnsten, *Psychopharmacology (Berl).*, 2004, **174**, 25–31.

38 K. Pytka, A. Partyka, M. Jastrzębska-Więsek, A. Siwek, M. Głuch-Lutwin, B. Mordyl, G. Kazek, A. Rapacz, A. Olczyk, A. Gałuszka, M. Błachuta, A. Waszkielewicz, H. Marona, J. Sapa, B. Filipek and A. Wesołowska, *PLoS One*, 2015, **10**, 1–24.

39 P. Panula and S. Nuutinen, *Nat. Rev. Neurosci.*, 2013, **14**, 472–487.

40 C. Y. Jin and P. Panula, *Neuroscience*, 2005, **132**, 137–149.

41 K. Meskanen, H. Ekelund, J. Laitinen, P. J. Neuvonen, J. Haukka, P. Panula and J. Ekelund, *J. Clin. Psychopharmacol.*, 2013, **33**, 472–478.

42 M. Hamon and P. Blier, *Prog. Neuropsychopharmacol. Biol. Psychiatry*, 2013, **45**, 54–63.

43 M. M. Uys, M. Shahid and B. H. Harvey, *Front. Psychiatry*, 2017, **8**.

44 S. Miyamoto, G. E. Duncan, C. E. Marx and J. A. Lieberman, *Mol. Psychiatry*, 2005, **10**, 79–104.

45 C. Cottingham and Q. Wang, *Neurosci. Biobehav. Rev.*, 2012, **36**, 2214–2225.

46 P. G. Strange, *Br. J. Pharmacol.*, 2010, **161**, 1238–1249.

47 C. Harrison and J. R. Traynor, *Life Sci.*, 2003, **74**, 489–508.

48 35S GTP Binding Assays Perkin Elmer, *http://www.perkinelmer.co.uk/lab-products-and-services/application-support-knowledgebase/radiometric/35s-gtp-binding-assays.html*.

49 T. D. Vieweg, W. V. R. Vieweg, Y. Aderibigbe and A. Aderibigbe, *Psychiatry Clin. Neurosci.*, 1999, **53**, 437–448.

50 T. C. Kyziridis, *Ger. J. Psychiatry*, 2005, **8**, 42–48.

51 R. Tandon, W. Gaebel, D. M. Barch, J. Bustillo, R. E. Gur, S. Heckers, D. Malaspina, M. J. Owen, S. Schultz, M. Tsuang, J. Van Os and W. Carpenter, *Schizophr. Res.*, 2013, **150**, 3–10.

52 N. C. Andreasen and S. Olsen, *Arch. Gen. Psychiatry*, 1982, **39**, 789–794.

53 J.-P. Lindenmayer, H. Nasrallah, M. Pucci, S. James and L. Citrome, *Schizophr. Res.*, 2013, **147**, 241–252.

54 S. Frangou, *Psychiatry*, 2005, **4**, 46–48.

55 WHO, *http://www.who.int/mental_health/management/schizophrenia/en/*.

56 J. McGrath, S. Saha, D. Chant and J. Welham, *Epidemiol. Rev.*, 2008, **30**, 67–76.

57 WHO Schizophrenia Fact sheet N°397 [Updated September 2015], *Http://Www.Who.Int/Mediacentre/Factsheets/Fs397/En/*.

58 S. Ripke, B. M. Neale, A. Corvin, J. T. R. Walters and et al., *Nature*, 2014, **511**, 421–427.

59 O. D. Howes, F. Vergunst, S. Gee, P. McGuire, S. Kapur and D. Taylor, *Br. J. Psychiatry*, 2012, **201**, 481–485.

60 L. A. McCollum, R. E. McCullumsmith and R. C. Roberts, *Brain Struct. Funct.*, 2016.

61 M. J. Owen and M. C. O'Donovan, *Psychiatry*, 2008, **7**, 415–420.

62 D. F. Levinson, *Curr. Opin. Psychiatry*, 2003, **16**, 157–170.

63 G. Modinos, C. Iyegbe, D. Prata, M. Rivera, M. J. Kempton, L. R. Valmaggia, P. C. Sham, J. van Os and P. McGuire, *Schizophr. Res.*, 2013, **150**, 356–365.

64 W. Yue, X. Yu and D. Zhang, *npj Schizophr.*, 2017, **3**, 24.

65 S. Prasad, T. Bhatia, P. Kukshal, V. L. Nimgaonkar, S. N. Deshpande and B. K. Thelma, *npj Schizophr.*, 2017, **3**, 28.

66 P. R. Ormel, H. C. van Mierlo, M. Litjens, M. E. van Strien, E. M. Hol, R. S. Kahn and L. D. de Witte, *npj Schizophr.*, 2017, **3**, 41.

67 I. Lena, A. Chessel, G. Le Pen, M. O. Krebs and R. Garcia, *Psychopharmacology (Berl).*, 2007, **192**, 373–383.

68 E. Scarr, M. Udawela and B. Dean, *npj Schizophr.*, 2018, **4**, 4.

69 F. Piras, M. Schiff, C. Chiapponi, P. Bossù, M. Mühlenhoff, C. Caltagirone, R. Gerardy-Schahn, H. Hildebrandt and G. Spalletta, *Transl. Psychiatry*, 2015, **5**, e658.

70 X. Caseras, K. E. Tansey, S. Foley and D. Linden, *Transl. Psychiatry*, 2015, **5**, e692.

71 J. van Os, G. Kenis and B. P. F. Rutten, *Nature*, 2010, **468**, 203–212.

72 K. Bakhshi and S. a. Chance, *Neuroscience*, 2015, **303**, 82–102.

73 O. D. Howes and S. Kapur, *Schizophr. Bull.*, 2009, **35**, 549–62.

74 O. Howes, R. McCutcheon and J. Stone, *J. Psychopharmacol.*, 2015, **29**, 97–115.

75 J. T. Coyle, *Schizophr. Bull.*, 2012, **38**, 920–926.

76 J. H. Krystal, D. C. D'Souza, D. Mathalon, E. Perry, A. Belger and R. Hoffman, *Psychopharmacology (Berl).*, 2003, **169**, 215–233.

77 K. Fukuda, *Med. Hypotheses*, 2014, **82**, 20–23.

78 G. K. Aghajanian and G. J. Marek, *Brain Res. Rev.*, 2000, **31**, 302–312.

79 J. Brosda, F. Jantschak and H. H. Pertz, *Psychopharmacology (Berl).*, 2014, **231**, 801–812.

80 M. J. Just, *Neuropsychiatr. Dis. Treat.*, 2015, **11**, 1655–61.

81 J. Kew and J. Kemp, *Psychopharmacol.*, 2005, **179**, 4–29.

82 C. a Paladini, C. D. Fiorillo, H. Morikawa and J. T. Williams, *Nat. Neurosci.*, 2001, **4**, 275–281.

83 F. Fazio, L. Lionetto, M. Curto, L. Iacovelli, M. Cavallari, C. Zappulla, M. Ulivieri, F. Napoletano, M. Capi, V. Corigliano, S. Scaccianoce, A. Caruso, J.

Miele, A. De Fusco, L. Di Menna, A. Comparelli, A. De Carolis, R. Gradini, R. Nisticò, A. De Blasi, P. Girardi, V. Bruno, G. Battaglia, F. Nicoletti and M. Simmaco, *Sci. Rep.*, 2015, **5**, 177–199.

84 A. E. Timms, M. O. Dorschner, J. Wechsler, K. Y. Choi, R. Kirkwood, S. Girirajan, C. Baker, E. E. Eichler, O. Korvatska, K. W. Roche, M. S. Horwitz and D. W. Tsuang, *JAMA Psychiatry*, 2013, **70**, 582–590.

85 J. D. Jentsch and R. H. Roth, *Neuropsychopharmacology*, 1999, **20**, 201–225.

86 V. Bubeníková-Valešová, J. Horáček, M. Vrajová and C. Höschl, *Neurosci. Biobehav. Rev.*, 2008, **32**, 1014–1023.

87 B. Moghaddam and D. Javitt, *Neuropsychopharmacology*, 2012, **37**, 4–15.

88 H. Y. Meltzer, Z. Li, Y. Kaneda and J. Ichikawa, *Prog. Neuro-Psychopharmacology Biol. Psychiatry*, 2003, **27**, 1159–1172.

89 H. Y. Meltzer and B. W. Massey, *Curr. Opin. Pharmacol.*, 2011, **11**, 59–67.

90 W. W. Shen, *Compr. Psychiatry*, 1999, **40**, 407–414.

91 S. Kapur and D. Mamo, *Prog. Neuro-Psychopharmacology Biol. Psychiatry*, 2003, **27**, 1081–1090.

92 K. V. G. C. Sekhar, D. R. K. Vyas, H. N. Nagesh and V. S. Rao, *Bull. Korean Chem. Soc.*, 2012, **33**, 2930–2936.

93 S. Kasper, J. Tauscher, B. Küfferle, C. Barnas, L. Pezawas and S. Quiner, *Eur. Arch. Psychiatry Clin. Neurosci.*, 1999, **249**, 83–89.

94 S. Mas, P. Gassó, M. A. Ritter, C. Malagelada, M. Bernardo and A. Lafuente, *Eur. Neuropsychopharmacol.*, 2015, **25**, 51–9.

95 L. S. Kegeles, M. Slifstein, W. G. Frankle, X. Xu, E. Hackett, S.-A. Bae, R. Gonzales, J.-H. Kim, B. Alvarez, R. Gil, M. Laruelle and A. Abi-Dargham, *Neuropsychopharmacology*, 2008, **33**, 3111–3125.

96 H. L. Cai, Q. Y. Tan, P. Jiang, R. L. Dang, Y. Xue, M. M. Tang, P. Xu, Y. Deng, H. D. Li and J. K. Yao, *Transl. Psychiatry*, 2015, **5**, 661.

97 A. Uçok and W. Gaebel, *World Psychiatry*, 2008, **7**, 58–62.

98 H. A. Nasrallah, *Mol. Psychiatry*, 2008, **13**, 27–35.

99 W. K. Kroeze, S. J. Hufeisen, B. A. Popadak, S. M. Renock, S. Steinberg, P. Ernsberger, K. Jayathilake, H. Y. Meltzer and B. L. Roth, *Neuropsychopharmacology*, 2003, **28**, 519–526.

100 M. Riedel, I. Spellmann, M. Strassnig, A. Douhet, S. Dehning, M. Opgen-Rhein, R. Valdevit, R. R. Engel, N. Kleindienst, N. Müller and H. J. Möller, *Eur. Arch. Psychiatry Clin. Neurosci.*, 2007, **257**, 360–370.

101 R. Tandon, *Hum Psychopharmacol*, 2004, **19**, 559–563.

102 T. Sharma, C. Hughes, W. Soni and V. Kumari, *Psychopharmacology (Berl).*, 2003, **169**, 398–403.

103 H. A. Nasrallah, *Mol. Psychiatry*, 2008, **13**, 27–35.

104 M. Lee, P. Thompson and H. Y. Meltzer, *J. Clin. Psychiatry*, 1994, **55**, 82–87.

105 R. S. E. Keefe, C. A. Young, S. L. Rock, S. E. Purdon, J. M. Gold and A. Breier, *Schizophr. Res.*, 2006, **81**, 1–15.

106 H. O. Kalkman and E. Loetscher, *Eur J Pharmacol*, 2003, **462**, 33–40.

107 T. H. Svensson, *Prog. Neuro-Psychopharmacology Biol. Psychiatry*, 2003, **27**, 1145–1158.

108 H. Y. Meltzer and B. W. Massey, *Curr. Opin. Pharmacol.*, 2011, **11**, 59–67.

109 A. E. Knaus, V. Muthig, S. Schickinger, E. Moura, N. Beetz, R. Gilsbach and L. Hein, *Neurochem. Int.*, 2007, **51**, 277–281.

110 J. W. Kable, L. C. Murrin and D. B. Bylund, 2000, **293**, 1–7.

111 M. M. Bücheler, K. Hadamek and L. Hein, *Neuroscience*, 2002, **109**, 819–26.

112 J. S. Franowicz, L. E. Kessler, C. M. D. Borja, B. K. Kobilka, L. E. Limbird and A. F. T. Arnsten, *J. Neurosci.*, 2002, **22**, 8771–8777.

113 E. M. Hecht and D. C. Landy, *Schizophr. Res.*, 2012, **134**, 202–206.

114 S. J. Cho, K. Yook, B. Kim, T. K. Choi, K. S. Lee, Y. W. Kim, J. E. Lee, S. Suh, K. H. Yook and S.-H. Lee, *Prog. Neuropsychopharmacol. Biol. Psychiatry*, 2011, **35**, 208–211.

115 S. V Phan and T.-J. M. Kreys, *Pharmacotherapy*, 2011, **31**, 1017–1030.

116 M. M. Marcus, C. Wiker, O. Franberg, A. Konradsson-Geuken, X. Langlois, K. Jardemark and T. H. Svensson, *Int J Neuropsychopharmacol*, 2010, **13**, 891–903.

117 B. J. Gertz, P. H. Vlasses, M. L. J. Rocci, L. D. Coker, V. Williams, T. D. Bjornsson and K. H. Jones, *Clin. Pharmacol. Ther.*, 1989, **46**, 566–575.

118 D. D. Schwartz and T. P. Clark, *J. Vet. Pharmacol. Ther.*, 1998, **21**, 342–347.

119 C. Porter and R. Neubig, *J. Pharmacol. Exp. Ther.*, 1994, **271**, 1558–1565.

120 J. Sallinen, J. Holappa, A. Koivisto, K. Kuokkanen, H. Chapman, J. Lehtimäki, P. Piepponen, J. Mijatovic, H. Tanila, R. Virtanen, J. Sirviö and A. Haapalinna, *Basic Clin. Pharmacol. Toxicol.*, 2013, **113**, 239–249.

121 M. D. Tricklebank, *Br. J. Pharmacol.*, 2007, **150**, 381–382.

122 J. Sallinen, I. Höglund, M. Engström, J. Lehtimäki, R. Virtanen, J. Sirviö, S. Wurster, J.-M. Savola and A. Haapalinna, *Br. J. Pharmacol.*, 2007, **150**, 391–402.

123 J. Imaki, Y. Mae, S. Shimizu and Y. Ohno, *Neurosci. Lett.*, 2009, **454**, 143–147.

124 V. Fagerholm, J. Rokka, L. Nyman, J. Sallinen, J. Tiihonen, E. Tupala, M. Haaparanta and J. Hietala, *Synapse*, 2008, **62**, 508–15.

125 S. Uhlen, *Brain Res.*, 1997, **770**, 261–266.

126 S. D. Patel, W. M. Habeski, H. Min, J. Zhang, R. Roof, B. Snyder, G. Bora, B. Campbell, C. Li, D. Hidayetoglu, D. S. Johnson, A. Chaudhry, M. E. Charlton and N. M. Kablaoui, *Bioorg. Med. Chem. Lett.*, 2008, **18**, 5689–5693.

127 W. Quaglia, F. Del Bello, M. Giannella and A. Piergentili, 2011, 455–481.

128 C. Dardonville, P. Goya, I. Rozas, A. Alsasua, M. I. Martín and M. J. Borrego, *Bioorg. Med. Chem.*, 2000, **8**, 1567–1577.

129 F. Rodriguez, I. Rozas, J. E. Ortega, J. J. Meana and L. F. Callado, *J. Med. Chem.*, 2007, **50**, 4516–4527.

130 F. Rodriguez, I. Rozas, J. E. Ortega, A. M. Erdozain, J. J. Meana and L. F. Callado, *J. Med. Chem.*, 2008, **51**, 3304–3312.

131 F. Rodriguez, I. Rozas, J. E. Ortega, A. M. Erdozain, J. J. Meana and L. F. Callado, *J. Med. Chem.*, 2009, **52**, 601–609.

132 B. Kelly, M. McMullan, C. Muguruza, J. E. Ortega, J. J. Meana, L. F. Callado and I. Rozas, *J. Med. Chem.*, 2015, **58**, 963–977.

133 C. Muguruza, F. Rodríguez, I. Rozas, J. J. Meana, L. Urigüen and L. F. Callado, *Neuropharmacology*, 2013, **65**, 13–19.

134 A. Flood, C. Trujillo, G. Sanchez-Sanz, B. Kelly, C. Muguruza, L. F. Callado and I. Rozas, *Eur. J. Med. Chem.*, 2017, **138**, 38–50.

135 D. H. O'Donovan, C. Muguruza, L. F. Callado and I. Rozas, *Eur. J. Med. Chem.*, 2014, **82**, 242–54.

136 M. Fujioka and N. Omori, *Drug Discov. Today*, 2012, **17**, 1133–1138.

137 P. I. Dosa and E. A. Amin, *J. Med. Chem.*, 2016, **59**, 810–840.

138 M. McMullan, A. García-Bea, P. Miranda-Azpiazu, L. F. Callado and I. Rozas, *Eur. J. Med. Chem.*, 2016, **123**, 48–57.

139 I. Rozas, M. McMullan and B. Kelly, 2016, Manuscript in Prep.

140 F. Rodriguez, I. Rozas, J. E. Ortega, A. M. Erdozain, J. J. Meana and L. F. Callado, *J. Med. Chem.*, 2008, **51**, 3304–3312.

141 D. H. O'Donovan, C. Muguruza, L. F. Callado and I. Rozas, *Eur. J. Med. Chem.*, 2014, **82**, 242–254.

142 F. Rodriguez, I. Rozas, J. E. Ortega, A. M. Erdozain, J. J. Meana and L. F.

Callado, *J. Med. Chem.*, 2009, **52**, 601–609.

143 T. S. Gujral, L. Peshkin and M. W. Kirschner, 2014, **111**.

144 D. R. Weiss, J. Karpiak, X. Huang, M. Flori, J. Lyu, B. L. Roth and B. K. Shoichet, 2018.

145 F. Gentili, M. Pigini, A. Piergentili and M. Giannella, *Curr. Top. Med. Chem.*, 2007, **7**, 163–186.

146 A. Jayaraman, K. Jamil and K. K. Kakarala, *J. Comput. Sci. Syst. Biol.*, 2013, **6**, 136–149.

147 L. Ostopovici-Halip, R. Curpân, M. Mracec and C. G. Bologa, *J. Mol. Graph. Model.*, 2011, **29**, 1030–1038.

148 V. Kumar, G. Bansal, J. Patel and C. Gopi Mohan, *Med. Chem. Res.*, 2014, **23**, 735–746.

149 B. Balogh, A. Szilágyi, K. Gyires, D. B. Bylund and P. Mátyus, *Neurochem. Int.*, 2009, **55**, 355–61.

150 T. Flock, A. S. Hauser, N. Lund, D. E. Gloriam, S. Balaji and M. M. Babu, *Nature*, 2017, **545**, 317–322.

151 H. Xhaard, T. Nyrönen, V.-V. Rantanen, J. O. Ruuskanen, J. Laurila, T. Salminen, M. Scheinin and M. S. Johnson, *J. Struct. Biol.*, 2005, **150**, 126–43.

152 J. M. M. Laurila, G. Wissel, H. Xhaard, J. O. Ruuskanen, M. S. Johnson and M. Scheinin, *Br. J. Pharmacol.*, 2011, **164**, 1558–72.

153 J. A. Ballesteros and H. Weinstein, *Methods Neurosci.*, 1995, **25**, 366–428.

154 A. J. Venkatakrishnan, X. Deupi, G. Lebon, C. G. Tate, G. F. Schertler and M. Madan Babu, *Nature*, 2013, **494**, 185–194.

155 J. M. Peltonen, T. Nyrönen, S. Wurster, M. Pihlavisto, A.-M. Hoffrén, A. Marjamäki, H. Xhaard, L. Kanerva, J.-M. Savola, M. S. Johnson and M. Scheinin, *Br. J. Pharmacol.*, 2003, **140**, 347–358.

156 E. Jnoff, B. Christophe, P. Collart, F. Coloretti, A. Debeuckelaere, M. De Ryck, B. Fuks, C. Genicot, M. Gillard, M. Guyaux, N. Price, M.-C. Vandergeten and C. Vermeiren, *ChemMedChem*, 2012, **7**, 385–390.

157 P.-A. Crassous, C. Cardinaletti, A. Carrieri, B. Bruni, M. DiVaira, F. Gentili, F. Ghelfi, M. Giannella, H. Paris, A. Piergentili, W. Quaglia, S. Schaak, C. Vesprini and M. Pigini, *J. Med. Chem.*, 2007, **50**, 3964–3968.

158 F. del Bello, L. Mattioli, F. Ghelfi, M. Giannella, A. Piergentili, W. Quaglia, C. Cardinaletti, M. Perfumi, R. J. Thomas, U. Zanelli, C. Marchioro, M. Dal Cin and M. Pigini, *J. Med. Chem.*, 2010, **53**, 7825–7835.

159 F. Gentili, P. Bousquet, L. Brasili, M. Caretto, A. Carrieri, M. Dontenwill, M. Giannella, G. Marucci, M. Perfumi, A. Piergentili, W. Quaglia, C. Rascente and M. Pigini, *J Med Chem*, 2002, **45**, 32–40.

160 D. Castagnolo, S. Schenone and M. Botta, *Chem. Rev.*, 2011, **111**, 5247–5300.

161 D. A. Powell, P. D. Ramsden and R. A. Batey, *J. Org. Chem.*, 2003, **68**, 2300–2309.

162 A. R. Katritzky and B. V Rogovoy, *ARKIVOC*, 2005, **2005**, 49–87.

163 C. Alonso-Moreno, A. Antiñolo, F. Carrillo-Hermosilla and A. Otero, *Chem. Soc. Rev.*, 2014, **43**, 3406–25.

164 S. Kim and L. Qian, *Tetrahedron Lett.*, 1993, **34**, 7677–7680.

165 S. Cunha, B. R. De Lima and A. R. De Souza, *Tetrahedron Lett.*, 2002, **43**, 49–52.

166 S. Cunha, M. T. R. Jr, C. Silva and H. B. Napolitano, *Tetrahedron*, 2005, **61**, 10536–10540.

167 S. Cunha and M. T. Rodrigues, *Tetrahedron Lett.*, 2006, **47**, 6955–6956.

168 K. Ohara, J. J. Vasseur and M. Smietana, *Tetrahedron Lett.*, 2009, **50**, 1463–1465.

169 S. Pape, P. Wessig and H. Brunner, *RSC Adv.*, 2015, **5**, 101408–101411.

170 B. R. Linton, A. J. Carr, B. P. Orner and A. D. Hamilton, *J. Org. Chem.*, 2000, **65**, 1566–1568.

171 Â. B. Costa, H. B. Napolitano, I. Vencato and S. Cunha, *Tetrahedron*, 2001, **57**, 1671–1675.

172 M. S. Bernatowicz, Y. Wu and G. R. Matsueda, *J. Org. Chem.*, 1992, **57**, 2497–2504.

173 S. Herres-Pawlis, A. Neuba, O. Seewald, T. Seshadri, H. Egold, U. Fl??rke and G. Henkel, *European J. Org. Chem.*, 2005, 4879–4890.

174 K. Tsubokura, T. Iwata, M. Taichi, A. Kurbangalieva, K. Fukase, Y. Nakao and K. Tanaka, *Synlett*, 2014, **25**, 1302–1306.

175 L. Xu, W. X. Zhang and Z. Xi, *Organometallics*, 2015, **34**, 1787–1801.

176 G. Evindar and R. A. Batey, *Org. Lett.*, 2003, **5**, 133–136.

177 H. Xing, Y. Zhang, Y. Lai, Y. Jiang and D. Ma, *J. Org. Chem.*, 2012, **77**, 5449–5453.

178 H. Hammoud, M. Schmitt, F. Bihel, C. Antheaume and J. J. Bourguignon, *J. Org. Chem.*, 2012, **77**, 417–423.

179 J. W. Shaw, D. H. Grayson and I. Rozas, *European J. Org. Chem.*, 2014, **2014**, 3565–3569.

180 P. S. Nagle, F. Rodriguez, A. Kahvedžić, S. J. Quinn and I. Rozas, *J. Med. Chem.*, 2009, **52**, 7113–7121.

181 C. Dardonville, I. Rozas, P. Goya, R. Giron, C. Goicoechea and M. I. Martin, *Bioorg Med Chem*, 2003, **11**, 1283–1291.

182 Z. P. Khan, C. N. Ferguson and R. M. Jones, *Anaesthesia*, 1999, **54**, 146–165.

183 C. B. Chapleo, R. C. Butler, D. C. England, P. L. Myers, a G. Roach, C. F. Smith, M. R. Stillings and I. F. Tulloch, *J. Med. Chem.*, 1989, **32**, 1627–30.

184 A. Gómez-Sanjuan, J. M. Botija, A. Méndez, N. Sotomayor and E. Lete, *Arch. Org. Chem.*, 2014, **2014**, 44–56.

185 S. R. Mundla, L. J. Wilson, S. R. Klopfenstein, W. L. Seibel and N. N. Nikolaides, *Tetrahedron Lett.*, 2000, **41**, 6563–6566.

186 Y. Shiraishi, S. Sumiya and T. Hirai, *Org. Biomol. Chem.*, 2010, **8**, 1310–1314.

187 H. K. Oh, J. E. Park, D. D. Sung and I. Lee, *J. Org. Chem.*, 2004, **69**, 3150–3153.

188 D. H. O'Donovan and I. Rozas, *Tetrahedron Lett.*, 2012, **53**, 4532–4535.

189 G. Giester, *Eur. J. Inorg. Chem.*, 2002, 171–180.

190 G. Pavlović, Z. Popović, Ž. Soldin and D. Matković-Čalogović, *Acta Crystallogr. Sect. C Cryst. Struct. Commun.*, 2000, **56**, 61–63.

191 F. Rodriguez, I. Rozas, J. E. Ortega, J. J. Meana and L. F. Callado, *J. Med. Chem.*, 2007, **50**, 4516–4527.

192 D. J. Hwang, J. Yang, H. Xu, I. M. Rakov, M. L. Mohler, J. T. Dalton and D. D. Miller, *Bioorganic Med. Chem.*, 2006, **14**, 6525–6538.

193 A. Meyer and K. Fischer, *Environ. Sci. Eur.*, 2015, **27**.

194 R. J. Vijn, H. J. Arts, P. J. Maas and A. M. Castelijns, *J. Org. Chem.*, 1993, **58**, 887–891.

195 B. Kelly, D. H. O'Donovan, J. O'Brien, T. McCabe, F. Blanco and I. Rozas, *J. Org. Chem.*, 2011, **76**, 9216–9227.

196 D. H. O'Donovan, C. Muguruza, L. F. Callado and I. Rozas, *Eur. J. Med. Chem.*, 2014, 82, 242–54.

197 M. McMullan, A. García-Bea, P. Miranda-Azpiazu, L. F. Callado and I. Rozas, *Eur. J. Med. Chem.*, 2016, 123, 48–57.

198 Y. Usuki, K. Matsumoto, T. Inoue, K. Yoshioka, H. Iio and T. Tanaka, *Bioorganic Med. Chem. Lett.*, 2006, **16**, 1553–1556.

199 B. L. Roth, *NIMH PDSP ASSAY Protoc. B.*, 2018, **3**.

200 J. Besnard, G. F. Ruda, V. Setola, K. Abecassis, R. M. Rodriguiz, X. P. Huang, S. Norval, M. F. Sassano, A. I. Shin, L. A. Webster, F. R. C. Simeons, L. Stojanovski, A. Prat, N. G. Seidah, D. B. Constam, G. R. Bickerton, K. D.

Read, W. C. Wetsel, I. H. Gilbert, B. L. Roth and A. L. Hopkins, *Nature*, 2012, **492**, 215–220.

201 Y. Haddad, Z. Heger and V. Adam, *ACS Chem. Neurosci.*, 2016, **7**, 1607–1613.

202 Z. Lin, J. J. Canales, T. Björgvinsson, M. M. Thomsen, Q. Liu, G. E. Torres and S. B. Caine, *Prog Mol Biol Transl Sci*, 2011, 1–40.

203 C. A. Obejero-Paz, A. Bruening-Wright, J. Kramer, P. Hawryluk, M. Tatalovic, H. C. Dittrich and A. M. Brown, *Sci. Rep.*, 2015, **5**, 1–12.

204 M. A. M. Subbaiah, *J. Med. Chem.*, 2017, acs.jmedchem.6b01827.

205 M.-L. Wadenberg, C. Wiker and T. H. Svensson, *Int. J. Neuropsychopharmacol.*, 2007, **10**, 191–202.

206 E. F. Torrey and J. M. Davis, *Clin. Schizophr. Relat. Psychoses*, 2012, **5**, 208–216.

207 T. Hayashi and T. Su, *Curr. Neuropharmacol.*, 2005, **3**, 267–280.

208 C. G. Rousseaux and S. F. Greene, *J. Recept. Signal Transduct.*, 2016, **36**, 327–388.

209 M. E. Parsons and C. R. Ganellin, *Br. J. Pharmacol.*, 2006, **147**, 127–135.

210 M. M. Kraus, H. Prast and A. Philippu, *Br. J. Pharmacol.*, 2013, **170**, 214–221.

211 S. Dove, S. Elz, R. Seifert and A. Buschauer, *Mini-Reviews Med. Chem.*, 2004, **4**, 941–954.

212 N. Kagermeier, K. Werner, M. Keller, P. Baumeister, G. Bernhardt, R. Seifert and A. Buschauer, *Bioorganic Med. Chem.*, 2015, **23**, 3957–3969.

213 S. Pockes, D. Wifling, M. Keller, A. Buschauer and S. Elz, *ACS Omega*, 2018, **3**, 2865–2882.

214 J. M. Arrang, *Int. Rev. Neurobiol.*, 2007, **78**, 247–287.

215 L. Di Cesare Mannelli, C. Ghelardini, L. Micheli, F. Del Bello, M. Giannella, A. Piergentili, M. Pigini and W. Quaglia, *Eur. J. Pharmacol.*, 2017, **810**, 128–133.

216 D. J. Haleem, *Behav. Pharmacol.*, 2015, **26**, 45–58.

217 V. M. Pogorelov, R. M. Rodriguiz, J. Cheng, M. Huang, C. M. Schmerberg, H. Y. Meltzer, B. L. Roth, A. P. Kozikowski and W. C. Wetsel, *Neuropsychopharmacology*, 2017, 1–15.

218 K. Alix, S. Khatri, P. D. Mosier, S. Casterlow, D. Yan, H. L. Nyce, M. M. White and M. K. Schulte, 2016, **3**.

219 M. H. P. Verheij, A. J. Thompson, J. E. van Muijlwijk-Koezen, S. C. R.

Lummis, R. Leurs and I. J. P. de Esch, *J. Med. Chem.*, 2012, **55**, 8603–14.

220 A. J. Thompson and S. C. R. Lummis, *Curr. Pharm. Des.*, 2006, **12**, 3615–30.

221 G. Mengod, J. M. Palacios and R. Cortés, *ACS Chem. Neurosci.*, 2015, **6**, 1089–1098.

222 A. Newman-Tancredi, J. P. Nicolas, V. Audinot, S. Gavaudan, L. Verrièle, M. Touzard, C. Chaput, N. Richard and M. J. Millan, *Naunyn. Schmiedebergs. Arch. Pharmacol.*, 1998, **358**, 197–206.

223 R. Sakhuja, K. Kondabolu, T. Córdova-Sintjago, S. Travers, A. S. Vincek, M. S. Kim, K. A. Abboud, L. Fang, Z. Sun, C. E. Canal and R. G. Booth, *Bioorganic Med. Chem.*, 2015, **23**, 1588–1600.

224 A. R. Knight, A. Misra, K. Quirk, K. Benwell, D. Revell, G. Kennett and M. Bickerdike, *Naunyn. Schmiedebergs. Arch. Pharmacol.*, 2004, **370**, 114–123.

225 C. E. Canal, T. Cordova-Sintjago, Y. Liu, M. S. Kim, D. Morgan and R. G. Booth, *J. Pharmacol. Exp. Ther.*, 2013, **347**, 705–716.

226 C. E. Canal and K. S. Murnane, *J. Psychopharmacol.*, 2017, **31**, 127–143.

227 G. A. Higgins and P. J. Fletcher, *ACS Chem. Neurosci.*, 2015, **6**, 1071–1088.

228 S. Ruiu, G. Marchese, P. L. Saba, G. L. Gessa and L. Pani, *Mol. Psychiatry*, 2000, **5**, 673–677.

229 S. Akhondzadeh, M. Malek-Hosseini, A. Ghoreishi, M. Raznahan and S. A. Rezazadeh, *Prog. Neuro-Psychopharmacology Biol. Psychiatry*, 2008, **32**, 1879–1883.

230 C. L. Schmid, J. M. Streicher, H. Y. Meltzer and L. M. Bohn, *Neuropsychopharmacology*, 2014, **39**, 1902–1913.

231 L. Peng, L. Gu, B. Li and L. Hertz, *Curr. Neuropharmacol.*, 2014, **12**, 365–379.

232 L. Maroteaux, E. Ayme-dietrich, G. Aubertin-kirch, S. Banas, E. Quentin, R. Lawson, L. Monassier, L. Maroteaux, E. Ayme-dietrich, G. Aubertin-kirch, S. Banas and E. Quentin, 2017.

233 S. L. Diaz, S. Doly, N. Narboux-Nme, S. Fernández, P. Mazot, S. M. Banas, K. Boutourlinsky, I. Moutkine, A. Belmer, A. Roumier and L. Maroteaux, *Mol. Psychiatry*, 2012, **17**, 154–163.

234 J. Brea, J. Castro-Palomino, S. Yeste, E. Cubero, A. Párraga, E. Domínguez and M. I. Loza, *Curr. Top. Med. Chem.*, 2010, **10**, 493–503.

235 D. Wacker, S. Wang, J. D. McCorvy, R. M. Betz, A. J. Venkatakrishnan, A. Levit, K. Lansu, Z. L. Schools, T. Che, D. E. Nichols, B. K. Shoichet, R. O. Dror and B. L. Roth, *Cell*, 2017, **168**, 377–389.e12.

236 D. Morgan, K. Kondabolu, A. Kuipers, R. Sakhuja, K. L. Robertson, N. E. Rowland and R. G. Booth, *Neuropharmacology*, 2013, **72**, 274–281.

237 V. Bubenikova-Valesova, A. Stuchlik, J. Svoboda, J. Bures and K. Vales, *Proc. Natl. Acad. Sci.*, 2008, **105**, 1061–1066.

238 H. S. Blaxall, M. F. O'Rourke, L. J. Iversen and D. B. Bylund, *J. Pharmacol. Exp. Ther.*, 1994, **268**, 1362–1367.

239 M. Holmberg, V. Fagerholm and M. Scheinin, *Neuroscience*, 2003, **117**, 875–898.

240 M. Halme, B. Sj, J. Savola and M. Scheinin, *Biochim. Biophys. Acta - Proteins Proteomics*, 1995, **1266**, 207–214.

241 M. Dukat, K. Alix, J. Worsham, S. Khatri and M. K. Schulte, *Bioorganic Med. Chem. Lett.*, 2013, **23**, 5945–5948.

242 M. Dukat, *Curr. Med. Chem. CNS agents*, 2004, **4**, 77–94.

243 M. Dukat, Y. Choi, M. Teitler, D. Pre, K. Herrick-davis and R. A. Glennon, *Bioorg. Med. Chem. Lett.*, 2001, **11**, 1599–1603.

244 J. U. Peters, T. Lübbers, A. Alanine, S. Kolczewski, F. Blasco and L. Steward, *Bioorganic Med. Chem. Lett.*, 2008, **18**, 262–266.

245 J. U. Peters, T. Lübbers, A. Alanine, S. Kolczewski, F. Blasco and L. Steward, *Bioorganic Med. Chem. Lett.*, 2008, **18**, 262–266.

246 K. Hinton, D. Jean, R. Cerutis and D. B. Bylund, *J. Pharmacol. Exp. Ther.*, 1996, **278**, 1215–1227.

247 J. R. Jasper, J. D. Lesnick, L. K. Chang, S. S. Yamanishi, T. K. Chang, S. a Hsu, D. a Daunt, D. W. Bonhaus and R. M. Eglen, *Biochem. Pharmacol.*, 1998, **55**, 1035–1043.

248 B. Kelly, Trinity College Dublin, 2012.

249 S. A. Munk, D. Harcourt, P. Arasasinghana, C. Gluchowski, H. Wong, J. Burke, A. Kharlamb, C. Manlapaz, E. Padillo, L. Williams, L. Wheeler and M. Garst, *Bioorganic Medicit~al Chem. Lett.*, 1995, **5**, 1745–1750.

250 S. Schann, H. Greney, V. Gasparik, M. Dontenwill, C. Rascente, G. Lacroix, L. Monassier, V. Bruban, J. Feldman, J. D. Ehrhardt and P. Bousquet, *Bioorganic Med. Chem.*, 2012, **20**, 4710–4715.

251 S. Okumura, C. H. Lin, Y. Takeda and S. Minakata, *J. Org. Chem.*, 2013, **78**, 12090–12105.

252 E. Merino, *Chem. Soc. Rev.*, 2011, **40**, 3835–3853.

253 O. B. Sandor, A. Georgiades, R. Meszaros, K. Kis, I. Palinko and F. Fulop, *J. Catal.*, 2017, **348**, 90–99.

254 B. Dutta, S. Biswas, V. Sharma, N. O. Savage, S. P. Alpay and S. L. Suib, *Angew. Chemie - Int. Ed.*, 2016, **55**, 2171–2175.

255 K. Orito, T. Hatakeyama, S. Uchiito, M. Tokuda and H. Suginome,

Tetrahedron, 1998, **54**, 8403–8410.

256 A. Antoine John and Q. Lin, *J. Org. Chem.*, 2017, **82**, 9873–9876.

257 WIPO International, WO2004052869 (A1), 2004, 243.

258 E. E. Kwan, Y. Zeng, H. A. Besser and E. N. Jacobsen, *Nat. Chem.*, 2018, 1–7.

259 F. Blanco, B. Kelly, I. Alkorta, I. Rozas and J. Elguero, *Chem. Phys. Lett.*, 2011, **511**, 129–134.

260 C. Schroif-Grégoire, K. Barale, A. Zaparucha and A. Al-Mourabit, *Tetrahedron Lett.*, 2007, **48**, 2357–2359.

261 M. Tian, M. Yan and P. S. Baran, *J. Am. Chem. Soc.*, 2016, **138**, 14234–14237.

262 C. A. Seipp, N. J. Williams, V. S. Bryantsev, R. Custelcean and B. A. Moyer, *RSC Adv.*, 2015, **5**, 107266–107269.

263 W. M. Kan, S. Lin and C. Chern, *Synth. Commun.*, 2005, **35**, 2633–2639.

264 A. R. Katritzky, N. M. Khashab and S. Bobrov, 2005, **88**, 1664–1675.

265 H. Shen, Y. Wang and Z. Xie, *Org. Lett.*, 2011, **13**, 4562–4565.

266 J. W. Shaw, D. H. Grayson and I. Rozas, *Arkivoc*, 2014, **ii**, 161–174.

267 P. O. Sullivan and I. Rozas, *ChemMedChem.*, 2014, **9**, 2065–2073.

268 N. Matsumura, A. Noguchi, A. Kitayoshi and H. Inoue, *J. Chem. Soc. Perkin Trans. I*, 1995, **4**, 2953–2954.

269 P. O'Sullivan and I. Rozas, *ChemMedChem*, 2014, **9**, 2065–2073.

270 E. Martini, M. Norcini, C. Ghelardini, D. Manetti, S. Dei, L. Guandalini, M. Melchiorre, S. Pagella, S. Scapecchi, E. Teodori and M. N. Romanelli, *Bioorganic Med. Chem.*, 2008, **16**, 10034–10042.

271 G. H. Kuo, A. DeAngelis, S. Emanuel, A. Wang, Y. Zhang, P. J. Connolly, X. Chen, R. H. Gruninger, C. Rugg, A. Fuentes-Pesquera, S. A. Middleton, L. Jolliffe and W. V. Murray, *J. Med. Chem.*, 2005, **48**, 4535–4546.

272 Y. T. Xia, X. T. Sun, L. Zhang, K. Luo and L. Wu, *Chem. - A Eur. J.*, 2016, **22**, 17151–17155.

273 M. K. Sahoo, G. Jaiswal, J. Rana and E. Balaraman, *Chem. - A Eur. J.*, 2017, **23**, 14167–14172.

274 S. B. Bang and J. Kim, *Synth. Commun.*, 2018, **48**, 1291–1298.

275 S. Chen, Q. Wan and A. K. Badu-Tawiah, *Angew. Chemie - Int. Ed.*, 2016, **55**, 9345–9349.

276 N. Zumbrägel, M. Sako, S. Takizawa, H. Sasai and H. Gröger, *Org. Lett.*,

2018, **20**, 4723–4727.

277 J. Zhang, S. Chen, F. Chen, W. Xu, G. J. Deng and H. Gong, *Adv. Synth. Catal.*, 2017, **359**, 2358–2363.

278 H. Zhang, *Struct. Bond.*, 2006, **120**, 37–79.

279 N. J. Leonard and A. G. Cook, *J. Am. Chem. Soc.*, 1959, **81**, 5627–5631.

280 N. J. Leonard and F. P. Hauck, *J. Am. Chem. Soc.*, 1957, **79**, 5279–5292.

281 S. A. Munk, C. Gluchowski, L. Dolby, H. Wong, J. Burke, A. Kharlamb, C. Manlapaz, E. Padillo, D. Rodgers, B. Ohta, L. Wheeler and M. Garst, *Bioorganic Med. Chem. Lett.*, 1994, **4**, 459–462.

282 C. B. Chapleo, J. C. Doxey and P. L. Myers, *J. Med. Chem.*, 1982, **25**, 821–824.

283 C. G. Barber, R. P. Dickinson and P. V. Fish, *Bioorganic Med. Chem. Lett.*, 2004, **14**, 3227–3230.

284 O. Alijevic, H. Hammoud, A. Vaithia, V. Trendafilov, M. Bollenbach, M. Schmitt, F. Bihel and S. Kellenberger, *ACS Chem. Neurosci.*, 2018, **9**, 1357–1365.

285 C. G. Barber, R. P. Dickinson and V. A. Horne, *Bioorganic Med. Chem. Lett.*, 2002, **12**, 181–184.

286 US6248738B1, 2001, 1–32.

287 N. K. Hien, P. T. Quy, N. T. Trung, V. Vien, D. Van Khanh, N. T. A. Nhung and D. T. Quang, *Chem. Lett.*, 2014, **43**, 1034–1036.

288 M. H. Lee, S. W. Lee, S. H. Kim, C. Kang and J. S. Kim, *Org. Lett.*, 2009, **11**, 2101–2104.

289 M. V. Costa, L. C. de Sequeira Aguiar, L. F. B. Malta, G. M. Viana and B. B. S. Costa, *Tetrahedron Lett.*, 2016, **57**, 1585–1588.

290 A. P. Carley, S. Dixon and J. D. Kilburn, *Synthesis (Stuttg).*, 2009, 2509–2516.

291 M. Calas, M. Ouattara, G. Piquet, Z. Ziora, Y. Bordat, M. L. Ancelin, R. Escale and H. Vial, *J. Med. Chem.*, 2007, **50**, 6307–6315.

292 P. Zlatušková, I. Stibor, M. Tkadlecová and P. Lhoták, *Tetrahedron*, 2004, **60**, 11383–11390.

293 S. Wangngae, M. Pattarawarapan and W. Phakhodee, *J. Org. Chem.*, 2017, **82**, 10331–10340.

294 P. S. Chaudhari, P. S. Dangate and K. G. Akamanchi, *Synlett*, 2010, 3065–3067.

295 Z. K. Wan, E. F. Ousman, N. Papaioannou and E. Saiah, *Tetrahedron Lett.*,

2011, **52**, 4149–4152.

296 A. Porcheddu, L. De Luca and G. Giacomelli, *Synlett*, 2009, 3368–3372.

297 D. H. O'Donovan and I. Rozas, *Tetrahedron Lett.*, 2011, **52**, 4117–4119.

298 P. S. Chaudhari, S. P. Pathare and K. G. Akamanchi, *J. Org. Chem.*, 2012, **77**, 3716−3723.

299 R. Wong and S. J. Dolman, *J. Org. Chem.*, 2007, **72**, 3969–3971.

300 J. Nath, L. Jamir and B. K. Patel, *Green Chem. Lett. Rev.*, 2011, **4**, 1–34.

301 U. R. Mandapati, S. Pinapati and R. R. Rudraraju, *Tetrahedron Lett.*, 2017, **58**, 125–128.

302 P. Liu, C. Li, J. Zhang and X. Xu, *Synth. Commun. An Int. J. Rapid Commun. Synth. Org. Chem.*, 2013, **43**, 3342–3351.

303 H. Munch, J. S. Hansen, M. Pittelkow, J. B. Christensen and U. Boas, *Tetrahedron Lett.*, 2008, **49**, 3117–3119.

304 V. Štrukil, *Beilstein J. Org. Chem.*, 2017, **13**, 1828–1849.

305 H. Minegishi, S. Fukashiro, H. S. Ban and H. Nakamura, *ACS Med. Chem. Lett.*, 2013, **4**, 297–301.

306 K. Hagihara, H. Kashima, K. Iida, J. Enokizono, S. ichi Uchida, H. Nonaka, M. Kurokawa and J. Shimada, *Bioorg. Med. Chem. Lett.*, 2007, **17**, 1616–1621.

307 M. M. Uys, M. Shahid, J. Sallinen and B. H. Harvey, *Behav. Pharmacol.*, 2017, **28**, 9–18.

308 B. Sun, S. Lockyer, J. Li, R. Chen, M. Yoshitake and J. Kambayashi, *J. Pharmacol. Exp. Ther.*, 2001, **299**, 652–658.

309 K. Orito, M. Kishi, T. Imaizumi, T. Nakazawa, A. Hashimoto, T. Mori and T. Kambe, *Br. J. Pharmacol.*, 2001, **134**, 763–770.

310 R. A. Wise, F. M. Wigley, B. White, G. Leatherman, J. Zhong, H. Krasa, J. I. Kambayashi, C. Orlandi and F. S. Czerwiec, *Arthritis Rheum.*, 2004, **50**, 3994–4001.

311 E. Arponen, S. Helin, P. Marjamaki, T. Gronroos, P. Holm, E. Loyttyniemi, K. Nagren, M. Scheinin, M. Haaparanta-Solin, J. Sallinen and O. Solin, *J. Nucl. Med.*, 2014, **55**, 1171–1177.

312 K. Kawamura, M. Akiyama, J. Yui, T. Yamasaki, A. Hatori, K. Kumata, H. Wakizaka, M. Takei, N. Nengaki, K. Yanamoto, T. Fukumura and M. R. Zhang, *ACS Chem. Neurosci.*, 2010, **1**, 520–528.

313 P. Luoto, S. Suilamo, V. Oikonen, E. Arponen, S. Helin, J. Herttuainen, J. Hietamäki, A. Holopainen, M. Kailajärvi, J. M. Peltonen, J. Rouru, J. Sallinen, M. Scheinin, J. Virta, K. Virtanen, I. Volanen, A. Roivainen and J.

O. Rinne, *Eur. J. Nucl. Med. Mol. Imaging*, 2014, **41**, 1947–1956.

314 J. Lehto, M. M. Hirvonen, J. Johansson, J. Kemppainen, P. Luoto, T. Naukkarinen, V. Oikonen, E. Arponen, J. Rouru, J. Sallinen, H. Scheinin, L. Vuorilehto, S. J. Finnema, C. Halldin, J. O. Rinne and M. Scheinin, *Synapse*, 2015, **69**, 172–181.

315 J. Lehto, J. Johansson, L. Vuorilehto, P. Luoto, E. Arponen, H. Scheinin, J. Rouru and M. Scheinin, *Psychopharmacology (Berl).*, 2015, **232**, 4169–4178.

316 J. Lehto, A. Scheinin, J. Johansson, P. Marjamäki, E. Arponen, H. Scheinin and M. Scheinin, *Synapse*, 2016, **70**, 57–65.

317 J. Lehto, J. R. Virta, V. Oikonen, A. Roivainen, P. Luoto, E. Arponen, S. Helin, J. Hietamäki, A. Holopainen, M. Kailajärvi, J. M. Peltonen, J. Rouru, J. Sallinen, K. Virtanen, I. Volanen, M. Scheinin and J. O. Rinne, *Eur. J. Nucl. Med. Mol. Imaging*, 2015, **42**, 120–127.

318 S. Silver, M. T. Engstro, H. Salo, A. Tauber, H. Kyyro and P. Saarenketo, *J. Med. Chem.*, 2006, **49**, 6351–6363.

319 M. Kamber, S. Flückiger-Isler, G. Engelhardt, R. Jaeckh and E. Zeiger, *Mutagenesis*, 2009, **24**, 359–366.

320 L. Janovec, M. Kozurkova, D. Sabolova, J. Ungvarsky, H. Paulikov, J. Plsikova, Z. Vantova and J. Imrich, *Bioorganic Med. Chem.*, 2011, **19**, 1790–1801.

321 F. Bouyer, J. Moretto, D. Pertuit, A. Szollosi, M.-A. Lacaille-Dubois, Y. Blache, B. Chauffert and N. Desbois, *J. Inorg. Biochem.*, 2012, **110**, 51–57.

322 M. Carland, M. J. Grannas, M. J. Cairns, V. J. Roknic, W. A. Denny, W. D. McFadyen and V. Murray, *J. Inorg. Biochem.*, 2010, **104**, 815–819.

323 A. Cordeiro, P. S. Nagle, C. McKeever and I. Rozas, *Unpublished results*, 2015.

324 L. F. Callado, J. J. Meana, B. Grijalba, a Pazos, M. Sastre and J. a García-Sevilla, *J. Neurochem.*, 1998, **70**, 1114–23.

325 A. Wróblewska, P. Paluch, E. Wielgus, G. Bujacz, M. K. Dudek and M. J. Potrzebowski, *Org. Lett.*, 2017, **19**, 5360–5363.

326 E. Valeur and M. Bradley, *Chem. Soc. Rev.*, 2009, **38**, 606–631.

327 D. Kloos, R. J. E. Derks, M. Wijtmans, H. Lingeman, O. A. Mayboroda, A. M. Deelder, W. M. A. Niessen and M. Giera, *J. Chromatogr. A*, 2012, **1232**, 19–26.

328 J. P. Hughes, S. S. Rees, S. B. Kalindjian and K. L. Philpott, *Br. J. Pharmacol.*, 2011, **162**, 1239–1249.

329 D. A. DeGoey, H.-J. Chen, P. B. Cox and M. D. Wendt, *J. Med. Chem.*, 2017, **61**, 2636–2651.

330 C. Dardonville, B. A. Caine, M. Navarro De La Fuente, G. Martín Herranz, B. Corrales Mariblanca and P. L. A. Popelier, *New J. Chem.*, 2017, **41**.

331 J. Sallinen, A. Haapalinna, J. Holappa, A. Koivisto, K. Kuokkanen, J. Lehtimäki, P. Piepponen, J. Mijatovic, H. Tanila, R. Virtanen, J. Sirviö and H. Chapman, *Basic Clin. Pharmacol. Toxicol.*, 2013, **113**, 239–249.

332 J. Wellbourne-Wood and J. Y. Chatton, *ACS Chem. Neurosci.*, 2018, **9**, 1975–1985.

333 H. G. Roweth, R. Yan, N. H. Bedwani, A. Chauhan, N. Fowler, A. H. Watson, J. D. Malcor, S. O. Sage and G. E. Jarvis, *Sci. Rep.*, 2018, **8**, 1–14.

334 K. Schrör, *Semin. Thromb. Hemost.*, 1997, **23**, 349–356.

335 Y. Ramot, A. Nyska and G. Spectre, *Drug Saf.*, 2013, **36**, 585–603.

336 R. E. Scharf, *Semin Thromb Hemost*, 2012, **38**, 865–883.

337 K. Koltai, G. Kesmarky, G. Feher, A. Tibold and K. Toth, *Int. J. Mol. Sci.*, 2017, **18**, 1–21.

338 D. E. Roberts, A. McNicol and R. Bose, *J. Biol. Chem.*, 2004, **279**, 19421–19430.

339 M. J. Santos-Martínez, A. Prina-Mello, C. Medina and M. W. Radomski, *Analyst*, 2011, **136**, 5120–5126.

340 K. Yamane, Y. Kato, J. Tazaki, T. Tada, T. Makiyama, M. Imai, T. Jinnai, T. Ikeda, R. Shirakawa, T. Kimura and H. Horiuchi, *J. Atheroscler. Thromb.*, 2012, **19**, 559–569.

341 K. Nakamura, H. Kariyazono, T. Shinkawa, T. Yamaguchi, T. Yamashita, O. Ayukawa, Y. Moriyama, G. Yotsumoto, H. Toyohira, a Taira and K. Yamada, *Hum. Exp. Toxicol.*, 1999, **18**, 487–92.

342 J. G. Baker, *Br. J. Pharmacol.*, 2008, **153**, 1011–1021.

343 R. Usha and T. Ramasami, *Colloids Surfaces B Biointerfaces*, 2008, **61**, 39–42.

344 B. Ahmad, M. Z. Ahmed, S. K. Haq and R. H. Khan, *Biochim. Biophys. Acta - Proteins Proteomics*, 2005, **1750**, 93–102.

345 M. Ishtikhar, A. Khan, C. K. Chang, L. T. W. Lin, S. S. S. Wang and R. H. Khan, *J. Biomol. Struct. Dyn.*, 2016, **34**, 1409–1420.

346 M. Cattaneo, A. Lecchi, M. Ohno, B. V. Joshi, P. Besada, S. Tchilibon, R. Lombardi, N. Bischofberger, T. K. Harden and K. A. Jacobson, *Biochem. Pharmacol.*, 2004, **68**, 1995–2002.

347 R. A. Nicholas, *Blood*, 2015, **125**, 893–896.

348 D. H. O'Donovan, B. Kelly, E. Diez-Cecilia, M. Kitson and I. Rozas, *New J. Chem.*, 2013, **37**, 2408.

349 M. E. Marketou, E. Kintsurashvili, N. E. Androulakis, J. Kontaraki, M. G. Alexandrakis, I. Gavras, P. E. Vardas and H. Gavras, *Int. J. Cardiol.*, 2013, **168**, 2561–2566.

350 I. M. L. W. Keularts, R. M. A. Van Gorp, M. A. H. Feijge, W. M. J. Vuist and J. W. M. Heemskerk, *J. Biol. Chem.*, 2000, **275**, 1763–1772.

351 F. Lanza, J. P. Cazenave, A. Beretz, A. Sutter-Bay, J. G. Kretz and R. Kieny, *Agents Actions*, 1986, **18**, 586–595.

352 D. Pinthong, P. Songsermsakul, P. Rattanachamnong and D. A. Kendall, *J Pharm Pharmacol*, 2004, **56**, 213–220.

353 P. Corporation, *Tech. Bull.*, 2009, **306**, 608–277.

354 R. Paniccia, R. Priora, A. A. Liotta and R. Abbate, *Vasc. Health Risk Manag.*, 2015, **11**, 133–148.

355 C. N. Floyd and A. Ferro, *JRSM Cardiovasc. Dis.*, 2012, **1**, 1–13.

356 J. F. Van Velzen, B. A. P. Laros-Van Gorkom, G. A. M. Pop and W. L. Van Heerde, *Thromb. Res.*, 2012, **130**, 92–98.

357 J. U. Peters, *J. Med. Chem.*, 2013, **56**, 8955–8971.

358 A. Talevi, *Front. Pharmacol.*, 2015, **6**, 1–7.

359 G. R. Fulmer, A. J. M. Miller, N. H. Sherden, H. E. Gottlieb, A. Nudelman, B. M. Stoltz, J. E. Bercaw and K. I. Goldberg, *Organometallics*, 2010, **29**, 2176–2179.

360 World Intellectual Property Organization, Patent Number:WO2006/94237, 2006.

361 B. Kelly and I. Rozas, *Tetrahedron Lett.*, 2013, **54**, 3982–3984.

362 WO2007099317 (A1), 2007, 96–106.

363 H. Zhao, X. Hu, K. Cao, Y. Zhang, K. Zhao, C. Tang and B. Feng, *Eur. J. Med. Chem.*, 2018, **157**, 935–945.

364 I. Armitage, M. Fu, F. Hicks, A. Kattuboina, J. S. N. Li, A. McCarron and L. Zhu, *J. Heterocycl. Chem.*, 2017, **54**, 728–734.

365 Z. Tu, S. Li, A. Li, M. Taylor, D. Ho, M. Malik, R. R. Luedtke and R. H. Mach, *Med.Chem.Comm.*, 2013, **4**, 1283–1289.

366 K. W. Jeong, J. H. Lee, S. M. Park, J. H. Choi, D. Y. Jeong, D. H. Choi, Y. Nam, J. H. Park, K. N. Lee, S. M. Kim and J. M. Ku, *Eur. J. Med. Chem.*, 2015, **102**, 387–397.

367 S. Park, B. L. Hayes, F. Marankan, D. C. Mulhearn, L. Wanna, A. D. Mesecar, B. D. Santarsiero, M. E. Johnson and D. L. Venton, *J. Med. Chem.*, 2003, **46**, 936–953.

368 M. Buchholz, U. Heiser, S. Schilling, A. J. Niestroj, K. Zunkel and H. U. Demuth, *J. Med. Chem.*, 2006, **49**, 664–677.

369 J. D. Bloom, M. J. DiGrandi, R. G. Dushin, K. J. Curran, A. A. Ross, E. B. Norton, E. Terefenko, T. R. Jones, B. Feld and S. A. Lang, *Bioorg. Med. Chem. Lett.*, 2003, **13**, 2929–2932.